The synthesis and study of titanium amidinate complexes as olefin polymerisation catalysts

Maren Theresa Scharbert

MChem, AMRSC

St Edmund Hall



Thesis submitted to the University of Oxford for the degree of Doctor of Philosophy in Inorganic Chemistry, August 2018.

Statement of confidentiality

Some of the work described in this Thesis is of a commercially sensitive nature. The examiners are requested to respect the confidentiality of this information and not to disclose the information to individuals outside the Board of Examiners.

The work described in this Thesis was carried out in the Chemistry Research Laboratory, University of Oxford from October 2015 to August 2018 under the supervision of Professor Philip Mountford. All work is my own unless stated to the contrary, and has not previously been submitted for any degree at this or any other university.



Maren Theresa Scharbert

August 2018

Abstract

Maren Theresa Scharbert Trinity 2018
St Edmund Hall D.Phil. Thesis

This Thesis is concerned with the synthesis of post-metallocene group 4 amidinate complexes as pre-catalysts for the polymerisation and oligomerisation of α-olefins. Activation of half-sandwich group 4 amidinate complexes with 1,3-conjugated dienes is also investigated and their underlying chemistry is explored.

Chapter 1 introduces homogeneous Ziegler-Natta catalysis, with a specific focus on group 4 compounds. A review of metallocene and post-metallocene complexes of group 4 will also be presented and their behaviour in olefin polymerisation will be discussed.

Chapter 2 describes the synthesis and characterisation of κ^1-amidinate supported titanium complexes. Base-free activation of the titanium cyclopentadienyl-amidinate dialkyl complexes will be investigated and the resulting cationic species will be further explored with commonly applied trapping agents. The synthesis and characterisation of new titanium cyclopentadienyl-amidinate diene complexes and their corresponding tri(pentafluorophenyl)borane-activated zwitterionic compounds will also be described and their performance in the co-polymerisation of ethylene and propylene will be discussed.

Chapter 3 explores the addition of 1,3-conjugated diene reagents to titanium cyclopentadienyl-amidinate and guanidinate alkyl cations. Mechanistic and computational studies of allyl and diene formation will also be described. The polymerisation capabilities of the newly formed complex will be discussed and compared to previously reported dialkyl complexes.

Chapter 4 describes the synthesis and characterisation of aminopyridinato titanium complexes and κ^1-κ^2-bis(amidinate) titanium complexes. The activation chemistry of the newly formed dialkyl complexes will be investigated. Furthermore, the synthesis of a new bis(aminopyridinato) titanium complex will also be discussed alongside their activity in EPM and EPDM polymerisation.

Chapter 5 describes the performance of the aminopyridinato titanium complexes (synthesised in Chapter 4) in EPDM polymerisation. The sensitivity of the

aforementioned complexes towards hindered phenols will also be discussed and their behaviour in ethylene oligomerisation will be explored.

Chapter 6 presents full experimental procedures and characterising data for the new complexes reported in this Thesis.

CD Appendix contains .cif files for all new crystallographically characterised complexes described.

Contents

	Statement of confidentiality	i
	Declaration	ii
	Abstract	iii
	Contents	iv
	Acknowledgements	ix
	Abbreviations	xi

Chapter One – Introduction

1.1	General introduction	1
1.2	Early metal catalysed polymerisation of olefin	1
1.3	Polymerisation mechanism	2
1.3.1	Propagation mechanism	3
1.3.2	Chain transfer and termination pathways	4
1.4	Polymer analysis	7
1.4.1	GPC analysis	7
1.4.2	Specific monomer incorporation	8
1.5	Homogeneous catalyst advances	9
1.5.1	*Ansa*-metallocene catalyst	9
1.5.2	CGC systems	10
1.5.3	Post-metallocene catalyst and the isolobal analogy	11
1.5.3.1	Half-sandwich group 4 complexes	11
1.5.3.2	Alternative face-capping ligands	16
1.5.3.3	Chelating amidinate ligands	17
1.5.3.4	Chelating aryloxide ligands	19

1.6	Activators	20
1.6.1	Aluminium-based activators	20
1.6.2	Protonolysis	21
1.6.3	Alkyl abstraction	23
1.6.4	BAr^F_3 activation of dialkyl complexes	24
1.6.5	BAr^F_3 activation of diene complexes	25
1.7	Metal alkyl cations	27
1.7.1	Non-classical interactions	27
1.7.2	Reactivity of metal alkyl cations	30
1.8	Project Introduction	33
1.8.1	Neutral κ^1-amidinate titanium diene complexes	33
1.8.2	Aminopyridinato titanium complexes and their activity in co-polymerisation	35
1.9	Summary and Objectives	35
1.10	References	36

Chapter Two – Synthesis, reactivity and polymerisation capabilities of cyclopentadienyl-amidinate complexes

2.1	Overview	50
2.2	Syntheses and characterisation of cyclopentadienyl-amidinate complexes	50
2.3	Activation chemistry of Cp*Ti{NCN(Dipp)$CH_2C_6H_4$}X_2 (**3** and **4**)	56
2.3.1	Activation with $[Ph_3C][BAr^F_4]$	56
2.3.2	Activation with BAr^F_3	59
2.3.3	Activation with $[HNMe_2Ph][BAr^F_4]$	60
2.4	Syntheses and characterisation of cyclopentadienyl-amidinate diene complexes	63
2.4.1	Cp*Ti{NCN(Dipp)$CH_2C_6H_4$}{η-2,3-$C_4H_4Me_2$} (**11**)	64
2.4.2	Cp*Ti{NCN(Dipp)$CH_2C_6H_4$}{η-$CH_2(CH)_2CHEt$} (**12**)	66
2.4.3	Cp*Ti{NCN(Dipp)$CH_2C_6H_4$}{η-1,4-$C_4H_4Me_2$} (**13**)	68
2.4.4	Synthesis and characterisation of zwitterionic cyclopentadienyl-amidinate complexes	70

2.4.4.1	Cp*Ti{NCN(Dipp)$CH_2C_6H_4$}{η^3-EtCH$(CH)_2CH_2BAr^F_3$} (**14**)	70
2.4.4.2	Attempted reaction of **11** with BAr^F_3	74
2.5	EPM co-polymerisation of **3**, **12** and **14**	75
2.6	Summary	77
2.7	References for Chapter 2	77

Chapter Three –Synthesis, mechanistic and polymerisation studies of cationic κ^1-amidiante diene and allyl complexes

3.1	Overview	81
3.2	Reaction of [Cp*Ti{NCN(Dipp)$CH_2C_6H_4$}Me][BAr^F_4] (**5-[BAr^F_4]**) with conjugated dienes	82
3.2.1	[Cp*Ti{HNCN(Dipp)$CH_2C_6H_4$}{η-$CH_2(CH)_3{}^iPr$}][BAr^F_4] (**15-[BAr^F_4]**)	83
3.2.2	[Cp*Ti{HNCN(Dipp)$CH_2C_6H_4$}{η-$CH_2(CH)_3Et$}][BAr^F_4] (**16-[BAr^F_4]**)	86
3.3	Experimental and DFT mechanistic studies of reaction pathway	90
3.4	Synthesis of activated diene complexes with other κ^1-amidinate and κ^1-guandinate titanium complexes	103
3.4.1	Variation of the κ^1-amidinate supporting ligand	104
3.4.2	Reaction of conjugated diene with κ^1-guanidinate half-sandwich complexes	107
3.5	Polymerisation studies	115
3.6	Addition of Lewis bases to **15-[BAr^F_4]** and **16-[BAr^F_4]**	125
3.7	Summary	126
3.8	References	127

Chapter Four – Synthesis, characterisation and reactivity of aminopyridinato- and κ^2-amidinate titanium complexes

4.1	Overview	129
4.2	Ligand synthesis	129
4.3	Synthesis of (Ap^R)Ti{NC(Ph)N^iPr_2}X_2 (R = 1, 2 or 3 and X = Cl, Me or CH_2Ph)	131
4.4	Attempted synthesis of alternative aminopyridinato, κ^1-amidinate titanium dichloride complex	142

4.5	Synthesis and characterisation of cationic mono-alkyl complexes	144
4.6	Synthesis of mixed κ^1- and κ^2-amidinate titanium complexes	148
4.6.1	Synthesis of Ti{NC(Ph)N^{i}Pr$_2$}{MeC(NDipp)$_2$}X$_2$ (X = Cl or Me)	149
4.6.2	Attempted synthesis of Ti{NC(Ph)N^{i}Pr$_2$}(hpp)Cl$_2$ (**52**)	154
4.7	Synthesis and characterisation of cationic mono-alkyl complexes of Ti{NC(Ph)N^{i}Pr$_2$}{MeC(NDipp)$_2$}Me$_2$ (**51**)	155
4.8	Synthesis of homo-bis(ligand) complexes	156
4.8.1	Synthesis of bis(aminopyridinato) complex (Ap^1)$_2$TiCl$_2$ (**55**)	156
4.8.2	Synthesis of previously reported bis(amidinate) (κ^1or κ^2) complexes	159
4.9	Polymerisation studies of the κ^2-amidinate complexes, **50**, **51**, and the bis(aminopyridinato) complex **55**	159
4.10	Summary	160
4.11	References	160

Chapter Five – High-throughput polymerisation and oligomerisation studies for mixed aminopyridinato, κ^1-amidinate titanium complexes

5.1	Overview	163
5.2	EPDM ter-polymerisation experiments using **1.75**–**1.77**, **4.02** and **32**–**34**	168
5.3	BHT-H sensitivity of **35** and **37**	171
5.4	Ethylene oligomerisation experiments with **35** and **37**	176
5.5	Summary	190
5.6	References	191

Chapter Six – Experimental details and characterising data

6.1	General methods and instrumentation	195
6.2	Literature preparations and reagent purification	195
6.3	X-ray data collection and processing parameters	196
6.4	General polymerisation procedure	196
6.4.1	General polymerisation reagents	197

6.4.2	Ethylene-Propylene copolymerisation	197
6.4.3	Parallel Polymerisation Reactor (PPR) procedure	198
6.4.4	1-hexene polymerisation	199
6.5	Computational details	199
6.6	Experimental details and characterising data for Chapter Two	200
6.7	Experimental details and characterising data for Chapter Three	214
6.8	Experimental details and characterising data for Chapter Four	227
6.9	Experimental details and characterising data for Chapter Five	246
6.9.1	Characterising data	246
6.9.2	Ethylene oligomerisation procedures	249
6.10	References	251
Appendix		253

CD Appendix

Acknowledgements

First and foremost, I would like to thank my supervisor Professor Philip Mountford for the support and advice provided throughout my DPhil. His dedication and precision to everything he does is unmatched. Thank you for all your support, DFT calculations and encouragement.

I would like to thank my collaborators at ARLANXEO. In particular Dr Gerard von Doremaele, Dr Alexandra Berthoud, Dr Maxence Valla and Dr Raffaele Bernardo who's constant help, interest in my project and encouragement has been crucial for this Thesis. A thank you also to Mr John van de Moosdijk, Mr Sander Niessen, Mr Bart van Weyde and Mr Wouter van Meerendonk who I had the pleasure to meet while spending time at Chemelot.

Furthermore, I would also like to thank Professor Christophe Copéret and Dr Alexey Fedorov who gave me access to their High Throughput Experimentation facility at ETH Zürich and provided support throughout the week I spent there.

A very important thank you must go to everyone in the Mountford group and friends across the CRL. A special thanks goes to Dr Richard Collins who supervised me at the start of my PhD and made sure I would never forget three of my crystals failing on a Sunday afternoon by playing "Why can't we be friends" on repeat for weeks. Also thanks to Dr Ben Clough and Dr Bowen Xie, who went above and beyond helping me to run and solve my crystal structures, while also always helping around the lab and proof-reading my Thesis. I have been lucky to meet Dr Matt Blake and Dr Insun Yun who provided wise scientific advice. Karen Gamero has been a great lab partner and friend throughout my time in the Mountford group, always making labs more fun with her continuous positive attitude and good mood which was infectious. Nichabhat Diteepeng, who was very supportive, especially in the last few months of writing, and was always up for a coffee break. I would also like to thank my two Part II students, Wilf Diment and Claire Nesbitt, I wish you both the best of luck in during your studies and working life. A thank you to David Ryan, his bottomless knowledge about literature and scientific discussion has been much appreciated. A thank you to Natalia Reis, Martin Sulsarczyk, Simona Mellino, Adan Reyes, Ross Green, Archie McNeills and past group members who made going to conferences, pub trips and discussion about the world cup always enjoyable.

A special thank you must go to Dr Jean-Charles Buffet and Dr Zoë Turner who appreciate geeky Star Wars jokes as much as I do and who always were around to give me scientific and life advice.

I would also like to thank the Green Impact team, especially Sue Henderson and Joy Cook. The endless cake exchanges and laughter's during our meetings and award ceremonies won't be forgotten.

I am very grateful for all those who keep the CRL safe and operating. I would like to thank Dr Nick Rees with NMR (and fun uni-club pub trips) and Dr Amber Thompson with crystallography.

I cannot be thankful enough for all the friends who I have met during my time at Oxford. Especially the lunches with Harriet Godwin at University Park and the endless committee meetings at Teddy Hall with Linde Wester I will remember fondly. Not to forget my friends from undergraduate and home, Natalie Keir, Jenny Peake, Miye Hong Thomé de Moura, Rebecca Muller Alcalay and Jasmine Bickel who have always made the effort to come and visit me wherever I moved to and showed great interest in my DPhil progress throughout the years.

An enormous thank you goes to the four people who have been the most patient and supporting through the last three years. My parents, Sabine and Bernd, who with their continuous support, trust and believing in me have made this possible. My sister, Annika, who spent Sundays working on the second floor of the CRL besides me and made sure I would also explore the UK going on road trips with me. And last but not least, my partner, Nicholas, who always lent me an ear and made me laugh in the toughest times. I cannot wait to see what the future holds for the two of us. Words cannot even describe how much the support from the four of you means to me and I hope you see this as much as your achievement as mine.

Abbreviations

General

Å	Ångstrom
avg.	average
ca.	*circa*, about
calcd.	calculated
Cp_{cent}	computed cyclopentadienyl ring carbon centroid
CSD	Cambridge Structural Database
°C	degrees Celsius
°	degrees
DFT	Density Functional Theory
Eq.	equivalent(s)
g	gram(s)
GPC	Gel Permeation Chromatography
η	hapticity
h	hour(s)
k	kilo
K	Kelvin
κ	denticity
kJ	kilojoule(s)
l	litre(s)
mbar	millibar(s)
mg	milligram(s)
min	minute(s)
ml	millilitre(s)
mmol	millimole(s)
psi	pounds per square inch
rpm	revolutions per minute
RT	room temperature

μ	bridging
μl	microlitre(s)
μmol	micromole(s)
vs.	*versus*

Chemical

Ap	aminopyridinato
Ar	aryl
Ar^{F_2}	2,6-$C_6H_3F_2$
$[BAr^{F}{}_3]^-$	tris(pentafluorophenyl)borane, $B(C_6F_5)_3$
$[BAr^{F}{}_4]^-$	tetra(pentafluorophenyl)borate, $[B(C_6F_5)_4]^-$
BHT-H	2,6-di-*tert*-butyl-4-methylphenol
Bn	benzyl
Bu	*n*-butyl
^{t}Bu	*tert*-butyl
CGC	constrained geometry catalyst
Cp	cyclopentadienyl
Cp^*	pentamethylcyclopentadienyl
DiBAlO	Bis-(diisobutylaluminum)oxide
Dipp	2,6-diisopropylphenyl
DMP	2,4-dimethyl-1-pentene
EPM	ethylene-propylene
EPDM	ethylene-propylene-diene monomer
ENB	5-ethylidenebicyclo[2.2.1]hept-2-ene
Et	ethyl
Et_2O	diethyl ether
H-hpp	1,3,4,6,7,8-hexahydro-2*H*-pyrimido[1,2-*a*]pyrimidine
L	a supporting ligand set
M	metal or mol dm^{-3}
MAO	methylaluminoxane

Me	methyl
Mes	mesityl, 2,4,6-trimethylphenyl
M_n	number average molecular weight
M_w	weight average molecular weight
PDI	polydispersity index
Ph	phenyl
PMH	pentamethylheptane
PPR	Parallel Polymerisation Reactor
^{i}Pr	*iso*-propyl
py	pyridine
R	generic alkyl group or hydrogen atom
TACN	triazacyclononane
TiBA	tri(isobutyl)aluminium
TMA	trimethylaluminium, $AlMe_3$
THF	tetrahydrofuran
TMEDA	*N*,*N*,*N´*,*N´*-tetramethylethylenediamine
Tp^{Ms*}	HB(3-mesityl-pyrazolyl)$_2$(5-mesityl-pyrazolyl)
TPM	tris(3,5-dimethylpyrazoyl)methane
Tripp	2,4,6-triisopropylphenyl
Trop	tropidinyl
VNB	5-vinylbicyclo[2.2.1]hept-2-ene
X	generic halide or alkyl ligand
Xyl	2,6-$C_6H_3Me_2$

Nuclear Magnetic Resonance Spectroscopy

app.	apparent
br	broad
$^{13}C\{^{1}H\}$	proton-decoupled ^{13}C
COSY	correlation spectroscopy
d	doublet

δ	chemical shift in ppm
HMBC	heteronuclear multiple bond correlation
HSQC	heteronuclear single quantum coherence
Hz	Hertz
i	*ipso*
J	coupling constant
m	*meta*
m	multiplet
MHz	Megahertz
NMR	Nuclear Magnetic Resonance
o	*ortho*
p	*para*
ppm	parts per million
q	quartet or quaternary
ROESY	rotating-frame nuclear Overhauser Effect spectroscopy
s	singlet
sept	septet
SST	spin saturation transfer
t	triplet
VT	variable temperature

Mass Spectrometry

EI	Electron Impact
ESI	Electrospray Ionisation
m/z	mass to charge ratio
MS	Mass spectrometry

Infrared Spectroscopy

cm^{-1}	wavenumbers
FT-IR	Fourier transform infrared

IR	Infrared
m	medium
s	strong
w	weak
ν	frequency

Notes

Literature compounds described in this Thesis are numbered **1.x**, **2.x**, **3.x**, **4.x**, **5.x** according to the Chapter in which they occur. The new compounds described in this Thesis are numbered **1–59**. Density functional theory (DFT) calculations were carried out by Professor Philip Mountford. DFT calculated compounds which were also obtained experimentally, are labelled with a Q before the compound number. Compounds only obtained by DFT calculations are labelled with letters from **A**–**T**. X-ray data was collected by Dr Richard Collins (**32** and **52**), Dr Ben Clough (**2**, **33**, **34**, **38**, **40**, **51** and **50**) or Dr Bowen Xie (**4** and **14**) and solved and refined by the author. In all cases the molecular drawings were produced by Prof Philip Mountford. Polymerisations were carried out by ARLANXEO under the supervision of Dr Alexandra Berthoud.

Chapter One

Introduction

1.1 General introduction

The discovery of group 4 metal catalysed polyolefin production in the 1950's by Ziegler and Natta shaped the research of the following decades. In 2015, 178 million tons of polyolefins were produced and over 300 grades of commercial polyolefins are available.[1-3] This emphasises the importance of research into heterogeneous and homogeneous catalytic systems, to provide economically and energy-efficient synthesis of polyolefins. This project was carried out in collaboration with ARLANXEO, a leading company in the production of ethylene, propylene and diene co-polymer (EPDM). The catalysts applied in this process are of homogeneous nature and research advancements will be highlighted throughout this Chapter.

This Thesis is concerned with the synthesis of novel group 4 κ^1-amidinate complexes, bearing at most one cyclopentadienyl supporting ligand, and their productivity in EPDM polymerisation. Fundamental research of the activation chemistry of half-sandwich complexes bearing a range of κ^1-amidinate and κ^1-guanidinate ligands in the presence of conjugated dienes will be explored in Chapters Two and Three. Furthermore, complexes bearing κ^1-amidinate moieties and a range of κ^2-binding mode ligands will be investigated and their productivity in EPDM polymerisation and ethylene oligomerisation will be discussed in Chapters Four and Five.

This Chapter will provide a concise summary of olefin polymerisation processes including a short overview of heterogeneous systems first applied in olefin polymerisation, the mechanistic role of the catalysts and the advancements of homogeneous catalysts over the last few decades. The further focus lies on the activation of those homogeneous catalysts and their behaviour as active species. Finally, a summary of research conducted within the Mountford group, relevant to this Thesis, will be given.

1.2 Early metal catalysed polymerisation of olefins

In 1963, Ziegler and Natta were awarded the Noble Prize for their ground-breaking research in the field of 'chemistry and technology of high polymers'. Ziegler's discovery of low pressure polymerisation of ethylene using a mixture of aluminium alkyls and metals from group 4 and 6,[4] and Natta's discovery of stereoselective polymerisation of propene with the same systems[5] triggered intensive research in academia and industry. To date, most olefin polymerisation processes in industry rely

on heterogeneous catalysis. However, those systems also have limitations, illustrated by the nature of the ill-defined active site, leading to broad molecular weight distributions and inhibiting good mechanistic understanding of the process. Wilkinson first introduced the synthesis of bis(cyclopentadienyl) (bis(Cp)) group 4 metal complexes in 1953 and hence opened up a new field of research for metallocene compounds.[6] Natta and Breslow independently studied Cp_2MX_2 (M = Ti (**1.01**) or Zr) sandwich complexes, showing that these systems were capable of polymerising ethylene in the presence of co-catalysts Et_2AlCl or Et_3Al.[7-9] However, their reactivity was lower compared to Ziegler systems and were prone to reduction of Ti(IV) to the inactive Ti(III) complex. Despite Vseley and co-workers suggesting that water acts as a poison to these systems,[10] an unexpected increase in productivity was discovered when a small amount of water was added to the aluminium activated metallocene systems. This enhancement was proposed to result from the *in situ* generation of methyl aluminoxane (MAO).[11-14] MAO, made by the reaction of trialkylaluminium and water, is an ill-defined species that is made up from a mixture of different oligomers including cyclic ones.[15] Sinn and co-workers have shown that the hexamethyl-tetraaluminoxane $[Al_4O_3Me_6]_4$ is a major component of MAO and therefore proposed a structure similar to the structure of *tert*-butylaluminoxane.[16-18]

1.3 Polymerisation mechanism

The mechanism for olefin polymerisation using homogeneous catalysts has been widely investigated. It was believed that the active species would be somewhat similar to the one for the heterogeneous Ziegler-Natta polymerisation resulting in a halide-bridged titanium aluminium mixed-metal species as suggested by Breslow and Newburg.[19] However, in 1961, Shilov and co-workers suggested the active species to be a cation of the type $[Cp_2TiMe]^+$.[20, 21] Even though, Dyachkovskii conducted electrochemical experiments and showed that ethylene polymerisation would only take place in the cathode chamber in dichloromethane, and no direct evidence for the active cationic species was given.[21] Direct evidence was provided by Eisch and co-workers by isolation and characterisation of $[Cp_2Ti\{C(SiMe_3)C(Ph)Me\}][AlCl_4]$ (**1.02**, Scheme 1.1).[22]

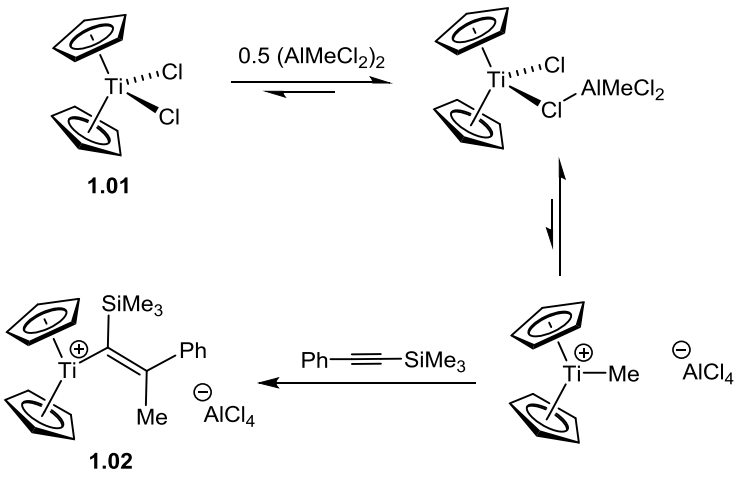

Scheme 1.1. Alkyne insertion into $[Cp_2TiMe]^+$.

Further evidence was provided by Jordan and co-workers as they reported the reaction of Cp_2ZrR_2 (R = alkyl) with $Ag[BPh_4]$ followed by recrystallisation from THF resulted in the cationic zirconium adduct $[Cp_2Zr(Me)(THF)][BPh_4]$. This complex was active in the polymerisation of ethylene and evidently encouraged the extension of the scope for co-catalysts beyond alkyl aluminium species.[23, 24]

1.3.1 Propagation mechanism

Historically, there have been four mechanistic proposals for the nature of the M-alkyl insertion essential for chain propagation (Figure 1.1).[25] Adapting the Cossee-Arlman mechanism from heterogeneous to homogenous catalysis suggests the active site is enclosed by a set of ancillary ligands.[26, 27] Firstly, an olefin coordinates to the electron deficient metal centre, giving a π-adduct. This is followed by migrating the alkyl group to the unsaturated ligand, resulting in an overall insertion reaction and the propagation of the polymer chain and simultaneous regeneration of the active species. Rooney and Green have adapted the Cossee-Arlman mechanism where a metal-alkylidene hydride species is generated *via* an oxidative 1,2-Hydrogen shift from the polymer chain to the metal centre.[28] The newly formed species undergoes [2+2] cycloaddition to give a metallocyclobutane with the incoming olefin and *via* reductive elimination propagates the chain. A further modification to the Green-Rooney mechanism is the presence of a α-H agostic interaction throughout the catalytic pathway.[29, 30] And the last proposed mechanism, shown in Figure 1.1, implies the stabilising α-H agostic interaction is only present in the transition state upon formation of metallocyclobutane. This is now the widely accepted general

mechanism, although the relative importance of the α-agostic interaction appears to be system-dependent as judged by mechanistic studies.[31]

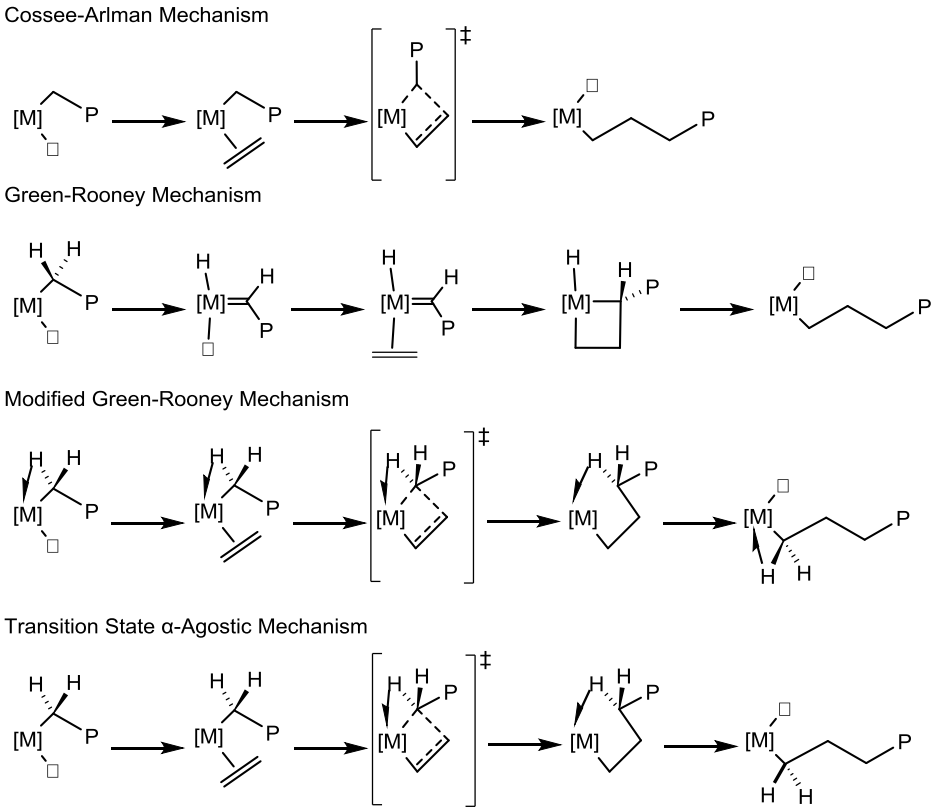

Figure 1.1. Proposed insertion mechanisms for Ziegler-Natta catalysis. P = polymeryl chain.[25] [M] represents a metal-ligand moiety.

1.3.2 Chain transfer and termination pathways

Chain transfer and termination pathways compete with propagation and are crucial in controlling the molecular weight of polymer. Chain transfer varies greatly with the nature of the monomer as well as the structure of catalyst.[32-34] There are several known chain transfer mechanisms, including β-H elimination,[35-37] β-H transfer to monomer,[32] β-Me elimination[38-40] and chain transfer to aluminium,[35, 36] all displayed in Figure 1.2.

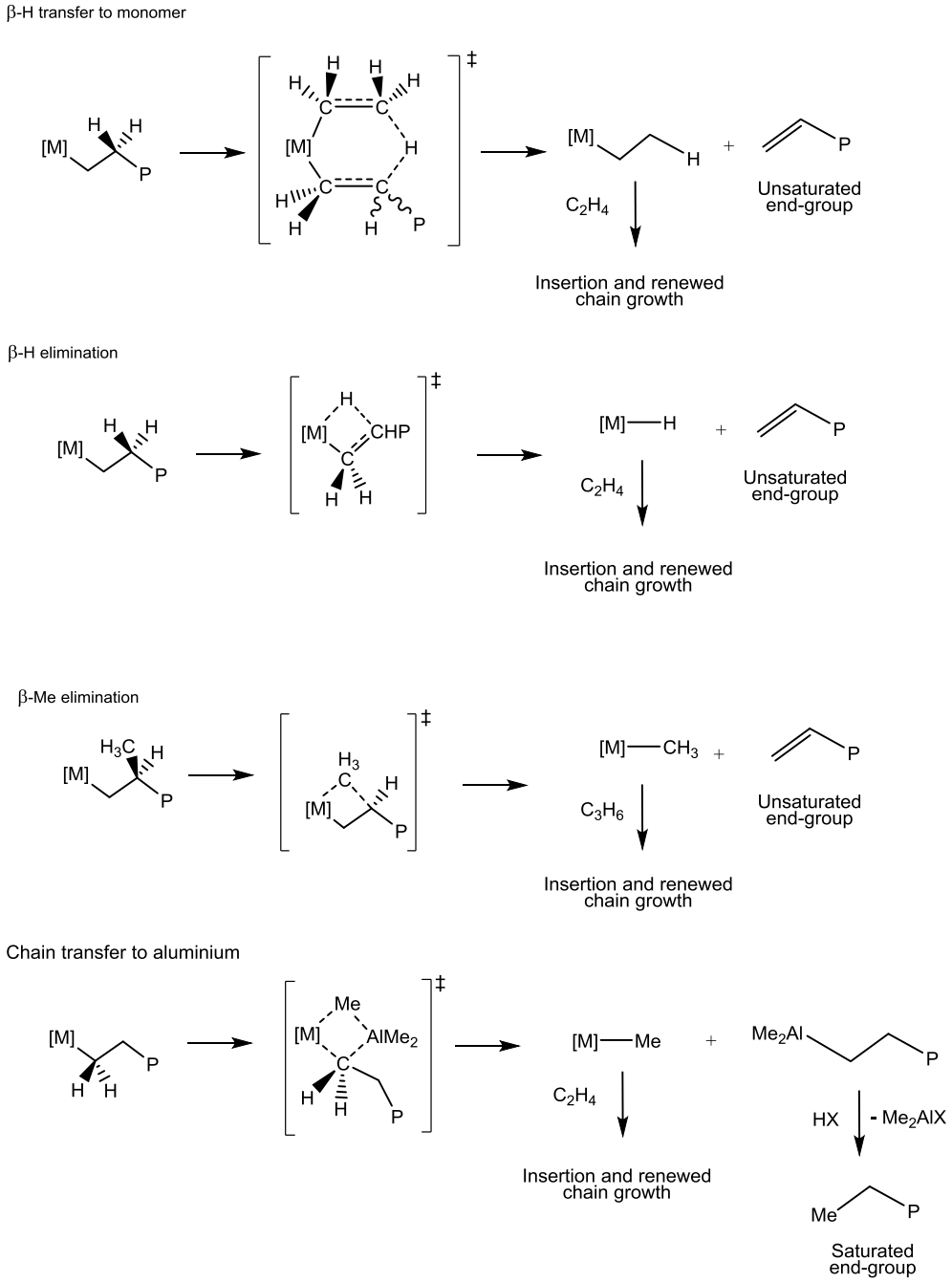

Figure 1.2. Chain transfer and termination pathways. P = polymeryl chain. [M] represents a metal-ligand moiety.

β-H transfer is a bimolecular process which proceeds *via* a 6-membered ring transition state while β-H elimination is a unimolecular process which progresses *via* a 4-membered ring transition state. However, both result in vinylic polymer end-groups and therefore are difficult to distinguish between.[41-43] DFT calculations conducted by Ziegler and co-workers[44] have shown that the energy barrier of β-H

transfer is always smaller than the one for β-H elimination. In agreement with experimental data, β-H transfer is the dominant mechanism for chain termination.[45]

However, it has been shown by Teuben *et al*.[38] that β-Me elimination dominates the chain termination step in the case of polypropylene. Resconi and co-workers disclosed that the preference for β-Me elimination can be credited to steric hindrance.[39, 46] The transition state of β-H elimination/transfer (**A**), implies that the β-Me group clashes sterically with the pentamethylcyclopentadienyl ligand (Cp*), while the transition state for β-Me elimination (**B**) pathway shows less steric crowding (Figure 1.3).

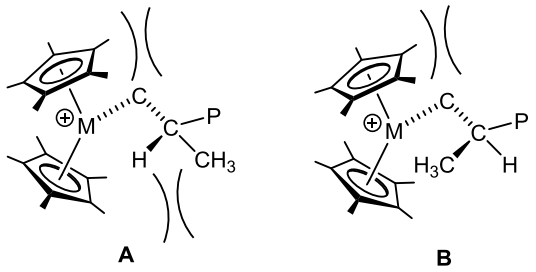

Figure 1.3. Steric hindrance of transition state **A** and **B**.[39]

MAO is known to be an effective activator and scavenger (*vide infra*). However, it provides another possible chain termination step *via* transfer to aluminium (Figure 1.2). The resulting polymer possesses saturated end-groups and can therefore be distinguished from the other termination pathways.[47] MAO contains residual amounts of $AlMe_3$ (TMA) which influences catalytic activity and is difficult to remove. Resconi *et al*.[48] have shown that upon polymerisation of propylene with TMA as the co-catalyst, polymer chain with *iso*butyl-terminated ends are seen and serve as direct evidence for chain transfer to aluminium. Furthermore, the heterodinuclear complexes formed with TMA, exemplified in Figure 1.2, can be resting states in olefin polymerisation with MAO.[49, 50] It has also been shown that residual amount of TMA can reduce Ti(IV) complexes to Ti(III) or Ti(II), both of which are inactive species.[51] There are several ways to prevent interference of TMA, discussed in Section 1.6.1.

On occasions, where the rate of propagation exceeds the rate of termination considerably, hydrogen can be introduced into the system to allow control of molecular weight.[52] Due to the high affinity of the metal cation to hydrogen, chain transfer is the preferred route over the other termination pathways and similar to β-H

elimination, a M–H species is thought to re-enter the catalytic cycle as an active species.[53-55]

1.4 Polymer analysis

Polymer analysis is important to identify the molecular weight, the polydispersity index, incorporation of the substrate in co-polymerisation and the tactiticy for stereoregulated polymerisation processes. The main technique relevant to this Thesis is gel permeation chromatography (GPC).

1.4.1 GPC analysis

GPC, a form of size exclusion chromatography, provides a convenient method to determine the molecular weight distribution and the molecular weight averages of a polymer.[56] The polymer is dissolved and passed through a column as a solution. The column contains pores of varying sizes resulting in the separation of small molecules from larger molecules, where larger molecules have shorter retention times.[57] The chromatogram displays the peak molecular weight (M_p), the number average molecular weight (M_n) and the weight average molecular weight (M_w), as displayed in Equations 1.1 and 1.2 respectively.

M_n is given by:

$$M_n = \frac{\sum N_i \times M_i}{\sum N_i} \qquad \textbf{Equation 1.1}$$

where N_i equals to the number of molecules having a molar mass of M_i.

M_w is given by:

$$M_w = \frac{\sum W_i \times M_i}{\sum W_i} \qquad \textbf{Equation 1.2}$$

where W_i is the mass of polymers having a molar mass of M_i, where $W_i = N_i \times M_i$.

Mark-Houwink parameters (K and α), relating the molecular weight to the polymers intrinsic viscosity, and calibration are necessary to obtain the absolute molecular weight.[58] The chromatogram also provides insight into the behaviour of the catalytic species. Mono-modal traces are observed if only one active single-site is present, while higher modality indicates the presence of multiple active species. Furthermore, the polydispersity index (PDI), obtained by the ratio of M_w to M_n, gives a value of 1.0 if all chains have the same lengths.[59] This indicates "living polymerisation" where no

termination pathways occur. A PDI of 2.0 is generally observed if chain transfer mechanisms are taking place.[60]

1.4.2 Specific monomer incorporation

Accessibility of olefin feedstock to other monomers such as propylene, 1-hexene and others, have allowed the scope to be widened beyond polyethylene. However, polyethylene (including high density, low density and linear low density polymers) and polypropylene are the main polymers produced on an industrial scale to date. The co-polymerisation of ethylene, propylene and diene is of particular importance to this Thesis. EPDM is a random terpolymer obtained from the co-polymerisation of ethylene and propylene and a non-conjugated diene (Figure 1.4). The diene, such as ENB (5-ethylidene-2-norbornene) or VNB (5-vinyl-2-norbornene) is incorporated typically in 2–10 wt% quantities.[61] For those dienes, the strained cyclic double bond is incorporated into the main chain, while the other double bond remains in the polymerisation and allows cross-linking of the polymers post polymerisation *via* sulphur vulcanisation or peroxide reagents.[62] ^{1}H NMR spectroscopy and FT-IR analysis can be used to identify the relative quantities of incorporation of the diene substrate.

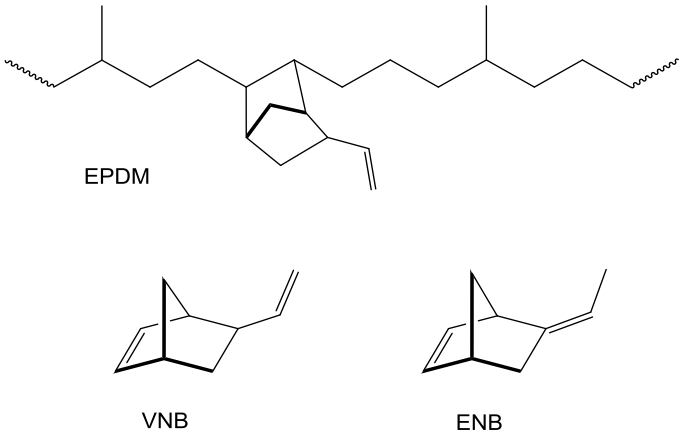

Figure 1.4. Representation of a segment of EPDM and the monomers VNB and ENB.

EPDM has good mechanical and elastic properties, as well as good resistance against heat, polar solvents, aqueous media and oxygen.[62, 63] Therefore its applications are wide ranged from roof sheeting, to wire and cable insulation and as part of the inlay of 2018's world cup football. A commonly applied catalyst for the co-polymerisation was the classical Vanadium-based Ziegler-Natta catalyst. However, due to low

productivity and low reactor temperature requirements to achieve high molecular weight, the scope shifted to homogeneous catalysis.[61, 62, 64-66]

1.5 Homogeneous catalyst advances

Despite the discovery of metallocenes in the presence of MAO polymerising ethylene and propylene, excessive research and patenting in the field combined with limited thermal stability and production of only low molecular weight polymers has triggered further exploration into the field of homogeneous early transition metal catalysed olefin polymerisation. For this Thesis, the main focus will lie on early transition state metals, especially group 4 metals. However, it should be noted that extensive research has been carried out on coordination compounds containing metals from across the periodic table.[67-74]

1.5.1 *Ansa*-metallocene catalysts

Introducing an *ansa*-bridging moiety to link the two supporting ligands on the metal centre, such as cyclopentadienyl or indenyl ligands, gave rise to a new class of compounds known as *ansa*-metallocenes. Brintzinger and co-workers prepared a range of stereorigid, chiral *ansa*-titanocene complexes utilising an $-CH_2CH_2-$ bridge (**1.03** and **1.04**, Figure 1.5).[75] The racemic mixture of **1.03** was employed by Ewen *et al*. in the polymerisation of propylene, resulting in atactic and isotactic polypropylene.[76] However, the enantiomer pure complex **1.04** gave only isotactic polypropylene.[77, 78]

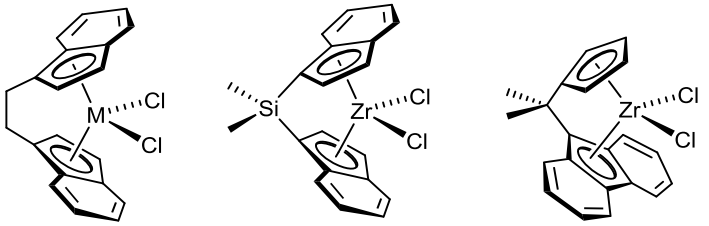

1.03 M = Ti
1.04 M = Zr

1.05

1.06

Figure 1.5. Example of *ansa*-metallocenes that exhibit tacticity control.

Replacing the $-CH_2CH_2-$ bridge with the smaller dimethyl silyl bridge, as shown for **1.05**, had beneficial impact on the molecular weight and isotacticity of polypropylene.[79] Introducing further variations in substitution on the ring ligands, such as a methyl substituent in 2-position of the indenyl ligand, led to an increase in molecular weight and isotacticity.[80, 81] *Ansa*-metallocenes containing C_s-symmetry, such as **1.06**, gave syndiotactic polypropylene.[82]

1.5.2 CGC systems

Introducing an *ansa*-cyclopentadienyl-amido ligand system with scandium (III) metal by Bercaw[83], followed shortly by a publication from Okuda utilising the same ligand system with titanium metal[84] led to the discovery of constrained geometry catalysts (CGC). Those catalysts are utilised by Dow[85-88] (Figure 1.6) and Exxon[89-91] and are defined as complexes where two ligands, coordinated to the same metal centre, are linked to one another. This results in a smaller bite angle between the auxiliary ligand, the metal and the centroid of the π-system than in non-linked complexes.[85] Overall, the new set of catalysts show high activity, thermal stability and high incorporation of co-monomers such as high length α-olefins.[92, 93] The rise in activity can be attributed to a more electrophilic metal centre arising from the possibility of the amide to act as a 3-electron donor.[94] However, studies also have shown the important role of the linker moiety on the activity of the catalyst. Dimethyl silyl or the $-CH_2CH_2-$ linkers result in small bite angles providing a more sterically open environment (**1.07** and **1.08**, respectively). Introducing 2-dimethysilyl linkers (**1.09**) leads to an increase in bite angle and consequently a reduction in activity and co-monomer incorporation was observed.[71]

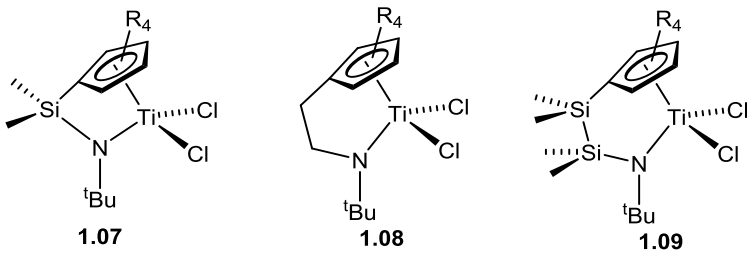

Figure 1.6. Example of Dow's constrained geometry catalysts.

Particularly interesting in the light of this project are the low-valent Ti(III) complex **1.10** and *o*-aryl bridged cyclopentadienyl-amide complex **1.11**, introduced by DSM[95, 96] and by Lanxess (now ARLANXEO), respectively.[97] Both were utilised in the preparation of EPDM polymer showing high thermal stability and molecular weight capacities (Figure 1.7).

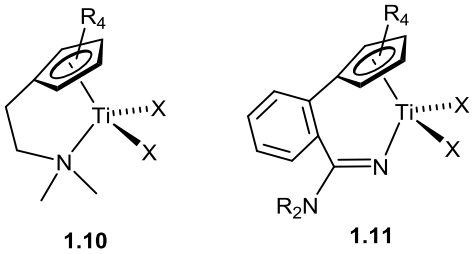

Figure 1.7. Structures of DSM's Lovacat (left) and Lanxess CGC Titanium compound (right).

1.5.3 Post-metallocene catalyst and the isolobal analogy

The concept of isolobal analogy, established by Hoffmann,[98] opened up a new era of group 4 complexes for olefin polymerisation, namely post-metallocene catalysts and offered alternatives to the heavily patented metallocene and CGC systems.[99] Isolobality relates two electronically defined systems by the similarity of symmetry, shape and energies of their frontier orbitals. Frontier orbitals of cyclopentadienyl ligands (Cp) consists of a single σ-donor and two π-donor orbitals, all three can interact with the metal centre (Figure 1.8). The aim of post-metallocene complexes is to replace at least one of the cyclopentadienyl ligands on the metal centre with an isolobal moiety. The focus of the following Section will be on anionic heteroatom moieties binding to the metal centre in a κ^1- and κ^2-mode and their advantages in polymerisation will be discussed.

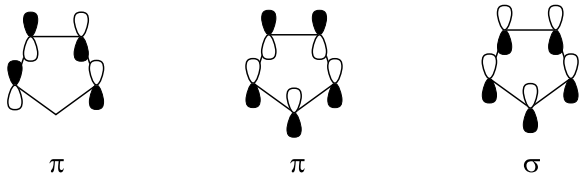

Figure 1.8. Frontier orbital symmetries of Cp moiety.

1.5.3.1 Half-sandwich group 4 complexes

A range of isolobal ligands have been investigated as alternatives for cyclopentadienyl ligands including aryl oxides (**1.12**), phosphinimides (**1.13**), non-*ansa* amides (**1.14**), ketimides (**1.15**), amidinates (**1.16**), iminoimidazolide (**1.17**) and guanidinates (**1.18**) to give non-*ansa* half-sandwich post-metallocene precatalysts (Figure 1.9).[73, 100]

Serrano introduced a range of halo- and alkyl-oxo half-sandwich titanium complexes.[101] But it was not until 1998, when Nomura *et al*. investigated the capability of these aryl-oxo half-sandwich complexes (**1.12**) as ethylene, propylene and styrene polymerisation catalysts in the presence of MAO.[102, 103] Nomura and co-workers have also investigated aryl-oxo compounds of the type $Cp^{R}Ti(O\text{-}2,6\text{-}C_6H_3{}^{i}Pr_2)Cl_2$ (R = Cp*, $C_5H_4{}^{t}Bu$ or 1,2,4-$C_5H_2Me_3$) in the co-polymerisation of ethylene with various α-olefins. The Cp* containing aryl-oxo complex displayed the highest activity for co-polymerisation of ethylene/1-hexene and ethylene/norbornene with high incorporation of the α-olefin.[104-107] In contrast, aryl-oxo complexes with either $C_5H_4{}^{t}Bu$ or 1,2,4-$C_5H_2Me_3$ substituent showed the highest activity and uniform incorporation of cyclohexene in the co-polymerisation of ethylene/cyclohexene.[108]

Phosphinimide post-metallocene complexes (**1.13**) were first introduced by Stephen and co-workers and showed to be electronically and sterically similar to cyclopentadienyl ligands.[109] In ethylene polymerisation, the systems such as $CpTi(NP^{t}Bu_3)Cl_2$ showed a higher activity than the parent metallocene complex under similar conditions.[110, 111] The newly fashioned post-metallocene pre-catalysts were thermally stable and the importance of steric bulk on the phosphinimide ligands has been emphasised by a *tert*-butyl substituted pre-catalyst preforming much better in polymerisation processes than isopropyl or cyclohexyl analogues.[109, 110]

Okuda and Nomura both investigated amide complexes **(1.14)** as post-metallocene catalysts.[112-114] When $Cp^*Ti(NMe_2)(CH_2Ph)_2$ was activated with $B(C_6F_5)_3$, highly syndiotactic polystyrene was obtained. Interestingly, this was not observed with the dimethyl silyl bridged constrained geometry catalyst (**1.07**), which is known to be inactive in the polymerisation of styrene. However, the analogues $Cp^*Ti(NMe_2)Cl_2$ when activated with MAO only poorly polymerised ethylene.[112] More recently, Nomura and co-workers explored pyrrolyl ligands as isoelectronic alternatives to cyclopentadienyl fragments and have shown that they usually bound in a η^1-fashion to the metal centre. Conversely, low steric demanding pyrrolyl ligands led to a higher activities when polymerising ethylene in the presence of MAO.[115]

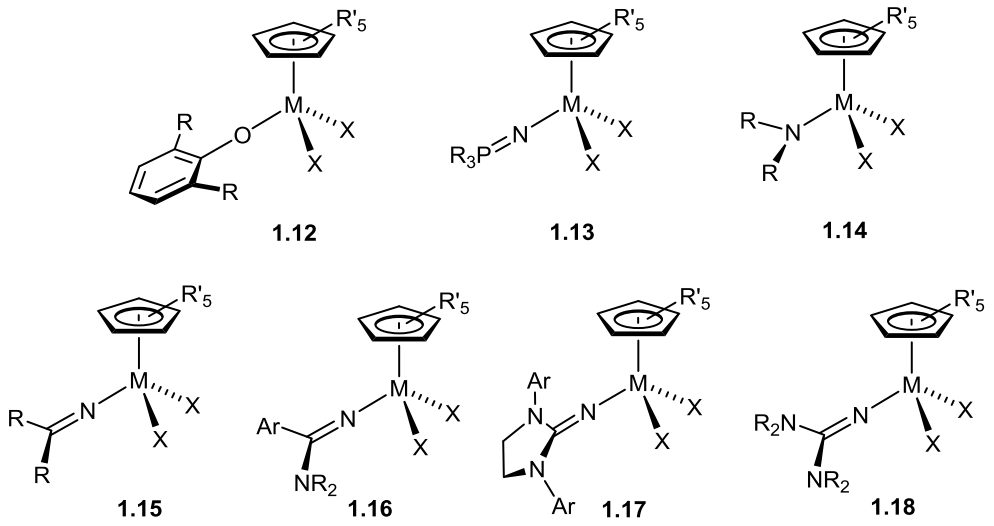

Figure 1.9. Non-*ansa* half-sandwich post-metallocene precatalysts.

The first ketimide complex was synthesised by Jibril *et al*. in 1986 but it was not until later that its activity in olefin polymerisation was discovered.[116] Nomura and co-workers have shown that ketimide complexes of the type $Cp^RTi(NC^tBu_2)Cl_2$ (Cp^R = Cp, $C_5H_4{}^tBu$ or Cp*) are highly active ethylene polymerisation and 1-hexene/ethylene co-polymerisation catalysts in the presence of MAO.[117] Changing the substituent on the cyclopentadienyl fragment of **1.15** did not seem to influence incorporation of 1-hexene, opposing observations for aryl oxide and amide complexes (**1.12** and **1.14,** respectively).[118] $Cp^*Ti(NC^tBu_2)Cl_2$ acts as a living co-polymerisation catalyst of ethylene and styrene.[119] The solid state structure showed an almost linear binding fashion and a short Ti–N bond length.[120, 121]

Replacing the alkyl substituents on the ketimide ligand with either one or two nitrogen atoms, results in amidinate (**1.16**), iminoimidazoldide (**1.17**) and guanidiante (**1.18**) ligand systems.

Kretschmer, Tamm and Nomura have independently investigated iminoimidazolide ligand systems (**1.17**, Figure 1.9).[122-125] Kretschmer *et al*. synthesised $CpTi\{1,3\text{-}(Xyl)_2(CH_2N)_2CN\}TiX_2$ (X= Cl or CH_2Ph) and showed in a comparative study relating iminoimidazolide post-metallocene complexes to ketimide complexes (**1.14**) in the presence of MAO, that $CpTi\{1,3\text{-}(Xyl)_2(CH_2N)_2CN\}Ti(CH_2Ph)_2$ was a highly efficient catalyst and more active than the equivalent ketimide species, $CpTi(NC^tBu_2)(CH_2Ph)_2$ (1600 *vs*. 464 kg mol^{-1} h^{-1} bar^{-1}).[122] The higher activity can

be derived from the significant π-bonding of these complexes compared to the ketimide systems. The enhanced π-bonding arises from formal lone pair donation of the amino nitrogen's towards the π_{CN} system. This allows the ligand to donate up to 5 electrons *via* a σ+2π interaction (Figure 1.10).

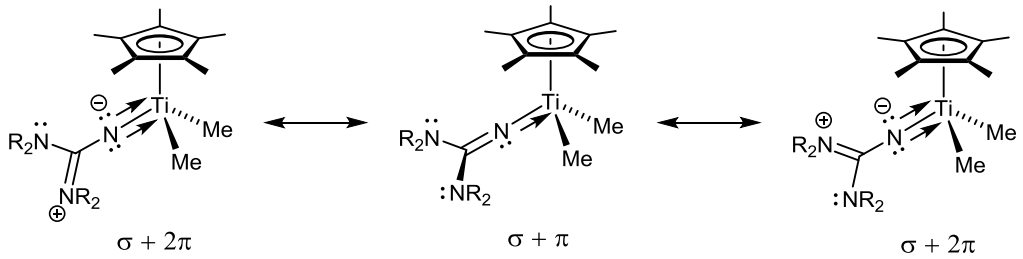

Figure 1.10. Metal-ligand bonding interactions for guanidinate supported complexes (**1.17** and **1.18**).

Various studies investigating substitution on the ligand backbone of **1.17**, have shown how ligand modification can be used as a tool to fine tune the catalysts for specific polymerisation. This is exemplified by *tert*-butyl substitution giving higher ethylene polymerisation activities over xylene substitution.[123] At the same time, the more bulky systems exhibited lower activity in syndiospecific styrene polymerisation.

In recent years, Mountford and co-workers have, in collaboration with ARLANXEO (formerly Lanxess and DSM), investigated κ^1-amidinates and non-cyclic κ^1-guanidinates ligands for EPDM co-polymerisation (**1.16** and **1.18**, respectively).[126, 127] κ^1-amidinate ligands are isolobal with ketimides, guanidinates and cyclopentadienyl type ligands and have the ability to act as σ+2π donors, as do iminoimidazolides; however, the system tends to be less basic as only one substituent can donate its lone pair to the nitrogen atom. The flexibility of aryl and alkyl substitution allows investigation of the influence of electronic and steric properties on the active polymerisation species. Titanium amidinate complexes are known to produce ultra-high molecular weight polyethylene and also have an outstanding performance in co-polymerisation of EPDM.[126, 128-130] Complex **1.16** is now marketed under the trade name Keltan ACE^{TM} and in 2015, a plant was built in Changzhou, China to implement the newly developed technology.[131] These systems are of relevance to this Thesis.

Another ligand set used in half-sandwich complexes are κ^2-bound amidinates. Unlike **1.16**, the monoanionic charge can be spread over the central NCN unit, and therefore

these systems are best considered to be isoelectronic to allyl and carboxylate ligands (Figure 1.11).[132]

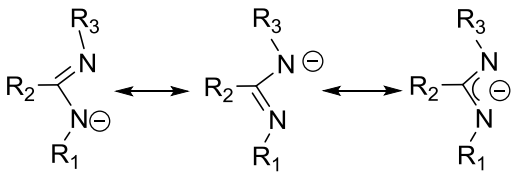

Figure 1.11. *N*,*N*'-disubstituted amidinate resonance forms.

Dehnicke was the first to report a zirconium(II) complex with a supporting κ^2-amidinate ligand, *viz. N,N´*(bis-trimethylsilyl)benzamidinate.[133] Shortly after, Edelmann and Green reported the metallocene analogues $(C_5R_5)M\{PhC(N(SiMe_3)_2\}Cl_2$ (R = H (**1.19**) or Me (**1.20**), Figure 1.12).[134-136] These systems were active in ethylene polymerisation in the presence of MAO however, overall, the activity was lower than of the parent metallocene complexes.

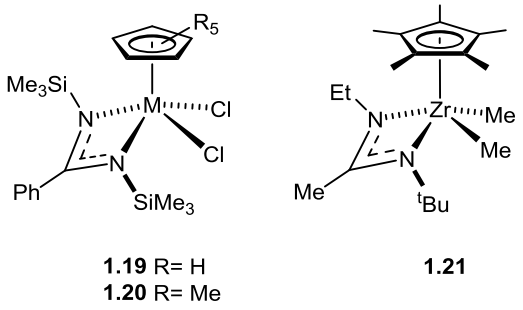

1.19 R= H
1.20 R= Me

1.21

Figure 1.12. Structure of κ^2-amidinate supported post-metallocene complexes **1.19**–**1.21** (where M = Zr or Ti and R = H or Me).

Sita and co-workers also investigated the catalytic activity of unsymmetrical substituted benzamidinate ligands, such as $Cp^*Zr\{MeC(N(^tBuC)(NEt)\}Me_2$ (**1.21**) by insertion of carbodiimides into the Zr–Me bond of Cp^*TiMe_3.[137, 138] Upon activation of **1.21** with $[HNMe_2Ph][BAr^F{}_4]$ (where $Ar^F = C_6F_5$), the resulting metal cation was highly active and stereoselective in the polymerisation of 1-hexene to give isotactic and high molecular weight poly(1-hexene).[139]

So far this section has focused on replacing just one of the cyclopentadienyl fragments with ligands in either η^1- or η^2-binding modes, however, non-cyclopentadienyl group 4 metal complexes have also been included in this research. Alternative element incorporation into the cyclopentadienyl ligand as well as face-capping ligands will be explored in the following Section.

1.5.3.2 Alternative face-capping ligands

In 1996, Bazan and co-workers investigated the electronic modification of group 4 metal complexes by replacing the cyclopentadienyl fragment with heterocyclic ligands. The main focus was on boratabenzene ligands, where the substitution of the boron moiety was varied, changing the electronics of the ligand backbone (**1.22** and **1.23**, Figure 1.13). Amine substitution gave a strong B–N π-orbital overlap, manifested in the molecular structure of **1.22** with a short bond distance. This weakened the metal–B interaction. In the presence of MAO, $(C_5H_5BN^iPr_2)_2ZrCl_2$ (**1.22**) gave similar activities to Cp_2ZrCl_2 in the polymerisation of ethylene.[140] On the other hand, substitution of the boron atom with an ethoxy group, $(C_5H_5BOEt)_2ZrCl_2$ (**1.23**) tuned the catalyst to oligomerise ethylene instead.[141] A potential reason for this observation, provided by Bazan *et al*., suggests an increase in the B–O bond length led to ultimately shorter B–Zr bond distance, allowing greater orbital overlap between B–Zr bond and therefore making the catalyst more electrophilic. This increases the rate of β-H elimination, favouring oligomerisation over polymerisation.[142] Replacing one of the carbon atoms in the cyclopentadienyl moiety with a phosphorus atom gives $(PC_4Me_4)_2ZrCl_2$ (**1.24**), which in the presence of MAO polymerises ethylene less readily compared to the parent metallocene complex, $Cp^*_2ZrCl_2$ (**1.26**).[143]

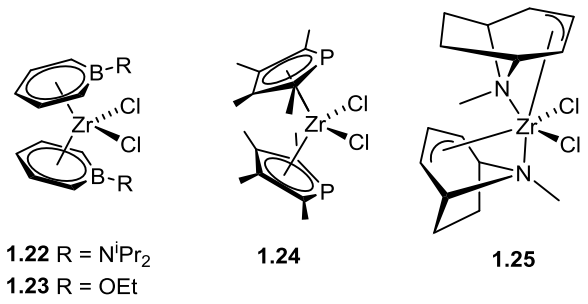

1.22 R = N^iPr_2
1.23 R = OEt

1.24

1.25

Figure 1.13. Group 4 cyclopentadienyl analogues.

Introducing two tropidinyl (trop) ligands to the metal centre, resulting in $(trop)_2ZrCl_2$ (**1.25**, Figure 1.13), where the allyl moiety acts as a 2π-donor and the amine moiety as a σ-donor.[144] Overall, this results in an isoelectronic but less symmetric complex compared to Cp_2ZrCl_2. **1.25** is only moderately active in ethylene polymerisation and shows bimodal behaviour, indicating the presence of more than one active site.[145]

Trofimenko[146-148] discovered tris(pyrazolyl)borate ligands as alternatives to Cp moieties and, more recently, Gil *et al*.[149-151] and Jordan *et al*.[152] used those ligand sets

to give a class of group 4 non-metallocene complexes with varying sterics, exemplified with $(Tp^{Ms*})TiCl_3$ (Tp^{Ms*} = HB(3-mesityl-pyrazolyl)$_2$(5-mesityl-pyrazolyl)). These systems showed comparable activity in ethylene polymerisation to the parent metallocene complexes.[151] Mountford and co-workers also explored the synthesis of a range of κ^1-amidinate titanium complexes with supporting tris(pyrazolyl)borate ligand (**1.27**, Figure 1.14), however, when activated with MAO only low activities in polymerisation of ethylene were observed.[153]

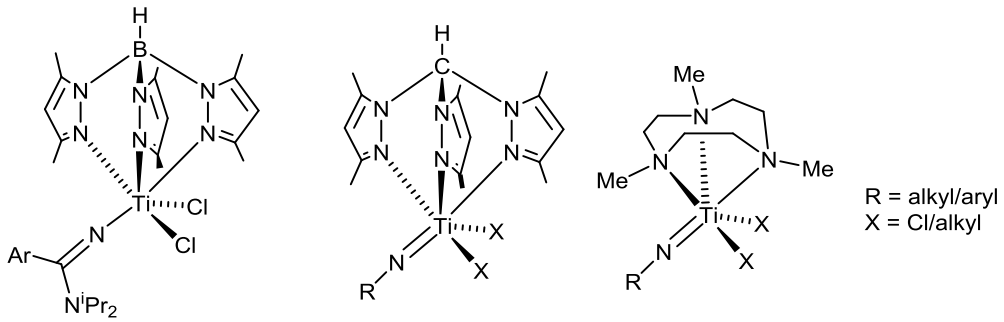

1.27 **1.28** **1.29**

Figure 1.14. Group 4 non-metallocene complexes with supporting face capping ligands.

Related systems using neutral face-capping ligands such as tri(3,5-dimethylpyrazoyl)methane (TPM) and triazacyclononane (TACN) in conjunction with a supporting imido ligand were also investigated (**1.28** and **1.29**, respectively).[154-157] An in-depth study of the substituent on the imido moiety of **1.29** showed that bulky and electron-donating alkyl groups led to highly active systems once activated with MAO.[158-160]

1.5.3.3 Chelating amidinate ligands

Bis-κ^2-amidinate complexes are also known in the field of post-metallocene catalysts. Eisen *et al*. synthesised the bis-(benzamidinate) zirconocene complex, $\{PhC(NSiMe_3)_2\}_2ZrCl_2$ (**1.30**), by reacting bis(trimethylsilyl)benzamidinate lithium-TMEDA (TMEDA = *N*,*N*,*N´*,*N´*-tetramethylethylenediamine) with $ZrCl_4$.[161] Arnold showed that **1.30** is also sterically similar to $Cp^*_2ZrCl_2$ (**1.26**), as the reaction with two equivalents of $(THF)_2LiTeSi(SiMe_3)_3$ gives only the mono-substituted complex, $R_2Ti\{TeSi(SiMe_3)_3\}Cl$ (R= Cp* or $PhC(NSiMe_3)_2$) in both cases.[162] It is known, however, that the same reaction using Cp_2ZrCl_2 leads instead to the bis-substituted product $Cp_2Ti\{TeSi(SiMe_3)_3\}_2$.[163] Furthermore, Richter *et al*. replaced the silyl-

fragment with an alkyl group as the Si–N bond is more prone to hydrogenation. This led to a series of group 4 complexes of the type $\{PhC(NR)_2\}_2MCl_2$ (M = Ti, Zr and R = ^{i}Pr or Cy), which possessed comparable catalytic activities of ethylene polymerisation to **1.20**.[164]

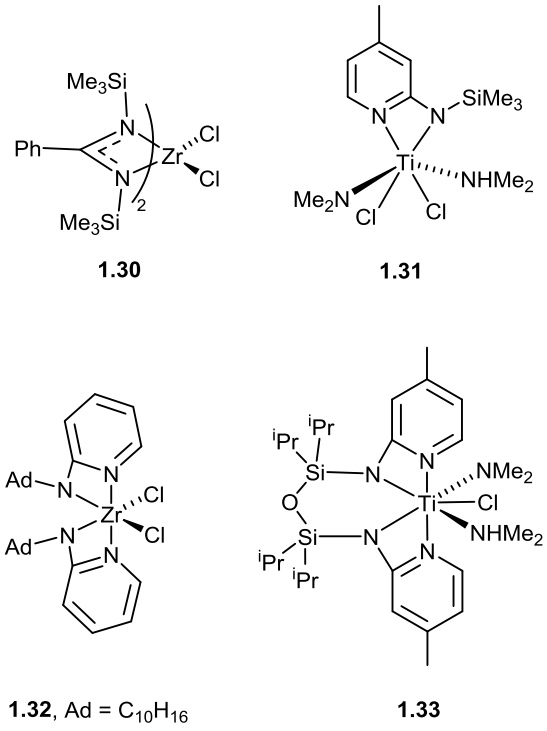

Figure 1.15. Group 4 metal complexes bearing at least one Ap ligand.

In 1991, Gambarotta and co-workers were the first to synthesise an early transition metal complex, carrying an aminopyridinato ligand (Ap).[165] The ligand is a monoanionic species, closely related to amidinate ligands and can bind to a metal centre in a η^2-mode.[166] The aminopyridinato ligands contained little steric demands as only the amide was substituted with methyl, phenyl or trimethylsilyl groups. Kempe and co-workers synthesised a mono(Ap) complex, namely $\{(C_5H_4N)N(SiMe_3)\}Ti(NMe_2)(NHMe_2)Cl_2$ (**1.31,** Figure 1.15), which was shown to be active in propylene and 1-butene polymerisation in the presence of MAO or BAr^F_3 ($Ar^F = C_6F_5$).[167] Scott *et al*. introduced adamantyl (Ad) as a substituent on the nitrogen amine resulting in a more sterically demanding Ap ligand.[168] The resulting zirconium complex **1.32** showed moderate activity in ethylene polymerisation when activated with MAO (Figure 1.15).[168]

Unlike amidinates, aminopyridinato ligands can be linked *via* a bridge between the two amido nitrogen atoms, giving an *ansa*-aminopyridinato complex. Titanium

containing siloxane-bridge bis(aminopyridinato) complexes, such as **1.33** (Figure 1.15), however, resulted in an overall low activity as polymerisation catalysts for ethylene.[169] This was attributed to the arrangement of the ligand around the metal centre, as the planar coordination mode separated the coordination site of olefins to that of the growing alkyl chain.[167]

1.5.3.4 Chelating aryloxide ligands

The independent discovery of phenoxy-imine ligands, by Fujita (group 4 metal complexes), Johnson and Grubbs (late transition metal complexes) created a new generation of non-metallocene olefin polymerisation catalysts.[70, 170-172] The ease of ligand synthesis, provided diversity and tunability to the new class of complexes, with the general structure (**1.34**) displayed in Figure 1.16. Complex **1.35**, developed by Fujita *et al*., showed to be a very efficient catalyst in ethylene polymerisation, with a TOF of 64,9000 s^{-1} bar^{-1} and two order of magnitude more active than the parent Cp_2ZrCl_2 complex.[170, 173] Furthermore, changing R^1 to a more electron-withdrawing substituent, such as C_6F_5, resulted in living polymerisation of ethylene and propylene, shown by a polydispersity index (PDI) close to 1.[174-176] Recently, Fujita and co-workers developed titanium complexes bearing phenoxy-imine ligand with a pendant aryl-OMe donor (**1.36**) which displayed especially high activity in the trimerisation of ethylene.[177, 178] These systems and others will be further discussed in Chapter Five.

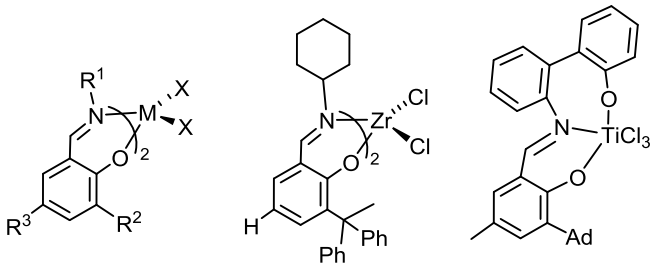

Figure 1.16. Group 4 FI catalysts polymerisation catalysts.

Related to that new generation of catalysts, Kol and co-workers synthesised a zirconium complex bearing a dianionic tetradentate chelating ligand of the type $[ONNO]^{2-}$ (**1.37**, Figure 1.17). Complex **1.37** is active in living and isospecific polymerisation of 1-hexene at room temperature in the presence of MAO.[179] Recently, Waymouth *et al*. have introduced octahedral bis(phenolate) ether Hafnium complex

(**1.38**) which yield a wide variety of highly isotactic propylene to amorphous material depending on the ligand and the aryl substitution.[180]

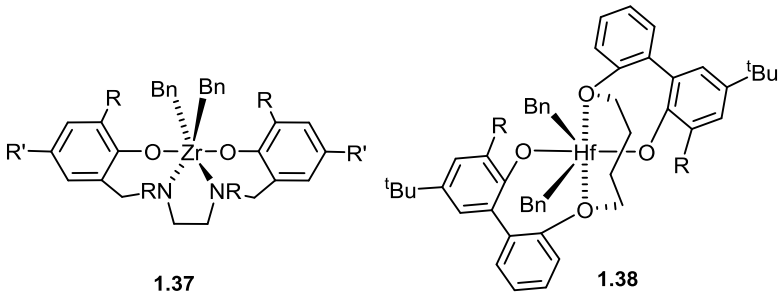

Figure 1.17. Group 4 polymerisation catalysts with tetradentate ligands.

1.6 Activators

Metal cations, known to be the active species in olefin polymerisation, can be obtained in a number of different ways. These include oxidative and abstractive cleave of M–R bonds, protonolysis of the M–R bond, alkyl or hydride abstraction and one-electron oxidation and reduction. These methods have been extensively reviewed.[50, 181] Of note to this Thesis are alkyl abstractive cleavage pathways and protonolysis of the M–R bond.

1.6.1 Aluminium-based activators

The discovery of MAO as a co-catalyst (Section 1.2) was crucial for olefin polymerisation and is still predominantly used in commercial applications. MAO can alkylate group 4 dichloride complexes to a monomethyl complex and subsequently abstract a chloride ligand forming the active cationic species. However, disadvantages of MAO include the large excess required to allow optimum performance, the low solubility in aliphatic solvents and the poor storage stability in solution as well as the presence of free trimethylaluminium (TMA).[51, 182-184] To improve the storage ability and solubility of MAO, modified methylaluminoxanes (MMAO) were introduced which for example can be prepared by the hydrolysis of TMA and triisobutylaluminium (TiBA).[181]

Although TMA can help the polymerisation process by acting as a water and oxygen scavenger, it is also a known reducing agent, leading to the formation of methyl-bridged heterodinuclear species which are inactive in polymerisation and also promote chain transfer.[185] In 1994, the heterodinuclear complex [$Cp_2Zr(\mu\text{-}Me_2)AlMe_2$] (**1.39**, Figure 1.18) of the reaction of TMA with Cp_2ZrMe_2 was first

reported by Bochmann *et al.*[49] It was not until 2006, that the first cationic group 4 metal compound possessing a M(μ-Me_2)$AlMe_2$-moiety was characterised by X-ray crystallography (**1.40,** Figure 1.18), reported by Mountford *et al.*[157]

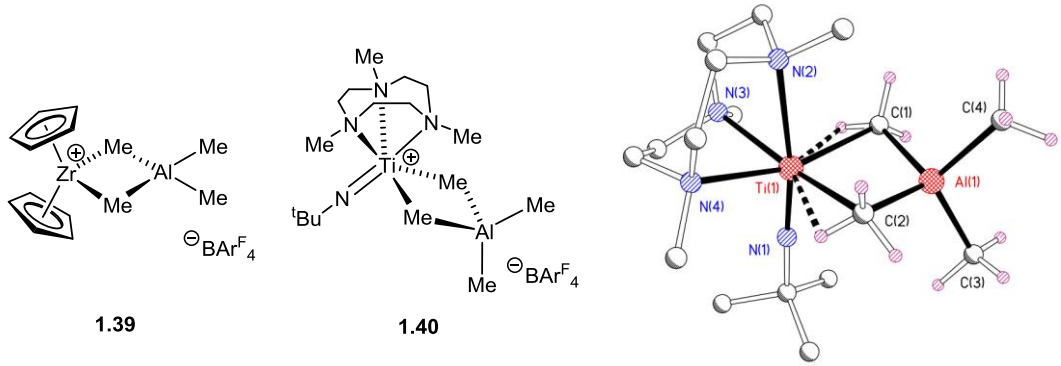

Figure 1.18. TMA adducts of alkyl cations.[157, 186]

An alternative way to remove free TMA from MAO is the addition of sterically hindered phenols such as 2,6-di-*tert*-butyl-4-methylphenol (BHT-H).[185, 187] resulting in the formation of (O-2,6-$^tBu_2C_6H_2Me)_2AlMe$ complexes. These alkylaluminium phenoxides are known as 'non-interacting scrubbing agents' and so do not interact with activators like BAr^F_3.[188-190] However, an excess of BHT-H can result in the formation of a dormant species. Youngs and co-workers have shown that the reaction of [Cp_2ZrMe][$MeBAr^F_3$] (**1.41**) with BHT-H, eliminates methane and slowly forms the phenoxide complex [Cp_2ZrBHT][$MeBAr^F_3$] (**1.42**, BHT = $OC_6H_2Me^tBu_2$) which is inactive in polymerisation of α-olefins.[188] Inclusion of BHT-H in polymerisation studies as well as synthetically will be discussed in Chapter Five.

Metal alkyl cation formation is not limited to using aluminium alkyl species and several alternative ways have been studied as described in the following section.

1.6.2 Protonolysis

Ammonium salts have been employed to generate alkyl cations, as shown by Bochmann and co-workers who synthesised [$Cp_2TiMe(NH_3)$][PF_6] from Cp_2TiMe_2 and ammonium hexafluorophosphate, releasing one equivalent of methane.[191] Turner *et al.* illustrated the protonolysis of Zr–Me bond with one equivalent of [NH^nBu_3][BPh_4] and subsequent C–H bond activation of the $[BPh_4]^-$ anion, leading to the further release of methane and formation of the zwitterion Cp^*_2Zr(μ-1,3-C_6H_4)BPh_3.[192, 193] To avoid the interference of the counter-anion with the alkyl

cations, new reagents were developed such as *N*,*N*´-dimethylanilinium- and tri-^{n}butylammonium tetrakis(pentafluorophenyl)borate salts ([$HNMe_2Ph$][BAr^F_4] and [$^{t}Bu_3NH$][BAr^F_4], $Ar^F = C_6F_5$, respectively).[194, 195] Horten and co-workers have shown that protonolysis of **1.43** with [$HNMe_2Ph$][BAr^F_4] provides a clean route to the cationic complex which is stabilised by the coordination of the aniline (Equation 1.3).[195] Depending on the electronics of the ligand backbone and the sterics of the metal complexes, the coproduct of the protonolysis can coordinate to the cationic metal centre.[196]

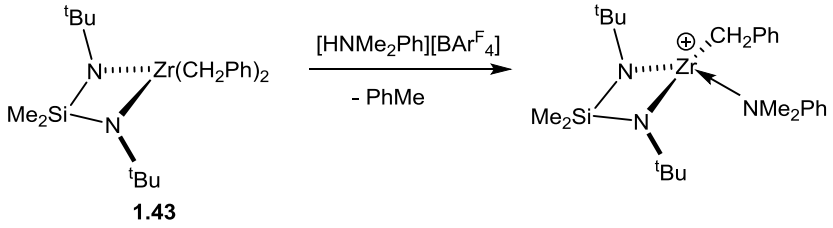

1.43

Equation 1.3

Upon investigation of siloxyaluminium alkyl compounds, Brintzinger *et al*. have shown that upon addition of [$HNMe_2Ph$][BAr^F_4] to a siloxyaluminium alkyl compound, methane is released and a new aluminium-methyl species is observed (**1.44**, Scheme 1.2). The reaction of the newly formed species **1.44** with Cp_2ZrMe_2, does not yield the assumed zirconium cation, but leads to the observation of a C–H bond activation product **1.45**.[197]

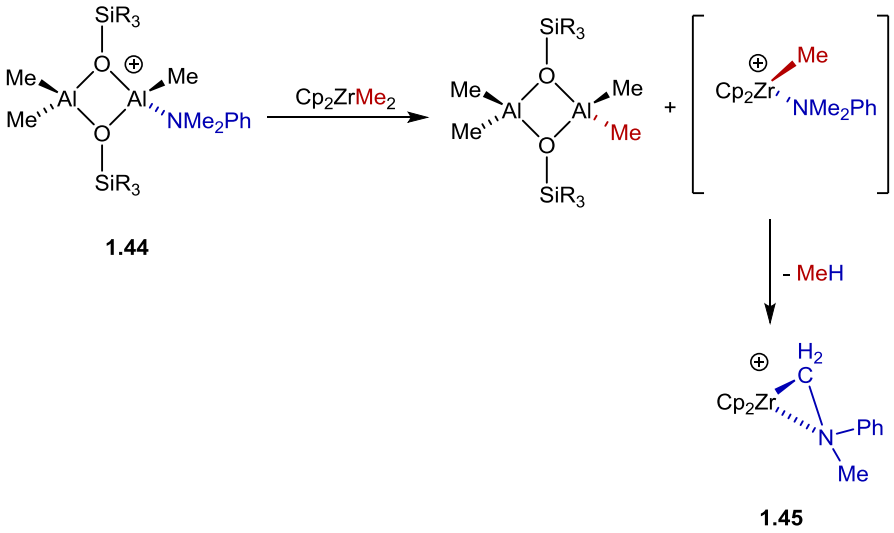

1.44 **1.45**

Scheme 1.2. Reaction of **1.44** with Cp_2ZrMe_2 to give **1.45** *via* C–H bond activation.

This is as the by-product of the reaction, *viz*. *N*,*N*´-dimethylaniline, acts as a Lewis base and can coordinate to the cationic metal centre as shown in Scheme 1.2.

1.6.3 Alkyl abstraction

In 1986, Jordan and co-workers were able to isolate the first cationic bis(cyclopentadienyl) zirconium complex $[Cp_2Zr(CH_2Ph)(THF)][BPh_4]$, by one-electron oxidation using $[Cp_2Fe][BPh_4]$ in THF with $Cp_2Zr(CH_2Ph)_2$. The resulting cation was active in the polymerisation of ethylene in the absence of alkyl aluminium reagents.[23, 198, 199] In the same year, Bochmann was able to isolate the cationic titanium analogue of the type $[Cp_2TiMe(L)][X]$ (L = NCR, pyridine, NH_3, $X^- = BPh_4$, PF_6). However, no activity towards ethylene polymerisation was observed due to the presence of stronger Lewis bases. It has also been shown that the counterion $[BPh_4]^-$ interacts strongly with the cationic metal centre and can also undergo unwanted C–H bond activation (*vide supra*).[192, 200] Rausch, Chien and co-workers combined the triphenylcarbenium cation with the aforementioned mentioned tetrakis(pentafluorophenyl)borate anion giving trityl tetrakis(pentafluorophenyl)borate salt ($[Ph_3C][BAr^F_4]$), now one of the most commonly employed activators in polymerisation chemistry.[201] They showed that *rac*-ethylene-bis(indenyl)dimethylzirconium (**1.46**) reacted cleanly with $[Ph_3C][BAr^F_4]$ to give the cationic species (**1.47**) and triphenylethane (Ph_3CMe) by abstracting a methyl group (Equation 1.4).[201, 202]

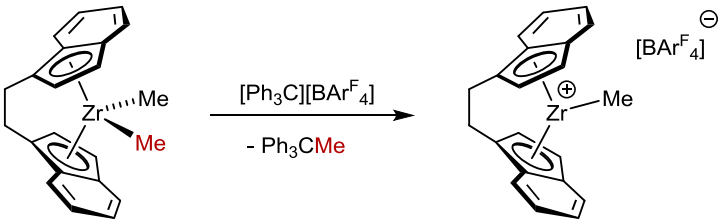

1.46 **1.47**

Equation 1.4

After the discovery of trityl tetrakis(pentafluorophenyl)borate, the combination of alkyl aluminium species and $[Ph_3C][BAr^F_4]$ resulted in a highly efficient polymerisation system, suggesting initial alkylation by the alkyl aluminium species and activation by $[Ph_3C][BAr^F_4]$, allowing the alkyl aluminium reagent to scavenge any impurities.[203, 204]

1.6.4 BAr^F_3 activation of dialkyl complexes

Tris(pentafluorophenyl)borane (BAr^F_3) was first synthesised by Massey and Park in 1964, but it was not implemented in olefin polymerisation until 1991.[205] Marks[206] and Jordan[207] have independently reacted a series of $(Cp^R)_2ZrMe_2$ species with BAr^F_3 (Cp^R = Cp, Cp* or 1,2-$C_5H_3Me_2$). All three compounds gave quantitatively the mono-methyl cation and a weakly coordinating methyl-tris(pentafluorophenyl)borate. The molecular structure of $[Cp_2ZrMe][MeBAr^F_3]$ (**1.41**) is displayed in Figure 1.19.[207] All three systems were highly active in the polymerisation of ethylene.

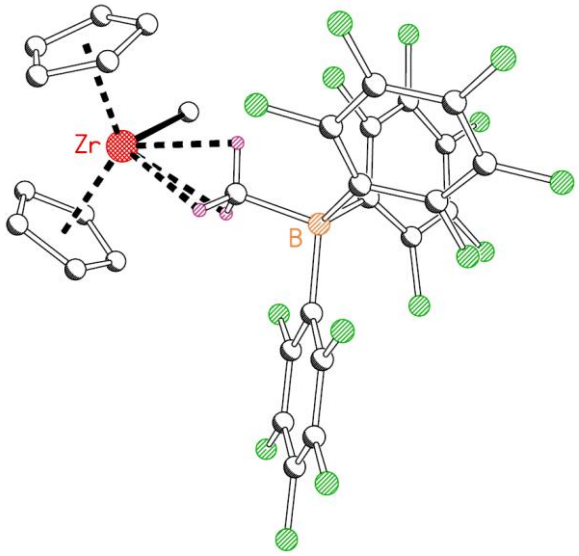

Figure 1.19. Molecular structure of **1.41**.

Horton and co-workers investigated the formation of the mono-alkyl cations of $\{Me_3SiN(CH_2CH_2NSiMe_3)_2\}ZrR_2$ (R = Me or CH_2Ph) with BAr^F_3.[208] The reaction with the dimethyl complex resulted in the expected mono-methyl cation $[\{Me_3SiN(CH_2CH_2NSiMe_3)_2\}ZrMe][MeBAr^F_3]$ (**1.48**, Figure 1.20) with coordination of the anion *via* a Zr···Me–B interaction.

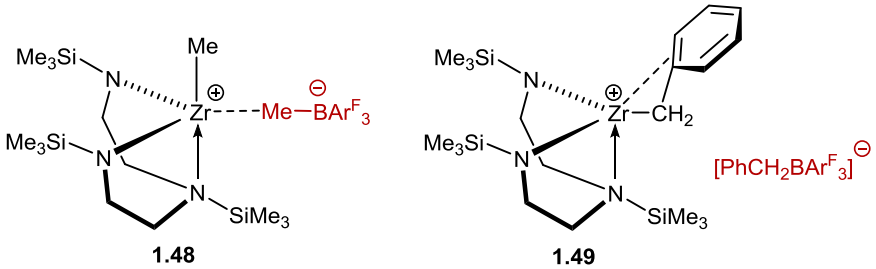

Figure 1.20. Activation products of $\{Me_3SiN(CH_2CH_2NSiMe_3)_2\}ZrR_2$ (R = Me or CH_2Ph) with BAr^F_3.

Horton *et al*. identified, that the coordination of the counterion to the cationic metal centre can be determined with help of the ^{19}F NMR spectrum. A larger chemical shift difference ($\Delta\delta_{(m,pF)}$), between 3 and 6 ppm, of the *meta*- and *para*-fluoro resonances implies coordination of the counterion. A difference smaller than 3, however, shows "noncoordination" of the counterion.[208]

The addition of BAr^F_3 to the dibenzyl complex also gave the short-lived mono-benzyl cation $[\{Me_3SiN(CH_2CH_2NSiMe_3)_2\}ZrCH_2Ph][CH_2PhBAr^F_3]$ (**1.49**). Interestingly, in the case of the mono-benzyl cation, no interaction between Zr···CH_2Ph–B was observed as shown by the ^{19}F NMR spectrum.[208]

1.6.5 BAr^F_3 activation of diene complexes

Neutral group 4 diene complexes have been known in literature over the last two decades (*vide infra*).[209, 210] The discovery of the formation of a zwitterionic group 4 complex by the reaction of a zirconocene butadiene complex with BAr^F_3 to give $[Cp_2Zr(\eta^3\text{-}(CH)_3CH_2BAr^F_3)]$ (**1.50**) and its high activity in ethylene polymerisation has prompted further research in this field.[211, 212] A weak interaction of the *ortho*-fluoro from the C_6F_5 moiety with the metal centre was identified by low temperature ^{19}F NMR due to the distinct up-field shift of a fluoro atom (Scheme 1.3). Reversible cleavage of the C–F···M interaction has been observed before the first insertion of ethylene.[213] Increasing the steric bulk on the metal centre, such as introducing pentamethylcyclopentadienyl ligands, prohibited the extra stabilisation *via* the *ortho*-fluorine.[214]

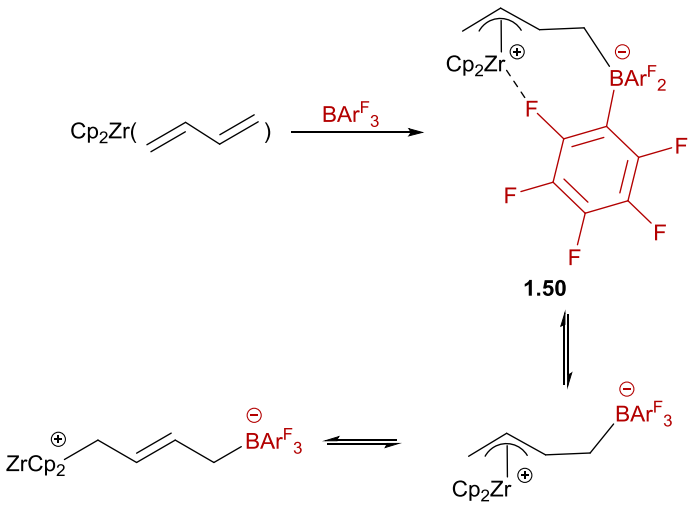

Scheme 1.3. Activation of Cp_2Zr(butadiene) complex with BAr^F_3.

Bochmann and co-workers synthesised a diallyl zirconium zwitterionic species Cp"Zr(η^3-C_3H_5)(η^3-$CH_2C(Me)C(Me)CH_2BAr^F_3$) (Cp" = 1,3-$C_5H_3(SiMe_3)_2$) where a possible C–H···M agostic interaction was observed, indicated by an upfield ^{1}H NMR chemical shift of the CH_2-moiety bonded to BAr^F_3. No up-field shift of an *ortho*-fluorine was observed in this case.[215] Marks *et al*. prepared the first example of a constrained geometry catalyst bearing a 1,3-pentadiene ligand known to be an efficient precatalyst for copolymerisation of ethylene and 1-octene.[216, 217] However, it was not until 1999 when Jones and co-workers presented the first structurally characterised example of a titanium borate zwitterion (**1.51**, Figure 1.21), revealing stabilisation *via* an agostic interaction between the $CH_2BAr^F_3$ methylene hydrogen and the metal centre.[218]

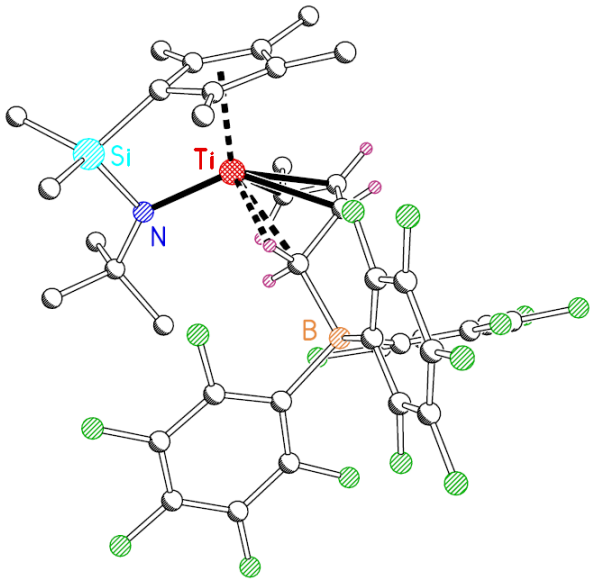

Figure 1.21. Molecular structure of **1.51**.

The reaction of titanium complexes, bearing a 1,4-$C_4H_4Me_2$ diene fragment, with BAr^F_3 led to the formation a zwitterionic allyl species, where the borate moiety is attached to a newly formed methylene carbon (Equation 1.5).

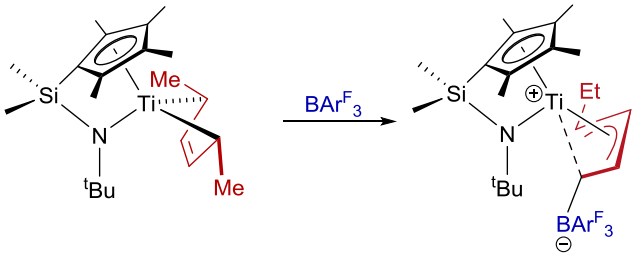

Equation 1.5

This final compound was observed as the migration of the borate moiety was accompanied by a concomitant hydrogen shift.[219, 220] Half-sandwich phosphinimide group 4 diene complexes were also investigated by Stephan and co-workers.[221, 222] The stoichiometric reaction of the 2,3-dimethylbutadiene zirconium complex with BAr^F_3 afforded a zwitterion $Cp^*Zr(NP^tBu_3)(CH_2C(Me)C(Me)CH_2BAr^F_3)$, similar to previously observed zwitterions of constrained geometry catalysts.

1.7 Metal alkyl cations

Due to the electrophilic nature of the metal alkyl cations, their reactivity has been widely explored.[50, 73, 223, 224] Solvent and agostic interactions, reactivity with Lewis bases and insertion products with α-olefins are an essential part of understanding the activity of these cations in olefin polymerisation and will be discussed further in this Section.

1.7.1 Non-classical interactions

Bochmann *et al*. investigated the reaction of $(Cp^R)_2ZrMe_2$ (Cp^R = Cp or $Me_2Si(Ind)_2$) with $[Ph_3C][BAr^F_4]$ at −60 °C in CD_2Cl_2, forming a dinuclear monocationic monomethyl bridged complex $[(Me_2Si(Ind)_2ZrMe)_2(\mu\text{-}Me)][BAr^F_4]$. The adduct formation suggests that the neutral dialkyl metallocene effectively stabilises the 14-electron species.[186, 225] Recently, van Doremaele and co-workers have isolated and structurally characterised the dication $[(Cp^*Ti\{NC(Ar^{F2})N^iPr_2\})_2\{\mu\text{-}Me\}_2][BAr^F_4]_2$ (**1.53**) from the reaction of $Cp^*Ti\{NC(Ar^{F2})N^iPr_2\}Me_2$ (**1.52**) with $[Ph_3C][BAr^F_4]$ (Scheme 1.4).[129] The addition of further **1.52** to **1.53** led to the formation of the dimeric monocation, with only one bridging methyl group (**1.54**), as previously observed by Bochmann *et al*. Addition of the strong Lewis base Ph_3PO gave the base-stabilised titanium methyl monocation (**1.55**), as shown in Scheme 1.4.

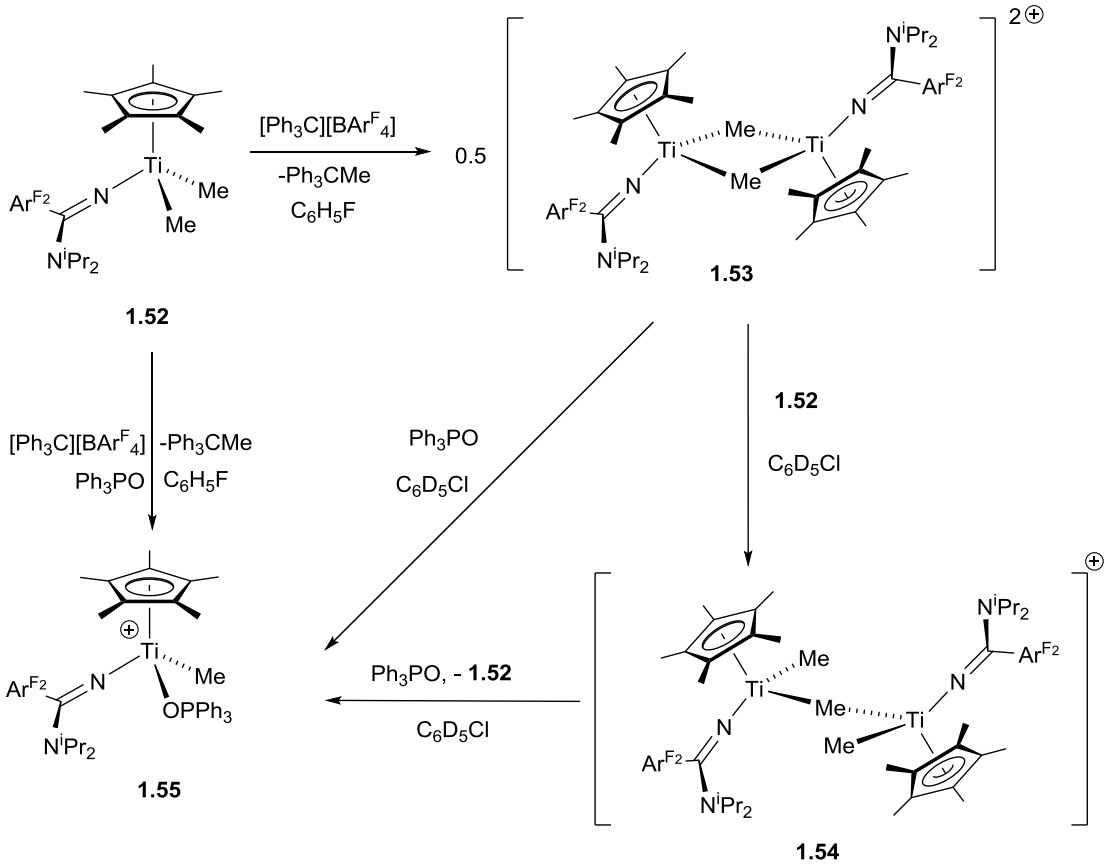

Scheme 1.4. Formation of cationic dimer **1.53** and further reactivity. Anion omitted for clarity.

The solid state structure of **1.53** shows *pseudo*-tetrahedral geometry around the titanium centres and the bond distances of Ti–Me are larger for the bridging dimer than the neutral species **1.52**, which is in agreement with the Ti–Me–Ti moiety acting as a 3-centre-2-electron bond.[129] Both bridging methyl groups form two α-agostic interactions, one with each titanium centre. The same interaction has been previously observed for a dinuclear methyl dication complex carrying a κ^2-amidinate supporting ligand $[(Cp^*Zr\{MeC(N^tBu)(NEt)\})_2\{\mu\text{-}Me\}_2][BAr^F{}_4]_2$.[226] More recently, the Mountford group also investigated the activation chemistry of the slightly less sterically demanding complex $CpTi\{NC(Ph)N^iPr_2\}Me_2$ with $[Ph_3C][BAr^F{}_4]$. In this case, a nitrogen-bridged dimeric cation was observed instead of a μ-Me bridged dimer due to different steric factors.[227] Similar behaviour was observed for the κ^1-guanidinate complexes, displayed in Scheme 1.5.[228]

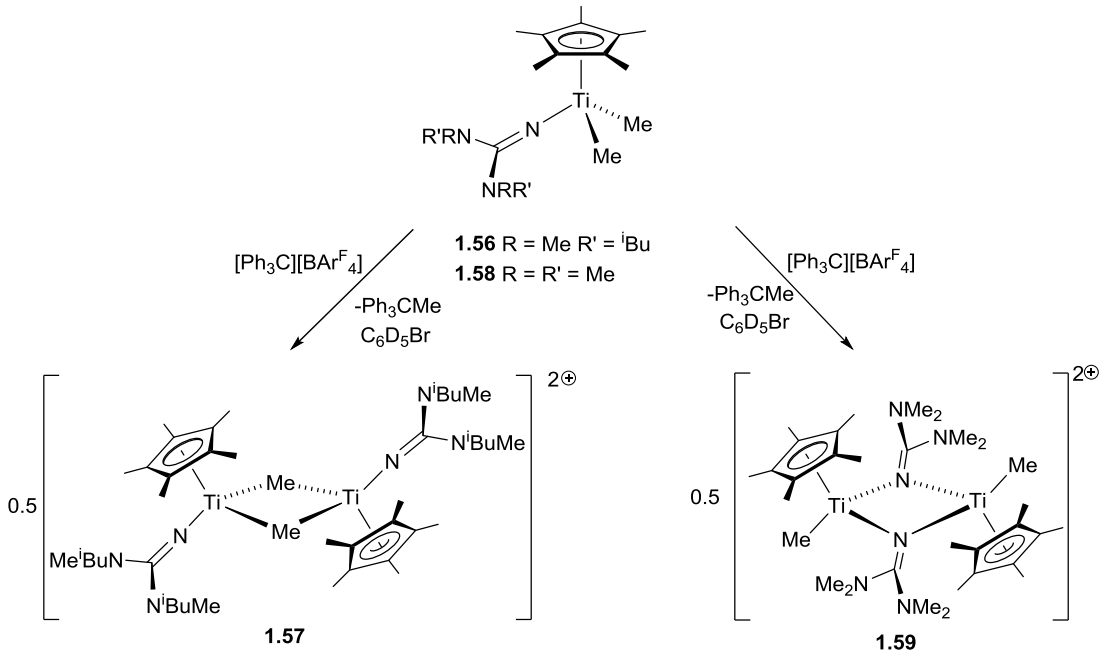

Scheme 1.5. Activation of **1.56** and **1.58** with $[Ph_3C][BAr^F_4]$ to form dimer **1.57** and **1.59**, respectively.

Upon activation of **1.56**, bearing a more sterically demanding ligand, the μ-Me bridged dimer was formed (**1.57**, Scheme 1.5). Moving to a less sterically demanding guanidinate system (**1.58**), results in immediate formation of an insoluble μ-guanidinate bridged dimer **1.59**. The newly formed dimer (**1.59**) shows no reactivity towards added Lewis bases or unsaturated reagents.[228]

On the contrary, in the presence of a benzyl ligand, the resulting cationic complexes, exemplified with $[Cp_2Zr(CH_2Ph)][BAr^F_4]$ (**1.60**), is thermally more stable than the respective monomethyl cation and does not result in dimer formation.[229, 230] The extra stability is attributed to the intramolecular interaction of the C_{ipso} with the metal centre (Figure 1.22). This is manifested in the NMR data where an increase in the $^1J_{CH}$ value and a high-field chemical shift of the C_{ipso} is observed in the ^{13}C NMR spectrum.[231-233] The solid state structure of $[Cp_2ZrCH_2Ph][BAr^F_4]$ provides further evidence for this η^2-coordination mode of the benzyl ligand. An acute $Zr–C_\alpha–C_\beta$ bond angle of 84.4(5)° is observed as well as close contact between the Zr metal and the phenyl substituent ($Zr–C_{ipso}$ distance = 2.627(9) Å).[233]

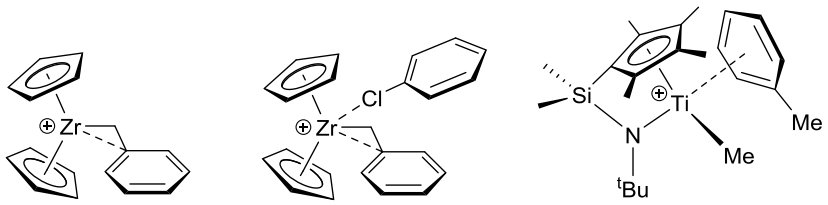

1.60 **1.61** **1.62**

Figure 1.22. Non-classical interaction of group 4 metal cations. $[BAr^F{}_4]^-$ omitted for clarity.

Upon further investigation of $[Cp_2Zr(CH_2Ph)][BAr^F{}_4]$ (**1.60**), Jordan *et al*. identified additional stabilisation of the cationic zirconocene complex by η^1-coordination of the chlorobenzene solvent *via* the chlorine atom (**1.61**, Figure 1.22).[200, 234] The coordination of the arene solvent does not influence the η^2-coordination mode of the benzyl ligand and the bond angle of $Zr–C_\alpha–C_\beta$ is comparable to **1.60**. Marks and co-workers[194] have also shown that arene solvent coordination stabilises CGC cationic species, exemplified with toluene coordination to $[C_5Me_4SiMe_2(N^tBu)ZrMe][BAr^F{}_4]$ (**1.62**).

In general, mono-alkyl cations, that do not possess any sorts of additional stabilisation of the type described (*vide supra*), tend to result in oily residues of a mixture of products, and are therefore difficult to analyse.[181] Addition of Lewis bases, such as triphenylphosphine oxide, THF, nitriles and pyridine, can result in base-stabilised adducts of the type $[Cp_2MR(L)]^+$ (L = Lewis base),[23] although C–H activation can occur with pyridine[235, 236] and migratory insertion with nitriles (*vide infra*).[191, 237] These systems can be characterised by spectroscopy and X-ray diffractometry.

1.7.2 Reactivity of metal alkyl cations

Insertion reactions with reagents such as ^{t}BuCN, CO and carbodiimides to group 4 cations have also been extensively investigated by Bochmann[129], Jordan[23] and Stephan.[238, 239] The resulting products are no longer active in olefin polymerisation. Of note for this Thesis is the insertion reaction with *N*,*N*´-diisopropylcarbodiimde (^{i}PrNCN^{i}Pr). Stephan and co-workers showed activation of $CpZr(NP^tBu_3)Me_2$ (**1.63**) with $BAr^F{}_3$ in the presence of carbodiimide resulted in the stable κ^2-amidinate product $[CpZr(NP^tBu_3)\{MeC(N^iPr)_2\}][MeBAr^F{}_3]$ (**1.64**, Equation 1.6).[238]

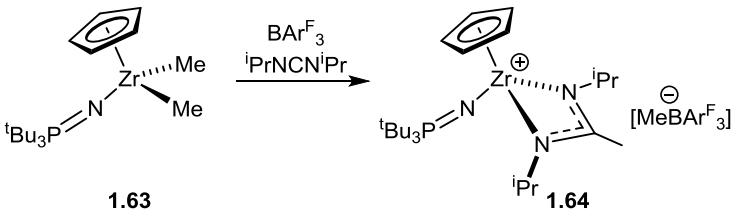

1.63 **1.64**

Equation 1.6

Insertion of the α-olefin into the metal-alkyl bond is essential for a growing polymer chain. Pellecchia and co-workers were the first to observe the insertion adduct of propylene to the non-metallocene complex [Cp*Zr(CH_2Ph)$_2$][η^6-$PhCH_2BAr^F_3$] at temperatures below 25 ºC.[240, 241] Propylene inserted into one of the Zr–CH_2Ph bonds, giving [Cp*Zr(CH_2Ph)($CH_2CHMeCH_2Ph$)][$PhCH_2BAr^F_3$] (**1.65,** Figure 1.23), where the counterion was no longer coordinated to the zirconium centre. As indicated by ^{1}H and ^{13}C NMR spectra, the complex is stabilised by a chelating π-coordination of the benzene ring of the inserted ligand. Furthermore, Horton *et al*. investigated the solvent and activator effect on the first insertion of alkynes and alkenes, exemplified with propylene, into the metal-alkyl bond of cationic zirconium diamide complexes, giving [{$Me_2Si(N^tBu)_2$}$ZrCH_2CH(Me)CH_2Ph$]$^+$ (**1.66**, Figure 1.23).

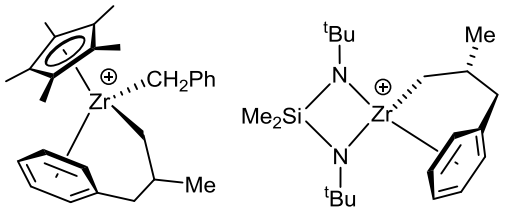

1.65 **1.66**

Figure 1.23. Insertion products of addition of propylene to group 4 metal cations. Counterions omitted.

The presence of anions, such as [$RBAr^F_3$]$^-$ (R = alkyl) or Lewis base (by-product of activation with [$HNMe_2Ph$][BAr^F_4], Section 1.6.2) showed that the relative rates of insertion of alkenes are dependent on the ease of displacement of those, where [BAr^F_4]$^-$ led to faster rates compared to NMe_2Ph and [$RBAr^F_3$]$^-$.[195]

Baird and co-workers investigated the reaction of 2,2-disubstituted alkenes, such as 2,4-dimethyl-1-pentene (DMP) with [Cp_2ZrMe]$^+$. They were able to observe the unprecedented η^1-vinylidene intermediate [$Cp_2ZrMe(\eta^1$-$CH_2CMeCH_2CHMe_2)$]$^+$ (**1.67**, Figure 1.24), as the alkenes are expected to disfavour migratory insertion.

However, **1.67** decomposed to methane and a zirconocene allyl complex even at low temperatures.[242, 243] Further investigation of $[Cp_2TiMe]^+$ with DMP showed considerably different behaviour. Complex $[Cp_2TiMe(DMP)]^+$ underwent migratory insertion to give the expected σ-alkyl complex, which rearranged *via* a cascade of reactions to give the C_8 allylic complex $[Cp_2TiMe(\eta^3\text{-}(CH_2)_2CCH_2CMe_3)]^+$ (**1.68**), free 2,4,4-trimethyl-1-pentene and the hydride complex $[Cp_2TiH]^+$.[244] The hydride complex, $[Cp_2TiH]^+$, reacted with free DMP to give the insertion product $[Cp_2Ti(CH_2CHMeCH_2CHMe_2)]^+$ (**1.69**), which is the one of the first examples of a β-H agostic interaction in a titanocene complex.

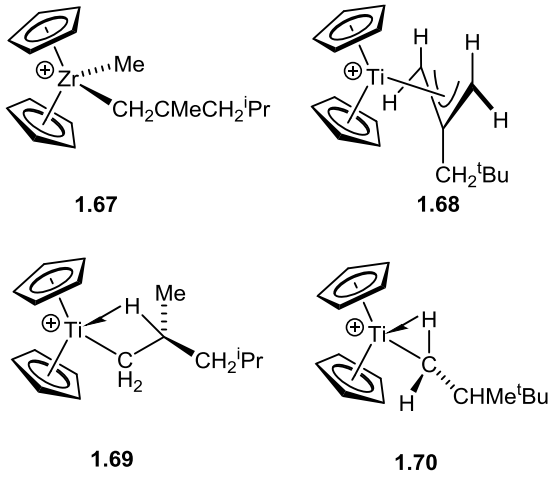

1.67 **1.68** **1.69** **1.70**

Figure 1.24. Reaction of $[Cp_2MMe]^+$ (M = Zr, Ti) with more sterically hindered alkenes.

Reacting $[Cp_2TiMe]^+$ with an even more sterically hindered olefin, 3,3-dimethyl-1-butene (DMB), provided the single 1,2-insertion product $[Cp_2TiCH_2CHMe^tBu]^+$ (**1.70**), which showed an α-agostic interaction as identified by NMR spectroscopy.[244] Complex **1.70** decomposed to 2,3,3-trimethyl-1-butene and $[Cp_2TiH]^+$ which inserted DMB to give $[Cp_2TiCH_2CH_2{}^tBu]^+$, featuring a β-H agostic interaction as previously observed for **1.69**. These examples show the complexity of reactivity of metal cations and will also be further discussed in Chapter Three.

1.8 Project introduction

1.8.1 Neutral κ^1-amidinate titanium diene complexes

Previous work done by the Mountford group, in collaboration with ARLANXEO, involved the synthesis of a range of neutral κ^1-amidinate supported titanium diene

complexes, as displayed in Figure 1.25. The reaction of Cp*Ti{NC(Ph)N^{i}Pr$_2$}Cl$_2$ (**1.71**) with two equivalents of ^{n}BuLi in the presence of 2,3-dimethyl-1,3-butadiene resulted in the formation of only the *supine* isomer (**1.72**, Figure 1.25). However, the reaction in the presence of 2,4-hexadiene or 1,4-diphenyl-1,3-butadiene always resulted in the formation of the *supine* (major) and *prone* (minor) isomer (**1.73** and **1.74**, respectively). A two-dimensional ROESY spectrum permitted a reliable way to distinguish between the *supine* and *prone* isomer, where the vinylic protons of the *prone* isomer, correlate through space to the Cp* moiety.

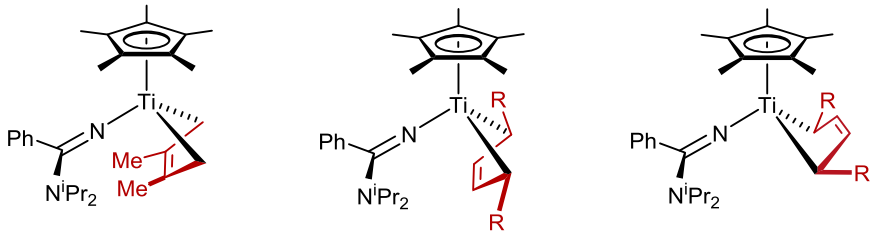

1.72 *supine* *prone*

1.73 R = Me
1.74 R = Ph

Figure 1.25. κ^1-amidinate supported titanium diene complexes **1.72**, **1.73** and **1.74**.

In these κ^1-amidinate supported titanium diene complexes, the diene coordinated in the *cis* fashion and the complexes **1.72–1.74** were characterised crystallographically, aiding the understanding of the nature of bonding. In solid state, the *supine* confirmation was adopted for all complexes. The solid state structure of **1.72** is shown in Figure 1.26. The bonding of the diene shows that the central C–C bond (1.395(3) Å) is shorter than the peripheral C–C bonds (1.427(3) and 1.419(4) Å), suggesting substantial 'ene-diyl' character of the diene fragment.[245] Furthermore the Ti(1)–Cp*$_{cent}$ distance measures 2.07 Å, which is typical for Ti(+4) half-sandwich complexes, suggesting that the extensive reduction of the diene ligand results in a significant dianionic character (ene-diyl) and predominantly σ-binding to the metal centre, bringing the oxidation state of titanium closer to +4 than +2.

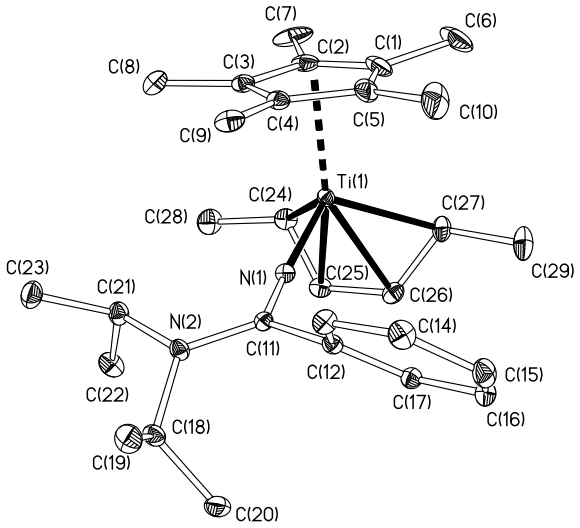

Figure 1.26. Solid state structure of Cp*Ti{NC(Ph)N^{i}Pr$_2$}{η-(Me)CH(CH)$_2$CH(Me)} (**1.73**).[227]

These neutral complexes were activated with BAr$^{F}_3$ to form zwitterionic allyl borate complex, allowing unique control over cation-anion interaction. The activation of **1.72** with BAr$^{F}_3$ generated a zwitterionic allylic borate complex Cp*Ti{NC(Ph)N^{i}Pr$_2$}{η^3-CH$_2$C(Me)C(Me)CH$_2$BAr$^{F}_3$} (**1.75**) as shown in Equation 1.7.

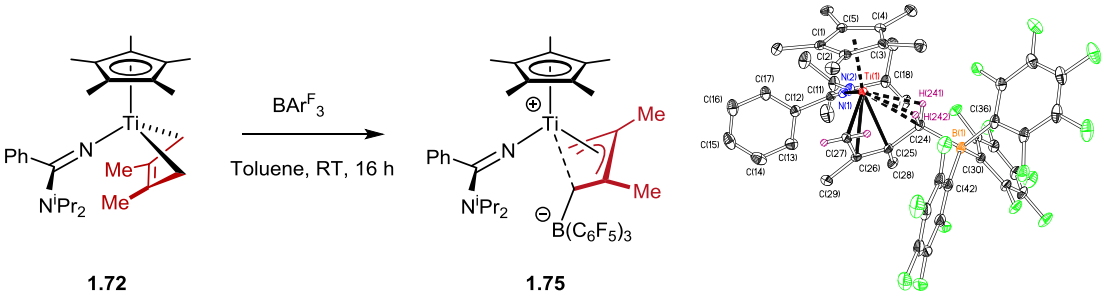

1.72 **1.75**

Equation 1.7

Similar to literature,[218] a Ti···H interaction is observed for the methylene protons adjacent to the borate moiety, which is also shown in the ^{1}H NMR spectrum with two shielded proton shifts.

The neutral diene complexes and their zwitterionic allylic borate counterparts were tested in the co-polymerisation of ethylene, propylene and non-conjugated diene (EPDM). The composition did not vary greatly between the different neutral diene complexes **1.72** and **1.73**, emphasising the role of the supporting ligand systems in the polymerisation process. However, lower productivity was observed between the

neutral diene complex **1.72** and zwitterionic allylic complex **1.75**. This is attributed to the greater sensitivity of the pre-activated complexes.[227]

1.8.2 Aminopyridinato titanium complexes and their activity in co-polymerisation

In 2004, Kempe and co-workers introduced more sterically crowded aminopyridinato ligands, by using 2,6- or 2,4,6-alkylphenyl substituents at the 6 position of the pyridine ring as well as at the amide nitrogen.[246, 247] More recently, Kempe *et al*. investigated aminopryidinato complexes **1.76–1.79** as catalytic systems for ethylene and propylene co-polymerisation (Figure 1.27). These complexes will be described in more detail in Chapter Four and Five.

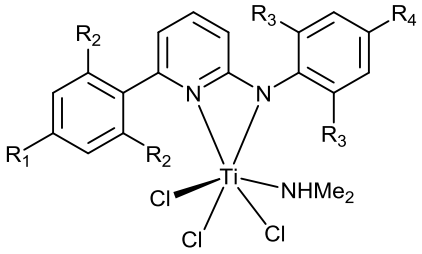

1.76 $R^1 = R^2 = R^3 = R^4 = Me$
1.77 $R^1 = R^2 = R^3 = {}^iPr$; $R^4 = H$
1.78 $R^1 = R^2 = {}^iPr$; $R^3 = R^4 = Me$
1.79 $R^1 = R^4 = H$; $R^2 = Me$; $R^3 = {}^iPr$

Figure 1.27. Aminopyridinato titanium complexes **1.76–1.79**.

Addition of three equivalents of $CH_2PhMgCl$ to **1.77** resulted in the tri-substituted benzyl complex $ApTi(CH_2Ph)_3$, however, the alkylated species was not stable in solution at room temperature. The co-polymerisation of ethylene and propylene with complexes **1.76–1.79** showed the most sterically crowded complex **1.77** gave the highest activity (32,000 kg_{PE} mol^{-1} h^{-1}) in the presence of dried MAO (*d*-MAO). Polymerisation of ethylene, propylene and ENB with **1.77** displayed moderate activity of 8000 kg_{PE} mol^{-1} h^{-1}.[248]

1.9 Summary and Objectives

This Chapter gave an overview of heterogeneous and homogeneous group 4 catalysts active in polymerisation of α-olefins, with a focus on post-metallocene systems. Synthesis of the metal cations *via* a range of activators and the reactivity of those cations towards Lewis bases and olefins has been discussed in detail. Chapter Two will explore the synthesis and activation of new κ^1-amidinate half-sandwich dialkyl

and diene precatalysts. In collaboration with ARLANXEO, all precatalysts were assessed for EP and EPDM co-polymerisation capabilities. The synthesis and mechanistic behaviour of cationic titanium-diene species will be discussed in Chapter Three. Chapter Four will introduce a new set of post-metallocene κ^1-amidinate supported titanium complexes, where the cyclopentadienyl moiety is replaced with either aminopyridinato or κ^2-amidinate ligands. Their activity and polymerisation capabilities will be investigated. Chapter Five will discuss the activity of aminopyridinato κ^1-amidinate supported titanium dialkyl complexes in ethylene oligomerisation.

1.10 References

1. M. M. Stalzer, M. Delferro and T. J. Marks, *Catal. Lett.*, 2015, **145**, 3-14.
2. T. J. Hutley and M. Ouederni, in *Polyolefin Compounds and Materials: Fundamentals and Industrial Applications*, eds. M. Al-Ali AlMa'adeed and I. Krupa, Springer International Publishing, Cham, 2016, pp. 13-50.
3. D. Sauter, M. Taoufik and C. Boisson, *Polymers*, 2017, **9**, 185.
4. K. Ziegler, E. Holzkamp, H. Breil and H. Martin, *Angew. Chem. Int. Ed.*, 1955, **67**, 541-547.
5. G. Natta, *Angew. Chem. Int. Ed.*, 1956, **68**, 393-403.
6. G. Wilkinson, P. L. Pauson, J. M. Birmingham and F. A. Cotton, *J. Am. Chem. Soc.*, 1953, **75**, 1011-1012.
7. G. Natta, P. Pino, G. Mazzanti, U. Giannini, E. Mantica and M. Peraldo, *J. Polym. Sci.*, 1957, **26**, 120-123.
8. D. S. Breslow and N. R. Newburg, *J. Am. Chem. Soc.*, 1957, **79**, 5072-5073.
9. G. Natta, P. Pino, G. Mazzanti and U. Giannini, *J. Am. Chem. Soc.*, 1957, **79**, 2975-2976.
10. K. Veselý, J. Ambrož, R. Vilím and O. Hamřík, *J. Polym. Sci.*, 1961, **55**, 25-32.
11. W. Kaminsky, M. Miri, H. Sinn and R. Woldt, *Makromol. Chem., Rapid Commun.*, 1983, **4**, 417-421.
12. K. H. Reichert and K. R. Meyer, *Makromol. Chem.*, 1973, **169**, 163-176.
13. W. P. Long and D. S. Breslow, *Justus Liebigs Ann. Chem.*, 1975, **1975**, 463-469.
14. P. Pino and R. Mülhaupt, *Angew. Chem. Int. Ed. Engl.*, 1980, **19**, 857-875.

15. W. Kaminsky, *Macromolecules*, 2012, **45**, 3289-3297.
16. H. Sinn, *Macromol. Symp.*, 1995, **97**, 27-52.
17. M. R. Mason, J. M. Smith, S. G. Bott and A. R. Barron, *J. Am. Chem. Soc.*, 1993, **115**, 4971-4984.
18. Y. Koide, S. G. Bott and A. R. Barron, *Organometallics*, 1996, **15**, 2213-2226.
19. D. S. Breslow and N. R. Newburg, *J. Am. Chem. Soc.*, 1959, **81**, 81-86.
20. A. K. Zefirova and A. E. Shilov, *Dokl. Akad. Nauk*, 1961, **136**, 599-602.
21. F. S. Dyachkovskii, A. K. Shilova and A. E. Shilov, *J. Polym. Sci., Polym. Symp.*, 1967, **16**, 2333-2339.
22. J. J. Eisch, A. M. Piotrowski, S. K. Brownstein, E. J. Gabe and F. L. Lee, *J. Am. Chem. Soc.*, 1985, **107**, 7219-7221.
23. R. F. Jordan, W. E. Dasher and S. F. Echols, *J. Am. Chem. Soc.*, 1986, **108**, 1718-1719.
24. R. F. Jordan, C. S. Bajgur, R. Willett and B. Scott, *J. Am. Chem. Soc.*, 1986, **108**, 7410-7411.
25. R. H. Grubbs and G. W. Coates, *Acc. Chem. Res.*, 1996, **29**, 85-93.
26. P. Cossee, *J. Catal.*, 1964, **3**, 80-88.
27. E. J. Arlman and P. Cossee, *J. Catal.*, 1964, **3**, 99-104.
28. K. J. Ivin, J. J. Rooney, C. D. Stewart, M. L. H. Green and R. Mahtab, *J. Chem. Soc., Chem. Commun.*, 1978, 604-606.
29. M. Brookhart and M. L. H. Green, *J. Organomet. Chem.*, 1983, **250**, 395-408.
30. Z. Dawoodi, M. L. H. Green, V. S. B. Mtetwa and K. Prout, *J. Chem. Soc., Chem. Commun.*, 1982, 802-803.
31. R. H. Grubbs and G. W. Coates, *Acc. Chem. Res.*, 1996, **29**, 85-93.
32. Z. Liu, E. Somsook, C. B. White, K. A. Rosaaen and C. R. Landis, *J. Am. Chem. Soc.*, 2001, **123**, 11193-11207.
33. I. Kim, J.-M. Zhou and H. Chung, *J. Polym. Sci., Part A: Polym. Chem.*, 2000, **38**, 1687-1697.
34. H. H. Brintzinger, D. Fischer, R. Mülhaupt, B. Rieger and R. M. Waymouth, *Angew. Chem. Int. Ed. Engl.*, 1995, **34**, 1143-1170.
35. W. Kaminsky, A. Ahlers and N. Möller-Lindenhof, *Angew. Chem. Int. Ed. Engl.*, 1989, **28**, 1216-1218.
36. Z. Guo, D. C. Swenson and R. F. Jordan, *Organometallics*, 1994, **13**, 1424-1432.

37. S. Hajela and J. E. Bercaw, *Organometallics*, 1994, **13**, 1147-1154.
38. J. J. W. Eshuis, Y. Y. Tan, J. H. Teuben and J. Renkema, *J. Mol. Catal.*, 1990, **62**, 277-287.
39. L. Resconi, F. Piemontesi, G. Franciscono, L. Abis and T. Fiorani, *J. Am. Chem. Soc.*, 1992, **114**, 1025-1032.
40. G. Sini, S. A. Macgregor, O. Eisenstein and J. H. Teuben, *Organometallics*, 1994, **13**, 1049-1051.
41. T. Tsutsui, K. Sugimura and T. Ueda, *EP436399A2*, 1991.
42. D. Fischer and R. Mülhaupt, *J. Organomet. Chem.*, 1991, **417**, C7-C11.
43. L. Resconi, F. Piemontesi, I. Camurati, D. Balboni, A. Sironi, M. Moret, H. Rychlicki and R. Zeigler, *Organometallics*, 1996, **15**, 5046-5059.
44. P. Margl, L. Deng and T. Ziegler, *Top. Catal.*, 1999, **7**, 187-208.
45. C. R. Landis, K. A. Rosaaen and D. R. Sillars, *J. Am. Chem. Soc.*, 2003, **125**, 1710-1711.
46. M. E. O'Reilly, S. Dutta and A. S. Veige, *Chem. Rev.*, 2016, **116**, 8105-8145.
47. N. Naga and K. Mizunuma, *Polymer*, 1998, **39**, 5059-5067.
48. L. Resconi, S. Bossi and L. Abis, *Macromolecules*, 1990, **23**, 4489-4491.
49. M. Bochmann and S. J. Lancaster, *Angew. Chem. Int. Ed. Engl.*, 1994, **33**, 1634-1637.
50. M. Bochmann, *Organometallics*, 2010, **29**, 4711-4740.
51. F. Zhu, Q. Huang and S. Lin, *J. Polym. Sci., Part A: Polym. Chem.*, 1999, **37**, 4497-4501.
52. S. W. Ewart, M. A. Parent and M. C. Baird, *J. Polym. Sci., Part A: Polym. Chem.*, 1999, **37**, 4386-4389.
53. Y. V. Kissin, R. I. Mink, T. E. Nowlin and A. J. Brandolini, *J. Polym. Sci., Part A: Polym. Chem.*, 1999, **37**, 4281-4294.
54. Y. V. Kissin and A. J. Brandolini, *J. Polym. Sci., Part A: Polym. Chem.*, 1999, **37**, 4273-4280.
55. H. Mori, M. Endo and M. Terano, *J. Mol. Catal. A: Chem.*, 1999, **145**, 211-220.
56. B. Dušan, *J. Sep. Sci.*, 2010, **33**, 315-335.
57. L. K. Kostanski, D. M. Keller and A. E. Hamielec, *J. Biochem. Bioph. Methods*, 2004, **58**, 159-186.

58. A. Rudin and H. L. W. Hoegy, *J. Polym. Sci., Part A: Polym. Chem.*, 1972, **10**, 217-235.
59. G. Odian, *Principles of Polymerisation*, Wiley-Interscience, 1992.
60. P. J. Flory, *Principles of Polymer Chemistry*, Cornell University Press, 1992.
61. G. H. J. van Doremaele, M. van Duin, M. Valla and A. Berthoud, *J. Polym. Sci., Part A: Polym. Chem.*, 2017, **55**, 2877-2891.
62. W. Kaminsky and M. Miri, *J. Polym. Sci.: Polym. Chem. Ed.*, 1985, **23**, 2151-2164.
63. R. A. Collins, A. F. Russell, R. T. W. Scott, R. Bernardo, G. H. J. van Doremaele, A. Berthoud and P. Mountford, *Organometallics*, 2017, **36**, 2167-2181.
64. A. Ostoja Starzewski, N. Steinhauser and B. S. Xin, *Macromolecules*, 2008, **41**, 4095-4101.
65. L. D'Agnillo, J. B. P. Soares and G. H. J. van Doremaele, *Macromol. Mater. Eng.*, 2005, **290**, 256-271.
66. M. C. Haag, J. H. Z. Dos Santos, F. C. Stedile and J. Dupont, *J. Appl. Polym. Sci.*, 1999, **74**, 1997-2003.
67. G. J. P. Britovsek, V. C. Gibson and D. F. Wass, *Angew. Chem. Int. Ed.*, 1999, **38**, 428-447.
68. L. Resconi, J. C. Chadwick and L. Cavallo, in *Comprehensive Organometallic Chemistry III*, eds. R. H. Crabtree and D. M. Mingos, Elsevier, Oxford, 2007, pp. 1005-1166.
69. G. W. Coates, *Chem. Rev.*, 2000, **100**, 1223-1252.
70. S. D. Ittel, L. K. Johnson and M. Brookhart, *Chem. Rev.*, 2000, **100**, 1169-1204.
71. M. C. Baier, M. Zuideveld and S. Mecking, *Angew. Chem. Int. Ed.*, 2014, **53**, 2-25.
72. J. Klosin, P. P. Fontaine and R. Figueroa, *Acc. Chem. Res.*, 2015, **48**, 2004-2016.
73. R. A. Collins, A. F. Russell and P. Mountford, *Appl. Petrochem. Res.*, 2015, **5**, 153-171.
74. O. Daugulis, A. H. R. MacArthur, F. C. Rix and J. L. Templeton, *ACS Catalysis*, 2016, **6**, 1518-1532.

75. F. R. W. P. Wild, L. Zsolnai, G. Huttner and H. H. Brintzinger, *J. Organomet. Chem.*, 1982, **232**, 233-247.
76. J. A. Ewen, *J. Am. Chem. Soc.*, 1984, **106**, 6355-6364.
77. W. Kaminsky, K. Külper, H. H. Brintzinger and F. Wild, *Angew. Chem. Int. Ed. Engl.*, 1985, **24**, 507-508.
78. M. C. Sacchi, E. Barsties, I. Tritto, P. Locatelli, H.-H. Brintzinger and U. Stehling, *Macromolecules*, 1997, **30**, 3955-3957.
79. W. Spaleck, M. Antberg, J. Rohrmann, A. Winter, B. Bachmann, P. Kiprof, J. Behm and W. A. Herrmann, *Angew. Chem. Int. Ed. Engl.*, 1992, **31**, 1347-1350.
80. W. Spaleck, F. Kueber, A. Winter, J. Rohrmann, B. Bachmann, M. Antberg, V. Dolle and E. F. Paulus, *Organometallics*, 1994, **13**, 954-963.
81. W. Spaleck, M. Aulbach, B. Bachmann, F. Küber and A. Winter, *Macromol. Symp.*, 1995, **89**, 237-247.
82. J. A. Ewen, R. L. Jones, A. Razavi and J. D. Ferrara, *J. Am. Chem. Soc.*, 1988, **110**, 6255-6256.
83. P. J. Shapiro, E. Bunel, W. P. Schaefer and J. E. Bercaw, *Organometallics*, 1990, **9**, 867-869.
84. J. Okuda, *Chem. Ber.*, 1990, **123**, 1649-1651.
85. J. C. Stevens, F. J. Timmers, D. R. Wilson, G. F. Schmidt, P. N. Nickias, R. K. Rosen, G. W. Knight and S. Y. Lai, *EP416815A2*, 1991.
86. J. C. Stevens and D. R. Neithamer, *EP418044A2*, 1991.
87. R. K. Rosen, P. N. Nickias, D. D. Devore and F. J. Timmers, *WO9319104A1*, 1993.
88. R. K. Rosen, P. N. Nickias, D. D. Devore, J. C. Stevens and F. J. Timmers, *US5374696A*, 1994.
89. J. A. M. Canich, *US5026798A*, 1991.
90. J. A. M. Canich, *EP420436A1*, 1991.
91. J. A. M. Canich, H. W. Turner and G. G. Hlatky, *US5621126A* 1997.
92. J. C. Stevens, in *Stud. Surf. Sci. Catal.*, Elsevier, 1996, vol. 101, pp. 11-20.
93. J. C. Stevens and T. Kazuo Soga and Minoru, in *Stud. Surf. Sci. Catal.*, Elsevier, 1994, vol. Volume 89, pp. 277-284.
94. H. Braunschweig and F. M. Breitling, *Coord. Chem. Rev.*, 2006, **250**, 2691-2720.

95. G. J. M. Gruter, M. Kranenburg and M. Herklots, *EP919571A1*, 1999.
96. J. A. M. Van Beek, G. H. J. Van Doremaele, G. J. M. Gruter, H. J. Arts and G. H. M. R. Eggels, *WO9613529A1*, 1996.
97. A. Berthoud, V. Q. Norambuena, G. H. J. Van Doremaele, M. A. Zuideveld, R. T. W. Scott and P. Mountford, *EP2801578A1*, 2014.
98. H. Roald, *Angew. Chem. Int. Ed. Engl.*, 1982, **21**, 711-724.
99. R. Hoffmann, *Angew. Chem. Int. Ed.*, 1982, **21**, 711-724.
100. V. C. Gibson and S. K. Spitzmesser, *Chem. Rev.*, 2003, **103**, 283-315.
101. P. Gómez-Sal, A. Martín, M. Mena, P. Royo and R. Serrano, *J. Organomet. Chem.*, 1991, **419**, 77-84.
102. K. Nomura, N. Naga, M. Miki, K. Yanagi and A. Imai, *Organometallics*, 1998, **17**, 2152-2154.
103. K. Nomura, N. Naga, M. Miki and K. Yanagi, *Macromolecules*, 1998, **31**, 7588-7597.
104. K. Nomura, K. Oya and Y. Imanishi, *J. Mol. Catal. A: Chem.*, 2001, **174**, 127-140.
105. K. Nomura, T. Komatsu and Y. Imanishi, *J. Mol. Catal. A: Chem.*, 2000, **152**, 249-252.
106. K. Nomura, M. Tsubota and M. Fujiki, *Macromolecules*, 2003, **36**, 3797-3799.
107. W. Wei, T. Tatsuo, T. Miki, F. Michiya, Y. Shozo and N. Kotohiro, *Adv. Synth. Catal.*, 2005, **347**, 433-446.
108. W. Wang, M. Fujiki and K. Nomura, *J. Am. Chem. Soc.*, 2005, **127**, 4582-4583.
109. D. W. Stephan, J. C. Stewart, F. Guérin, R. E. v. H. Spence, W. Xu and D. G. Harrison, *Organometallics*, 1999, **18**, 1116-1118.
110. D. W. Stephan, J. C. Stewart, F. Guerin, S. Courtenay, J. Kickham, E. Hollink, C. Beddie, A. Hoskin, T. Graham, P. Wei, R. E. v. H. Spence, W. Xu, L. Koch, X. Gao and D. G. Harrison, *Organometallics*, 2003, **22**, 1937-1947.
111. D. W. Stephan, *Organometallics*, 2005, **24**, 2548-2560.
112. P.-J. Sinnema, T. P. Spaniol and J. Okuda, *J. Organomet. Chem.*, 2000, **598**, 179-181.
113. K. Nomura and K. Fujii, *Organometallics*, 2002, **21**, 3042-3049.
114. K. Nomura and K. Fujii, *Macromolecules*, 2003, **36**, 2633-2641.
115. I. Saeed, S. Katao and K. Nomura, *Organometallics*, 2009, **28**, 111-122.

116. I. A. Latham, G. J. Leigh, G. Huttner and I. Jibril, *J. Chem. Soc., Dalton Trans.*, 1986, 377-383.
117. K. Nomura, K. Fujita and M. Fujiki, *Catal. Commun.*, 2004, **5**, 413-417.
118. K. Nomura, K. Fujita and M. Fujiki, *J. Mol. Catal. A: Chem.*, 2004, **220**, 133-144.
119. H. Zhang and K. Nomura, *J. Am. Chem. Soc.*, 2005, **127**, 9364-9365.
120. A. R. Dias, M. T. Duarte, A. C. Fernandes, S. Fernandes, M. M. Marques, A. M. Martins, J. F. da Silva and S. S. Rodrigues, *J. Organomet. Chem.*, 2004, **689**, 203-213.
121. M. J. Ferreira and A. M. Martins, *Coord. Chem. Rev.*, 2006, **250**, 118-132.
122. W. P. Kretschmer, C. Dijkhuis, A. Meetsma, B. Hessen and J. H. Teuben, *Chem. Commun.*, 2002, 608-609.
123. K. Nomura, H. Fukuda, S. Katao, M. Fujiki, H. J. Kim, D.-H. Kim and S. Zhang, *Dalton Trans.*, 2011, **40**, 7842-7849.
124. M. Tamm, S. Randoll, T. Bannenberg and E. Herdtweck, *Chem. Commun.*, 2004, 876-877.
125. M. Tamm, S. Randoll, E. Herdtweck, N. Kleigrewe, G. Kehr, G. Erker and B. Rieger, *Dalton Trans.*, 2006, 459-467.
126. E. G. Ijpeij, P. J. H. Windmuller, H. J. Arts, F. Van der Burgt, G. H. J. Van Doremaele and M. A. Zuideveld, *WO2005090418*, 2005.
127. G. H. J. Van Doremaele, M. Zuideveld, V. Quiroga Norambuena and A. Leblanc, *US8987393B2*, 2015.
128. E. G. Ijpeij, M. A. Zuideveld, H. J. Arts and G. H. J. Van Doremaele, *WO2007059881A1*, 2007.
129. E. G. Ijpeij, B. Coussens, M. A. Zuideveld, G. H. J. van Doremaele, P. Mountford, M. Lutz and A. L. Spek, *Chem. Commun.*, 2010, **46**, 3339-3341.
130. A. Berthoud, G. H. J. Van Doremaele, V. Quiroga Norambuena, R. T. W. Scott, M. Zuideveld and H. J. Arts, *EP2816050B2816051*, 2013.
131. http://www.keltan.com/en/home).
132. E. Smolensky and M. S. Eisen, *Dalton Trans.*, 2007, 5623-5650.
133. K. Merzweiler, D. Fenske, E. Hartmann and K. Dehnicke, *Z. Naturforsch., B: J. Chem. Sci.*, 1989, **44**, 1003-1006.
134. A. N. Chernega, R. Gomez and M. L. H. Green, *J. Chem. Soc., Chem. Commun.*, 1993, 1415-1417.

135. F. T. Edelmann, *Coord. Chem. Rev.*, 1994, **137**, 403-481.
136. R. Gomez, R. Duchateau, A. N. Chernega, J. H. Teuben, F. T. Edelmann and M. L. H. Green, *J. Organomet. Chem.*, 1995, **491**, 153-158.
137. L. R. Sita and J. R. Babcock, *Organometallics*, 1998, **17**, 5228-5230.
138. L. A. Koterwas, J. C. Fettinger and L. R. Sita, *Organometallics*, 1999, **18**, 4183-4190.
139. K. C. Jayaratne and L. R. Sita, *J. Am. Chem. Soc.*, 2000, **122**, 958-959.
140. G. C. Bazan, G. Rodriguez, A. J. Ashe, S. Al-Ahmad and C. Müller, *J. Am. Chem. Soc.*, 1996, **118**, 2291-2292.
141. J. S. Rogers, G. C. Bazan and C. K. Sperry, *J. Am. Chem. Soc.*, 1997, **119**, 9305-9306.
142. G. C. Bazan, G. Rodriguez, A. J. Ashe, S. Al-Ahmad and J. W. Kampf, *Organometallics*, 1997, **16**, 2492-2494.
143. C. Janiak, K. C. H. Lange, U. Versteeg, D. Lentz and P. H. M. Budzelaar, *Chem. Ber.*, 1996, **129**, 1517-1529.
144. G. G. Lavoie and R. G. Bergman, *Angew. Chem. Int. Ed. Engl.*, 1997, **36**, 2450-2452.
145. S. J. Skoog, C. Mateo, G. G. Lavoie, F. J. Hollander and R. G. Bergman, *Organometallics* 2000, **19**, 1406-1421.
146. S. Trofimenko, *J. Am. Chem. Soc.*, 1966, **88**, 1842-1844.
147. S. Trofimenko, *J. Am. Chem. Soc.*, 1967, **89**, 3904-3905.
148. S. Trofimenko, *J. Am. Chem. Soc.*, 1967, **89**, 6288-6294.
149. L. G. Furlan, M. P. Gil and O. L. Casagrande, Jr., *Macromol. Rapid Commun.*, 2000, **21**, 1054-1057.
150. M. P. Gil, S. J. H. Z. Dos and O. L. Casagrande, Jr., *Macromol. Chem. Phys.*, 2001, **202**, 319-324.
151. M. P. Gil and O. L. Casagrande, *J. Organomet. Chem.*, 2004, **689**, 286-292.
152. K. Michiue and R. F. Jordan, *Organometallics*, 2004, **23**, 460-470.
153. H. Bigmore, *DPhil Thesis*, University of Oxford, 2007.
154. H. R. Bigmore, S. C. Lawrence, P. Mountford and C. S. Tredget, *Dalton Trans.*, 2005, 635-651.
155. H. R. Bigmore, M. A. Zuideveld, R. M. Kowalczyk, A. R. Cowley, M. Kranenburg, E. J. L. McInnes and P. Mountford, *Inorg. Chem.*, 2006, **45**, 6411-6423.

156. N. Adams, H. J. Arts, P. D. Bolton, D. Cowell, S. R. Dubberley, N. Friederichs, C. M. Grant, M. Kranenburg, A. J. Sealey, B. Wang, P. J. Wilson, M. Zuideveld, A. J. Blake, M. Schroeder and P. Mountford, *Organometallics*, 2006, **25**, 3888-3903.
157. P. D. Bolton, E. Clot, N. Adams, S. R. Dubberley, A. R. Cowley and P. Mountford, *Organometallics*, 2006, **25**, 2806-2825.
158. B. D. Ward, G. Orde, E. Clot, A. R. Cowley, L. H. Gade and P. Mountford, *Organometallics*, 2004, **23**, 4444-4461.
159. N. Adams, H. J. Arts, P. D. Bolton, D. Cowell, S. R. Dubberley, N. Friederichs, C. M. Grant, M. Kranenburg, A. J. Sealey, B. Wang, P. J. Wilson, A. R. Cowley, P. Mountford and M. Schroder, *Chem. Commun.*, 2004, 434-435.
160. P. D. Bolton and P. Mountford, *Adv. Synth. Catal.*, 2005, **347**, 355-366.
161. D. Herskovicskorine and M. S. Eisen, *J. Organomet. Chem.*, 1995, **503**, 307-314.
162. J. R. Hagadorn and J. Arnold, *Organometallics*, 1994, **13**, 4670-4672.
163. V. Christou, S. P. Wuller and J. Arnold, *J. Am. Chem. Soc.*, 1993, **115**, 10545-10552.
164. J. Richter, F. T. Edelmann, M. Noltemeyer, H.-G. Schmidt, M. Shmulinson and M. S. Eisen, *J. Mol. Catal. A: Chem.*, 1998, **130**, 149-162.
165. J. J. H. Edema, S. Gambarotta, A. Meetsma, A. L. Spek and N. Veldman, *Inorg. Chem.*, 1991, **30**, 2062-2066.
166. Q. Sadaf, H. Kristina, F. C. M., J. P. C., D. G. B. and K. Rhett, *Eur. J. Inorg. Chem.*, 2008, **2008**, 557-562.
167. R. Kempe, *Eur. J. Inorg. Chem.*, 2003, **2003**, 791-803.
168. C. Morton, P. O'Shaughnessy and P. Scott, *Chem. Commun.*, 2000, 2099-2100.
169. O. Markus, A. Perdita and K. Rhett, *Chem. Ber.*, 1996, **129**, 1087-1091.
170. H. Makio, H. Terao, A. Iwashita and T. Fujita, *Chem. Rev.*, 2011, **111**, 2363-2449.
171. V. C. Gibson and S. K. Spitzmesser, *Chem. Rev.*, 2003, **103**, 283-316.
172. S. Mecking, *Angew. Chem. Int. Ed.*, 2001, **40**, 534-540.

173. S. Matsui, M. Mitani, J. Saito, Y. Tohi, H. Makio, N. Matsukawa, Y. Takagi, K. Tsuru, M. Nitabaru, T. Nakano, H. Tanaka, N. Kashiwa and T. Fujita, *J. Am. Chem. Soc.*, 2001, **123**, 6847-6856.

174. J. Tian, P. D. Hustad and G. W. Coates, *J. Am. Chem. Soc.*, 2001, **123**, 5134-5135.

175. J. Saito, M. Mitani, J.-I. Mohri, Y. Yoshida, S. Matsui, S.-I. Ishii, S.-I. Kojoh, N. Kashiwa and T. Fujita, *Angew. Chem. Int. Ed.*, 2001, **40**, 2918-2920.

176. M. Mitani, J.-i. Mohri, Y. Yoshida, J. Saito, S. Ishii, K. Tsuru, S. Matsui, R. Furuyama, T. Nakano, H. Tanaka, S.-i. Kojoh, T. Matsugi, N. Kashiwa and T. Fujita, *J. Am. Chem. Soc.*, 2002, **124**, 3327-3336.

177. Y. Suzuki, S. Kinoshita, A. Shibahara, S. Ishii, K. Kawamura, Y. Inoue and T. Fujita, *Organometallics*, 2010, **29**, 2394-2396.

178. F. F. Karbach, J. R. Severn and R. Duchateau, *ACS Catalysis*, 2015, **5**, 5068-5076.

179. E. Y. Tshuva, I. Goldberg and M. Kol, *J. Am. Chem. Soc.*, 2000, **122**, 10706-10707.

180. E. T. Kiesewetter, S. Randoll, M. Radlauer and R. M. Waymouth, *J. Am. Chem. Soc.*, 2010, **132**, 5566-5567.

181. E. Y.-X. Chen and T. J. Marks, *Chem. Rev.*, 2000, **100**, 1391-1434.

182. I. Tritto, S. X. Li, M. C. Sacchi and G. Zannoni, *Macromolecules*, 1993, **26**, 7111-7115.

183. I. Tritto, S. X. Li, M. C. Sacchi, P. Locatelli and G. Zannoni, *Macromolecules*, 1995, **28**, 5358-5362.

184. A. R. Barron, *Organometallics*, 1995, **14**, 3581-3583.

185. V. Busico, R. Cipullo, F. Cutillo, N. Friederichs, S. Ronca and B. Wang, *J. Am. Chem. Soc.*, 2003, **125**, 12402-12403.

186. M. Bochmann and S. J. Lancaster, *Angew. Chem. Int. Ed. Engl.*, 1994, **33**, 1634-1637.

187. A. P. Shreve, R. Mulhaupt, W. Fultz, J. Calabrese, W. Robbins and S. D. Ittel, *Organometallics*, 1988, **7**, 409-416.

188. R. A. Stapleton, B. R. Galan, S. Collins, R. S. Simons, J. C. Garrison and W. J. Youngs, *J. Am. Chem. Soc.*, 2003, **125**, 9246-9247.

189. V. C. Williams, C. Dai, Z. Li, S. Collins, W. E. Piers, W. Clegg, M. R. J. Elsegood and T. B. Marder, *Angew. Chem. Int. Ed.*, 1999, **38**, 3695-3698.

190. M. Bochmann and M. J. Sarsfield, *Organometallics*, 1998, **17**, 5908-5912.
191. M. Bochmann, L. M. Wilson, M. B. Hursthouse and R. L. Short, *Organometallics*, 1987, **6**, 2556-2563.
192. G. G. Hlatky, H. W. Turner and R. R. Eckman, *J. Am. Chem. Soc.*, 1989, **111**, 2728-2729.
193. M. Bochmann and S. J. Lancaster, *J. Organomet. Chem.*, 1992, **434**, C1-C5.
194. L. Jia, X. Yang, C. L. Stern and T. J. Marks, *Organometallics*, 1997, **16**, 842-857.
195. A. D. Horton and J. de With, *Organometallics*, 1997, **16**, 5424-5436.
196. X. Bei, D. C. Swenson and R. F. Jordan, *Organometallics*, 1997, **16**, 3282-3302.
197. O. Wrobel, F. Schaper, U. Wieser, H. Gregorius and H. H. Brintzinger, *Organometallics*, 2003, **22**, 1320-1325.
198. R. F. Jordan, C. S. Bajgur, R. Willett and B. Scott, *J. Am. Chem. Soc.*, 1986, **108**, 7410-7411.
199. R. F. Jordan, R. E. LaPointe, C. S. Bajgur, S. F. Echols and R. Willett, *J. Am. Chem. Soc.*, 1987, **109**, 4111-4113.
200. M. Bochmann, A. J. Jagger and J. C. Nicholls, *Angew. Chem. Int. Ed. Engl.*, 1990, **29**, 780-782.
201. J. C. W. Chien, W. M. Tsai and M. D. Rausch, *J. Am. Chem. Soc.*, 1991, **113**, 8570-8571.
202. J. C. W. Chien, W. Song and M. D. Rausch, *J. Polym. Sci., Part A: Polym. Chem.*, 1994, **32**, 2387-2393.
203. J. C. W. Chien, W. Song and M. D. Rausch, *Macromolecules*, 1993, **26**, 3239-3240.
204. J. C. W. Chien and B. Xu, *Makromol. Chem., Rapid Commun.*, 1993, **14**, 109-114.
205. A. G. Massey and A. J. Park, *J. Organomet. Chem.*, 1964, **2**, 245-250.
206. X. Yang, C. L. Stern and T. J. Marks, *J. Am. Chem. Soc.*, 1994, **116**, 10015-10031.
207. I. A. Guzei, R. A. Stockland, Jr and R. F. Jordan, *Acta Crystallogr. Sect. C-Cryst. Struct. Commun*, 2000, **56**, 635-636.
208. A. D. Horton, J. de With, A. J. van der Linden and H. van de Weg, *Organometallics*, 1996, **15**, 2672-2674.

209. H. Yasuda, K. Tatsumi and A. Nakamura, *Acc. Chem. Res.*, 1985, **18**, 120-126.
210. H. Yasuda and A. Nakamura, *Angew. Chem. Int. Ed. Engl.*, 1987, **26**, 723-742.
211. B. Temme, G. Erker, J. Karl, H. Luftmann, R. Frohlich and S. Kotila, *Angew. Chem. Int. Ed. Engl.*, 1995, **34**, 1755-1757.
212. M. Bochmann, *J. Chem. Soc., Dalton Trans.*, 1996, 255-270.
213. J. Karl, G. Erker and R. Froehlich, *J. Am. Chem. Soc.*, 1997, **119**, 11165-11173.
214. J. Karl, G. Erker and R. Froehlich, *J. Organomet. Chem.*, 1997, **535**, 59-62.
215. P. G. Jimenez, M. Thompson-Pett, M. Bouwkamp, A. Meetsma, B. Hessen and M. Bochmann, *Angew. Chem. Int. Ed.*, 1997, **36**, 2358-2361.
216. D. D. Devore, F. J. Timmers, D. L. Hasha, R. K. Rosen, T. J. Marks, P. A. Deck and C. L. Stern, *Organometallics*, 1995, **14**, 3132-3134.
217. D. D. Devore, L. H. Crawford, J. C. Stevens, F. J. Timmers, R. D. Mussell, D. R. Wilson and R. K. Rosen, *WO9500526A1*, 1995.
218. A. H. Cowley, G. S. Hair, B. G. McBurnett and R. A. Jones, *Chem. Commun.*, 1999, 437-438.
219. G. S. Hair, R. A. Jones, A. H. Cowley and V. Lynch, *Organometallics*, 2000, **20**, 177-181.
220. G. S. Hair, R. A. Jones, A. H. Cowley and V. Lynch, *Inorg. Chem.*, 2001, **40**, 1014-1019.
221. N. Yue, E. Hollink, F. Guerin and D. W. Stephan, *Organometallics*, 2001, **20**, 4424-4433.
222. T. W. Graham, J. Kickham, S. Courtenay, P. Wei and D. W. Stephan, *Organometallics*, 2004, **23**, 3309-3318.
223. R. F. Jordan, in *Adv. Organomet. Chem.*, eds. F. G. A. Stone and R. West, Academic Press, 1991, vol. 32, pp. 325-387.
224. M. Bochmann, *J. Organomet. Chem.*, 2004, **689**, 3982-3998.
225. M. Bochmann, S. J. Lancaster, M. B. Hursthouse and K. M. A. Malik, *Organometallics*, 1994, **13**, 2235-2243.
226. R. J. Keaton, K. C. Jayaratne, J. C. Fettinger and L. R. Sita, *J. Am. Chem. Soc.*, 2000, **122**, 12909-12910.
227. R. Scott, *DPhil Thesis*, University of Oxford, 2013.
228. A. F. Russell, *DPhil Thesis*, University of Oxford, 2014.

229. M. Bochmann and S. J. Lancaster, *Organometallics*, 1993, **12**, 633-640.
230. R. F. Jordan, P. K. Bradley, N. C. Baenziger and R. E. LaPointe, *J. Am. Chem. Soc.*, 1990, **112**, 1289-1291.
231. Y.-X. Chen and T. J. Marks, *Organometallics*, 1997, **16**, 3649-3657.
232. Y. W. Alelyunas, R. F. Jordan, S. F. Echols, S. L. Borkowsky and P. K. Bradley, *Organometallics*, 1991, **10**, 1406-1416.
233. R. F. Jordan, R. E. LaPointe, N. Baenziger and G. D. Hinch, *Organometallics*, 1990, **9**, 1539-1545.
234. F. Wu, A. K. Dash and R. F. Jordan, *J. Am. Chem. Soc.*, 2004, **126**, 15360-15361.
235. R. F. Jordan, D. F. Taylor and N. C. Baenziger, *Organometallics*, 1990, **9**, 1546-1557.
236. R. F. Jordan and A. S. Guram, *Organometallics*, 1990, **9**, 2116-2123.
237. M. Bochmann and L. M. Wilson, *J. Chem. Soc., Chem. Commun.*, 1986, 1610-1611.
238. E. Hollink, P. Wei and D. W. Stephan, *Organometallics*, 2004, **23**, 1562-1569.
239. L. Cabrera, E. Hollink, J. C. Stewart, P. Wei and D. W. Stephan, *Organometallics*, 2005, **24**, 1091-1098.
240. C. Pellecchia, A. Immirzi, A. Grassi and A. Zambelli, *Organometallics*, 1993, **12**, 4473-4478.
241. C. Pellecchia, A. Grassi and A. Zambelli, *J. Chem. Soc., Chem. Commun.*, 1993, 947-949.
242. M. Vatamanu, G. Stojcevic and M. C. Baird, *J. Am. Chem. Soc.*, 2008, **130**, 454-456.
243. F. Sauriol, E. Wong, A. M. H. Leung, I. E. Donaghue, M. C. Baird, T. Wondimagegn and T. Ziegler, *Angew. Chem. Int. Ed.*, 2009, **48**, 3342-3345.
244. A. F. Dunlop-Brière, P. H. M. Budzelaar and M. C. Baird, *Organometallics*, 2012, **31**, 1591-1594.
245. S. Pillet, G. Wu, V. Kulsomphob, B. G. Harvey, R. D. Ernst and P. Coppens, *J. Am. Chem. Soc.*, 2003, **125**, 1937-1949.
246. N. M. Scott, T. Schareina, O. Tok and R. Kempe, *Eur. J. Inorg. Chem.*, 2004, 3297-3304.
247. W. P. Kretschmer, A. Meetsma, B. Hessen, T. Schmalz, S. Qayyum and R. Kempe, *Chem. - Eur. J.*, 2006, **12**, 8969-8978.

248. A. Noor, W. P. Kretschmer, G. Glatz and R. Kempe, *Inorg. Chem.*, 2011, **50**, 4598-4606.

Chapter Two

Synthesis, reactivity and polymerisation capabilities of cyclopentadienyl-amidinate complexes

2.1 Overview

This Chapter describes the syntheses, characterisation and ethylene and propylene (EPM) co-polymerisation of a range of cyclopentadienyl κ^1-amidinate supported titanium complexes. The activation chemistry of dialkyl complexes is also reported and a series of trapping agents are used to allow further investigation of the cationic species. The synthesis and characterisation of κ^1-amidinate supported titanium diene complexes is presented and their reactivity with tris(pentafluorophenyl)borane (BAr^F_3, $Ar^F = C_6F_5$) to form well-defined zwitterionic species is explored. The X-ray solid state structures of $Cp^*Ti\{NCN(Dipp)CH_2C_6H_4\}Cl_2$ (**2**), $Cp^*Ti\{NCN(Dipp)CH_2C_6H_4\}(CH_2Ph)_2$ (**4**) and $Cp^*Ti\{NCN(Dipp)CH_2C_6H_4\}\{\eta\text{-}EtCH(CH)_2CH_2BAr^F_3\}$ (**14**) are described and various structural parameters are used to further understand the bonding in these complexes. High temperature co-polymerisation of ethylene, propylene and a non-conjugated diene, such as 5-ethylidene-2-norbornene (ENB), were conducted in collaboration with ARLANXEO. A comparison of the productivities of the dialkyl, neutral diene and zwitterionic species is presented.

2.2 Synthesis and characterisation of cyclopentadienyl-amidinate complexes

In 2005, Lanxess Elastomers (now ARLANXEO), published a patent evolving the synthesis of an amidine and its complexation with group 4 metals to afford a range of post-metallocene κ^1-amidinate supported pre-catalysts for olefin polymerisation.[1] The synthesis of isoindolin-1-imine ligand (**1**) was achieved by the reaction of 2-(bromomethyl)benzonitrile with diisopropylaniline under reflux for 90 hours. The resulting hydrobromide salt was stirred over a concentrated NaOH solution overnight, resulting in the desired protio-ligand **1** as an off-white solid in 84% yield (Scheme 2.1). Removal of HBr is essential, as previous work within the Mountford group has shown its negative influence upon any subsequent reactions with group 4 metal complexes.[2]

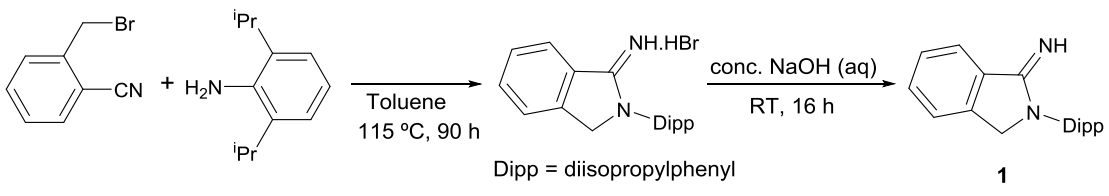

Scheme 2.1. Synthesis of 2-(2,6-diisopropylphenyl)isoindolin-1-imine (**1**).

The room temperature ^{1}H NMR spectrum of **1** shows a broad signal corresponding to the amidine N–H proton at 6.64 ppm. The synthesis of this isoindolin-1-imine ligand provides flexibility regarding substituents on the aryl backbone of the aniline reagent, allowing variation of steric and electronic properties. However, for the scope of this Thesis, only the diisopropylphenyl group was investigated.

Stoichiometric reaction of Cp*$TiCl_3$ with **1** in the presence of excess triethylamine offered a convenient route to synthesise the dichloride complex **2**, isolated as a yellow powder in 79% yield (Equation 2.1).

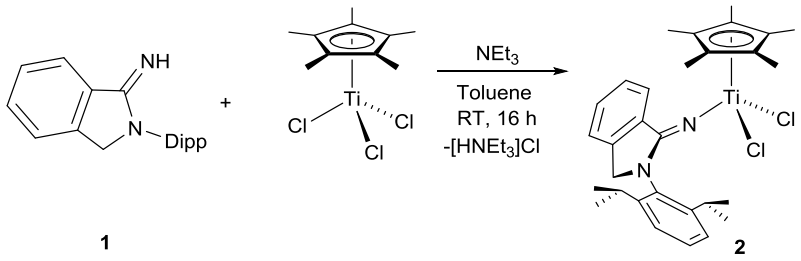

1 **2**

Equation 2.1

The room temperature ^{1}H NMR spectrum of **2** shows a sharp singlet at 2.10 ppm belonging to the Cp* methyl groups (Figure 2.1).

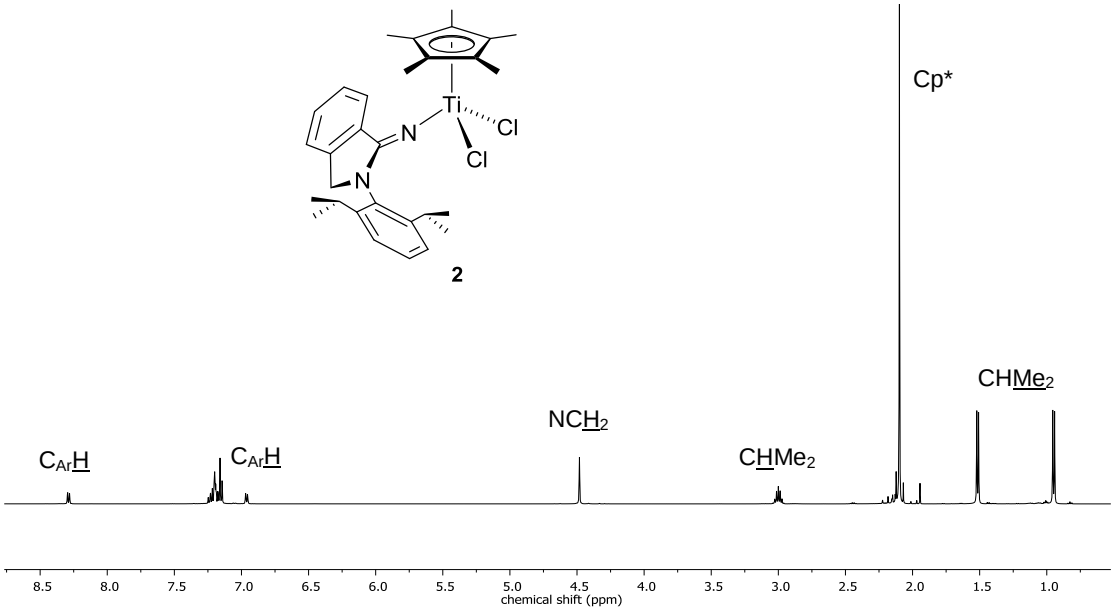

2

Figure 2.1. ^{1}H NMR spectrum (499.9 MHz, C_6D_6, 298 K) of **2**.

The aromatic protons of the ligand backbone appear in overlapping multiplets at 7.25–7.14 ppm and with two doublets at 8.28 and 6.96 ppm. The resonance of the NCH_2 moiety of the amidinate ligand is observed as a singlet at 4.48 ppm, and a septet at 3.00 ppm along with two doublets at 1.50 and 0.95 ppm correspond to the methine and methyl protons of the isopropyl substituents, respectively. The latter observation suggests free rotation around the C–N bond.

Compound **2** was further characterised by single crystal X-ray diffraction. Diffraction-quality crystals were grown from a benzene solution at room temperature. The molecular structure is shown in Figure 2.2. Selected bond distances and angles are listed in Table 2.1. For comparison the selected distances of the known complex $Cp^*Ti\{NC(Ph)N^iPr_2\}Cl_2$ (**1.71**) are also listed in Table 2.1.

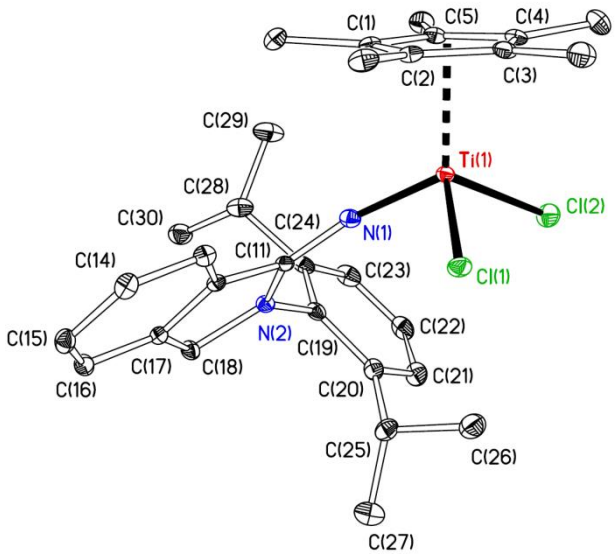

Figure 2.2. Displacement ellipsoid plot of $Cp^*Ti\{NCN(Dipp)CH_2C_6H_4\}Cl_2$ (**2**). Ellipsoids are drawn at 20% probability level and H atoms are omitted for clarity.

Table 2.1. Selected bond lengths (Å) and angles (º) for complex **2**, and **1.71**. Cp^*_{cent} refers to the computed Cp* ring centroid as depicted in Figure 2.2.

	1.71	**2**
Ti(1)–N(1)	1.800(3)	1.816(1)
$Ti(1)–Cp^*_{cent}$	2.05	2.04
Ti(1)–Cl(1)	2.314(1)	2.293(1)
Ti(1)–Cl(2)	2.305(1)	2.299(1)
N(1)–C(11)	1.310(4)	1.284(2)
N(2)–C(11)	1.340(4)	1.357(2)
Ti(1)–N(1)–C(1/11)	165.2(3)	157.5(1)

The molecular structure of **2** shows the expected *pseudo*-tetrahedral three-legged piano stool arrangement around the titanium centre, supported by κ^1-amidinate and η^5-cyclopentadienyl ligands with two chloride ligands occupying the other coordination sites in line with **1.71**. The Ti(1)–N(1) bond distance (1.816(1) Å) is significantly shorter than what is expected for a Ti–N single bond (1.96 Å),[3] but also is slightly longer than observed for a formal $Ti{\equiv}N_{imide}$ triple bond (ranges from 1.69–1.76 Å).[4, 5] A close to linear bond angle between Ti(1)–N(1)–C(11) (157.5(1)º) suggests an sp hybridised N(1) atom and metal-amidinate dπ–pπ bonding contributions.[4, 6] However, the bond angle deviates further from linearity in complex **2** than in **1.71** (157.5(1) *vs.* 165.2(3)º, respectively) which might be attributed to the increase in steric profile pertaining to the amidinate backbone of **2**, and explain the modest lengthening of the Ti(1)–N(1) bond distance (1.816(1) *vs.* 1.800(3) Å in **2** and **1.71**, respectively).

Dialkyl complexes of the type Cp^*TiLX_2 (X= alkyl) are known as important precursors in olefin polymerisation.[6-8] Alkylation of **2** with two equivalents of the respective Grignard reagent (MeMgBr and $PhCH_2MgCl$) proceeded smoothly to give **3** and **4** as dark red solids in 67 and 54% yield, respectively (Equation 2.2).

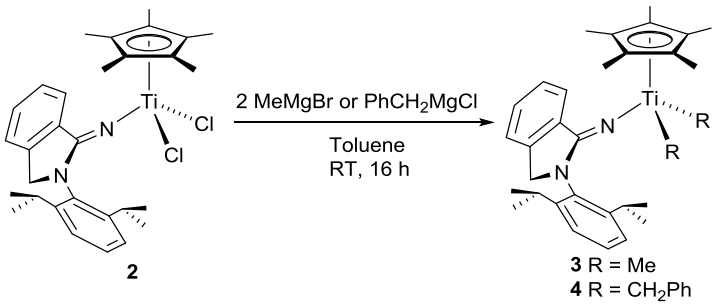

Equation 2.2

The ^{1}H NMR spectrum of **3** shows the expected signal corresponding to the Ti–Me protons at 0.40 ppm, with an HSQC correlation to a ^{13}C signal at 47.7 ppm. A $^{1}J_{CH}$ of 122 Hz, belonging to the Ti–Me moiety is within the range of monomeric neutral titanium dialkyl complexes.[9]

The ^{1}H NMR spectrum of **4** shows two doublets corresponding to the diastereotopic CH_2 protons of the benzyl group at 2.88 and 1.98 ppm ($^{2}J_{HH}$ = 9.8 Hz), with an HSQC correlation to a ^{13}C signal at 79.2 ppm. The $^{1}J_{CH}$ values belonging to the Ti–CH_2 moiety are 123 and 122.6 Hz. The aromatic protons of the benzyl group were identified as a doublet at 6.71 ppm for the *ortho*-protons, a triplet at 6.80 ppm for the *para*-protons and an overlapping multiplet of the *meta*-protons with the aromatic protons of the ligand backbone at 6.95–6.92 ppm (Figure 2.3).

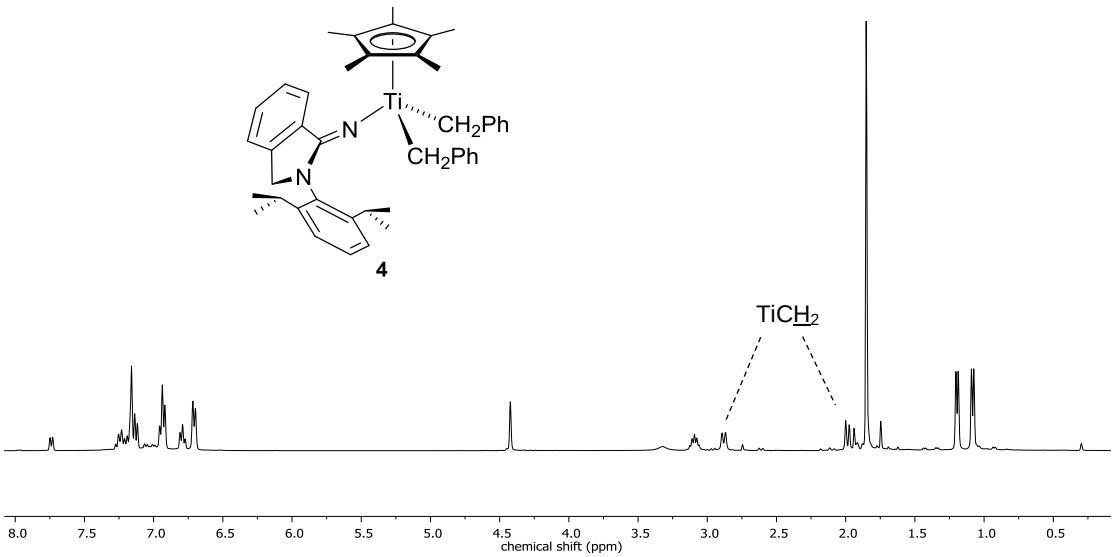

Figure 2.3. ^{1}H NMR spectrum (400.2 MHz, C_6D_6, 298 K) of Cp*Ti{NCN(Dipp)-$CH_2C_6H_4$}$(CH_2Ph)_2$ (**4**).

Compound **4** was further characterised by single crystal X-ray diffraction. Diffraction-quality crystals were grown from a concentrated benzene solution at room temperature. The molecular structure of **4** is shown in Figure 2.4. Selected bond distances and angles are listed in Table 2.2. For comparison the selected distances of the known complex Cp*Ti{NC(Ph)N^{i}Pr$_2$}(CH$_2$Ph)$_2$ (**2.01**) are also listed in Table 2.2.

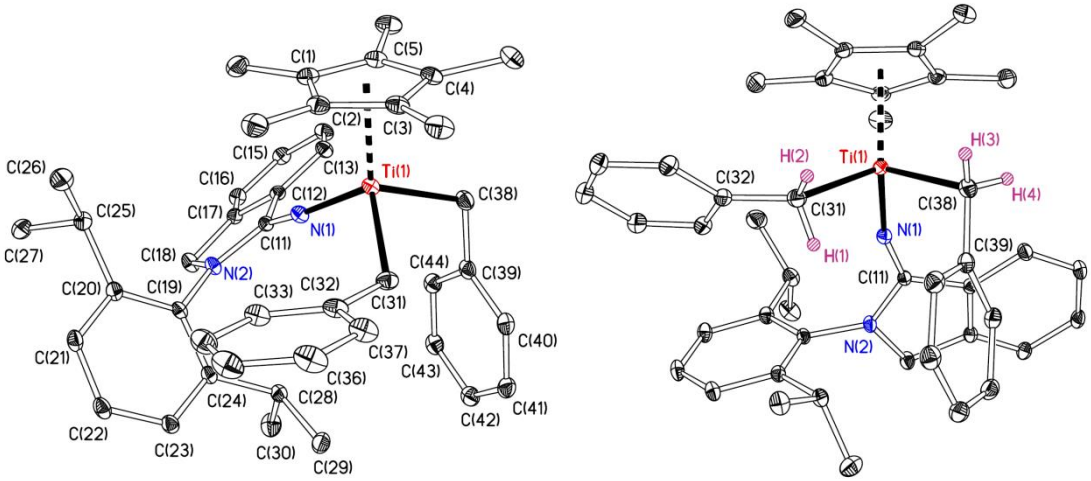

Figure 2.4. Displacement ellipsoid plots, 2 views (20% probability) of Cp*Ti{NCN(Dipp)CH$_2$C$_6$H$_4$}(CH$_2$Ph)$_2$ (**4**). H atoms except those for C(38) and C(31) omitted for clarity.

Table 2.2. Selected bond lengths (Å) and angles (º) for complex **4**, and **2.01**. Cp*$_{cent}$ refers to the computed Cp* ring centroid as depicted in Figure 2.4.

	2.01	**4**
Ti(1)–N(1)	1.838(2)	1.861(1)
Ti(1)–Cp*$_{cent}$	2.05	2.06
Ti(1)–C(31)	2.158(2)	2.148(1)
Ti(1)–C(24/38)	2.180(2)	2.177(1)
N(1)–C(11)	1.295 (3)	1.273(2)
N(2)–C(11)	1.356(3)	1.377(2)
Ti(1)–C(31)–C32)	126.2(2)	125.5(1)
Ti(1)–C(24/38)–C(25/39)	110.5(2)	111.7(1)
Ti(1)–N(1)–C(11)	172.2 (2)	162.8 (1)

Similar to **2**, the molecular structure of **4** also shows a three-legged piano stool arrangement of the amidinate and alkyl ligands around the titanium centre and possesses an overall *pseudo*-tetrahedral geometry. In comparison to the structure of **2**, the introduction of the benzyl ligands results in a lengthening of the Ti(1)–N(1) bond from 1.816(1) to 1.861(1) Å, reflecting the enhanced σ-donation from the benzyl ligands. It also leads to a change in the Ti(1)–N(1)–C(11) bond angle, which in **4** is closer to linearity compared to **2** (162.8(1) *vs.* 157.5(1)º respectively). The orientation of the metal bound benzyl ligands is of particular interest; instead of the usually employed 'riding' model for hydrogens, the position of C(38)–H(4) was found from a Fourier distance map and has been positionally and isotropically refined. The more acute bond angle (111.7(1)º) pertaining to Ti(1)–C(38)–C(39) in comparison to Ti(1)–C(31)–C(32) (125.5(1)º), as well as the shortening of the Ti–C(38) bond length (2.148(1) *vs.* 2.177(1) Å) suggests a C_{ipso} interaction between the benzyl group and metal centre.[10] The bond distances of Ti(1)–C(31) and Ti(1)–C(38) are both shorter in compound **4** compared to compound **2.01** which complements the difference in the bond distances of Ti(1)–N(1) (1.861(1) *vs.* 1.838(1) Å, respectively).

2.3 Activation chemistry of 3 and 4

To study the catalytically active species in polymerisation, base-free cationic complexes were synthesised and fully characterised. Reagents such as BAr^F_3, $[Ph_3C][BAr^F_4]$ or $[HNMe_2Ph][BAr^F_4]$ were used to obtain cationic species by alkyl abstraction and protonolysis, respectively.[6] The reactions were either prepared in bromobenzene-d_5 or in fluorobenzene. Whilst different from those solvents typically used in the reactor for polymerisation catalysis, such solvents are ideal for study of generated cationic complexes, due to their solubilising, yet relatively non-coordinating properties.

2.3.1 Activation with $[Ph_3C][BAr^F_4]$

$[Ph_3C][BAr^F_4]$ has been shown to be an efficient co-catalyst in conjunction with MAO and is regularly employed by ARLANXEO in the co-polymerisation of ethylene, propylene and non-conjugated diene (EPDM).[11, 12] Therefore, the activation with $[Ph_3C][BAr^F_4]$ with the dialkyl species **3** and **4** is of relevance for this Thesis. On NMR tube scale, treatment of **3** with one equivalent of $[Ph_3C][BAr^F_4]$ in C_6D_5Br led to the immediate and quantitative formation of the monoalkyl cation **5-$[BAr^F_4]$**,

which was subsequently characterised by ^{1}H, ^{11}B and ^{19}F NMR spectroscopy. The ^{1}H NMR spectrum showed the expected resonance of Ph_3CMe, the by-product of the methyl abstraction at 2.24 ppm. The Cp* moiety appears at a more downfield shift (1.93 ppm) compared to its neutral counterpart **3**. The Ti–Me resonance is overlapping with the isopropyl moiety of the amidinate ligand at 1.25–1.27 ppm (Figure 2.5).

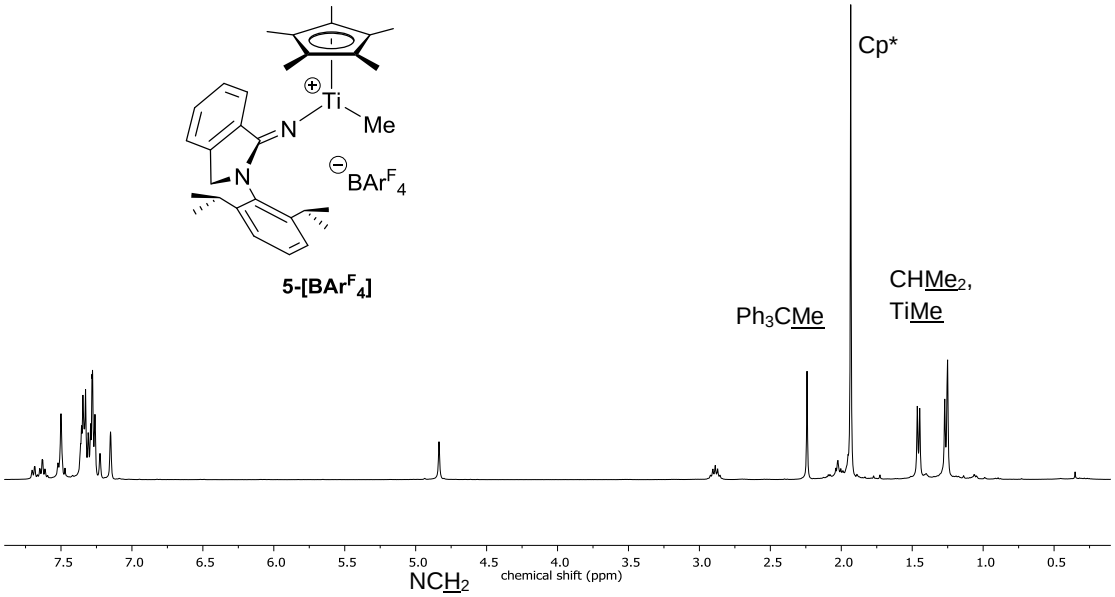

Figure 2.5. ^{1}H NMR spectrum (400.2 MHz, C_6D_5Br, 298 K) of [Cp*Ti{NCN(Dipp)$CH_2C_6H_4$}Me][BAr$^F_4$] (**5-[BAr$^F_4$]**).

Early examples of alkyl cations were obtained as Lewis base adducts (Section 1.7.3).[7] Lewis bases, such as triphenylphosphine oxide (Ph_3PO) are commonly used to form a more stable adduct which can be subsequently isolated and further characterised.

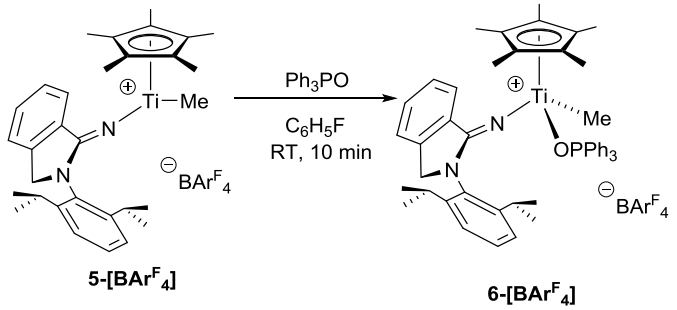

Equation 2.3

On a preparative scale, addition of stoichiometric amounts of Ph_3PO to **5-[BAr$^F_4$]** resulted in the immediate and quantitative formation of a single product, namely

[Cp*Ti{NCN(Dipp)$CH_2C_6H_4$}(OPPh_3)Me][$BAr^F{}_4$] (**6-[$BAr^F{}_4$]**, Equation 2.3), which was isolated as a pale yellow solid in 70% yield. The room temperature ^{1}H NMR spectrum of **6-[$BAr^F{}_4$]** is consistent with C_1 symmetry in solution, as the NCH_2 protons are diastereotopic (5.08 and 4.90 ppm). This is suggestive of an increase in steric crowding around the metal centre when introducing the Ph_3PO fragment and therefore hinders rotation around the Ti–N bond. This is also manifested in the four resonances of the methyl moieties of the Dipp fragment. The Ti–Me resonance shifts more upfield to 0.46 and 52.1 ppm in the ^{1}H and ^{13}C NMR spectra, respectively. The ^{31}P{^{1}H} NMR spectrum reveals a single resonance at 50.2 ppm in contrast to free Ph_3PO normally observed at 26 ppm, in support of coordination by the Lewis base.

On the NMR tube scale, complex **4** was treated with one equivalent of [Ph_3C][$BAr^F{}_4$] in C_6D_5Br which resulted in the quantitative formation of [Cp*Ti{NCN(Dipp)$CH_2C_6H_4$}(CH_2Ph)][$BAr^F{}_4$] (**7-[$BAr^F{}_4$]**). The ^{1}H NMR spectrum of **7-[$BAr^F{}_4$]** features a resonance at 4.04 ppm, corresponding to $Ph_3CC\underline{H}_2Ph$.

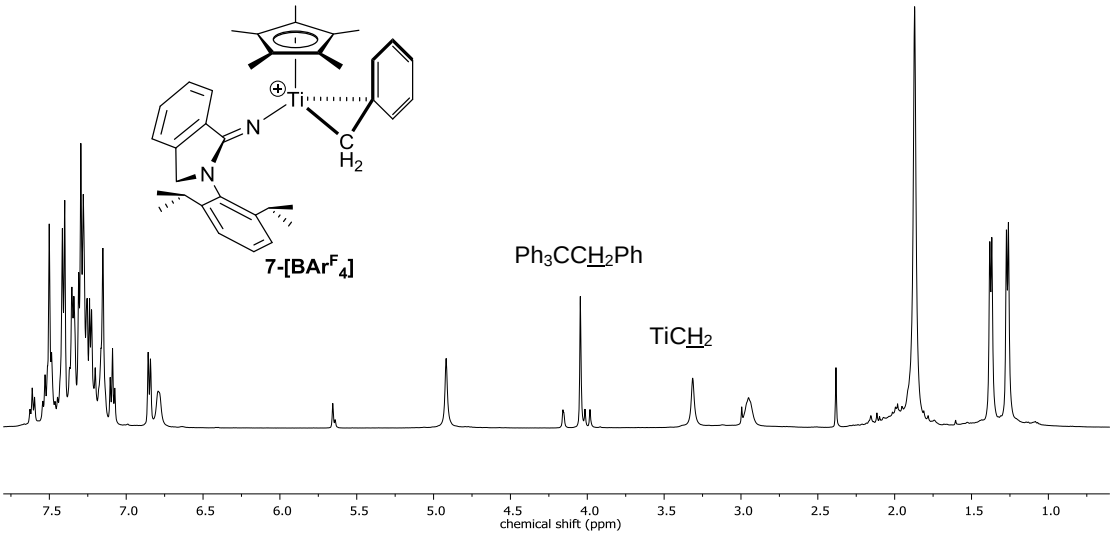

Figure 2.6. ^{1}H NMR spectrum (400.2 MHz, C_6D_5Br, 298 K) of **7-[$BAr^F{}_4$]** and Ph_3CCH_2Ph.

The titanium-benzyl group produces the expected aromatic resonances and a $TiC\underline{H}_2$ signal as a broad singlet at 3.31 ppm, which could be accidental overlap of the otherwise diastereotopic methylene protons (Figure 2.6). The $^1J_{CH}$ coupling constant of the benzyl methylene protons increases upon activation to 149 Hz in comparison to the values of 123 and 122.6 Hz in the neutral complex **4**, which supports the model of

an η^2-benzylic ligand coordination. This coordination leads to re-hybridisation of the CH_2 orbitals involved in bonding to the metal, submitting more π-character to its titanium bonding orbital, causing the other orbitals to gain more s character. The increase in s character leads to the higher coupling constant observed.[10, 13]

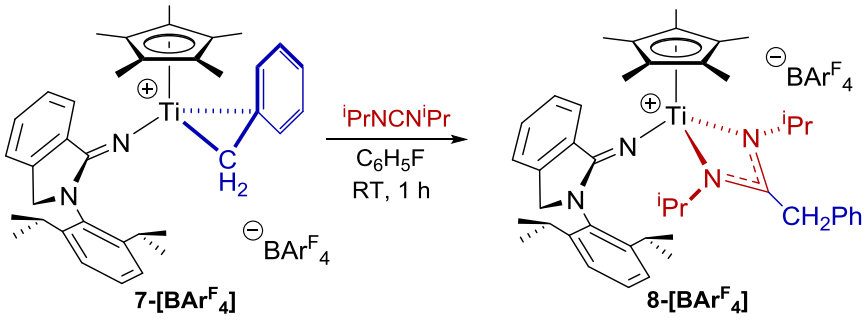

Equation 2.4

To investigate the ease of insertion into the Ti–CH_2 and to allow further characterisation of the cationic species, stoichiometric amounts of *N,N´*-diisopropylcarbodiimide (^{i}PrNCN^{i}Pr) was added to complex **7-[BAr$^F_4$]** giving [Cp*Ti{NCN(Dipp)$CH_2C_6H_4$)}{$PhCH_2C(N^iPr)_2$}][BAr$^F_4$] (**8-[BAr$^F_4$]**) (Equation 2.4). NMR spectroscopy confirmed that the carbodiimide substrate inserted into the Ti–CH_2 bond, as the migrated C<u>H</u>$_2$Ph moiety appears at a more downfield chemical shift of 3.85 ppm in the ^{1}H NMR spectrum, with an HSQC correlation to a ^{13}C signal at 32.2 ppm.

2.3.2 Activation with BAr$^F_3$

Another activator used in the co-polymerisation of ethylene and propylene is BAr$^F_3$. It is also well-known for activating neutral diene complexes to give zwitterionic allylic species which polymerise α-olefins (*vide infra*).[14] Furthermore, activation with BAr$^F_3$ in the polymerisation of propylene gives highly isotactic polypropylene, while the with MAO-activated complex results in atactic polymer.[15] Therefore the cation formed upon activation with BAr$^F_3$ was also of interest for this Thesis (*vide infra*). The stoichiometric reaction on NMR tube scale of **3** with one equivalent of the strong Lewis acid BAr$^F_3$ in C_6D_5Br gave an immediate colour change to a darker red (Equation 2.5). The ^{1}H NMR spectrum of **5-[BAr$^F_3$]** showed two singlets at 1.91 and 1.89 ppm corresponding to the Ti–Me and [<u>Me</u>BAr$^F_3$]$^-$ environments, respectively. The ^{11}B NMR spectrum shows a signal at –14.1 ppm, indicating a four-coordinate

geometry around the boron atom. Horton *et al*. showed that the separation of the *meta*- and *para*-fluorine ^{19}F NMR chemical shift ($\Delta_{(m,p)}$) of $[MeB\underline{Ar}^{F}{}_{3}]^{-}$ provides a good indication of its degree of association to the cationic titanium centre.[16] The ^{19}F NMR shifts of **5-[MeBAr$^{F}_{3}$]** are –132.1 (*o*-C_6F_5), –159.2 (*p*-C_6F_5) and –164.1 (*m*-C_6F_5), giving $\Delta_{(m,p)}$ = 4.9, indicating coordination of $[MeBAr^{F}{}_{3}]^{-}$ to the cation.

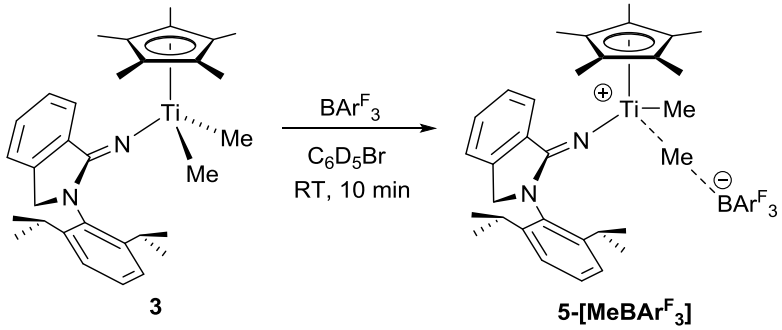

3 **5-[MeBAr$^{F}_{3}$]**

Equation 2.5

In order to check the ease of displacement of the coordinating anion $[MeBAr^{F}{}_{3}]^{-}$ in **5-[MeBAr$^{F}_{3}$]**, Ph_3PO was added to the reaction. Treatment of **5-[MeBAr$^{F}_{3}$]** with Ph_3PO leads to the formation of **6-[MeBAr$^{F}_{3}$]**. The ^{1}H and ^{31}P NMR spectrum were identical to **6-[BAr$^{F}_{4}$]**, with the exception of the $[MeBAr^{F}{}_{4}]^{-}$ counterion. The ^{11}B NMR spectrum shows a resonance at –14.3 ppm. In the ^{19}F NMR spectrum, the *meta*- and *para*-C_6F_5 chemical shifts of $[MeB\underline{Ar}^{F}{}_{3}]^{-}$ result in a $\Delta_{(m,p)}$ of 2.8, indicating "non-coordination" of the $[MeBAr^{F}{}_{3}]^{-}$ anion in respect to the cationic titanium centre.

2.3.3 Activation with [HNMe$_2$Ph][BAr$^{F}_{4}$]

The addition of a proton source, such as $[HNMe_2Ph][BAr^{F}{}_{4}]$, to dimethyl group 4 complexes releases methane and provides an alternative route to the mono-methyl cationic species. In some cases, the same cation is formed as in the activation with $[Ph_3C][BAr^{F}{}_{4}]$;[16] however, the side product of the protonolysis reaction, *viz*. *N*,*N*-dimethylaniline (NMe_2Ph), can act as a Lewis base and coordinate to the particularly electrophilic and sterically open cationic metal centres. Protonation of the metal-bound nitrogen of the κ^1-amidinate moiety has been observed for **3** when activated with $[Ph_3C][BAr^{F}{}_{4}]$ in the presence of 2,4-hexadiene (Chapter Three). Thus the reaction of $[HNMe_2Ph][BAr^{F}{}_{4}]$ to **3** was of interest for this Thesis.

Treatment of **3** with one equivalent of $[HNMe_2Ph][BAr^F{}_4]$ led to a colour change of the solution from orange to dark red. The ^1H NMR spectrum was recorded within 10 minutes of the reaction, showing eliminated methane at 0.35 ppm and a new Ti–Me resonance is observed at 1.25–1.27 ppm, similar to **5-[BAr$^F{}_4$]** (Figure 2.7, a). The methylene protons of amidinate backbone (NCH_2) are diastereotopic, appearing as an AB quartet as a resultant of the small coupling constant $^2J_{HH}$. This is not observed in **5-[BAr$^F{}_4$]**, therefore suggesting coordination of NMe_2Ph.

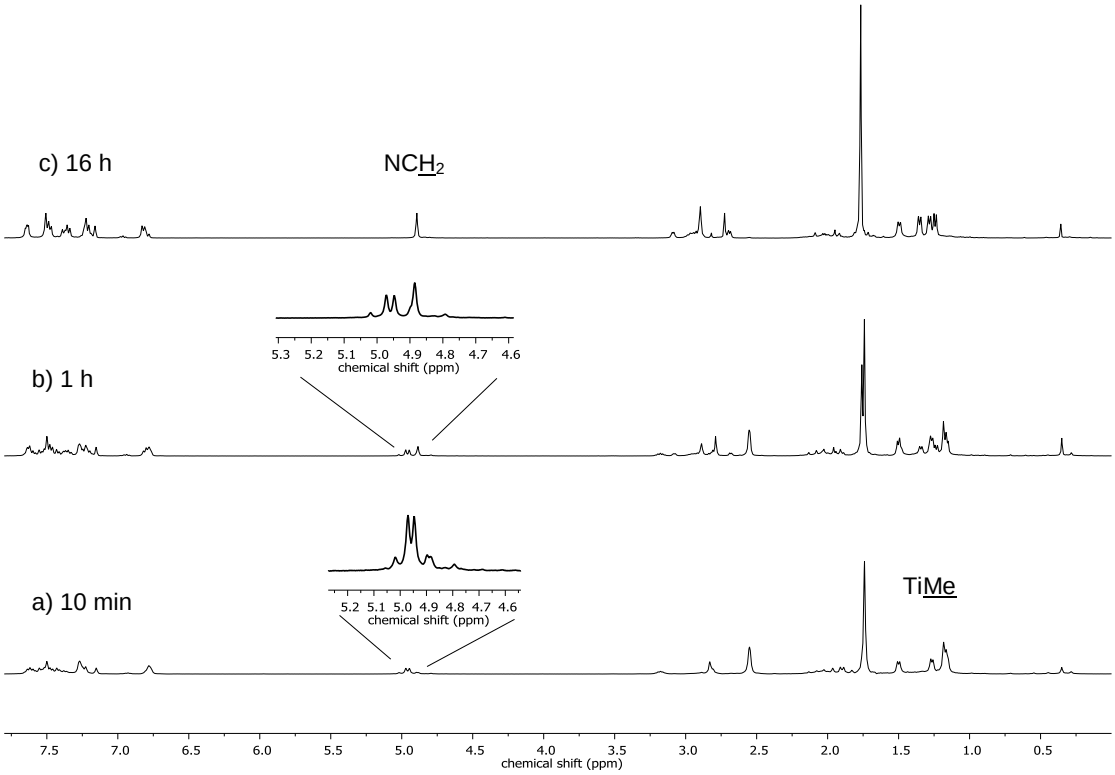

Figure 2.7. ^1H NMR spectrum (400.2 MHz, C_6D_5Br, 298 K) of reaction **3** with $[HNMe_2Ph][BAr^F{}_4]$ recorded at a) 10 minutes, b) 1 hour and c) 16 hours.

The reaction was monitored for a further hour, over which time the formation of a second product was observed (Figure 2.7, b). After 16 hours, only one product was detected, originating from two consecutive C–H bond activations, eliminating two equivalents of methane (Figure 2.7, c, Scheme 2.2). A similar reaction has been previously observed by Wrobel and co-workers, albeit for a zirconium cation.[17]

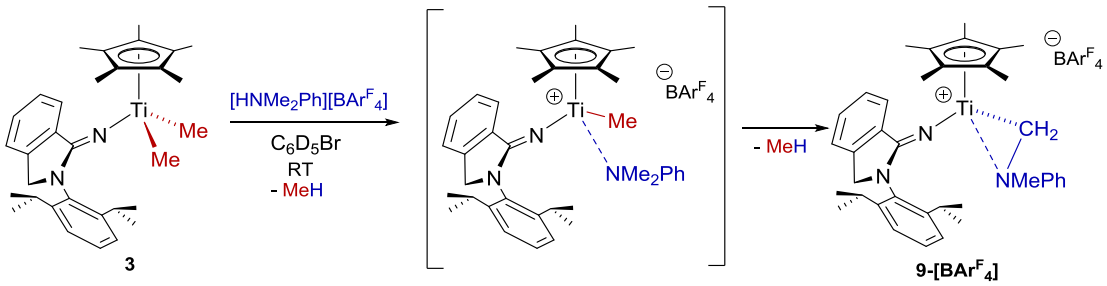

Scheme 2.2. Synthesis of [Cp*Ti{NCN(Dipp)$CH_2C_6H_4$}{CH_2NMe(Ph)}][BAr^F_4] (**9-[BAr^F_4]**).

The final product was isolated as a dark red solid in a 46% yield. ^{1}H NMR spectrum of **9-[BAr^F_4]** showed two doublets at 3.08 and 2.69 ppm belonging to the TiCH_2 moiety, with an HSQC correlation to a ^{13}C signal at 77.6 ppm. Interestingly, despite observing a singlet for the NCH_2 proton, four different signals are observed for the methyl groups of the Dipp fragment. Having two different substituents on the titanium centre, in this case a –CH_2 and a –NMePh group, suggests even with fast rotation around the Ti–N bond, that the methyl groups of the Dipp moiety cannot be interconverted. **9-[BAr^F_4]** was also independently synthesised from the reaction of *N*,*N*-dimethylaniline with **5-[BAr^F_4]**.

On the NMR tube scale, within 5 minutes Ph_3PO was added to the reaction of **3** with [$HNMe_2Ph$][BAr^F_4] to replace the NMe_2Ph moiety. The ^{1}H NMR spectrum shows the same signals as for **6-[BAr^F_4]** alongside signals for NMe_2Ph, exemplified by the singlet at 2.87 ppm of the NMe_2 moiety. The ^{31}P{^{1}H} spectrum displays a signal at 50.2 ppm further confirming the formation of the Lewis base adduct.

On a preparative scale, treatment of **9-[BAr^F_4]** with one equivalent of diisopropylcarbodiimide, resulted in the insertion of the unsaturated substrate into the Ti–CH_2 bond, and formation of the κ^2-bound moiety [Cp*Ti{NCN(Dipp)$CH_2C_6H_4$}-{(NMePh)$CH_2C(N^iPr)_2$}][BAr^F_4] (**10-[BAr^F_4]**) as a red solid in 43% yield (Equation 2.6).

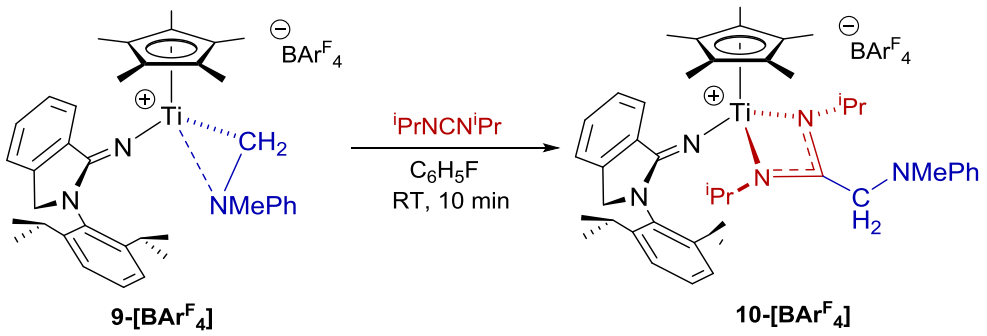

9-[BAr$^F_4$] **10-[BAr$^F_4$]**

Equation 2.6

The NCH_2 protons of the imidazolidine moiety are diastereotopic and correspond to an AB quartet at 5.01 to 4.92 ppm in the ^{1}H NMR spectrum. Two doublets at 4.19 and 4.00 ppm belong to the methylene protons of the migrated $CH_2N(Ph)Me$ moiety, with an HSQC correlation to a ^{13}C resonance at 53.9 ppm, a more upfield shift than that in complex **9-[BAr$^F_4$]**. These observations, alongside four chemically different environments of the methyl groups of the Dipp moiety, provide evidence for restricted rotation around the Ti–N bond induced by the newly formed κ^2-amidinate ligand.

2.4 Synthesis and characterisation of cyclopentadienyl-amidinate diene complexes

Neutral diene complexes of metallocene and post-metallocene group 4 complexes have been widely explored in the literature.[18, 19] There are several ways of synthesising neutral group 4 diene complexes, such as photolysis of diarylmetallocenes in the presence of conjugated dienes, reaction of cyclopentadienyl metal halides with 'ene-diyl' magnesium reagents, or reduction of cyclopentadienyl metal halides with two equivalents of ^{n}BuLi in the presence of 1,3-diene compounds.[20, 21] Coordination of conjugated diene moieties to group 4 metals can occur *via* different binding modes, *viz*. *cis* and *trans*.[18, 20, 22, 23] The *cis* geometry of the diene can bind to the metal centre in either η^4-cis-diene (middle to late transition metals) or 'ene-diyl' coordination mode.[18, 22, 24] The latter has been previously reported to be favoured for group 4 metal complexes and results in two possible isomers, *viz*. *supine* and *prone*.[25] These two isomers differ in the orientation of the coordinated diene with respect to the cyclopentadienyl ligand (Scheme 2.3) and the relative ratios of either depend on the metal complex.[19]

Erker *et al*. discovered in the early 1990s, that upon the addition of BAr^F_3 to the neutral diene species, a well-defined zwitterionic species is formed which is active in olefin polymerisation and provides unique control over cation-anion interactions during catalysis.[14] Diene activation since then has been exploited for a variety of catalyst systems, including constrained geometry-type catalysts and post-metallocene precatalysts.[26, 27] Over the last decade, collaborative research between the Mountford group and ARLANXEO has focused on cyclopentadienyl-amidinate diene complexes and their activity in EPDM polymerisation for the complex **1.71**–**1.74** as shown in Section 1.8.1.[28]

2.4.1 Cp*Ti{NCN(Dipp)$CH_2C_6H_4$}(η-2,3-$C_4H_4Me_2$) (11)

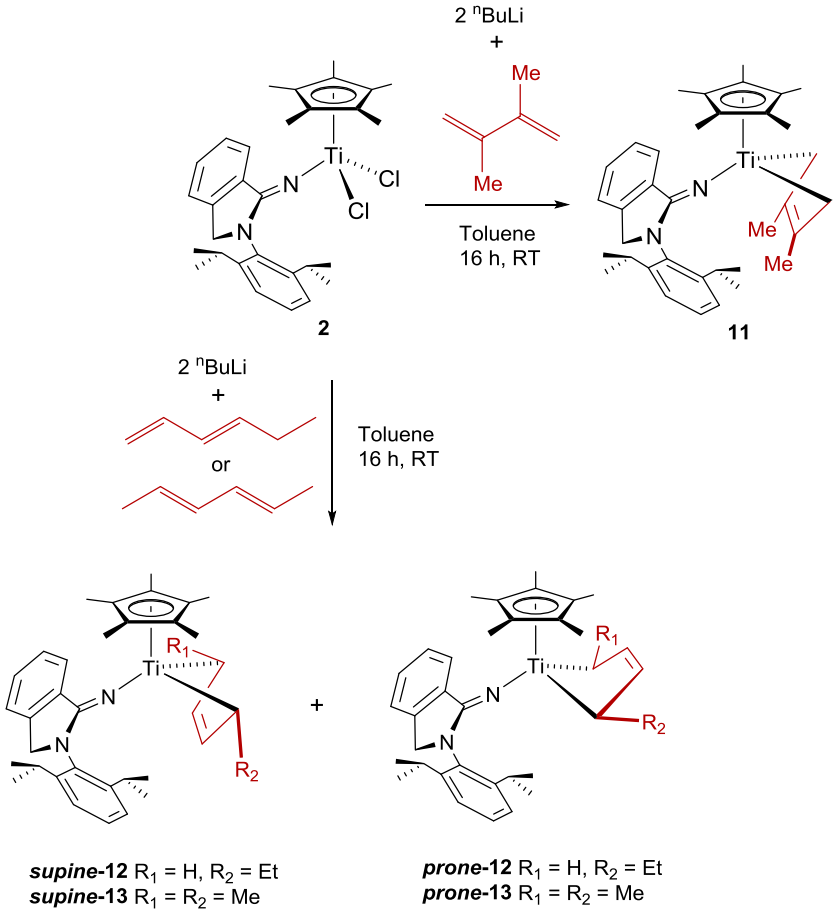

Scheme 2.3. Synthesis of neutral diene complexes, Cp*Ti{NCN(Dipp)$CH_2C_6H_4$}{X} (X = η-2,3-$C_4H_4Me_2$, **11**; η-$CH_2(CH)_2CHEt$, **12**; η-1,4-$C_4H_4Me_2$, **13**).

The reactive intermediates in the reaction of group 4 metal dichloride complexes with ^{n}BuLi are still unclear.[29] The mechanism is thought to go *via* alkylation of the metal

centre, followed by α, β, or γ-H elimination resulting in alkane loss and formation of a metal-alkene species.[30, 31] Even in the absence of conjugated diene reagents, Harrod and Dioumaev have shown that $Cp_2Zr^nBu_2$ forms 'ene-diyl' metallacyclic bonds after undergoing a number of organometallic rearrangements. This suggested a thermodynamic preference and a driving force towards diene coordination.[29]

During the reduction of **3** with two equivalents of ^{n}BuLi in the presence of 2,3-dimethyl-1,3-butadiene, only the *supine* isomer **11** is observed. Upon substitution at the 'vinylic' 2,3-positions, the *prone* isomer becomes highly disfavoured as a resultant of the steric repulsion with the Cp* ligand. This has also been confirmed by DFT calculations conducted by Professor Philip Mountford, where the *supine* isomer of this system is 7.5 kcal mol^{-1} more favoured compared to the *prone* isomer at 298 K. Complex **11** was isolated as a dark green solid in 80% yield. The room temperature ^{1}H NMR spectrum shows that the coordination of the diene to **2** results in restricted rotation on the NMR timescale: this is manifested in the splitting of the NCH_2 moiety into an AB quartet at 4.50 ppm as well as four distinct environments for methyl groups of the Dipp moiety (Figure 2.8).

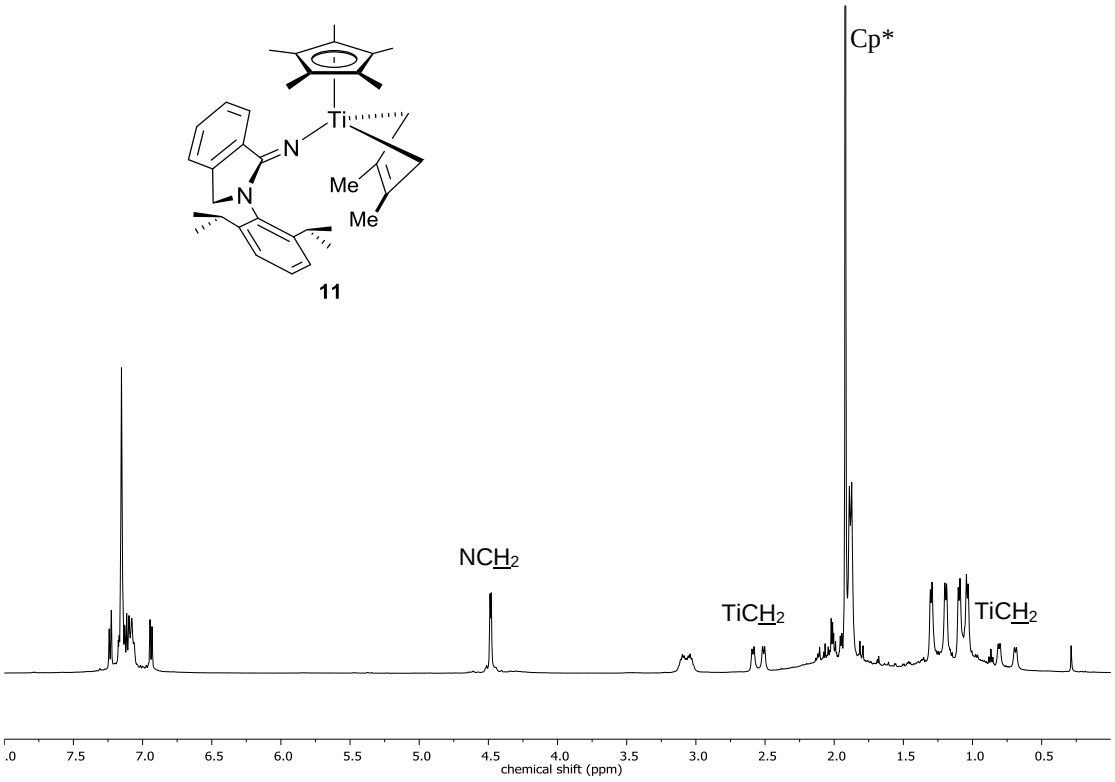

Figure 2.8. ^{1}H NMR spectrum (499.9 MHz, C_6D_5Br, 298 K) of Cp*Ti{NCN(Dipp)$CH_2C_6H_4$}(η-2,3-$C_4H_4Me_2$) (**11**).

Two low field doublets at 2.59 and 2.52 ppm and two high field doublets at 0.81 and 0.70 ppm belong to the four diastereotopic diene protons, assigned *syn* and *anti* protons, respectively. The chemical shift difference can be attributed to the *anti* protons experiencing enhanced shielding due to the close proximity of the Cp* moiety.[25, 32] The geminal coupling constants (7.2 and 7.1 Hz, respectively) of the methylene protons are further support for the coordinated *s-cis*-diene, with similar values reported in literature.[18, 23, 33] The ^{13}C shifts at 71.2 and 69.2 ppm are assigned to the CH_2 group adjacent to the titanium centre, while the vinylic ^{13}C resonances are observed at 128.2 and 128.0 ppm. The large difference in the ^{13}C resonances of the diene fragment emphasises the presence of sp^3 and sp^2 hybridised carbons, supporting the 'ene-diyl' metallacylic structure of the complex.[33-35] This is further supported by the $^1J_{CH}$ coupling constants obtained for the diene methylene groups, ranging from 140.0 to 149.3 Hz, showing a considerable smaller value than for usual sp^2-hybridised carbon atoms (155–160 Hz).[20] The *supine* confirmation of **11** was further supported as the methylene *anti* protons are the only protons from the diene fragment to correlate-through space to the Cp* moiety at 1.93 ppm.

2.4.2 Cp*Ti{NCN(Dipp)$CH_2C_6H_4$}(η-$CH_2(CH)_2$CHEt) (12)

Reaction of **2** with two equivalents of ^{n}BuLi in the presence of excess 1,3-hexadiene at room temperature results in the formation of the unsymmetrical compound Cp*Ti{NCN(Dipp)$CH_2C_6H_4$}(η-$CH_2(CH)_2$CHEt) (***supine***- and ***prone***-**12**, Scheme 2.3) which was isolated as a dark green solid in 78% yield.

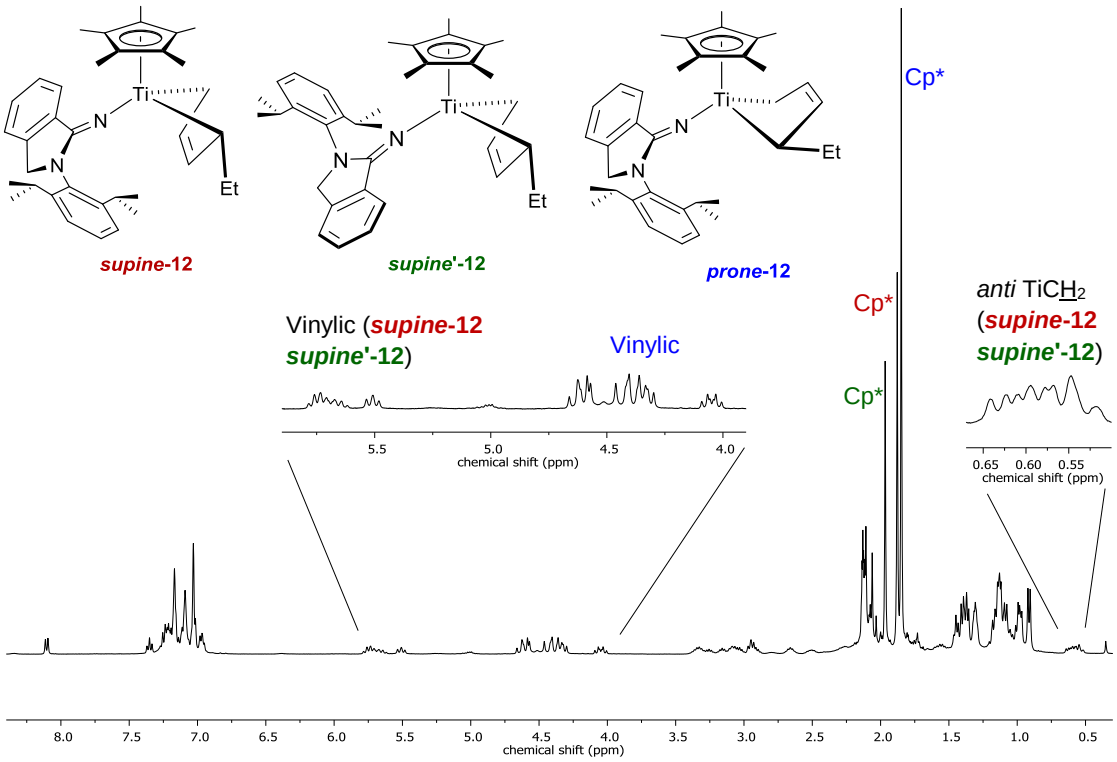

Figure 2.9. ^{1}H NMR spectrum (400.2 MHz, toluene-d_8, 243 K) of ***supine***- and ***prone***-**12**.

Unlike compound **11**, *supine* (***supine*-12**) and *prone* (***prone*-12**) isomers are observed in a 2:1 ratio. Attempts to separate these isomers *via* sublimation or crystallisation have thus far been unsuccessful. Characterisation by NMR spectroscopy was recorded at –30 ºC in order to 'freeze out' any exchange of isomers (Figure 2.9), since the room temperature ^{1}H NMR spectrum exhibited broad resonances.

A total of three isomers are observed in the spectra recorded at –30 ºC, as revealed mainly by the presence of three different Cp* resonances from 1.98 to 1.85 ppm in the ^{1}H NMR spectrum. The presence of two *supine* isomers (***supine*-12** and ***supine*'-12**) in the reaction mixture is due to the asymmetric nature of the supporting κ^{1}-amidinate ligand and diene moiety. The backbone of the diene fragment is orientated towards the amidinate ligand, which subsequently hinders rotation around the Ti–N bond, resulting in two different conformations of the amidinate ligand with respect to the titanium-diene fragment (Figure 2.10). The two *supine* isomers could not be individually assigned using NMR spectroscopy. DFT calculations show that one *prone* isomer is more disfavoured compared to the other isomers, which is consistent with the experimental observation.

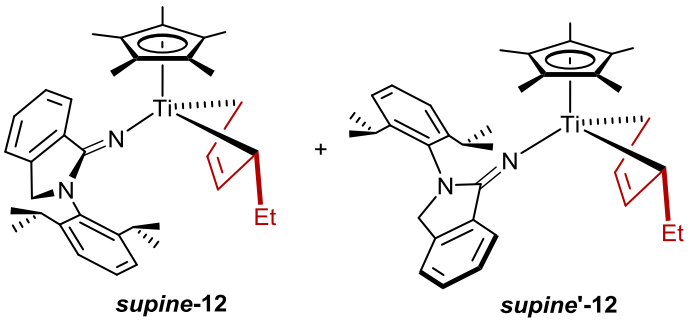

Figure 2.10. Lewis structure of ***supine*-12** and ***supine*'-12**.

A ROESY spectrum was obtained in order to allow reliable assignments of the *supine* (***supine*-12** and ***supine*'-12**) and *prone* (***prone*-12**) isomers. The vinylic protons of ***prone*-12** at 4.35 and 4.04 ppm correlate through-space to the Cp* methyl groups at 1.85 ppm. The same signals exhibit through-bond correlations to the diastereotopic methylene and methine protons adjacent to the titanium centre at 3.02, 1.39–1.36 and 1.74–1.72 ppm, respectively. In contrast, the resonances belonging to the *anti* protons of the methylene moieties of ***supine*-12** and ***supine*'-12** (overlapping multiplet at 0.61–0.54 ppm) correlate through-space to the Cp* moiety at 1.95 and 1.98 ppm, respectively. The same signals exhibit through-bond correlations to the vinylic protons at 5.80 to 5.51 ppm. The upfield shift of the vinylic resonances of ***prone*-12** in comparison to ***supine***- and ***supine*'-12** can be attributed towards the enhanced shielding effect through the close proximity to the Cp* moiety (*vide supra*). For all three isomers, the ^{13}C resonances of the vinylic carbons are shifted downfield from those adjacent to the titanium centre, suggesting, as previously observed, a substantial 'ene-diyl' character of the diene, further supporting the resultant +4 oxidation state of the metal centre.[32]

2.4.3 Cp*Ti{NCN(Dipp)$CH_2C_6H_4$}(η-1,4-$C_4H_4Me_2$) (13)

Reacting **2** with two equivalents of ^{n}BuLi in the presence of excess 2,4-hexadiene results in the formation of Cp*Ti{NCN(Dipp)$CH_2C_6H_4$}(η-1,4-$C_4H_4Me_2$) **(*supine*-** and ***prone*-13**) (Scheme 2.3), which was isolated as a brown solid in a 70% yield.

The low temperature ^{1}H NMR spectrum (Figure 2.11) reveals the presence of two major isomers, namely ***supine*-13** and ***prone*-13**, as well as the three isomers of complex **12** (*vide supra*). The presence of **12** indicates that another rearrangement took place during the reaction and could be related to the metal-alkene complex

presumably formed as an intermediate (*vide supra*). Olefin/diene isomerisation catalysts are well established and may operate *via* a range of mechanisms.[36-38]

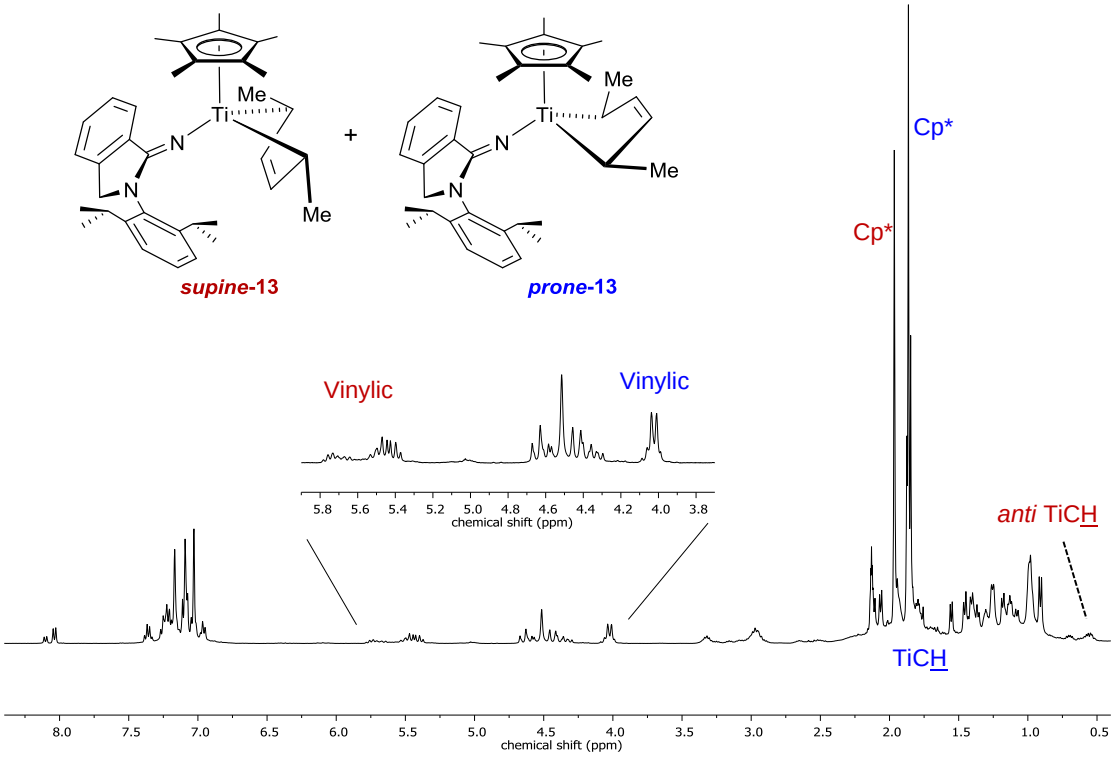

Figure 2.11. ^{1}H NMR spectrum (499.9 MHz, toluene-d_8, 243 K) of ***supine***- and ***prone*-13**.

Overall, both isomers possess C_1 symmetry in solution. A ROESY experiment was obtained at –30 ºC assign the *supine* (***supine*-13**) and *prone* (***prone*-13**) isomer. The vinylic protons of ***prone*-13** at 4.06 to 3.99 ppm correlate through space to the Cp* methyl groups at 1.86 ppm. The same signals exhibit through-bond correlation to the methine protons adjacent to the metal centre at 1.81–1.79 ppm.

In contrast, the methine protons of ***supine*-13**, adjacent to the metal centre, appear as a multiplet at an upfield shift (0.69–0.52 ppm). This resonance correlates through space to the Cp* moiety at 1.96 ppm. This suggests, in agreement with the chemical shifts, that these protons are in the *anti* position.

Similar as for structure **11** and **12**, the differences in chemical shift between the internal carbons and the terminal carbons imply significant σ-bonding character of the diene fragment.

2.4.4 Synthesis and characterisation of zwitterionic cyclopentadienyl-amidinate complexes

Erker and co-workers were the first to discover the formation of a zwitterionic species of group 4 metal diene complexes and their activity in olefin polymerisation.[14] The structurally characterised complex showed an interaction between one of the *ortho*-fluorine on the borate anion and the cationic metal centre. This was also manifested in the ^{19}F NMR spectrum with a particularly shielded *ortho*-fluorine shift. The first structurally characterised titanium zwitterionic complex showed an agostic interaction between the methylene protons adjacent to the borate and the titanium cationic centre, suggesting that an increase in steric hindrance in the supporting ligands (cyclopentadienyl *vs*. geometry-constrained ligand systems) alters the interaction in the apparent free coordination site.[26]

2.4.4.1 Synthesis of Cp*Ti{NCN(Dipp)$CH_2C_6H_4$}{η^3-EtCH$(CH)_2CH_2BAr^F_3$} (14)

On a preparative scale, stoichiometric reaction of ***supine*-12, *supine*'-12** and ***prone*-12** with BAr^F_3 immediately generates a single zwitterionic species, *viz.* Cp*Ti{NCN(Dipp)$CH_2C_6H_4$}{η^3-EtCH$(CH)_2CH_2BAr^F_3$} (**14**) which was isolated as a dark green solid in 53% yield. The borate moiety is found to be located on the terminal CH_2 with the remaining three diene carbons forming a π-coordinated allylic moiety (Equation 2.7).

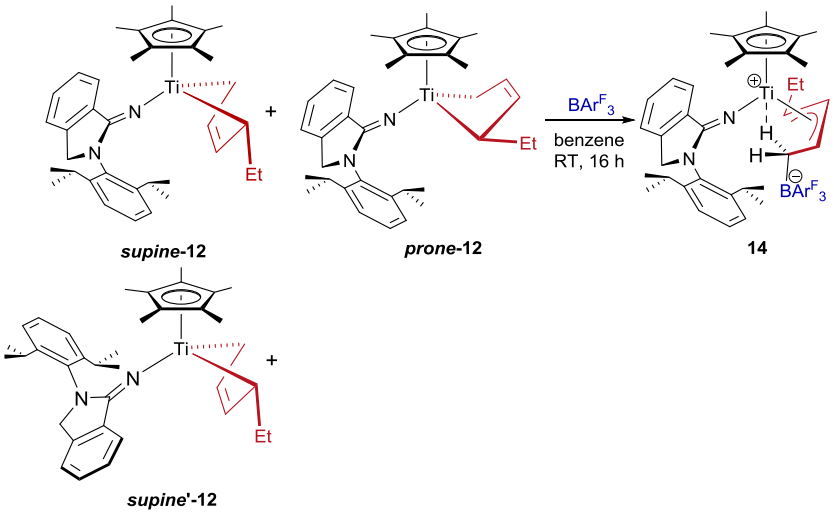

Equation 2.7

The three allylic protons correspond to the resonances at 5.51, 3.69 and 3.38 ppm assigned to the central allylic CH, CH adjacent to the ethyl group and CH adjacent to $CH_2BAr^F_3$, respectively (Figure 2.12). The diastereotopic methylene protons correspond to the broad signals at 1.31 and –1.32 ppm. The large difference of chemical shifts for the two methylene protons is indicative of an agostic interaction with the cationic titanium centre. This was also confirmed by structural characterisation (*vide infra*). Such large chemical shift differences are also present in previously investigated compounds that also show analogous agostic interactions.[26, 28] The $^1J_{CH}$ coupling constant for the proton at –1.32 ppm is shown to be 93.6 Hz. This value is significantly lower than the typical range of $^1J_{CH}$ coupling constants relating to sp^3 hybridised CH bonds (normally between 120–130 Hz), but matches values of previously reported $^1J_{CH}$ coupling constants of CH moieties involved in an agostic interactions.[9, 39, 40]

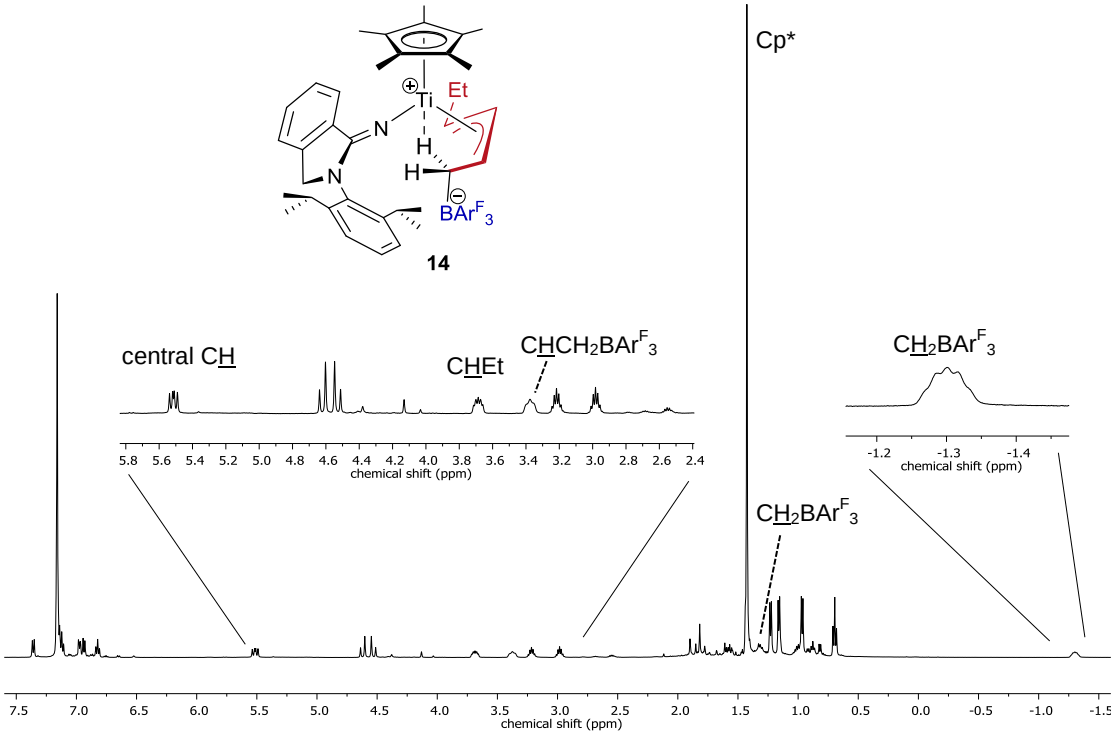

Figure 2.12. ^{1}H NMR spectrum (499.9 MHz, C_6D_6, 298 K) of Cp*Ti{NCN(Dipp)$CH_2C_6H_4$}{η^3-EtCH$(CH)_2CH_2BAr^F_3$} (**14**).

A ROESY experiment was carried out to give insight into the confirmation of the allyl borate ligand. The central allylic proton and the proton adjacent to the $CH_2BAr^F_3$ moiety correlate through-space to the Cp* methyl groups, indicating an *exo*-type

conformation in **14**. This was also observed in the solid state structure and in the previously reported related complex Cp*Ti{NC(Ph)NiPr$_2$}{η^3-CH$_2$C(Me)C(Me)CH$_2$BAr$^F_3$} (**1.75**).[28]

The ^{19}F NMR spectrum showed 15 different fluorine environments, indicating highly hindered rotation around the B–CH$_2$ and B–Ar bonds. This was also observed with the zwitterionic species (η^5-1,3-C$_5$H$_3$(SiMe$_3$)$_2$)Zr{η^3-CH$_2$CHCH$_2$}{η^3-CH$_2$C(Me)C(Me)CH$_2$BAr$^F_3$} reported by Bochmann *et al.*[41] Unlike Erker's zirconocene zwitterion, no high field fluorine shift was observed in the ^{19}F NMR spectrum suggesting the absence of the Ti···F interaction, as supported by the crystal structure (*vide infra*). The room temperature ^{11}B NMR spectrum displays a sharp singlet at –12.5 ppm corresponding to the expected tetracoordinate boron.

On a preparative scale, stoichiometric reaction of the mixture of isomers of **13** with BAr$^F_3$ at room temperature also forms the zwitterionic allylic complex **14**. The reaction occurs *via* the migration of the borane moiety accompanied with a hydrogen shift, resulting in the borate being attached to a newly formed methylene group. The methylene group is bound to the allylic moiety, leaving the other peripheral allylic carbon now bearing an ethyl group. The same rearrangement has been previously observed for the reaction of Cp*Ti{NC(Ph)N^{i}Pr$_2$}{η-1,4-C$_4$H$_4$Me$_2$} (**1.73**) with BAr$^F_3$ as well as for the reaction of (η^5,η^1-C$_5$Me$_4$SiMe$_2$N^{t}Bu)Ti(η-1,4-C$_4$H$_4$Me$_2$) with BAr$^F_3$.[26, 28]

Single crystals of **14** suitable for X-ray diffraction were grown from a benzene solution at room temperature. The molecular structure is shown in Figure 2.13 and full crystallographic data can be found in the CD appendix. Selected distances and angles are listed in Table 2.3. For comparison selected distances of the known complex Cp*Ti{NC(Ph)N^{i}Pr$_2$}{η^3-EtCH(CH)$_2$CH$_2$BAr$^F_3$} (**2.02**) are also listed in Table 2.3. The solid state structure of **14** is in agreement with the spectroscopic data, showing an agostic interaction between the cationic titanium centre and one of the methylene protons on the allyl moiety. The *anti*-substituted allyl moiety, allows C(31) to be in a favourable position for the observed agostic interaction, which has also been previously observed for (η^5-C$_5$Me$_4$SiMe$_2$N^{t}Bu)Zr{η^3-CH$_3$(CH)$_3$CH$_2$BAr$^F_3$}.[27]

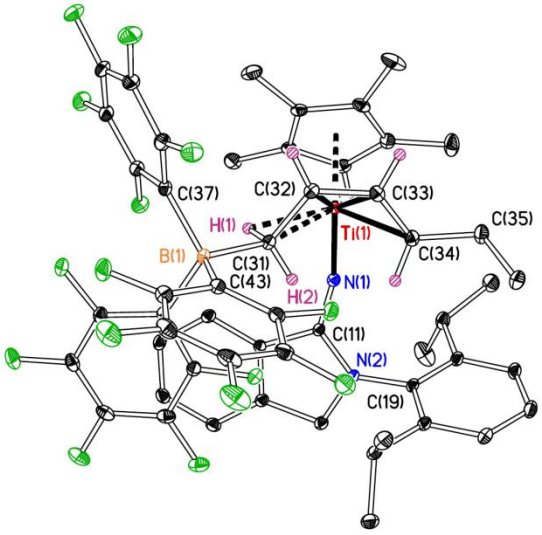

Figure 2.13. Displacement ellipsoid plots (20% probability) Cp*Ti{NCN(Dipp)$CH_2C_6H_4$}{η^3-EtCH$(CH)_2CH_2BAr^F{}_3$} (**14**). H atoms except those for C(31) to C(34) omitted for clarity.

Table 2.3. Selected bond lengths (Å) and angles (º) for complex **14**, and **2.02**. Cp^*_{cent} refers to the computed Cp* ring centroid as depicted in Figure 2.4.

	2.02	**14**
Ti(1)–N(1)	1.852(4)	1.848(2)
Ti(1)–Cp^*_{cent}	2.05	2.04
Ti(1)–C(24/31)	2.445(4)	2.385(2)
Ti(1)–H(241/1)	2.47(5)	2.16(2)
Ti(1)–C(25/32)	2.243(4)	2.269(2)
Ti(1)–C(26/33)	2.331(5)	2.339(2)
Ti(1)–C(27/34)	2.308(5)	2.313(2)
Ti(1)–C(24/31)–B(1)	166.1(3)	162.8(1)
Ti(1)–N(1)–C(11)	170.8(4)	163.5(1)
N(1)–Ti(1)–H(241/1)	97.9(1)	89.8(6)
C(24/31)–B(1)–C(30/37)	99.9(3)	114.1(2)
C(24/31)–B(1)–C(36/43)	114.0(4)	113.3(2)
C(24/31)–B(1)–C(42/49)	113.4(4)	109.6(2)

H(1) and H(2) atoms of C(31) were located from a Fourier difference map and positionally and isotropically refined. The Ti(1)–H(1) bond length is relatively short (2.16(2) Å) and lies within the typical range of an agostic interaction (1.8–2.3 Å).[42] Furthermore, the apparent linearity of the Ti(1)–C(31)–B(1) (163.(5)º) is triggered through the favourable arrangement of the CH_2 moiety participating in the agostic interaction. Similar near linearity has been previously observed in **1.74** (166.1(6)º).[28] The distances between the terminal allyl carbons to titanium Ti(1)–C(32) and Ti(1)–C(34) (2.269(2) and 2.313(2) Å, respectively) are shorter than the distance of the central allyl carbon to titanium Ti(1)–C(33) (2.339(2) Å). This agrees with reports in the literature of early transition metal η^3-allylic zwitterions.[14, 26, 27] The bond angle of C(31)–B(1)–C(49) is considerably more acute (109.6(2)º) than in C(31)–B(1)–C(37)/C(43) (114.1(2) and 113.3(2)º, respectively), which might reasonably be attributed to π-stacking interaction between the perfluorinated aryl ring and the aromatic ring of the supporting κ^1-amidinate ligand. The arene-perfluoroarene interactions, arising from the large negative quadrupole moment of the arene (part of the imidazolidine moiety) and the large positive quadrupole moment of the perfluoroarene (due to the presence of electronegative fluorine substituents), have been calculated to be up to *ca*. 5 kcal mol^{-1} more favourable than arene-arene and perfluoroarene-perfluoroarene interactions.[43-45] The separation of the planes of the arene and perfluoroarene is calculated as 3.58 Å, close to the typical π-stacking range of 3.34–3.50 Å.[46]

2.4.4.2 Attempted reaction of Cp*Ti{NCN(Dipp)$CH_2C_6H_4$}(η-2,3-$C_4H_4Me_2$) (11) with BAr^F_3

Unlike the aforementioned diene complexes, **12** and **13**, Cp*Ti{NCN(Dipp)$CH_2C_6H_4$}(η-2,3-$C_4H_4Me_2$) (**11**) did not react cleanly with BAr^F_3 to form a well-defined zwitterionic species. The ^1H, ^{19}F and ^{11}B NMR spectra showed a mixture of products, where for example, four resonances for the borate moiety were observed at –2.0, –8.7, –12.6 and –25.0 ppm in the ^{11}B NMR spectrum. Changing reaction conditions, such as low temperature addition of BAr^F_3 or heating of the reaction did not result in characterisable reaction mixtures.

2.5 EPM co-polymerisation experiments

Ethylene and propylene co-polymerisation testing of complexes Cp*Ti{NCN(Dipp)$CH_2C_6H_4$}Me_2 (**3**), Cp*Ti{NCN(Dipp)$CH_2C_6H_4$}{η-$CH_2(CH)_2CHEt$} (**12**) and Cp*Ti{NCN(Dipp)$CH_2C_6H_4$}{η^3-$EtCH(CH)_2CH_2BAr^F_3$} (**14**) were all performed in a small-scale batch reactor under industrially relevant conditions at ARLANXEO, The Netherlands. Activations of the dialkyl complexes were achieved by triisobutylaluminium (TiBA) and either $[Ph_3C][BAr^F_4]$ or $[BAr^F_3]$. A large excess of the aluminium reagent was used in conjunction with the addition of two equivalents of 4-methyl-2,6-di-*tert*-butylphenol (BHT-H) per aluminium centre to allow effective scavenging of any trace water or other reactive impurities in the reactor without introducing chain-termination pathways.[47-50] The composition of the polymers was analysed using FT-IR and the polydispersity index (PDI) and molecular weight were obtained from GPC data.

A slightly lower productivity in the co-polymerisation of ethylene and propylene is observed when complex **3** is activated with TiBA/ $[BAr^F_3]$ compared to activation with TiBA/ $[Ph_3C][BAr^F_4]$ (Entry 1 and 2, Table 2.4). The small discrepancy in productivity could be explained by the need to displace the coordinating $[MeBAr^F_3]^-$ counteranion (*vide supra*), resulting in a slightly longer induction period than with the non-coordinating $[BAr^F_4]^-$ counteranion. A similar observation has been made in literature for the compounds of the type Cp*Ti{NC(4-C_6H_4R)N^iPr_2}Me_2 (R = H, CF_3, ^{t}Bu or NMe_2) in the co-polymerisation of ethylene, propylene and ENB.[4, 8, 51] The composition of the resultant polymer does not vary significantly between the different activated systems (Entry 1 and 2, Table 2.4). Under similar conditions, the complex Cp*Ti{NC(Ar^{F2})N^iPr_2}Me_2 (**1.52**) gives an overall lower productivity (40,100 kg mol^{-1} Ti h^{-1} bar^{-1})[52] when activated with $[Ph_3C][BAr^F_4]$ compared to the productivity obtained with Cp*Ti{NCN(Dipp)$CH_2C_6H_4$}Me_2 (**3**).

The productivity of **12** is considerably lower compared to **14** which could hint towards a less clean *in situ* activation of **12** under the industrially relevant conditions (Entry 3 and 4, Table 2.4).

Table 2.4. EPM co-polymerisation results for Cp*Ti{NCN(Dipp)$CH_2C_6H_4$}Me_2 (**3**) and Cp*Ti{NCN(Dipp)$CH_2C_6H_4$}{η-$CH_2(CH)_2CHEt$} (**12**) and Cp*Ti{NCN(Dipp)$CH_2C_6H_4$}{η^3-$EtCH(CH)_2CH_2BAr^F_3$} (**14**).

Entry	Precatalyst	Cocatalyst	Productivity (kg mol^{-1} Ti h^{-1} bar^{-1})	C_2 (wt%)	C_3(wt%)	M_n (g mol^{-1})	M_w (g mol^{-1})	PDI
1	**3**	TiBA / $[BAr^F_3]$	77,100	58.7	41.2	599,000	1,293,000	2.4
2	**3**[b]	TiBA / $[Ph_3C][BAr^F_4]$	102,800	60.6	39.4	594,000	1,438,000	2.2
3	**12**[c]	TiBA/ $[BAr^F_3]$	42,400	56.4	43.3	621,000	1,337,000	2.2
4	**14**	TiBA	97,800	60.8	39.0	621,000	1,297,000	2.1

Polymerisation conditions. T = 90 °C, Pressure = 7 bar, Cat loading = 0.1 μmol ([b]Cat loading = 0.05 μmol, [c] Cat = 0.2 μmol), [Al]:[Cat] = 4500, [Al]:[BHT-H] = 0.5, [Cat]:[B] = 1, 10 minute reaction time. Solvent = pentamethylheptane (1L), C_3/C_2 = 400/200 Nl/h.

Polymer characterisation. Polymer molecular weight and molecular weight distribution have been analysed with Freeslate Rapid GPC in 1,2,4-Trichlorobenzene against PS standards. The average composition have been determined *via* transmission IR spectroscopy on a pressed polymer film.

Furthermore, the productivity of **14** is slightly higher than for the *in situ* generated cation when BAr^F_3 is used as a co-catalyst (Entry 1 and 4, Table 2.4). The small discrepancy could be related to the $[MeBAr^F_3]^-$ anion being able to interact with the metal centre throughout the polymerisation process, while the steric bulk around the metal centre prohibits the $BAr^F_3{}^-$ on the allyl moiety to interact with it in the first place and throughout polymerisation. No real discrepancy is observed in the composition of the resulting polymer, suggesting that after the first insertions, a similar active species polymerises ethylene and propylene in all cases. Entries 1–4 all display a similar PDI (2.0–2.2), indicating the presence of only one active site.

2.6 Summary

This Chapter has described the synthesis and characterisation of a range of κ^1-amidinate titanium complexes. The solid state structure of the dichloride and dibenzyl complex (**2** and **4**, respectively) provided an insight into the bonding of the amidinate ligand and the influence of the electron-withdrawing or electron-donating ligands on the metal centre. Activation chemistry of the dialkyl systems with a range of activators ($[Ph_3C][BAr^F_4]$, $[BAr^F_3]$, $[HNMe_2Ph][BAr^F_4]$) was investigated and the behaviour upon addition of Lewis bases and carbodiimides was explored. Detailed NMR studies at variable temperatures were presented to distinguish between the *supine* and *prone* isomers of the neutral diene systems. Reactions of **12** and **13** with BAr^F_3 afforded the identical well-defined zwitterionic species (**14**). **14** gave a higher productivity in the co-polymerisation of ethylene and propylene compared to the dimethyl complex **3** and the neutral diene complex **12** when activated in the presence of $[BAr^F_3]$. This evidently shows the unique control of the cation-anion interaction in the zwitterionic allylic species **14**. No substantial difference in composition was observed when **3** was activated in the presence of $[BAr^F_3]$ or $[Ph_3C][BAr^F_4]$, however a slight difference in productivity was observed.

2.7 References for Chapter 2

1. E. G. Ijpeij, P. J. H. Windmuller, H. J. Arts, F. Van der Burgt, G. H. J. Van Doremaele and M. A. Zuideveld, *WO2005090418*, 2005.
2. R. A. Collins, *DPhil Thesis*, University of Oxford, 2016.
3. J. R. Hagadorn and J. Arnold, *Organometallics*, 1998, **17**, 1355-1368.

4. R. A. Collins, A. F. Russell, R. T. W. Scott, R. Bernardo, G. H. J. van Doremaele, A. Berthoud and P. Mountford, *Organometallics*, 2017, **36**, 2167-2181.
5. P. Mountford, *Chem. Commun.*, 1997, 2127-2134.
6. R. A. Collins, A. F. Russell and P. Mountford, *Appl. Petrochem. Res.*, 2015, **5**, 153-171.
7. M. Bochmann, *Organometallics*, 2010, **29**, 4711-4740.
8. E. Y.-X. Chen and T. J. Marks, *Chem. Rev.*, 2000, **100**, 1391-1434.
9. M. Brookhart and M. L. H. Green, *J. Organomet. Chem.*, 1983, **250**, 395-408.
10. X. Bei, D. C. Swenson and R. F. Jordan, *Organometallics*, 1997, **16**, 3282-3302.
11. J. C. W. Chien and B. Xu, *Makromol. Chem., Rapid Commun.*, 1993, **14**, 109-114.
12. J. C. W. Chien, W. Song and M. D. Rausch, *Macromolecules*, 1993, **26**, 3239-3240.
13. Y.-X. Chen and T. J. Marks, *Organometallics*, 1997, **16**, 3649-3657.
14. B. Temme, G. Erker, J. Karl, H. Luftmann, R. Frohlich and S. Kotila, *Angew. Chem. Int. Ed. Engl.*, 1995, **34**, 1755-1757.
15. V. Volkis, E. Nelkenbaum, A. Lisovskii, G. Hasson, R. Semiat, M. Kapon, M. Botoshansky, Y. Eishen and M. S. Eisen, *J. Am. Chem. Soc.*, 2003, **125**, 2179-2194.
16. A. D. Horton, J. de With, A. J. van der Linden and H. van de Weg, *Organometallics*, 1996, **15**, 2672-2674.
17. O. Wrobel, F. Schaper, U. Wieser, H. Gregorius and H. H. Brintzinger, *Organometallics*, 2003, **22**, 1320-1325.
18. H. Yasuda and A. Nakamura, *Angew. Chem. Int. Ed. Engl.*, 1987, **26**, 723-742.
19. H. Yasuda, K. Tatsumi and A. Nakamura, *Acc. Chem. Res.*, 1985, **18**, 120-126.
20. G. Erker, J. Wicher, K. Engel, F. Rosenfeldt, W. Dietrich and C. Krueger, *J. Am. Chem. Soc.*, 1980, **102**, 6344-6346.
21. H. Yasuda, Y. Kajihara, K. Mashima, K. Nagasuna, K. Lee and A. Nakamura, *Organometallics*, 1982, **1**, 388-396.
22. J. Blenkers, B. Hessen, F. Van Bolhuis, A. J. Wagner and J. H. Teuben, *Organometallics*, 1987, **6**, 459-469.

23. C. Krueger, G. Mueller, G. Erker, U. Dorf and K. Engel, *Organometallics*, 1985, **4**, 215-223.
24. E. Meléndez, R. Ilarraza, G. P. A. Yap and A. L. Rheingold, *J. Organomet. Chem.*, 1996, **522**, 1-7.
25. N. Yue, E. Hollink, F. Guerin and D. W. Stephan, *Organometallics*, 2001, **20**, 4424-4433.
26. A. H. Cowley, G. S. Hair, B. G. McBurnett and R. A. Jones, *Chem. Commun.*, 1999, 437-438.
27. G. S. Hair, R. A. Jones, A. H. Cowley and V. Lynch, *Inorg. Chem.*, 2001, **40**, 1014-1019.
28. R. Scott, *DPhil Thesis*, University of Oxford, 2013.
29. V. K. Dioumaev and J. F. Harrod, *Organometallics*, 1997, **16**, 1452-1464.
30. R. J. Keaton, L. A. Koterwas, J. C. Fettinger and L. R. Sita, *J. Am. Chem. Soc.*, 2002, **124**, 5932-5933.
31. A. Epshteyn, E. F. Trunkely, D. A. Kissounko, J. C. Fettinger and L. R. Sita, *Organometallics*, 2009, **28**, 2520-2526.
32. T. W. Graham, J. Kickham, S. Courtenay, P. Wei and D. W. Stephan, *Organometallics*, 2004, **23**, 3309-3318.
33. H. Yamamoto, H. Yasuda, K. Tatsumi, K. Lee, A. Nakamura, J. Chen, Y. Kai and N. Kasai, *Organometallics*, 1989, **8**, 105-119.
34. J. Chen, Y. Kai, N. Kasai, H. Yamamoto, H. Yasuda and A. Nakamura, *Chem. Lett.*, 1987, 1545-1548.
35. K. Mashima and A. Nakamura, *J. Organomet. Chem.*, 2002, **663**, 5-12.
36. N. Chinkov, S. Majumdar and I. Marek, *J. Am. Chem. Soc.*, 2002, **124**, 10282-10283.
37. J. R. Clark, J. R. Griffiths and S. T. Diver, *J. Am. Chem. Soc.*, 2013, **135**, 3327-3330.
38. Y. Chen, M.-Y. Wang, S. Fang, T. Wang and J.-Y. Liu, *Organometallics*, 2015, **34**, 4864-4870.
39. F. Sauriol, J. F. Sonnenberg, S. J. Chadder, A. F. Dunlop-Brière, M. C. Baird and P. H. M. Budzelaar, *J. Am. Chem. Soc.*, 2010, **132**, 13357-13370.
40. M. B. Harney, R. J. Keaton, J. C. Fettinger and L. R. Sita, *J. Am. Chem. Soc.*, 2006, **128**, 3420-3432.

41. P. G. Jimenez, M. Thompson-Pett, M. Bouwkamp, A. Meetsma, B. Hessen and M. Bochmann, *Angew. Chem. Int. Ed.*, 1997, **36**, 2358-2361.
42. M. Brookhart, M. L. H. Green and G. Parkin, *Proc. Natl. Acad. Sci. U. S. A.*, 2007, **104**, 6908-6914.
43. C. R. Patrick and G. S. Prosser, *Nature*, 1960, **187**, 1021-1021.
44. C. A. Hunter, K. R. Lawson, J. Perkins and C. J. Urch, *J. Chem. Soc. Perk. Trans. 2*, 2001, 651-669.
45. O. R. Lozman, R. J. Bushby and J. G. Vinter, *J. Chem. Soc., Perk. Trans. 2*, 2001, 1446-1452.
46. C. Rajesh, C. Majumder, H. Mizuseki and Y. Kawazoe, *J. Chem. Phys.*, 2009, **130**, 124911.
47. V. Busico, R. Cipullo, F. Cutillo, N. Friederichs, S. Ronca and B. Wang, *J. Am. Chem. Soc.*, 2003, **125**, 12402-12403.
48. A. P. Shreve, R. Mulhaupt, W. Fultz, J. Calabrese, W. Robbins and S. D. Ittel, *Organometallics*, 1988, **7**, 409-416.
49. V. C. Williams, C. Dai, Z. Li, S. Collins, W. E. Piers, W. Clegg, M. R. J. Elsegood and T. B. Marder, *Angew. Chem. Int. Ed.*, 1999, **38**, 3695-3698.
50. G. J. Pindado, S. J. Lancaster, M. Thornton-Pett and M. Bochmann, *J. Am. Chem. Soc.*, 1998, **120**, 6816-6817.
51. A. D. Horton and J. de With, *Organometallics*, 1997, **16**, 5424-5436.
52. E. G. Ijpeij, B. Coussens, M. A. Zuideveld, G. H. J. van Doremaele, P. Mountford, M. Lutz and A. L. Spek, *Chem. Commun.*, 2010, **46**, 3339-3341.

Chapter Three

Synthesis, mechanistic and polymerisation studies of cationic κ^1-amidinate diene and allyl complex

3.1 Overview

Titanium allyl species have been investigated as dormant species in the heterogeneous polymerisation of propylene with $MgCl_2$ supported Ziegler catalysts. The absence of terminal double bonds in titanium catalysed heterogeneous polymerisation of propylene, led to the discovery of a dormant titanium allyl species, formed by the C–H activation of the coordinated monomer.[1] The titanium allyl species could be reactivated by either alkyl aluminium reagents or by the addition of dihydrogen.[2] Richardson[3] and Feichtinger[4] discovered that in homogeneous catalysis, metallocene complexes such as Cp_2ZrX_2 (X = Me or Cl), can also result in an allylic dormant state of the type $[Cp_2Zr(allyl)]^+$ (**3.01**). Eshuis and co-workers showed that these allyl systems can be reactivated by addition of H_2 analogous to the heterogeneous systems (Scheme 3.1).[5, 6] This was also confirmed by theoretical calculations conducted by Ziegler and co-workers on metallocene and CGC species.[7, 8] Ziegler *et al*. also demonstrated that reactivation *via* reinsertion of small α-olefins is also possible.[8]

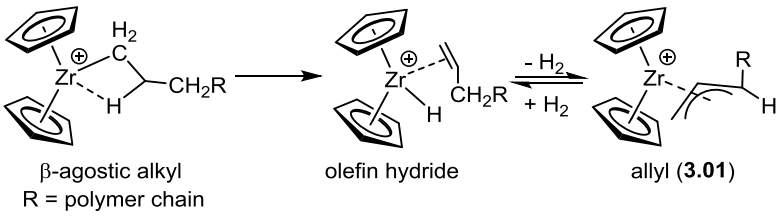

Scheme 3.1. Allyl formation process *via* β-H transfer and H_2 release.

Recently, Brintzinger *et al*. discovered that $[\{Me_2Si(1\text{-indenyl})_2\}Zr(allyl)]^+$ (**3.02**) is active in the polymerisation of propylene, one possible isomer shown in Figure 3.1.[9-11] After a dramatic colour change from bright red to purple on addition of excess 1-hexene, Brintzinger and co-workers saw only 15% of the starting heterobinuclear cation $[\{Me_2Si(1\text{-indenyl})_2\}Zr(\mu\text{-}Me)_2AlMe_2]^+$ left. Simultaneously **3.02** was observed by ^1H NMR and UV/Vis spectroscopy. A second addition of 1-hexene within 20 minutes resulted in the same half-life of 1-hexene consumption, showing that the new η^3-allyl species **3.02** polymerises 1-hexene at the same rate.[10, 11]

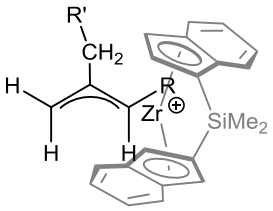

3.02, R = ^{n}Pr, R' = CH(^{n}Bu)-polyhexyl
3.03, R = R' = ^{n}Pr

Figure 3.1. [{Me_2Si(1-indenyl)$_2$}Zr(allyl)]$^+$ (**3.02,** R = ^{n}Pr, R´ = CH(^{n}Bu)-polyhexyl; **3.03**, R = R´ = ^{n}Pr).

To allow further investigation of the allyl cation formation and its activity in polymerisation, Brintzinger *et al*. used a more sterically demanding alkene, *viz*. 2-butyl-1-hexene. The resulting zirconium allyl species (**3.03**) polymerises 1-hexene and concomitantly **3.02** is observed. When using **3.03** the rate of polymerisation was indistinguishable compared to the *in situ* formed allyl complex (**3.02**).[10]

The recent discovery of active zirconium allyl systems and the established activity of group 4 allylic zwitterions in polymerisation of a range of α-olefins (Chapter 1), led to an interest in κ^1-amidinate supported titanium allyl cations. The previous Chapter has shown the high productivity of the zwitterionic allylic titanium species Cp*Ti{NCN(Dipp)$CH_2C_6H_4$}{η^3-EtCH$(CH)_2CH_2BAr^F_3$} (**14**) in the co-polymerisation of ethylene and propylene. This Chapter, therefore, describes the reaction of κ^1-amidinate and κ^1-guanidinate supported titanium dimethyl complexes with conjugated dienes and $[Ph_3C][BAr^F_4]$. Mechanistic and computational studies of allyl and diene formation will also be described. Furthermore, the behaviour in α-olefin polymerisation of the newly formed complexes is investigated.

3.2 Reaction of [Cp*Ti{NCN(Dipp)$CH_2C_6H_4$}Me][BAr^F_4] (5-[BAr^F_4]) with conjugated dienes

Reaction of neutral diene complexes with BAr^F_3 has been shown to form allylic zwitterionic species that are active in olefin polymerisation (Chapter 2), and especially in the co-polymerisation of ethylene, propylene and non-conjugated diene.[12] The study of an allylic cationic species which do not contain a coordinated counteranion, and therefore potentially provide a more open coordination site, is of interest for this Thesis.

3.2.1 [Cp*Ti{HNCN(Dipp)$CH_2C_6H_4$}{η-$CH_2(CH)_3{}^iPr$}][$BAr^F{}_4$] (**15-[$BAr^F{}_4$]**)

Addition of 2,4-hexadiene to [Cp*Ti{NCN(Dipp)$CH_2C_6H_4$}Me][$BAr^F{}_4$] (**5-[$BAr^F{}_4$]**) at room temperature, did not result in an observable cationic allyl species as expected, but instead underwent C–H bond activation of 2,4-hexadiene and protonation of the metal-bound nitrogen of the κ^1-amidinate supporting ligand, giving [Cp*Ti{HNCN(Dipp)$CH_2C_6H_4$}{η-$CH_2(CH)_3{}^iPr$}][$BAr^F{}_4$] (**15-[$BAr^F{}_4$]**, Scheme 3.2). The compound was isolated as a dark green solid in 40% yield.

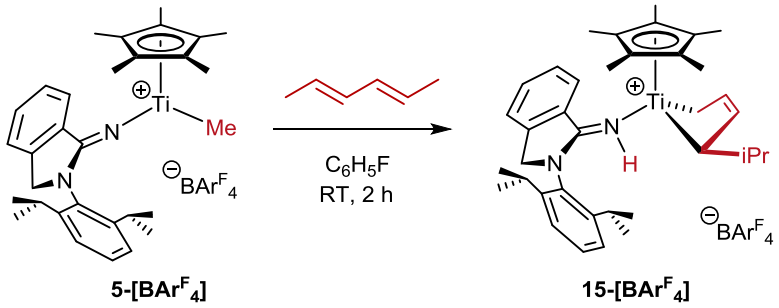

Scheme 3.2. Synthesis of [Cp*Ti{HNCN(Dipp)$CH_2C_6H_4$}{η-$CH_2(CH)_3{}^iPr$}]-[$BAr^F{}_4$] (**15-[$BAr^F{}_4$]**).

In the ^{1}H NMR spectrum, a singlet at 3.90 ppm is observed which is assigned to the migrating proton, bound to the nitrogen of the amidine ligand (Figure 3.2). Multiple bond correlation of the aforementioned resonance to the ^{13}C resonances of N$\underline{C}$ and the N$C\underline{C}_{Ar}$ of the supporting ligand are observed. Furthermore, a one-dimensional ^{15}N-^{1}H HSQC experiment revealed a $^1J_{NH}$ coupling constant of 63 Hz, while a two-dimensional ^{15}N-^{1}H HSQC identified the chemical shift of the ^{15}N at 153 ppm. Further evidence for the presence of the NH peak is shown in the IR spectrum, where a sharp NH peak is observed at 3264 cm^{-1}.

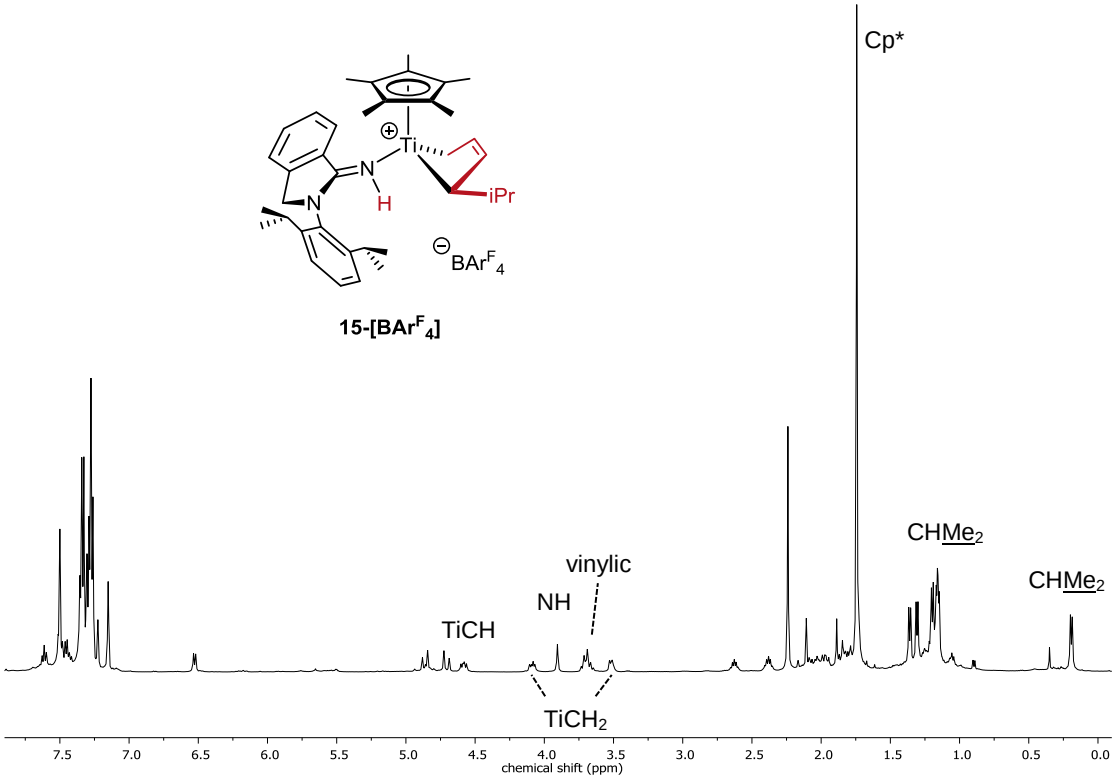

Figure 3.2. ^{1}H NMR spectrum (400.2 MHz, C_6D_5Br, 298 K) of [Cp*Ti{HNCN(Dipp)$CH_2C_6H_4$}{η-CH_2(CH)$_3^i$Pr}][BAr$^F_4$] (**15-[BAr$^F_4$]**).

The vinylic protons of **15-[BAr$^F_4$]**, observed as overlapping multiplets at 3.70–3.64 ppm, show NOE correlations to the Cp* methyl groups at 1.73 ppm, establishing the selective formation of the *prone* isomer. This differs to the observations made for the neutral diene systems, where either the *supine* isomer Cp*Ti{NCN(Dipp)$CH_2C_6H_4$}(η-2,3-$C_4H_4Me_2$) (**11**) or both isomers Cp*Ti{NCN(Dipp)$CH_2C_6H_4$}(η-CH_2(CH)$_2$CHEt) (***supine***- and ***prone*-12**) were observed. This might be attributed to the certain mechanistic requirements of the cationic diene formation (*vide infra*) or to thermodynamic preferences.

The DFT structures of the *prone* and *supine* isomer of **15-[BAr$^F_4$]** are depicted in Figure 3.3 (***prone*-15Q$^+$** and ***supine*-15Q$^+$**, respectively). The Ti(1)–N(1)–C_{Ar} bond angle is smaller for ***supine*-15Q$^+$**, compared to ***prone*-15Q$^+$** (135.1 *vs.* 140.1°). This is indicative of the Dipp group bending slightly more away from the diene fragment in the *supine* isomer which can be related to increase in steric crowding. ***Prone*-15Q$^+$** was computed to be 2.4 kcal mol^{-1} more stable than ***supine*-15Q$^+$**.

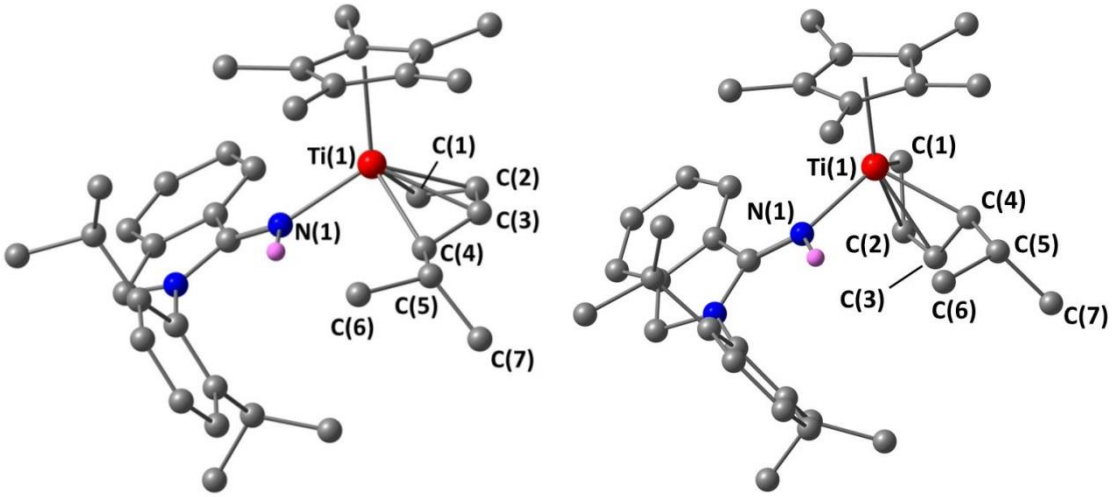

***prone*-15Q$^+$** ***supine*-15Q$^+$**

Figure 3.3. DFT structures of ***prone*-15Q$^+$** (left) and one of its supine isomers (***supine*-15Q$^+$**, right). Selected distances (Å) and angles (^{o}) for ***prone*-15Q$^+$**: Ti(1)–N(1) 2.102, Ti(1)–C(1) 2.139, Ti(1)–C(2) 2.270, Ti(1)–C(3) 2.279, Ti(1)–C(4) 2.151, C(1)–C(2) 1.429, C(2)–C(3) 1.401, C(3)–C(4) 1.423, Ti(1)–N(1)–C_{Ar} 140.1; for ***supine*-15Q$^+$**: Ti(1)–N(1) 2.081, Ti(1)–C(1) 2.152, Ti(1)–C(2) 2.281, Ti(1)-C(3) 2.268, Ti(1)–C(4) 2.148, C(1)–C(2) 1.430, C(2)–C(3) 1.393, C(3)–C(4) 1.438, Ti(1)–N(1)–C_{Ar} 135.1. C-bound H atoms omitted.

The ^{13}C NMR calculated chemical shifts, referenced internally with respect to the experimental values of the Cp* ligand, show that only the ^{13}C chemical shifts obtained from ***prone*-15Q$^+$** fit the experimental data, while the ***supine*-15Q$^+$** results in more deshielded ^{13}C chemical shifts of the vinylic carbons than observed (TiCH_2CH and TiCHCH, Table 3.1).

Table 3.1. ^{13}C{^{1}H} chemical shifts of the diene fragment of **15-[BAr$^F_4$]**, ***prone*-15Q$^+$** and ***supine*-15Q$^+$**.

	δ TiCH_2CH (ppm)	δ TiCH_2CH (ppm)	δ TiCHCH (ppm)	δ TiCHCH (ppm)
15-[BAr$^F_4$]	84.0	117.3	117.4	110.7
***prone*-15Q$^+$**	79.9	119.4	117.2	108.6
***supine*-15Q$^+$**	81.8	135.5	133.0	106.9

The cationic diene complex $[Cp´´Hf(2,3\text{-}Me_2C_4H_4)(OEt_2)]^+$, synthesised by Bochman *et al*., results in the *supine* isomer, confirmed with the solid-state structure.[13] The ^{13}C chemical shifts of the diene fragment of $[Cp´´Hf(2,3\text{-}Me_2C_4H_4)(OEt_2)]^+$ appear at 123.4 and 129.2 ppm, more deshielded than for the *prone* isomer **15-[BAr$^F_4$]**. The differences between the vinylic ^{13}C resonances of the diene fragment and those resonances adjacent to the titanium centre are indicative of a dianionic 'ene-diyl' ligand and η^2-binding mode.[13, 14] This is further confirmed by the bond distances obtained from the calculated structures ***prone-*** and ***supine*-15Q$^+$**, where the C(2)–C(3) bond distance is shorter than the C(1)–C(2) and C(3)–C(4) bond distances (Figure 3.3).

The isopropyl methyls of the diene fragment appear as an overlapping multiplet at 1.16–1.14 ppm and as a doublet at 0.20 ppm in the ^1H NMR spectrum (Figure 3.2). The shielding of one of these groups, labelled as C(6) in ***prone*-15Q$^+$**, can be explained by its relative position leading to enhanced anisotropic shielding from the diisopropylphenyl (Dipp) aromatic ring (Figure 3.3). The deuterium NMR of the addition of 2,4-hexadiene to **5-[BAr$^F_4$]-*d*$_3$** displayed a resonance at 1.16–1.14 ppm suggesting that the migrated methyl group is the one *not* experiencing enhanced shielding, labelled as C(7) in ***prone*-15Q$^+$**. The ^1H NMR calculated chemical shifts further support this observation: C(6) has a calculated shift of 0.0 ppm while C(7) is calculated at 1.0 ppm.

The addition of two or more equivalents of 2,4-hexadiene, did not give further reactions and complex **15-[BAr$^F_4$]** is observed with unreacted 2,4-hexadiene starting material, even after heating the reaction up to 60 ºC.

3.2.2 [Cp*Ti{HNCN(Dipp)CH$_2$C$_6$H$_4$}{η-CH$_2$(CH)$_3$Et}][BAr$^F_4$] (16-[BAr$^F_4$])

Addition of 1,3-pentadiene to **5-[BAr$^F_4$]** also resulted in C–H bond activation, giving $[Cp*Ti\{HNCN(Dipp)CH_2C_6H_4\}\{\eta\text{-}CH_2(CH)_3Et\}][BAr^F{}_4]$ (**16-[BAr$^F_4$]**). **16-[BAr$^F_4$]** was isolated as a dark green solid in 57% yield. Similar to **15-[BAr$^F_4$]**, a singlet at 3.89 ppm is observed in the ^1H NMR spectrum assigned to the NH proton (Figure 3.4). With the help of a one-dimensional ^{15}N-^1H HSQC experiment, the $^1J_{NH}$ coupling constant was evaluated at 62 Hz while a two-dimensional ^{15}N-^1H HSQC identified the

chemical shift of the ^{15}N at 154 ppm. A sharp peak in the IR spectrum was observed at 3235 cm^{-1}, analogues to compound **15-[BAr$^F_4$]**.

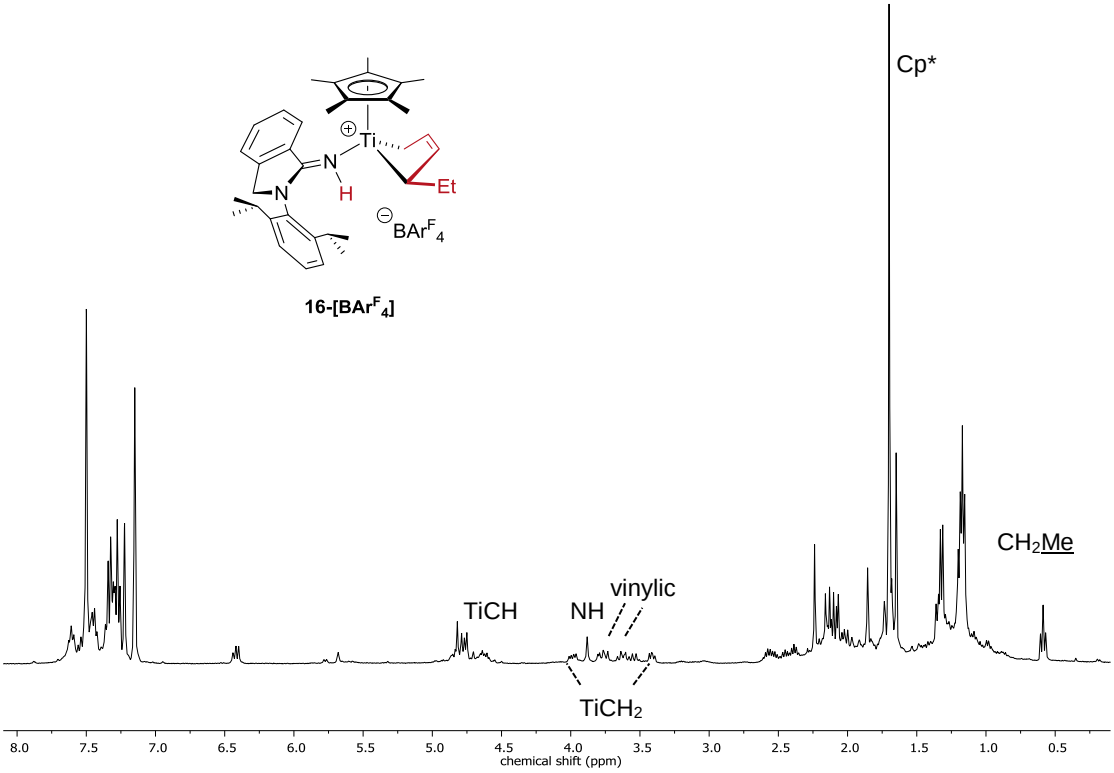

Figure 3.4. ^1H NMR spectrum (400.2 MHz, C_6D_5Br, 298 K) of [Cp*Ti{HNCN(Dipp)$CH_2C_6H_4$}{η-$CH_2(CH)_3Et$}][BAr$^F_4$] (**16-[BAr$^F_4$]**).

The vinylic protons of **16-[BAr$^F_4$]**, observed as multiplets at 3.80–3.74 and 3.59–3.52 ppm, correlate through-space to the Cp* methyl groups at 1.71 ppm and so again shows the selective formation of the *prone* isomer. The methylene protons adjacent to the titanium centre appear at 4.00–3.97 and 3.44–3.40 ppm, correlate to a ^{13}C signal at 83.9 ppm. The more deshielded ^{13}C resonance in comparison to the neutral diene systems, exemplified by ***prone*-12** (59.0 ppm), could be due to titanium carrying a positive charge and therefore increasing its electrophilicity. The triplet at 0.59 ppm corresponds to the migrating methyl group, confirmed by the reaction of [Cp*Ti{NCN(Dipp)$CH_2C_6H_4$}(CD_3)][BAr$^F_4$] (**5-[BAr$^F_4$]-*d*$_3$**) and 1,3-pentadiene (Scheme 3.3).

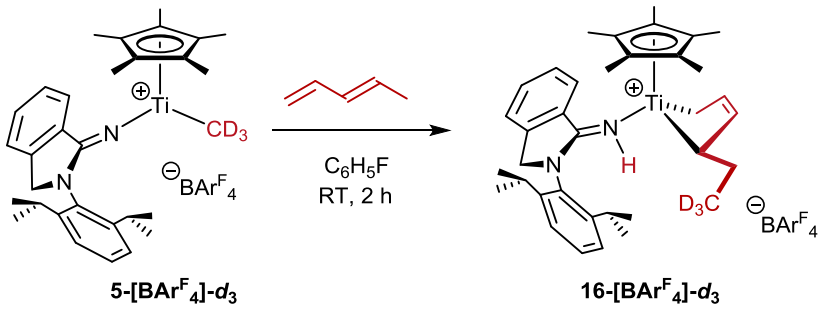

5-[BAr$^F_4$]-*d*$_3$ **16-[BAr$^F_4$]-*d*$_3$**

Scheme 3.3. Reaction of [Cp*Ti{NCN(Dipp)CH$_2$C$_6$H$_4$}(CD$_3$)][BAr$^F_4$] (**5-[BAr$^F_4$]-*d*$_3$**) with 1,3-pentadiene.

The somewhat shielded ^{1}H chemical shift of the migrating methyl group can be explained by the presence of two rotation isomers of **16-[BAr$^F_4$]** through rotation of the C(4)–C(5) bond (**16Qa**$^+$ and **16Qb**$^+$, Figure 3.5). Isomer **16Qb**$^+$ is –0.8 kcal mol^{-1} more stable than **16Qa**$^+$, showing no thermodynamic preference for either. The experimentally observed ^{1}H NMR chemical shift of the methyl group of the ethyl fragment agrees with the average (0.4 ppm) of the calculated chemical shifts of **16Qa**$^+$ (1.0 ppm) and **16Qb**$^+$ (–0.2 ppm). As observed for **15-[BAr$^F_4$]**, the calculated average ^{13}C NMR chemical shifts (range 118–120 ppm) of C(2) and C(3) agree with the observed *prone* isomer.

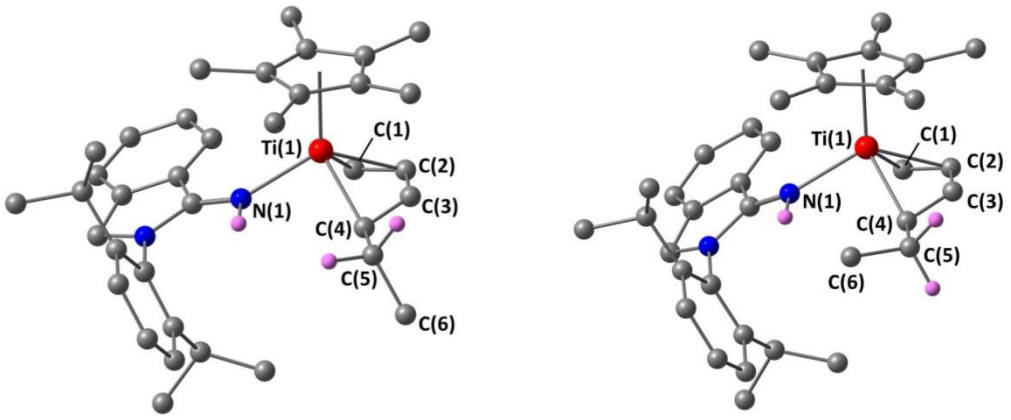

16Qa$^+$ **16Qb**$^+$

Figure 3.5. DFT structure of the two C(4)–C(5) bond rotation isomers (**a**,**b**) of **16Q**$^+$. C-bound H atoms omitted except for those attached to C(5).

Simultaneous addition of excess 2,4-hexadiene and 1,3-pentadiene (1 : 1 ratio) to **5-[BAr$^F_4$]**, resulted in the formation of both complexes, **15-[BAr$^F_4$]** and **16-[BAr$^F_4$]** (0.38 : 0.62, respectively). The slight preference for **16-[BAr$^F_4$]** is presumably observed due to steric factors in the initial migratory-insertion step. Addition of 2,4-

hexadiene to **16-[BAr$^F_4$]** or *vice versa* did not result in any exchange between the two diene complexes even after extended heating at 60 ºC.

Salzer *et al*. have previously observed allyl complex formation from CpIr(diene) upon protonation. The formed allyl cation was in equilibrium with a metal-hydride species.[15] The protonation of a metal-bound nitrogen of a κ^1-amidinate ligand, however, has previously not been observed to our knowledge.

To test the principal of N–H protonation, the neutral dichloride species, Cp*Ti{NCN(Dipp)$CH_2C_6H_4$}Cl_2 (**2**), was reacted with [$HNMe_2Ph$][BAr$^F_4$], a well-established proton source with a non-coordinating anion. The addition of [$HNMe_2Ph$][BAr$^F_4$] to **2** led to a colour change from orange to deep red, forming [Cp*Ti{HNCN(Dipp)$CH_2C_6H_4$}Cl_2][BAr$^F_4$] (**17-[BAr$^F_4$]**). Even though decomposition was observed upon attempted isolation, **17-[BAr$^F_4$]** was characterised by NMR spectroscopy. The ^{1}H NMR spectrum displayed a resonance at 7.81 ppm, assigned to the newly formed NH fragment. Similar to **15-[BAr$^F_4$]** and **16-[BAr$^F_4$]**, the HMBC NMR spectrum showed multiple bond correlation to the resonances at 170.9 (N<u>C</u>) and 142.3 (NC<u>C</u>$_{Ar}$) ppm. One-dimensional ^{15}N-^{1}H HSQC experiment measured the $^1J_{NH}$ coupling constant at 66 Hz, comparable to the observed coupling constants of complexes **15-[BAr$^F_4$]** and **16-[BAr$^F_4$]**. The two-dimensional ^{15}N-^{1}H HSQC experiment identified the chemical shift of the ^{15}N at 190 ppm. A similar ^{15}N{^{1}H} NMR chemical shift (196 ppm) was calculated for structure **17Q$^+$** (Figure 3.6).

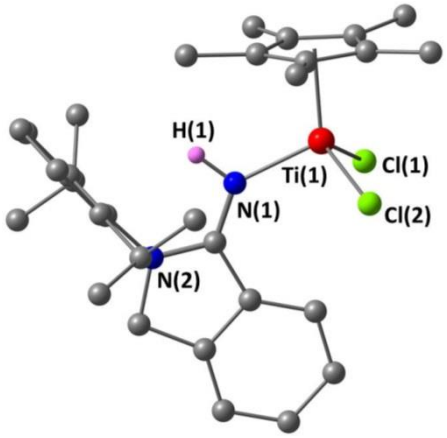

Figure 3.6. DFT structure of **17Q$^+$**. Selected distances (Å) and angles (^{o}): Ti(1)-Cl(1) 2.211, Ti(1)–Cl(2) 2.213, Ti(1)–N(1) 2.005, Ti(1)–N(1)–C 134.7. C-bound H atoms

omitted. Selected computed distances (Å) and angles (°) for the dichloride complex **2Q**: Ti(1)–Cl(1) 2.279, Ti(1)–Cl(2) 2.278, Ti(1)–N(1) 1.796, Ti(1)–N(1)–C_{Ar} 166.5.

$[DNMe_2Ph][BAr^F{}_4]$ was synthesised by reacting $[HNMe_2Ph][BAr^F{}_4]$ in dichloromethane with D_2O and catalytic amounts of NaOD, obtaining $[DNMe_2Ph][BAr^F{}_4]$ in 78% deuteriation. Reaction of **2** with $[DNMe_2Ph][BAr^F{}_4]$ showed a resonance at 7.8 ppm in the deuterium NMR spectrum. **17Q**$^+$ shows that the proton ends up on the Dipp "side" of the κ^1-amidinate ligand, while the other isomer (proton on the other side) is 3.7 kcal mol^{-1} less stable. This results in the bulky Dipp group bending away from the metal centre and the Ti(1)–N(1)–C_{Ar} bond angle becomes more acute in the protonated structure **17Q**$^+$ compared to the neutral complex **2Q** (134.7 *vs.* 166.5º, respectively). This is also observed for ***prone*-15Q**$^+$. The Ti(1)–N(1) bond distance shows the expected increase upon protonation from 1.796 Å in **2Q** to 2.211 Å in **17Q**$^+$ (Figure 3.6).

The DFT calculations also show that the protonation on the isoindoline nitrogen (N(2) in Figure 3.6) is disfavoured by 25.6 kcal mol^{-1} and also gives a lower calculated ^{15}N chemical shift of 116 ppm.

Attempted deprotonation of **17-[BAr$^F{}_4$]** with strong bases such as lithium bis(trimethylsilyl)amide or trimethyl aluminium were unsuccessful giving a complex mixture. However, using *N*,*N*,*N*´,*N*´-tetramethyl-1,8-naphthalenediamine (**3.04**) successfully deprotonated **17-[BAr$^F{}_4$]** to regenerate complex **2** (Equation 3.1).

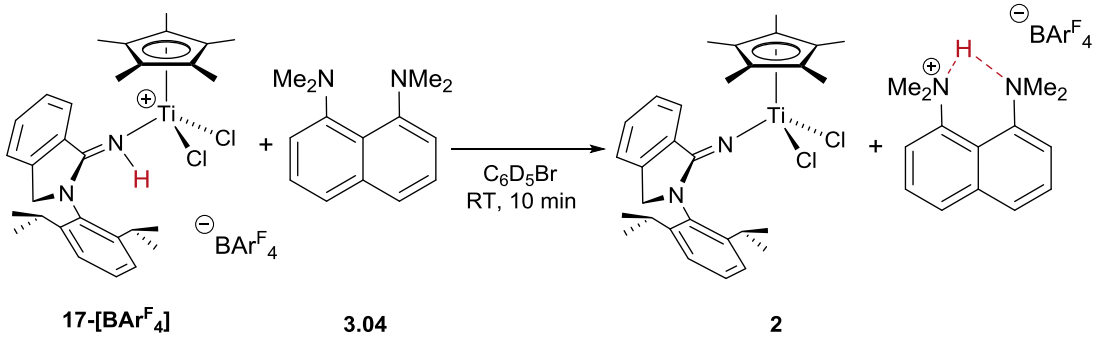

17-[BAr$^F{}_4$] **3.04** **2**

Equation 3.1

3.3 Experimental and DFT mechanistic studies of reaction pathway

In order to study the mechanism of diene formation (**15-[BAr$^F{}_4$]**), low temperature NMR studies were conducted. The NMR probe was pre-cooled to –30 ºC and 2,4-

hexadiene was added to **5-[BAr$^F_4$]** in bromobenzene-d_5 at –30 ºC. The ^{1}H NMR spectra showed a mixture of products, identified as unreacted 2,4-hexadiene, and two titanium allyl isomers, *viz*. *endo*,*syn*,*syn*-η^3-allyl and *exo*,*syn*,*syn*-η^3-allyl (***endo*-18-[BAr$^F_4$]** and ***exo*-18-[BAr$^F_4$]** respectively, Scheme 3.4).

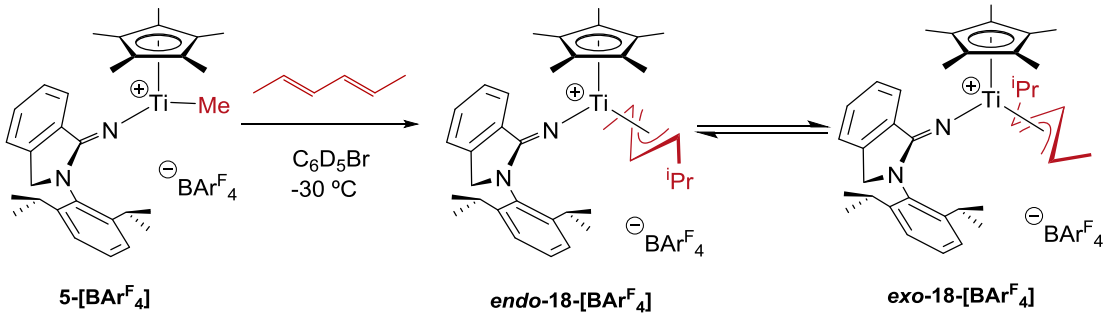

Scheme 3.4. Reaction of **5-[BAr$^F_4$]** with 2,4-hexadiene at –30 ºC. Only one rotamer of the *endo*- and *exo*,*syn*,*syn*-η^3-allyl complexes are shown for simplicity.

Endo and *exo* refer to the relative orientation of the central allylic proton (*meso* proton), and *syn*,*syn* to the relative arrangement of the two end groups to the allylic centre.

Even at –30 ºC, both isomers are short-lived, and convert to **15-[BAr$^F_4$]** over time, without any other observable intermediates. Therefore, a ROESY experiment was obtained in CD_2Cl_2 at –70 ºC, in order to permit reliable assignments of the *endo* and *exo* allyl isomers (***endo*-18-[BAr$^F_4$]** and ***exo*-18-[BAr$^F_4$]**, respectively). The *anti* 1,3-allylic protons of the *endo* isomer (***endo*-18-[BAr$^F_4$]**) at 4.94–4.34 and 4.03 ppm correlate through-space to the Cp* methyl groups at 2.01 ppm (Figure 3.7). The same signals exhibit through-bond correlations to the *meso* proton triplet at 8.06 ppm. The latter experiment also revealed through-bond correlations between a second set of allylic protons at 6.15–6.10 and 5.60–5.53 ppm to a triplet at 6.91 ppm, assigning this resonance to the *meso* proton of the *exo* allyl isomer (***exo*-18-[BAr$^F_4$]**, Figure 3.7).

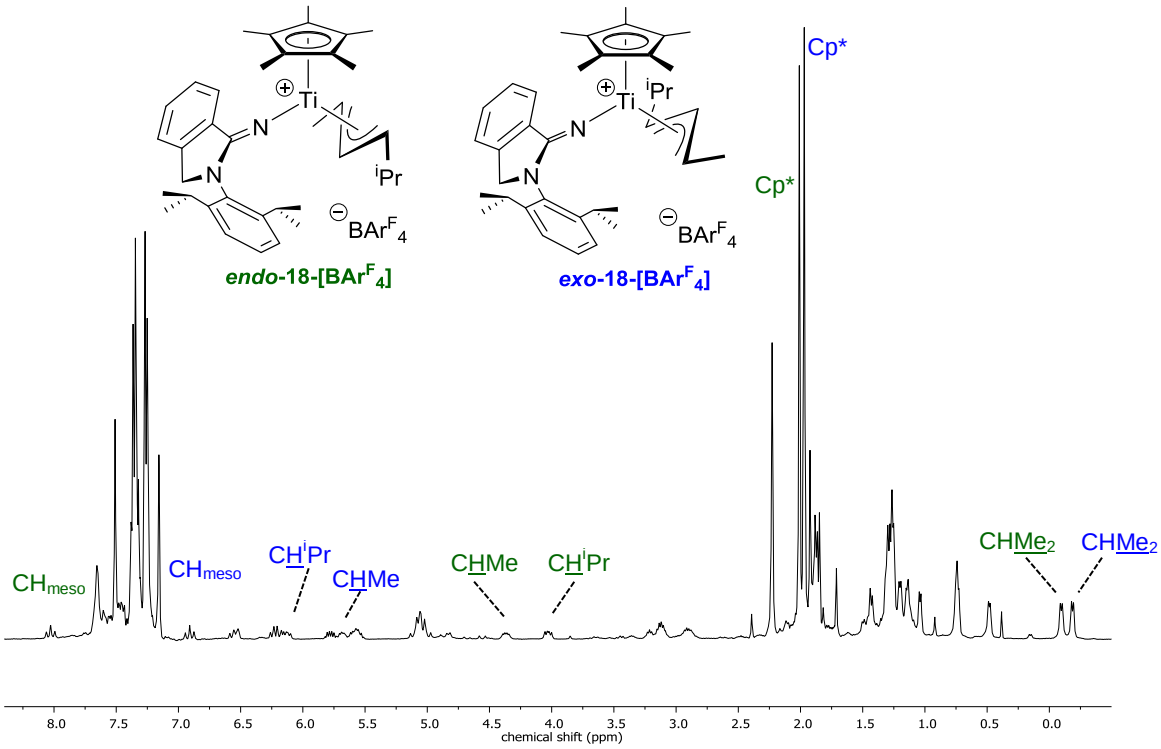

Figure 3.7. ^{1}H NMR spectrum (400.2 MHz, C_6D_5Br, 243 K) of ***endo*-18-[BAr$^{F}_{4}$]** and ***exo*-18-[BAr$^{F}_{4}$]**.

Overall, the chemical shifts agree with the relative chemical shifts of cationic titanium allyl complexes previously reported in literature by Budzelaar and co-workers.[16] However, the chemical shifts of these cationic allyl systems vary greatly from other cationic metal allyl systems, such as for palladium, the *meso* proton has a more upfield shift (*ie*. 5.36 ppm).[17]

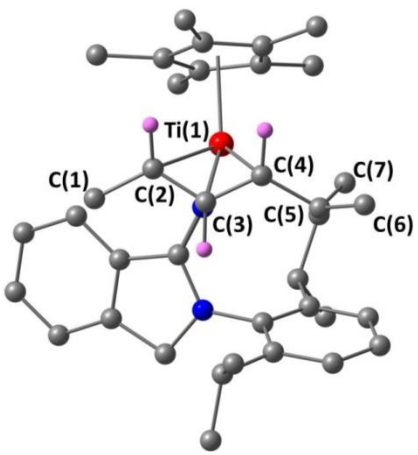

***endo*-18Qa^{+}**

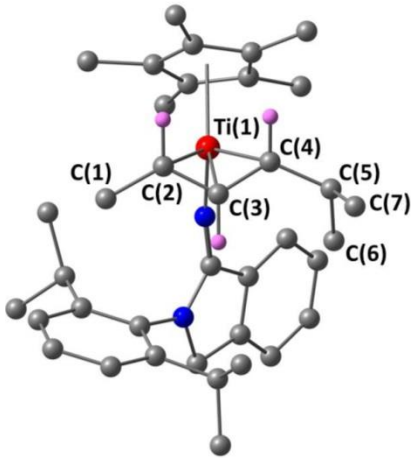

***endo*-18Qb^{+}**

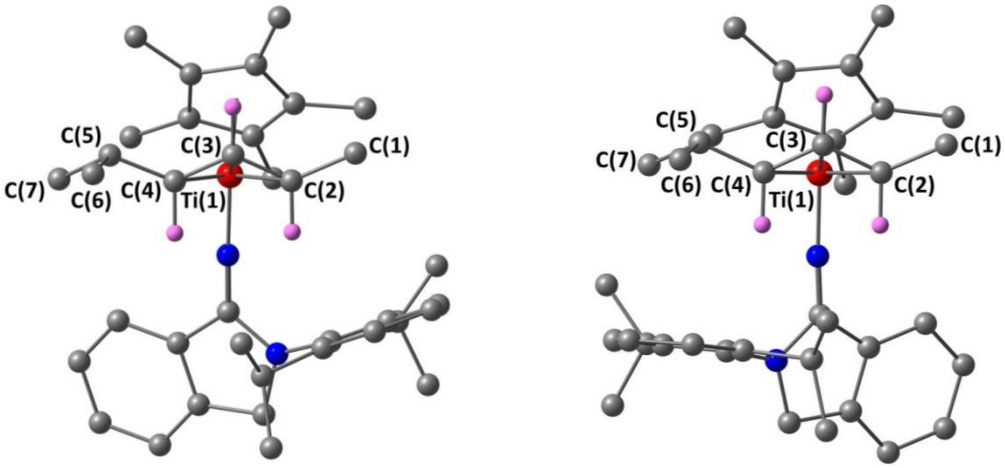

***exo*-18Qa$^+$** ***exo*-18Qb$^+$**

Figure 3.8. DFT structure of the four isomers of the allyl cation **18Q$^+$**. H atoms except for those of the allyl methine carbons omitted. Representative selected distances (Å) for ***endo*-18Qa$^+$**: Ti(1)–C(2) 2.306, Ti(1)–C(3) 2.296, Ti(1)–C(4) 2.278, C(2)–C(3) 1.406, C(3)–C(4) 1.391; for ***endo*-18Qb$^+$**: Ti(1)–C(2) 2.333, Ti(1)–C(3) 2.297, Ti(1)–C(4) 2.259, C(2)–C(3) 1.392, C(3)–C(4) 1.410.

Both allyl systems show fluxional behaviour at room temperature. But as the rotation around the Ti(1)–N(1) bond is fast, no broadening is observed. Two different orientations of the κ^1-amidinate ligand are possible. The rotamers (donated **a** and **b**) for the *endo*,*syn*,*syn*- and *exo*,*syn*,*syn*-η^3-allyl complexes are shown in Figure 3.8.

The calculated ^{1}H NMR chemical shifts (Table 3.2) of ***endo*-18Qa,b$^+$** and ***exo*-18Qa,b$^+$** emphasise the impact the Dipp fragment has on the chemical shifts of either the methyl (C(1)) or isopropyl moiety (C(6) and C(7)) of the diene fragment. When the methyl group (MeCH) sits above the Dipp ring (***endo*-18Qb$^+$**), the calculated chemical ^{1}H NMR shift is shielded, while in the rotamer (***endo*-18Qa$^+$**), the chemical ^{1}H NMR shift of one of the isopropyl methyls ($CHMe_2$) is shielded (–1.64 ppm, Table 3.2). The average of both isomers (assuming a 50:50 contribution) agrees with the experimental values obtained for ***endo*-18-[BAr$^F_4$]**. A similar trend is observed for the calculated ^{1}H NMR shifts of the *exo*-allyl complex.

Table 3.2. ^{1}H NMR chemical shifts of the *endo*- and *exo*-allyl fragment of ***endo*-18-[BAr$^{F}_{4}$]**, ***endo*-18Qa,b^{+}**, ***endo*-18-[BAr$^{F}_{4}$]** and ***exo*-18Qa,b^{+}**.

Complexes	δ CH_{meso} (ppm)	δ $CH\underline{Me}_2$ (ppm)	δ $CH\underline{Me}_2$ (ppm)	δ $CH\underline{Me}$ (ppm)
***endo*-18Qa^{+}**	6.98	-1.64	0.51	1.05
***endo*-18Qb^{+}**	8.69	0.63	0.51	-0.45
***Av. endo*-18Qa,b^{+}**	7.84	-0.50	0.51	0.30
***endo*-18-[BAr$^{F}_{4}$]**	8.06	-0.09	0.74	0.49
***exo*-18Qa^{+}**	7.21	0.77	0.77	0.82
***exo*-18Qb^{+}**	6.72	-0.91	0.56	1.19
***Av. exo*-18Qa,b^{+}**	6.96	-0.07	0.67	1.01
***exo*-18-[BAr$^{F}_{4}$]**	6.91	-0.18	0.74	1.04

To further probe the migratory-insertion step, a low-temperature reaction of Cp*Ti{NCN(Dipp)$CH_2C_6H_4$}$(CD_3)_2$ (**3-*d*$_6$**) with 2,4-hexadiene and $[Ph_3C][BAr^{F}_{4}]$ was monitored by NMR spectroscopy. The deuterium NMR spectrum shows the expected $Ph_3CC\underline{D}_3$ resonance at 2.24 ppm, the by-product of the activation, alongside a broad resonance at –0.12 ppm, corresponding to the two CD_3 groups of ***endo*-18-[BAr$^{F}_{4}$]-*d*$_3$** and ***exo*-18-[BAr$^{F}_{4}$]-*d*$_3$**. This shows that the *shielded* methyl group observed in the ^{1}H NMR spectrum of ***endo***- and ***exo*-18-[BAr$^{F}_{4}$]** is the migrating methyl group, labelled as C(7) in the calculated structures (Figure 3.8). Upon allowing the reaction to warm to room temperature, a new signal at 1.15 ppm is observed in the deuterium NMR spectrum which corresponds to the migrating methyl group (C(7)) in the final product **15-[BAr$^{F}_{4}$]**. This was also independently observed from the room temperature reaction of **3-*d*$_6$** with 2,4-hexadiene.

Interconversion between the ***endo***- and ***exo*-18-[BAr$^{F}_{4}$]** isomers is slow on the NMR timescale, such that the separate sets of allylic signals belonging to each respective isomer do not broaden due to exchange at the set temperature. However, with the help of spin-spin saturation transfer experiments, whereby the selective irradiation of the *meso* proton of the *endo*,*syn*,*syn*-η^3-allyl (***endo*-18-[BAr$^{F}_{4}$]**), results in spin-saturation transfer to the corresponding *meso* proton on the *exo*,*syn*,*syn*-η^3-allyl system (***exo*-18-[BAr$^{F}_{4}$]**), showed that both allyl systems do interconvert (Scheme 3.4).[17] This implies

that these two systems are in equilibrium. The optimised geometries of ***endo*-18Qb$^+$** and ***exo*-18b$^+$** highlight how close in energy (−19.0 *vs.* −19.5 kcal mol^{-1} respectively) they both are, showing no obvious thermodynamic preference as is also implied by the NMR data (*vide supra*). The question arises if the insertion is favoured for one allyl system over the other, only obtaining the other system through interconversion; Or if both allyl complexes are formed first, followed by interconversion. The current experimental data does not allow to unambiguously assign this. Molecular modelling, however, is suggestive of a favoured insertion to give the *endo*,*syn*,syn-η^3-allyl (***endo*-18-[BAr$^F_4$]**) over the *exo*,*syn*,syn-η^3-allyl (***exo*-18-[BAr$^F_4$]**) due to steric clash of the Cp* moiety and the methyl end-group of 2,4-hexadiene in the latter.

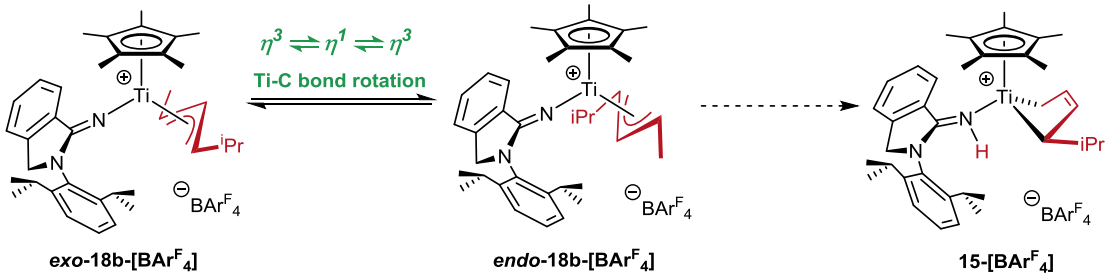

Scheme 3.4. Interconversion between the *exo*- and *endo*,*syn*,*syn*-η^3-allyl systems *via* Ti–C bond rotation in an η^1-allyl intermediate (not shown).

In order to gain understanding of the underlying electronic preferences in cationic *endo*- and *exo*-allyl formation and the cationic *supine*- and *prone*-diene formation, computational studies were carried out by Professor Philip Mountford on a series of small model complexes (Figure 3.9). Neutral small model systems of *supine*- and *prone*-diene complexes were also investigated.

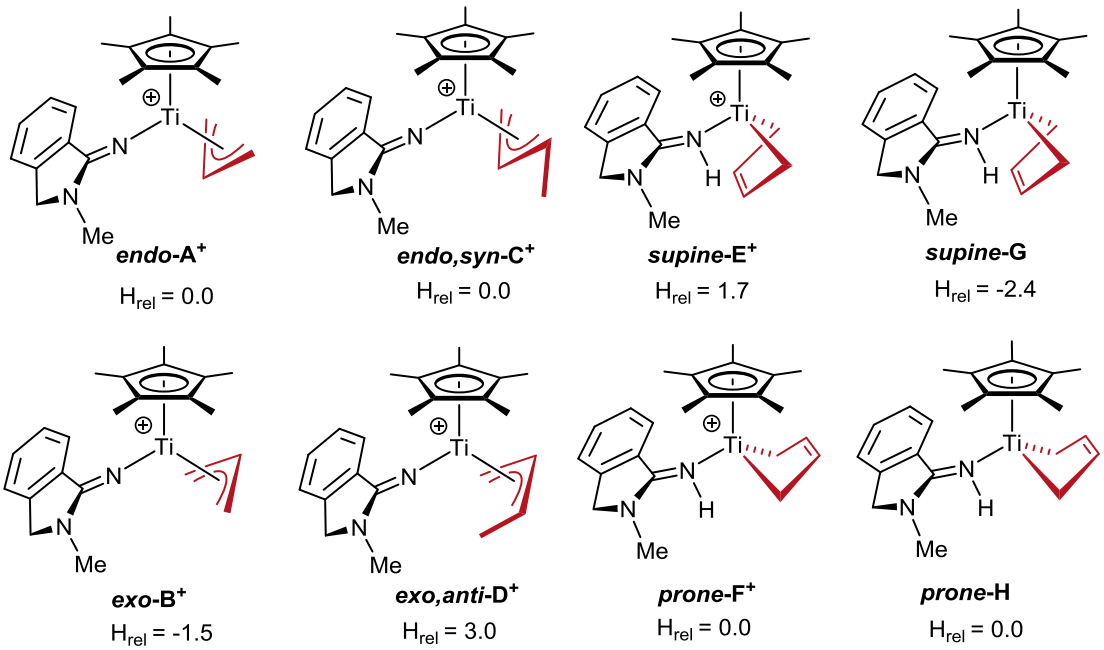

Figure 3.9. Structures of calculated small model cationic allyl, cationic diene and neutral diene complexes. The relative enthalpies were calculated in the units kcal mol^{-1}.

The computational results show in terms of electronic preferences there is a potential reverse in the favoured diene isomer between the neutral diene systems (***supine*-G** and ***prone*-H**) and the cationic diene systems (***supine*-E^+** and ***prone*-F^+**). Overall, the results suggests that each set of cationic allyl isomers or cationic diene isomers show no real strong preference for one over the other, as exemplified by the small relative enthalpy differences depicted in Figure 3.9. Energetically, there is a small preference for ***prone*-F^+** compared to its mechanistic precursor (*vide infra*) ***exo,anti*-D^+** by 2.6 kcal mol^{-1}. This implies that any final positions in the equilibrium of the reaction, notwithstanding mechanistic limitations, will be a fine balance.

Further DFT calculations were carried out to probe the mechanism of the real systems (Figure 3.10).

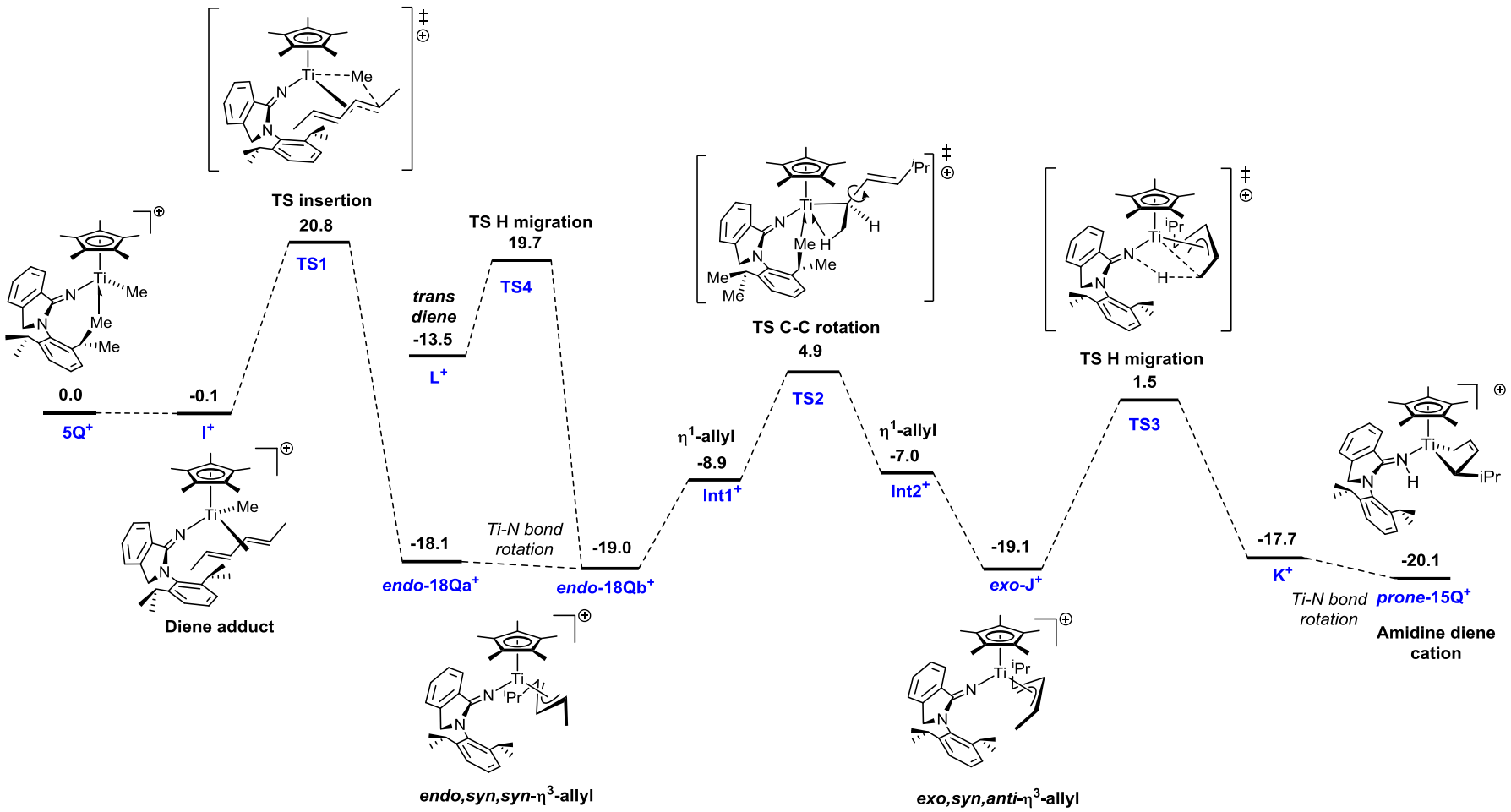

Figure 3.10. DFT reaction pathway from **5Q**$^+$ to ***prone*-15Q**$^+$. Gibb free energies (kcal mol^{-1}, T = 298 K) for minima, maxima and transition states (labelled **TSx**) are shown in bold relative to **5Q**$^+$.

The reaction pathway identifies the *endo*- and *exo*-*syn*,*syn*-η^3-allyl intermediates (***endo*-18Qa,b**$^+$ and ***exo*-18Qa,b**$^+$) after the migratory-insertion step (**TS1**), as determined experimentally. As the following steps only consider ***endo*-18Qa,b**$^+$ to obtain the final product, the *exo*-allyls are not represented in the reaction pathway. The reaction pathway above shows the isomerisation of the ***endo*-18Qa**$^+$ to ***endo*-18Qb**$^+$ *via* Ti–N bond rotation, with the latter being slightly more stable. ***Endo*-18Qb**$^+$ then undergoes isomerisation *via* C–C bond rotation to give the *exo*,*syn*,*anti*-η^3-allyl system (***exo*-J**$^+$) *via* **TS2**. ***Exo*-J**$^+$ can undergo C–H bond activation and H-migration to the metal-bound nitrogen of the κ^1-amidinate to give **K**$^+$. The difference between **K**$^+$ and ***prone*-15Q**$^+$ is the orientation of the κ^1-amidinate ligand. The rotation around the Ti(1)–N(1) bond gives the final observed product. Each step is discussed in more detail below.

The DFT structure of the methyl cation **5Q**$^+$ shows an extra stabilisation by one isopropyl methyl group (Figure 3.11). The Ti(1)–H(1) and Ti(1)–H(2) distances are 2.054 and 2.297 Å, respectively. This could explain why no α-agostic stabilisation is observed by the mono-methyl substituent on the metal centre (Chapter Two).

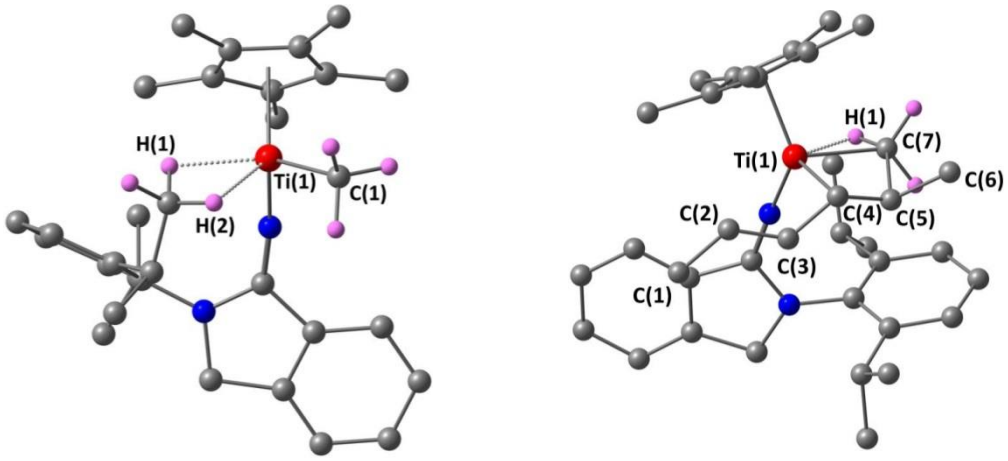

5Q$^+$ **TS1**

Figure 3.11. DFT structure of the methyl cation **5Q**$^+$ (left) and transition state **TS1** (right) for *trans*-2,4-hexadiene insertion into the Ti–Me bond of **5Q**$^+$. H atoms except for those of the titanium methyl and agostic Dipp methyl groups omitted. Selected distances (Å) and angles (^{o}) for **5Q**$^+$: Ti(1)–C(1) 2.087, Ti(1)–H(1) 2.054, Ti(1)–H(2) 2.297; for **TS1**: Ti(1)–C(7) 2.196, Ti(1)–C(4) 2.214, Ti(1)–H(1) 2.200, C(2)–C(3) 1.360, C(3)–C(4) 1.445, C(4)–C(5) 1.402, C(5)–C(7) 2.198, Ti(1)–C(7)–H(1) 75.6.

The migratory-insertion transition state **TS1** shows an elongation of the bond distance of titanium to the migrating methyl group (C(1)/(7)) compared to the mono-methyl cation **5Q**$^+$ from 2.087 to 2.196 Å. The transition state (**TS1**) also shows that the Dipp group is no longer involved in stabilising the metal centre, but is rather pointing away from it. Instead an α-agostic interaction is observed from the migrating methyl group (C(7)–H(1)) which is confirmed by the acute bond angle of Ti(1)–C(7)–H_α (75.6º) and a close Ti(1)–H(1) bond distance of 2.200 Å. **TS1** followed potentially by interconversion (*vide supra*) results in the formation, and experimentally observable, *syn*,*syn*-η^3-allyl intermediates (***endo*-18-[BAr$^F_4$]** and ***exo*-18-[BAr$^F_4$]**).

The reaction pathway suggests that the ***endo*-18Qb**$^+$ undergoes isomerisation to give the *exo*,*syn*,*anti*-η^3-allyl (***exo*-J**$^+$) *via* C–C bond rotation with a relative high energy barrier. ***Exo*-J**$^+$ is not observed experimentally which suggests that the isomerisation *via* Ti–C bond rotation is more accessible than the isomerisation *via* C-C bond rotation.

Int1$^+$, representing the η^1-allyl intermediate from ***endo*-18Qb**$^+$, shows the expected smaller Ti(1)–C(2) bond distance compared to ***endo*-18Qb**$^+$ (2.110 *vs.* 2.333 Å, Figure 3.12). Furthermore, more double bond character is observed in the η^1-allyl system, as shown by the shorter bond distance of C(3)–C(4) and longer bond distance of C(2)–C(3) (1.345 and 1.466 Å, respectively) compared to the η^3-allyl ***endo*-18Qb**$^+$.

Soling and Szabo have investigated allyl palladium complexes and their isomerisation *via* $\eta^3 \rightarrow \eta^1 \rightarrow \eta^3$ with C–C bond rotation. With the help of DFT calculations, they identified η^1-allyl coordination to Palladium results in hyperconjugative interactions between the σ(Pd–C1) and the π*(C2–C3) molecular orbitals.[18] Furthermore, investigation into the rotation of the C–C bond showed its disruptive effect on the aforementioned conjugative interaction, which was assumed to trigger the particularly high energy barrier.[18]

Similar deductions could be made for this system. A potential delocalisation could take place involving the σ(Ti(1)–C(2)) and π*(C(3)–C(4)), similar to the study from Szabo *et al*. (Figure 3.12).[18] The DFT calculated structure of the η^1-allyl system (**Int1**$^+$) of ***endo*-18Qb**$^+$ gives a slightly shorter C(2)–C(3) bond distance compared to the elongated bond when rotating around the C(2)–C(3) bond in **TS2** (1.466 *vs.*

1.494 Å). Furthermore, the Ti(1)–C(2) bond distance becomes shorter in the transition state **TS2** compared to the η^1-allyl system (**Int1**$^+$) (2.077 *vs.* 2.110 Å), suggesting more donation to titanium in **TS2**. A direct comparison can be drawn between these bond distances as the sp^2-hydridisation of C(2) does not change as shown with the almost identical sum of angles subtended at C(2). This all points towards loss of delocalisation upon rotation and indeed could explain the higher barrier observed when interconverting to the *syn*,*anti*-η^3-allyl systems.

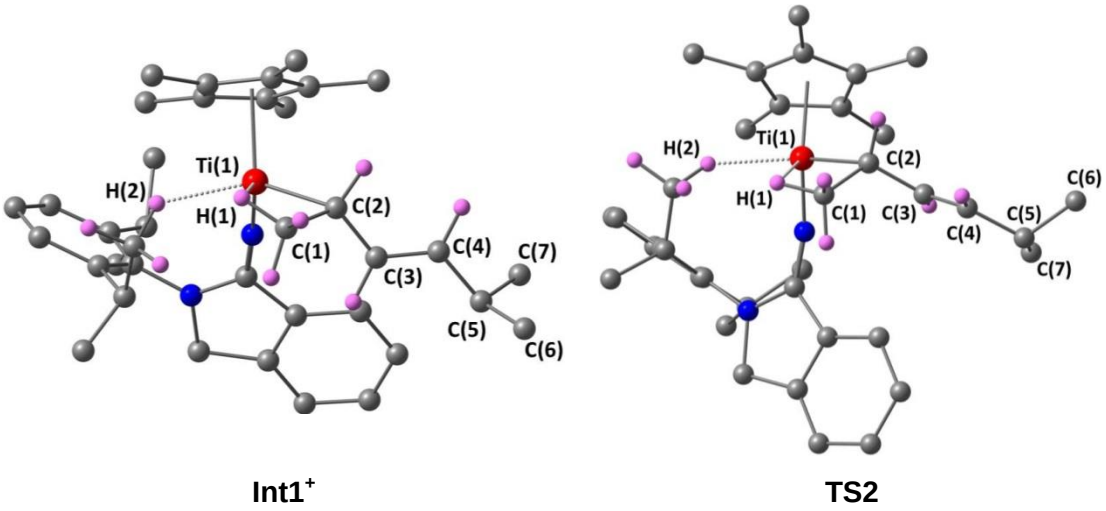

Figure 3.12. DFT structure of the η^1-allyl isomer (**Int1**$^+$, left) of ***endo*-18Qb**$^+$and the transition state (**TS2**, right) for rotation about C(2)–C(3). C-bound H atoms omitted except for those of the methyl groups involved in agostic interactions and the methine hydrogens of the allyl group. Selected distances (Å) and angles (^{o}) for **Int1**$^+$: Ti(1)–C(2) 2.110, Ti(1)–H(1) 2.091, Ti(1)–H(2) 2.166, C(2)–C(1) 1.513, C(2)-C(3) 1.466, C(3)–C(4) 1.345, Ti(1)–C(2)–C(1) 81.0; for **TS2**: Ti(1)–C(2) 2.077, Ti(1)–H(1) 2.127, Ti(1)–H(2) 2.161, C(2)–C(1) 1.513, C(2)–C(3) 1.494, C(3)–C(4) 1.340, Ti(1)–C(2)–C(1) 85.0. The sum of the angles subtended at C(2) are 340.3 and 340.6 ^{o}, respectively.

The spectroscopic data obtained for **15-[BAr$^F{}_4$]**, shows that the *prone*-diene isomer is obtained exclusively. The selectivity for only the *prone* isomer is derived from the geometry of the previous intermediate: *exo*,*syn*,*anti*-η^3-allyl (***exo*-J**$^+$, Figure 3.10). The *supine* isomer could in theory be formed from the *endo*,*syn*,*anti*-η^3-allyl (***endo*-M**$^+$). To understand this selectivity further, both allyl systems, ***exo*-J**$^+$ and ***endo*-M**$^+$, were calculated (Figure 3.13). No thermodynamic preference was observed for either of these allyl systems, but the C(1), from which the H-migration takes place (**TS3**,

vide infra) is in the wrong orientation in ***endo*-M$^+$** to allow C–H bond activation. While for ***exo*-J$^+$**, C(1) is in the correct orientation.

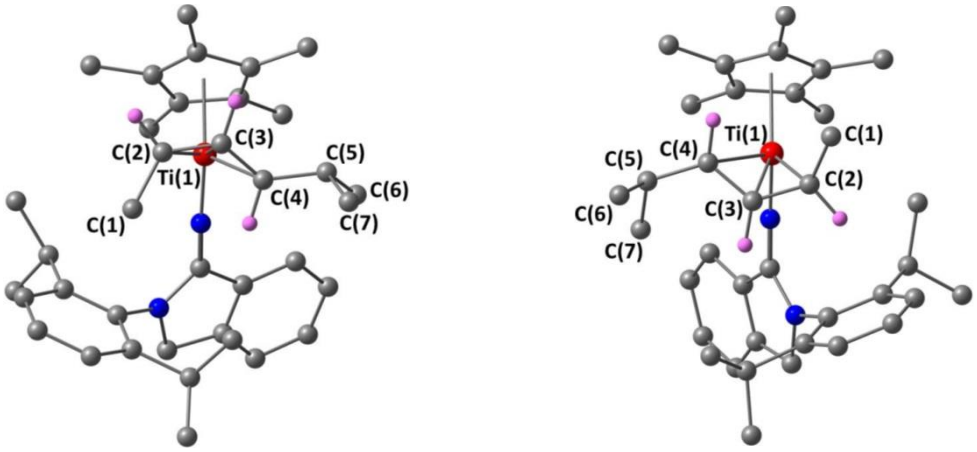

***exo*-J$^+$** ***endo*-M$^+$**

Figure 3.13. DFT structure of the *exo,syn,anti*-η^3-allyl species (***exo*-J$^+$**) and one of its *exo,syn,anti*-η^3-allyl isomers (***endo*-M$^+$**). H atoms except for those of the allyl methine carbons omitted. Selected distances (Å) for ***exo*-J$^+$**: Ti(1)–C(2) 2.263, Ti(1)–C(3) 2.325, Ti(1)–C(4) 2.310, C(2)–C(3) 1.412, C(3)–C(4) 1.390; for ***endo*-M$^+$**: Ti(1)–C(2) 2.336, Ti(1)–C(3) 2.282, Ti(1)–C(4) 2.317, C(2)–C(3) 1.404, C(3)-C(4) 1.399.

Another pathway to obtain the *supine* isomer of ***prone*-15Q$^+$** is isomerisation *via* ring flipping, which is described in literature.[19-21] However, for complex ***prone*-15Q$^+$** a ring flip would put the isopropyl group in the *anti* position and therefore pointing towards the sterically demanding cyclopentadienyl fragment as well as resulting in 1,4-strain across the diene fragment.

The transition state **TS3** shows an almost linear Ti(1)–N(1)–C_{Ar} bond angle compared to the bond angle of **K$^+$**(177.4 *vs*. 142.1º, respectively, Figure 3.14). This suggests that during the C–H bond activation the Dipp fragment is in closer proximity to the metal centre. As previously observed for ***prone*-15Q$^+$** and **17Q$^+$**, the proton ends up on the Dipp "side" of the κ^1-amidinate in **K$^+$**. The Ti(1)–C(1) bond distance expectably decreases from the transition state (**TS3**) to **K$^+$** (2.231 *vs*. 2.115 Å). The newly formed *prone* complex **K$^+$** has a shorter C(2)–C(3) bond distance and a longer C(3)–C(4) bond distance compared to the *exo,syn,anti*-η^3-allyl (***exo*-J$^+$**), supporting the formation of a diene complex with an 'ene-diyl' bonding mode.

The first formed *cis*-diene product $\mathbf{K}^+$ is less stable than the final, observed product ***prone*-15Q**$^+$ where the Ti–N bond rotation results in the Dipp fragment lying below the isopropyl moiety of the diene fragment.

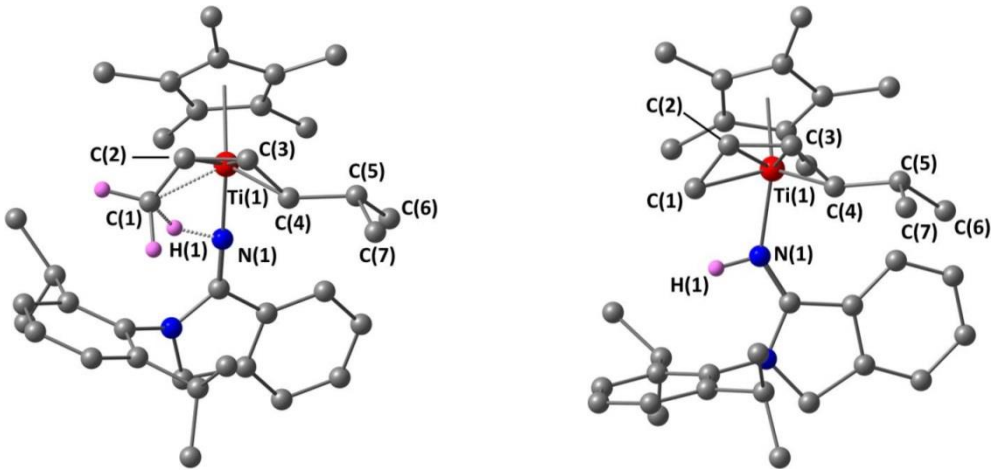

Figure 3.14. DFT structure of the first-formed *cis*-diene product ($\mathbf{K}^+$, right) and the associated transition state (**TS3**, left) originating from ***exo*-J**$^+$. C-bound H atoms omitted except for those of C(1) or N(1). Selected distances (Å) and angles (^{o}) for **TS3**: Ti(1)–C(1) 2.231, Ti(1)–C(2) 2.217, Ti(1)–C(3) 2.287, Ti(1)–C(4) 2.206, C(1)-C(2) 1.463, C(2)–C(3) 1.401, C(3)–C(4) 1.410, C(1)–H(1) 1.510, N(1)–H(1) 1.380, C(1)–H(1)–N(1) 150.3, Ti(1)–N(1)–C_{Ar} = 177.4; for $\mathbf{K}^+$: Ti(1)–C(1) 2.155, Ti(1)–C(2) 2.275, Ti(1)–C(3) 2.269, Ti(1)–C(4) 2.156, C(1)–C(2) 1.425, C(2)–C(3) 1.398, C(3)–C(4) 1.427, N(1)–H(1) 1.023, Ti(1)–N(1)–C_{Ar} = 142.1.

One further possibility is to obtain the *trans*-diene product $\mathbf{L}^+$ from the C–H activation of the C(1) methyl group from the ***endo*-18Qb**$^+$ intermediate (Figure 3.15). *Cis*- and *trans*-diene complexes of group 4 metals have been previously observed, including isomerisation from one to the other.[22] The coordination mode seems dependent on the metal itself, the supporting ligand and the substituent on the diene fragment.[20] The computational results however show, that in this case, the C–H bond activation, as well as the *trans*-diene product ($\mathbf{L}^+$), are substantially thermodynamically disfavoured in comparison to the final experimentally observed product ***prone*-15Q**$^+$ (Figure 3.10). Similar as for the transition state **TS3**, the Ti(1)–N(1)–C_{Ar} bond angle is close to linearity when going from ***exo*-J**$^+$ to $\mathbf{L}^+$ of 168.8º.

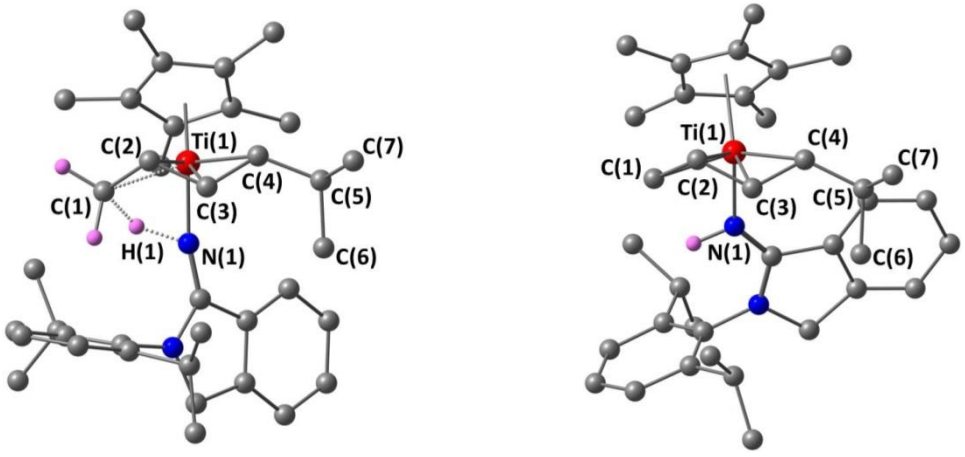

TS4 **L$^+$**

Figure 3.15. DFT structure of the *trans*-diene product (**L**$^+$, right) and the associated transition state (**TS4**, left) originating from ***endo*-18b**$^+$. C-bound H atoms omitted except for those of C(1) or N(1). Selected distances (Å) and angles (^{o}) for **TS4**: Ti(1)–C(1) 2.322, Ti(1)–C(2) 2.141, Ti(1)–C(3) 2.247, Ti(1)–C(4) 2.352, C(1)–C(2) 1.446, C(2)–C(3) 1.419, C(3)–C(4) 1.396, C(1)–H(1) 1.534, N(1)–H(1) 1.357, C(1)–H(1)–N(1) 149.1, Ti(1)–N(1)–C_{Ar} = 168.8; for **L**$^+$: Ti(1)–C(1) 2.222, Ti(1)–C(2) 2.164, Ti(1)–C(3) 2.220, Ti(1)–C(4) 2.391, C(1)–C(2) 1.418, C(2)–C(3) 1.423, C(3)–C(4) 1.398, N(1)–H(1) 1.024, Ti(1)–N(1)–C_{Ar} = 138.1.

3.4 Synthesis of activated diene complexes with other κ^1-amidinate and κ^1-guandinate titanium complexes

κ^1-amidinate and κ^1-guanidiante ligands can both act as potential σ+2π donors. But the presence of two donor nitrogen atoms in κ^1-guanidinate ligand makes them more donating than κ^1-amidinate ligands. This Section explores to what extent steric and electronic properties of the supporting ligand play a role in the preferential formation of the titanium allyl and diene systems. The complexes relevant for this Section (Figure 3.16) were kindly provided by ARLANXEO or synthesised by students under the Author's supervision.

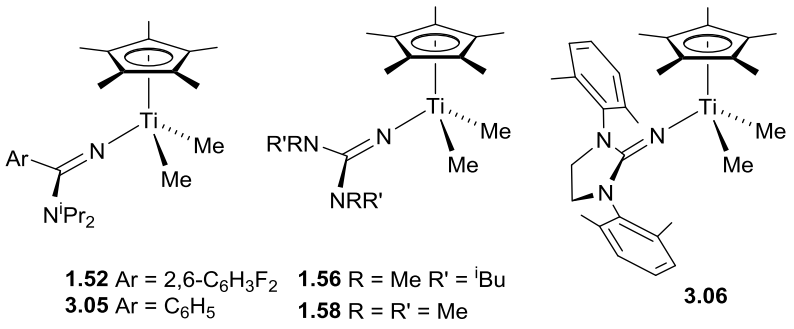

1.52 Ar = 2,6-$C_6H_3F_2$ **1.56** R = Me R' = ^{i}Bu
3.05 Ar = C_6H_5 **1.58** R = R' = Me

Figure 3.16. Range of κ^1-amidinate and κ^1-guanidinate half-sandwich titanium complexes.

Activation chemistry of **1.52**, **1.56** and **1.58** has been discussed in Section 1.7. To prevent dimer formation when activated with $[Ph_3C][BAr^F{}_4]$ (*vide supra*), complexes **1.52**, **1.56** and **1.58** were only activated in the presence of 2,4-hexadiene.

3.4.1 Variation of the κ^1-amidinate supporting ligand

The reaction of **1.52** or **3.05** with 2,4-hexadiene and $[Ph_3C][BAr^F{}_4]$ shows the formation of a cationic diene adduct **19-[BAr$^F{}_4$]** and **21-[BAr$^F{}_4$]**, respectively, (Equation 3.2) as the major product. However, the *endo*,*syn*,*syn*-η^3-allyl and the *exo*,*syn*,*syn*-η^3-allyl are observed in small quantities at room temperature with complex **1.52** (***endo***- and ***exo***-**20-[BAr$^F{}_4$]**). Low temperature NMR studies of the reaction with **3.05** revealed the presence of ***endo***-**22-[BAr$^F{}_4$]** at –30 ºC, observed by the characteristic downfield triplet at 8.12 ppm, corresponding to the *meso* proton thereof. ***Exo***-**22-[BAr$^F{}_4$]** was only present in trace amounts. **21-[BAr$^F{}_4$]** started forming at –20 ºC and quantitative conversion was observed.

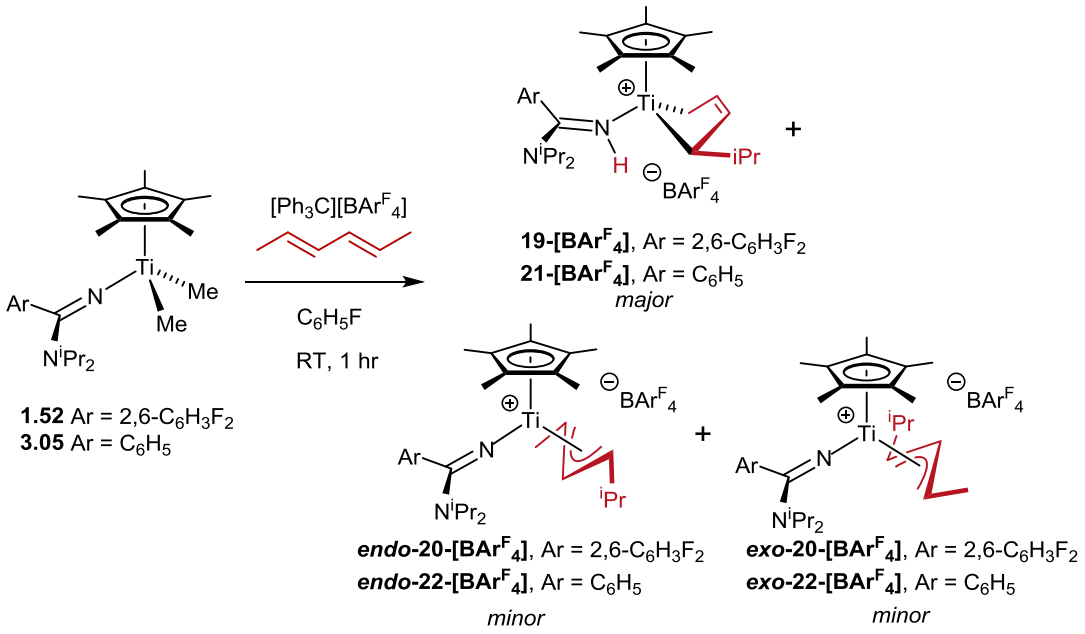

Equation 3.2

The room temperature ^{1}H NMR spectrum of the reaction of **1.52** with $[Ph_3C][BAr^{F}_4]$ and 2,4-hexadiene displays the diene cation (**19-[BAr$^{F}_4$]**), alongside small amounts of the *endo*- and *exo*-allyl complexes (***endo*-and *exo*-20-[BAr$^{F}_4$]**). The singlet at 4.80 ppm is assigned to the NH moiety of the supporting amidine ligand of **19-[BAr$^{F}_4$]** (Figure 3.17). Similar as for **15-[BAr$^{F}_4$]**, the proton correlates through multiple bond to the quaternary carbons NC and NAr^{F_2}. A J_{NH} coupling constant of 60.4 Hz also agrees with previous findings of migration of the proton to the metal-bound nitrogen of the amidine ligand (*vide supra*). The vinylic protons, observed at 3.70–3.61 and 3.28 ppm in the ^{1}H NMR spectrum, correlate through-space to the Cp* moiety at 1.73 ppm, again confirming the *prone* configuration (Figure 3.17). The differences in the ^{13}C chemical shifts of the vinylic group and the terminal groups of the diene fragment are indicatives of an ‘ene-diyl’ bonding mode (*vide supra*).

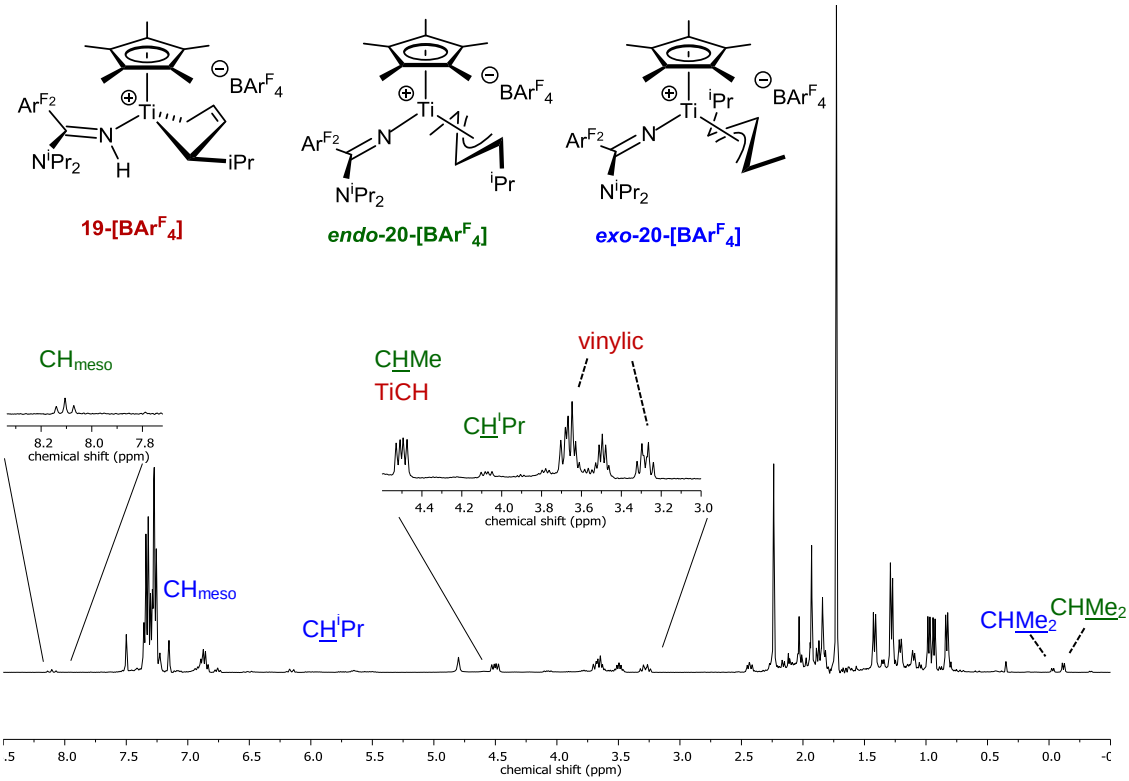

Figure 3.17. ^{1}H NMR spectrum (499.9 MHz, C_6D_5Br, 298 K) of **19-[BAr$^{F}_{4}$]**, ***endo*-20-[BAr$^{F}_{4}$]** and ***exo*-20-[BAr$^{F}_{4}$]**.

In contrast to the reaction of **5-[BAr$^{F}_{4}$]** with 2,4-hexadiene, the room temperature ^{1}H NMR spectrum evidently exhibits resonances for the *endo*,*syn*,*syn*-η^3-allyl and the *exo*,*syn*,*syn*-η^3-allyl (***endo*-** and ***exo*-20-[BAr$^{F}_{4}$]**, respectively). The downfield triplet at 8.11 ppm, correlates to the *anti* 1,3-allylic protons at 4.50 and 4.08 ppm. These two allylic protons correlate through-space to the Cp* moiety at 1.94 ppm, assigning those resonances to the *endo*,*syn*,*syn*-η^3-allyl (***endo*-20-[BAr$^{F}_{4}$]**). The *meso* proton of ***exo*-20-[BAr$^{F}_{4}$]** is overlapping with other aromatic resonances at 7.11–7.09 ppm. The relative ratios of the diene complex **19-[BAr$^{F}_{4}$]**, the *endo*,*syn*,*syn*-η^3-allyl (***endo*-20-[BAr$^{F}_{4}$]**) and the *exo*,*syn*,*syn*-η^3-allyl (***exo*-20-[BAr$^{F}_{4}$]**) are 0.80 : 0.14 : 0.06, respectively. The relative Gibbs free energy can be calculated using $\Delta G = -RT\ln(K)$, where R is the ideal gas constant (1.987 kcal mol^{-1} K^{-1}), T is the reaction temperature and *K* is the equilibrium constant, for each compound. With respect to ***endo*-20-[BAr$^{F}_{4}$],** the relative Gibbs free energy of ***exo*-20-[BAr$^{F}_{4}$]** equals to +0.50 kcal mol^{-1} and of **19-[BAr$^{F}_{4}$]** is –1.0 kcal mol^{-1}. This shows the fine balance between the cationic allyl and diene species of compound **1.52**, and is consistent with the

difference in Gibbs free energy (1.1 kcal mol^{-1}) between ***endo*-18Qb^{+}** and ***prone*-15Q^{+}** (Figure 3.10).

Interestingly, modification of the electronic and steric requirement of the κ^1-amidinate ligand results in different stabilities of the allyl and diene complexes formed upon the reaction with conjugated dienes.

3.4.2 Reaction of conjugated diene with κ^1-guanidinate half-sandwich complexes

Activation of Cp*Ti{NC(NMe$_2$)$_2$}Me$_2$ (**1.58**) with [Ph$_3$C][BAr$^F_4$] in the presence of 2,4-hexadiene in C$_6$D$_5$Br resulted in a short-lived mixture of products, identified as the cationic diene adduct (**23-[BAr$^F_4$]**) and the *endo*,*syn*,*syn*-η^3-allyl (***endo*-24-[BAr$^F_4$]**, Equation 3.3). The *exo*,*syn*,*syn*-η^3-allyl (***exo*-24-[BAr$^F_4$]**) can only be observed in trace amounts, preventing characterisation of this complex.

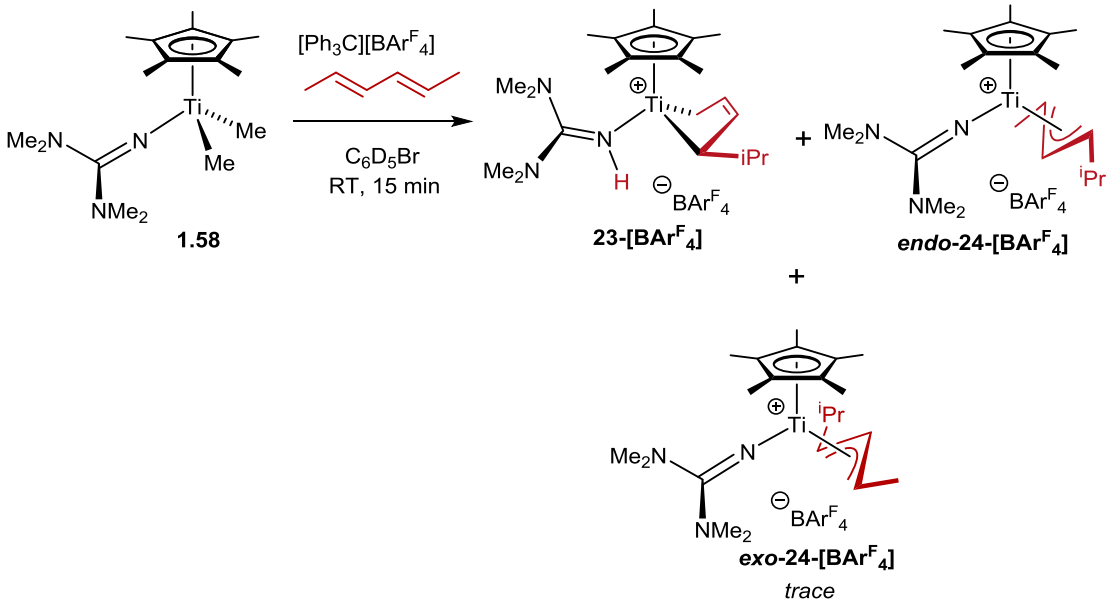

Equation 3.3

The newly formed NH resonance is observed at 3.24 ppm, but due to the short living nature of the complex, no J_{NH} coupling constant could be obtained. The vinylic protons of **23-[BAr$^F_4$]** are observed as multiplets at 3.95–3.91 and 3.62–3.56 ppm (Figure 3.18). The *anti* 1,3-allylic protons of ***endo*-24-[BAr$^F_4$]** at 4.55–4.50 and 4.31 ppm exhibit through-bond correlation to the *meso* proton at 8.11 ppm (Figure 3.18). The chemical shifts agree with the previous observed *endo*,*syn*,*syn*-η^3-allyl complexes (*vide supra*).

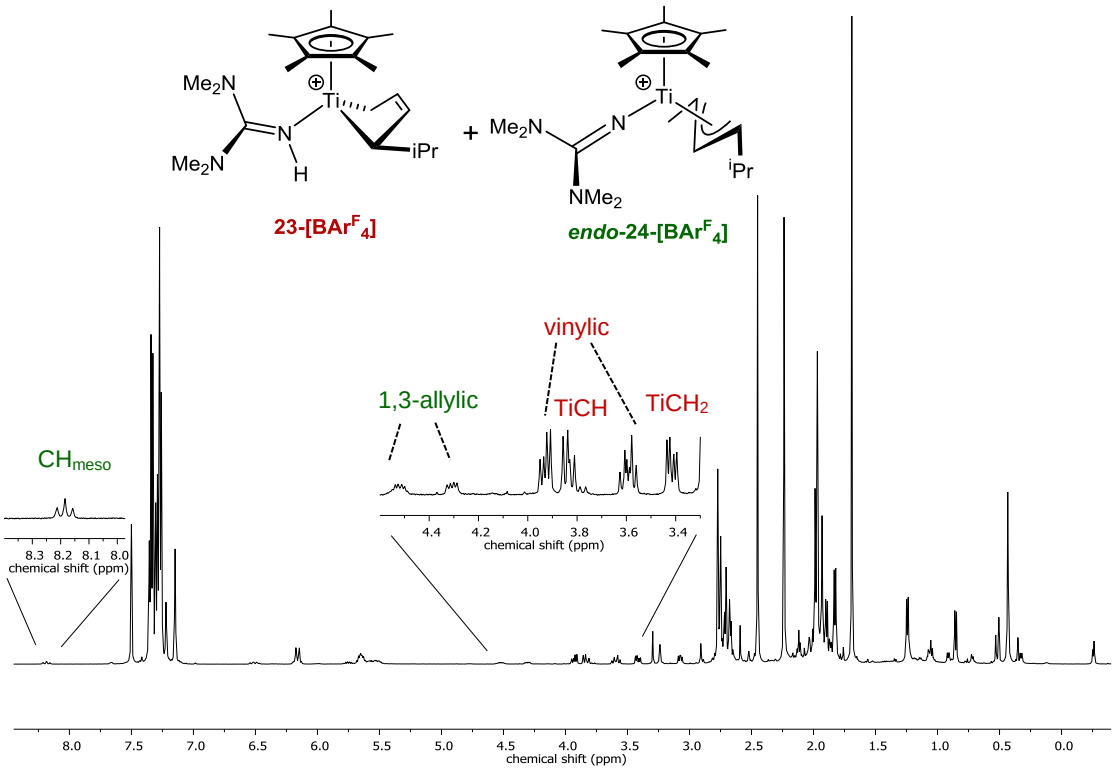

Figure 3.18. ^{1}H NMR spectrum (400.2 MHz, C_6D_5Br, 298 K) of **23-[BAr$^{F}_{4}$]** and ***endo*-24-[BAr$^{F}_{4}$]**.

Further low temperature NMR experiments were conducted to gain insight into the formation of the allyl and diene species. At –30 ºC, only ***endo*-24-[BAr$^{F}_{4}$]** was observed alongside unreacted 2,4-hexadiene and triphenylethane. Slowly warming the reaction to room temperature, small amounts of **23-[BAr$^{F}_{4}$]** and simultaneously a precipitate was observed accounted for by the formation of insoluble dimer (Section 1.7). Changing the solvent system to CD_2Cl_2 in an attempt to increase solubility, gives the immediate formation of ***endo*-24-[BAr$^{F}_{4}$]** at room temperature. Within 30 minutes, however, **23-[BAr$^{F}_{4}$]** was more abundant alongside unidentified species.

The *endo*,*syn*,*syn*-η^3-allyl (***endo*-24-[BAr$^{F}_{4}$]**) is the only allyl species observed at the start of the reaction. This indicates that **Insertion A** is favoured and therefore suggests that the *endo*-allyl is formed, followed by interconversion to the *exo*-allyl (Figure 3.19).

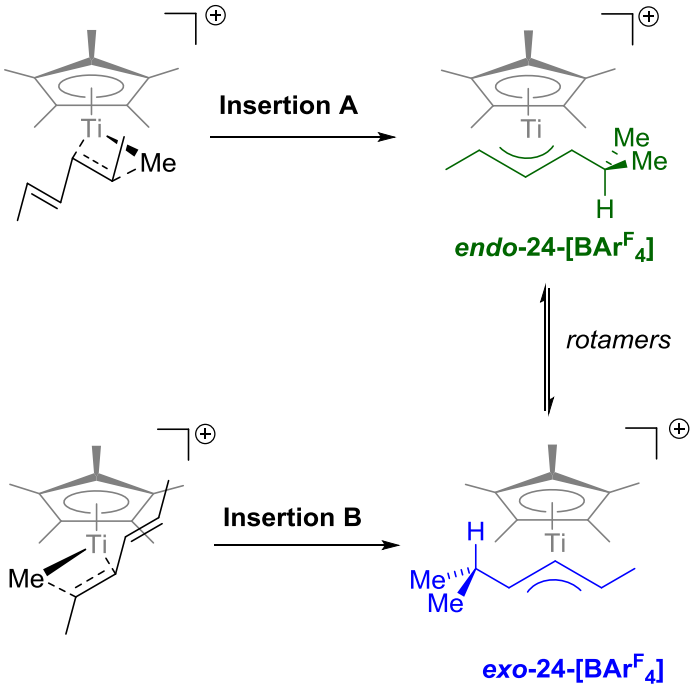

Figure 3.19. Insertion of 2,4-hexadiene into the Ti–Me bond. $[BAr^F_4]^-$ omitted for clarity.

An increase in steric requirement of the supporting ligand system was achieved by replacing one methyl group on each nitrogen atom with an *iso*-butyl group (**1.56**). Reacting **1.56** with $[Ph_3C][BAr^F_4]$ in the presence of 2,4-hexadiene gives *endo*,*syn*,*syn*-η^3-allyl $[Cp^*Ti\{NC(NMe^iBu)_2\}\{\eta^3\text{-}CH(Me)(CH)_2{}^iPr\}][BAr^F_4]$ (***endo*-25-[BAr$^F_4$]**) as major product (Equation 3.4). The *exo*,*syn*,*syn*-η^3-allyl and cationic diene adduct are the minor products of this reaction (***exo*-25-[BAr$^F_4$]** and **26-[BAr$^F_4$]**, respectively). The relative ratios of ***endo*-25-[BAr$^F_4$]**, ***exo*-25-[BAr$^F_4$]** and **26-[BAr$^F_4$]** are 0.53: 0.13 : 0.34, respectively. As shown previsouly, the relative Gibbs free energy of each compound can be calculated using $\Delta G = -RT\ln(K)$. With respect to ***endo*-25-[BAr$^F_4$],** the relative Gibb free energy of ***exo*-25-[BAr$^F_4$]** equals to +0.83 kcal mol^{-1} and of **26-[BAr$^F_4$]** is +0.26 kcal mol^{-1}. This shows the fine balance between the cationic allyl and diene species of compound **1.56**, and shows a smaller energy differences between ***endo*-25-[BAr$^F_4$]** and **26-[BAr$^F_4$]** compared to the ***endo*-18Qb$^+$** and ***prone*-15Q$^+$** (Figure 3.10).

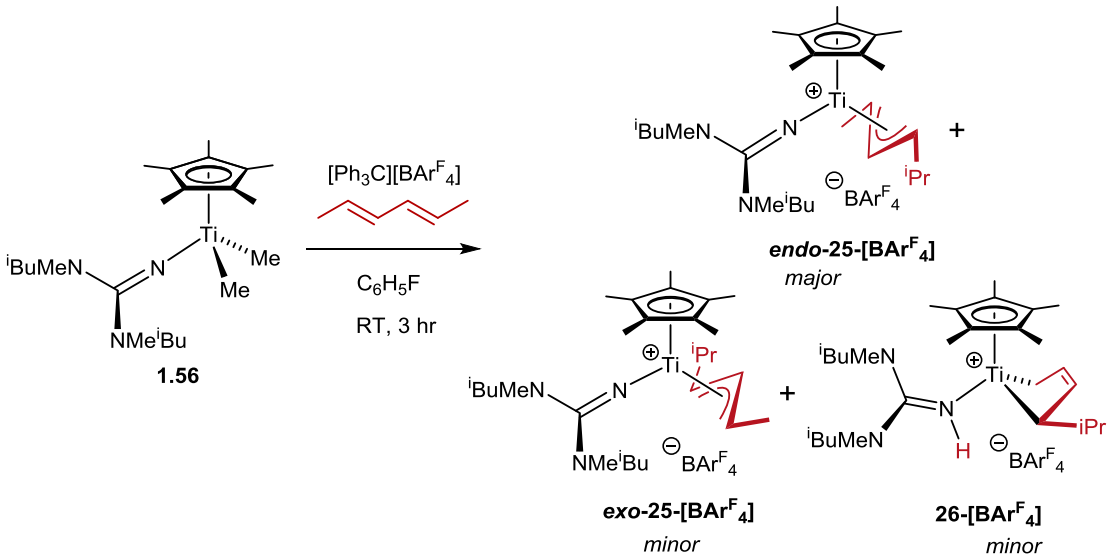

Equation 3.4

These reactions were run in collaboration with a Part II student under the Author's supervision. The *anti* 1,3-allylic protons of ***endo*-25-[BAr$^F_4$]** correlate through-space to the Cp* moiety at 1.95 ppm. The same resonances correlate through-bond to the *meso* proton at 8.23 ppm, assigning it to the *endo*,*syn*,*syn*-η^3-allyl (Figure 3.20).

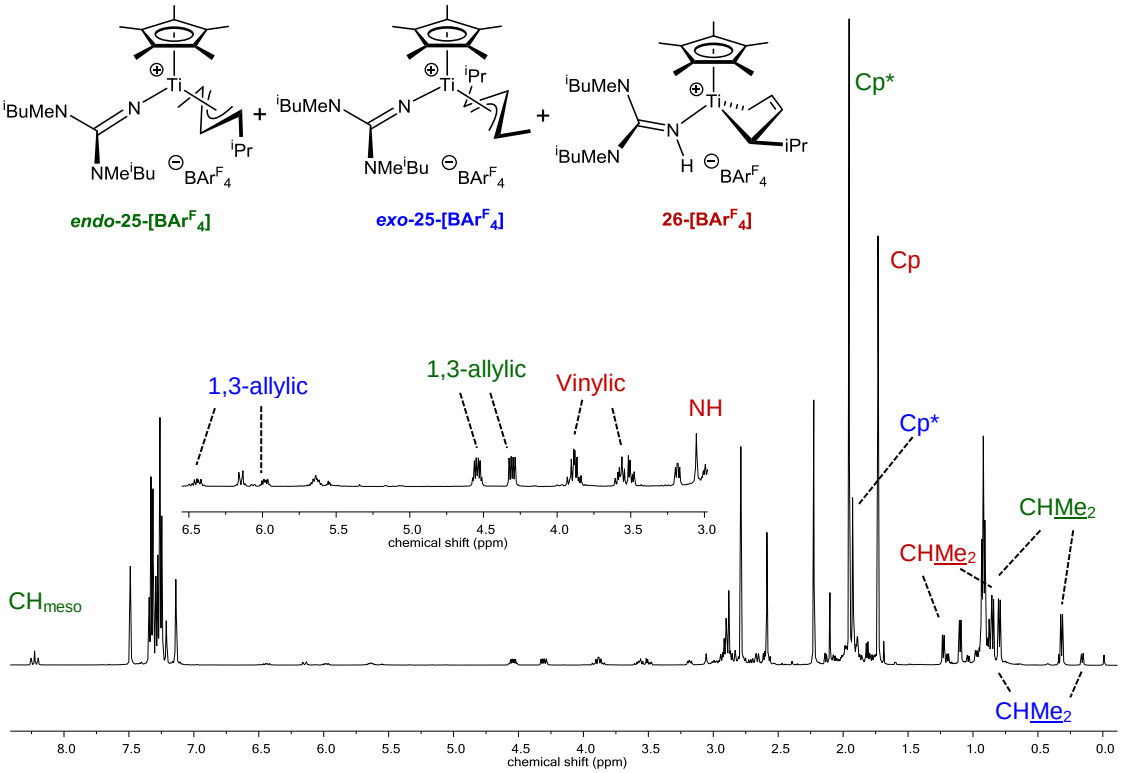

Figure 3.20. ^{1}H NMR spectrum (499.9 MHz, C_6D_5Br, 298 K) of ***endo*-25-[BAr$^F_4$]**, ***exo*-25-[BAr$^F_4$]** and **26-[BAr$^F_4$]**.

The *meso* proton of ***exo*-25-[BAr$^{F}_{4}$]** is overlapping with aromatic resonances of the by-product triphenylethane but was located in a COSY experiment through the bond correlation to the 1,3-allylic protons at 6.44 and 5.98 ppm. The difference in chemical shifts of the 1,3-allylic protons of the *endo*- and *exo*,*syn*,*syn*-η^3-allyl can be attributed to the enhanced shielding effect experienced by the close proximity of the Cp* moiety.

The vinylic protons at 3.93–3.84 and 3.61–3.54 ppm of **26-[BAr$^{F}_{4}$]** correlate through-space to the Cp* fragment at 1.73 ppm, confirming the suspected *prone* configuration of the diene moiety. The NH is assigned to the resonance at 3.05 ppm, a more upfield shift than observed for **15-[BAr$^{F}_{4}$]** and **19-[BAr$^{F}_{4}$]**. With a one-dimensional ^{15}N-^{1}H HSQC experiment, the $^{1}J_{NH}$ coupling constant was determined as 60.9 Hz. To further investigate the regiochemistry of the methyl migration, deuterium-labelled NMR studies using **1.56-*d*$_6$** were conducted. Analogously to **15-[BAr$^{F}_{4}$]-*d*$_3$**, the diene complex **26-[BAr$^{F}_{4}$]-*d*$_3$** was deuterated at the more deshielded doublet (1.23 ppm) only. However, the allyl isomers, ***endo*-25-[BAr$^{F}_{4}$]-*d*$_3$** and ***exo*-25-[BAr$^{F}_{4}$]-*d*$_3$**, showed deuteration exclusively at the more upfield doublets at 0.32 and 0.16 ppm, respectively. The upfield shift of the migrating methyl group cannot be explained by an enhanced shielding effect due to the absence of an aromatic ring. An alternative explanation is the proximity of the electrophilic metal centre to the methyl group as well as the potential influence of the Cp* moiety.

Introducing the cyclic, C_2-symmetric, κ^1-coordinated guanidinate ligand giving Cp*Ti{NC(N(Xyl)$_2$(CH$_2$)$_2$}Me$_2$ (**3.06**) increases the steric crowding around the titanium center considerably in comparison to **1.58**.

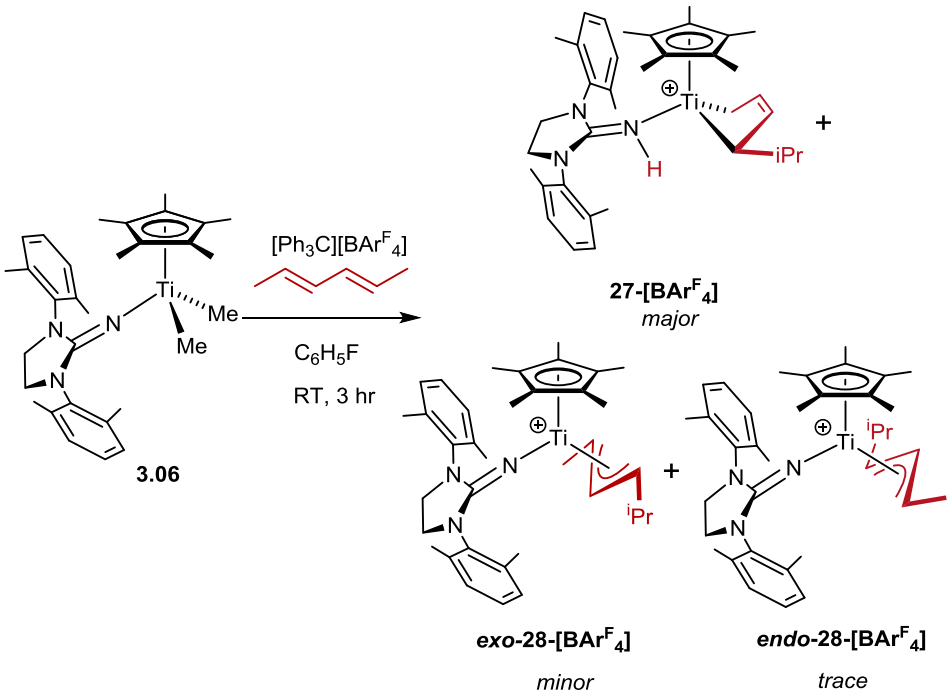

Equation 3.5

Upon activation of **3.06** with $[Ph_3C][BAr^F{}_4]$ in the presence of 2,4-hexadiene at room temperature, the cationic diene complex (**27-[BAr$^F{}_4$]**), identified as the major product, and ***endo***- and ***exo*-28-[BAr$^F{}_4$]** were observed (Equation 3.5). Conversely to previous observation, the dominant isomer was the *exo*,*syn*,*syn*-η^3-allyl (***exo*-28-[BAr$^F{}_4$]**), while the *endo*,*syn*,*syn*-η^3-allyl isomer (***endo*-28-[BAr$^F{}_4$]**) was only observed in trace amounts at room temperature.

The ^{1}H NMR spectrum (Figure 3.21) features clearly a major Cp* resonance at 1.36 ppm, which correlates through space to the vinylic protons at 3.55–3.42 and 3.25 ppm of **27-[BAr$^F{}_4$]**. This confirms the selective *prone* confirmation of the diene. The NH moiety appears in an overlapping mutliplet with the diastereotopic NCH_2 ligand backbone resonances at 3.64–3.61 ppm and the $^1J_{NH}$ coupling constant was determined as 61.9 Hz.

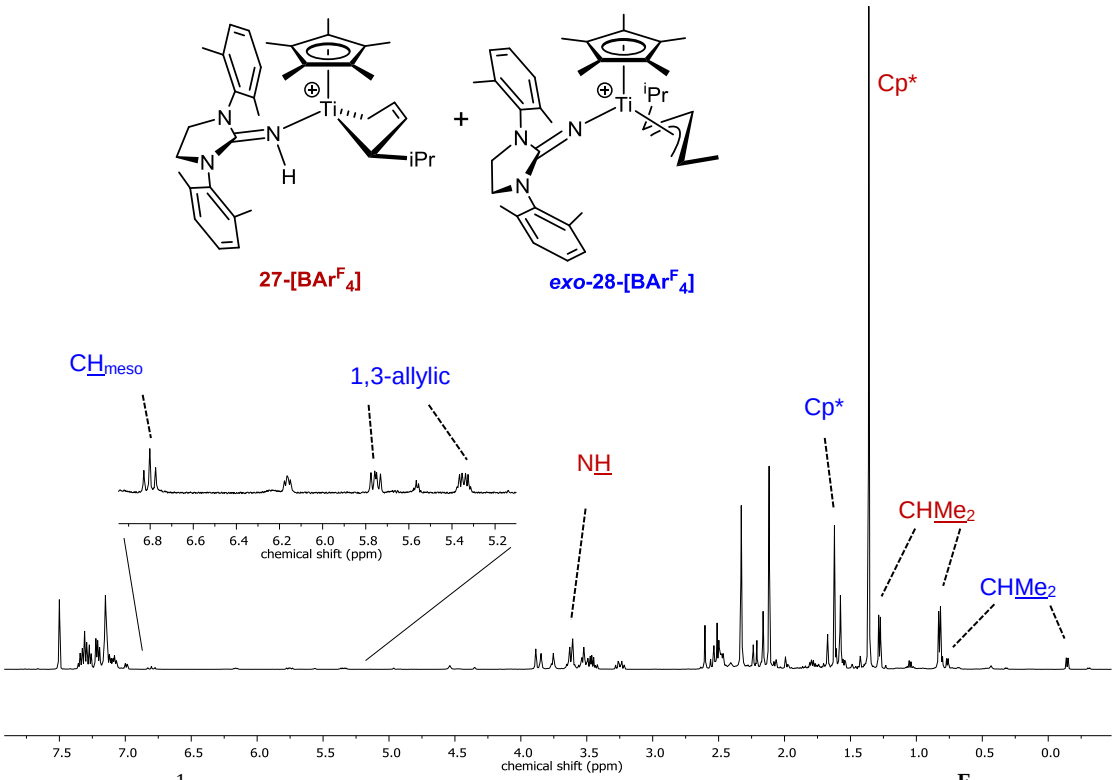

Figure 3.21. ^{1}H NMR spectrum (499.9 MHz, C_6D_5Br, 298 K) of **27-[BAr$^F_4$]** and ***exo*-28-[BAr$^F_4$]**.

A triplet at 6.81 ppm, assigned to the *meso* proton of ***exo*-28-[BAr$^F_4$]** correlates through-space to the Cp* moiety at 1.63 ppm. The former resonance also correlates through-bond to the 1,3-allylic protons at 5.79–5.72 and 5.36 ppm. Similarly, to ***exo*-25-[BAr$^F_4$]**, an upfield doublet at –0.14 ppm is assigned to one of the methyl groups of the isopropyl moiety of ***exo*-28-[BAr$^F_4$]** and was identified as the migrating methyl group with help of deuterium labelling studies.

Low temperature NMR studies of the reaction of **3.06** with 2,4-hexadiene and [Ph_3C][BAr$^F_4$] were conducted in order to investigate the diene formation further. At –30 °C, only the *endo,syn,syn*-η^3-allyl isomer (***endo*-28-[BAr$^F_4$]**) was observed, identified by a downfield triplet at 7.78 ppm, assigned to the *meso* proton. When slowly warming the reaction to –10 °C, an increased amount of ***endo*-28-[BAr$^F_4$]** was shown while simultaneously, ***exo*-28-[BAr$^F_4$]** started to appear and within 2 minutes at 0 °C, both allyl systems were observed in a 1:1 ratio (Figure 3.22). At 0 °C, the diene complex **27-[BAr$^F_4$]** began to appear, with decreasing amounts of ***endo*-28-[BAr$^F_4$]** while the amount of ***exo*-28-[BAr$^F_4$]** continued to increase. The immediate observation of the *endo,syn,syn*-η^3-allyl isomer (***endo*-28-[BAr$^F_4$]**) agrees with the

observation made for **1.56** and further supports that **Insertion A** is favoured over **Insertion B** (Figure 3.19). The *exo*,*syn*,*syn*-η^3-allyl isomer (***exo*-28-[BAr$^F_4$]**) is then either observed due to slow insertion of the conjugated diene into the Ti–Me bond (**Insertion B**) or by interconversion of the *endo*,*syn*,*syn*-η^3-allyl (*vide supra*). This suggests that ***endo*-28-[BAr$^F_4$]** is the kinetic product, while the *exo*,*syn*,*syn*-η^3-allyl isomer (***exo*-28-[BAr$^F_4$]**) is the thermodynamically favoured product supported by its prevalent nature at room temperature.

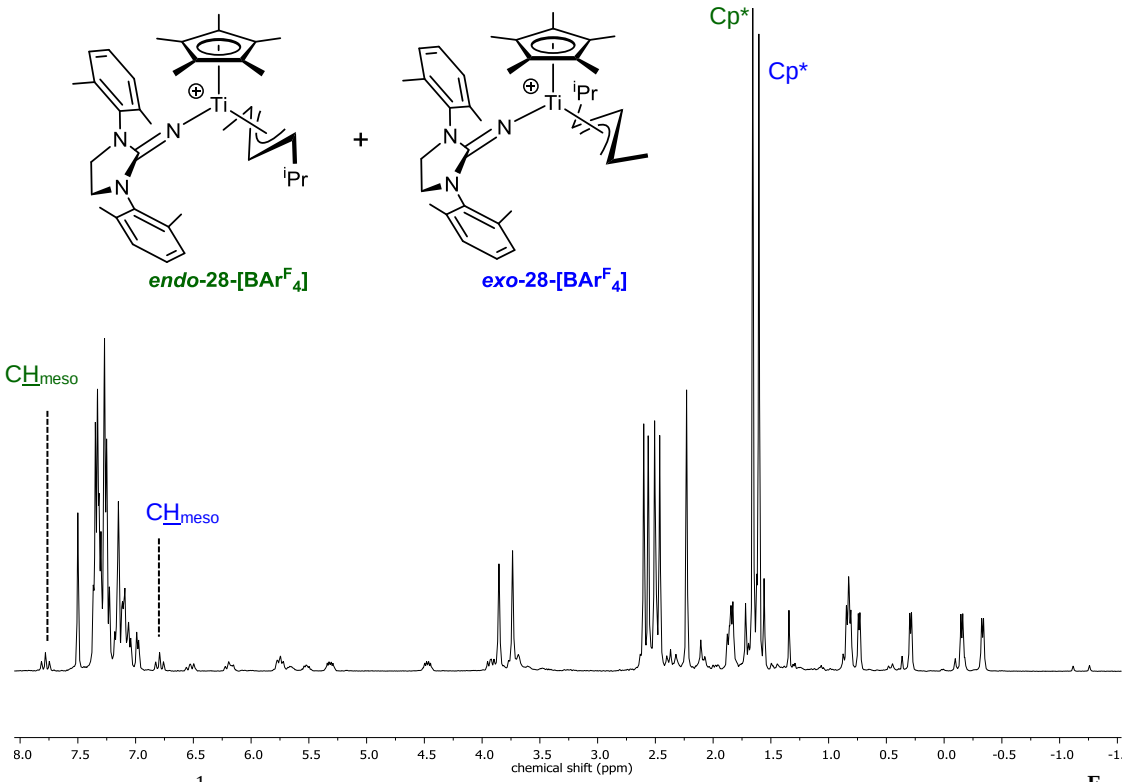

Figure 3.22. ^{1}H NMR spectrum (400.2 MHz, C_6D_5Br, 273 K) of ***endo*-28-[BAr$^F_4$]** and ***exo*-28-[BAr$^F_4$]**.

Changing the electronic and steric requirements simultaneously, in comparison to Cp*Ti{NCN(Dipp)$CH_2C_6H_4$}Me_2 **(3)**, resulted in change of ratio of the cationic allyl-complexes compared the cationic diene complex. The reaction with complex **1.58** gave the *endo*,*syn*,*syn*-η^3-allyl (***endo*-25-[BAr$^F_4$]**) as the major product. This is surprising, as the nitrogen on the guanidinate is more basic, which should more readily facilitate H-migration and therefore form the diene complex. Changing the substitution on the two nitrogen atoms led to the observation of **27-[BAr$^F_4$]** as major product. However, the *exo*,*syn*,*syn*-η^3-allyl isomer (***exo*-28-[BAr$^F_4$]**) was present (and

persisted) at room temperature which is in stark contrast to observations made for the reaction of the [Cp*Ti{NCN(Dipp)$CH_2C_6H_4$}Me][BAr^F_4] (**5-[BAr^F_4]**) with 2,4-hexadiene (*vide supra*).

3.5 Polymerisation studies

Co-polymerisation of ethylene and propylene with complexes Cp*Ti{NCN(Dipp)$CH_2C_6H_4$}Me_2 (**3**) and [Cp*Ti{NCN(Dipp)$CH_2C_6H_4$}{η-$CH_2(CH)_3$Et}][BAr^F_4] (**16-[BAr^F_4]**) were performed in a small-scale batch reactor under industrially relevant conditions at ARLANXEO, The Netherlands. This allowed direct comparison of the productivity and the resulting polymer of the *in situ* activated dimethyl complex and the preactivated cationic diene complex (**5-[BAr^F_4]** and **16-[BAr^F_4]**, respectively). A large excess of triisobutyl aluminium (TiBA) was used ([Al]:[Cat] = 4500:1, where [Al] is the relative concentration of the aluminium metal centres, and [Cat] is the precatalyst concentration) simultaneously with two equivalents of BHT-H per aluminium centre. BHT-H can react with TiBA to give $(BHT)_2Al(^iBu)$ which acts as an innocent scavenger of any trace amounts of impurities present in the reactor (Section 1.6). One equivalent of [Ph_3C][BAr^F_4] was used as cocatalyst. The composition of the resulting polymer was analysed using FT-IR and the molecular weight and polydispersity index (PDI) were obtained from GPC measurements (Chapter 6). The polymerisation data of Cp*Ti{NCN(Dipp)$CH_2C_6H_4$}{η-EtCH$(CH)_2CH_2BAr^F_3$} (**14**) is also mentioned for comparison purpose (Chapter 2).

Both, the dimethyl precatalyst **3** and the cationic diene complex **16-[BAr^F_4]**, show high productivity in the co-polymerisation of ethylene and propylene (Table 3.3). Greater sensitivity towards decomposition is expected of the preactivated complex **16-[BAr^F_4]** which can account for the discrepancy in productivity observed for **16-[BAr^F_4]** and **3**. Furthermore, the allyl species is the expected initial active polymerisation species, as shown by DFT calculations (*vide infra*). Therefore the diene complex has to undergo reversible H-migration to regenerate the allyl intermediate leading to potential longer induction time than for the *in situ* activated complex **3**, which may give lower productivity overall. This could also explain the higher productivity observed for **14** compared to **16-[BAr^F_4]**, as **14** does not have to undergo rearrangement to another intermediate before polymerisation can take place.

Table 3.3. EPM co-polymerisation results for Cp*Ti{NCN(Dipp)$CH_2C_6H_4$}Me_2 (**3**) and [Cp*Ti{HNCN(Dipp)$CH_2C_6H_4$}{$CH_2(CH)_3Et$}]-[$BAr^F{}_4$] (**16-[$BAr^F{}_4$]**) and Cp*Ti{NCN(Dipp)$CH_2C_6H_4$}{η^3-$EtCH(CH)_2CH_2BAr^F{}_3$} (**14**).

Entry[a]	Precatalyst	Cocatalyst	Productivity (kg mol^{-1} Ti h^{-1} bar^{-1})	C_2 (wt%)	C_3(wt%)	M_n (g mol^{-1})	M_w (g mol^{-1})	PDI
1	**3**	TiBA / $[Ph_3C][BAr^F{}_4]$	102,800	60.6	39.4	594,000	1,438,000	2.2
2	**16-[$BAr^F{}_4$]**	TiBA	60,800	65.5	34.5	688,000	1,498,000	2.2
3	**14**	TiBA	97,800	60.8	39.0	621,000	1,297,000	2.1

Polymerisation conditions. [a]T = 90 ºC, Pressure = 7 bar, Cat loading = 0.1 μmol, [Al]:[Cat] = 4500, [Al]:[BHT-H] = 0.5, [Cat]:[B] = 1, 10 minute reaction time. Solvent = pentamethylheptane (1L), C_3/C_2 = 400/200 Nl/h.

Polymer characterisation. Polymer molecular weight and molecular weight distribution have been analysed with Freeslate Rapid GPC in 1,2,4-Trichlorobenzene against PS standards. The average composition have been determined *via* transmission IR spectroscopy on a pressed polymer film.

The composition of the resulting polymer is very similar for **16-[BAr$^{F}_{4}$]** and **3**. This may suggest, that after the first insertion of α-olefin into the metal-alkyl bond, the active propagation species of **3** and **16-[BAr$^{F}_{4}$]** are identical. To investigate this matter further, DFT calculations on the first and consecutive insertion were conducted by Professor Philip Mountford (Figure 3.23). The computational results show that ethylene can be coordinated to the titanium centre from the η^1-allyl intermediate (**Int2**$^{+}$), originating from ***exo*-J**$^{+}$, followed by the insertion of the ethylene unit into the η^1-allyl unit (**TS5**, Figure 3.24). A relative Gibbs free energy of less than 20 kcal mol^{-1} suggests that the insertion is energetically accessible. Furthermore, the DFT calculations show that the 2nd insertion into the Ti–C bond gives a more stable complex (**Q**$^{+}$) indicating that propagation readily takes place (Figure 3.23).

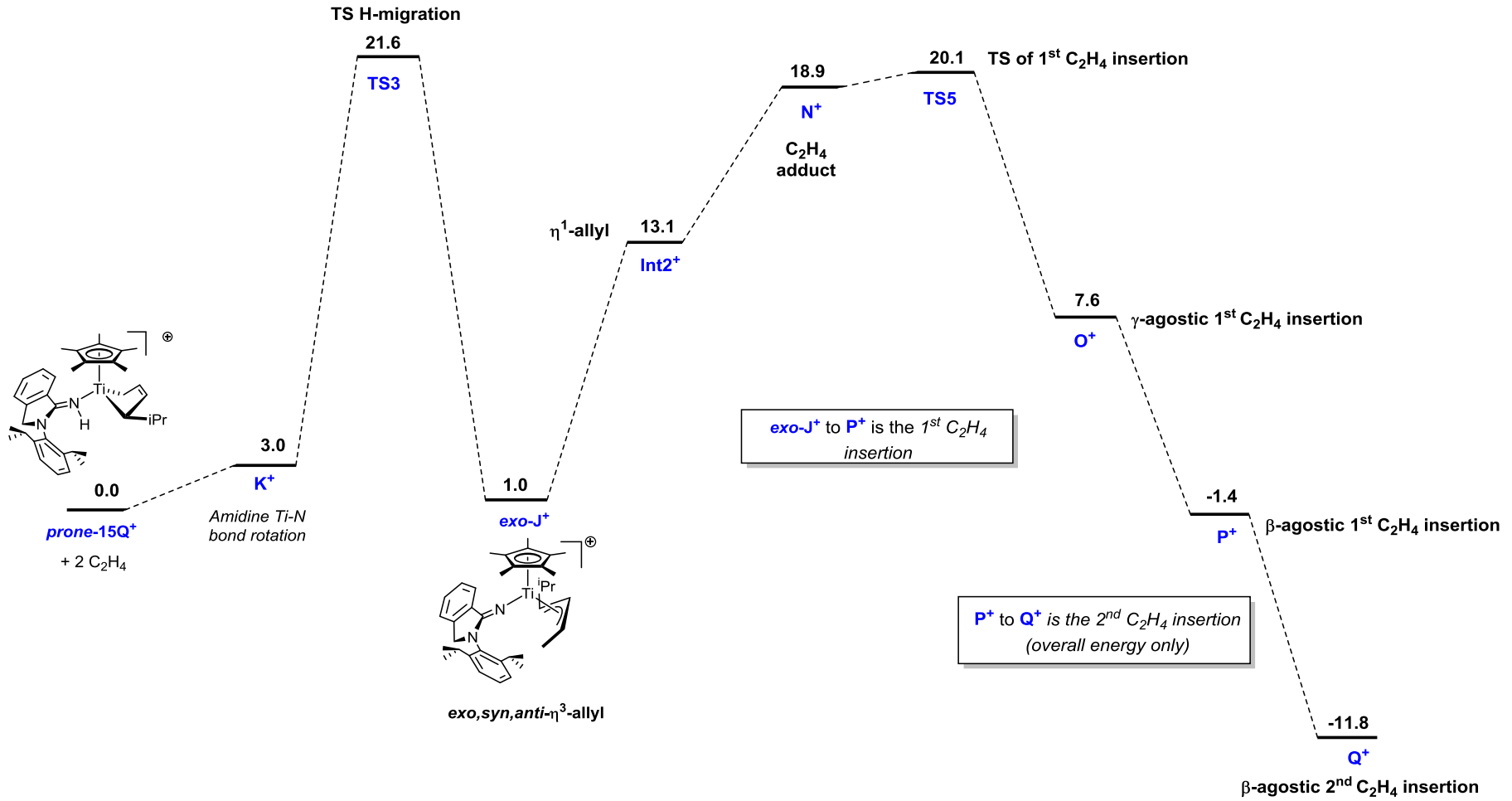

Figure 3.23. DFT reaction pathway of first (and second) insertion of ethylene, starting from ***prone*-15Q$^+$**. Gibb free energies (kcal mol^{-1}, T = 298 K) for minima, maxima and transition states (labelled **TSx**) are shown in bold relative to ***prone*-15Q$^+$**.

The transition state of the insertion into the Ti–C bond of $\mathbf{N}^+$ is shown in Figure 3.24, alongside the stable β-agostic insertion product $\mathbf{P}^+$. The change from $\mathbf{N}^+$ in **TS5** is shown by the lengthening of the Ti(1)–C(1) bond from 2.103 to 2.183 Å, respectively, and by the increase in the bond length of C(2)–C(3) to 1.399 Å from 1.350 Å. Comparing $\mathbf{Int2}^+$ with $\mathbf{P}^+$ shows analogous behaviour; The Ti(1)–C(2)/C(3) bond distance is similar in both cases, evaluated as 2.099 Å for $\mathbf{Int2}^+$ and 2.050 Å for $\mathbf{P}^+$. A β-agostic interaction is also observed in the η^1-allyl intermediate ($\mathbf{Int2}^+$), where in this case H(1) is based on the C(1) of the allyl and the distance to titanium is 2.137 Å.

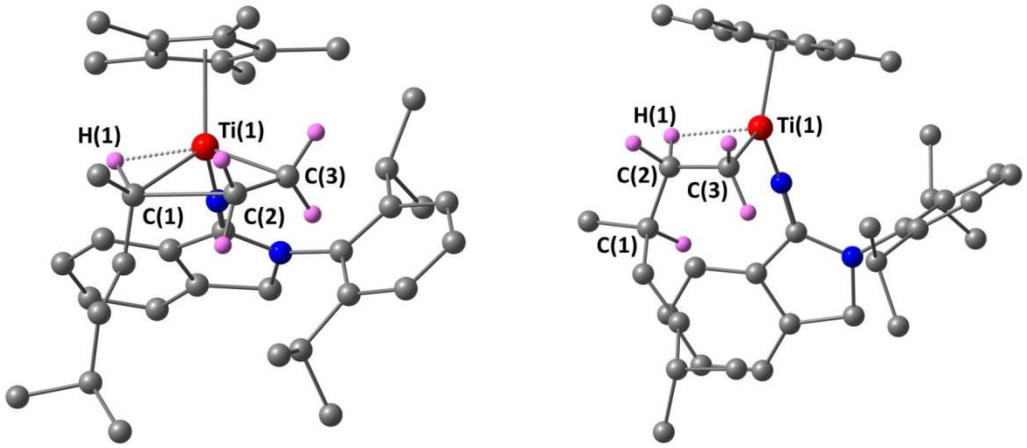

TS5 $\mathbf{P}^+$

Figure 3.24. Transition state **TS5** (left) for C_2H_4 insertion into the Ti-CH(Me)C(H)C(H)^{i}Pr bond of $\mathbf{Int2}^+$ and the corresponding β-agostic product $\mathbf{P}^+$ (right). Most H atoms omitted. Selected distances (Å) and angles (^{o}) for **TS5**: Ti(1)–C(1) 2.183, Ti(1)–H(1) 1.908, C(1)–C(2) 2.231, C(2)–C(3) 1.399, Ti(1)–C(3) 2.206, Ti(1)–C(1)–H(1) 60.9; for $\mathbf{P}^+$: Ti(1)–C(3) 2.050, Ti(1)–H(1) 1.969, C(3)-C(2) 1.501, Ti(1)–C(3)–C(2) 83.1.

The second insertion product, $\mathbf{Q}^+$, shows analogous interactions with the alkyl chain and the metal centre, compared to the first insertion product $\mathbf{P}^+$. However, one major difference is that $\mathbf{Q}^+$ (Figure 3.25) is also stabilised by a further agostic interaction with one of the methyl groups of the Dipp fragment (Ti(1)–H(2) = 2.166 Å), as observed previously for $\mathbf{5Q}^+$. The difference observed is potentially due to the longer chain, pushing the Dipp group towards the metal centre in $\mathbf{Q}^+$.

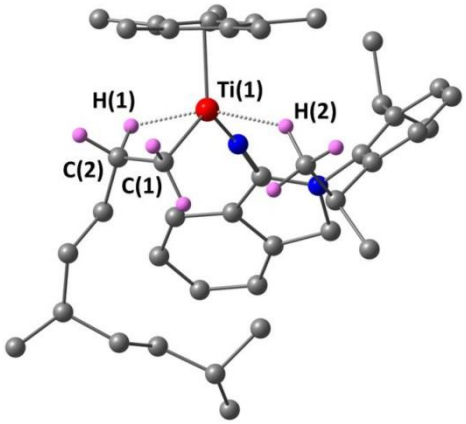

Figure 3.25. The β-agostic product $\mathbf{Q}^+$ after the second C_2H_4 insertion step. Most H atoms omitted. Selected distances (Å) and angles (°): Ti(1)–C(1) 2.080, Ti(1)–H(1) 1.916, Ti(1)–H(2) 2.166, C(1)–C(2) 1.494, Ti(1)–C(1)–C(2) 82.5.

Alongside the EP co-polymerisation experiments and DFT mechanistic calculations, 1-hexene polymerisation studies of **5-[BAr$^F_4$]**, **7-[BAr$^F_4$]** and **15-[BAr$^F_4$]** (Figure 3.26) were performed to allow further investigation into the polymer end-groups. On the NMR tube scale, the cationic complexes were generated *in situ* in C_6D_5Br and various amounts of 1-hexene added at room temperature. The NMR tube was vigorously shaken and a ^1H NMR spectrum was recorded within 5 minutes.

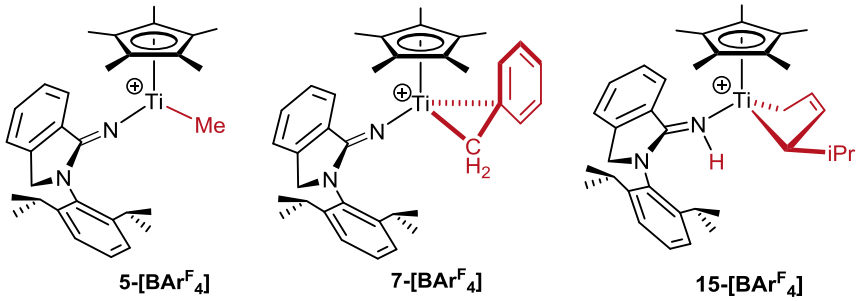

Figure 3.26. Complexes [Cp*Ti{NCN(Dipp)$CH_2C_6H_4$}Me][BAr$^F_4$] (**5-[BAr$^F_4$]**), [Cp*Ti{NCN(Dipp)$CH_2C_6H_4$}CH_2Ph][BAr$^F_4$] (**7-[BAr$^F_4$]**) and [Cp*Ti{HNCN-(Dipp)$CH_2C_6H_4$}{η-$CH_2(CH)_3{}^iPr$}][BAr$^F_4$] (**15-[BAr$^F_4$]**). [BAr$^F_4$]$^-$omitted for clarity.

In all cases, resonances corresponding to poly(1-hexene) were observed, showing immediate consumption of 1-hexene. The resulting polymers were isolated to allow chain end-group analysis by NMR and the determination of molecular weight and PDI by GPC measurements (Table 3.4). All three cations result in a mono-modal distribution of poly(1-hexene) with a PDI close to 2, which is indicative of non-living

behaviour (or other non-ideal characteristics). Interestingly, higher amounts of 1-hexene led to broader PDIs in all cases. **5-[BAr$^F_4$]** with 200 and 300 equivalents of 1-hexene did not give significant increase of molecular weight, being smaller than expected. The same trend is observed for **7-[BAr$^F_4$]** and **15-[BAr$^F_4$]**. This could be attributed to steady chain transfer events, such as β-H elimination, since the productivity stays constant for **7-[BAr$^F_4$]** and **15-[BAr$^F_4$]**. On the other hand, **5-[BAr$^F_4$]** shows an irregular dependence of productivity on [1-hexene] as judged by the isolated poly(1-hexene).

Table 3.4. 1-hexene polymerisation results of [Cp*Ti{NCN(Dipp)$CH_2C_6H_4$}Me]-[BAr^F_4] (**5-[BAr$^F_4$]**), [Cp*Ti{NCN(Dipp)$CH_2C_6H_4$}CH_2Ph][BAr^F_4] (**7-[BAr$^F_4$]**) and [Cp*Ti{HNCN(Dipp)$CH_2C_6H_4$}{η-$CH_2(CH)_3{}^iPr$}][BAr^F_4] (**15-[BAr$^F_4$]**).[a]

Pre-catalyst[a]	Equiv. of 1-hexene	Yield (g)	Productivity (kg mol^{-1} Ti mol^{-1} 1-hexene h^{-1})	Calculated M_n[b] (g mol^{-1})	Observed M_n (g mol^{-1})	M_w/M_n
5-[BAr$^F_4$]	25	0.020	97,800	2,120	4,670	2.5
5-[BAr$^F_4$]	50	0.050	122,200	4,220	5,110	2.3
5-[BAr$^F_4$]	100	0.120	146,600	8,430	6,090	2.0
5-[BAr$^F_4$]	200	0.160	97,800	16,850	7,630	2.6
5-[BAr$^F_4$]	300	0.170	69,200	25,260	6,530	3.1
7-[BAr$^F_4$][b]	25	0.020	166,200	2,200	4,750	1.9
7-[BAr$^F_4$][b]	50	0.040	166,200	4,300	6,020	2.1
7-[BAr$^F_4$][b]	100	0.080	166,200	8,510	7,950	2.0
7-[BAr$^F_4$][b]	200	0.150	155,800	16,920	12,240	2.0
7-[BAr$^F_4$][b]	300	0.200	138,500	25,340	8,900	3.0
15-[BAr$^F_4$]	25	0.020	97,800	2,200	14,630	1.8
15-[BAr$^F_4$]	50	0.040	97,700	4,310	16,470	2.2
15-[BAr$^F_4$]	100	0.120	146,600	8,510	16,230	2.2
15-[BAr$^F_4$]	200	0.190	116,100	16,930	10,260	2.6
15-[BAr$^F_4$]	300	0.300	122,200	25,350	9,270	3.3

[a]*Polymerisation conditions*. Cat loading = 9.9 μmol [b](Cat loading = 7.6 μmol), solvent = C_6D_5Br, total solution volume: 0.5 mL, room temperature, time = 5 minutes. Molecular weight measurements obtained with GPC. [b] M_n = [(equiv. of 1-hexene × M_w 1-hexene) + H + R], R = alkyl chain.

However, the ^{1}H NMR monitoring of all three catalyst confirmed that all of the 1-hexene was consumed within 5 minutes even at [Ti]:[1-hexene] = 1 : 300. Therefore, within this range, all of the catalysts are equally productive.

Overall, the observed molecular weight of poly(1-hexene) is higher for **15-[BAr$^{F}_{4}$]** compared to mono-alkyl cations. A potential reason for this observation is that fewer titanium centres are active in the polymerisation of 1-hexene at the start (i.e. a longer overall induction period) with complex **15-[BAr$^{F}_{4}$]**. DFT calculations have shown that the rate of initiation for **15-[BAr$^{F}_{4}$]** is controlled by **TS3** (21.6 kcal mol^{-1}, Figure 3.23) and the insertion of the α-olefin (calculated for ethylene) is controlled by **TS5** (20.1 kcal mol^{-1}). In contrast, the C_2H_4 insertion into the Ti–Me^{+} cation (**5-[BAr$^{F}_{4}$]**) has a computed $\Delta G^{\ddagger}$ of 17 kcal mol^{-1}. This suggests that the initiation is more efficient for the mono-methyl cation and therefore more [Ti] centres are involved in the catalytic process. Once all the centres get underway, the usual chain transfer events are taking place (>200 equiv.) resulting in a more similar behaviour.

In the case of **15-[BAr$^{F}_{4}$],** the decay of the complex upon addition of various amounts of 1-hexene can be monitored (Figure 3.27). This is not possible for **5-[BAr$^{F}_{4}$]** and **7-[BAr$^{F}_{4}$]** because of the complexity of the resulting ^{1}H NMR spectrum. After the consumption of 25 equivalents of 1-hexene, 81% of **15-[BAr$^{F}_{4}$]** is still observed (Figure 3.27). After 50 equivalents of 1-hexene, 58% of the cationic diene complex still present and after 100 equivalents of 1-hexene, only 18% of the original complex is seen in the ^{1}H NMR spectrum. The 82% now participating in the polymerisation process is likely to be a Ti–H species or polymeryl bearing complexes. Overall, this strengthens the suggestion that not all titanium centres participate in the polymerisation of 1-hexene at lower equivalents in case of **15-[BAr$^{F}_{4}$]**, leading to longer chains and to higher molecular weights (*vide infra*).

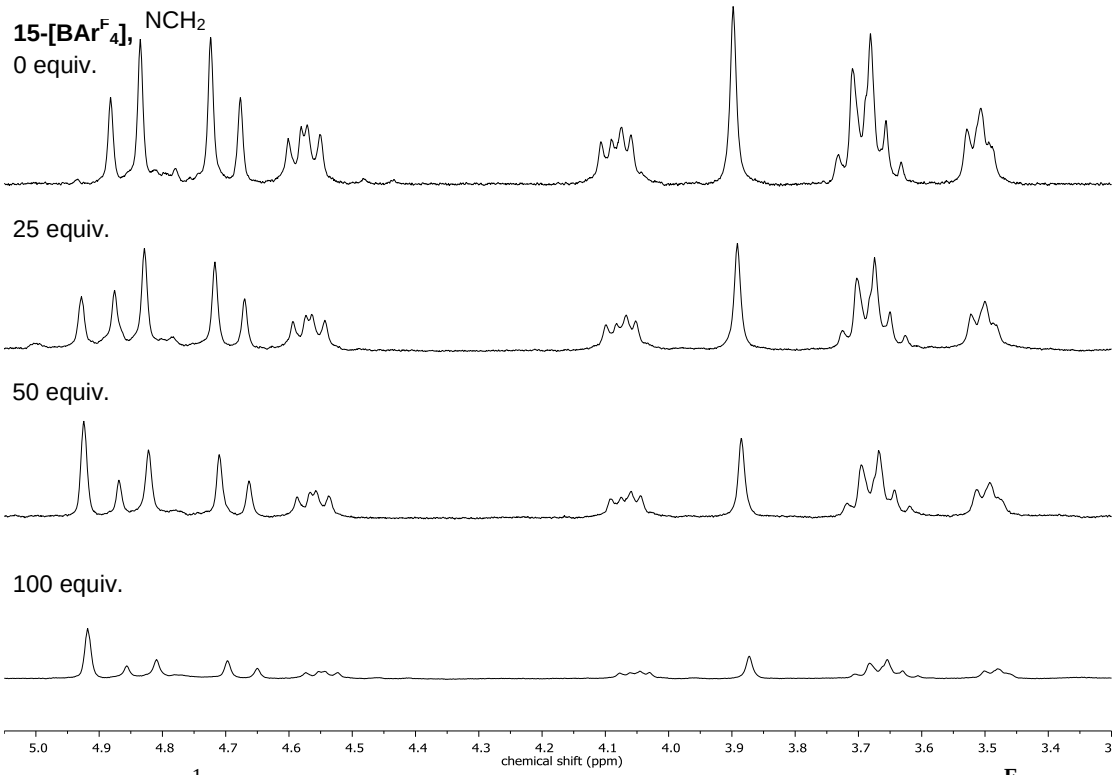

Figure 3.27. ^{1}H NMR spectra (400.2 MHz, C_6D_5Br, 298 K) of **15-[BAr^F_4]** with various amounts of 1-hexene.

NMR analysis of the atactic poly(1-hexene) formed showed the expected signals of the –Me group, the methylene protons –CH_2– and the protons bonded to a tertiary carbon of the polymer chains between 0.8 to 2.1 ppm (Figure 3.28).[23]

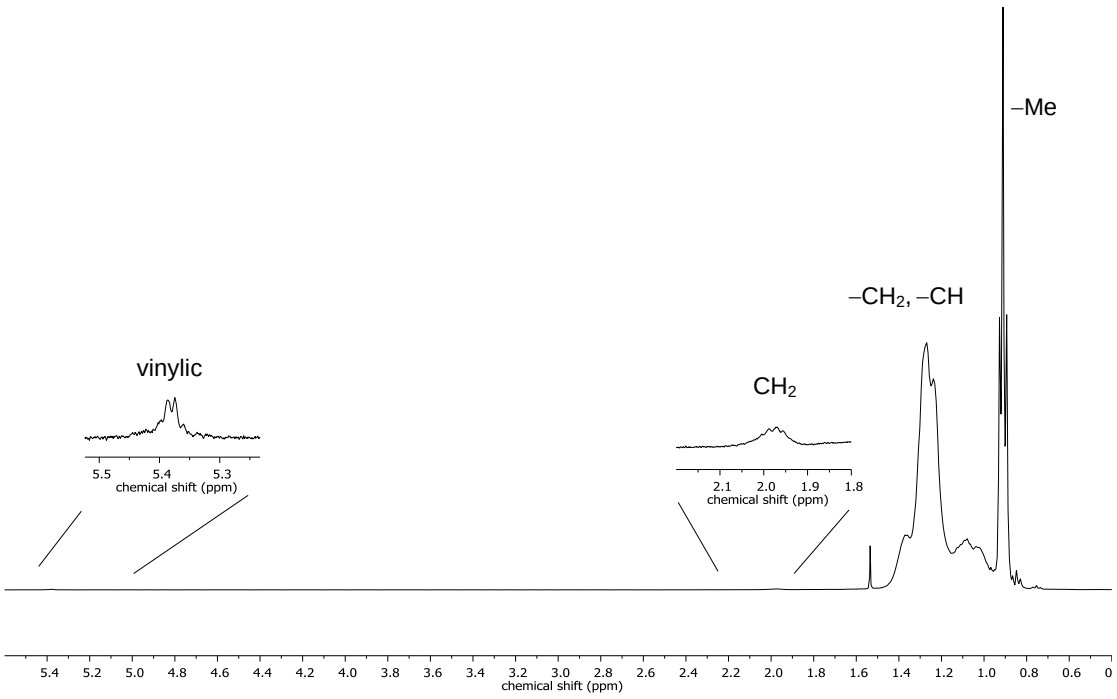

Figure 3.28. ^{1}H NMR spectrum (400.2 MHz, $CDCl_3$, 298 K) of poly(1-hexene).

The other regions of the NMR spectrum provided further insight into the chain end-groups. The poly(1-hexene) formed with these three half-sandwich systems showed only di-substituted vinylene end groups. The vinylic protons were assigned to the multiplet at 5.43–5.34 ppm with corresponding carbon resonances at 128.1 and 131.8 ppm (Figure 3.28). The downfield shift confirmed the vinylic character of this moiety.

To obtain these chain end-groups, the termination reaction ought to mainly occur at the 2,1-inserted chain-end *via* β-H elimination to a monomer or the metal centre (Equation 3.6). This termination mechanism is known to be the main termination pathway in polymerisation of 1-hexene with a range of metallocene catalysts.[24, 25]

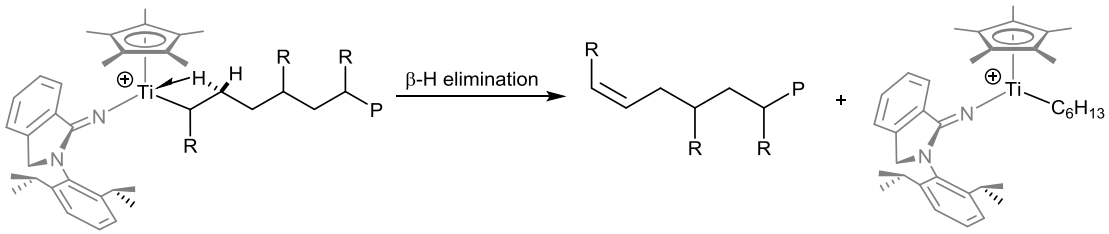

Equation 3.6

The alkyl/aryl groups bonded to the metal centre before the first insertion of monomer account for another chain end-group. In the case of **7-[BAr$^F_4$]**, the chain end-group is a benzyl group, where the aromatic moiety appears in a part of the ^{1}H NMR spectrum which is not obscured by the resulting polymer. The ^{1}H NMR spectrum in CD_2Cl_2 shows a triplet at 7.16 ppm, assigned to the *ortho*-protons and a multiplet at 7.08–7.05 ppm of the *para*- and *meta*-protons, verifying the presence of the benzyl group in the polymer chain. **5-[BAr$^F_4$]** and **15-[BAr$^F_4$]**, however, only consist of –CH_2, –Me and –CH groups that are obscured by the polymer. Therefore, the polymerisation of 1-hexene was repeated with the deuterium labelled analogues **5-[BAr$^F_4$]-*d*$_3$** and **15-[BAr$^F_4$]-*d*$_3$**. The deuterium NMR clearly displays the presence of a labelled methyl group (CD_3) in the isolated polymer in both cases. This shows that 1-hexene does insert into the titanium allyl bond.

The affinity of the mono-methyl cation **5-[BAr$^F_4$]** for polymerising 1-hexene or to form the cationic complex **15-[BAr$^F_4$]** was investigated. The simultaneous addition of 1-hexene (100 equiv.) and 2,4-hexadiene (5 equiv.) to preactivated complex **5-[BAr$^F_4$]** led to formation of poly(1-hexene) and unreacted 2,4-hexadiene starting

material. Addition of 2,4-hexadiene to the reaction mixture after 1-hexene (30 equiv.) was polymerised, led to 'trapping' of unreacted **5-[BAr$^F_4$]** to give 34% of **15-[BAr$^F_4$]**. This demonstrated that in the polymerisation of 30 equivalents of 1-hexene, 66% of **5-[BAr$^F_4$]** was involved, which is substantially higher participation than previously observed for **15-[BAr$^F_4$]** (*vide supra*).

3.6 Addition of Lewis bases to 15-[BAr$^F_4$] and 16-[BAr$^F_4$]

Addition of excess Lewis bases, such as Ph_3PO to **15-[BAr$^F_4$]** and **16-[BAr$^F_4$]** resulted in evolution of free diene, *viz*. (*E*)-5-methylhexa-1,3-diene and (*E*)-1,3-hexadiene, respectively. Concomitantly, a broad peak at *ca*. 11 ppm appears in the ^{1}H NMR spectrum, suggestive of a paramagnetic species. No other species could be identified. The NMR tube scale reaction of three equivalents of Ph_3PO with **15-[BAr$^F_4$]** at −30 ºC showed the formation of a new titanium species (**29-[BAr$^F_4$]**). The amidine is no longer coordinating to the metal centre, exemplified by the loss of diastereotopicity of the NCH_2 moiety. Furthermore, no sharp NH resonance is observed (Figure 3.29).

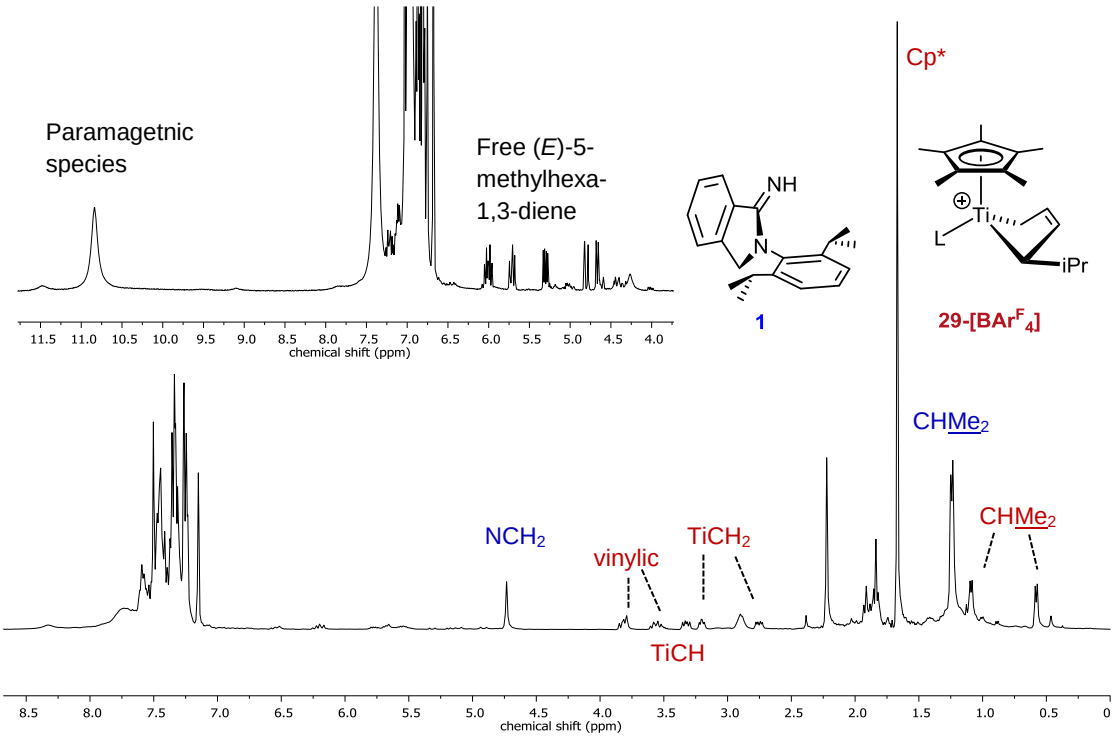

Figure 3.29. ^{1}H NMR spectrum (499.9 MHz, C_6D_5Br, 243 K) of [Cp*Ti{η-$CH_2(CH)_3{}^iPr$}($OPPh_3$)][BAr$^F_4$] (**29-[BAr$^F_4$]**) and HNCN(Dipp)$CH_2C_6H_4$ (**1**). Inset: ^{1}H

NMR spectrum (499.9 MHz, C_6D_5Br, 298 K) showing paramagnetic species at 11 ppm.

Through-space correlation of the vinylic protons at 3.85–3.79 ppm and 3.60–3.51 ppm of the diene moiety to the Cp* fragment provides evidence for coordination of the two aforementioned moieties to the metal centre. The $^{31}P\{^1H\}$ NMR spectrum shows a major peak at 53.1 ppm, suggesting coordination of the Lewis base (*vide supra*). However, other minor resonances are observed as well, implying the reaction does not proceed cleanly. Once the reaction mixture was brought to room temperature, free diene and a paramagnetic species were observed (*vide supra*).

Addition of a different amidine ligand, $HNC(Ph)N^iPr_2$ (**3.06**), to **15-[BAr$^F_4$]** gives (*E*)-5-methylhexa-1,3-diene as a major product, while **15-[BAr$^F_4$]** is observed alongside the newly formed complex $[Cp^*Ti\{HNC(Ph)N^iPr_2\}\{CH_2(CH)_3{}^iPr][BAr^F_4]$ (**21-[BAr$^F_4$]**). This shows the protonated amidine is less basic and can be displaced by other donor atoms. No interconversion from the diene to the allyl upon addition of other donor ligands is observed.

3.7 Summary

This Chapter has described the synthesis and characterisation of a range of cationic κ^1-amidinate and κ^1-guanidinate titanium diene and allyl complexes. Low temperature NMR spectroscopy and DFT calculations were used in order to identify the reaction pathway from the mono-methyl cation **5-[BAr$^F_4$]** to the final observed cationic diene complex **15-[BAr$^F_4$]**. The low temperature ^1H NMR spectrum reveals the presence of the *endo*,*syn*,*syn*-η^3- and *exo*,*syn*,*syn*-η^3-allyl complexes. The computational studies showed the conversion of the *endo*,*syn*,*syn*-η^3allyl to the *exo*,*syn*,*anti*-η^3-allyl from where C–H bond activation can take place to give the experimentally observed final product. Complexes bearing different κ^1-amidinate supporting ligands showed the steric and electronic influence on the diene formation. A more electron withdrawing aryl group led to the observation of the *endo*- and *exo*-allyl at room temperature, alongside the diene complex as the major product. Complexes with κ^1-guanidinate supporting ligands showed a distinct difference in the relative ratio of the allyl complexes and the diene complex, compared to metal complexes with κ^1-amidinate

supporting ligands. Despite possessing more basic nitrogen, C–H bond activation did not take place readily for complex **1.56**. The co-polymerisation of ethylene and propylene showed a good productivity for complex **16-[BAr$^{F}_{4}$]**, however, slightly lower productivity compared to the dimethyl complex (**3**) and the previously synthesised zwitterionic allylic species **14**. The difference could be related to a longer induction period for **16-[BAr$^{F}_{4}$]**, as computational studies have shown that the diene converts to the allyl system before ethylene inserts into the Ti–C bond. Despite the lower productivity, the resulting polymer did not differ greatly in composition and molecular weight distribution between **3** and **16-[BAr$^{F}_{4}$]**. Further investigation in the chain end-groups from the polymerisation of 1-hexene of **16-[BAr$^{F}_{4}$]** and **5-[BAr$^{F}_{4}$]** showed incorporation of the diene into the polymer chain, as shown with deuterium labelled NMR studies. Attempted reactions to reverse diene coordination to allyl coordination by addition of Lewis base resulted in displacement of the amidine at low temperatures.

3.8 References

1. R. Spitz, P. Masson, C. Bobichon and A. Guyot, *Makromol. Chem.*, 1988, **189**, 1043-1050.
2. A. Guyot, R. Spitz, J.-P. Dassaud and C. Gomez, *J. Mol. Catal.*, 1993, **82**, 29-36.
3. D. E. Richardson, N. G. Alameddin, M. F. Ryan, T. Hayes, J. R. Eyler and A. R. Siedle, *J. Am. Chem. Soc.*, 1996, **118**, 11244-11253.
4. D. Feichtinger, D. A. Plattner and P. Chen, *J. Am. Chem. Soc.*, 1998, **120**, 7125-7126.
5. J. J. W. Eshuis, Y. Y. Tan, J. H. Teuben and J. Renkema, *J. Mol. Catal.*, 1990, **62**, 277-287.
6. J. J. W. Eshuis, Y. Y. Tan, A. Meetsma, J. H. Teuben, J. Renkema and G. G. Evens, *Organometallics*, 1992, **11**, 362-369.
7. P. M. Margl, T. K. Woo, P. E. Blöchl and T. Ziegler, *J. Am. Chem. Soc.*, 1998, **120**, 2174-2175.
8. P. M. Margl, T. K. Woo and T. Ziegler, *Organometallics*, 1998, **17**, 4997-5002.
9. D. E. Babushkin and H. H. Brintzinger, *J. Am. Chem. Soc.*, 2010, **132**, 452-453.

10. D. E. Babushkin, V. N. Panchenko and H. H. Brintzinger, *Angew. Chem. Int. Ed.*, 2014, **53**, 9645-9649.
11. V. N. Panchenko, D. E. Babushkin and H. H. Brintzinger, *Macromol. Rapid Commun.*, 2015, **36**, 249-253.
12. R. Scott, *DPhil Thesis*, University of Oxford, 2013.
13. G. Jiménez Pindado, M. Thornton-Pett, M. B. Hursthouse, S. J. Coles and M. Bochmann, *J. Chem. Soc., Dalton Trans.*, 1999, 1663-1668.
14. T. W. Graham, J. Kickham, S. Courtenay, P. Wei and D. W. Stephan, *Organometallics*, 2004, **23**, 3309-3318.
15. U. Piantini, W. Von Philipsborn, A. Salzer and B. Buchmann, *Helv. Chim. Acta*, 1987, **70**, 1487-1506.
16. F. Sauriol, J. F. Sonnenberg, S. J. Chadder, A. F. Dunlop-Brière, M. C. Baird and P. H. M. Budzelaar, *J. Am. Chem. Soc.*, 2010, **132**, 13357-13370.
17. B. Laurent, R. Shailesh, O. John A., C. Claire, T. Francis, D. C. André and F. Jean, *Eur. J. Inorg. Chem.*, 2000, **2000**, 2523-2532.
18. N. Solin and K. J. Szabó, *Organometallics*, 2001, **20**, 5464-5471.
19. H. Yasuda, K. Tatsumi and A. Nakamura, *Acc. Chem. Res.*, 1985, **18**, 120-126.
20. H. Yasuda and A. Nakamura, *Angew. Chem. Int. Ed. Engl.*, 1987, **26**, 723-742.
21. D. D. Devore, F. J. Timmers, D. L. Hasha, R. K. Rosen, T. J. Marks, P. A. Deck and C. L. Stern, *Organometallics*, 1995, **14**, 3132-3134.
22. G. Erker, J. Wicher, K. Engel, F. Rosenfeldt, W. Dietrich and C. Krueger, *J. Am. Chem. Soc.*, 1980, **102**, 6344-6346.
23. I. Kim, J.-M. Zhou and H. Chung, *J. Polym. Sci., Part A: Polym. Chem.*, 2000, **38**, 1687-1697.
24. N. Kawahara, J. Saito, S. Matsuo, H. Kaneko, T. Matsugi, Y. Toda and N. Kashiwa, *Polymer*, 2007, **48**, 425-428.
25. K. Il, Z. Jia-Min and C. Hoeil, *J. Polym. Sci., Part A: Polym. Chem.*, 2000, **38**, 1687-1697.

Chapter Four

Synthesis, characterisation and reactivity of aminopyridinato- and κ^2-amidinate titanium complexes

4.1 Overview

Aminopyridinato[1-5] and mono- and bis-κ^2-amidinate[6-10] complexes are known to polymerise α-olefins (Section 1.5.3). Recently, Kretschmer *et al*. have shown that the complexes $(Ap^x)TiCl_3(NHMe_2)$ (**1.76**–**1.78**) polymerise ethylene, propylene and ENB.[5] It was of interest to this project, to investigate the influence on the activity in EPM and EPDM polymerisation when replacing the Cp* moiety in complex $Cp^*Ti\{NC(Ph)N^iPr_2\}Cl_2$ (**1.71**) with either an aminopyridinato or κ^2-amidinate ligand. This Chapter describes the synthesis and characterisation of a series of κ^2-aminopyridinato, κ^2-amidinate and bis(κ^2-aminopyridinato) post-metallocene titanium complexes. The X-ray solid state structures of $(Ap^1)Ti\{NC(Ph)N^iPr_2\}Cl_2$ (**32**), $(Ap^2)Ti\{NC(Ph)N^iPr_2\}Cl_2$ (**33**), $(Ap^3)Ti\{NC(Ph)N^iPr_2\}Cl_2$ (**34**), $(Ap^1)Ti\{NCN(Dipp)CH_2C_6H_4\}(NHMe_2)Cl_2$ (**40**), $Ti\{NC(Ph)N^iPr_2\}$-$\{(NDipp)_2CMe\}Me_2$ (**51**) and $(Ap^1)_2TiCl_2$ (**55**) are described and structural parameters are discussed. The activation chemistry of the dialkyl complexes is also reported and a range of trapping agents is used to allow further investigation of the active species in polymerisation of α-olefins. The activity of the κ^2-amidinate and bis(κ^2-aminopyridinato) titanium complexes in the polymerisation of α-olefins is discussed.

4.2 Ligand synthesis

Collaborative research between the Mountford group and ARLANXEO has resulted in a wide range of dichloride or dialkyl κ^1-amidinate titanium complexes applied in EPDM polymerisation. The amidine relevant to this Thesis is *N*,*N*-diisopropylbenzimidamide. The silylated amidine (**4.01**) can react directly with titanium tetrachloride eliminating Me_3SiCl giving a wide range of Ti(+4) complexes, exemplified by **4.02** (Scheme 4.1).

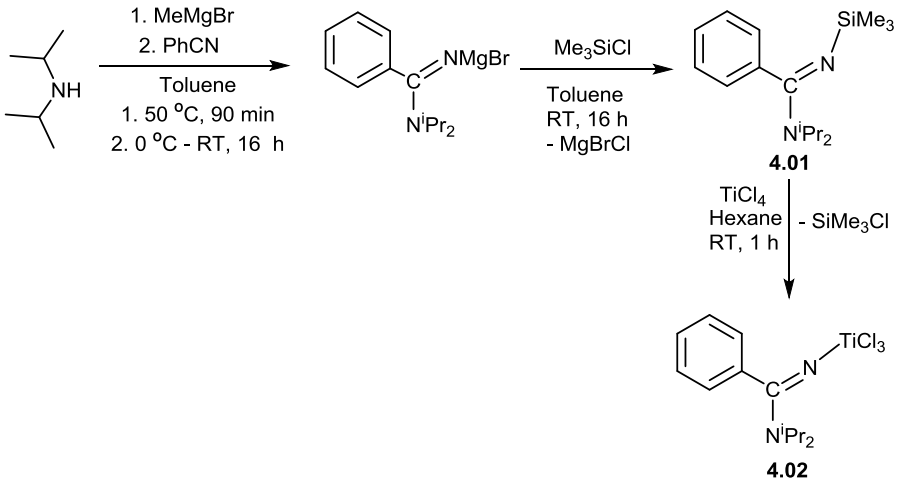

Scheme 4.1. Synthesis of a κ^1-amidine and complexation to titanium.

However, for more sterically crowded systems, such as bearing a Cp* moiety, this pathway did not prove successful. Instead, the parent amidine was reacted with Cp^*TiCl_3 in the presences of excess NEt_3 to trap the eliminated HCl (Chapter Two). This route was shown to be higher yielding in the synthesis of, for example, $Cp^*Ti\{NC(Ph)N^iPr_2\}Cl_2$ (**1.71**).

The aminopyridine compounds were synthesised according to literature procedures.[3, 4] A tri-substituted aryl Grignard was formed *in situ*, and in the presence of catalytic amounts of [$NiBr_2$(dme)] and tricyclohexylphosphine; the corresponding aryl bromo-pyridine was formed as a pale yellow solid. The aryl bromo-pyridine underwent a Buchwald-Hartwig amination in the presence of an aniline with catalytic amounts of tris(dibenzylideneacetone)dipalladium and 1,3-bis(diphenylphosphino)propane (dppp) to give the final ligands (2,4,6-trimethylphenyl)[6-(2,4,6-trimethylphenyl)pyridine-2-yl]amine (Ap^1, **4.03**), (2,6-diisopropylphenyl)[6-(2,4,6-triisopropylphenyl)pyridin-2-yl]amine (Ap^2, **4.04**) and (2,4,6-trimethylphenyl)[6-(2,4,6-triisopropylphenyl) pyridine-2-yl]amine (Ap^3, **4.05**) as off-white solids in 63–75% yield (Scheme 4.2).[3, 4]

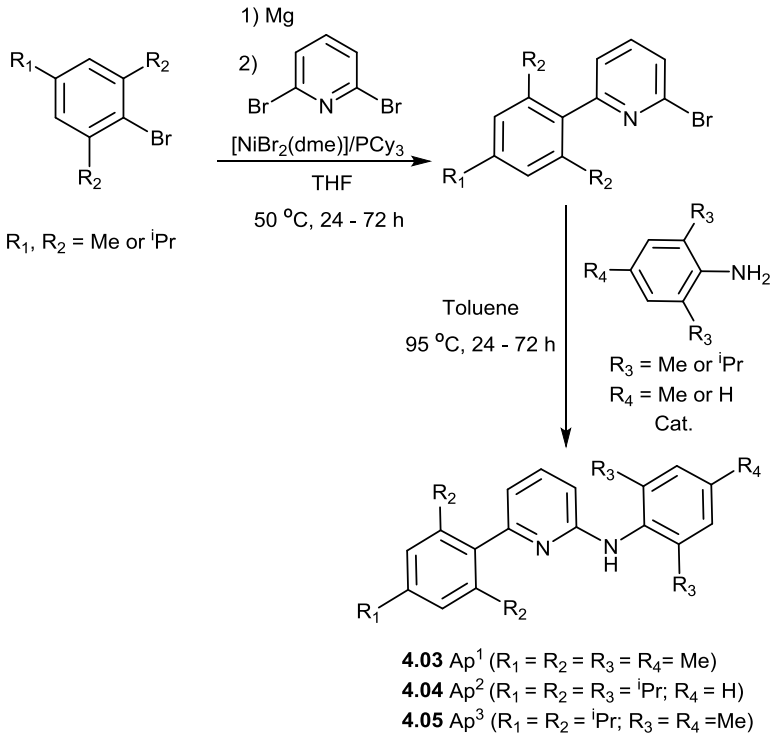

Scheme 4.2. Synthesis of aminopyridine ligands (**4.03**–**4.05**) with varying aryl substituents.

4.3 Synthesis of $(Ap^{R})Ti\{NC(Ph)N^{i}Pr_2\}X_2$ (R = 1, 2 or 3 and X = Cl, Me or CH_2Ph)

The complexation reaction of $Ti(NMe_2)Cl_3$ with aminopyridine ligands *via* protonolysis of the amine is known in the literature.[5, 11, 12] The neutral amine ligand stays tethered to the metal centre (**1.76**–**1.78**, Scheme 4.3). However, upon addition of $Me_3SiNC(Ph)N^{i}Pr_2$ (**4.01**) to the κ^2-aminopyridinato titanium complexes (**1.76**–**1.79**), the mixed κ^1-amidinate κ^2-aminopyridinato titanium complexes could not be obtained cleanly (Scheme 4.3).

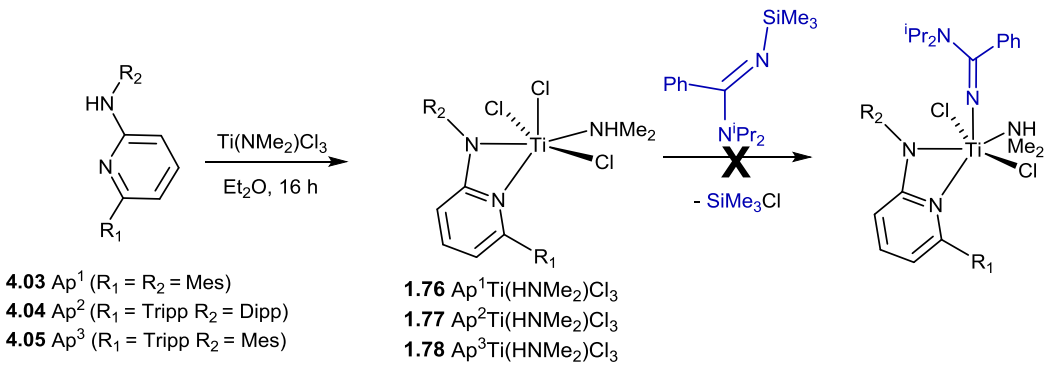

Scheme 4.3. Attempted synthesis of κ^1-amidinate κ^2-aminopyridinato titanium dichloride complexes.

Alternatively, the aminopyridine ligand was lithiated using *n*-butyl lithium, following a literature procedure,[3] and Ap^1Li, Ap^2Li and Ap^3Li (**30**, **4.06** and **31**, respectively) were isolated as off-white solids in 40–84% yield. Those newly formed ligand systems were reacted further with the previously synthesised κ^1-amidinate titanium complex (**4.02**) and a colour change from orange to red was observed. The resulting complexes (**32**–**34**) were isolated in 40–83% yield (Scheme 4.4).[13]

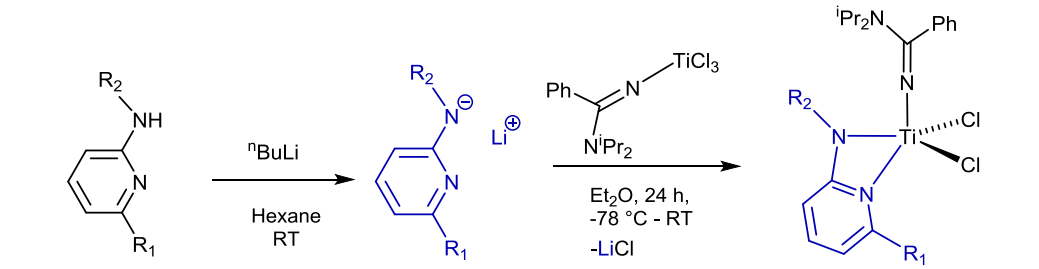

4.03 Ap^1 (R_1 = R_2 = Mes)
4.04 Ap^2 (R_1 = Tripp R_2 = Dipp)
4.05 Ap^3 (R_1 = Tripp R_2 = Mes)

30 Ap^1Li
4.06 Ap^2Li
31 Ap^3Li

32 $Ap^1Ti\{NC(Ph)NiPr_2\}Cl_2$
33 $Ap^2Ti\{NC(Ph)NiPr_2\}Cl_2$
34 $Ap^3Ti\{NC(Ph)NiPr_2\}Cl_2$

Scheme 4.4. Successful synthesis of complexes **32**–**34** *via* salt metathesis.

The ^{1}H NMR spectrum of **32** at –60 ºC shows two distinct doublets at 6.30 and 5.32 ppm corresponding to the *meta*-protons of the pyridine moiety (Figure 4.1). The *para*-proton is overlapping with the other aromatic protons in the region of 6.86–6.79 ppm.

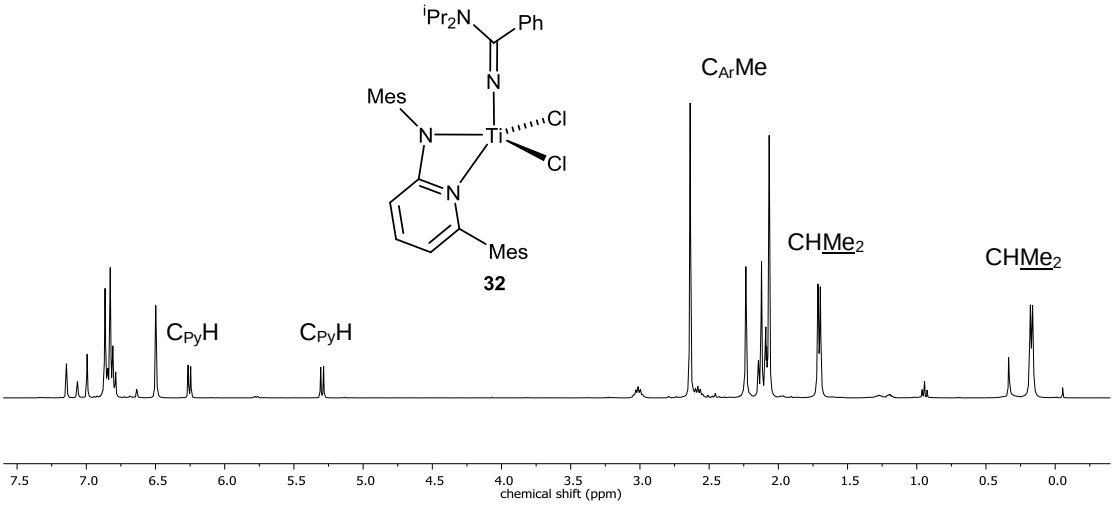

Figure 4.1. ^{1}H NMR spectrum (400.2 MHz, toluene-d_8, 213 K) of $Ap^1Ti\{NC(Ph)N^iPr_2\}Cl_2$ (**32**).

Four distinct C_{Ar}–Me environments are observed; the *ortho*-methyl moieties appear as two singlets at 2.64 and 2.07 ppm and the *para*-methyl protons appear as two singlets at 2.23 and 2.13 ppm. Interestingly, the room temperature ^{1}H NMR spectrum shows one broad and one sharp doublet at 1.62 and 0.40 ppm corresponding to the isopropyl methyl on the amidinate ligand, while at low temperatures, two sharp doublets at 1.70 and 0.18 ppm are observed instead.

Diffraction-quality crystals of **32–34** were grown from a benzene solution at room temperature. The molecular structures are shown in Figure 4.2. Selected distances and angles are listed in Table 4.1. Compounds **32–34** possess distorted pentacoordinate geometries. The τ parameter, first defined by Addison *et al*. as (A-B)/60, where A and B are the two greatest L–M–L angles in the complex,[14] gives an indication whether a complex either adapts a square base pyramidal (SBP) or trigonal bipyramidal (TBP) geometry. For an ideal trigonal bipyramidal geometry, τ = 1 while for an ideal square-based pyramidal geometry, τ = 0. Complex **32** has a τ value of 0.58, therefore the geometry of **32** may be described as 58% along the pathway of distortion between SBP and TBP geometries.

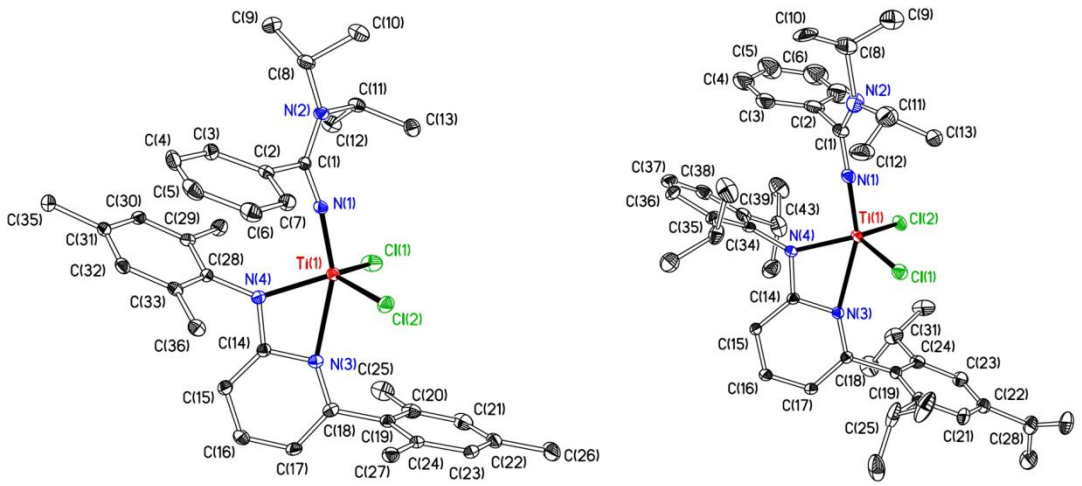

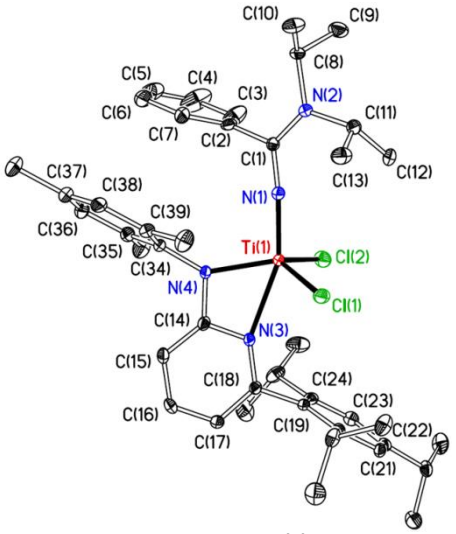

(c)

Figure 4.2. Displacement ellipsoid plots of (a) (Ap^1)Ti{NC(Ph)N^{i}Pr$_2$}Cl$_2$ (**32**), (b) (Ap^2)Ti{NC(Ph)N^{i}Pr$_2$}Cl$_2$ (**33**) and (c) (Ap^3)Ti{NC(Ph)N^{i}Pr$_2$}Cl$_2$ (**34**). Ellipsoids are drawn at 20% probability level and H atoms are omitted.

Table 4.1. Selected bond lengths (Å) and angles (°) for complexes **32–34**.

	32	**33**	**34**
Ti(1)–N(1)	1.773(3)	1.793(2)	1.797(2)
Ti(1)–N(3)	2.318(3)	2.360(2)	2.330(2)
Ti(1)–N(4)	1.978(3)	1.976(2)	1.969(2)
Ti(1)–Cl(1)	2.296(1)	2.294(1)	2.279(1)
Ti(1)–Cl(2)	2.271(1)	2.274(1)	2.276(1)
N(1)–C(1)	1.325(4)	1.287(4)	1.303(3)
N(2)–C(1)	1.335(4)	1.304(4)	1.328(3)
Ti(1)–N(1)–C(1)	161.2 (2)	169.6 (2)	159.7 (1)
N(1)–Ti(1)–N(4)	96.36(13)	97.40(9)	97.85(8)
N(3)–Ti(1)–N(4)	61.57(12)	61.28(7)	62.03(7)

The aforementioned distortion is caused by an acute bond angle, N(3)–Ti(1)–N(4), in all three complexes. Compound **32** exhibits π-stacking interaction between the mesityl group of the Ap^1 ligand and the phenyl of the amidinate ligand giving an approximate

inter-plane separation of 3.40 Å, which lies within the typical π-stacking range of 3.34–3.50 Å.[15] This is not observed for **33**, indicating that an increase in steric bulk prohibits the close approach of the two planes. A near linear Ti(1)–N(1)–C(1) bond angle for complexes **32–34** (161.2(2), 169.6(2) and 159.7(1)º, respectively) suggests an sp hybridised N(1) atom and metal-amidinate dπ–pπ bonding contributions.[16, 17]

The Ti–$N(4)_{amide}$ distances in $(Ap^2)Ti(NHMe_2)Cl_3$ (**1.77**) and **33** (1.981(4) *vs* 1.976(2) Å) are equivalent within error, whereas the Ti–$N(3)_{py}$ is significantly elongated in **33** compared to **1.77** (2.360(2) *vs* 2.233(5) Å, respectively). One possible explanation is that the neutral pyridyl donor ($N(3)_{py}$) is *trans* to the amidinate nitrogen, possibly as a result of the strong donor nitrogen atoms N(1) and N(4) avoiding being *trans* to one another (*vide infra*). Furthermore, increasing the steric bulk on the aminopyridinato ligands leads to the expected lengthening of the Ti(1)–$N(3)_{py}$ bond from **32** to **33** (2.318(3) to 2.360(2) Å, respectively) which is also observed for the literature compounds $(Ap^x)Ti(NHMe_2)Cl_3$ (x = 1 or 2, **1.76** and **1.77**, respectively).[5]

The Ti(1)–N(1) bond lengths (av. 1.788(1), range 1.773(3)–1.797(2) Å) are significantly shorter than the typical values for a Ti–N_{amide} ($\sigma^2\pi^2$) partial double bond (typically 1.90–2.00 Å),[18] and closer to those of Ti≡N ($\sigma^2\pi^4$) triple bonds, such as are found in titanium imido compounds (L)Ti≡NR, which lie in the range *ca.* 1.69–1.76 Å.[19, 20] This is observed due to the ability of the amidinate to act as a σ+2π donor while amides can only act as σ+π donors.[16]

DFT calculations by Professor Philip Mountford, suggest that the sterically demanding substituents on the κ^2-aminopyridinato ligand are crucial in dictating the geometry preferences of these complexes. Calculations of a sterically less demanding complex {MeN-2-C_5H_4N}Ti{$NC(Ph)NMe_2$}Cl_2 (**R**) showed only a slight preference for the SBP geometry over TBP geometry by 0.7 kcal mol^{-1}. However, an increase in the steric demand of the substituents on the amide and pyridyl moiety to xylyl groups (**S**) or mesityl groups (**32Q**) favours the TBP isomer considerably by 6.5 kcal mol^{-1} and 4.8 kcal mol^{-1}, respectively. This change in preference is triggered by two interactions. In the TBP geometry, π-stacking between the aryl groups of the aminopyridinato and amidinate can take place (inter-plane distance = 3.3 Å), as also seen in the molecular structure (*vide supra*). Secondly, the close proximity of the

ortho-methyl groups of the Ap[1] fragment to the amidinate moiety in the square-based pyramidal geometry is highly disfavoured (Figure 4.3).

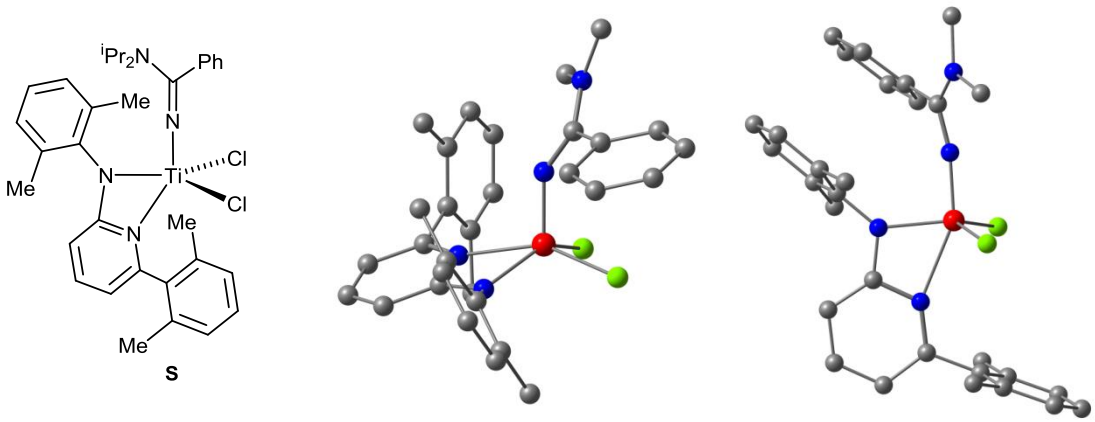

Figure 4.3. Optimised geometries for **S** with dispersion corrections included. Average inter-plane spacing between the phenyl ring and the xylyl is *ca.* 3.3 Å in the TBP isomer. Hydrogen atoms omitted for clarity.

The MOs of TBP ML_5 compounds are well known (Figure 4.4).[21, 22] The 3a' MO of ML_5 possesses mainly d_{z^2} character and is strongly σ* anti-bonding and therefore does not engage in any metal-ligand π-interactions. In the presence of two strongly π-donor ligands (N_{amide} and $N_{amidinate}$ of the supporting ligands) three $2p_\pi \rightarrow 3d_\pi$-π bonds originate from separate, non-conflicting titanium acceptor atomic orbitals (AOs) as displayed in Figure 4.4, resulting in a 16 valence electron compound formally.

The labels of the d-based orbitals are in fact shown for local C_s symmetry rather than the exact D_{3h} symmetry of a TBP ML_5 compound. The 1a' and 1a" orbitals on the metal are π-acceptors and are equivalent to one another. These two orbitals have the best energy match with amide nitrogen 2p lone pairs. However, even though 2a' and 2a" are slightly σ* anti-bonding, the *n*d/(*n*+1)p mixing allows the 2a" orbital to polarise favourable towards incoming π-donor group in the equatorial position. Therefore, the π-donor orbital of the Ap amide (1a") finds an even better interaction with the strongly π-bonding 2a" orbital of the titanium.

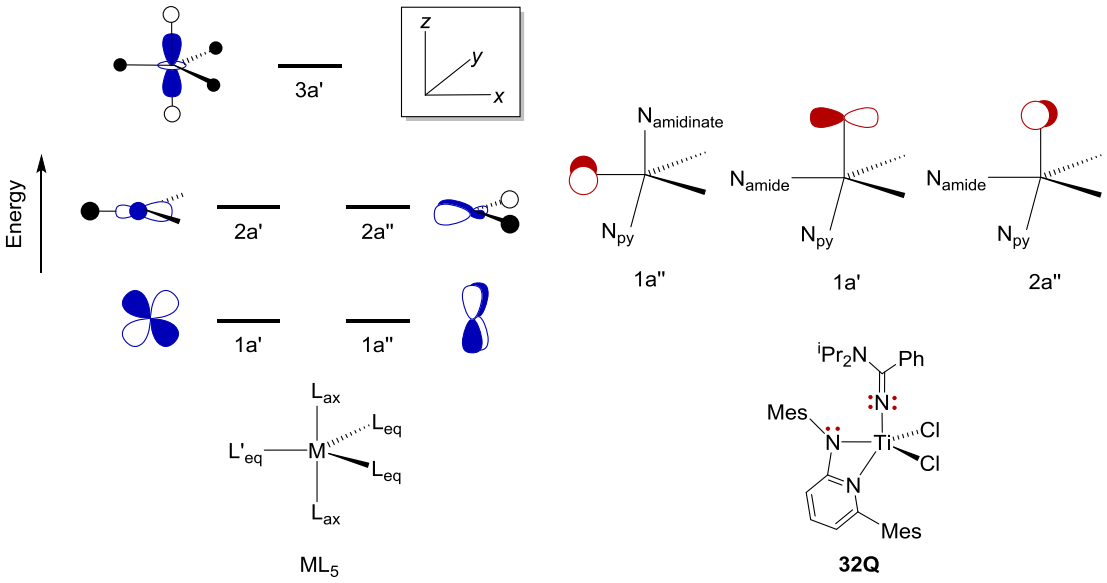

Figure 4.4. Left: the σ-only frontier MOs (d orbitals only, arbitrary energies) for a hypothetical ML_5 system. Right: representation of the compound $(Ap^1)Ti\{NC(Ph)N^iPr_2\}Cl_2$ (**32Q**) emphasising the 2p(π) lone pairs for the equatorial N_{amide} (from Ap ligand) and axial $N_{amidinate}$ nitrogens.

The two π-donor orbitals of the imine nitrogen of the amidinate (1a' and 2a", Figure 4.4) find a good match with 1a' and 1a" orbitals of the titanium and so make up HOMO, HOMO–1 and HOMO–2 as depicted in Figure 4.5. This is then in agreement with a 16-valence electron compound and the DFT calculations support the qualitative conclusions reached above.

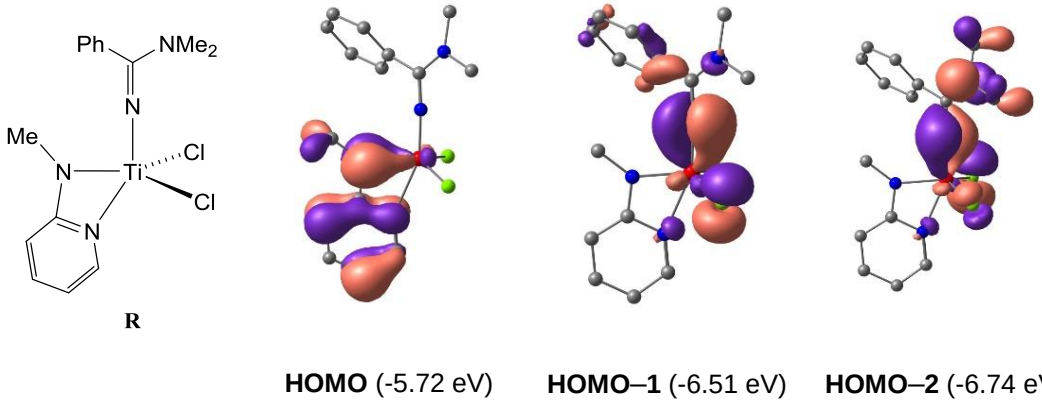

Figure 4.5. DFT computed frontier molecular orbitals of $\{MeN\text{-}2\text{-}C_5H_4N\}Ti\{NC(Ph)NMe_2\}Cl_2$ (**R**). Isosurfaces are drawn at the 0.004 au level. H atoms omitted.

To allow investigation of the cationic species on the NMR scale, believed to be the active species in polymerisation of α-olefins, complexes **32–34** were alkylated by treatment with two equivalents of Grignard or alkyl lithium reagents (Equation 4.1).

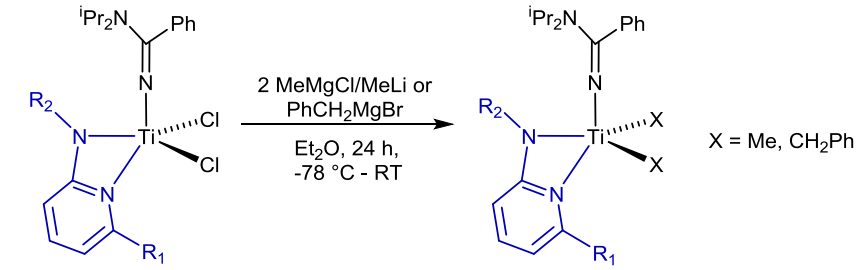

32 $R_1 = R_2$ = Mes
33 R_1 = Tripp R_2 = Dipp
34 R_1 = Tripp R_2 = Mes

35 $Ap^1Ti\{NC(Ph)N^iPr_2\}Me_2$
36 $Ap^1Ti\{NC(Ph)N^iPr_2\}(CH_2Ph)_2$
37 $Ap^2Ti\{NC(Ph)N^iPr_2\}Me_2$
38 $Ap^2Ti\{NC(Ph)N^iPr_2\}(CH_2Ph)_2$
39 $Ap^3Ti\{NC(Ph)N^iPr_2\}Me_2$

Equation 4.1

$(Ap^x)Ti\{NC(Ph)N^iPr_2\}Me_2$ (**35**, **37** and **39**, x = 1, 2, or 3) were isolated as olive green solids in moderate yield (66, 69 and 72% yield, respectively). The ^{1}H NMR spectra of $(Ap^x)Ti\{NC(Ph)N^iPr_2\}Me_2$ (**35**, **37** and **39**) show similar distinct features and therefore only **37** will be discussed in detail (Figure 4.6).

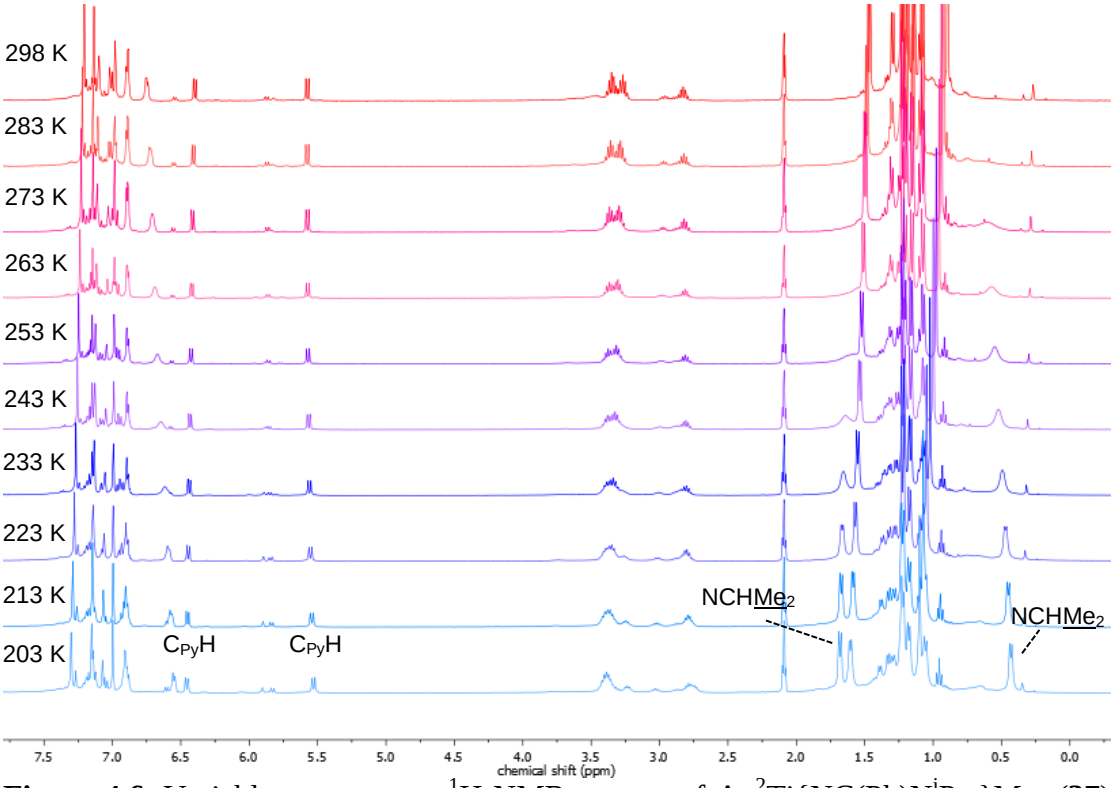

Figure 4.6. Variable temperature ^{1}H NMR spectra of $Ap^2Ti\{NC(Ph)N^iPr_2\}Me_2$ (**37**) (400.2 MHz, toluene-d_8).

All three complexes displayed fluxionality at room temperature as observed by the broad resonances corresponding to the isopropyl moiety of the amidinate ligand, overlapping with the isopropyl fragments of the aminopyridinato ligand (Figure 4.6, top spectrum). This is indicative of restricted rotation around the C–N^{i}Pr$_2$ bond on the NMR timescale. A variable low temperature ^{1}H NMR study was carried out. Below 263 K, the methyl and methine resonance of the isopropyl fragment of the amidinate ligand decoalesces into a pair of doublets and septets, respectively, by freezing out the rotation. At 203 K, two distinct doublets, assigned to the isopropyl methyl of the amidinate moiety, are observed at 1.67 and 0.45 ppm. As discussed in Chapter One, the amidinate ligand can act as a 5-electron donor ligand which results in a partial double bond character between the central carbon atom and the amine nitrogen (Equation 4.2). The extent of double bond character leads to the fluxionality observed.

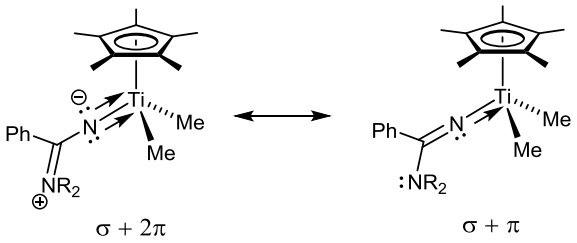

Equation 4.2

At low temperature, the Ti–Me resonance appears as a singlet at 1.07 ppm with a corresponding ^{13}C NMR resonance at 57.3 ppm. Two doublets at 6.58 and 6.45 ppm are assigned to the *meta*-protons on the pyridine ring.

The dibenzyl complexes, (Ap^1)Ti{NC(Ph)N^{i}Pr$_2$}(CH$_2$Ph)$_2$ (**36**) and (Ap^2)Ti{NC(Ph)N^{i}Pr$_2$}(CH$_2$Ph)$_2$ (**38**), were isolated as orange solids in 62 and 42% yield, respectively. The ^{1}H NMR spectrum of **36** shows an apparent singlet at 3.06 ppm, assigned to the TiCH$_2$ moiety, from accidental overlap of the diastereotopic methylene protons. The previous mentioned signal correlates to a ^{13}C resonance at 82.0 ppm in the HSQC (Figure 4.7, b)). The isopropyl fragment of the κ^1-amidinate ligand appears as four broad resonances at 4.49, 3.39, 1.13 and 0.83 ppm, corresponding to the methine and methyl groups, which implies free rotation about the Ti–N$_{amidinate}$ bond.

The room temperature ^{1}H NMR spectrum of **38** shows an apparent AB quartet at 2.68 ppm corresponding to the diastereotopic TiCH$_2$ moiety (Figure 4.7, a)).

Furthermore, the isopropyl methyl of the amidinate appear as two sharp doublets at 0.85 and 0.66 ppm in the room temperature ^{1}H NMR spectrum of **38**. In contrast to the dimethyl complexes **35** and **37**, the isopropyl methyl of the amidinate moiety are already decoalesced at room temperature for both dibenzyl complexes (**36** and **38**). A possible explanation could be the increase in steric bulk on the alkyl substituent (Me to CH_2Ph) with simultaneous increase in steric hindrance on the aminopyridinato ligand (for **38**) leads to more hindered rotation.

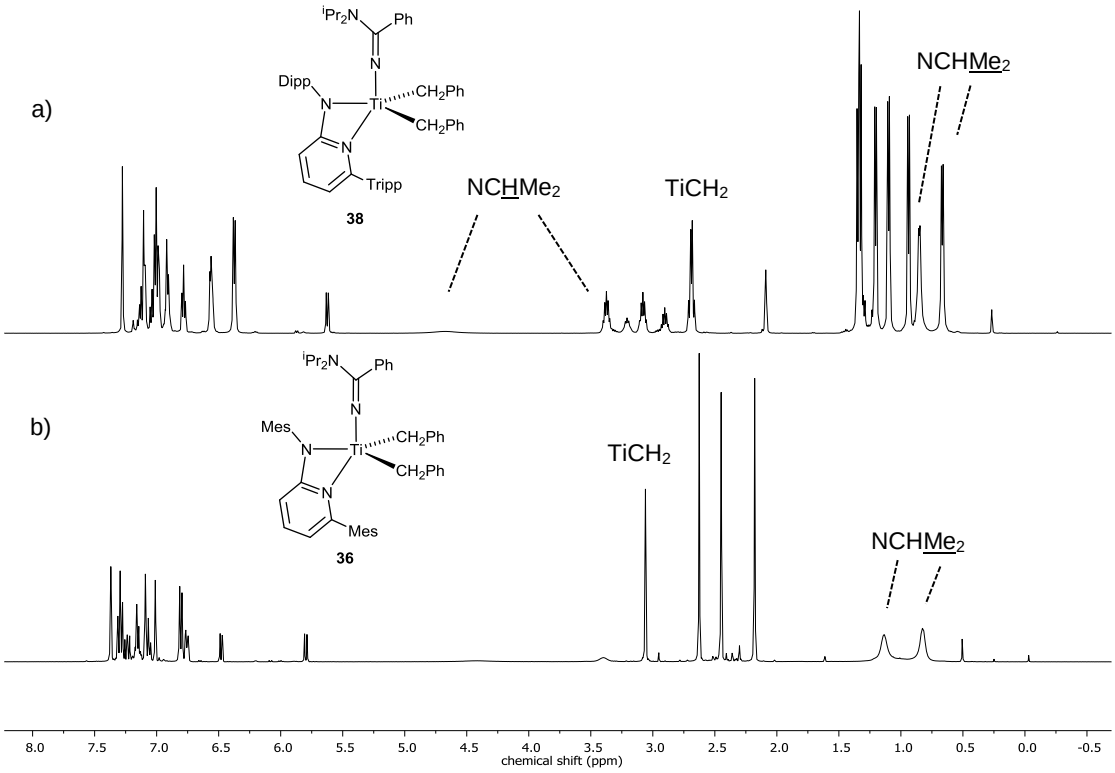

Figure 4.7. ^{1}H NMR spectrum (400.2 MHz, toluene-d_8, 298 K) of (a) (Ap^2)Ti{NC(Ph)N^{i}Pr$_2$}(CH_2Ph)$_2$ (**38**) and (b) (Ap^1)Ti{NC(Ph)N^{i}Pr$_2$}(CH_2Ph)$_2$ (**36**).

Interestingly, one of the methine protons has a distinct downfield chemical shift (4.76 ppm for **38**) and remains broad even at low temperatures, which could be linked to quadrupolar relaxation from the proximate nitrogen atom and was only assigned based on its ^{13}C chemical shift at 51.6 ppm.[23] Both dibenzyl complexes are stable in solution at room temperature. This is in stark contrast to (Ap^2)Ti(CH_2Ph)$_3$, which is known to decompose when left in solution at room temperature.[5]

Diffraction-quality crystals of complex **38** were grown from a solution in pentane at –30 ºC. The molecular structure is shown in Figure 4.8. Selected distances and angles are listed in Table 4.2. The τ value of **38** was determined as 0.68, suggesting that the

geometry of **38** is slightly closer to distorted trigonal bipyramidal geometry than SBP geometry.

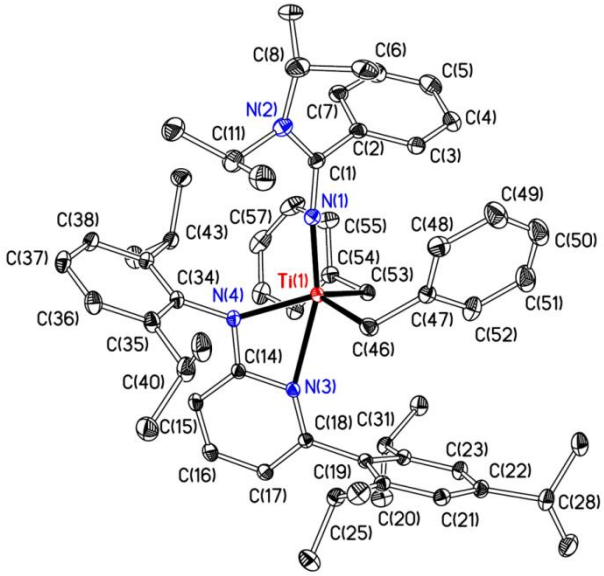

Figure 4.8. Displacement ellipsoid plot of $(Ap^2)Ti\{NC(Ph)N^iPr_2\}(CH_2Ph)_2$ (**38**). Ellipsoids are drawn at 20% probability level and H atoms are omitted.

Table 4.2. Selected bond lengths (Å) and angles (°) for complex **38**.

Ti(1)–N(1)	1.819(2)	N(1)–Ti(1)–C(46)	100.8(1)
Ti(1)–N(3)	2.376(1)	N(1)–Ti(1)–C(53)	101.0(1)
Ti(1)–N(4)	2.013(1)	Ti(1)–C(46)–C(47)	111.1(1)
Ti(1)–C(46)	2.131(2)	Ti(1)–C(53)–C(54)	106.9(1)
Ti(1)–C(53)	2.152(2)	Ti(1)–N(1)–C(1)	171.4(1)
N(1)–C(1)	1.294(2)	N(3)–Ti(1)–N(4)	60.54(5)
N(2)–C(1)	1.368(2)		

The Ti(1)–N(1) bond in **38** is slightly elongated in comparison to the dichloride complex **33** (1.818(2) *vs*. 1.793(2) Å, respectively) reflecting the enhanced σ-donation from the benzyl ligands. Furthermore, the N(2)–C(1) bond distance also lengthens compared to the dichloride complex **33** (1.368(2) *vs*. 1.304(4) Å), which is indicative of less partial double bond character present in **38** (*vide supra*). The bond angle of

Ti(1)–C(46)–C(47) is close to the expected tetrahedral angle (111.1º) and therefore pointing away from the metal centre. This suggests no interaction with the titanium centre. The smaller bond angle of Ti(1)–C(53)–C(54) (106.9º) is associated with the phenyl group that is oriented towards the metal centre and suggests that there might be some interaction with the otherwise 16 valence electron centre.[24]

4.4 Attempted synthesis of alternative aminopyridinato, κ^1-amidinate titanium dichloride complex

Reaction of $(Ap^1)Ti(HNMe_2)Cl_3$ with $Me_3SiNCN(Dipp)CH_2C_6H_4$ resulted in a mostly clean reaction on the NMR tube scale (Figure 4.9). Despite the observation of one major product, displayed by the singlet at 4.19 ppm, assigned to the NCH_2 of the amidinate backbone and the two major resonances of the *meta*-protons of the pyridine backbone at 6.28 and 5.49 ppm, other species were formed in up to 30% spectroscopic yield (Figure 4.9). On a preparative scale, the impurities became more apparent and even after optimising reaction conditions and work-up procedure, the pure compound **40** could not be obtained.

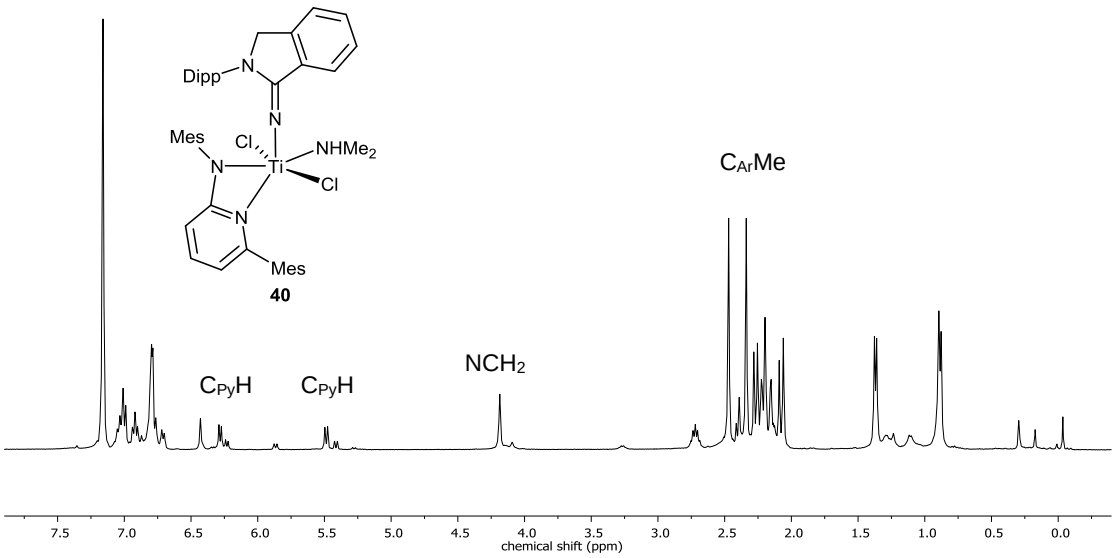

Figure 4.9. ^{1}H NMR spectrum (400.2 MHz, C_6D_6, 298 K) of attempted synthesis of compound **40**.

In the attempt to purify compound **40**, the mixture was recrystallised in a solution of pentane at −30 °C resulting in diffraction-quality crystals and a pale orange solid, containing impurities and complex **40**. The molecular structure is shown in Figure 4.10. Selected distances and angles are listed in Table 4.3.

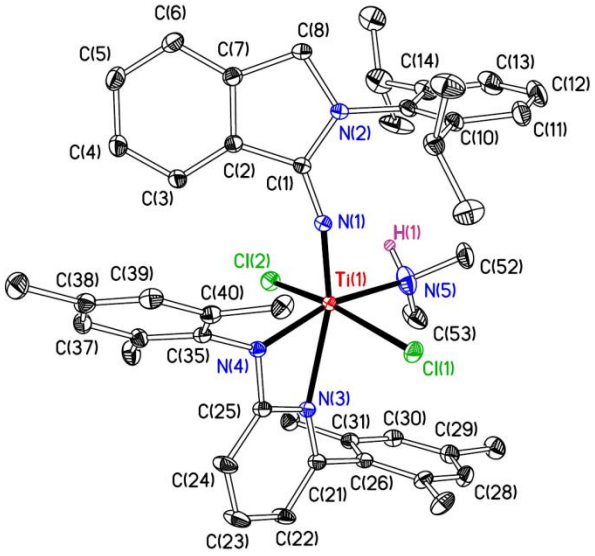

Figure 4.10. Displacement ellipsoid plot of $(Ap^1)Ti\{NCN(Dipp)CH_2C_6H_4\}(NHMe_2)Cl_2$ (**40**). Ellipsoids are drawn at 20% probability level and selected H atoms are omitted.

Table 4.3. Selected bond lengths (Å) and angles (°) for complex **40**.

Ti(1)–N(1)	1.800(2)	Ti(1)–Cl(2)	2.364(1)
Ti(1)–N(3)	2.377(1)	N(1)–C(1)	1.294(2)
Ti(1)–N(4)	2.013(1)	N(1)–Ti(1)–N(3)	161.9(1)
Ti(1)–N(5)	2.274(2)	N(3)–Ti(1)–N(4)	60.9(1)
Ti(1)–Cl(1)	2.367(1)	Cl(1)–Ti(1)–Cl(2)	158.4(1)

The molecular structure of **40** shows that the amine stays tethered to the metal centre resulting in a distorted octahedral arrangement around the metal centre. Comparing the structure of **40** to the known compound $(Ap^1)Ti(NHMe_2)Cl_3$ (**1.75**) emphasises the influence of the amidinate ligand on the bonding of the aminopyridinato to the titanium centre. In **40**, the $Ti(1)–N(3)_{py}$ bond is significantly elongated due to the *trans* influence from the κ^1-amidinate nitrogen. The amine-titanium bonds are equivalent within error for **40** and **1.75**. Two chloride ligands are in both cases *trans* to one another. However, in **40**, the bond distances are elongated in comparison to **1.75** (2.367(1) and 2.364(1) *vs*. 2.283(2) and 2.316(2) Å, respectively).

4.5 Synthesis and characterisation of cationic mono-alkyl complexes

The synthesis and reactivity of catalytically active group 4 mono-alkyl cations have been extensively explored throughout the literature.[16, 17, 25] Activation of Cp*Ti{NC(Ph)N^{i}Pr$_2$}Me$_2$ (**3.05**) with [Ph$_3$C][BAr$^F_4$] results in a mixture of products, including dimer formation (Section 1.7).[16] However, addition of Lewis base to the mixture of complexes results in formation of a single Lewis base adduct (Scheme 4.5). The main route of activation relevant in this Chapter is *via* alkyl abstraction.

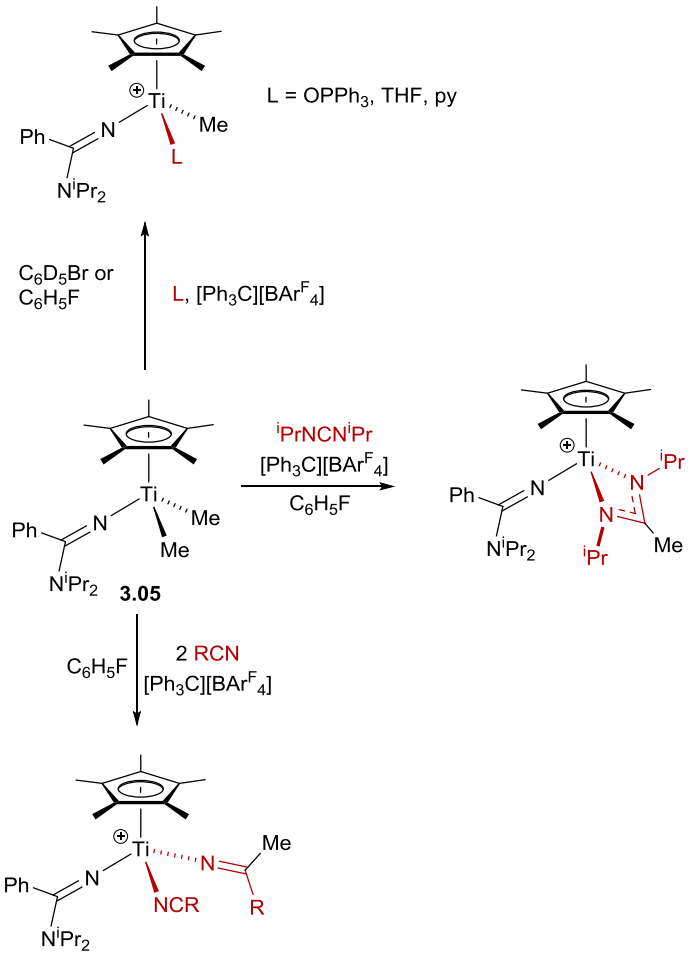

Scheme 4.5. Syntheses of Lewis base adducts and insertion products of cyclopentadienyl titanium complex **3.05**.[16] Anion omitted for clarity.

The reactions were performed in either bromobenzene-d_5 or fluorobenzene due to their solubilising, yet relatively non-coordinating properties. To investigate the potentially active species in the polymerisation process, the activation chemistry of the least and most sterically crowded complexes, **35** and **37** respectively, was explored. On the NMR tube scale, treatment of **35** and **37** with one equivalent of

$[Ph_3C][BAr^F{}_4]$ led to the immediate formation of the monomethyl cation $[(Ap^1)Ti\{NC(Ph)N^iPr_2\}Me][BAr^F{}_4]$ and $[(Ap^2)Ti\{NC(Ph)N^iPr_2\}Me][BAr^F{}_4]$ (**41-[BAr$^F{}_4$]** and **42-[BAr$^F{}_4$]**, respectively, Equation 4.3).

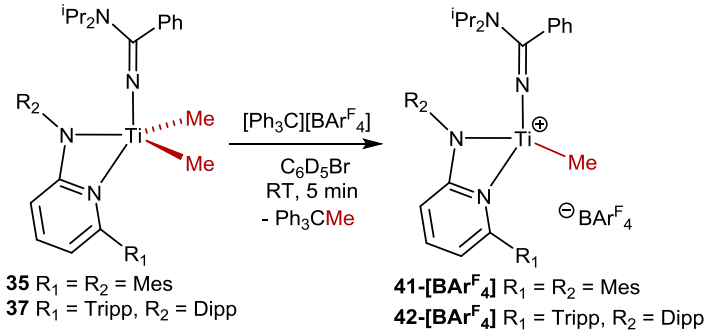

Equation 4.3

The room temperature ^1H NMR spectrum of **41-[BAr$^F{}_4$]** displays a singlet at 1.62 ppm, assigned to the Ti–Me moiety. The resonance is further downfield compared to the neutral dimethyl complex (**35**, 1.07 ppm). However, overall, neither cation, **41-[BAr$^F{}_4$]** or **42-[BAr$^F{}_4$]**, were stable in solution at room temperature, and decomposition was observed within 5 minutes.

In order to stabilise the cationic species and prevent decomposition, the dimethyl complexes were activated in the presence of a trapping agent, Ph_3PO, forming $[(Ap^1)Ti\{NC(Ph)N^iPr_2\}(Me)(OPPh_3)][BAr^F{}_4]$ and $[(Ap^2)Ti\{NC(Ph)N^iPr_2\}$-$(Me)(OPPh_3)][BAr^F{}_4]$ (**43-[BAr$^F{}_4$]** and **44-[BAr$^F{}_4$]**, respectively, Equation 4.4).

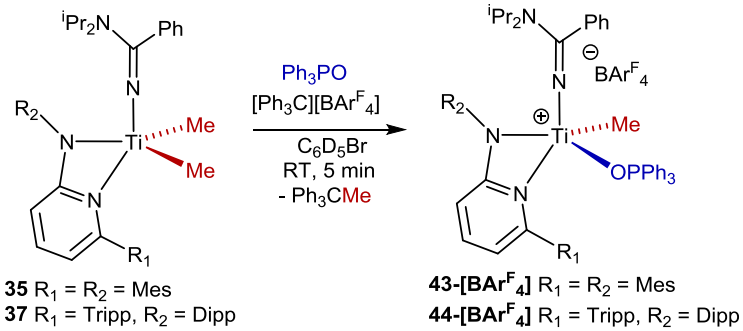

Equation 4.4

However, the NMR spectra of both complexes also display the presence of other unidentified products, manifested in the $^{31}P\{^1H\}$ NMR spectrum showing a major peak at 48.5 ppm, belonging to **43-[BAr$^F{}_4$]**, and minor resonances at 41.4 and 40.6 ppm.

As the mono-methyl cations **41-[BAr$^{F}_{4}$]** and **42-[BAr$^{F}_{4}$]** as well as their Lewis base adducts (**43-[BAr$^{F}_{4}$]** and **44-[BAr$^{F}_{4}$]**, respectively) were not stable in solution, *N*,*N*´-diisopropylcarbodiimide was used instead, resulting in migratory insertion into the Ti–Me bond. On the NMR tube scale **35** and **37** were activated in the presence of *N*,*N*´-diisopropylcarbodiimide forming the κ^2-amidinate insertion product [(Ap^1)Ti{NC(Ph)N^{i}Pr$_2$}{MeC(N^{i}Pr$_2$)$_2$}][BAr$^{F}_{4}$] and [(Ap^2)Ti{NC(Ph)N^{i}Pr$_2$}-{MeC(N^{i}Pr$_2$)$_2$}][BAr$^{F}_{4}$] (**45-[BAr$^{F}_{4}$]** and **46-[BAr$^{F}_{4}$]**, respectively, Equation 4.5).

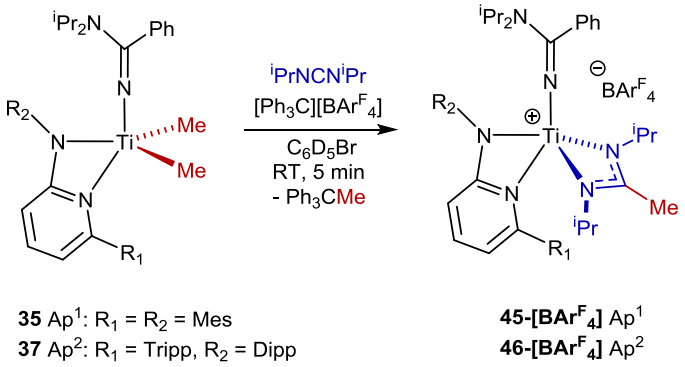

Equation 4.5

NMR spectroscopy (Figure 4.11) confirmed that the carbodiimide substrate inserted into the Ti–Me bond.

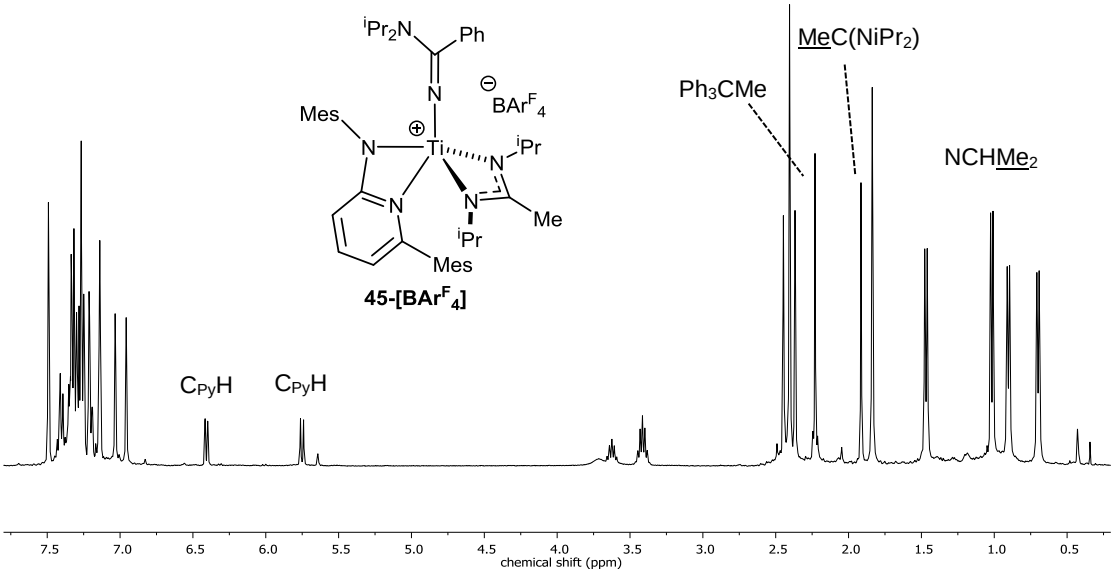

Figure 4.11. ^{1}H NMR spectrum (400.2 MHz, C_6D_5Br, 298 K) of [(Ap^2)Ti{NC(Ph)N^{i}Pr$_2$}{MeC(N^{i}Pr$_2$)$_2$}][BAr$^{F}_{4}$] (**45-[BAr$^{F}_{4}$]**).

The migrated methyl moiety appears at a more downfield chemical shift at 1.93 ppm in the ^{1}H NMR spectrum, with an HSQC correlation to a ^{13}C signal at 12.1 ppm for **45-[BAr$^{F}_{4}$]**. Four distinct environments of the isopropyl groups of the κ^{1}- and κ^{2}-amidinate are observed and were differentiated by two-dimensional NMR experiments (Figure 4.11). Even though both complexes were stable in solution, allowing full characterisation by NMR spectroscopy, neither of the complexes could be successfully isolated without undergoing considerable decomposition. This is indicative of the very sensitive nature of this series of complexes.

On the NMR tube scale, complexes **36** and **38** were also treated with one equivalent of [Ph$_3$C][BAr$^{F}_{4}$]. **38** resulted in a clean activation giving the monobenzyl cation, [Ap^{2}Ti{NC(Ph)N^{i}Pr$_2$}(CH$_2$Ph)][BAr$^{F}_{4}$] (**47-[BAr$^{F}_{4}$]**). The ^{1}H NMR spectrum of **47-[BAr$^{F}_{4}$]** shows a singlet at 4.04 ppm assigned to the by-product 1,1,1,2-tetraphenylethane (Ph$_3$CCH$_2$Ph) of the reaction. The TiCH$_2$ moiety appears as a multiplet at 3.22–2.99 ppm, overlapping with the methine protons of the κ^{2}-aminopyridinato aryl substituent.

The activation of **36** with [Ph$_3$C][BAr$^{F}_{4}$] resulted in an intractable mixture of products. Alternatively, on the NMR tube scale, **36** was activated with one equivalent of [Ph$_3$C][BAr$^{F}_{4}$] in the presence of Ph$_3$PO (Equation 4.6). In contrast to the reaction of the dimethyl analogue **35** with Ph$_3$PO and [Ph$_3$C][BAr$^{F}_{4}$] (*vide supra*), the Lewis base adduct **48-[BAr$^{F}_{4}$]** was formed quantitatively (Figure 4.12).

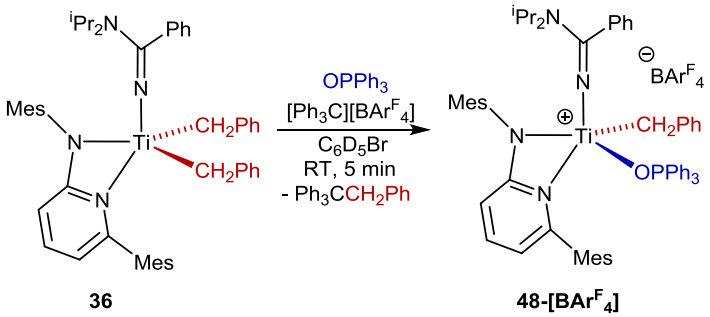

Equation 4.6

The diastereotopic methylene protons of the benzyl moiety correspond to two mutually-coupled doublets at 3.15 and 2.70 ppm in the room temperature ^{1}H NMR spectrum of **48-[BAr$^{F}_{4}$]**. The isopropyl moiety of the κ^{1}-amidinate ligand, as well as the methyl substituents on the aromatic ring of the κ^{2}-aminopyridinato ligand appear

as inequivalent resonances (Figure 4.12), indicating restricted rotation. This evidently, along with the downfield chemical shift of the Ph_3PO group in the $^{31}P\{^1H\}$ NMR spectrum at 50.1 ppm, supports the coordination of the sterically demanding Ph_3PO group.

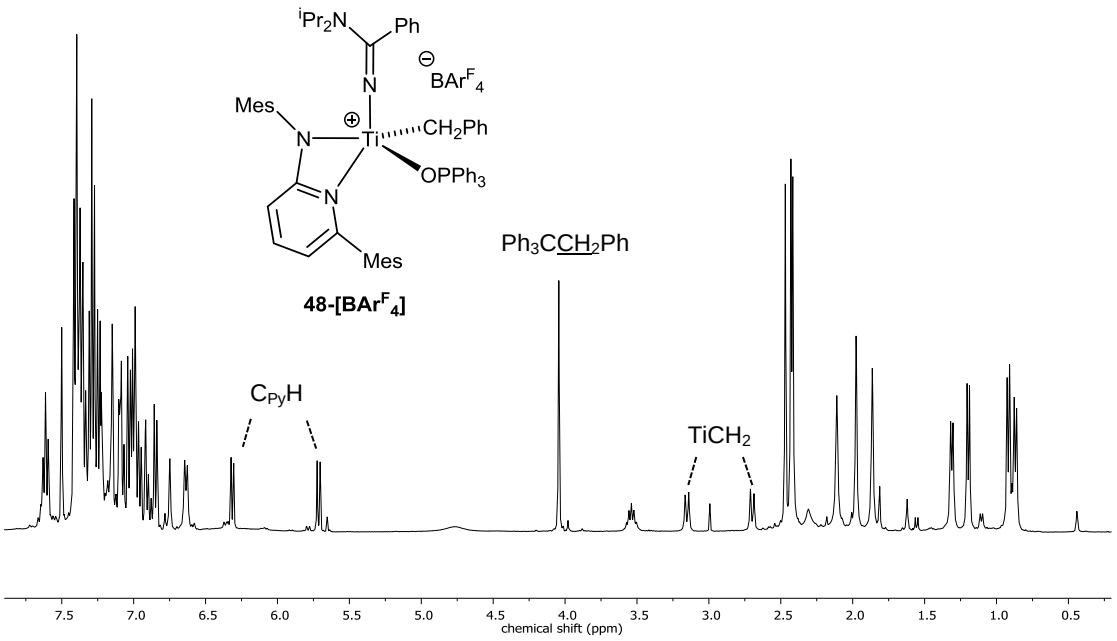

Figure 4.12. ^1H NMR spectrum (400.2 MHz, C_6D_5Br, 298 K) of $[Ap^1Ti\{NC(Ph)N^iPr_2\}(CH_2Ph)(OPPh_3)][BAr^F{}_4]$ (**48-[BAr$^F{}_4$]**).

Even in the presence of trapping agents, the cationic complexes (**45-[BAr$^F{}_4$]**–**48-[BAr$^F{}_4$]**) decomposed upon attempted isolation. The behaviour of these systems in the co-polymerisation of ethylene, propylene and non-conjugated diene (EPDM) will be discussed in Chapter Five.

4.6 Synthesis of mixed κ^1- and κ^2-amidinate titanium complexes

κ^2-amidinate ligands are well established in literature and the first mono-substituted benzamidinato complex was synthesised by Dehnicke *et al*. in 1988.[6] The anionic moiety $[RC(NR')_2]^-$ (where R, R´ = alkyl, aryl or $SiMe_3$) acts as a four-electron donor resulting in a more electrophilic metal centre than in its parent metallocene complex (Section 1.5.3).[26-29] An advantage of these ligand systems is that substitution on the backbone or on the nitrogen atoms allows an investigation of the influence of steric and electronic factors on the polymerisation process.[30]

4.6.1 Synthesis of Ti{NC(Ph)N^{i}Pr$_2$}{MeC(NDipp)$_2$}X$_2$ (X = Cl or Me)

The lithium metal amidinate precursor was synthesised by the addition of methyl lithium to bis(diisopropylphenyl)carbodiimide yielding Li[MeC(NDipp)$_2$] (**49**). **49** was isolated as an off-white solid in 80% yield (Scheme 4.6). The ^{1}H NMR spectrum of compound **49** shows a singlet at 1.39 ppm assigned to the methyl of the MeC(NDipp)$_2$ fragment with a corresponding ^{13}C resonance at 16.9 ppm.

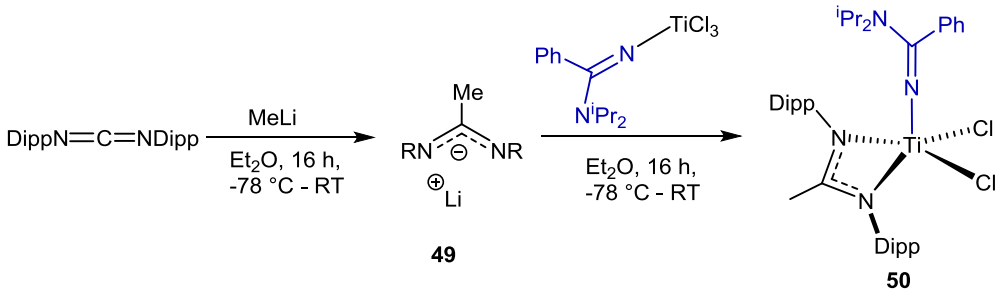

Scheme 4.6. Synthesis of Ti{NC(Ph)N^{i}Pr$_2$}{MeC(NDipp)$_2$}Cl$_2$ (**50**).

One equivalent of **49** was added to Ti{NC(Ph)iPr$_2$}Cl$_3$ (**4.02**) giving Ti{NC(Ph)N^{i}Pr$_2$}{MeC(NDipp)$_2$}Cl$_2$ (**50**) as a dark yellow solid in 67% yield (Scheme 4.6).

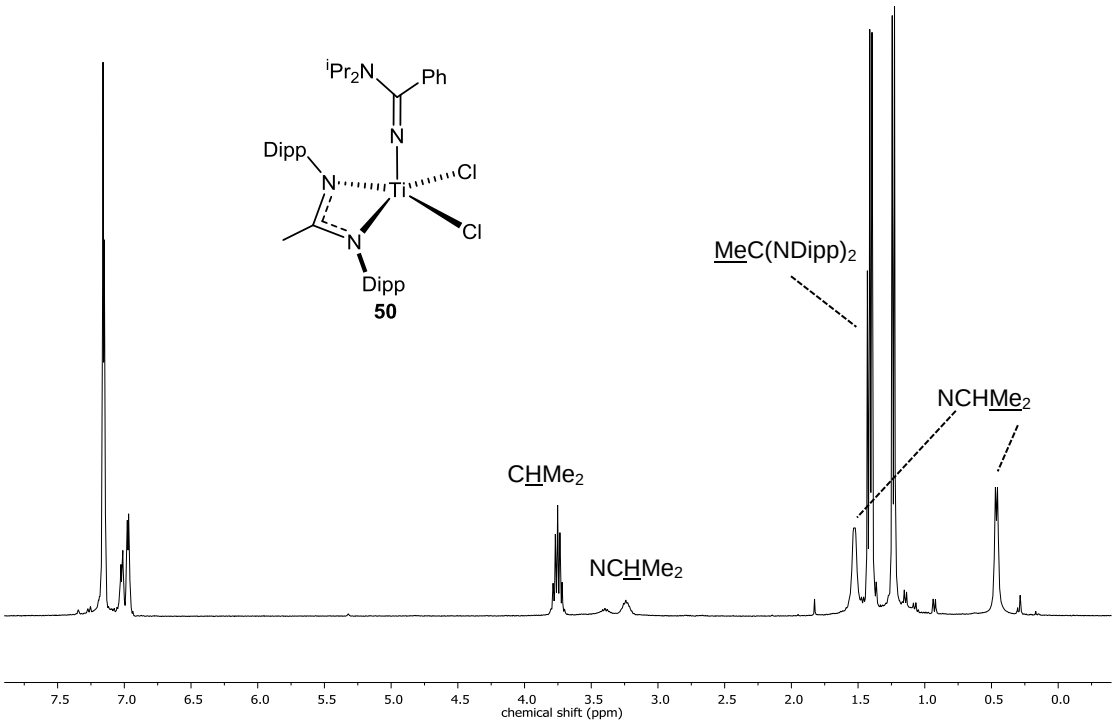

Figure 4.13. ^{1}H NMR spectrum (400.2 MHz, C$_6$D$_6$, 298 K) of Ti{NC(Ph)N^{i}Pr$_2$}-{MeC(NDipp)$_2$}Cl$_2$ (**50**).

The room temperature ^{1}H NMR spectrum (Figure 4.13) shows a sharp septet at 3.70 ppm and two sharp doublets at 1.36 and 1.22 ppm corresponding to the diisopropylphenyl moiety of the κ^2-amidinate ligand. As for previously synthesised compounds,[16] the signals at 3.39 to 3.21 ppm are assigned to the overlapping methine protons of the diisopropyl moiety of the κ^1-amidinate ligand. The aforementioned resonance correlates through-bond (COSY) to the doublets at 1.53 and 0.55 ppm, assigned to the isopropyl methyls of the κ^1-amidinate ligand. The singlet displayed at 1.42 ppm corresponds to the methyl of the κ^2-amidinate backbone.

The dichloride complex (**50**) was reacted further with two equivalents of methyl lithium yielding the dimethyl complex Ti{NC(Ph)N^{i}Pr$_2$}{MeC(NDipp)$_2$}Me$_2$ (**51**), isolated as an olive green solid in 60% yield. The ^{1}H NMR spectrum shows a singlet at 1.50 ppm, assigned to the TiMe moiety, with a corresponding ^{13}C resonance at 58.2 ppm. As previously observed, the diisopropyl moiety of the κ^1-amidinate is broad at room temperature due to fluxionality. To resolve the desired signals, a variable temperature NMR study was carried out (Figure 4.14).

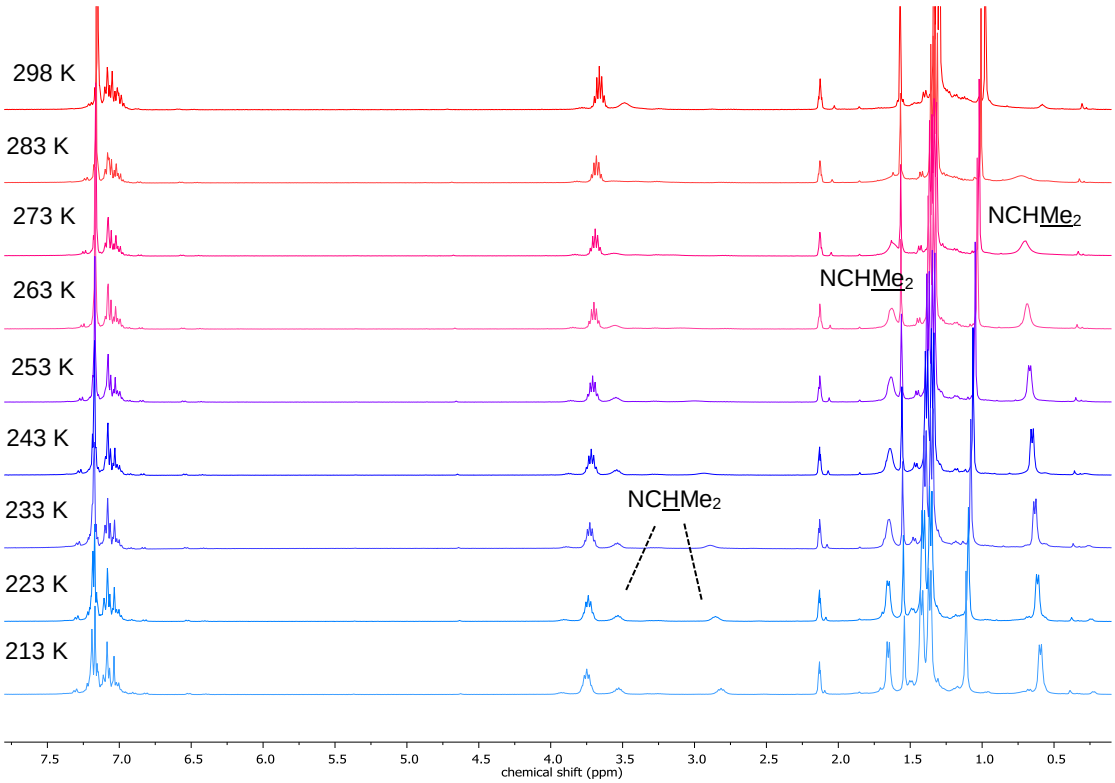

Figure 4.14. Variable temperature ^{1}H NMR spectra of Ti{NC(Ph)N^{i}Pr$_2$}-{MeC(NDipp)$_2$}Me$_2$ (**51**) (400.2 MHz, toluene-d_8).

At 263 K the isopropyl methyls decoalesce into two broad peaks and at 213 K two sharp doublets are observed at 1.61 and 0.55 ppm. The methine group, a broad peak at room temperature also decoalesces into two sharper signals at 3.50 and 2.79 ppm when reaching 243 K.

Diffraction-quality crystals of Ti{NC(Ph)N^{i}Pr$_2$}{CMe(NDipp)$_2$}Me$_2$ (**51**) were grown from a pentane solution at room temperature and the molecular structure is shown in Figure 4.15. Selected distances and angles are listed in Table 4.4. The τ value was determined as 0.09 for **51**, suggesting that **51** adopts an almost ideal square based pyramidal geometry. **51** shows an alternative arrangement of the supporting ligands around the metal centre. The methyl group (C(41)) is best considered to sit in the axial position, while the κ^1-amidinate (π-donor) is in the equatorial position which is generally disfavoured.[22] The alternative arrangement is observed because of the steric crowding around the metal centre caused by the Dipp moiety.

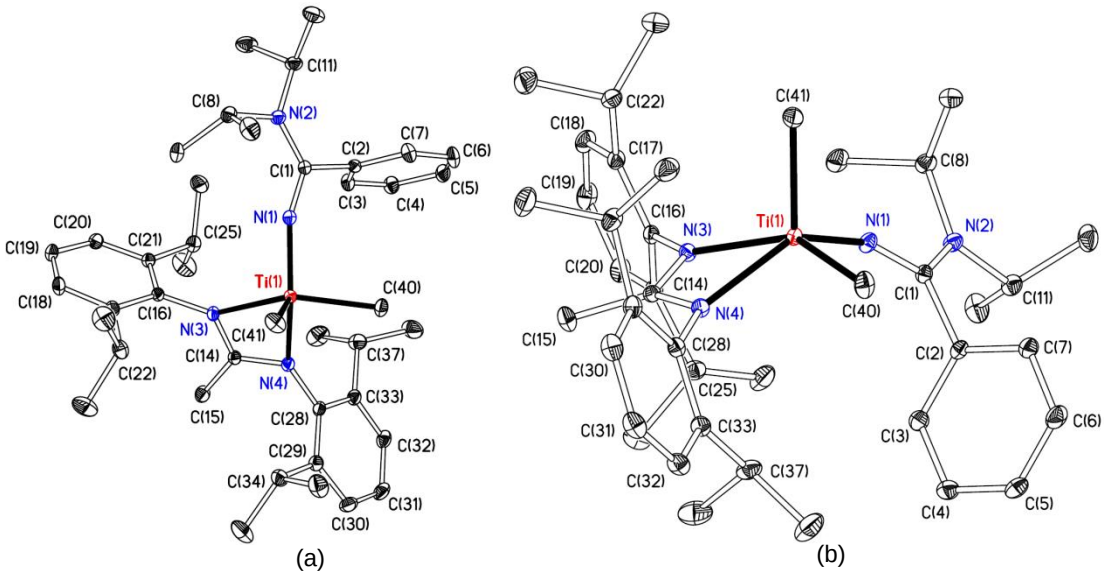

Figure 4.15. Displacement ellipsoid plots of Ti{NC(Ph)N^{i}Pr$_2$}-{MeC(NDipp)$_2$}Me$_2$ (**51**) in two different views (a) κ^1-amidinate in the axial position (b) C(41) in the axial position. Ellipsoids are drawn at 20% probability level and H atoms are omitted.

Table 4.4. Selected bond lengths (Å) and angles (°) for complex **51**.

Ti(1)–N(1)	1.822(1)	Ti(1)–N(1)–C(1)	156.8(1)
Ti(1)–N(3)	2.149(1)	Ti(1)–N(3)–C(14)	93.6(1)
Ti(1)–N(4)	2.156(1)	Ti(1)–N(4)–C(14)	93.5(1)
Ti(1)–C(40)	2.120(1)	N(3)–T(1)–N(4)	61.1(1)
Ti(1)–C(41)	2.106(1)	N(3)–C(14)–N(4)	111.5(1)

The Ti(1)–N(1) bond is elongated in **51** compared to **32** (1.822(1) *vs*. 1.791(1) Å, respectively), which foremost reflects the enhanced σ-donating ability of the methyl substituents. Furthermore, the Ti(1)–N(1)–C(1) bond angle in **51** deviates further from linearity than in complex Ti{NC(Ph)N^{i}Pr$_2$}{PhC(NSiMe$_3$)$_2$}Cl$_2$ (**4.07**) (156.8(1) *vs*. 165.4(2)º, respectively), which could be attributed to an increase steric demand of the κ^2-amidinate ligand in **51**.[31] The bond angles of Ti(1)–N(3)–C(14) and Ti(1)–N(4)–C(14) are comparable (93.6(1) *vs*. 93.5(1)º, respectively) and suggestive of a κ^2 σ,σ-symmetrical bonding mode of κ^2-amidinate.

Calculations done by Professor Mountford have shown that for small κ^2-amidiante model systems, such as Ti{MeC(NMe)$_2$}{NC(Ph)NMe$_2$}Cl$_2$ (**T**), SBP geometry is slightly favoured by 3.1 kcal mol^{-1} over TBP geometry (Figure 4.16).

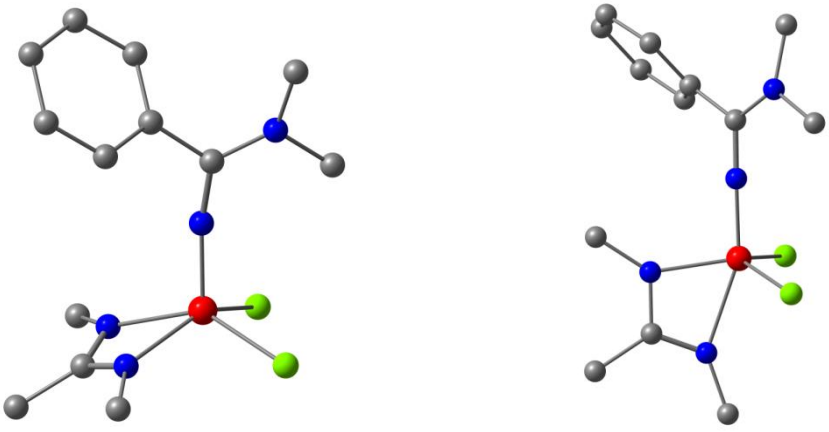

SBP (0.0 kcal mol^{-1}) **TBP** (+3.1 kcal mol^{-1})

Figure 4.16. Optimised geometries for the model κ^2-amidinate system Ti{MeC(NMe)$_2$}{NC(Ph)NMe$_2$}Cl$_2$ (**T**). Hydrogen atoms omitted for clarity.

This is different to the observations made for the small model system of the κ^2-aminopyridinato complex, where both geometries were close in energy (**R**, *vide supra*). The bond distances of the MeC–N are very similar in the SBP geometry (1.324 and 1.329 Å), suggesting a symmetrical bonding mode, allowing two σ-donor symmetry adapted linear combinations to interact with the metal centre. The two π-donor orbitals of the κ^1-amidinate can interact with the 1a' and 1a" orbitals on the metal centre (Figure 4.17). Neither of the π-acceptor MOs (2a' and 2a") would be suitable to interact with the δ-symmetry HOMO of the κ^2-amidinate ligand due to symmetry mis-match.

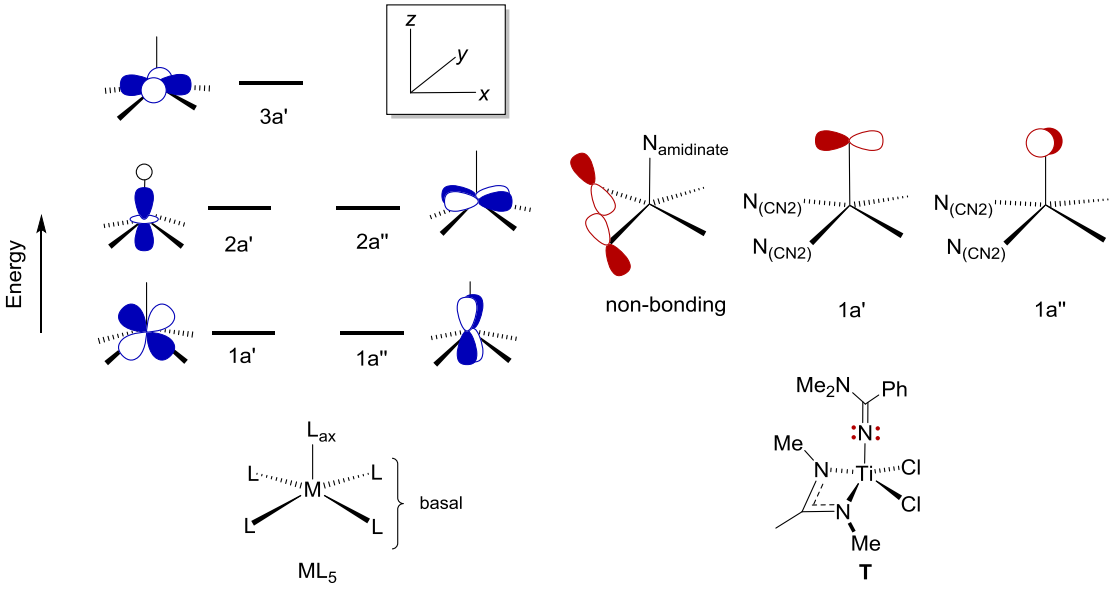

Figure 4.17. Left: the σ-only frontier MOs (d orbitals only, arbitrary energies) for a hypothetical ML_5 system. Right: representation of the compound $Ti\{MeC(NMe)_2\}\{NC(Ph)NMe_2\}Cl_2$ (**T**).

For the TBP geometry, however, different MeC–N bond lengths are observed (1.362 Å (equatorial) and 1.299 Å (axial)) indicating that the amide-imine resonance form of the ligand is stabilised (Figure 4.16). This implies that the "amide"-moiety (in the equatorial position) can now interact with the d-bonding orbitals of the metal centre, as discussed previously. However, the structure shows an elongation in the $Ti–N_{amidinate}$ bond length in TBP compared to SBP (1.799 *vs.* 1.775 Å, respectively) and hence disfavours the TBP geometry.

To study the influence of steric and electronic properties of the κ^2-supporting ligand on the polymerisation of ethylene and propylene, $Ti\{NC(Ph)N^iPr_2\}\{MeC(N^iPr)_2\}Cl_2$

(**4.07**) and Ti{NC(Ph)N^{i}Pr$_2$}{PhC(NSiMe$_3$)$_2$}Cl$_2$ (**4.08**) were prepared according to an in-house synthesis.[31] **4.07** results in a smaller steric profile compared to **50**, while **4.08** carries a trimethylsilyl substituent. Their behaviour in the co-polymerisation of ethylene and propylene will be discussed in Section 4.8.

4.6.2 Attempted synthesis of Ti{NC(Ph)N^{i}Pr$_2$}(hpp)Cl$_2$ (52)

H-hpp (1,3,4,6,7,8-hexahydro-2*H*-pyrimido[1,2-*a*]pyrimidine), a bicyclic-guanidinate ligand was also of interest for this Thesis. The anionic hpp ligand is known to coordinate to the metal centre in a κ^2-fashion, similar to the κ^2-amidinate ligands previously mentioned.[32] The substituents of N(5) (*vide infra*) are tied into the ring and therefore generating a sterically non-demanding ligand set.[32]

The NMR tube reaction of one equivalent of Li[hpp], synthesised according to literature,[33] with **4.02** yielded a mixture of products which could not be separated, even after extensive work-up procedures. However, a few diffraction-quality crystals were successfully grown from a benzene solution at room temperature. The molecular structure is shown in Figure 4.18. Selected distances and angles are listed in Table 4.5, and show that in the absence of any significant steric effects a non-distorted SBP geometry ($\tau = 0$), with the κ^1-amidinate sitting in the axial position, is formed.

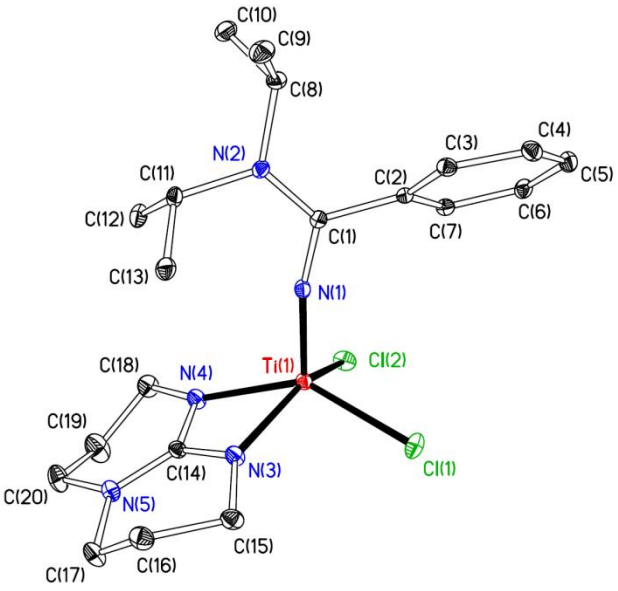

Figure 4.18. Displacement ellipsoid plots of Ti{NC(Ph)N^{i}Pr$_2$}(hpp)Cl$_2$ (**52**). Ellipsoids are drawn at 20% probability level and H atoms are omitted.

Table 4.5. Selected bond lengths (Å) and angles (°) for complex **52**.

Ti(1)–N(1)	1.773(2)	C(14)–N(5)	1.341(3)
Ti(1)–N(3)	2.038(2)	Ti(1)–N(1)–C(1)	167.4(1)
Ti(1)–N(4)	2.075(2)	Ti(1)–N(3)–C(14)	93.2(1)
Ti(1)–Cl(1)	2.315(1)	Ti(1)–N(4)–C(14)	91.7(1)
Ti(1)–Cl(2)	2.326(1)	N(3)–T(1)–N(4)	64.4(1)
C(14)–N(3)	1.336(3)	N(3)–C(14)–N(4)	110.5(1)
C(14)–N(4)	1.333(3)		

The near linear Ti(1)–N(1)–C(1) bond angle (167.4(1)º) and the short Ti(1)–N(1) bond distance (1.773(2) Å) show that the smaller steric hindrance of the hpp ligand allows efficient orbital overlap between the metal orbitals and the π-donor orbitals of the amidinate ligand. Though complex **51** carries more electron-donating substituents and therefore direct comparison between the bond distance of **51** and **52** cannot be drawn. However, the Ti(1)–N(1)–C(1) bond angle deviates further from linearity in **51** compared to **52** which is attributed to the increase in the steric demand of the κ^2-amidinate ligand in **51**. The comparable bond distances of C(14)–N(3), C(14)–N(4) and C(14)–N(5) suggests even delocalisation across the system and the bond angles of Ti(1)–N(3)–C(14) and Ti(1)–N(4)–C(14) are similar (93.2(1) *vs*. 91.7(1)º, respectively) and suggestive of a κ^2 σ,σ-symmetrical bonding mode to the metal centre.[34]

4.7 Synthesis and characterisation of cationic mono-alkyl complexes of Ti{NC(Ph)N^{i}Pr$_2$}{MeC(NDipp)$_2$}Me$_2$ (51)

On the NMR tube scale, treatment of **51** with $[Ph_3C][BAr^F{}_4]$ in C_6D_5Br led to the immediate and quantitative formation of the mono-methyl cation $[Ti\{NC(Ph)N^iPr_2\}\{MeC(NDipp)_2\}Me][BAr^F{}_4]$ (**53-[BAr$^F{}_4$]**). The Ti–Me moiety of **53-[BAr$^F{}_4$]** appears at a more downfield shift compared to the neutral complex **51** (1.87 *vs*. 1.50 ppm, respectively).

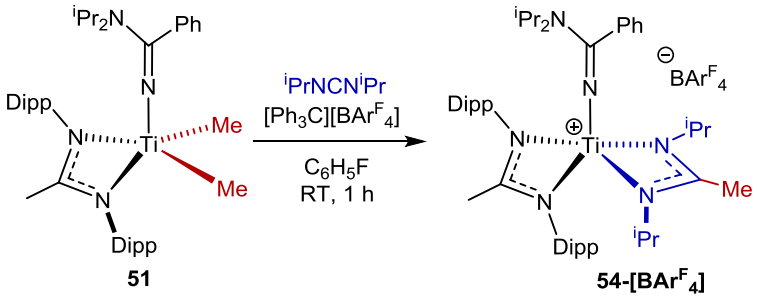

Equation 4.7

In order to stabilise the resulting cation and to allow further characterisation, **51** was activated with $[Ph_3C][BAr^F{}_4]$ in the presence of *N*,*N´*-diisopropylcarbodiimide on a preparative scale (Equation 4.7). $[Ti\{NC(Ph)N^iPr_2\}\{MeC(NDipp)_2\}\{CMe(N^iPr)_2\}][BAr^F{}_4]$ (**54-[BAr$^F{}_4$]**) was isolated as a red solid in 52% yield. In the room temperature ^1H NMR spectrum the newly formed C–Me moiety appears as a singlet at 1.98 ppm with a corresponding ^{13}C resonance at 12.5 ppm, further confirming migratory insertion into the Ti–Me bond.

4.8 Synthesis of homo-bis(ligand) complexes

The first bis(benzamidinato)metal dichloride complex was synthesised by Roesky *et al*. in 1988 and since a wide range of bis(benzamidinato) group 4 metal dichloride complexes have shown to polymerise ethylene, propylene, styrene and sometimes norbornene. [29, 30, 35-37] However, to our knowledge, those complexes have not been tested in the co-polymerisation of ethylene, propylene and ENB.

4.8.1 Synthesis of bis(aminopyridinato) complex $(Ap^1)_2TiCl_2$ (55)

Complex **55** was successfully synthesised by addition of two equivalents of lithiated aminopyridinato (**30**) to a solution of titanium tetrachloride in toluene (Equation 4.8). Immediately upon addition, a purple precipitate was observed, identified as **55** and isolated in 52% yield.

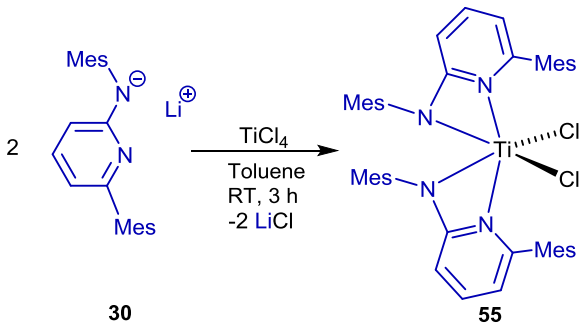

Equation 4.8

The ^{1}H NMR spectrum displays two resonances for the *meta*-protons of the pyridine backbone (6.43 and 6.24 ppm) and four singlets from 2.40 to 2.16 ppm corresponding to the methyl substituents on the aromatic ring (Figure 4.19).

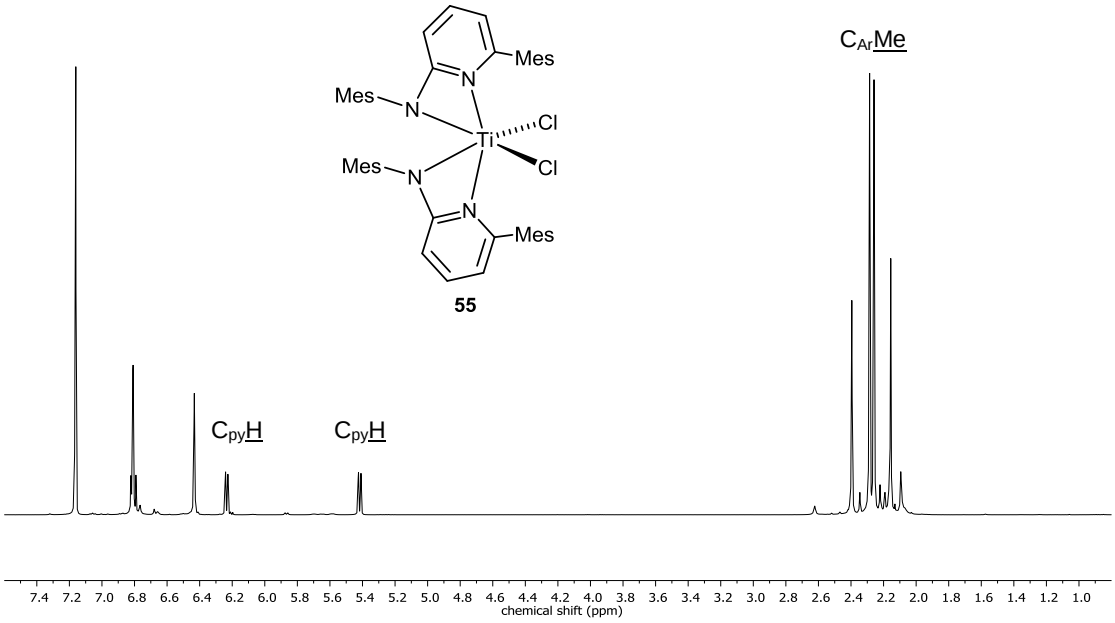

Figure 4.19. ^{1}H NMR spectrum (400.2 MHz, C_6D_6, 298 K) of $(Ap^1)_2TiCl_2$ (**55**).

Diffraction-quality crystals of **55** were obtained from a concentrated toluene solution at –78 °C and the molecular structure is shown in Figure 4.20. Selected distances and angles are listed in Table 4.6.

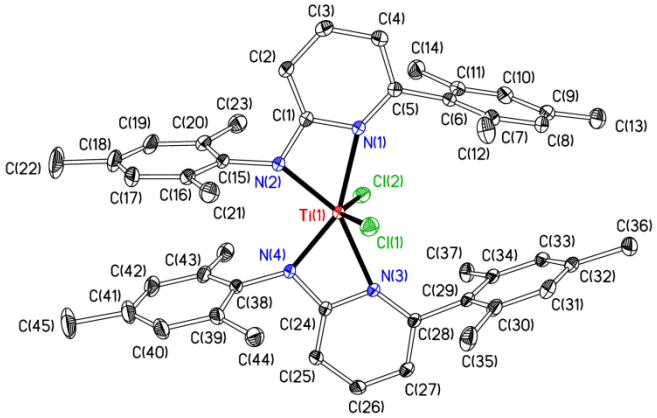

Figure 4.20. Displacement ellipsoid plot of $(Ap^1)_2TiCl_2$ (**55**). Ellipsoids are drawn at 20 % probability level and H atoms are omitted.

Table 4.6. Selected bond lengths (Å) and angles (°) for complex **55**.

Ti(1)–N(1)	2.232(1)	N(1)–T(1)–N(2)	63.39(5)
Ti(1)–N(2)	1.976(1)	N(3) –T(1)–N(4)	63.31(5)
Ti(1)–N(3)	2.234(1)	Cl(1)–Ti(1)–Cl(2)	145.06(2)
Ti(1)–N(4)	1.986(1)	N(2)–Ti(1)–N(4)	90.22(5)
Ti(1)–Cl(1)	2.290(1)	N(1)–Ti(1)–N(3)	143.05(4)
Ti(1)–Cl(2)	2.297(1)		

The molecular structure of **55** shows a distorted octahedral arrangement around the titanium centre with two chelating aminopyridinato ligands and *cis*-orientation of the two chloride ligands. The *cis* arrangement is favourable as it reduces the steric clash between the mesityl groups on the aminopyridinato. A similar trend has been observed for $Ti\{PhC(NSiMe_3)_2\}_2Cl_2$ (**4.09**).[37] Potential π-stacking of the two mesityl groups on the amine nitrogen of the aminopyridinato ligand is observed, with a distance of 3.52 Å between the two planes.[15] This has been also observed for complex **32**.

Two equivalents of methyl lithium or MeMgCl were added to $(Ap^1)_2TiCl_2$ (**55**) in attempt to dialkylate the complex. However, in both instances, the reaction resulted in a complex mixture. An alternative route was also attempted by the addition of the

protio aminopyridine ligand (Ap^1, **4.03**) to titanium tetrabenzyl, which has been proven successful for the bis(benzamidine) ligand.[38] However, again a complex mixture was observed.

4.8.2 Synthesis of previously reported bis(amidinate) (κ^1or κ^2) complexes

$Ti\{PhC(NSiMe_3)_2\}_2Cl_2$ and $Ti\{PhC(NSiMe_3)_2\}Me_2$ (**4.09** and **4.10**, respectively) were prepared following literature procedures.[32, 35-37] $Ti\{PhC(NSiMe_3)_2\}_2Cl_2$ (**4.09**) was isolated as an orange solid in 76% yield and reacted further with two equivalents of MeLi to generate $Ti\{PhC(NSiMe_3)_2\}Me_2$ (**4.10**), as a red solid 70% yield.

The bis(κ^1-amidinate) complexes, $Ti\{NC(Ph)N^iPr_2\}_2Cl_2$ and $Ti\{NC(Ph)N^iPr_2\}_2Me_2$ (**4.11** and **4.12**) have been previously made in the Mountford group and the synthesis was followed accordingly.[39] $Ti\{NC(Ph)N^iPr_2\}_2Cl_2$ (**4.11**) was isolated as a light brown solid in 65% yield and reacted further with two equivalents of MeMgCl to give the dimethyl compound $Ti\{NC(Ph)N^iPr_2\}_2Me_2$ (**4.12**) in 61% yield.

4.9 Polymerisation studies of the κ^2-amidinate complexes, 50, 51, and the bis(aminopyridinato) complex 55

To study the influence of steric and electronic properties of the κ^2-supporting ligand on the polymerisation of ethylene and propylene, $Ti\{NC(Ph)N^iPr_2\}\{MeC(N^iPr)_2\}Cl_2$ (**4.07**) and $Ti\{NC(Ph)N^iPr_2\}\{PhC(NSiMe_3)_2\}Cl_2$ (**4.08**) were also tested under the same industrially relevant conditions as for **50** and **51**.

The co-polymerisation of ethylene and propylene was performed in a small-scale batch reactor under industrially relevant conditions (90 ºC, 10 minutes) at ARLANXEO, The Netherlands. MAO-10T/BHT-H was added as co-catalyst as scavenger. Unfortunately, **50**, **51**, **4.07** and **4.08** did not polymerise ethylene and propylene under the industrially required conditions. Further tests were conducted with complex **51**. Research has emphasised a certain sensitivity of activated complexes towards BHT-H (Chapter Five). BHT-H can react with the cationic species, leading to release of methane and forming a new phenoxide complex, which is inactive towards ethylene polymerisation.[40] In the absence of any alkyl aluminium and BHT-H with $[Ph_3C][BAr^F_4]$ as the only activator, **51** did not successfully polymerise ethylene and propylene.

The bis(aminopyridinato) complex $(Ap^1)_2TiCl_2$ (**55**) was tested in the co-polymerisation of ethylene, propylene and ENB (EPDM) and for comparison, **4.09** and **4.11** were also tested under the same conditions. Unfortunately, none of these species showed any activity. The activation chemistry of **4.11** has been investigated extensively by a former DPhil student in the Mountford group, emphasising the complex behaviour of **4.11** upon activation.[39]

4.10 Summary

This Chapter has described the synthesis and characterisation of a range of aminopyridinato and κ^2-amidiante supported titanium complexes. This has included a comprehensive discussion of their structures in both, the solution phase through variable temperature NMR studies and their solid state structures. The synthetic limitations when using a different sterically demanding κ^1-aminidate in conjunction with aminopyridinato ligands and the dialkylation of a bis(aminopyridinato) complex have been discussed. The activation chemistry of aminopyridinato dimethyl complexes has been explored and the sensitivity of the resulting cations showed difficulties in isolation in general. The κ^2-amidinate bearing complexes (**50** and **51**) were shown to be inactive in the co-polymerisation of ethylene and propylene. Furthermore, $(Ap^1)TiCl_2$ (**55**) was inactive in EPDM polymerisation under industrially relevant conditions. The same observation was made for the analogues $Ti\{PhC(NSiMe_3)_2\}_2Cl_2$ and $Ti\{MeC(N^iPr)_2\}_2Cl_2$ (**4.09** and **4.11**).

4.11 References

1. R. Kempe, *Eur. J. Inorg. Chem.*, 2003, **2003**, 791-803.
2. C. Morton, P. O'Shaughnessy and P. Scott, *Chem. Commun.*, 2000, 2099-2100.
3. N. M. Scott, T. Schareina, O. Tok and R. Kempe, *Eur. J. Inorg. Chem.*, 2004, 3297-3304.
4. W. P. Kretschmer, A. Meetsma, B. Hessen, T. Schmalz, S. Qayyum and R. Kempe, *Chem. - Eur. J.*, 2006, **12**, 8969-8978.
5. A. Noor, W. P. Kretschmer, G. Glatz and R. Kempe, *Inorg. Chem.*, 2011, **50**, 4598-4606.
6. K. Merzweiler, D. Fenske, E. Hartmann and K. Dehnicke, *Z. Naturforsch., B: J. Chem. Sci.*, 1989, **44**, 1003-1006.

7. F. T. Edelmann, *Coord. Chem. Rev.*, 1994, **137**, 403-481.
8. R. Gomez, R. Duchateau, A. N. Chernega, J. H. Teuben, F. T. Edelmann and M. L. H. Green, *J. Organomet. Chem.*, 1995, **491**, 153-158.
9. L. A. Koterwas, J. C. Fettinger and L. R. Sita, *Organometallics*, 1999, **18**, 4183-4190.
10. K. C. Jayaratne and L. R. Sita, *J. Am. Chem. Soc.*, 2000, **122**, 958-959.
11. M. Hafeez, W. P. Kretschmer and R. Kempe, *Eur. J. Inorg. Chem.*, 2011, **2011**, 5512-5522.
12. J. Obenauf, W. P. Kretschmer, T. Bauer and R. Kempe, *Eur. J. Inorg. Chem.*, 2013, **2013**, 537-544.
13. H. Bigmore, *DPhil Thesis*, University of Oxford, 2007.
14. A. W. Addison, T. N. Rao, J. Reedijk, J. van Rijn and G. C. Verschoor, *J. Chem. Soc., Dalton Trans.*, 1984, 1349-1356.
15. C. Rajesh, C. Majumder, H. Mizuseki and Y. Kawazoe, *J. Chem. Phys.*, 2009, **130**, 124911.
16. R. A. Collins, A. F. Russell, R. T. W. Scott, R. Bernardo, G. H. J. van Doremaele, A. Berthoud and P. Mountford, *Organometallics*, 2017, **36**, 2167-2181.
17. R. A. Collins, A. F. Russell and P. Mountford, *Appl. Petrochem. Res.*, 2015, **5**, 153-171.
18. P. Mountford, *Chem. Commun.*, 1997, 2127-2134.
19. D. A. Fletcher, R. F. McMeeking and D. Parkin, *J. Chem. Inf. Comput. Sci.*, 1996, **36**, 746 (The UK Chemical database Service: CSD updated May 2015).
20. F. H. Allen, O. Kennard, J. J. Galloy, O. Johnson and D. G. Watson, *Chem. Des. Autom. News*, 1993, **8**, 1 & 31.
21. T. A. Albright, J. K. Burdett and M.-H. Whangbo, *Orbital Interactions in Chemistry*, Wiley-Interscience, New York, 1985.
22. A. R. Rossi and R. Hoffmann, *Inorg. Chem.*, 1975, **14**, 365-374.
23. R. A. Collins, *DPhil Thesis*, University of Oxford, 2016.
24. M. Bochmann, *Organometallics 1*, Oxford University Press, Oxford, UK, 1994.
25. E. Y.-X. Chen and T. J. Marks, *Chem. Rev.*, 2000, **100**, 1391-1434.
26. D. Walther, R. Fischer, M. Friedrich, P. Gebhardt and H. Görls, *Chem. Ber.*, 1996, **129**, 1389-1393.

27. R. Gomez, R. Duchateau, A. N. Chernega, A. Meetsma, F. T. Edlmann, J. H. Teuben and M. L. H. Green, *J. Chem. Soc., Dalton Trans.*, 1995, 217-225.
28. J. R. Hagadorn and J. Arnold, *Organometallics*, 1994, **13**, 4670-4672.
29. D. Herskovicskorine and M. S. Eisen, *J. Organomet. Chem.*, 1995, **503**, 307-314.
30. J. Richter, F. T. Edelmann, M. Noltemeyer, H.-G. Schmidt, M. Shmulinson and M. S. Eisen, *J. Mol. Catal. A: Chem.*, 1998, **130**, 149-162.
31. L. Clark, *Part II Thesis*, University of Oxford, 2008.
32. M. P. Coles, *Chem. Commun.*, 2009, 3659-3676.
33. M. P. Coles and P. B. Hitchcock, *Organometallics*, 2003, **22**, 5201-5211.
34. B. A. Clough, S. Mellino, A. V. Protchenko, M. Slusarczyk, L. C. Stevenson, M. P. Blake, B. Xie, E. Clot and P. Mountford, *Inorg. Chem.*, 2017, **56**, 10794-10814.
35. D. Walther, R. Fischer, H. Görls, J. Koch and B. Schweder, *J. Organomet. Chem.*, 1996, **508**, 13-22.
36. J. C. Flores, J. C. W. Chien and M. D. Rausch, *Organometallics*, 1995, **14**, 1827-1833.
37. H. W. Roesky, B. Meller, M. Noltemeyer, H.-G. Schmidt, U. Scholz and G. M. Sheldrick, *Chem. Ber.*, 1988, **121**, 1403-1406.
38. K.-H. Thiele, H. Windisch, H. Windisch, F. T. Edelmann, U. Kilimann and M. Noltemeyer, *Z. Anorg. Allg. Chem.*, 1996, **622**, 713-716.
39. A. Heath, *DPhil Thesis*, University of Oxford, 2011.
40. R. A. Stapleton, B. R. Galan, S. Collins, R. S. Simons, J. C. Garrison and W. J. Youngs, *J. Am. Chem. Soc.*, 2003, **125**, 9246-9247.

Chapter Five

High-throughput polymerisation and oligomerisation studies for mixed aminopryidinato, κ^1-amidinate titanium complexes

Chapter 5.1 Overview

Linear α-olefins (LAOs) are essential chemical intermediates in the synthesis of low- and high density polyethylenes (LDPE and HDPE respectively), household detergents and lubricants.[1, 2] There are a variety of methods employed to obtain LAOs but the focus of this introduction is synthesis of LAOs *via* oligomerisation. C_4–C_{40} oligomers are obtained in the Shell higher olefin process (SHOP), resulting in a Schulz-Flory distribution.[3, 4, 5] This distribution is established as the oligomerisation follows the Cossee-Arlman mechanism. The ethylene monomer coordinates to the nickel catalyst and inserts into the Ni–H bond. This is followed by further ethylene insertion and β-H elimination to give a wide range of α-olefins (Scheme 5.1). The oxidation state of the metal is maintained throughout the process. The α-olefins in the range of C_6–C_{18} are separated from the product mixture by distillation, while the heavier and lighter alkenes are isomerised and undergo cross-metathesis reaction to give a wide range of linear internal alkenes with odd and even number of carbons.[3, 4]

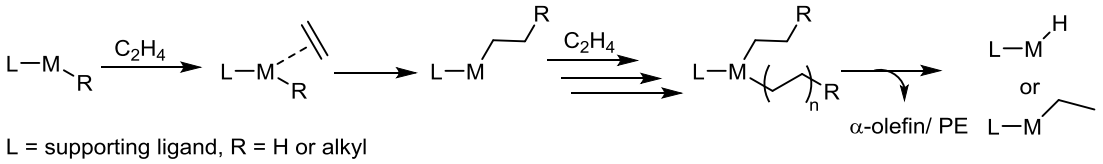

Scheme 5.1. Mechanism of ethylene oligomerisation in the SHOP process.

Despite the success of synthesising LAOs on the industrial scale, further research was directed towards a narrower product distribution and synthesis of single α-olefins with a higher market value.

Selective trimerisation of ethylene to give 1-hexene with chromium catalysts has been explored by a range of industries. Union Carbide discovered that a Cr(III) 2-ethylhexanoate system with partially hydrolysed TiBA gave polyethylene as well as 1-hexene.[6-9] A range of ligands in conjunction with a chromium metal and alkyl aluminium reagent are employed as for example Phillips uses a dimethylpyrrole supporting ligand (**5.01**, Figure 5.1),[10] and BP a bis(arylphosphine)amine ligand (**5.02**).[11, 12] The BP system achieves selectivity greater than 99% for 1-hexene at 110 °C and 8 bar ethylene pressure.[11, 12] Sasol introduced mixed heteroatomic systems

(**5.03** and **5.04**, Figure 5.1),[13-15] to give highly active trimerisation or tetramerisation catalysts, respectively.

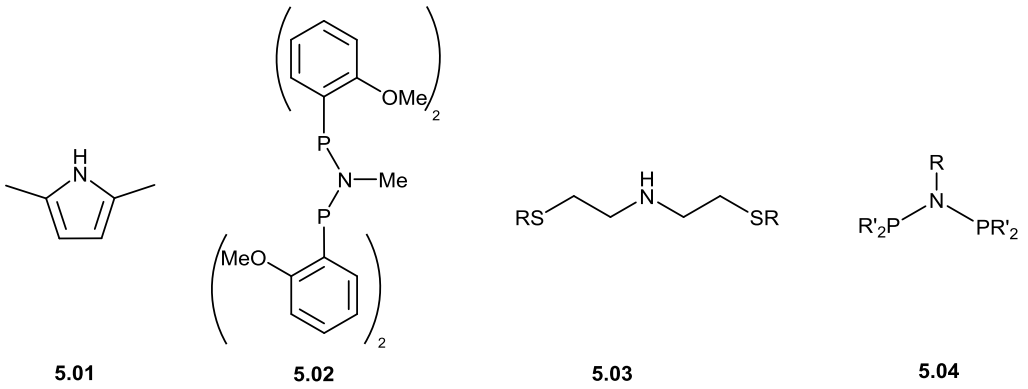

Figure 5.1. Ligand sets (**5.01–5.04**) for ethylene trimerisation catalysts.

Due to the unique selectivity for 1-hexene, the trimerisation is unlikely to operate *via* the chain growth mechanism (*vide supra*, Section 1.3). Instead, it was suggested that the mechanism follows a metallacyclic pathway.[16] This includes the coordination of two molecules of ethylene, giving a diolefin species (**I**, Scheme 5.2). This then undergoes oxidative addition to yield a metallacyclopentane complex (**II**, Scheme 5.2) and further insertion of ethylene into the metallacyclopentane moiety takes place resulting in a metallacycloheptane analogue (**III**, Scheme 5.2). β-H elimination gives a hydride-alkyl species which reductively eliminates 1-hexene and the resulting chromium species can re-enter the catalytic cycle. The oxidation state of the metal changes throughout the pathway.[16] Recently, Britovsek *et al*. have shown by experimental and DFT mechanistic studies that tetramerisation can take place *via* bis-ethylene chromacyclopentanes, in competition with mono-ethylene coordination (giving 1-hexene).[17, 18]

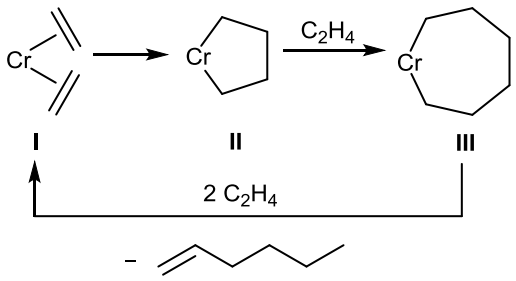

Scheme 5.2. Mechanism of trimerisation of ethylene.

The relative stability of the metallacyclopentane *versus* the metallacycloheptane ring plays a crucial role in the selectivity of 1-hexene and it has been shown that elimination of olefins from metallacycloheptane is more rapid compared to smaller rings, as the required dihedral angle of the M–β-H elimination is more accessible.[19-21] Furthermore, mechanistic studies conducted by Bercaw and co-workers have shown that trimerisation of a 1:1 mixture of C_2H_4 and C_2D_4 following a metallacyclic mechanism would give no H/D scrambling and therefore only even deuterons would be observed,[22] while for the Cossee-Arlman mechanism, H/D scrambling would be observed giving isotopomers with odd and even numbers of deuterons.[23] In the case of chromium catalysts, no H/D scrambling was observed upon trimerisation of ethylene, providing further evidence for the metallacyclic mechanism (Scheme 5.2).[22, 23]

Interestingly, Gibson *et al*. have shown that a (benzimidazol)pyridine chromium catalyst, oligomerises ethylene to give a Schulz-Flory distribution with an chain propagation probability (α) of 0.84, following a large metallacyclic ring pathway, as a 1:1 experiment of C_2H_4 and C_2D_4 did not result in H/D scrambling.[24]

Relevant to this Thesis are the homogeneous group 4 based systems capable of oligomerising ethylene. Olivé *et al*. discovered in 1970, that the system $Cp_2Ti(R)Cl/RAlCl_2$ (R = alkyl) can act as an ethylene oligomerisation catalyst to give C_4–C_{40} olefins at −20 °C and with 12 bar of ethylene.[25] However, it was not until 2001 when Hessen *et al*. discovered the selective trimerisation of ethylene with $\{Me_2C(C_5H_4)(C_6H_5)\}TiCl_3$ (**5.05**) in the presence of MAO, the first highly selective system not based on chromium.[26] The hemilabile ligand accounted for the switch of polymerisation catalyst to trimerisation catalyst. This is believed due to its ability to stabilise the low valent Ti(+2) oxidation state (Scheme 5.3). This has been confirmed experimentally and by DFT.[27, 28]

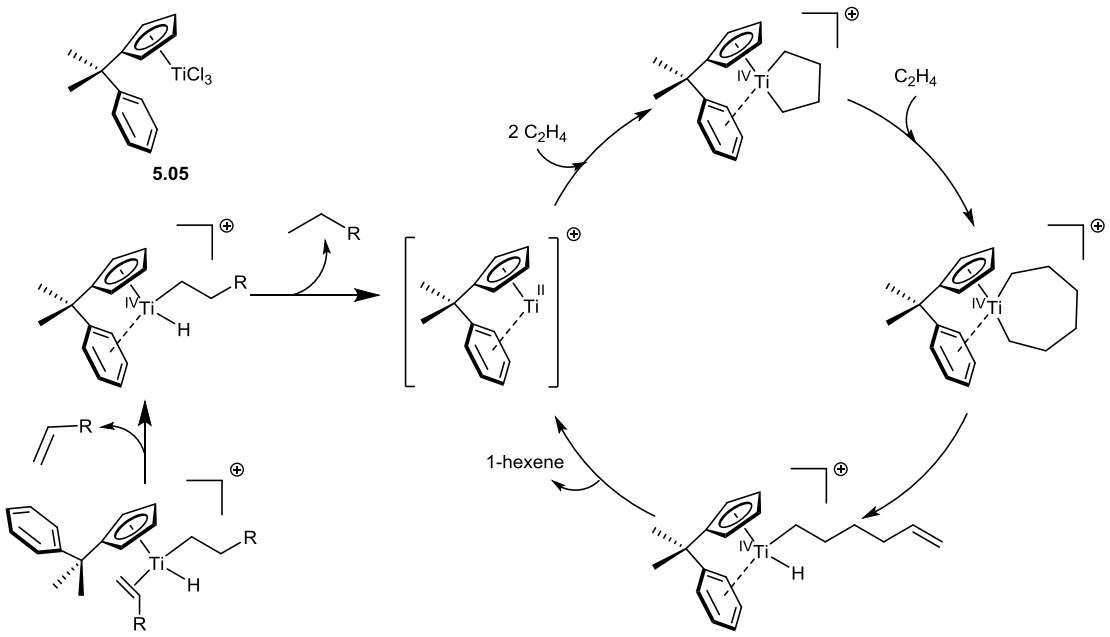

Scheme 5.3. Mechanism of trimerisation of ethylene with titanium-based catalysts.[28]

More recently, Fujita *et al*. introduced a highly active titanium-based catalyst bearing a phenoxy-imine-ether ligand (**1.36**) for ethylene trimerisation, which gave high activities of 6.59 × 10^6 g of 1-hexene/(g of Ti)/ h.[29, 30] Severn and co-workers have shown that immobilising these systems on MAO pre-treated silica alongside silica-supported scavengers resulted in a highly active trimerisation of 1-hexene while preventing any reactor fouling.[31]

To obtain branched low density polyethylene (LLDPE) most commonly required two monomers, such as ethylene and 1-hexene. However, Bazan and co-workers have shown that the combination of two catalysts can give branched polyethylene with only ethylene as feedstock (Figure 5.2).[32]

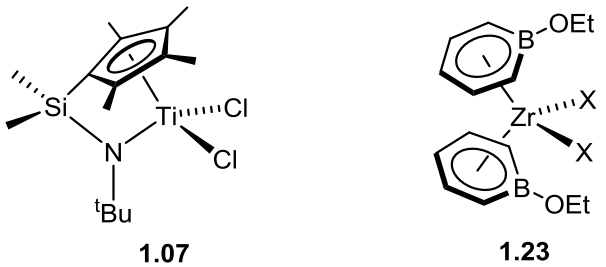

1.07 **1.23**

Figure 5.2. 1.07 and **1.23** employed as catalysts in the manufacturing of LLDPE.

The constrained geometry catalyst {$C_5Me_4SiMe_2(N^tBu)$}$TiCl_2$ (**1.07**), copolymerising ethylene and 1-alkenes,[33, 34] alongside the boratabenzene substituted zirconium

dichloride complex, $(C_5H_5BOEt)_2ZrCl_2$ (**1.23**), oligomerising ethylene,[35] have been shown to give LLDPE in the presence of MAO and ethylene.[32] Shortly after, Gruter *et al*. achieved co-polymerisation of ethylene and 1-hexene with $[Cp^*TiMe_2][MeBAr^F{}_3]$ from a simple ethylene feed using high concentration of titanium and low monomer pressure (under 1 atm). It was proposed that 1-hexene is generated *in situ via* titana(IV)cycles (*vide supra*) followed by co-polymerisation of ethylene and 1-hexene, easily achieved due to the open coordination sphere of the catalyst.[36]

The selective dimerisation of ethylene to 1-butene was first discovered by Ziegler in 1952.[37, 38] However, it was the cooperation of IFP and Sabic that led to the development and implementation of the Alphabutol process, which is responsible for a significant proportion of the world's high purity 1-butene supply. The Alphabutol process uses titanium alkoxide systems, of the type $Ti(OR)_4$ (R = alkyl groups), with triethylaluminium to successfully dimerise ethylene to 1-butene in good yield and high selectivity (>93%) at moderate temperatures (50–60 ºC).[39-41] Titanium aryloxide complexes of the type $Ti(OAr)_4$ (Ar = aryl) have also been successfully employed in combination with trialkylaluminium in the Toso 1-butene process.[42] More recently, titanium systems bearing aryloxide and alkyloxide ligands have been investigated and show promising results for the selective formation of 1-butene.[43, 44] There are controversies concerning the mechanism of the dimerisation. It was generally believed that the dimerisation occurs *via* a metallacyclic mechanism.[45] However, certain studies have shown that the metallacyclopentane complexes can be more stable than its metallacycloheptane analogues due to the relative rigidity of the 5-membered ring and therefore the difficulty to obtain the correct M–β-H dihedral angle to allow β-H elimination (*vide supra*).[19, 21] More recently, mechanistic studies were performed by Suttil and McGuinness on the $Ti(OBu)_4/AlMe_3$ catalyst system.[46] Analysis by GC-MS of dimerisation of a 1:1 mixture of C_2H_4 and C_2D_4, resulted in H/D scrambling, providing further evidence for the Cossee-Arlman mechanism taking place (*vide supra*).[46]

This Chapter describes the activity of the aminopyridinato-based complexes $(Ap^x)Ti\{NC(Ph)N^iPr_2\}Cl_2$ (**32**–**34**) in the polymerisation of ethylene, propylene and ENB as well as the capability of $(Ap^1)Ti\{NC(Ph)N^iPr_2\}Me_2$ (**35**) and

(Ap^2)Ti{NC(Ph)N^{i}Pr$_2$}Me$_2$ (**37**) to oligomerise ethylene. The sensitivity of these systems towards BHT-H, a common additive in polymerisation, will also be explored.

5.2 EPDM ter-polymerisation experiments using 1.75–1.77, 4.02 and 32–34

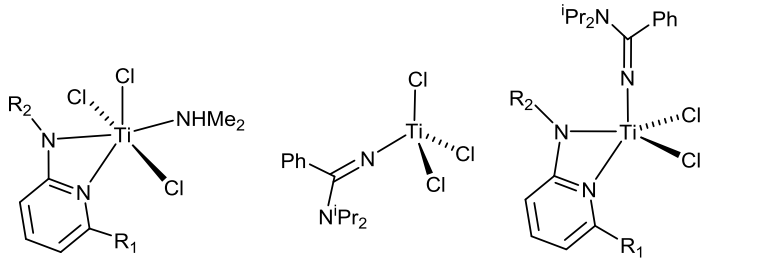

1.75 $Ap^1Ti(HNMe_2)Cl_3$
1.76 $Ap^2Ti(HNMe_2)Cl_3$
1.77 $Ap^3Ti(HNMe_2)Cl_3$

4.02

32 $Ap^1Ti\{NC(Ph)NiPr_2\}Cl_2$
33 $Ap^2Ti\{NC(Ph)NiPr_2\}Cl_2$
34 $Ap^3Ti\{NC(Ph)NiPr_2\}Cl_2$

Figure 5.3. Structures of 1.75–1.77, 4.02 and 32–34.

EPDM (ethylene, propylene and 5-ethylidenebicyclo[2.2.1]hept-2-ene (ENB)) ter-polymerisation testing of the aminopyridinato bearing complexes (**32**–**34**) were performed in Parallel Pressurised Reactors (PPR, Freeslate) under industrially relevant conditions at ARLANXEO, The Netherlands. A comparison made with the known complexes, bearing only aminopyridinato or amidinato supporting ligands (**1.75**–**1.77** and **4.02**, respectively) under identical conditions. [Ph_3C][BAr^F_4] and MMAO-3A/BHT-H were used as co-catalysts to achieve efficient activation of the aforementioned dichloride complexes. One equivalent of BHT-H per aluminium centre was added in order to scavenge any residual TMA and TiBA by making (BHT)$_2$AlR (R = Me or ^{i}Bu) which can further scavenge impurities in the reactor. BHT-H is thought to be essential, as NMR tube experiments with complex **37** have shown the transfer of the aminopyridinato ligand from titanium to aluminium to give (Ap^2)$AlMe_2$. Similar observations have been made by Kretschmer *et al*. for the complex (Ap^2)$ZrCl_2$ with MAO.[47]

Complexes **1.75** and **4.02** gave significant higher incorporation of propylene in the resulting polymer compared to **32**. The wt% of ENB for polymers produced with **32–34** could not be determined accurately as the resonances in the IR spectrum overlapped with the resonances of the vinyl end-groups. The high level of vinyl measured by FT-IR for **32**–**34** is surprising but can be explained by these systems to

also act as oligomerisation and subsequently as polymerisation catalysts, resulting in vinyl chain-ends (*vide infra*).

The productivities obtained for all complexes are low, especially in comparison to other known EPDM catalysts (Chapter 2).[48] Complex **1.76** was also tested in the ter-polymerisation of ethylene, propylene and ENB by Kempe *et al*. at 50 ºC. The resulting productivity (1145 kg mol^{-1} h^{-1} bar^{-1}) is comparable to the productivity obtained under industry relevant conditions for ARLANXEO (Table 5.1, Entry 2).[49] For all complexes, the yield of the isolated polymer was low, ranging from 31.1 mg to 13.3 mg, and therefore at the limit for accurate characterisation of the molecular weight and polydispersity index (PDI) by GPC measurements (Table 5.1). To allow GPC measurements for the lower yielding polymers, the experiments were repeated for 10 minutes (Table 5.1, Entry 4, 6 and 7). All complexes show multi-modal behaviour, as seen with PDIs larger than 2 in all cases. The molecular weight traces show a low molecular weight component for complexes **32**–**34**, which could be representing oligomers (C_{14} and above) or poly(oligomer) formed during the process (Figure 5.4). This will be discussed further in Section 5.4. The composition and GPC values reflect the bulk of a multi-modal polymer blend therefore conclusions on monomer affinities cannot be drawn.

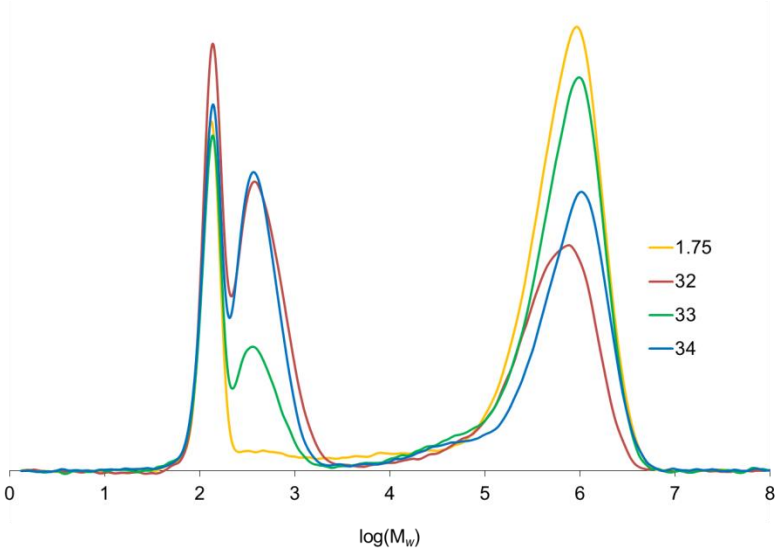

Figure 5.4. Molecular weight traces (log(M_w) *vs*. detector response) of multi-modal polymer blend synthesised with compounds **1.75** and **32**–**34**. The lowest M_w peak corresponds to BHT reference marker.

Table 5.1. EPDM copolymerisation results for **1.75**–**1.77**, **4.02** and **32**–**34**.

Entry	Precatalyst	Productivity (kg mol^{-1} Ti h^{-1} bar^{-1})	C_2 (wt%)	C_3 (wt%)	ENB (wt%)	Vinyl (wt%)	M_n (g mol^{-1})	M_w (g mol^{-1})	PDI
1	**1.75**[a]	2,560	38	56	5	<1	257,000	798,000	3.6
2	**1.76**[a]	1,230	41	52	6	<1	97,000	805,000	8.3
3	**1.77**[a]	1,200	37	54	8	<1	144,000	765,000	5.3
4	**4.02**[b,c]	3,150	29	64	8	<1	38,000[c]	470,000	12.2
5	**32**[b]	4,705	31	38	*d*	10	184,000	576,000	3.7
6	**33**[b,c]	1,430	32	48	*d*	6	155,000[c]	880,000	6.3
7	**34**[b,c]	2,340	32	51	*d*	5	253,000[c]	938,000	3.7

Polymerisation conditions.[a] T = 90 ºC, Pressure = 8.8 bar, Cat loading = 0.02 μmol, cocatalyst = MMAO-3A/BHT ([Al]:[BHT-H] = 0.5, [Al]:[Cat] = 500), $[Ph_3C][BAr^F{}_4]$: [Cat] = 2, 5 minute reaction time. Solvent = toluene (4.1 mL), $P_{C_3H_6}$ = 7.5 bar, $P_{C_2H_4}$ = 1.3 bar, C_2/C_3 (liquid phase) = 0.025 molar ratio, ENB = 185 μmol. [b] Cat loading = 0.016 μmol, [Al]:[Cat] = 625.[c] 10 minute reaction time.[d] Could not be accurately determined due to overlapping IR resonances from the vinyl end-groups.

Polymer characterisation. Polymer molecular weight and molecular weight distribution have been analysed with Freeslate Rapid GPC in 1,2,4-Trichlorobenzene against PS standards. The average composition have been determined *via* transmission IR spectroscopy on a pressed polymer film.

An increase in the steric requirement of the Ap ligand results in a higher PDI as for example **33** gives a PDI of 6.3, while **32** gives a PDI of 3.7 (Table 5.1, Entry 5 and 6). The highest molecular weight was achieved with compound **34** (Table 5.1, Entry 7). Compound **4.02**, bearing only a κ^1-amidinate ligand, gives the lowest productivity along with a very high PDI, emphasising the broad molecular weight distribution of the resulting polymer (Table 5.1, Entry 4).

5.3 BHT-H sensitivity of 35 and 37

Initial studies of the activation of metallocene complexes in the presence of MAO showed that residual amounts of $AlMe_3$ would trigger lower productivity due to the adduct formation with the cationic group 4 complex (Section 1.6). Addition of 2,6-di-*tert*-butyl-4-methylphenol (BHT-H) led to the formation of $MeAl(BHT)_2$,[50-52] which has shown to be a non-interacting scavenger.[53, 54] Collins *et al*. reported the reaction of BHT-H with $[Cp_2ZrMe][MeBAr^F_3]$ (**1.41**) resulted in the formation of an aryloxide complex $[Cp_2ZrBHT][MeBAr^F_3]$ (**1.42**, BHT = O-2,6-$^tBu_2C_6H_3Me$).[55] However, when Collins and co-workers compared the relative rate of reaction of BHT-H with the rate of insertion of ethylene with complex **1.41**, it showed that ethylene inserted more readily than the reaction with BHT-H and therefore free BHT-H did not influence the productivity.[55]

Under industrially relevant conditions, BHT-H is added to the small scale reactor in a 2:1 ratio to aluminium centres. Ittel *et al*. have shown that TiBA reacts with two equivalents of BHT-H to give $^iBuAl(BHT)_2$ in a step-wise reaction,[52] while NMR tube scale reactions of DiBAlO ($(^iBu_2Al)_2O$) with one equivalent of BHT-H showed the formation of $\{Al(^iBu)_2\}O\{^iBuAl(BHT)\}$ (**56**). Addition of two or four equivalents of BHT-H gave $\{^iBuAl(BHT)\}_2O$ (**57**) as a major product alongside unreacted BHT-H and **56**, even under continuous heating. This could suggest that some free BHT-H is present in the reactor during polymerisation.

The co-polymerisation of ethylene and propylene with **35** was tested in a small scale reactor under industrially relevant conditions at ARLANXEO, the Netherlands. Two equivalents of $[Ph_3C][BAr^F_4]$ were added as co-catalyst throughout to allow efficient activation of the dimethyl complex.

Table 5.2. EPM co-polymerisation results for $(Ap^1)Ti\{NC(Ph)N^iPr_2\}Me_2$ (**35**).

Entry	Precatalyst[a]	Alkyl Al	BHT	$[Ph_3C][BAr^F{}_4]$	Yield (g)	ΔT (ºC)
1	**35**	TiBA	2 eq wrt Al	2 eq wrt Ti	0.25	0.06
2	**35**[b]	DiBAlO	2 eq wrt Al	2 eq wrt Ti	0.29	0.52
3	**35**[b,c]	–	1 eq wrt Ti	2 eq wrt Ti	0.1	0.06
4	**35**[b,d]	–	5 eq wrt Ti	2 eq wrt Ti	0.06	0.02
5	**35**[b,e]	DiBAlO	–	2 eq wrt Ti	0.99	>11
6	**35**[f]	–	–	2 eq wrt Ti	1.43	>10
7	**35**[b,f]	–	–	2 eq wrt Ti	1.3	6.13

Polymerisation conditions. [a] T = 90 ºC, Pressure = 7 bar, Cat loading = 10.0 μmol, [Al]:[Cat] = 4500, [Al]:[BHT] = 0.5, [Cat]:[B] = 2, 10 minute reaction time. Solvent = pentamethylheptane (1L), C_3/C_2 = 200/400 Nl/h. [b] Cat loading = 5 μmol. [c] [Al]:[Cat] = 0, [BHT]:[Ti] = 1. [d] [Al]:[Cat] = 0, [BHT]:[Ti] = 5. [e] [Al]:[Ti] = 4500, [Al]:[BHT] = 0. [f] no Al/BHT additives.

To investigate the influence of BHT-H on the polymerisation process, two equivalents of BHT-H per aluminium centre were added (Table 5.2, Entry 1 and 2). Only a low yield was obtained and no significant change in temperature was observed. ΔT is the only parameter that allows an insight into the reactivity of these systems, as most of the products are in the gas phase. Addition of various amounts of BHT-H to the reactor, in the absence of alkyl aluminium reagents, also showed no significant increase in temperature (Table 5.2, Entry 3 and 4).

The sensitivity of **35** and **37** towards BHT-H was tested with the NMR tube scale reaction of **35** or **37** with $[Ph_3C][BAr^F_4]$ in the presence of BHT-H (Equation 5.1). The new complex $[(Ap^x)Ti\{NC(Ph)N^iPr_2\}(BHT)][BAr^F_4]$ is formed upon release of methane (x = 1 or 2, **58-[BAr$^F_4$]** and **59-[BAr$^F_4$]** respectively). The reaction proceeded cleanly for **37** and was also prepared on a preparative scale, isolated as a pale red complex in 55% yield. Complex **58-[BAr$^F_4$]** was only investigated on the NMR tube scale as isolation on a preparative scale was not successful.

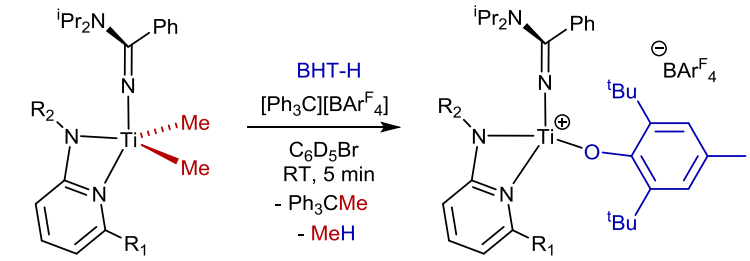

35 $R_1 = R_2$ = Mes
37 R_1 = Tripp R_2 = Dipp

58-[BAr$^F_4$] $R_1 = R_2$ = Mes
59-[BAr$^F_4$] R_1 = Tripp R_2 = Dipp

Equation 5.1

The ^{1}H NMR spectrum of **59-[BAr$^F_4$]** displays two singlets at 2.43 and 1.23 ppm assigned to the methyl and *tert*-butyl group of the BHT moiety (Figure 5.5). The region between 1.49 to 0.90 ppm corresponds to the isopropyl methyl groups on both supporting ligands. Through-space correlation of the *tert*-butyl group to a methine group on the Ap-moiety at 2.51 ppm is observed in the ROESY experiment, confirming coordination of the BHT fragment.

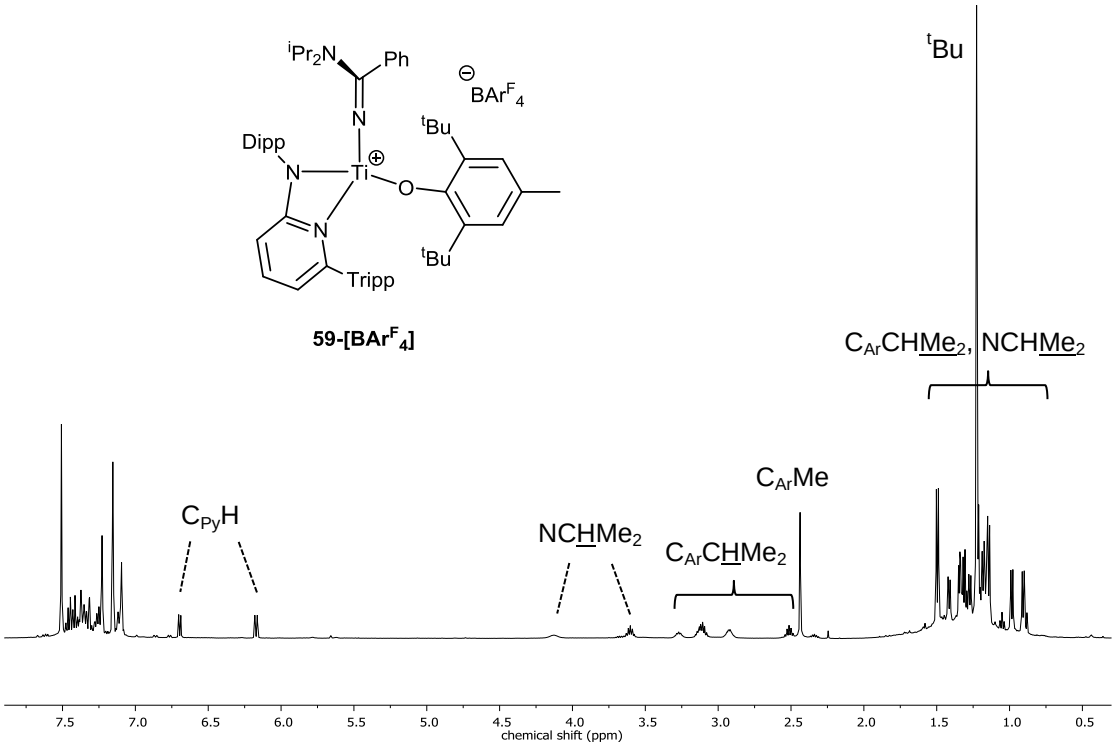

Figure 5.5. ^{1}H NMR spectrum (400.2 MHz, C_6D_5Br, 298 K) of [(Ap^{2})Ti{NC(Ph)N^{i}Pr$_2$}(BHT)][BAr$^{F}_4$] (**59-[BAr$^{F}_4$]**).

The newly formed aryloxide complexes **58-[BAr$^{F}_4$]** and **59-[BAr$^{F}_4$]** were investigated in their activity towards ethylene by NMR tube scale reactions. A degassed C_6D_5Br solution of *in situ* prepared [(Ap^{2})Ti{NC(Ph)N^{i}Pr$_2$}(BHT)][BAr$^{F}_4$] (**59-[BAr$^{F}_4$]**) in an NMR tube was exposed to two atmosphere of ethylene and the ^{1}H NMR spectrum was recorded within 3 minutes. No colour change or precipitate was observed. The room temperature ^{1}H NMR spectrum clearly shows **59-[BAr$^{F}_4$]** as the major compound alongside small amounts of unreacted ethylene at 5.65 ppm (Figure 5.6). Interestingly, new multiplets are observed in the region between 5.00 to 6.10 ppm and also between 2.10 to 2.20 ppm. These were assigned to the methylene and methine moieties of α-olefins and agreed with the chemical shifts of 1-butene[56] and 1-hexene. The resonances of –CH_2 and –Me moieties are obstructed by isopropyl groups of the supporting ligand system. Similar observations were made for **58-[BAr$^{F}_4$]**.

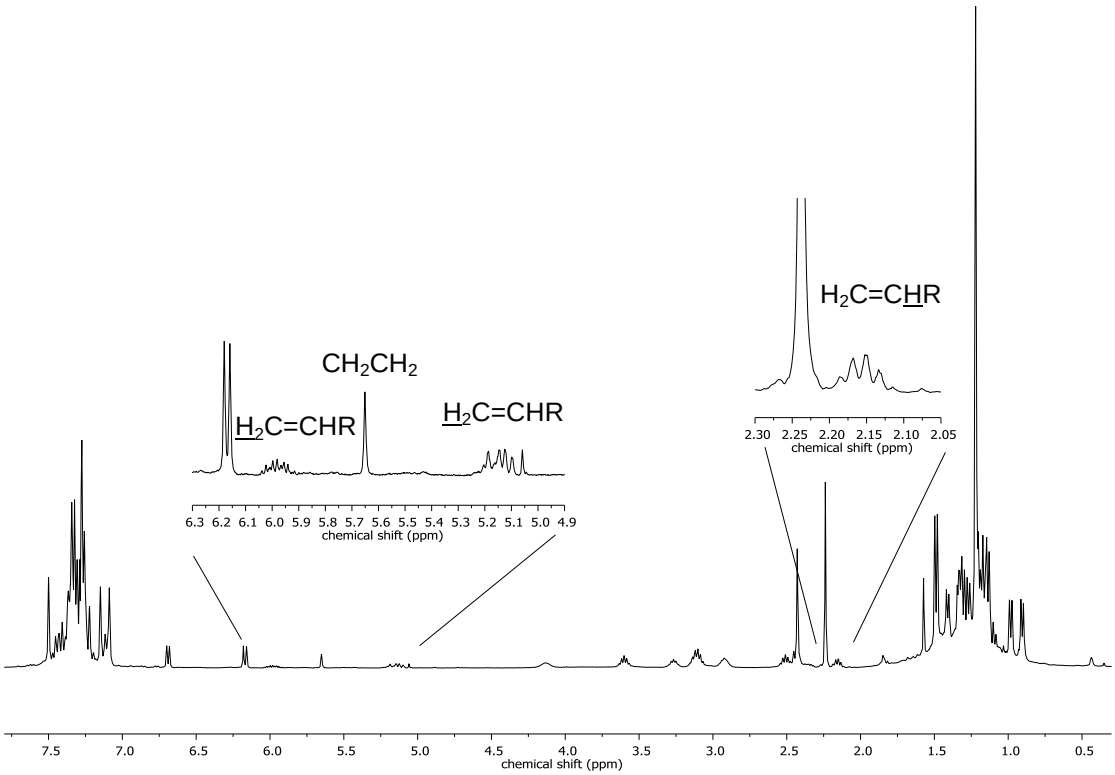

Figure 5.6. ^{1}H NMR spectrum (400.2 MHz, C_6D_5Br, 298 K) of **58-[BAr$^{F}_{4}$]** and ethylene.

Further experiments on the small scale reactor at ARLANXEO showed that in the co-polymerisation of ethylene and propylene, a significant temperature increase is observed in the absence of BHT-H, with or without alkyl aluminium as co-catalyst (Table 5.2, Entry 5–7). This is suggestive of a highly active system. The isolated polymer, however, results in a lower yield than what would be expected for an exothermic reaction. To investigate this further, ARLANXEO analysed the reaction medium by gas chromatography (GC) and observed a range of oligomers. This provides a reasonable explanation of the low yield of isolated polymer, the low molecular weight component and the high vinyl wt% observed. However, the pentamethylheptane obscured most of the important region in the chromatogram, and therefore the oligomerisation capabilities of **35** and **37** were further investigated at the High Throughput Experimentation facility of ETH Zürich (HTE@ETH) and on the NMR tube scale in Oxford.

5.4 Ethylene oligomerisation experiments with 35 and 37

Upon exposure of two atmosphere of ethylene to a degassed C_6D_5Br solution of the *in situ* prepared [(Ap[1])Ti{NC(Ph)N[i]Pr$_2$}Me][BAr$^F_4$] (**41-[BAr$^F_4$]**), no precipitate was observed, nor any resonances for oligomers. Instead a soluble polymer was formed, as indicated by the broad resonances from 1.10 to 1.90 ppm. The solution was quenched with methanol and the resulting polymer was isolated (Chapter Three) and analysed by NMR spectroscopy and GPC measurements. No polyethylene was observed, indicating oligomerisation of ethylene before polymerising the oligomers. To assign the ^{13}C resonances of the resultant polymer, DEPT and 2-D experiments were carried out (Figure 5.7). The repeating units of the –CH$_2$ and –CH appear at 40.2 and 32.3 ppm (**f** and **e**, respectively). The resonances corresponding to the final –Me groups come around 14 ppm (**a**, Figure 5.7), followed by the adjacent –CH$_2$ group at around 22–23 ppm (**b**), showing multiple peaks in each region.

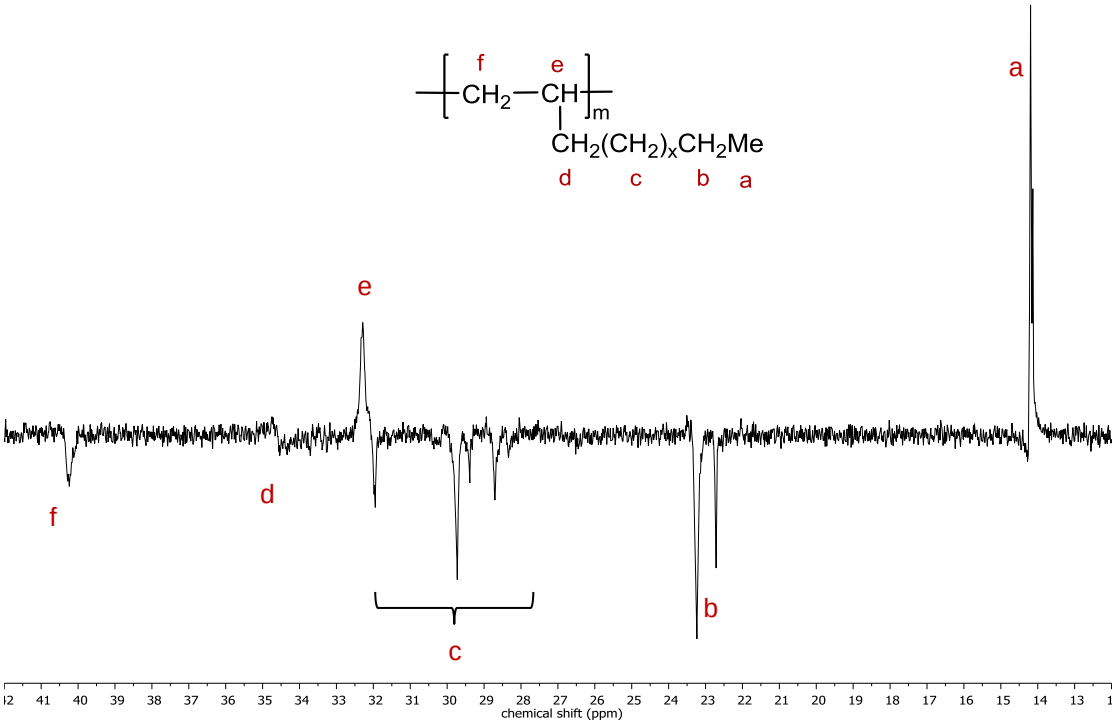

Figure 5.7. DEPT-135 spectrum ($CDCl_3$, 298 K) of the isolated poly(oligomer).

The ^{13}C NMR spectrum therefore shows that the polymer is made from more than just one oligomer. These assignments are similar to the literature of poly(1-hexene) and poly(1-octene).[57, 58]

The GPC trace of the poly(oligomer) shows bimodal distribution with a PDI of 7.0 (Table 5.3, Figure 5.8). For comparison, poly(1-hexene) was prepared on the NMR tube scale with $[(Ap)^1Ti\{NC(Ph)N^iPr_2\}Me][BAr^F{}_4]$ **41-[BAr$^F{}_4$]**. The resulting polymer was isolated and characterised by NMR spectroscopy and GPC.

Table 5.3. GPC data of poly(1-hexene) and poly(oligomer) obtained with **41-[BAr$^F{}_4$]**.

	M_n (g mol^{-1})	M_w (g mol^{-1})	PDI	M_p(1) (g mol^{-1})	M_p(2) (g mol^{-1})	Yield (g)
Poly(1-hexene)	1,200	8,500	7.0	1,800[a]	18,700[b]	0.02
Poly(oligomer)	2,200	15,300	7.0	2,300[c]	18,712[d]	0.04

[a] M_n = 990, M_w = 1,700. [b] M_n = 19,000, M_w = 39,200. [c] M_n = 1,600, M_w = 2,600. [d] M_n = 20,400, M_w = 39,600.

Similar bimodal behaviour was observed of poly(1-hexene) (PDI of 7.0). However, the second component is slightly more pronounced in poly(oligomer), which is also reflected in the individual M_n values (Table 5.3, Figure 5.8).

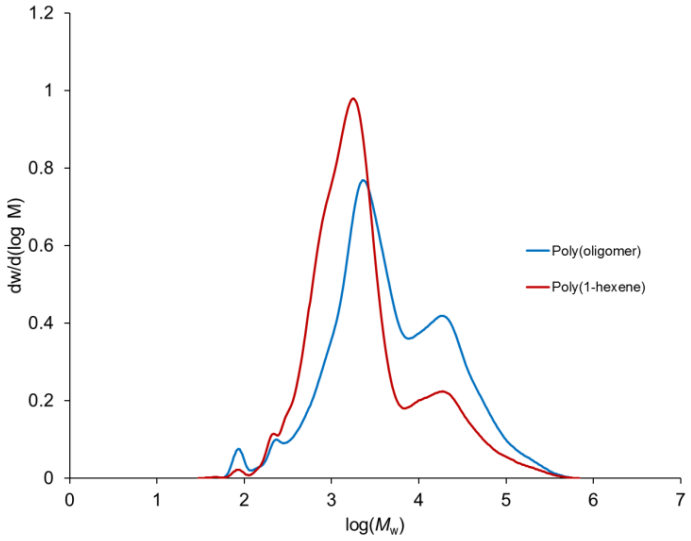

Figure 5.8. Molecular weight trace (log(M_w) *vs.* detector response of poly(1-hexene) and poly(oligomer) in THF at 303 K.

To observe oligomers before they are polymerised, the NMR tube scale reaction of ethylene addition to a degassed C_6D_5Br solution of **41-[BAr$^F{}_4$]** at –30 ºC was investigated and monitored by ^{1}H NMR spectroscopy at –30 ºC. The first addition of two atmosphere of ethylene showed only polymer formation in the ^{1}H NMR

spectrum. However, further addition of two atmosphere of ethylene (to the degassed sample) at –30 ºC displayed originally the formation of oligomers in the ^{1}H NMR spectrum which were converted to the polymer. This suggests that when using high concentrations of **35** and **37** (16 mM) with only one addition of two atmosphere of ethylene (*ie* "starving" the catalyst) at room temperature, the catalyst forms oligomers which are then immediately polymerised. This is similar to observations made by Gruter *et al*. with [Cp*TiMe$_2$][MeBAr$^{F}_3$] (*vide supra*).[36]

To investigate if the polymer is only formed under "starving" conditions, the reaction was repeated in a Schlenk tube and ethylene was added to the vigorously stirring solution under continuous flow for 30 minutes and afterwards stirred for another 30 minutes. The room temperature ^{1}H NMR spectrum of the resulting reaction mixture, showed the presence of a considerable amount of oligomers, alongside the formation of polymer and some residual ethylene (Figure 5.9).

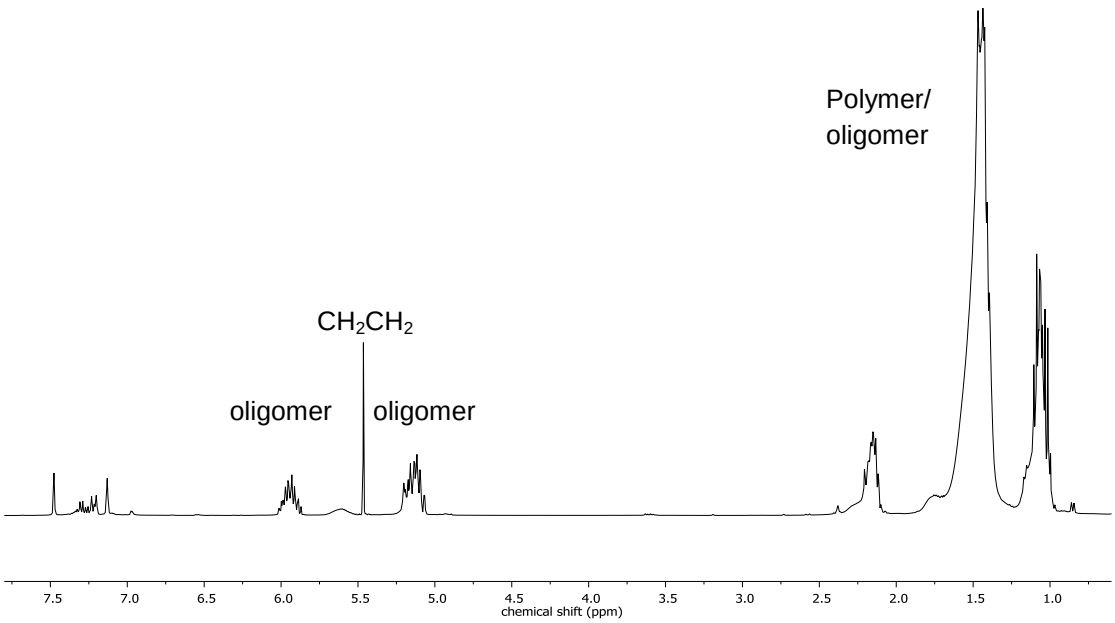

Figure 5.9. ^{1}H NMR spectrum (400.2 MHz, C_6D_5Br, 298 K) of the reaction of **41-[BAr$^{F}_4$]** under continuous flow of ethylene.

This suggests that the polymer is also formed under continuous feed of ethylene. It also shows that within one hour, the catalyst is no longer active.

To investigate the distribution of the oligomers formed, catalytic ethylene oligomerisation experiments were performed at the High Throughput Experimentation

facility of ETH Zürich (HTE@ETH) in collaboration with Dr. Alexey Fedorov and Prof. Christophe Copéret. Glass liners were charged with appropriate amounts of DiBAlO, decaline (internal standard) and $[Ph_3C][BAr^F_4]$ in toluene and loaded into an 8-parallel autoclave in a glove box. The cells were heated and pressurised with ethylene to the desired conditions and once those conditions were reached, a toluene solution containing the metal complex was injected. A full experimental description is provided in Chapter Six and the Appendix.

The reaction was quenched by purging the autoclave with nitrogen. The GC-MS samples were prepared by taking a 1 mL solution from the glass vials and diluted with further 0.5 mL of toluene. The GC was calibrated, allowing the quantitative analysis of liquid oligomers (C_6–C_{22}) formed during the reaction. However, the provided experimental set up did not allow for quantitative determination of 1-butene and poly(oligomer) formed in the reactor. The GC chromatograms obtained for **35** and **37** both show a non-selective, Schulz-Flory distribution of oligomers, ranging from C_4–C_{22} for **35** and **37** (Figure 5.10, Table 5.4).

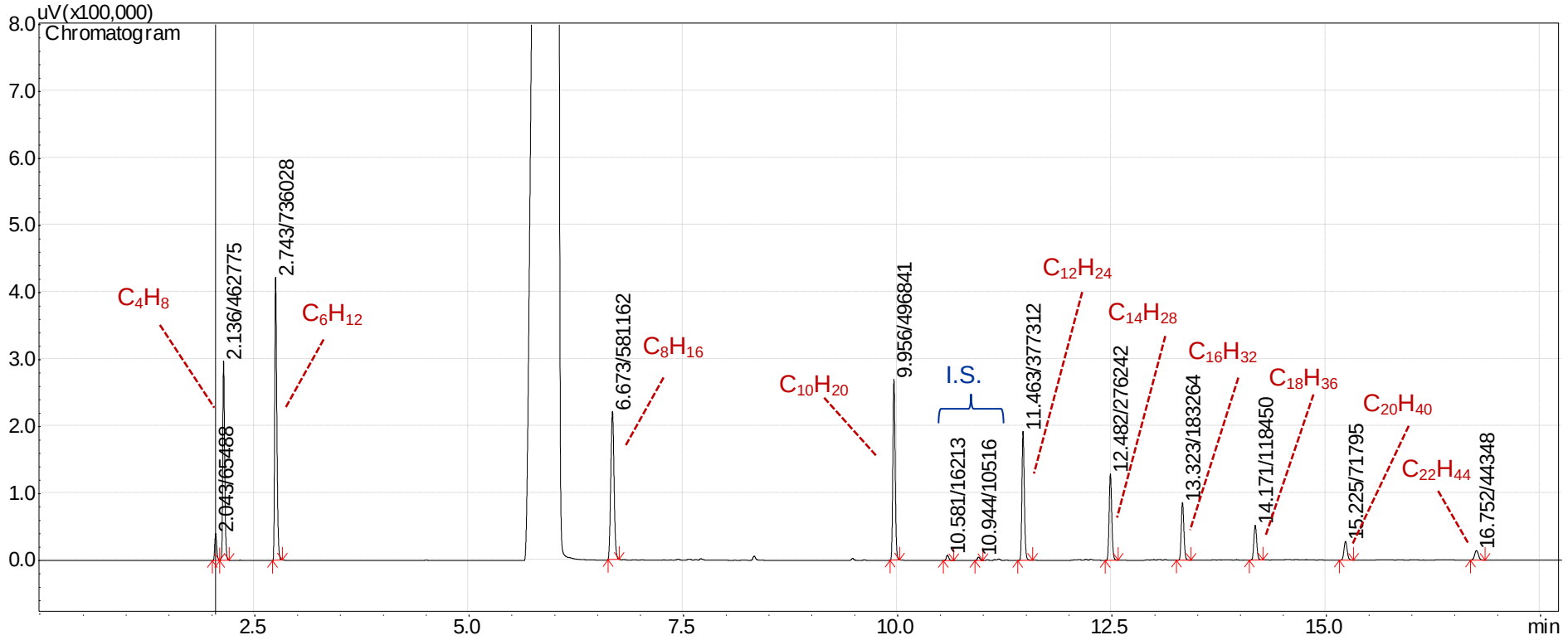

Figure 5.10. GC chromatogram of oligomers formed for **35** under conditions summarised in Table 5.4, Entry 1. I.S. (*trans*- and *cis*-Decalin) retention time at 10.58 and 10.94 min.

The weight percentages (wt%), mol(*n*) fractions (mol(n)/*R*), the chain propagation probability (α) for the experiments giving the highest productivity for complexes **35** and **37** are all summarised in Table 5.4. The mol(*n*) fractions are obtained by dividing the molar amounts (mol(n)), with the total molar amount of oligomers produced (*R*). α, which represents the probability of chain propagation, is defined by the rate of propagation divided by the sum of rate of propagation and termination. It can be determined by the Schulz-Flory equation mol(*n*) = $(1-\alpha)\alpha^{n-1}R$, where *n* is the number of ethylene units in the oligomer and *R* is the total molar amount of oligomer made. Alternatively, it can be derived by plotting [ln(mol(*n*)/*R*)] *versus n* (Figure 5.11).[17, 24, 59]

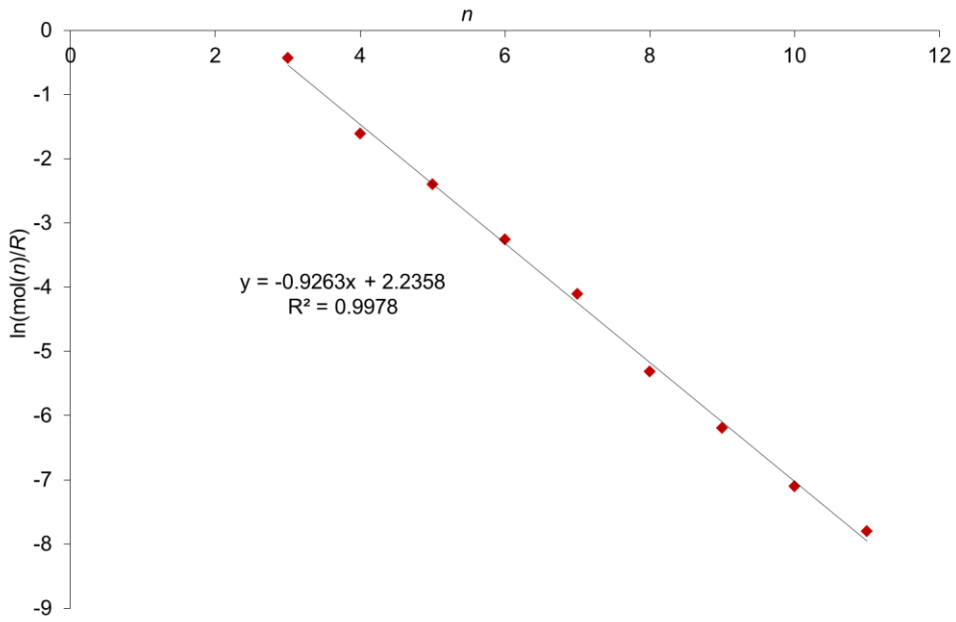

Figure 5.11. ln(mol(*n*)/R) *versus* ethylene units in oligomer (*n*). $\alpha = e^{-0.9263} = 0.40$.

The probability of chain propagation (α) is evaluated as 0.40 for **37** at 40 °C with 5 bar ethylene pressure, which also implies that the probability of chain termination is 0.60. The GC did not account for the gaseous oligomers formed (1-butene) nor for the poly(oligomer) formed during the reaction. However, α can be used to determine how much mol(*n*) of C_4 is present by applying the Schulz-Flory equation (*vide supra*). The calculated mol(*n*) fractions are also summarised in Table 5.4 (and Appendix A5). When only considering liquid oligomers (C_6–C_{22}), the data suggests that the complex **37** offers some selectivity towards C_6 with a mol(*n*) fraction of 0.64 (Table 5.4, Entry 3). However, once including the C_4 fragment, the mol(*n*) fraction changes to show a

greater selectivity towards C_4 (0.60, wt% = 45.5) compared to the newly identified mol(*n*) fraction of C_6 as 0.24 (wt% = 27.0). A similar trend is observed for **35**. In this case, the mol(*n*) fraction for C_6 is 0.43, when only considering the experimentally obtained values of the liquid oligomers. The calculated mol(*n*) fractions (including C_4) show a decrease in the mol(*n*) fraction for C_6 to 0.25 (wt% = 23.1), while the mol(*n*) fraction for C_4 is identified as 0.45 (27.8 wt, Table 5.4, Entry 1). No significant change is seen in the observed weight percentage (wt%), mol(*n*) fraction and calculated mol(*n*) fraction of the self-scavenging experiment of **35** (Table 5.4, Entry 2).compared to the experiment in the presence of DiBAlO

The α value obtained for complex **35** is 0.56 under similar conditions compared to **37** (Entry 1 and 3, respectively). This agrees with the GC data observed for either complex, a higher α value indicates a smaller chain termination probability and therefore higher wt% of higher oligomers are observed (C_4–C_{22}) for **35.** A smaller α (0.40), as observed for **37** allows for a bigger probability of chain termination, this is reflected by the distribution of C_6–C_{22} and smaller weight percentages and mol(*n*) fractions for higher oligomers. A typical value of α in the SHOP process is around 0.80, showing a higher probability of chain propagation in comparison to chain termination and therefore also resulting in the wider distribution ranging from C_4 to C_{40}.[60] While other complexes, such as 1,1-bis(1H-benzimidazol-2-ylmethyl)ethane chromium(III) chloride resulted in LAO synthesis with a Schulz-Flory distribution and a similar chain propagation probability (α = 0.55) was observed as for **35**.[59]

The productivities shown in Table 5.4 are based on liquid oligomers only. A drop in productivity is observed in the self-scavenging experiment (Entry 2) which is believed due to the less efficient scavenging of impurities in the system. The sterically more crowded system (**37**) gives a higher productivity than the less sterically demanding system (**35**). It should be emphasised that the productivities obtained do not consider any 1-butene or the potential oligomers that were polymerised and therefore higher productivities can potentially be reached.

Table 5.4. Ethylene oligomerisation conditions for complex **35** and **37**.

Entry	Cat loading (μmol)[a]	parameters	*n*									
			2	3	4	5	6	7	8	9	10	11
1	**35**, 0.08	wt%	–	30.6	19.9	17.0	12.9	9.5	4.3	2.8	1.9	1.0
		mol(*n*)/*R*	–	0.44	0.22	0.15	0.09	0.06	0.02	0.01	0.008	0.004
		α, Productivity[d]	0.55, 1.44×10^5									
		calc. normalised mol(*n*)	0.45	0.25	0.14	0.08	0.04	0.02	0.01	0.007	0.004	0.002
2	**35**[b], 0.08	wt%	–	29.8	19.8	17.1	13.3	9.8	4.4	2.8	1.9	1.0
		mol(*n*)/*R*	–	0.43	0.22	0.15	0.10	0.06	0.02	0.01	0.008	0.004
		α, Productivity[d]	0.56, 6.11×10^4									
		calc. normalised mol(*n*)	0.44	0.25	0.13	0.08	0.04	0.02	0.01	0.008	0.004	0.002
3	**37**[c], 0.08	wt%	–	53.8	22.1	12.5	6.4	3.2	1.1	0.5	0.2	0.1
		mol(*n*)/*R*	–	0.64	0.20	0.09	0.04	0.02	0.005	0.002	0.008	0.0004
		α, Productivity[d]	0.40, 5.15×10^5									
		calc. normalised mol(*n*)	0.60	0.24	0.09	0.04	0.01	0.005	0.002	0.0009	0.0004	0.0001

[a] Pressure C_2 = 5 bar, temperature (°C) = 40, [B]:[Ti] = 2:1, DiBAlO = 0.4 μmol, time = 14.0 min. [b] no DiBAlO, time = 9.50 min. [c] time = 10.3 min. [d] mmol liquid oligomers mol^{-1} h^{-1} bar^{-1}

The system $Cp_2Ti(R)Cl/RAlCl_2$, investigated by Olivé *et al.*, gave a similar weight percentage for C_6, C_8, C_{12}, C_{20} and C_{22} oligomers (between 12.0–16.0 wt%),[25] while for the complexes **35** and **37**, a decline in wt% is observed with increasing number of ethylene units in the oligomer. Hessen's system, $\{Me_2C(C_5H_4)_2\}TiCl_3$ (**5.05**), a selectivity for C_6 (93 wt%) is observed, alongside C_{10} and polyethylene as minor products (5 and 1.3 wt%, respectively).[26]

The thermal stability of **35** and **37** was also investigated in the oligomerisation of ethylene. The ethylene uptake was monitored for temperatures from 40 to 70 ºC and the productivity was calculated from the GC data obtained for the liquid oligomers. The ethylene uptake (Figure 5.12) shows a significant drop when the temperature is increased to 50 from 40 ºC, showing low thermal stability of the complexes **35** under these relevant conditions and experimental set up. Minimal uptake was observed for the higher temperatures, suggesting catalyst degradation. This is confirmed by the calculated productivity from the GC traces, where a considerable drop in productivity is observed from 40 to 50 ºC (1.44×10^5 *vs*. 5.95×10^4 mol of liquid oligomers mol^{-1} Ti h^{-1} bar^{-1}, respectively). The α value obtained for 50 °C is 0.59 and is comparable to the α value at 40 ºC.

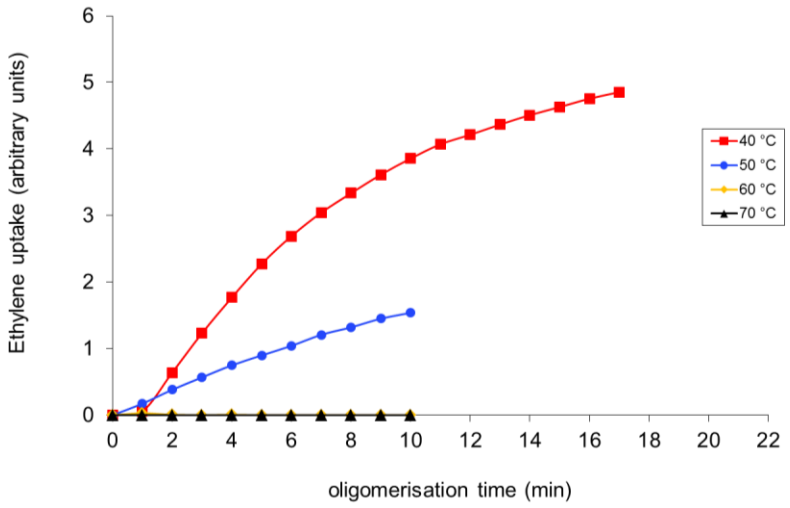

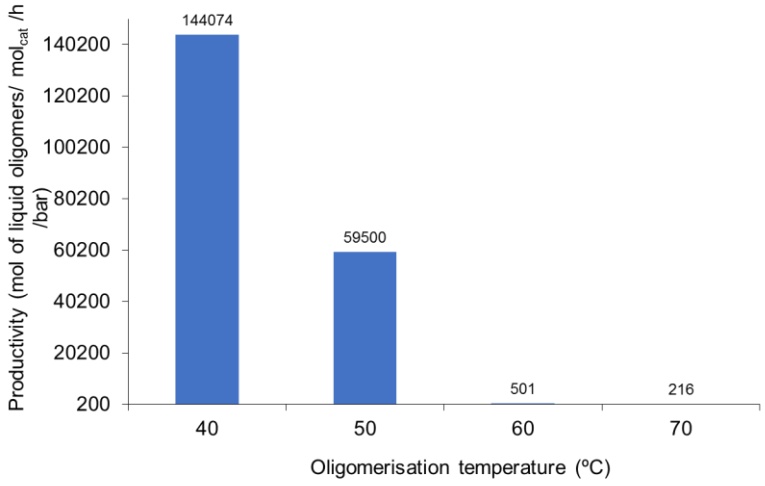

Figure 5.12. Ethylene uptake and productivity of ethylene oligomerisation with (Ap[1])Ti{NC(Ph)N^{i}Pr$_2$}Cl$_2$ (**35**, 0.08 μmol) in the presence of [Ph$_3$C][BAr$^{F}_4$] (0.16 μmol) and DiBAlO (0.4 μmol) at varying temperature.

Other known titanium based systems, active in ethylene oligomerisation, uses variable temperatures from –20 to 50 ºC to achieve highest productivity.[25, 26, 31, 36] Compound **5.05**, for example, possesses modest thermal stability, where an increase in temperature led to a decrease in ethylene uptake.[26] While chromium based systems have shown to possess a greater thermal stability in some cases, where for example [CrCl$_3$(THF)$_3$] with **5.02** can trimerise ethylene successfully at 80 to 110 ºC.[11]

Compound **37** also displays modest thermal stability. At 60 and 70 ºC ethylene uptake is still observed, suggesting higher persistence of the catalyst before it degrades. This is also illustrated by the increase in ethylene uptake at 70 ºC in the first minute followed by a sharp decline (Figure 5.13). The α value changes from 0.40 to 0.43 from 40 to 60 °C, respectively and are therefore comparable to one another. Even though the α obtained are comparable, temperature seems to have a small influence on the distribution, as for example at 60°C no C$_{22}$ oligomer was observed anymore.

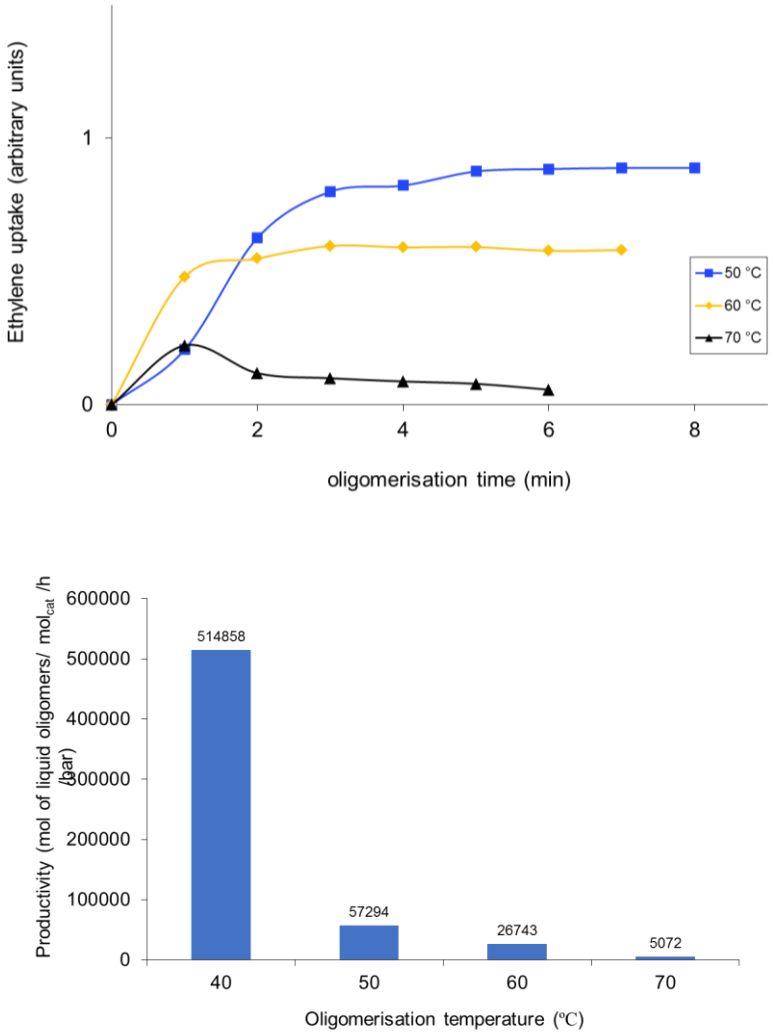

Figure 5.13. Ethylene uptake and productivity of ethylene oligomerisation with $(Ap^2)Ti\{NC(Ph)N^iPr_2\}Cl_2$ (**37**, 0.02 μmol) in the presence of $[Ph_3C][BAr^F{}_4]$ (0.08 μmol) and DiBAlO (0.4 μmol) at varying temperature.

To test the influence of pressure on the activity and productivity of complex **35**, parallel experiments were ran at 2, 5 and 10 bar ethylene. The productivity is comparable at 2 and 5 bar, which is also reflected in the yield obtained for the liquid oligomers (3.6 and 8.1 mmol of liquid oligomers, respectively, Figure 5.14). The productivity drops considerably at 10 bar, however a small increase in yield is still observed (10.0 mmol of liquid oligomers). This is suggestive of mass-transport limitation observed at higher pressures. The pressure change in each reactor cell, shows efficient refilling of each cell and more frequent refilling at 5 and 10 bar compared to 2 bar, which is in agreement with the observation of greater yields of liquid oligomers at higher pressures.

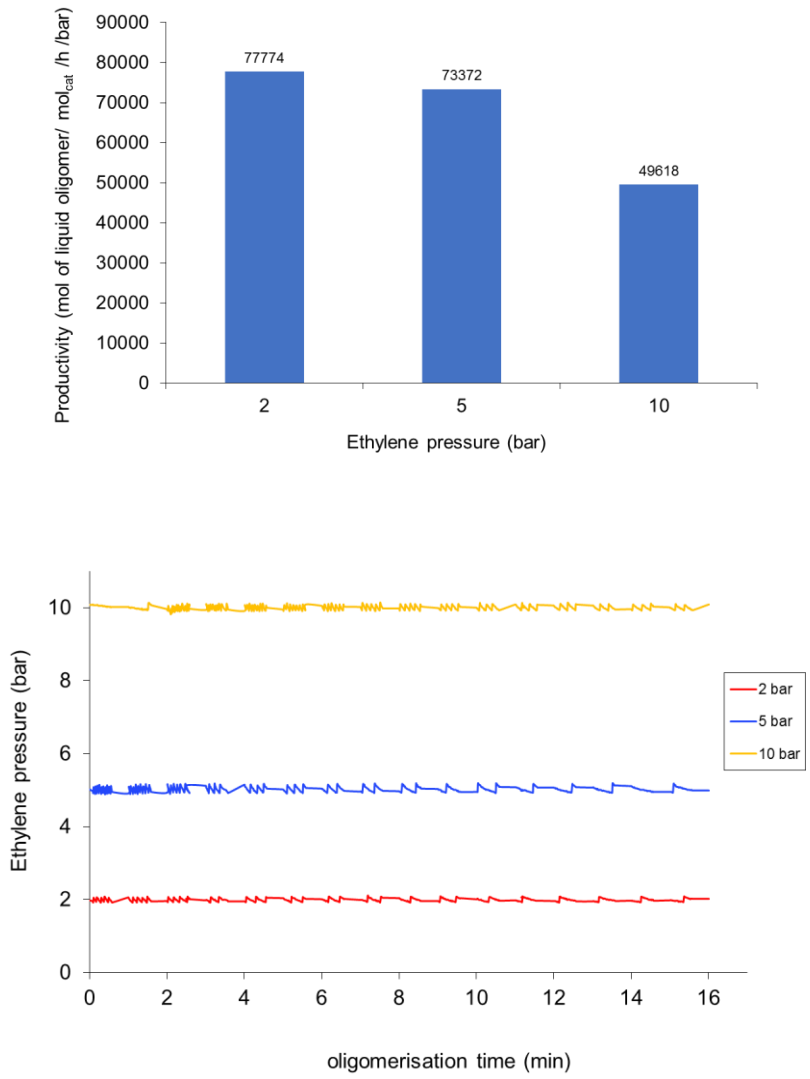

Figure 5.14. Productivity and pressure change of reactor cell of ethylene oligomerisation with (Ap^2)Ti{NC(Ph)N^{i}Pr$_2$}Cl$_2$ (**35**, 0.08 μmol) in the presence of [Ph$_3$C][BAr$^F{}_4$] (0.16 μmol) and DiBAlO (0.4 μmol) at varying pressure.

To test the influence of pressure on the activity and productivity of complex **37**, parallel experiments were ran at 2, 4 and 8 bar. At 2 and 4 bar, comparable productivities are obtained (Figure 5.15).

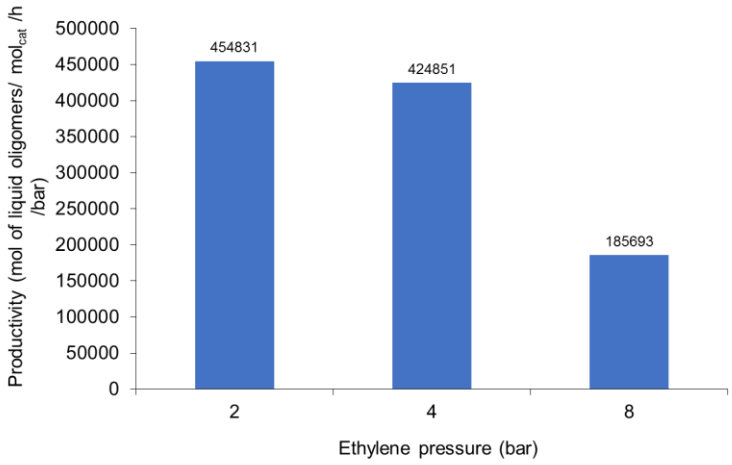

Figure 5.15. Productivity in the oligomerisation of ethylene with compound **37** (0.02 μmol) with $[Ph_3C][BAr^F_4]$ (0.04 μmol) and DiBAlO (0.4 μmol) at varying ethylene pressures.

However, the productivity at 8 bar is considerably lower than at 2 and 4 bar. However, in this case a lower yield was also determined (6.1 mmol of liquid oligomers at 8 bar compared to 7.2 mmol of liquid oligomers at 4 bar). This can be partially explained by looking at the pressure change of each reactor cell, displayed in Figure 5.16.

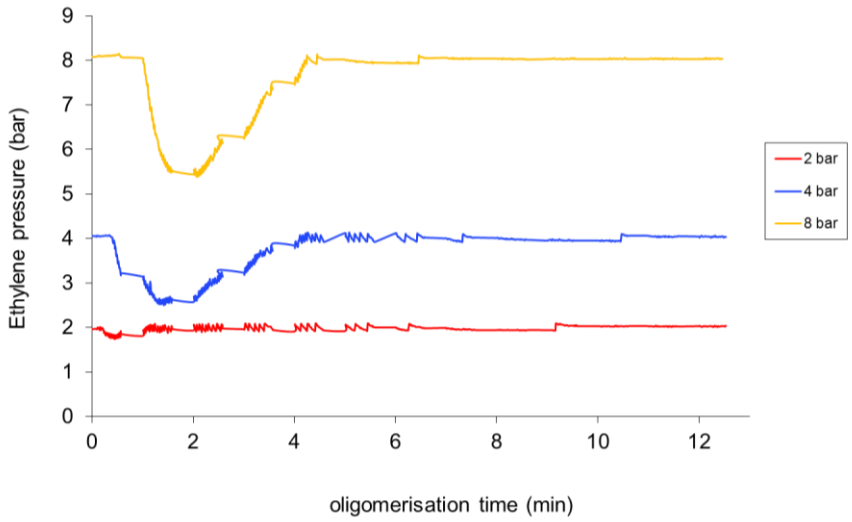

Figure 5.16. Ethylene uptake and pressure of the reactor cells in the oligomerisation of ethylene with compound **37** (0.02 μmol) with $[Ph_3C][BAr^F_4]$ (0.04 μmol) and DiBAlO (0.4 μmol) at varying ethylene pressures.

The ethylene pressure could not be kept constant at 4 and 8 bar, hinting towards a highly active system overall. The calculated productivity might therefore be slightly underestimated, as for example the average pressure from 1 minute to 4 ½ minutes of the reaction at 8 bar was only 6.5 bar. However, after 4 minutes the reactor cell was only refilled a few more times at 8 bar, while more frequent refills were observed at 2 and 4 bar (Figure 5.16). This is suggestive of a lower activity and potentially the presence of a dormant state at 8 bar. This is surprising as in the literature, it has been shown that an increase in pressure leads to an increase in activity.[26] However, due to limited time access to the facilities, no repeat experiments could be performed.

The sensitivity of the complexes **35** and **37** towards BHT-H in ethylene oligomerisation was also tested at the High Throughput Experimentation facility of ETH Zürich. Two and four equivalents of BHT-H relative to DiBAlO were added, giving a 1:1 and 2:1 ratio of [BHT]:[Al], respectively. In both cases, a considerable lower ethylene uptake was observed compared to the experiment in the absence of BHT-H, the uptake curve with complex **35** is displayed in Figure 5.17. The same trend was observed in the calculated productivity, based on the liquid oligomers obtained, where the productivity dropped to 2.01×10^4 and 8.64×10^3 mol of liquid oligomers mol^{-1} Ti h^{-1} bar^{-1}, for two and four equivalents of BHT-H, respectively. Interestingly, a small increase in the α value to 0.59 is observed in the presence of BHT.

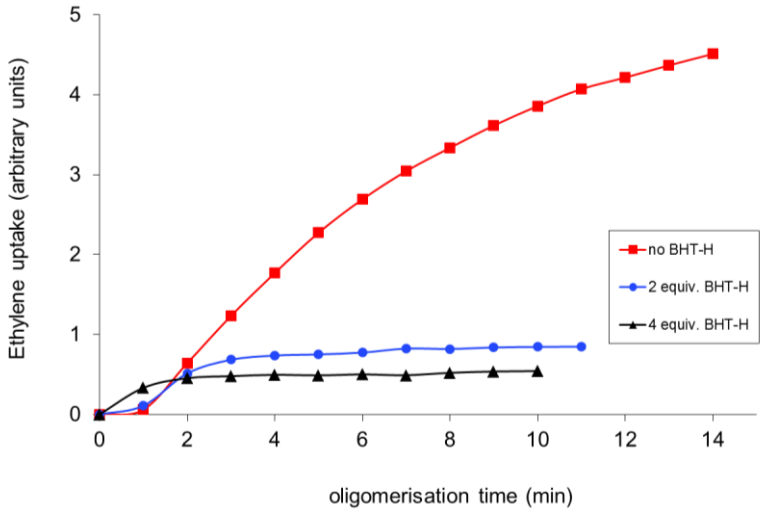

Figure 5.17. Ethylene uptake of compound **35** (0.08 μmol) with $[Ph_3C][BAr^F_4]$ (0.16 μmol) and DiBAlO (0.4 μmol) with varying amounts of BHT-H.

Similar observations were made for the productivity and ethylene uptake for the self-scavenging experiment of **35**, where the productivity decreased from 6.11×10^4 to 1.15×10^3 mol of liquid oligomers mol^{-1} Ti h^{-1} bar^{-1} upon addition of 5 equivalents of BHT-H relative to titanium metal (Appendix).

Overall, the non-selectivity of these systems together with the observation of polymer, is suggestive that these systems operate according to the Cossee-Arlman mechanism (Scheme 5.1) rather than the metallacyclic mechanism which can be highly selectivity for C_6 (*vide supra*). Despite the fact that literature has shown a Schulz-Flory distribution can take place *via* large metallacyclic rings,[24] it is less likely to occur in this system due to the disfavoured formation of a Ti(+2) species, in the absence of stabilising ligands such as η-C_5R_5.

5.5 Summary

This Chapter has provided a short literature overview about oligomerisation of ethylene, with focus on group 4 metal complexes. The behaviour of the mixed aminopyridinato- and amidinato systems (**32**–**34**) in the ter-polymerisation of ethylene, propylene and ENB was described, showing low productivities. The capability of the dimethyl complexes **35** and **37** to oligomerise ethylene has also been investigated and a Schulz-Flory distribution of LAOs was determined (α = 0.55 and 0.40 for **35** and **37** respectively). Both compounds show only modest thermal stability, indicated by the sharp drop in productivity and ethylene uptake at higher temperatures. The increase in pressure shows mass-transport limitation in the case of **35**, but interestingly shows a drop in productivity for **37** accompanied with a potential dormant state. NMR tube scale reactions have shown that **35** and **37** also subsequently polymerise the oligomers formed. This process is more abundant under starving conditions. The sensitivity towards BHT-H was investigated and showed the formation of an aryloxide complex when BHT-H is reacted with the monomethyl cation **41-[BAr$^F_4$]** and **42-[BAr$^F_4$]**. The newly formed complexes showed only poor productivity in the oligomerisation of ethylene, which was also confirmed on the NMR tube scale.

5.6 References

1. A. de Klerk, S. W. Hadebe, J. R. Govender, D. Jaganyi, A. B. Mzinyati, R. S. Robinson and N. Xaba, *Ind. Eng. Chem. Res.*, 2007, **46**, 400-410.
2. G. R. Lappin, in *Alpha olefins applications handbook*, eds. G. R. Lappin and J. D. Saue, Marcel Dekker, New York, 1990, pp. 1-35.
3. J. C. Mol, *J. Mol. Catal. A: Chem.*, 2004, **213**, 39-45.
4. K. Wilhelm, *Angew. Chem. Int. Ed.*, 2013, **52**, 12492-12496.
5. B. Reuben and H. Wittcoff, *J. Chem. Educ.*, 1988, **65**, 605.
6. R. M. Manyik, W. E. Walker and T. P. Wilson, *J. Catal.*, 1977, **47**, 197-209.
7. R. M. Manyik, W. E. Walker and T. P. Wilson, *US3300458A*, 1967.
8. R. M. Manyik, W. E. Walker, T. P. Wilson and G. F. Hurley, *US3231550A*, 1966.
9. R. M. Manyik, W. E. Walker, T. P. Wilson and G. F. Hurley, *US3242099A*, 1966.
10. J. W. Freeman, J. L. Buster and R. D. Knudsen, *US5856257A*, 1999.
11. A. Carter, S. A. Cohen, N. A. Cooley, A. Murphy, J. Scutt and D. F. Wass, *Chem. Commun.*, 2002, 858-859.
12. D. F. Wass, *WO0204119A1*, 2002.
13. D. S. McGuinness, P. Wasserscheid, W. Keim, D. Morgan, J. T. Dixon, A. Bollmann, H. Maumela, F. Hess and U. Englert, *J. Am. Chem. Soc.*, 2003, **125**, 5272-5273.
14. A. Bollmann, K. Blann, J. T. Dixon, F. M. Hess, E. Killian, H. Maumela, D. S. McGuinness, D. H. Morgan, A. Neveling, S. Otto, M. Overett, A. M. Z. Slawin, P. Wasserscheid and S. Kuhlmann, *J. Am. Chem. Soc.*, 2004, **126**, 14712-14713.
15. D. S. McGuinness, P. Wasserscheid, W. Keim, C. Hu, U. Englert, J. T. Dixon and C. Grove, *Chem. Commun.*, 2003, 334-335.
16. J. R. Briggs, *J. Chem. Soc., Chem. Commun.*, 1989, 674-675.
17. G. J. P. Britovsek, D. S. McGuinness, T. S. Wierenga and C. T. Young, *ACS Catalysis*, 2015, **5**, 4152-4166.
18. G. J. P. Britovsek and D. S. McGuinness, *Chem. Eur. J.*, 2016, **22**, 16891-16896.

19. J. X. McDermott, J. F. White and G. M. Whitesides, *J. Am. Chem. Soc.*, 1976, **98**, 6521-6528.
20. R. Emrich, O. Heinemann, P. W. Jolly, C. Krüger and G. P. J. Verhovnik, *Organometallics*, 1997, **16**, 1511-1513.
21. J. X. McDermott, J. F. White and G. M. Whitesides, *J. Am. Chem. Soc.*, 1973, **95**, 4451-4452.
22. T. Agapie, S. J. Schofer, J. A. Labinger and J. E. Bercaw, *J. Am. Chem. Soc.*, 2004, **126**, 1304-1305.
23. T. Agapie, J. A. Labinger and J. E. Bercaw, *J. Am. Chem. Soc.*, 2007, **129**, 14281-14295.
24. A. K. Tomov, J. J. Chirinos, D. J. Jones, R. J. Long and V. C. Gibson, *J. Am. Chem. Soc.*, 2005, **127**, 10166-10167.
25. G. Henrici-Olivé and S. Olivé, *Angew. Chem. Int. Ed. Engl.*, 1970, **9**, 243-243.
26. P. J. W. Deckers, B. Hessen and J. H. Teuben, *Angew. Chem. Int. Ed.*, 2001, **40**, 2516-2519.
27. S. Tobisch and T. Ziegler, *Organometallics*, 2003, **22**, 5392-5405.
28. E. Otten, A. A. Batinas, A. Meetsma and B. Hessen, *J. Am. Chem. Soc.*, 2009, **131**, 5298-5312.
29. S. Ishii, T. Nakano, K. Kawamura, S. Kinoshita, S. Ichikawa and T. Fujita, *Catal. Today*, 2018, **303**, 263-270.
30. Y. Suzuki, S. Kinoshita, A. Shibahara, S. Ishii, K. Kawamura, Y. Inoue and T. Fujita, *Organometallics*, 2010, **29**, 2394-2396.
31. F. F. Karbach, J. R. Severn and R. Duchateau, *ACS Catalysis*, 2015, **5**, 5068-5076.
32. R. W. Barnhart, G. C. Bazan and T. Mourey, *J. Am. Chem. Soc.*, 1998, **120**, 1082-1083.
33. J. C. Stevens, F. J. Timmers, D. R. Wilson, G. F. Schmidt, P. N. Nickias, R. K. Rosen, G. W. Knight and S. Y. Lai, *EP416815A2*, 1991.
34. J. C. Stevens and D. R. Neithamer, *EP418044A2*, 1991.
35. G. C. Bazan, G. Rodriguez, A. J. Ashe, S. Al-Ahmad and J. W. Kampf, *Organometallics*, 1997, **16**, 2492-2494.
36. C. Pellecchia, D. Pappalardo and G.-J. Gruter, *Macromolecules*, 1999, **32**, 4491-4493.
37. K. Ziegler, *GB787438A*, 1957.

38. K. Ziegler and H. Martin, *US2943125A*, 1960.
39. A. Forestière, H. Olivier-Bourbigou and L. Saussine, *Oil Gas Sci. Technol. Rev. IFP*, 2009, **64**, 649-667.
40. A. W. Al-Sa'doun, *Appl. Catal., A*, 1993, **105**, 1-40.
41. F. A. Al-Sherehy, in *Stud. Surf. Sci. Catal.*, eds. M. Absi-Halabi, J. Beshara and A. Stanislaus, Elsevier, 1996, vol. 100, pp. 515-523.
42. S. Yamada and I. Ono, *Bull. Japan Pet. Inst.*, 1970, **12**, 160-163.
43. F. Grasset, J.-B. Cazaux, L. Magna, P. Braunstein and H. Oliver-Bourbigou, *Dalton Trans.*, 2012, **41**, 10396-10404.
44. J.-B. Cazaux, P. Braunstein, L. Magna, L. Saussine and H. Olivier-Bourbigou, *Eur. J. Inorg. Chem.*, 2009, **2009**, 2942-2950.
45. A. M. Al-Jarallah, J. A. Anabtawi, M. A. B. Siddiqui, A. M. Aitani and A. W. Al-Sa'doun, *Catal. Today*, 1992, **14**, 1-121.
46. J. A. Suttil and D. S. McGuinness, *Organometallics*, 2012, **31**, 7004-7010.
47. W. P. Kretschmer, B. Hessen, A. Noor, N. M. Scott and R. Kempe, *J. Organomet. Chem.*, 2007, **692**, 4569-4579.
48. R. A. Collins, A. F. Russell, R. T. W. Scott, R. Bernardo, G. H. J. van Doremaele, A. Berthoud and P. Mountford, *Organometallics*, 2017, **36**, 2167-2181.
49. A. Noor, W. P. Kretschmer, G. Glatz and R. Kempe, *Inorg. Chem.*, 2011, **50**, 4598-4606.
50. E. Jeffery and T. Mole, *Aust. J. Chem.*, 1968, **21**, 2683-2686.
51. M. D. Healy, D. A. Wierda and A. R. Barron, *Organometallics*, 1988, **7**, 2543-2548.
52. A. P. Shreve, R. Mulhaupt, W. Fultz, J. Calabrese, W. Robbins and S. D. Ittel, *Organometallics*, 1988, **7**, 409-416.
53. S. S. Reddy, G. Shashidhar and S. Sivaram, *Macromolecules*, 1993, **26**, 1180-1182.
54. R. K. Rosen, J. C. Stevens and J. C. Tracy, *WO9727228A1*, 1997.
55. R. A. Stapleton, B. R. Galan, S. Collins, R. S. Simons, J. C. Garrison and W. J. Youngs, *J. Am. Chem. Soc.*, 2003, **125**, 9246-9247.
56. C. M. R. Wright, T. J. Williams, Z. R. Turner, J.-C. Buffet and D. O'Hare, *Inorg. Chem. Front.*, 2017, **4**, 1048-1060.

57. K. Sukhdeep, N. D. G., S. Gurmeet, P. H. R., K. A. V. and G. V. K., *J. Appl. Polym. Sci.*, 2010, **115**, 229-236.
58. B. D. Ward, S. Bellemin-Laponnaz and L. H. Gade, *Angew. Chem. Int. Ed.*, 2005, **44**, 1668-1671.
59. A. K. Tomov, J. D. Nobbs, J. J. Chirinos, P. K. Saini, R. Malinowski, S. K. Y. Ho, C. T. Young, D. S. McGuinness, A. J. P. White, M. R. J. Elsegood and G. J. P. Britovsek, *Organometallics*, 2017, **36**, 510-522.
60. P. W. N. M. van Leeuwen, N. D. Clément and M. J. L. Tschan, *Coord. Chem. Rev.*, 2011, **255**, 1499-1517.

Chapter Six

Experimental details and characterising data

6.1 General methods and instrumentation

All manipulations were carried out using standard Schlenk line or dry-box techniques under an atmosphere of argon or dinitrogen. Solvents were degassed by sparging with dinitrogen and dried by passing through a column of the appropriate drying agent or refluxed over sodium (toluene, xylene), potassium (THF), Na/K (Et_2O) or CaH_2 (fluorobenzene) and distilled. Deuterated solvents were dried over sodium (C_6D_6 and toluene-d_8), potassium (THF- d_8), P_2O_5 ($CDCl_3$ and CD_2Cl_2) or CaH_2 (C_6D_5Br) distilled under reduced pressure and stored under argon in Teflon valve ampoules. NMR samples were prepared under dinitrogen in 5 mm Wilmad 507-PP tubes fitted with *J*. Young Teflon valves. ^{1}H, $^{13}C\{^{1}H\}$, $^{11}B\{^{1}H\}$, $^{19}F\{^{1}H\}$, $^{31}P\{^{1}H\}$ and ^{2}H NMR spectra were recorded on a Bruker Ascend 400 NMR spectrometer, Bruker Avance III 500 NMR spectrometer or on a Bruker AVC 500 spectrometer fitted with a ^{13}C cryoprobe. Spectra are referenced internally to residual protio-solvent (^{1}H) or solvent (^{13}C) resonances, and are reported relative to tetramethylsilane (δ = 0 ppm). ^{19}F spectra were referenced externally to $CFCl_3$ and ^{11}B spectra were referenced externally to $Et_2O{\cdot}BF_3$. Assignments were confirmed using one- or two-dimensional ^{1}H-^{1}H and ^{13}C-^{1}H and ^{15}N-^{1}H NMR correlation experiments. Chemical shifts are quoted in δ (ppm) and coupling constants in Hz. Mass spectra were recorded by the mass spectrometry service of the University of Oxford. IR spectra were recorded on a Thermo Scientific Nicolet iS5 FTIR spectrometer. Samples were prepared in a dry-box as Nujol mulls between NaCl plates or as a thin film, and the data are quoted in wavenumbers (cm^{-1}) within the range 4000−400 cm^{-1}. Elemental analyses were carried out by the Elemental Analysis Service at the London Metropolitan University.

6.2 Literature preparations and reagent purification

$HNC(N^iPr_2)Ph$,[1] $C(NDipp)_2$,[2, 3] $TiBn_4$,[4] were prepared to literature procedures. $Ti\{NC(Ph)N^iPr_2\}Cl_3$ (**4.02**) was prepared following an in-house preparation.[5] Cp*$TiCl_3$, Trityl-tetrakis(pentafluorophenyl)borate ($[Ph_3C][BAr^F_4]$), Tris(pentafluorophenyl) borane (BAr^F_3), $[HNMe_2Ph][BAr^F_4]$ and $Cp^*Ti\{NC(Ar^{F_2})N^iPr_2\}Me_2$ (**1.52**) were kindly donated by ARLANXEO. $Cp^*Ti\{NC(NMe_2)_2\}Me_2$ (**1.58**) was kindly donated by Wilf Diment and $Cp^*Ti\{NC(Ph)N^iPr_2\}Me_2$ (**3.05**), $Cp^*Ti\{NC(NMe^iBu)_2\}Me_2$ (**1.56**) and $Cp^*Ti\{NC(N(Xyl)CH_2)_2\}Me_2$ (**3.06**) were synthesised by a student under the

Author's supervision. All other reagents required for the isolation of the novel compounds described below were purchased directly from Alfa Aesar or Sigma-Aldrich and used directly or dried as appropriate before use.

Procedure for deuteration of [HNMe$_2$Ph][BAr$^F_4$]. Air sensitive techniques were used throughout. To a solution of [HNMe$_2$Ph][BAr$^F_4$] (0.500 g, 0.62 mmol) in CH_2Cl_2 (5 mL) was added D_2O (10 mL) and NaOD (40% solution in D2O, 0.006 mL, 0.081 mmol). The resultant mixture was left to stir for 3 days and then quenched with DCl (45% solution in D_2O, 0.011 mL). The 2 layers were then separated and the aqueous layer was extracted with CH_2Cl_2 (2 × 5 mL). The combined organic layers were dried over Na_2SO_4 and CH_2Cl_2 was reduced to half its volume. The product was recrystallized in CH_2Cl_2 at 5 ºC. Yield: 0.300 g (60%). ^{1}H NMR analysis indicated 78% deuteration.

Procedure for deuteration of (^{t}Bu$_2$C$_6$H$_2$(Me))OH. Air sensitive techniques were used throughout. To a solution of (^{t}Bu$_2$C$_6$H$_2$(Me))OH (2.00 g, 9.1 mmol) in benzene (10 mL) was added D_2O (10 mL) and the resulting mixture was stirred vigorously for 12 h. The solution was allowed to settle. The top layer was decanted away, dried over $MgSO_4$ and solvent removed *in vacuo*. Yield: 1.6 g (80%). ^{1}H NMR analysis indicated 83% deuteration.

6.3 X-ray data collection and processing parameters

Crystals were mounted on glass fibers using perfluoropolyether oil and cooled rapidly in a stream of cold N_2 using an Oxford Cryosystems Cryostream unit. Diffraction data were measured using either an Enraf-Nonius KappaCCD or Agilent Technologies Supernova diffractometer using Mo-Kα or Cu-Kα radiation, respectively. As appropriate, absorption and decay corrections were applied to the data and equivalent reflections merged.[6] The structures were solved with SIR92[7] or Superflip[8], and further refinements and all other crystallographic calculations were performed using the CRYSTALS program suite.[9] Other details of the structure solution and refinements are given in the Supporting Information (CIF data – see CD Appendix).

6.4 General polymerisation procedure

Polymerisation testing was carried out at ARLANXEO, The Netherlands, by Dr Raffaele Bernardo and Dr Maxence Valla under the supervision of Dr Alexandra

Berthoud. The analytics were carried out by Mr Sander Niessen at ARLANXEO, Geleen.

6.4.1 General polymerisation reagents

Methylaluminoxane (MAO) was purchased from Chemtura as a 10 wt.% Aluminium solution in toluene and was dosed as a 0.10 M or 1.0 M Aluminium solution in toluene. Triisobutylaluminium (TiBA, 10 wt.% Al hexane solution) was purchased from Akzo Nobel and dosed as 0.10 M (Al based) solutions in hexane. 4-Methyl-2,6-di-tert-butylphenol (BHT-H, +99.0%) was purchased from Sigma-Aldrich and dosed as a 0.20 M solution in hexane. The catalyst precursor solutions were dosed as 1.0 mM solutions in toluene or hexane. $[CPh_3][BAr^F_4]$ was dosed as a 2.0 mM solution in toluene. BAr^F_3 was dosed as a 2.0 mM solution in toluene or hexane. The feed streams (ethylene, propylene, hydrogen, nitrogen) were purified by contacting with various absorption media to remove catalyst killing impurities such as water, oxygen and polar compounds (Molsieves 4Å (Merck, nitrogen, ethylene, hydrogen), Molsieves 13-X (Merck, propene, PMH), Cu-catalyst BTS R311 (BASF, nitrogen, ethylene, propylene, nitrogen)). 2,2,4,6,6-Pentamethylheptane (PMH) solvent was additionally stripped with nitrogen. 5-ethylidenebicyclo[2.2.1]hept-2-ene was purchased from Ineos and dosed to the reactor as liquid after stripping with nitrogen. After opening the reactor, the reactor was dried using 450 μmol L^{-1} triisobutylaluminium. In order to avoid mass transfer limitation problems, the total polymer yield in each polymerization was limited to approximately 10 g after a total polymerization time of 10 minutes. The total aluminium (i.e. scavenger) concentration in the reactor was kept above 0.45 mM to ensure efficient scavenging.

6.4.2 Ethylene-Propylene co-polymerisation

Ethylene-propylene batch copolymerisation reactions were carried out in a 2 L autoclave equipped with a double intermig stirrer and baffles. The reaction temperature was set to 90 ºC and regulated by a Lauda LTH303 Thermostat. Ethylene and propylene monomers were continuously fed to the gas cap of the reactor during the conditioning period and the polymerisation time. The total monomer flow was kept constant during each experiment (either 600 NL h^{-1}). The pressure of the reactor was kept constant by a back-pressure valve. In an inert atmosphere of nitrogen (1.8 bar), the reactor was filled with 950 mL of PMH solvent, BHT-H and scavenger

(TiBA, DiBAlO) (Chapter Two, Three, Four and Five). The reactor was heated to 90 ºC, while stirring at 1350 rpm. The reactor was pressurised to 7 bar by feeding ethylene and propylene and the reactor was conditioned applying a fixed ratio of ethylene and propylene for 15 minutes. Then, the catalyst components were added as PMH solutions to the reactor and the catalyst vessel was rinsed with an additional 50 mL of PMH. After 10 minutes of polymerisation time, the monomer flow was stopped, and the solution was carefully transferred in a 2 L Erlenmeyer flask, containing a solution of Irganox-1076 in isopropanol and dried over night at 100 ºC under reduced pressure (< 20 mbar).

6.4.3 Parallel Polymerisation Reactor (PPR) procedure

Polymerisation experiments were carried out with a high throughput parallel reactor setup (PPR48 available from Freeslate), with six reactor modules each containing eight reaction cells (5 mL working volume per cell). The whole system is housed in a glovebox maintaining a pure nitrogen atmosphere. The monomer gas and quench gas lines are plumbed directly into the reactors and controlled by automatic valves; ethylene or propylene is fed after purification by passing through columns containing a BASF/Molecular sieves mixed bed. Liquid reagents are robotically added to individual cells by syringes. Solvents are previously purified in an MBraun SPS unit. The cells are fitted with a pre-weighed glass vial insert and a disposable stirring paddle. The reactor is then closed, and 4.1 mL of toluene/scavenger mixture are fed (10 μmol of scavenger, i.e. MMAO-3A from Akzo Nobel, 7 wt.% Al in hexane conditioned with 2,6-ditertbutyl,4-me-phenol, [Al]:[BHT-H] = 2) are injected into each cell through a valve. The reactors are pressurised with propene at 50 psi at 800 rpm for 30 mins. Afterward the modules are thermostated at 90 °C, and the cells are over pressurised with ethene (Propene and Ethene from Praxair) at 1.4 bar. The precatalyst and activator (activator $[Ph_3C][BAr^F{}_4]$, [B]:[Ti] = 2.0) are injected sequentially in to the cells, allowing no mixing via a nitrogen bubble of 50 μL. The polymerization is run at constant temperature and monomer partial pressure for 5 minutes, then quenched with N_2/O_2 mixture (2%v/v O_2) at 50 psi (3.4 bar) overpressure. The reactors are cooled, vented and purged with dinitrogen, in order to prevent the glove box pollution with air from the quenching. After purging with inert gas, the reactors are opened and the glass inserts are unloaded from the cells, transferred to a centrifuge/vacuum drying station (Genevac EZ-2 Plus) for overnight

treatment. The polymer samples are recovered and weighed on a Freeslate Weighting station unit, the polymer yields are automatically stored for polymer analysis.

6.4.4 1-hexene polymerisation

Typical procedure for 1-hexene polymerisation

To a C_6D_5Br solution containing the catalyst and activator was added the required amount of 1-hexene. The total volume was always 0.5 mL. The mixture was immediately transferred to a *J.* Young NMR tube and a ^1H NMR was recorded within 3 minutes. The sample was quenched with MeOH (0.2 mL) and run through a silica plug in pentane to remove any residual titanium species. The resulting polymer was analysed by GPC, by weight and NMR spectroscopy.

Polymer molecular weights (M_n, M_w and PDI) were determined by GPC using a Polymer Laboratories PL-GPC50 Plus instrument equipped with a Polymer Laboratories PLgel Mixed-D column (300 mm length, 7.5 mm diameter) and a refractive index (RI) detector. THF (Fisher, HPLC grade, stabilised with BHT-H, 2.5 ppm) was used as an eluent at 30 ºC with a flow rate of 1.0 mL min^{-1}. Samples were dissolved in THF (Fisher, HPLC grade, stabilised with BHT-H, 2.5 ppm) at a concentration of 2.0 mg mL^{-1} and filtered before injection. Linear polystyrenes (Polymer Laboratories) were used as primary calibration standards and the appropriate Mark-Houwink corrections for poly(1-hexene) in THF at 30 ºC were applied ($K = 23.2\ \mu L\ g^{-1}$ and $\alpha = 0.69$) to calculate the experimental molecular weights.[10, 11]

6.5 Computational details

Geometry optimizations for all systems were performed with the Gaussian09 package (rev. D.01)[12] at the B3PW91 level of hybrid density functional theory in the gas phase with all atoms represented by the def2-svp basis set.[13] Dispersion was taken into account both at the optimization and single point stages using Grimme's d3(bj) corrections[14] as implemented in Gaussian09. In addition, the solvent (treated as bromobenzene) influence was taken into consideration in the single point calculations with the def2-tzvp basis set applied to all atoms in the gas-phase optimised geometry with SCRF calculations within the SMD model. Gibbs free energies and enthalpies

were obtained by summing the SMD energy and the gas-phase Gibbs or enthalpy contribution at 298.15 K obtained from the geometry optimisations, and the d3(bj) correction. For the sterically pruned systems additional single point calculations were carried out on the optimised geometry using the def2-tzvp basis set also in the gas phase, and dispersion was not accounted for in either the optimisation or single point calculations. NMR chemical shifts were computed using the GIAO method[15, 16] as implemented in Gaussian09 at the B3PW91 level. All non-Ti atoms were described with the IGLO-II NMR basis set,[17] and Ti was described using the def2-tzvp basis set. The ^{1}H and ^{13}C NMR shifts were referenced internally with respect to the experimental values of the Cp* ligand.

6.6 Experimental details and characterising data for Chapter Two

2-(2,6-di*iso*propylphenyl)isoindolin-1-imine (1). To a round bottom flask, equipped with a magnetic stirrer bar, 2-(bromomethyl)benzonitrile (6.25 g, 31.8 mmol) was added under nitrogen flow. Dry toluene (50 mL) was added and to the stirred solution, a slight excess of 2,6-diisopropylaniline (6.11 mL, 32.4 mmol) was added. The reaction mixture was heated to reflux for 90 h and a white solid is formed in an orange/pink solution. The solution was allowed to cool to room temperature and the solid was filtered off and washed with cold toluene (3 × 10 mL). The off-white solid was dried *in vacuo* affording the HBr salt of the title compound. The solid was dissolved diethyl ether (50 mL) and an aqueous solution of NaOH was added (50 mL). The resulting layered solution was stirred for 24 h. The organic phase was separated from the aqueous layer which was then back-extracted with diethyl ether (3 × 10 mL). The combined organic phases were dried over $MgSO_4$, filtered and the volatiles removed under reduced pressure to give 2-(2,6-diisopropylphenyl)isoindolin-1-imine as an off-white solid. Yield: 7.20 g (84%).

^{1}H NMR (C_6D_6, 499.9 MHz, 298 K): 8.21 (1 H, s, $C_{Ar}\underline{H}$), 7.30–7.27 (1 H, m, $C_{Ar}\underline{H}$), 7.17–7.11 (3 H, m, $C_{Ar}\underline{H}$), 7.14 (1 H, s, $C_{Ar}\underline{H}$), 7.06 (1 H, d, $C_{Ar}\underline{H}$, $^{3}J_{HH}$ = 7.1 Hz), 6.64 (1 H, br.s, N$\underline{H}$), 4.43 (2 H, s, NC$\underline{H}_2$), 2.89 (2 H, sept, C$\underline{H}$Me$_2$, $^{3}J_{HH}$ = 6.8 Hz), 1.17 (6 H, d, CH$\underline{Me}_2$, $^{3}J_{HH}$ = 6.8 Hz), 1.08 (6 H, d, CH$\underline{Me}_2$, $^{3}J_{HH}$ = 6.8 Hz) ppm. ^{13}C{^{1}H} NMR (C_6D_6, 125.7 MHz, 298 K): 163.0 (N$\underline{C}$), 149.3 (N$\underline{C}_{Dipp}$), 140.3 (NC$\underline{C}_{Ar}$), 135.3 (CH$_2\underline{C}_{Ar}$), 133.3 ($\underline{C}_{Ar}$CH), 130.2 ($\underline{C}_{Ar}$H), 129.4 ($\underline{C}_{Dipp}$H), 128.2 ($\underline{C}_{Ar}$H), 124.5 ($\underline{C}_{Dipp}$H × 2), 123.8 ($\underline{C}_{Ar}$H × 2), 122.5 ($\underline{C}_{Ar}$H), 55.9 (N$\underline{C}$H$_2$), 28.6

(C<u>H</u>Me$_2$), 24.4 (CH<u>Me</u>$_2$), 24.1 (CH<u>Me</u>$_2$) ppm. EI-MS: *m/z* = 292 [*M*]$^+$, 249 [*M*–^{i}Pr]$^+$. Anal. Found (calcd. for $C_{20}H_{24}N_2$): C, 81.92 (82.15); N, 9.67 (9.58); H, 8.15 (8.27)%. IR (NaCl plates, Nujol mull, cm^{-1}): 3286 (br w, NH), 2922 (m), 2852 (m), 1632 (m), 1582 (w), 1452 (m), 1403 (w), 1379 (w), 1311 (w), 1245 (w), 1178 (w), 1094 (w), 1051 (w), 1019 (w), 795 (m), 729 (w).

Cp*Ti{NCN(Dipp)CH$_2$C$_6$H$_4$}Cl$_2$ (2). A Schlenk tube, under inert atmosphere, was charged with 2-(2,6-diisopropylphenyl)isoindolin-1-imine (**1**, 4.00g, 13.7 mmol) and Cp*TiCl$_3$ (3.96 g, 13.7 mmol). Dry Toluene (30 mL) was added and to the stirred solution triethylamine (5.2 mL, 37.0 mmol) was added dropwise. The resulting mixture was heated to 50 ºC for 20 h. The solution was allowed to cool to room temperature and filtered away from the trimethylamine salt. The solution was concentrated to 15 mL and stored for 2 h at –30 ºC after which time the product had crystallised as an orange needles which were washed with cold pentane (2 × 10 mL) and dried *in vacuo*. Yield: 5.33 g (79%).

^{1}H NMR (C$_6$D$_6$, 499.9 MHz, 298 K): 8.28 (1 H, d, C$_{Ar}$<u>H</u>, $^3J_{HH}$ = 7.1 Hz), 7.25–7.14 (5 H, m, C$_{Ar}$<u>H</u>, C$_{Dipp}$<u>H</u>), 6.96 (1 H, d, C$_{Ar}$<u>H</u>, $^3J_{HH}$ = 7.1 Hz), 4.48 (2 H, s, NC<u>H</u>$_2$), 3.00 (2 H, sept, C<u>H</u>Me$_2$, $^3J_{HH}$ = 6.9 Hz), 2.10 (15 H, s, C$_5$<u>Me</u>$_5$), 1.50 (6 H, d, CH<u>Me</u>$_2$, $^3J_{HH}$ = 6.9 Hz), 0.95 (6 H, d, CH<u>Me</u>$_2$, $^3J_{HH}$ = 6.9 Hz) ppm. ^{13}C{^{1}H} NMR (C$_6$D$_6$, 125.7 MHz, 298 K): 161.4 (<u>C</u>N), 147.5 (N<u>C</u>$_{Dipp}$), 140.2 (<u>C</u>$_{Ar}$), 135.5 (<u>C</u>$_{Ar}$), 134.3 (<u>C</u>$_{Dipp}$CHMe$_2$), 131.6 (<u>C</u>$_{Ar}$H), 129.7 (<u>C</u>$_{Ar}$H), 128.8 (<u>C</u>$_{Ar}$H), 127.6 (<u>C</u>$_5$Me$_5$), 125.9 (<u>C</u>$_{Ar}$H), 124.3 (<u>C</u>$_{Ar}$H × 2), 122.7 (<u>C</u>$_{Ar}$H), 56.6 (N<u>C</u>H$_2$), 29.0 (<u>C</u>HMe$_2$), 26.5 (CH<u>Me</u>$_2$), 23.5 (CH<u>Me</u>$_2$), 13.4 (C$_5$<u>Me</u>$_5$) ppm. EI-MS: *m/z* = 291 [NCN(Dipp)CH$_2$C$_6$H$_4$]$^+$, 542 [*M*]$^+$. Anal. found (calcd. for $C_{30}H_{38}N_2TiCl_2$): C, 65.93 (66.07); N, 5.26 (5.14); H, 7.15 (7.02)%. IR (NaCl plates, Nujol mull, cm^{-1}): 1614 (w), 1598 (m), 1573 (m), 1563 (m), 1463 (m), 1377 (m), 1300 (w), 1259 (w), 1217 (w), 1056 (w), 869 (w), 759 (w), 727 (w), 686 (w), 607 (w). Diffraction-quality crystals were grown from a benzene solution at room temperature.

Cp*Ti{NCN(Dipp)CH$_2$C$_6$H$_4$}Me$_2$ (3). To a stirring benzene (20 mL) solution of Cp*Ti{NCN(Dipp)CH$_2$C$_6$H$_4$}Cl$_2$ (**2**, 3.03 g, 6.2 mol) at 5 ºC was added dropwise MeLi (7.75 mL, 1.6 M in Et$_2$O, 12.4 mmol) and the resulting solution was allowed to warm up to room temperature and stirred for a further 16 h. The volatiles were then

removed *in vacuo* and the oily wax was then extracted into hexane (20 mL) to filter away from the insoluble LiCl salt. Cp*Ti{NCN(Dipp)$CH_2C_6H_4$}Me_2 was isolated as a dark red solid following removal of pentane *in vacuo*. Yield: 1.80 g (67%).

^{1}H NMR (C_6D_6, 499.9 MHz, 298 K): 7.93 (1 H, d, $C_{Ar}\underline{H}$, $^3J_{HH}$ = 6.6 Hz), 7.25–7.14 (5 H, m, $C_{Ar}\underline{H}$, $C_{Dipp}\underline{H}$), 7.01 (1 H, d, $C_{Ar}\underline{H}$, $^3J_{HH}$ = 7.6 Hz), 4.52 (2 H, s, NC$\underline{H}_2$), 3.11 (2 H, sept, C$\underline{H}Me_2$, $^3J_{HH}$ = 6.8 Hz), 1.99 (15 H, s, $C_5\underline{Me}_5$), 1.42 (6 H, d, CH$\underline{Me}_2$, $^3J_{HH}$ = 6.9 Hz), 1.04 (6 H, d, CH$\underline{Me}_2$, $^3J_{HH}$ = 6.9 Hz), 0.40 (6 H, s, Ti$\underline{Me}$) ppm. ^{13}C{^{1}H} NMR (C_6D_6, 125.7 MHz, 298 K): 156.3 ($\underline{C}$N), 148.0 (N$\underline{C}_{Dipp}$), 141.3 (NC$\underline{C}_{Ar}$), 136.5 (NC$H_2\underline{C}_{Ar}$), 135.9 ($\underline{C}_{Dipp}$), 134.1 ($\underline{C}_{Dipp}$CHMe_2), 130.7 ($\underline{C}_{Ar}$H), 129.2 ($\underline{C}_{Dipp}$H), 128.4 ($\underline{C}_{Ar}$H), 128.3 ($\underline{C}_{Ar}$H), 124.3 ($\underline{C}_{Ar}$H), 124.2 ($\underline{C}_{Dipp}$H), 122.9 ($\underline{C}_{Ar}$H), 120.2 ($\underline{C}_5Me_5$), 55.5 (N$\underline{C}H_2$), 47.7 (Ti$\underline{Me}$, $^1J_{CH}$ = 121.9 Hz), 29.0 ($\underline{C}HMe_2$), 25.8 (CH$\underline{Me}_2$), 24.1 (CH$\underline{Me}_2$), 12.4 ($C_5\underline{Me}_5$) ppm. EI-MS: *m/z* = 389 [*M*–C_5Me_5]$^+$, 474 [*M*–2 Me]$^+$, 542 [*M*]$^+$. IR (NaCl plates, Nujol mull, cm^{-1}): 2923 (br s), 1614 (m), 1584 (m), 1456 (m), 1378 (m), 1332 (w), 1295 (w), 1258 (w), 1216 (w), 1177 (m), 1099 (w), 1057 (w), 876 (w), 863 (m), 801 (w), 759 (w), 723 (w), 614 (w). A satisfactory elemental analysis could not be obtained.

Cp*Ti{NCN(Dipp)$CH_2C_6H_4$}$(CD_3)_2$ (3-*d*$_6$) was prepared analogously to **3**, using Cp*Ti{NCN(Dipp)$CH_2C_6H_4$}Cl_2 (**2**, 0.500 g, 0.92 mmol) and CD_3MgI (1.8 mL, 1.0 M in Et_2O, 1.83 mmol). Yield: 0.35 (76%). The ^{1}H NMR spectrum was identical to that of **3**, other than the absence of the TiMe resonance.

Cp*Ti{NCN(Dipp)$CH_2C_6H_4$}$(CH_2Ph)_2$ (4). To a stirring toluene (10 mL) solution of Cp*Ti{NCN(Dipp)$CH_2C_6H_4$}Cl_2 (**2**, 0.81 g, 1.6 mmol) at 0 ºC was added dropwise $PhCH_2MgCl$ (3.33 mL, 1.0 M in hexane, 3.3 mmol) and the resulting solution was allowed to warm up to room temperature and stirred for 16 h. The volatiles were then removed *in vacuo* and the oily wax was then extracted into benzene (20 mL) to filter away from the insoluble LiCl salt. The product, Cp*Ti{NCN(Dipp)$CH_2C_6H_4$}$(CH_2Ph)_2$, was isolated as a dark red solid following removal of pentane *in vacuo*. Yield: 0.61 g (54%).

^{1}H NMR (C_6D_6, 400.2 MHz, 298 K): 7.74 (1 H, d, $C_{Ar}\underline{H}$, $^3J_{HH}$ = 7.5 Hz), 7.27–7.21 (2 H, m, $C_{Ar}\underline{H}$, $C_{Dipp}\underline{H}$), 7.14–7.11 (2 H, m, $C_{Dipp}\underline{H}$), 6.94 (6 H, m, *m*-$\underline{Ph}CH_2$, $C_{Ar}\underline{H}$), 6.80 (2 H, t, *p*-$\underline{Ph}CH_2$, $^3J_{HH}$ = 7.5 Hz), 6.71 (4 H, d, *o*-$\underline{Ph}CH_2$, $^3J_{HH}$ = 7.5 Hz), 4.42

(2 H, s, NC$\underline{H}_2$), 3.09 (2 H, sept, C$\underline{H}$Me$_2$, $^3J_{HH}$ = 6.5 Hz), 2.88 (2 H, d, PhC$\underline{H}_2$, $^2J_{HH}$ = 9.8 Hz, $^1J_{CH}$ = 122.6 Hz), 1.98 (2 H, d, PhC$\underline{H}_2$, $^2J_{HH}$ = 9.8 Hz, $^1J_{CH}$ = 123.0 Hz) 1.98 (15 H, s, C$_5\underline{Me}_5$), 1.20 (6 H, d, CH$\underline{Me}_2$, $^3J_{HH}$ = 6.5 Hz), 1.08 (6 H, d, CH$\underline{Me}_2$, $^3J_{HH}$ = 6.5 Hz) ppm. ^{13}C{^{1}H} NMR (C_6D_6, 75.4 MHz, 298 K): 159.2 ($\underline{C}$N), 151.4 (TiCH$_2\underline{C}_{Ar}$), 148.0 (N$\underline{C}_{Dipp}$), 140.6 ($\underline{C}_{Ar}$CN), 136.6 (NCH$_2\underline{C}_{Ar}$), 135.9 (NC$_{Ar}\underline{C}$), 133.9 ($\underline{C}_{Dipp}$CHMe$_2$), 130.9 ($\underline{C}_{Ar}$H), 129.8 ($\underline{C}_{Dipp}$H), 128.1 (*m*-CH$_2$C$\underline{C}_{Ar}$H), 128.0 (*o*-CH$_2$C$\underline{C}_{Ar}$H), 124.9 ($\underline{C}_{Dipp}$H), 124.8 ($\underline{C}_{Ar}$H), 122.9 ($\underline{C}_{Ar}$H), 121.8 ($\underline{C}$Me), 120.9 (*p*-CH$_2$C$\underline{C}_{Ar}$H), 79.2 (Ti$\underline{C}$H$_2$), 56.5 (N$\underline{C}$H$_2$), 28.9 ($\underline{C}$HMe$_2$), 25.5 (CH$\underline{Me}_2$), 24.2 (CH$\underline{Me}_2$), 12.5 (C$_5\underline{Me}_5$) ppm. EI-MS: *m/z* = 91 [PhCH$_2$]$^+$, 565 [*M*–CH$_2$Ph]$^+$. IR (NaCl plates, Nujol mull, cm^{-1}): 1606 (s), 1582 (s), 1464 (m), 1376 (m), 1335 (w), 1294 (w), 1207 (m), 1172 (w), 855 (w), 746 (m), 729 (m), 695 (w), 675 (w), 605 (w). A satisfactory elemental analysis could not be obtained. Diffraction-quality crystals were grown from a benzene solution at room temperature.

NMR tube scale synthesis of [Cp*Ti{NCC(Dipp)CH$_2$C$_6$H$_4$}Me][BAr$^F_4$] (5-[BAr$^F_4$]). To a solution of Cp*Ti{NCN(Dipp)CH$_2$C$_6$H$_4$}Me$_2$ (**3**, 0.01 g, 0.02 mmol) in C_6D_5Br (0.5 mL) was added [Ph$_3$C][BAr$^F_4$] (0.018 g, 0.02 mmol) resulting in the formation of a dark red solution. The solution was transferred to an NMR tube and the NMR spectra recorded after 5 minutes, showing the quantitative formation of [Cp*Ti{NCC(Dipp)CH$_2$C$_6$H$_4$}Me][BAr$^F_4$].

^{1}H NMR (C_6D_5Br, 400.2 MHz, 298 K): 7.70–7.61 (3 H, m, C$_{Ar}\underline{H}$), 7.35–7.26 (19 H, m, C$_{Ar}\underline{H}$, $\underline{Ph}$CMe), 4.84 (2 H, s, NC$\underline{H}_2$), 2.89 (2 H, sept, C$\underline{H}$Me$_2$, $^3J_{HH}$ = 7.0 Hz), 2.24 (3 H, s, Ph$_3$C$\underline{Me}$), 1.93 (15 H, s, C$_5\underline{Me}_5$), 1.45 (6 H, d, CH$\underline{Me}_2$, $^3J_{HH}$ = 7.0 Hz), 1.27-1.25 (9 H, s, CH$\underline{Me}_2$, Ti$\underline{Me}$, $^1J_{CH}$ = 128.6 Hz) ppm. ^{19}F NMR (C_6D_5Br, 376.5 MHz, 298 K): –131.1 (m, *o*-C$_6\underline{F}_5$), –161.3 (m, *p*-C$_6\underline{F}_5$), –165.3 (m, *m*-C$_6\underline{F}_5$) ppm. ^{11}B NMR (C_6D_5Br, 128.4 MHz, 298 K): –16.0 ppm.

Cp*Ti{NCN(Dipp)CH$_2$C$_6$H$_4$}(CD$_3$)][BAr$^F_4$] (5-[BAr$^F_4$]-*d*$_3$) was prepared analogously to **5-[BAr$^F_4$]**, using Cp*Ti{NCN(Dipp)CH$_2$C$_6$H$_4$}Me$_2$ (0.01 g, 0.02 mmol) and [Ph$_3$C][BAr$^F_4$] (0.018 g, 0.02 mmol). The ^{1}H NMR spectrum was identical to that of **5-[BAr$^F_4$]**, other than the absence of the TiMe and Ph$_3$CMe resonances.

[Cp*Ti{NCN(Dipp)$CH_2C_6H_4$}Me($OPPh_3$)][BAr^F_4] (6-[BAr^F_4]). To a solution of Cp*Ti{NCN(Dipp)$CH_2C_6H_4$}Me_2 (**3**, 0.040 g, 0.08 mmol) and Ph_3PO (0.022 g, 0.08 mmol) in fluorobenzene (2 mL), was added [Ph_3C][BAr^F_4] (0.074 g, 0.08 mmol) in fluorobenzene (1 mL), resulting in the formation of a red solution. After 10 min, pentane (10 mL) was added resulting in the formation of a yellow solid. The pentane/fluorobenzene was decanted and the solid washed further with pentane (5 mL). The pale yellow solid was dried *in vacuo* yielding [Cp*Ti{NCN(Dipp)$CH_2C_6H_4$}Me($OPPh_3$)][BAr^F_4]. Yield: 0.081 g (70 %).

^{1}H NMR (C_6D_5Br, 400.2 MHz, 298 K): 7.63–7.54 (10 H, m, $C_{Ar}\underline{H}$, *o*-OP$\underline{Ph}_3$, *p*-OP$\underline{Ph}_3$), 7.42–7.24 (12 H, m, $C_{Dipp}\underline{H}$, $C_{Ar}\underline{H}$, *m*-OP$\underline{Ph}_3$), 5.08 (1 H, d, N$C\underline{H}_2$, $^3J_{HH}$ = 18.8 Hz), 4.90 (1 H, d, N$C\underline{H}_2$, $^3J_{HH}$ = 18.8 Hz), 3.06–2.97 (2 H, overlapping sept, $C\underline{H}Me_2$), 1.87 (15 H, s, $C_5\underline{Me}_5$), 1.43 (3 H, d, $CH\underline{Me}_2$, $^3J_{HH}$ = 6.6), 1.29 (3 H, d, $CH\underline{Me}_2$, $^3J_{HH}$ = 6.6), 1.14 (3 H, d, $CH\underline{Me}_2$, $^3J_{HH}$ = 6.6), 1.05 (3 H, d, $CH\underline{Me}_2$, $^3J_{HH}$ = 6.6), 0.47 (3 H, s, Ti$\underline{Me}$) ppm. ^{13}C{^{1}H} NMR (C_6D_5Br, 75.4 MHz, 298 K): 161.7 (N$\underline{C}$), 149.2 (N$\underline{C}_{Dipp}$), 148.9 (br. d, *o*-$\underline{C}_6F_5$, $^1J_{CF}$= 244.8 Hz), 146.9 ($\underline{C}_{Dipp}CHMe_2$), 146.6 ($\underline{C}_{Dipp}CHMe_2$), 140.9 (NC$\underline{C}_{Ar}$), 138.7 (br. d, *p*-$\underline{C}_6F_5$, $^1J_{CF}$ = 235.6 Hz), 136.7 (br. d, *m*-$\underline{C}_6F_5$, $^1J_{CF}$= 234.7 Hz), 134.8 (*p*-OP$\underline{Ph}_3$), 134.4 (*i*-OP$\underline{Ph}_3$), 133.7 ($\underline{C}_{Ar}CH_2$), 132.8 (d, $^2J_{CP}$ = 11.6 Hz, *o*-OP$\underline{Ph}_3$), 131.8 ($\underline{C}_{Ar}H$), 130.0 ($\underline{C}_{Ar}H$), 129.5 ($\underline{C}_{Ar}H$), 128.6 (*m*-OP$\underline{Ph}_3$), 128.2 ($\underline{C}_{Dipp}H$), 124.9 ($\underline{C}_5Me_5$), 124.4 ($\underline{C}_{Dipp}H$), 124.3 ($\underline{C}_{DIpp}H$), 132.6 ($C_{Ar}\underline{H}$), 56.9, (N$\underline{C}H_2$), 52.1 (Ti$\underline{Me}$), 29.0 ($\underline{C}HMe_2$), 28.7 ($\underline{C}HMe_2$), 27.1 ($CH\underline{Me}_2$), 26.2 ($CH\underline{Me}_2$), 23.5 ($CH\underline{Me}_2$), 23.0 ($CH\underline{Me}_2$), 12.41 ($C_5\underline{Me}_5$) ppm (*i*-$\underline{C}_6F_5$ were not observed). ^{19}F NMR (C_6D_5Br, 376.5 MHz, 298 K): –131.4 (m, *o*-$C_6\underline{F}_5$), –161.9 (m, *p*-$C_6\underline{F}_5$), –165.7 (m, *m*-$C_6\underline{F}_5$) ppm. ^{11}B NMR (C_6D_5Br, 128.4 MHz, 298 K): –16.0 ppm. ^{31}P-{^{1}H} NMR (C_6D_5Br, 121.4 MHz, 298 K): 50.2 ppm. Anal. found (calcd. for $C_{73}H_{56}B_1F_{20}N_2OPTi$): C 60.49, (60.60); N, 2.03 (1.94); H, 3.80 (3.90)%. IR (NaCl plates, Nujol mull, cm^{-1}): 1643 (m), 1600 (w), 1575 (M), 1513 (s), 1455 (s), 1378 (m), 1274 (w), 1123 (s), 1084 (s), 979 (s), 775 (w), 750 (w), 692 (w), 683 (w), 661 (w).

NMR tube scale synthesis of [Cp*Ti{NCN(Dipp)$CH_2C_6H_4$}CH_2Ph][BAr^F_4] (7-[BAr^F_4]). To a solution of Cp*Ti{NCN(Dipp)$CH_2C_6H_4$}($CH_2Ph)_2$ (**4**, 0.020 g, 0.03 mmol) in C_6D_5Br (0.5 mL) was added [Ph_3C][BAr^F_4] (0.028 g, 0.03 mmol) resulting in the formation of a dark red solution. The solution was transferred to an

NMR tube and the NMR spectra recorded after 5 minutes, showing the quantitative formation of [Cp*Ti{NCN(Dipp)$CH_2C_6H_4$}CH_2Ph][$BAr^F{}_4$].

^{1}H NMR (C_6D_5Br, 400.2 MHz, 298 K): 7.61 (1H, t, $C_{Ar}\underline{H}$, $^3J_{HH}$ = 7.1 Hz), 7.42-7.24 (26 H, m, $C_{Ar}\underline{H}$ $\underline{Ph}_3CCH_2\underline{Ph}$), 7.09 (2H, t, $C_{Ar}\underline{H}$, $^3J_{HH}$ = 7.4 Hz), 6.85 (2H, d, $\underline{Ph}_3CCH_2\underline{Ph}$, $^3J_{HH}$ = 7.4 Hz), 6.80 (1H, br. s, $C_{Ar}\underline{H}$), 4.92 (2H, s, $NC\underline{H}_2$), 4.04 (2H, s, $Ph_3CC\underline{H}_2Ph$), 3.31 (2H, s, $PhC\underline{H}_2$, $^1J_{CH}$ = 149.1 Hz), 2.95 (2H, br s., $C\underline{H}Me_2$), 1.87 (15H, s, $C_5\underline{Me}_5$), 1.38 (6H, d, $CH\underline{Me}_2$, $^3J_{HH}$ = 6.1 Hz), 1.27 (6H, d, $CH\underline{Me}_2$, $^3J_{HH}$ = 6.1 Hz). ^{19}F NMR (C_6D_5Br, 376.5 MHz, 298 K): –131.3 (m, *o*-$C_6\underline{F}_5$), –161.8 (m, *p*-$C_6\underline{F}_5$), –165.5 (m, *m*-$C_6\underline{F}_5$) ppm. ^{11}B NMR (C_6D_5Br, 128.4 MHz, 298 K): -15.9 ppm.

[Cp*Ti{NCN(Dipp)$CH_2C_6H_4$}{($PhCH_2C(N^iPr)_2$}][$BAr^F{}_4$] (8-[$BAr^F{}_4$]). To a stirring fluorobenzene (3 mL) solution of Cp*Ti{NC(Dipp)$CH_2C_6H_4$}$(CH_2Ph)_2$ (**4**, 0.033 g, 0.046 mmol) and ^{i}PrNCN^{i}Pr (7.1 µL, 0.046 mmol) was added dropwise a fluorobenzene (2 mL) solution of [Ph_3C][$BAr^F{}_4$] (0.042 g, 0.046 mmol). After 1 h, pentane (10 mL) was added resulting in the formation of a dark red oil. The pentane/fluorobenzene was decanted away and the oil washed with pentane (3 × 5 mL). The remaining solid was dried *in vacuo* to yield [Cp*Ti{NCN(Dipp)$CH_2C_6H_4$}{($PhCH_2C(N^iPr)_2$}][$BAr^F{}_4$] as a red solid. Yield: 0.026 g (41%).

^{1}H NMR (C_6D_6, 499.9 MHz, 298 K): 7.69–7.64 (2 H, m, $C_{Ar}\underline{H}$), 7.61–7.58 (1 H, t, $C_{Ar}\underline{H}$, $^3J_{HH}$ = 7.8 Hz), 7.48 (1 H, br m, *p*-$\underline{Ph}CH_2$), 7.45–7.38 (3 H, m, $C_{Ar}\underline{H}$, *m*-$\underline{Ph}Ch_2$), 7.31–7.28 (2 H, m, *o*-$\underline{Ph}CH_2$), 7.24 (1 H, br s, $C_{Dipp}\underline{H}$), 7.22 (2 H, br. s, $C_{Dipp}\underline{H}$), 4.73 (2 H, s, $NC\underline{H}_2$), 3.85 (2 H, s, $PhC\underline{H}_2$), 3.50 (2 H, br. s, $NC\underline{H}Me_2$), 2.75 (2 H, br. s, $C\underline{H}Me_2$), 2.18 (15 H, s, $C_5\underline{Me}_5$), 1.32 (6 H, d, $CH\underline{Me}_2$, $^3J_{HH}$ = 6.2 Hz), 1.24 (6 H, d, $CH\underline{Me}_2$, $^3J_{HH}$ = 6.2 Hz), 0.89 (6 H, d, $NCH\underline{Me}_2$, $^3J_{HH}$ = 6.2 Hz), 0.40 (6 H, br. s, $NCH\underline{Me}_2$) ppm. ^{13}C{^{1}H} NMR (C_6D_6, 125.7 MHz, 298 K): 169.2 (N$\underline{C}$N), 165.8 (N$\underline{C}$), 148.8 (br., d, *o*-$\underline{C}_6F_5$, $^1J_{CF}$ = 245.2 Hz), 146.3 (N$\underline{C}_{Dipp}$), 140.7 (NC$\underline{C}_{Ar}$), 138.7 (br., d, *p*-$\underline{C}_6F_5$, $^1J_{CF}$ = 231.1 Hz), 136.7 (br., d, *m*-$\underline{C}_6F_5$, $^1J_{CF}$ = 235.7 Hz), 134.1 (*i*-$\underline{C}(NCHMe_2)_2$), 133.5 ($\underline{C}_{Dipp}CHMe_2$), 133.3 ($C_{Ar}\underline{H}$), 131.7 (*p*-$\underline{Ph}CH_2$), 130.7 ($\underline{C}_{Ar}H$), 130.6 ($\underline{C}_5Me_5$), 128.7 ($\underline{C}_{Ar}H$), 128.1 (*o*-$\underline{Ph}CH_2$), 128.0 (*m*-$\underline{Ph}CH_2$), 124.9 ($\underline{C}_{Dipp}H$), 124.7 ($\underline{C}_{Dipp}H$), 123.7 ($\underline{C}_{Dipp}H$, $\underline{C}_{Ar}H$), 57.6 ($N\underline{C}H_2$), 51.7 $C(N\underline{C}HMe_2)_2$), 32.8 ($Ph\underline{C}H_2$), 28.8 ($\underline{C}HMe_2$), 25.4 ($CH\underline{Me}_2$, $C(NCH\underline{Me}_2)_2$), 24.5 $C(NCH\underline{Me}_2)_2$), 24.2

(CH$\underline{Me}_2$), 13.7 ($C_5\underline{Me}_5$) ppm (*i*-$\underline{C}_6F_5$ were not observed). ^{19}F NMR (C_6D_5Br, 470.4 MHz, 298 K): –131.3 (m, *o*-$C_6\underline{F}_5$), –161.9 (m, *p*-$C_6\underline{F}_5$), –165.7 (m, *m*-$C_6\underline{F}_5$) ppm. ^{11}B NMR (C_6D_5Br, 160.4 MHz, 298 K): -15.9 ppm. IR (NaCl plates, Nujol mull, cm^{-1}): 1643 (m), 1597 (w), 1556 (w), 1513 (w), 1463 (s), 1378 (w), 1275 (w), 1023 (w), 1085 (m), 979 (m), 804 (w), 756 (w), 728 (w), 684 (w), 661 (w). A satisfactory elemental analysis could not be obtained.

NMR tube scale synthesis of [Cp*Ti{NCN(Dipp)CH$_2$C$_2$H$_4$}Me][MeBAr$^F_3$] (5-[MeBAr$^F_3$]). To a solution of Cp*Ti{NCN(Dipp)CH$_2$C$_6$H$_4$}Me$_2$ (**3**, 0.020 g, 0.04 mmol) in C_6D_5Br (0.5 mL) was added B(C_6F_5)$_3$ (0.021 g, 0.04 mmol) resulting in the formation of a red solution. The solution was transferred to an NMR tube and the NMR spectra recorded after 5 minutes, showing quantitative formation of the titled compound.

^{1}H NMR (C_6D_5Br, 400.2 MHz, 298 K): 7.63–7.53 (2 H, m, $C_{Ar}\underline{H}$, $C_{Dipp}\underline{H}$), 7.46–7.28 (5 H, m, $C_{Ar}\underline{H}$, $C_{Dipp}\underline{H}$), 4.91 (2 H, s, NC$\underline{H}$), 3.14–2.88 (2 H, br, C$\underline{H}$Me$_2$), 1.94 (15 H, s, $C_5\underline{Me}_5$), 1.91–1.89 (6 H, overlapping singlets, Ti$\underline{Me}$, B$\underline{Me}$), 1.46 (6 H, br, CH$\underline{Me}_2$), 1.23 (6 H, d, $^3J_{HH}$ = 6.4 Hz) ppm. ^{19}F NMR (C_6D_5Br, 376.5 MHz, 298 K): –132.1 (m, *o*-$C_6\underline{F}_5$), –159.2 (m, *p*-$C_6\underline{F}_5$), –164.1 (m, *m*-$C_6\underline{F}_5$) ppm. ^{11}B NMR (C_6D_5Br, 128.4 MHz, 298 K): –13.8 ppm.

NMR tube scale reaction [Cp*Ti{NCN(Dipp)CH$_2$C$_6$H$_4$}Me(OPPh$_3$)][MeBAr$^F_3$] (6-[MeBAr$^F_3$]). To a solution of Cp*Ti{NCN(Dipp)CH$_2$C$_6$H$_4$}Me$_2$ (**3**, 0.010 g, 0.002 mmol) and Ph_3PO (0.006 g, 0.02 mmol) in C_6D_5Br (0.3 mL) was added a C_6D_5Br solution(0.2 mL) of [BAr$^F_3$] (0.010 g, 0.02 mmol) and the NMR spectra recorded after 5 min revealing quantitative conversion to **6-[MeBAr$^F_3$]**. The same ^{31}P{^{1}H} NMR and ^{1}H NMR spectra were observed as for **(6-[BAr$^F_4$])** except for the additional Ph_3CMe resonances at 7.59–7.09 (15H, m, $\underline{Ph}_3$CMe) and 2.24 (3H, s, $Ph_3C\underline{Me}$). ^{19}F NMR (C_6D_5Br, 376.5 MHz, 298 K): –131.3 (m, *o*-$C_6\underline{F}_5$), –163.8 (m, *p*-$C_6\underline{F}_5$), –166.2 (m, *m*-$C_6\underline{F}_5$) ppm. ^{11}B NMR (C_6D_5Br, 128.4 MHz, 298 K): -14.3 ppm.

NMR tube scale synthesis of [Cp*Ti{NCN(Dipp)CH$_2$C$_6$H$_4$}-{CH$_2$N(Ph)Me}][BAr$^F_4$]

Route A: To a solution of Cp*Ti{NCN(Dipp)CH$_2$C$_6$H$_4$}Me$_2$ (**3**, 0.020 g, 0.039 mmol) in C_6D_5Br (0.5 mL) was added [HNMePh][BAr$^F_4$] (0.036 g, 0.039 mmol) resulting in

the formation of a red solution. The solution was left standing for 12 h and transferred to an NMR tube and the NMR spectra recorded.

Route B: To a solution of Cp*Ti{NC(Dipp)$CH_2C_6H_4$}Me_2 (0.020 g, 0.039 mmol) and *N,N'*-dimethyl aniline (5.7 µL, 0.039 mmol) in C_6D_5Br (0.5 mL) was added $[Ph_3C][BAr^F{}_4]$ (0.037 g, 0.039 mmol) resulting in the formation of a red solution. The solution was left standing for 12 h and transferred to an NMR tube and the NMR spectra recorded revealing quantitative conversion of the mixture of cations to **9-[$BAr^F{}_4$]**.

[Cp*Ti{NCN(Dipp)$CH_2C_6H_4$}{CH_2N(Ph)Me}][$BAr^F{}_4$] (9-[$BAr^F{}_4$]). A solution of Cp*Ti{NCN(Dipp)$CH_2C_6H_4$}Me_2 (**3**, 0.050 g, 0.099 mmol) and [$HNMe_2Ph$][$BAr^F{}_4$] (0.079 g, 0.099 mmol) in fluorobenzene (3 mL) was left stirring for 12 h. Pentane (6 mL) was added resulting in the formation of a dark red oil. The pentane/fluorobenzene was decanted away and the oil washed with pentane (3 × 3 mL). The remaining solid was dried *in vacuo* to yield [Cp*Ti{NCN(Dipp)$CH_2C_6H_4$}{CH_2N(Ph)Me}][$BAr^F{}_4$] as a red solid. Yield: 0.058 g (46%).

^{1}H NMR (C_6D_5Br, 499.9 MHz, 298 K): 7.64–7.62 (2 H, m $C_{Ar}\underline{H}$), 7.48–7.46 (2 H, m, $C_{Ar}\underline{H}$), 7.38–7.33 (3 H, m, $C_{Ar}\underline{H}$, $C_{Dipp}\underline{H}$), 7.22–7.15 (2 H, C_{Ar}H), 6.82–6.77 (3 H, m, $C_{Ar}\underline{H}$, $C_{Dipp}\underline{H}$), 4.89 (2 H, s, N$C\underline{H}_2$), 3.08 (1 H, d, Ti$C\underline{H}_2$, $^3J_{HH}$ = 4.9 Hz), 2.96–2.89 (5 H, m, C$\underline{H}Me_2$, N$\underline{Me}$), 2.69 (1 H, d, Ti$C\underline{H}_2$, $^3J_{HH}$ = 4.9 Hz), 1.76 (15 H, s, $C_5\underline{Me}_5$), 1.49 (3 H, d, CH$\underline{Me}_2$, $^3J_{HH}$ = 6.7 Hz), 1.34 (3 H, d, CH$\underline{Me}_2$, $^3J_{HH}$ = 6.8 Hz), 1.27 (3 H, d, CH$\underline{Me}_2$, $^3J_{HH}$ = 6.8 Hz), 1.23 (3 H, d, CH$\underline{Me}_2$, $^3J_{HH}$ = 6.7 Hz) ppm. ^{13}C{^{1}H} NMR (C_6D_6, 125 MHz, 298 K): 162.7 ($\underline{C}$N), 150.0 ($\underline{Ph}$N), 148.8 (br. d, *o*-$\underline{C}_6F_5$, $^1J_{CF}$ = 242.9 Hz), 147.1 (N$\underline{C}_{Dipp}$),147.0 ($\underline{C}_{Dipp}CHMe_2$), 140.8 (NC$\underline{C}_{Ar}$), 138.7 (br. d, *p*-$\underline{C}_6F_5$, $^1J_{CF}$ = 236.6 Hz), 136.7 (br. d, *m*-$\underline{C}_6F_5$, $^1J_{CF}$ = 232.8 Hz), 133.2 ($\underline{C}_{Ar}$CH), 132.7 ($\underline{C}_{Ar}$H), 130.6 ($\underline{C}_{Dipp}$H), 128.9 ($\underline{C}_{Ar}$H), 128.6 ($\underline{C}_{Ar}$H), 124.9 (*m*-$\underline{Ph}$N), 124.1 ($\underline{C}_{Dipp}$H), 123.9 ($\underline{C}_5Me_5$), 123.8 ($C_{Ar}\underline{H}$, $C_{Dipp}\underline{H}$), 120.9 (*p*-$\underline{Ph}$N) 113.8 (*o*-$\underline{Ph}$N), 77.6 (Ti$\underline{C}H_2$), 57.2 (N$\underline{C}H_2$), 57.1 (N$\underline{Me}$), 28.8 ($\underline{C}HMe_2$), 26.4 (CH$\underline{Me}_2$), 26.2 (CH$\underline{Me}_2$), 23.9 (CH$\underline{Me}_2$), 23.0 (CH$\underline{Me}_2$), 12.5 ($C_5\underline{Me}_5$) ppm (*i*-$\underline{C}_6F_5$ were not observed). ^{19}F NMR (C_6D_5Br, 470.4 MHz, 298 K): –131.5 (m, *o*-$C_6\underline{F}_5$), –161.8 (m, *p*-$C_6\underline{F}_5$), –165.7 (m, *m*-$C_6\underline{F}_5$) ppm.^{11}B NMR (C_6D_5Br, 160.4 MHz, 298 K): –16.0 ppm. IR (NaCl plates, Nujol mull, cm^{-1}): 1643 (m), 1596 (w), 1555 (m), 11512 (m), 1455 (m), 1378 (w),

1273(w), 1213 (w), 1084 (m), 1056 (w), 978 (m), 755 (w), 774 (m), 727 (w), 683 (w), 660 (w), 609 (w), 572 (w), 545 (w). A satisfactory elemental analysis could not be obtained.

[Cp*Ti{NCN(Dipp)$CH_2C_6H_4$}{(NPhMe)$CH_2C(N^iPr)_2$}][BAr^F_4] (10-[BAr^F_4]). A solution of Cp*Ti{NCN(Dipp)$CH_2C_6H_4$}Me_2 (**3**, 0.050 g, 0.099 mmol) and [$HNMe_2Ph$][BAr^F_4] (0.079 g, 0.099 mmol) in fluorobenzene (5mL) was left stirring for 12 h. To the resulting mixture $^iPrNCN^iPr$ (15.1 µL, 0.099 mmol) was added. After 10 minutes, pentane (10 mL) was added resulting in the formation of a dark green oil. The pentane/fluorobenzene was decanted away and the oil washed with pentane (3 × 5 mL). The remaining solid was dried *in vacuo* to yield [Cp*Ti{NCN(Dipp)$CH_2C_6H_4$}{(NPhMe)$CH_2C(N^iPr)_2$}][BAr^F_4] as a green solid. Yield: 0.060 g (43%).

^{1}H NMR (C_6D_5Br, 499.9 MHz, 298 K): 7.82 (1 H, d, $C_{Ar}\underline{H}$, $^3J_{HH}$ = 7.5 Hz), 7.70 (1 H, t, $C_{Ar}\underline{H}$, $^3J_{HH}$ = 7.7 Hz), 7.63 (1 H, t, $C_{Ar}\underline{H}$, $^3J_{HH}$ = 7.5 Hz), 7.53–7.51 (1 H, m, $C_{Ar}\underline{H}$), 7.40–7.27 (7 H, m, $CH_2NMe\underline{Ph}$, $C_{Dipp}\underline{H}$), 7.06 (1 H, d, $C_{Dipp}\underline{H}$, $^3J_{HH}$ = 7.8 Hz), 5.01, 4.93 (2 H, ABq, $NC\underline{H}_2$, $^2J_{HH}$ = 19.2 Hz), 4.19 (1 H, d, $C\underline{H}_2NMePh$, $^2J_{HH}$ = 13.5 Hz), 4.00 (1 H, d, $C\underline{H}_2NMePh$, $^2J_{HH}$ = 13.5 Hz), 3.78 (1 H, sept, $C(NC\underline{H}Me_2)_2$, $^3J_{HH}$ = 6.0 Hz), 3.47 (1 H, sept, $C(NC\underline{H}Me_2)_2$, $^3J_{HH}$ = 6.6 Hz), 3.37 (1 H, sept, $C\underline{H}Me_2$, $^3J_{HH}$ = 6.6 Hz), 2.77–2.72 (1 H, m, $C\underline{H}Me_2$), 2.35 (3 H, s, $CH_2N\underline{Me}Ph$), 1.82 (15 H, s, $C_5\underline{Me}_5$), 1.78 (3 H, d, $C(NC\underline{H}Me_2)_2$, $^3J_{HH}$ = 6.6 Hz), 1.67 (3 H, d, $CH\underline{Me}_2$, $^3J_{HH}$ = 6.6 Hz), 1.40 (3 H, d, $C(NC\underline{H}Me_2)_2$, $^3J_{HH}$ = 6.0 Hz), 1.34–1.28 (9 H, m, $CH\underline{Me}_2$, $C(NC\underline{H}Me_2)_2$), 1.11 (3 H, d, $CH\underline{Me}_2$, $^3J_{HH}$ = 6.5 Hz), 1.06 (3 H, d, $CH\underline{Me}_2$, $^3J_{HH}$ = 6.5 Hz) ppm. $^{13}C\{^1H\}$ NMR (C_6D_6, 125.7 MHz, 298 K): 164.6 ($\underline{C}N$), 151.3 ($CH_2NMe\underline{Ph}$, 148.8 (br. d, *o*-$\underline{C}_6F_5$, $^1J_{CF}$ = 245.2 Hz), 146.7 ($\underline{N}C_{Dipp}$), 146.5 ($\underline{C}_{Dipp}CHMe_2$), 140.4 ($NC\underline{C}_{Ar}$), 138.7 (br. d, *p*-$\underline{C}_6F_5$, $^1J_{CF}$ = 231.1 Hz), 136.7 (br. d, *m*-$\underline{C}_6F_5$, $^1J_{CF}$ = 235.7 Hz), 133.9 ($NC\underline{C}_{Ar}$), 133.2 ($CH_2\underline{C}_{Ar}$), 133.0 ($\underline{C}_{Ar}H$), 132.7 ($CH_2NMe\underline{Ph}$), 130.6 ($CH_2NMe\underline{Ph}$), 129.2 ($\underline{C}_5Me_5$), 129.1 ($\underline{C}_{Ar}H$), 128.6 ($CH_2NMe\underline{Ph}$), 127.9 ($\underline{C}_{Dipp}H$), 127.7 ($\underline{C}_{Ar}H$), 124.7 ($\underline{C}_{Dipp}H$), 124.1 ($\underline{C}_{Dipp}H$), 123.6 ($C_{Ar}\underline{H}$), 123.4 ($\underline{C}_{Ar}H$), 121.0 ($\underline{C}_{Ar}H$), 58.4 ($CH_2N\underline{Me}Ph$), 57.1 ($N\underline{C}H_2$), 53.9 ($\underline{C}H_2NMePh$), 50.4 ($C(N\underline{C}HMe_2)_2$), 49.9 ($C(N\underline{C}HMe_2)_2$), 28.9 ($\underline{C}HMe_2$), 28.8 ($\underline{C}HMe_2$), 26.8 ($CH\underline{Me}_2$), 26.2 ($C(NCH\underline{Me}_2)_2$), 25.1 ($C(NCH\underline{Me}_2)_2$), 24.9 ($CH\underline{Me}_2$), 24.1 ($C(NCH\underline{Me}_2)_2$), 23.2 ($CH\underline{Me}_2$), 21.6 ($C(NCH\underline{Me}_2)_2$), 21.8 ($CH\underline{Me}_2$), 12.5

($C_5\underline{Me}_5$) ppm (*i*-$\underline{C}_6F_5$ were not observed).^{19}F NMR (C_6D_5Br, 470.4 MHz, 298 K): -131.4 (m, *o*-$C_6\underline{F}_5$), –161.7 (m, *p*-$C_6\underline{F}_5$), –165.7 (m, *m*-$C_6\underline{F}_5$) ppm. ^{11}B NMR (C_6D_5Br, 160.4 MHz, 298 K): –16.0 ppm. IR (NaCl plates, Nujol mull, cm^{-1}): 1642 (w), 1614 (w), 1596 (w), 1548 (m), 1511 (m), 1455 (m), 1399 (w), 1274(w), 1213 (w), 1159 (w), 1083 (m), 977 (m), 887 (w), 804 (w), 755 (w), 774 (m), 726 (w), 682 (w), 660 (w), 606 (w), 554 (w). A satisfactory elemental analysis could not be obtained.

Cp*Ti{NCN(Dipp)$CH_2C_6H_4$}(η-2,3-$C_4H_4Me_2$) (11). To a stirring solution of Cp*Ti{NCN(Dipp)$CH_2C_6H_4$}Cl_2 (**2**, 0.200 g, 0.41 mmol) and 2,3-dimethyl-1,3-butadiene (0.069 mL, 0.61 mmol) in toluene (15 mL) at 0 ºC was added dropwise two equivalents of ^{n}BuLi (0.51 mL, 1.6 M in hexane, 0.82 mmol) which resulted in the solution changing colour from orange/red to brown. The reaction mixture was allowed to warm slowly to room temperature and was stirred for 16 h upon the solution turned green. Removal of the volatiles *in vacuo* afforded a green solid which was extracted into pentane (4 × 10 mL). The solvent was removed *in vacuo* giving Cp*Ti{NCN(Dipp)$CH_2C_6H_4$}(η-2,3-$C_4H_4Me_2$) as a green solid. Yield: 0.407 g (80%).

^{1}H NMR (C_6D_6, 499.9 MHz, 298 K): 7.24 (1 H, d, $C_{Ar}\underline{H}$, $^3J_{HH}$ = 7.1 Hz), 7.15–7.17 (1 H, m, $C_{Dipp}\underline{H}$), 7.14–7.05 (4 H, $C_{Ar}\underline{H}$, $C_{Dipp}\underline{H}$) 6.94 (1 H, d, $C_{Ar}\underline{H}$, $^3J_{HH}$ = 7.1 Hz), 4.50 (2 H, ABq, $NC\underline{H}_2$, $^2J_{HH}$ = 4.2 Hz), 3.13–3.02 (2 H, m, $C\underline{H}Me_2$,), 2.59 (1 H, d, η-2,3-$C_4\underline{H}_4Me_2$, $^2J_{HH}$ = 7.2 Hz, $^1J_{CH}$ = 148.6 Hz), 2.52 (1 H, d, η-2,3-$C_4\underline{H}_4Me_2$, $^2J_{HH}$ = 7.1 Hz, $^1J_{CH}$ = 149.3 Hz), 1.93 (15 H, s , C_5Me_5), 1.89 (3 H, app s, η-2,3-$C_4H_4\underline{Me}_2$), 1.87 (3 H, app s, η-2,3-$C_4H_4\underline{Me}_2$), 1.32–1.28 (3 H, d, $CH\underline{Me}_2$, $^3J_{HH}$ = 6.5 Hz), 1.22–1.19 (3 H, d, $CH\underline{Me}_2$, $^3J_{HH}$ = 6.5 Hz), 1.11–1.04 (6 H, m, $CH\underline{Me}_2$), 0.81 (1 H, d, η-2,3-$C_4\underline{H}_4Me_2$, $^2J_{HH}$ = 7.2 Hz, $^1J_{CH}$ = 140.5 Hz), 0.70 (1 H, d, η-2,3-$C_4\underline{H}_4Me_2$, $^2J_{HH}$ = 7.1 Hz, $^1J_{CH}$ = 140.0 Hz) ppm. $^{13}C\{^1H\}$ NMR (C_6D_6, 125.7 MHz, 298 K): 154.0 ($N\underline{C}N$), 148.4 ($N\underline{C}_{Dipp}$), 140.0 ($NC\underline{C}_{Ar}$), 138.8 ($\underline{C}_{Dipp}CHMe_2$), 136.4 ($\underline{C}_{Dipp}CHMe_2$), 129.4 ($NCH_2\underline{C}_{Ar}$), 128.6 ($\underline{C}_{Dipp}H$), 128.2, η-2,3-$\underline{C}_4H_4Me_2$ (vinylic)), 128.0 (η-2,3-$\underline{C}_4H_4Me_2$ (vinylic)), 124.3 ($\underline{C}_{Ar}H$), 124.1 ($\underline{C}_{Dipp}H$), 124.0 ($\underline{C}_{Dipp}H$), 122.7 ($\underline{C}_{Ar}H$), 117.9 ($\underline{C}_5Me_5$), 71.2 (η-2,3-$\underline{C}_4H_4Me_2$ (adjacent to Ti), 69.2 (η-2,3-$\underline{C}_4H_4Me_2$ (adjacent to Ti), 56.0 ($N\underline{C}H_2$), 28.6 ($\underline{C}HMe_2$), 25.1 (η-2,3-$C_4H_4\underline{Me}_2$), 24.0 (η-2,3-$C_4H_4\underline{Me}_2$), 23.9 ($CH\underline{Me}_2$), 23.6 ($CH\underline{Me}_2$), 12.4 ($C_5\underline{Me}_5$) ppm. EI-MS *m/z*:

292 $[NCN(C_6H_2iPr_2)CH_2C_6H_4]^+$. IR (NaCl plates, Nujol mull, cm^{-1}): 1633 (m), 1587 (w), 1464 (m), 1376 (w), 1349 (w), 1333 (w), 1286 (w), 1260 (w), 1221 (w), 1182 (w), 1139 (w), 1091 (m), 1051 (w), 1016 (w), 875 (w), 771 (w), 760 (m), 727 (m), 658 (w), 604 (w). A satisfactory elemental analysis could not be obtained.

Cp*Ti{NCN(Dipp)$CH_2C_6H_4$}{η-$CH_2(CH)_3CH_2$Me} (12). To a stirring solution of Cp*Ti{NCN(Dipp)$CH_2C_6H_4$}Cl_2 (**2**, 0.500 g, 0.92 mmol) and 1,3-hexadiene (160 μL, 1.4 mmol) in toluene (5 mL) at 0 ºC was added dropwise two equivalents of ^{n}BuLi (1.1 mL, 1.6 M in hexane, 1.8 mmol) which resulted in the solution turning a darker colour. The reaction mixture was allowed to warm slowly to room temperature and stirred for further 16 h. Removal of volatiles *in vacuo* afforded a dark green solid which was extracted into pentane (4 × 5 mL). The solvent was removed *in vacuo* yielding the *supine* and *prone* isomer of Cp*Ti{NCN(Dipp)$CH_2C_6H_4$}{η-$CH_2(CH)_3CH_2$Me} as a dark green solid. Yield: 0.40 g (78%).

***supine*-12**. ^{1}H NMR (toluene-d_8, 400.2 MHz, 233 K): 5.80–5.63 (1 H, m, η-$CH_2(C\underline{H})_3CH_2$Me (vinylic)), 5.51 (1 H, app. t, η-$CH_2(C\underline{H})_3CH_2$Me (vinylic), $^2J_{HH}$ = 10.6 Hz), 4.66–4.57 (2 H, m, N$C\underline{H}_2$) 3.26 (1 H, m, $C\underline{H}Me_2$), 2.98–2.87 (1 H, m, η-$C\underline{H}_2(CH)_3CH_2$Me), 2.54–2.49 (1 H, m, η-$CH_2(CH)_3C\underline{H}_2$Me), 2.12–2.08 (1 H, m, η-$CH_2(CH)_3C\underline{H}_2$Me), 1.88 (15 H, s, C_5Me_5), 1.44–1.39 (3 H, m, $CH\underline{Me}_2$), 1.31 (3 H, br, η-$CH_2(CH)_3CH_2\underline{Me}$), 1.18 (3 H, m, $CH\underline{Me}_2$), 0.61–0.54 (2 H, m, η-$C\underline{H}_2(CH)_3CH_2$Me, η-$CH_2(C\underline{H})_3CH_2$Me (adjacent to Ti)) ppm. $^{13}C\{^1H\}$ NMR (toluene-d_8, 100.6 MHz, 233 K): 124.2 (η-$CH_2(\underline{C}H)_3CH_2$Me (vinylic)), 118.2 (η-$CH_2(\underline{C}H)_3CH_2$Me (vinylic)), 116.7($\underline{C}_5Me_5$), 81.9 (η-$CH_2(\underline{C}H)_3CH_2$Me (adjacent to Ti)), 65.0 (η-$\underline{C}H_2(CH)_3CH_2$Me), 54.8 (N$\underline{C}H_2$), 28.4 ($\underline{C}HMe_2$), 27.7 (η-$CH_2(CH)_3\underline{C}H_2$Me), 23.3 ($CH\underline{Me}_2$), 20.6 (η-$CH_2(CH)_3CH_2\underline{Me}$), 19.4 ($CH\underline{Me}_2$), 11.8 ($C_5\underline{Me}_5$) ppm. Remaining resonances could not be distinguished between the two *supine* isomers.

***supine´*-12.** ^{1}H NMR (toluene-d_8, 400.2 MHz, 233 K): 5.80–5.63 (2 H, m, η-$CH_2(C\underline{H})_3CH_2$Me (vinylic)), 4.46–4.36 (2 H, m, N$C\underline{H}_2$), 2.98–2.87 (1 H, m, η-$C\underline{H}_2(CH)_3CH_2$Me), 2.84–2.82 (1 H, m, η-$CH_2(CH)_3C\underline{H}_2$Me), 2.12–2.08 (1 H, m, η-$CH_2(CH)_3C\underline{H}_2$Me), 1.98 (15 H, s, C_5Me_5), 1.84–1.82 (1 H, m, η-$CH_2(CH)_3C\underline{H}_2$Me), 1.00–0.96 (4 H, m, η-$CH_2(CH)_3CH_2\underline{Me}$, η-$CH_2(C\underline{H})_3CH_2$Me (adjacent to Ti)),

0.61-0.54 (1 H, m, η-C$\underline{H}_2$(CH)$_3$CH$_2$Me) ppm. ^{13}C{^{1}H} NMR (toluene-d_8, 100.6 MHz, 233 K): 124.3 (η-CH$_2$(C$\underline{H}$)$_3$CH$_2$Me (vinylic)), 119.8 (η-CH$_2$(C$\underline{H}$)$_3$CH$_2$Me (vinylic)), 116.8 (C$_5$Me$_5$), 81.7 (η-CH$_2$(C$\underline{H}$)$_3$CH$_2$Me (adjacent to Ti)), 63.9 (η-C$\underline{H}_2$(CH)$_3$CH$_2$Me), 27.2 (η-CH$_2$(CH)$_3$C$\underline{H}_2$Me), 14.6 (η-CH$_2$(CH)$_3$CH$_2$C$\underline{H}_3$), 12.0 (C$_5$C$\underline{H}_3$) ppm. Remaining resonances could not be distinguished between the two *supine* isomers.

***prone*-12**. ^{1}H NMR (toluene-d_8, 400.2 MHz, 233 K): 8.10 (1 H d, C$_{Ar}\underline{H}$, $^3J_{HH}$ = 6.9 Hz), 7.35 (1 H, t, C$_{Ar}\underline{H}$, $^3J_{HH}$ = 6.9 Hz), 7.25–6.98 (3 H, m, C$_{Ar}\underline{H}$), 6.98-6.94 (2 H, m, C$_{Ar}\underline{H}$), 4.41–4.30 (3 H, m, NC$\underline{H}_2$, η-CH$_2$(C$\underline{H}$)$_3$CH$_2$Me (vinylic)), 4.04 (1 H, dt, η-CH$_2$(C$\underline{H}$)$_3$CH$_2$Me (vinylic)), $^3J_{HH}$ = 14.2 Hz, 10.3 Hz), 3.11–3.02 (1 H, m, η-C$\underline{H}_2$(CH)$_3$CH$_2$Me), 2.69–2.66 (2 H, m, C$\underline{H}$Me$_2$), 2.08 (2 H, m, C$\underline{H}_2$Me), 1.85 (15 H, s, C$_5$C$\underline{H}_3$), 1.74–1.72 (1 H, m, η-CH$_2$(C$\underline{H}$)$_3$CH$_2$Me (adjacent to Ti)), 1.39–1.36 (1 H, m, η-C$\underline{H}_2$(CH)$_3$CH$_2$Me) 1.09–1.07 (6 H, m, CHC$\underline{H}_3$), 0.99–0.97 (3 H, m, CH$_2$C$\underline{H}_3$), 0.91 (6 H, d, CHC$\underline{H}_3$, $^3J_{HH}$ = 6.7 Hz). ^{13}C{^{1}H} NMR (toluene-d_8, 100.6 MHz, 233 K): 155.1 (NCN), 148.0 (NC$_{Dipp}$), 147.8 (C$_{Dipp}$CHMe$_2$), 141.0 (NCC$_{Ar}$), 136.1 (NCH$_2$C$_{Ar}$), 129.7 (C$_{Ar}$H), 128.2 (C$_{Dipp}$H), 127.3 (C$_{Ar}$H), 124.0 (C$_{Ar}$H), 123.6 (C$_{Dipp}$H), 123.3 (C$_{Dipp}$H), 122.7 (C$_{Ar}$H), 114.9 (C$_5$Me$_5$), 114.6 (η-CH$_2$(CH)$_3$CH$_2$Me (vinylic)), 106.8 (η-CH$_2$(CH)$_3$CH$_2$Me (vinylic)), 81.4 (η-CH$_2$(CH)$_3$CH$_2$Me (adjacent to Ti)), 59.0 (η-CH$_2$(CH)$_3$CH$_2$Me), 55.2 (NCH$_2$), 28.9 (CHMe$_2$), 27.3 (η-CH$_2$(CH)$_3$CH$_2$Me), 26.7 (CHMe$_2$), 23.6 (CHMe$_2$), 19.1 (η-CH$_2$(CH)$_3$CH$_2$Me), 12.3 (C$_5$Me$_5$) ppm.

Common Data: EI-MS *m/z*: 421 [*M*–C$_5$Me$_5$]$^+$. IR (NaCl plates, Nujol mull, cm^{-1}): 1648 (m), 1584 (m), 1514 (m), 1457 (m), 1378 (m), 1332 (w), 1278 (w), 1215 (w), 1151 (w), 1092 (w), 1017 (w), 800 (m), 726 (w). A satisfactory elemental analysis could not be obtained.

Cp*Ti{NCN(Dipp)CH$_2$C$_6$H$_4$}{η-1,4-C$_4$H$_4$Me$_2$} (13). To a stirring solution of Cp*Ti{NCN(Dipp)CH$_2$C$_6$H$_4$}Cl$_2$ (**2**, 0.50 g, 0.92 mmol) and 2,4-hexadiene (158 μL, 1.4 mmol) in toluene (5 mL) at 0 ºC was added dropwise two equivalents of ^{n}BuLi (1.1 mL, 1.6 M in hexane, 1.8 mmol) which resulted in the solution turning a darker colour. The reaction mixture was allowed to warm slowly to room temperature and stirred for further 16 h. Removal of volatiles *in vacuo* afforded a dark green solid which was extracted into pentane (4 × 5 mL). The solvent was removed *in vacuo*

yielding the *supine* and *prone* isomer of Cp*Ti{NCN(Dipp)$CH_2C_6H_4$}{η-1,4-$C_4H_4Me_2$} as a brown solid. Yield: 0.39 g (70%).

***supine*-13**. ^{1}H NMR ($C_6D_5CD_3$, 499.9 MHz, 243 K): 7.33–6.95 (7 H, overlapping m, $C_{Ar}\underline{H}$), 5.53–5.37 (2 H, m, η-1,4-$C_4\underline{H}_4Me_2$ (vinylic)), 4.67–4.57 (2 H, overlapping m, $NC\underline{H}_2$), 3.36–3.33 (1 H, m, $C\underline{H}Me_2$), 2.98–2.95 (1 H, m, $C\underline{H}Me_2$), 2.07 (3 H, d, η-1,4-$C_4H_4\underline{Me}_2$), 1.96 (15 H, s, $C_5\underline{Me}_5$), 1.56 (3 H, d, η-1,4-$C_4H_4\underline{Me}_2$), 1.45 (3 H, d, $CH\underline{Me}_2$, $^3J_{HH}$ = 6.7 Hz), 1.36 (3 H, d, $CH\underline{Me}_2$, $^3J_{HH}$ = 6.8 Hz), 1.30 (3 H, br, $CH\underline{Me}_2$), 1.17 (3 H, d, $CH\underline{Me}_2$, $^3J_{HH}$ = 6.6 Hz) 0.72–0.68 (1 H, η-1,4-$C_4\underline{H}_4Me_2$ (adjacent to Ti)), 0.62–0.52 (1 H, η-1,4-$C_4\underline{H}_4Me_2$ (adjacent to Ti)) ppm. $^{13}C\{^1H\}$ NMR (C_6D_6, 125.7 MHz, 243 K): 154.0 ($N\underline{C}$), 147.9 ($N\underline{C}_{Dipp}$), 138.5 ($NC\underline{C}_{Ar}$), 136.6 ($\underline{C}_{Dipp}CHMe_2$), 123.4 (η-1,4-$\underline{C}_4H_4Me_2$ (vinylic)), 123.3 (η-1,4-$\underline{C}_4H_4Me_2$ (vinylic)), 116.2 ($\underline{C}_5Me_5$), 74.6 (η-1,4-$\underline{C}_4H_4Me_2$ (adjacent to Ti)), 73.3 (η-1,4-$\underline{C}_4H_4Me_2$ (adjacent to Ti)), 55.2 ($N\underline{C}H_2$), 18.6 (η-1,4-$C_4H_4\underline{Me}_2$), 18.6 (η-1,4-$C_4H_4\underline{Me}_2$), 11.4 ($C_5\underline{Me}_5$) ppm. Remaining resonances (aromatic ^{13}C) could not be assigned unambiguously.

***prone*-13**. ^{1}H NMR ($C_6D_5CD_3$, 499.9 MHz, 243 K): 8.04 (1 H, d, $C_{Ar}\underline{H}$, $^3J_{HH}$ = 7.1 Hz), 7.39–7.33 (2 H, m, $C_{Ar}\underline{H}$), 7.33–6.95 (4 H, m, $C_{Ar}\underline{H}$), 4.51 (2 H, s, $NC\underline{H}_2$) 4.06–3.99 (2 H, m, η-1,4-$C_4\underline{H}_4Me_2$ (vinylic)), 2.98–2.95 (2 H, m, $C\underline{H}Me_2$), 1.86 (15 H, s, $C_5\underline{Me}_5$), 1.81–1.79 (2 H, m, (η-1,4-$C_4\underline{H}_4Me_2$ (adjacent to Ti)), 1.25 (6 H, d, $CH\underline{Me}_2$, $^3J_{HH}$ = 6.6 Hz), 1.01–0.98 (12 H, br m, η-1,4-$C_4H_4\underline{Me}_2$, $CH\underline{Me}_2$) ppm. $^{13}C\{^1H\}$ NMR (C_6D_6, 125.7 MHz, 243 K): 154.4 ($N\underline{C}$), 148.1 ($N\underline{C}_{Dipp}$),141.0 ($NC\underline{C}_{Ar}$), 136.7 ($NCH_2\underline{C}_{Ar}$), 136.6 ($\underline{C}_{Dipp}CHMe_2$), 129.6 ($\underline{C}_{Ar}H$), 127.6 (2 × $\underline{C}_{Ar}H$), 122.7 ($\underline{C}_{Ar}H$), 125.4 ($\underline{C}_{Ar}H$), 124.5 ($\underline{C}_{Ar}H$), 122.6 ($\underline{C}_{Ar}H$), 114.9 ($\underline{C}_5Me_5$), 110.7 (2× (η-1,4-$\underline{C}_4H_4Me_2$ (vinylic)), 71.0 ((η-1,4-$\underline{C}_4H_4Me_2$ (adjacent to Ti)), 54.8 ($N\underline{C}H_2$), 18.9 (η-1,4-$C_4H_4\underline{Me}_2$), 12.0 ($C_5\underline{Me}_5$) ppm.

Common data: EI-MS *m/z*: 474 (*M*–CH(Me)$(CH)_2$CH(Me))$^+$. IR (NaCl plates, Nujol mull, cm^{-1}): 1655 (m), 1583(m), 1521 (m), 1449 (m), 1375 (w), 1331 (m), 1278 (w), 1215 (w), 1085 (m), 943 (w), 803 (m), 730 (w). A satisfactory elemental analysis could not be obtained. Also observe isomerisation to **12**.

Cp*Ti{NCN(Dipp)$CH_2C_6H_4$}{η^3-$CH_3CH_2(CH)_3CH_2BAr^F_3$} (14). To a solution of stirring solution of Cp*Ti{NCN(Dipp)$CH_2C_6H_4$}Cl_2 (**2**, 0.400 g, 0.79 mmol) and 1,3 hexadiene (0.13 mL, 1.19 mmol) in toluene (10 mL) at 0 ºC was added dropwise two equivalents of ^{n}BuLi (1.0 mL, 1.6 M in hexane, 1.59 mmol) which resulted in the solution changing colour from orange/red to brown. The reaction mixture was allowed to warm slowly to room temperature and was stirred for 16 h upon the solution turned green. Removal of the volatiles *in vacuo* afforded a green solid which was extracted into pentane (4 × 10 mL). The pentane was removed under reduced pressure leaving the crude diene complex as a dark green sticky solid. This was extracted into benzene (10 mL) and a solution of $B(C_6F_5)_3$ (0.41g, 0.79 mmol) in benzene (5 mL) was added. After 1 h the solution changed to a darker green colour. The solution was stirred for a further 16 h and the solvent was removed under reduced pressure, dried *in vacuo* and the titled compound was isolated as a dark green solid. Yield: 0.46 g (53%).

^{1}H NMR (C_6D_6, 499.9 MHz, 298 K): 7.36 (1 H, d, $C_{Ar}\underline{H}$, $^3J_{HH}$ = 7.6 Hz), 7.14–7.11 (3 H, m, $C_{Ar}\underline{H}$), 6.97 (1 H, d, $C_{Dipp}\underline{H}$, $^3J_{HH}$ = 7.0 Hz), 6.93 (1 H, d, $C_{Dipp}\underline{H}$, $^3J_{HH}$ = 7.6 Hz), 6.82 (1 H, t, $C_{Dipp}\underline{H}$, $^3J_{HH}$ = 7.6 Hz), 5.51 (1 H, dd, (allylic central C$\underline{H}$), $^3J_{HH}$ = 9.6 Hz, 14.6 Hz, $^1J_{CH}$ = 155.2 Hz), 4.62 (1 H, d, NC$\underline{H}_2$, $^2J_{HH}$ = 17.5 Hz), 4.53 (1 H, d, NC$\underline{H}_2$, $^2J_{HH}$ = 17.5 Hz), 3.69 (1 H, br m, (allylic adjacent to Et), $^1J_{CH}$ = 152.3 Hz), 3.38 (1 H, br m, (allylic adjacent to CH_2-BAr^F_3), $^1J_{CH}$ = 159.6 Hz), 3.22 (1 H, sept, C$\underline{H}Me_2$, $^3J_{HH}$ = 6.6 Hz), 2.98 (1 H, sept, C$\underline{H}Me_2$, $^3J_{HH}$ = 6.7 Hz), 1.56 (1 H, m, C$\underline{H}_2$Me), 1.43 (18 H, br. s, $C_5\underline{Me}_5$, CH$\underline{Me}_2$), 1.31 (1 H, m, C$\underline{H}_2$-BAr^F_3), 1.23 (3 H, d, CH$\underline{Me}_2$, $^3J_{HH}$ = 6.7 Hz), 1.16 (3 H, d, CH$\underline{Me}_2$, $^3J_{HH}$ = 6.6 Hz), 0.98 (1 H, br m, C$\underline{H}_2$Me), 0.97 (3 H, d, CH$\underline{Me}_2$, $^3J_{HH}$ = 6.7 Hz), 0.70 (3 H, t, $CH_2\underline{Me}$, $^3J_{HH}$ = 7.4 Hz), –1.32 (1 H, br m, C$\underline{H}_2$-BAr^F_3, $^1J_{CH}$ = 93.2 Hz) ppm. ^{13}C{^{1}H} NMR (C_6D_6, 125.7 MHz, 298 K): 161.0 (N$\underline{C}$N), 148.3 (br. d, *o*-$\underline{C}_6F_5$, $^1J_{CF}$ = 231.7 Hz), 148.2 (N$\underline{C}_{Dipp}$), 148.1 ($\underline{C}_{Dipp}CHMe_2$), 146.8 ($\underline{C}_{Dipp}CHMe_2$), 140.0 ($NCH_2\underline{C}_{Ar}$), 139.7 (br. d, *p*-$\underline{C}_6F_5$, $^1J_{CF}$ = 243.8 Hz), 137.0 (br. d, *m*-$\underline{C}_6F_5$, $^1J_{CF}$ = 235.7 Hz), 134.4 (diene (allylic central C)), 134.1 (NC$\underline{C}_{Ar}$), 131.0 ($\underline{C}_{Ar}$H), 127.2 ($\underline{C}_{Dipp}$H), 124.6 ($\underline{C}_{Ar}$H), 124.5 ($\underline{C}_{Ar}$H), 123.3 ($\underline{C}_{Dipp}$H), 123.2 ($\underline{C}_{Ar}$H), 123.1 ($\underline{C}_{Dipp}$H), 123.0 ($\underline{C}_5Me_5$), 109.6 (diene (allylic C adjacent to CH_2-BAr^F_3)), 94.3 (diene (allylic C adjacent to Et)), 56.6 (N$\underline{C}H_2$), 28.2 ($\underline{C}HMe_2$), 28.0 ($\underline{C}HMe_2$), 26.3 (CH$\underline{Me}_2$), 26.2 (CH$\underline{Me}_2$), 25.9 (diene $\underline{C}H_2$Me), 22.9 (CH$\underline{Me}_2$), 22.8 (CH$\underline{Me}_2$), 16.4 (diene $CH_2\underline{Me}$), 11.7 ($C_5\underline{Me}_5$) ppm (*i*-$\underline{C}_6F_5$ and $CH_2BAr^F_3$ were not observed). ^{19}F NMR (C_6D_6, 376.5 MHz, 298 K): –128.8 (m),

–131.5 (m), –132.8 (m), –133.1 (m), –133.2 (m), –134.3 (m), –157.0 (m), –158.9 (m), –160.0 (m), –160.8 (m), –163.2 (m), –164.1 (m), –165.2 (m), –165.9 (m) ppm. ^{11}B NMR (C_6D_6, 128.4 MHz, 298 K): –12.5 ppm. IR (NaCl plates, Nujol mull, cm^{-1}): 2922 (s), 1644 (m), 1580 (m), 1514 (m), 1455 (m), 1377 (m), 1334 (w), 1278 (w), 1215 (w), 1297 (w), 1170 (w), 1085 (m), 1023 (w), 973 (m), 878 (w), 866 (w), 843 (w), 760 (w), 781 (w), 728 (m), 676 (m), 665 (w), 605 (w). A satisfactory elemental analysis could not be obtained. Diffraction-quality crystals were grown from a benzene solution at room temperature.

6.7 Experimental details and characterising data for Chapter Three

[Cp*Ti{HNCN(Dipp)$CH_2C_6H_4$}{(η-CH_2(CH)$_3$^{i}Pr}][BAr^F_4] (15-[BAr^F_4]). To a stirring fluorobenzene (4 mL) solution of Cp*Ti{NCN(Dipp)$CH_2C_6H_4$}Me_2 (**3**, 0.100 g, 0.223 mmol) and 2,4-hexadiene (25.6 µL, 0.223 mmol) was added dropwise a fluorobenzene (4 mL) solution of [Ph_3C][BAr^F_4] (0.206 g, 0.223 mmol). After 2 h, pentane (10 mL) was added resulting in the formation of a dark green oil. The pentane/fluorobenzene was decanted away and the oil washed with pentane (3 × 5 mL). The remaining solid was dried *in vacuo* to yield [Cp*Ti{HNCN(Dipp)$CH_2C_6H_4$}{(CH_2(CH)$_3$^{i}Pr}][BAr^F_4] (**15-[BAr^F_4]**) as a green solid. Yield: 0.112 g (40%).

^{1}H NMR (C_6D_5Br, 400.2 MHz, 298 K): 7.60 (1 H, t, $C_{Dipp}\underline{H}$, $^3J_{HH}$ = 7.7 Hz), 7.45–7.30 (5 H, m, $C_{Ar}\underline{H}$, $C_{Dipp}\underline{H}$), 6.51 (1 H, d, $C_{Dipp}\underline{H}$, $^3J_{HH}$ = 7.7 Hz), 4.85 (1 H, d, N$C\underline{H}_2$, $^2J_{HH}$ = 18.7 Hz), 4.70 (1 H, d, N$C\underline{H}_2$, $^2J_{HH}$ = 18.7 Hz), 4.57 (1 H, dd, TiC$\underline{H}$CH, $^3J_{HH}$ = 12.0 Hz, 8.2 Hz), 4.10–4.06 (1 H, m, TiC$\underline{H}_2$CH), 3.90 (1 H, s, N$\underline{H}$), 3.70–3.64 (2 H, m, TiCHC$\underline{H}$, TiCH_2C$\underline{H}$), 3.52–3.50 (1 H, m, TiC$\underline{H}_2$CH), 2.62 (1 H, sept, C$\underline{H}Me_2$, $^3J_{HH}$ = 6.7 Hz), 2.37 (1 H, sept, C$\underline{H}Me_2$,$^3J_{HH}$ = 6.7 Hz), 1.77–1.74 (1 H, m, TiCHC$\underline{H}Me_2$), 1.73 (15 H, s, $C_5\underline{Me}_5$), 1.35 (3 H, d, CH$\underline{Me}_2$, $^3J_{HH}$ = 6.7 Hz), 1.29 (3 H, d, CH$\underline{Me}_2$, $^3J_{HH}$ = 6.7 Hz), 1.18 (3 H, d, CH$\underline{Me}_2$, $^3J_{HH}$ = 6.7 Hz), 1.16–1.14 (6 H, m, TiCHCH$\underline{Me}_2$, CH$\underline{Me}_2$), 0.20 (3 H, d, TiCHCH$\underline{Me}_2$, $^3J_{HH}$ = 6.5 Hz) ppm. ^{13}C{^{1}H} NMR (C_6D_5Br, 100.6 MHz, 298 K): 166.9 (C$\underline{N}$), 148.9 (N$\underline{C}_{Dipp}$), 148.4 (br. d, *o*-$\underline{C}_6F_5$, $^1J_{CF}$ = 247.4 Hz), 147.2 ($\underline{C}_{Dipp}CHMe_2$), 147.1 ($\underline{C}_{Dipp}CHMe_2$), 141.4 (NC$\underline{C}_{Ar}$), 138.4 (br. d, *p*-$\underline{C}_6F_5$, $^1J_{CF}$ = 230.6 Hz), 136.5 (br. d, *m*-$\underline{C}_6F_5$, $^1J_{CF}$ = 232.6 Hz), 133.8 ($\underline{C}_{Dipp}$H), 131.7 ($\underline{C}_{Ar}$H), 128.2 ($\underline{C}_{Ar}$H), 128.0 ($\underline{C}_{Ar}$H), 127.7 ($H_2C\underline{C}_{Ar}$), 127.1 ($\underline{C}_{Dipp}$H), 125.8 ($\underline{C}_5Me_5$), 123.7 ($C_{Ar}\underline{H}$), 123.5 ($\underline{C}_{Dipp}$H), 117.4 (TiCH$\underline{C}$H), 117.3 (TiC$H_2\underline{C}$H),

110.7 (TiCHCH), 84.0 (TiCH$_2$CH), 57.4 (NCH$_2$), 31.1 (TiCHCHMe$_2$), 28.4 (CHMe$_2$), 28.3 (CHMe$_2$), 27.2 (TiCHCHMe$_2$), 25.7 (CHMe$_2$), 25.0 (CHMe$_2$), 22.9 (CHMe$_2$), 22.3 (TiCHCHMe$_2$), 12.4 (C$_5$Me$_5$) ppm (*i*-C$_6$F$_5$ were not observed). ^{19}F NMR (C$_6$D$_5$Br, 376.5 MHz, 298 K): –131.6 (m, *o*-C$_6$F$_5$), –161.7 (m, *p*-C$_6$F$_5$), –165.7 (m, *m*-C$_6$F$_5$) ppm. ^{11}B NMR (C$_6$D$_5$Br, 128.4 MHz, 298 K): –16.0 ppm. IR (NaCl plates, Nujol mull, cm^{-1}): 3264 (m, (NH)), 2923 (s), 1643 (m), 1602 (m), 1575 (m), 1513 (m), 1463 (m), 1410 (w), 1378 (m), 1330 (m), 1272 (w), 1085 (w), 1056 (m), 1022 (w), 978 (m), 827 (w), 804 (w), 774 (m), 726 (w), 683 (w), 661 (w), 602 (w), 573 (w), 544 (w). A satisfactory elemental analysis could not be obtained.

Cp*Ti{HNCN(Dipp)CH$_2$C$_6$H$_4$}{η-(CH$_2$(CH)$_3$CH(CH$_3$)(CD$_3$)}][BAr$^F_4$] (15-[BAr$^F_4$]-*d*$_3$) was prepared analogously to **15-[BAr$^F_4$]**, using Cp*Ti{NCN(Dipp)CH$_2$C$_6$H$_4$}(CD$_3$)$_2$ (**3-*d*$_6$**, 0.020 g, 0.04 mmol), [Ph$_3$C][BAr$^F_4$] (0.036 g, 0.04 mmol) and 2,4-hexadiene (4.6 μL, 0.04 mmol). The ^{1}H NMR spectrum was identical to that of **15-[BAr$^F_4$]**, other than the absence of a resonance corresponding to one Me group of the ^{i}Pr moiety at 1.15 ppm.

Low temperature NMR tube scale reaction of 3 with [Ph$_3$C][BAr$^F_4$] and 2,4-hexadiene. To a solution of [Cp*Ti{NCN(Dipp)CH$_2$C$_6$H$_4$}Me$_2$ (**3**, 0.020 g, 0.04 mmol) and [Ph$_3$C][BAr$^F_4$] (0.036 g, 0.04 mmol) in C$_6$D$_5$Br (0.3 mL) at –30 ºC was added a solution of 2,4-hexadiene (4.6 μL, 0.04 mmol) in C$_6$D$_5$Br (0.2 mL) at –30 ºC resulting in the formation of a dark green solution. The NMR spectra were recorded within 3 minutes at –30 ºC indicating formation of ***endo***- and ***exo*-18-[BAr$^F_4$]**.

***endo*-18-[BAr$^F_4$]**: ^{1}H NMR (C$_6$D$_5$Br, 400.2 MHz, 243 K): 8.06 (1 H, t, CH$_{meso}$, $^3J_{HH}$ = 12.7 Hz), 4.39–4.34 (1 H, m, MeCH), 4.03 (1 H, dd, CHCHMe$_2$, $^3J_{HH}$ = 13.8 Hz, 8.1 Hz), 2.12–2.04 (1 H, m, CHCHMe$_2$), 2.01 (15 H, s, C$_5$Me$_5$), 0.74 (3 H, br, CHCHMe$_2$), 0.48 (3 H, d, MeCH, $^3J_{HH}$ = 5.9 Hz), -0.09 (3 H, d, CHCHMe$_2$, $^3J_{HH}$ = 6.5 Hz) ppm.

***exo*-18-[BAr$^F_4$]**: ^{1}H NMR (C$_6$D$_5$Br, 400.2 MHz, 243 K): 6.91 (1 H, t, CH$_{meso}$, $^3J_{HH}$ = 13.8 Hz), 6.15–6.10 (1 H, m, CHCHMe$_2$), 5.60-5.53 (1 H, br , MeCH), 2.12–2.04 (1 H, m, CHCHMe$_2$), 1.97 (15H, s, C$_5$Me$_5$), 0.74 (3 H, br, CHCHMe$_2$), 1.04 (3 H, d, MeCH, $^3J_{HH}$ = 5.9 Hz), -0.18 (3 H, d, CHCHMe$_2$, $^3J_{HH}$ = 6.4 Hz) ppm.

[Cp*Ti{HNCN(Dipp)$CH_2C_6H_4$}{η-$CH_2(CH)_3$Et}][BAr^F_4] (16-[BAr^F_4]). To a stirring fluorobenzene (3 mL) solution of Cp*Ti{NCN(Dipp)$CH_2C_6H_4$}Me_2 (**3**, 0.050 g, 0.099 mmol) and 1,3-pentadiene (9.9 μL, 0.099 mmol) was added dropwise a fluorobenzene (2 mL) solution of [Ph_3C][BAr^F_4] (0.091 g, 0.099 mmol). After 3 h, pentane (10 mL) was added resulting in the formation of a dark green oil. The pentane/fluorobenzene was decanted away and the oil washed with pentane (3 × 5 mL). The remaining solid was dried *in vacuo* to yield compound **16-[BAr^F_4]** as a green solid. Yield: 0.070 g (57%).

^{1}H NMR (C_6D_5Br, 400.2 MHz, 298 K): 7.63–7.60 (1 H, m, $C_{Ar}\underline{H}$), 7.46–7.42 (1 H, m, $C_{Dipp}\underline{H}$), 7.34–7.26 (4 H, m, $C_{Ar}\underline{H}$, $C_{Dipp}\underline{H}$), 6.42 (1 H, d, $C_{Ar}\underline{H}$, $^3J_{HH}$ = 7.3 Hz), 4.84–4.78 (2 H, m, NC$\underline{H}_2$), 4.66–4.60 (1 H, m, TiC$\underline{H}$CH), 4.00–3.97 (1 H, m, TiC$\underline{H}_2$CH), 3.89 (1 H, s, N$\underline{H}$), 3.80–3.74 (1 H, m, TiCHC$\underline{H}$), 3.59–3.52 (1 H, m, TiCH_2C$\underline{H}$), 3.44–3.40 (1 H, m, TiC$\underline{H}_2$CH), 2.59–2.45 (2 H, m, C$\underline{H}Me_2$), 2.18–2.08 (1 H, m, C$\underline{H}_2$Me), 1.86–1.78 (1 H, m, TiCHC$\underline{H}_2$Me), 1.71 (15 H, s, $C_5\underline{Me}_5$), 1.37–1.32 (6 H, m, CH$\underline{Me}_2$), 1.19–1.17 (6 H, m, CH$\underline{Me}_2$), 0.59 (3 H, t, TiCHC$H_2\underline{Me}$, $^3J_{HH}$ = 7.5 Hz) ppm. ^{13}C{^{1}H} NMR (C_6D_5Br, 100.6 MHz, 298 K): 166.8 (C$\underline{C}$N), 148.3 (N$\underline{C}_{Dipp}$), 148.8 (br. d, *o*-$\underline{C}_6F_5$, $^1J_{CF}$ = 244.6 Hz), 147.5 ($\underline{C}_{Dipp}CHMe_2$), 147.1 ($\underline{C}_{Dipp}CHMe_2$), 140.9 (NC$\underline{C}_{Ar}$), 138.3 (br. d, *p*-$\underline{C}_6F_5$, $^1J_{CF}$ = 235.3 Hz), 136.4 (br. d, *m*-$\underline{C}_6F_5$, $^1J_{CF}$ = 230.6 Hz), 134.1 ($\underline{C}_{Ar}$H), 132.2 ($\underline{C}_{Ar}$H), 128.6 ($\underline{C}_{Ar}$H), 128.4 ($\underline{C}_{Dipp}$H), 128.0 ($\underline{C}_{Dipp}$H), 127.5 ($H_2C\underline{C}_{Ar}$), 125.8 ($\underline{C}_5Me_5$), 124.4 ($\underline{C}_{Ar}$H), 123.9 ($\underline{C}_{Dipp}$H), 119.5 (TlCH$\underline{C}$H), 117.3 (TiC$H_2\underline{C}$H), 104.3 (Ti$\underline{C}$HCH), 83.9 (Ti$\underline{C}H_2$CH), 57.8 (N$\underline{C}H_2$), 28.7 ($\underline{C}HMe_2$), 28.6 ($\underline{C}HMe_2$), 25.7 (CH$\underline{Me}_2$), 25.6 (TiCH$\underline{C}H_2$Me), 25.5 (CH$\underline{Me}_2$), 23.5 (CH$\underline{Me}_2$), 23.4 (CH$\underline{Me}_2$), 16.5 (TiCHC$H_2\underline{Me}$), 12.4 ($C_5\underline{Me}_5$) ppm (*i*-$\underline{C}_6F_5$ were not observed). ^{19}F NMR (C_6D_5Br, 376.5 MHz, 298 K): –131.4 (m, *o*-$C_6\underline{F}_5$), –161.8 (m, *p*-$C_6\underline{F}_5$), –165.7 (m, *m*-$C_6\underline{F}_5$) ppm. ^{11}B NMR (C_6D_5Br, 128.4 MHz, 298 K): –16.0 ppm. Anal. found (calcd. for $C_{60}H_{49}B_1F_{20}N_2Ti$): C 58.12, (58.27); N, 2.20 (2.27); H, 3.85 (3.99)%. IR (NaCl plates, Nujol mull, cm^{-1}): 3235 (m, NH), 2921 (s), 1643 (m), 1600 (m), 1573 (m), 1513 (m), 1455 (w), 1377 (m), 1330 (w), 1274 (m), 1084 (m), 1022 (w), 977 (m), 805 (w), 774 (w), 743 (w), 726 (w), 683 (w), 660 (w), 609 (w), 601 (w), 545 (w).

NMR Scale synthesis of [Cp*Ti{HNCN(Dipp)$CH_2C_6H_4$}Cl_2][BAr^F_4] (17-[BAr^F_4]). To a solution of [$HNMe_2Ph$][BAr^F_4] (0.037 g, 0.046 mmol) in C_6D_5Br (0.3 mL) was added dropwise a C_6D_5Br solution (0.2 mL) of Cp*Ti{NCN(Dipp)$CH_2C_6H_4$}Cl_2 (**2**,

0.025 g, 0.046 mmol). The NMR spectra were recorded after 12 h indicating formation of **17-[BAr$^{F}_{4}$]** and one equivalent of NMe_2Ph.

^{1}H NMR (C_6D_5Br, 499.9 MHz, 298 K): 8.21 (1 H, d, $C_{Ar}\underline{H}$, $^{3}J_{HH}$ = 8.1 Hz), 7.84 (1 H, s, N$\underline{H}$), 7.65 (1 H, t, *p*-$C_{Ar}\underline{H}$, $^{3}J_{HH}$ = 7.0 Hz), 7.60 (1 H, t, *p*-$C_{Ar}\underline{H}$, $^{3}J_{HH}$ = 7.0 Hz), 7.53–7.50 (1 H, m, $C_{Ar}\underline{H}$), 7.44–7.37 (5 H, m, *m*-$\underline{Ph}NMe_2$, $C_{Ar}\underline{H}$, $C_{Dipp}\underline{H}$), 7.31 (1 H, d, $C_{Dipp}\underline{H}$, $^{3}J_{HH}$ = 8.0 Hz), 6.93 (1 H, t, *p*-$\underline{Ph}NMe_2$, $^{3}J_{HH}$ = 8.0 Hz), 6.81 (2 H, *o*-$\underline{Ph}NMe_2$), 4.48 (2 H, s, $NC\underline{H}_2$), 2.86 (6 H, s, $PhN\underline{Me}_2$), 2.40–2.33 (2 H, m, $C\underline{H}Me_2$), 2.06 (15 H, s, $C_5\underline{Me}_5$), 1.21–1.17 (12 H, overlapping doublets, $CH\underline{Me}_2$) ppm. $^{13}C\{^{1}H\}$ NMR (C_6D_5Br, 125.7 MHz, 298 K): 170.9 ($\underline{C}N$), 150.1 ($\underline{Ph}NMe_2$), 148.8 (br. d, *o*-$\underline{C}_6F_5$, $^{1}J_{CF}$ = 245.2 Hz), 147.8 ($NC\underline{C}_{Dipp}$), 142.3 ($NC\underline{C}_{Ar}$), 140.0 ($\underline{C}_5Me_5$), 138.7 (br. d, *p*-$\underline{C}_6F_5$, $^{1}J_{CF}$ = 231.7 Hz), 136.7 (br. d, *m*-$\underline{C}_6F_5$, $^{1}J_{CF}$ = 235.8 Hz), 135.5 ($H_2C\underline{C}_{Ar}$), 133.2 ($\underline{C}_{Dipp}CHMe_2$), 129.1 ($\underline{C}_{Ar}H$), 128.8 ($\underline{C}_{Ar}H$), 127.8 ($\underline{C}_{Dipp}H$) 127.5 ($\underline{C}_{Ar}H$), 126.8 (*m*-$\underline{Ph}NMe_2$), 126.4 ($\underline{C}_{Dipp}H$), 126.3 ($\underline{C}_{Dipp}H$), 123.4 ($\underline{C}_{Ar}H$), 117.4 (*p*-$\underline{Ph}NMe_2$), 113.2 (*o*-$\underline{Ph}NMe_2$), 58.2 ($NC\underline{H}_2$), 40.7 ($PhN\underline{Me}_2$), 28.9 ($C\underline{H}Me_2$), 24.9 ($CH\underline{Me}_2$), 23.8 ($CH\underline{Me}_2$), 13.8 ($C_5\underline{Me}_5$) (*i*-$\underline{C}_6F_5$ were not observed) ppm. ^{19}F NMR (C_6D_5Br, 470.4 MHz, 298 K): –131.2 (m, *o*-$C_6\underline{F}_5$), –161.4 (m, *p*-$C_6\underline{F}_5$), –165.9 (m, *m*-$C_6\underline{F}_5$) ppm. ^{11}B NMR (C_6D_5Br, 160.4 MHz, 298 K): –15.8 ppm.

Cp*Ti{DNCN(Dipp)CH$_2$C$_6$H$_4$}Cl$_2$][BAr$^{F}_{4}$] (17-[BAr$^{F}_{4}$]-*d*$_1$) was prepared analogously to **17-[BAr$^{F}_{4}$]**, using Cp*Ti{NCN(Dipp)$CH_2C_6H_4$}Cl_2 (**2**, 0.010 g, 0.02 mmol) and [$DNMe_2Ph$][BAr$^{F}_{4}$] (0.016 g, 0.02 mmol). The ^{1}H NMR spectrum was identical to that of **17-[BAr$^{F}_{4}$]**, other than the decline (only 22% present) of the resonance representing the NH moiety at 7.81 ppm.

NMR tube reaction of [Cp*Ti{HNCN(Dipp)CH$_2$C$_6$H$_4$}Cl$_2$][BAr$^{F}_{4}$] (17-[BAr$^{F}_{4}$]) with *N,N,N´,N´*-tetramethyl-1,8-naphthalenediamine (**3.04**)**.** To a solution of **17-[BAr$^{F}_{4}$]** in C_6D_5Br (0.3 mL), prepared *in situ* by combination of **2** (0.015 g, 0.028 mmol) and [$HNMe_2Ph$[BAr$^{F}_{4}$] (0.022 g, 0.028 mmol), was added a solution of **3.04** (0.006 g, 0.028 mmol) in C_6D_5Br (0.2 mL). The NMR spectra were recorded within 5 minutes. The ^{1}H NMR spectrum was identical to that of **2** with the extra resonances of protonated *N,N,N´,N´*-tetramethyl-1,8-naphthalenediamine.

Reaction of Cp*Ti{NC(Ar^{F2})N^{i}Pr$_2$}Me$_2$ (1.52) with [Ph$_3$C][BAr$^{F}_{4}$] and 2,4-hexadiene. To a stirring fluorobenzene (3 mL) solution of

Cp*Ti{NC(Ar^{F_2})N^{i}Pr$_2$}Me$_2$ (**1.52**, 0.050 g, 0.10 mmol) and 2,4-hexadiene (11.5 μL, 0.10 mmol) was added dropwise a fluorobenzene (2 mL) solution of [Ph_3C][BAr^F_4] (0.092 g, 0.10 mmol). After 1 hour, pentane (10 mL) was added resulting in the formation of a dark green oil. The pentane/fluorobenzene was decanted away and the oil was washed with pentane (3 × 5 mL). The remaining solid was dried *in vacuo* to yield [Cp*Ti{NC(Ar^{F_2})N^{i}Pr$_2$}{η-$CH_2(CH)_2CH^iPr$}][BAr^F_4] and the *endo*- and *exo*-allyl of [Cp*Ti{NC(Ar^{F_2})N^{i}Pr$_2$}{η^3-$CH(Me)(CH)_2CH^iPr$}][BAr^F_4] in a 0.80 : 0.14 : 0.06 ratio as a green solid. Yield: 0.071 g (59%).

Major species, [Cp*Ti{HNC(Ar^{F_2})N^{i}Pr$_2$}{η-$CH_2(CH)_2CH^iPr$}][BAr^F_4] (19-[BAr^F_4])

^{1}H NMR (C_6D_5Br, 499.9 Hz, 298 K): 7.36–7.26 (2 H, m, $C_{Ar}\underline{H}$), 6.88–6.86 (1 H, m, $C_{Ar}H$), 4.80 (1 H, s, N$\underline{H}$, $^1J_{NH}$ = 60.4 Hz), 4.50 (1 H, dd, TiC$\underline{H}$CH, $^3J_{HH}$ = 7.8 Hz, 14.2 Hz), 3.70–3.61 (2 H, m, NC$\underline{H}$Me$_2$, TiCHC$\underline{H}$), 3.50 (1 H, sept, NC$\underline{H}$Me$_2$, $^3J_{HH}$ = 6.8 Hz), 3.28 (1 H, dt, TiCH$_2$C$\underline{H}$, $^3J_{HH}$ = 9.4 Hz, 12.8 Hz), 2.44 (1 H, m, TiC$\underline{H}_2$CH), 2.17–2.11 (1 H, m, TiC$\underline{H}_2$CH), 1.89–1.82 (1 H, m, C$\underline{H}$Me$_2$), 1.73 (15 H, s, $C_5\underline{Me}_5$), 1.42 (3 H, d, NCH$\underline{Me}_2$, $^3J_{HH}$ = 6.8 Hz), 1.28 (6 H, appt. d, NCH$\underline{Me}_2$, TiCHCH$\underline{Me}_2$, $^3J_{HH}$ = 7.2 Hz), 0.98 (3 H, d, NCH$\underline{Me}_2$, $^3J_{HH}$ = 6.8 Hz), 0.93 (3 H, d, NCH$\underline{Me}_2$, $^3J_{HH}$ = 6.8 Hz), 0.83 (3 H, d, TiCHCH$\underline{Me}_2$, $^3J_{HH}$ = 6.8 Hz) ppm. ^{13}C{^{1}H} NMR (C_6D_5Br, 125.7 MHz, 298 K): 160.8 (N$\underline{C}$), 156.7 (*o*-$\underline{C}_6H_3F_2$), 148.5 (br. d, *o*-$\underline{C}_6F_5$, $^1J_{CF}$ = 245.7 Hz), 138.6 (br. d, *p*-$\underline{C}_6F_5$, $^1J_{CF}$ = 231.7 Hz), 136.1 (br. d, *m*-$\underline{C}_6F_5$, $^1J_{CF}$ = 230.6 Hz), 128.2 (*p*-$\underline{C}_6H_3F_2$), 124.8 ($\underline{C}_5Me_5$), 117.5 (TiCH$\underline{C}$H), 114.0 (TiCH$_2\underline{C}$H), 112.2 (d, *m*-$\underline{C}_6H_3F_2$, $^2J_{CF}$ = 10.3 Hz), 110.7 (Ti$\underline{C}$HCH), 83.2 (Ti$\underline{C}$H$_2$CH), 56.0 (N$\underline{C}$HMe$_2$), 46.4 (N$\underline{C}$HMe$_2$), 32.7 (TiCH$\underline{C}$HMe$_2$), 27.4 (NCH$\underline{Me}_2$), 24.8 (TiCHCH$\underline{Me}_2$), 20.3 (NCH$\underline{Me}_2$), 19.5 (TiCHCH$\underline{Me}_2$), 19.4 (2 × NCH$\underline{Me}_2$), 12.0 ($C_5\underline{Me}_5$) (*i*-$\underline{C}_6F_5$ and *i*-$C_6H_3F_2$ were not observed). ppm. ^{19}F NMR (C_6D_5Br, 470.4 MHz, 298 K): –112.0 (d, *o*-$C_6H_3\underline{F}_2$, $^1J_{CF}$ = 109.1 Hz), –131.7 (m, *o*-$C_6\underline{F}_5$), –162.1 (m, *p*-$C_6\underline{F}_5$), –166.0 (m, *m*-$C_6\underline{F}_5$) ppm. ^{11}B NMR (C_6D_5Br, 160.4 MHz, 298 K): -16.3 ppm. IR (NaCl plates, Nujol mull, cm^{-1}): 3410 (m, (NH)), 3351 (w), 2923 (s), 2619 (w), 2359 (w), 2282 (w), 1644 (m), 1455 (s), 1377 (m), 1261 (w), 1086 (m), 1019 (w), 908 (w), 797 (m), 726 (w), 683 (w), 659 (w), 640 (w), 602 (w). A satisfactory elemental analysis could not be obtained.

Minor species: *endo*- and *exo*-allyl [Cp*Ti{NC(Ar^{F_2})N^{i}Pr$_2$}{η^3-CH(Me)(CH)$_2$CH^{i}Pr}][BAr$^F{}_4$] (*endo*- and ***exo*-20-[BAr$^F{}_4$])**

***Endo*-20-[BAr$^F{}_4$]**: ^{1}H NMR (C_6D_5Br, 499.9 Hz, 298 K): 8.11 (1 H, t, C<u>H</u>$_{meso}$, $^3J_{HH}$ = 14.1 Hz), 4.50 (1 H, overlapping m, MeC<u>H</u>), 4.08 (1 H, dd, C<u>H</u>CHMe$_2$, $^3J_{HH}$ = 13.8 Hz, 8.1 Hz), 2.19–2.16 (1 H, m, CHC<u>H</u>Me$_2$), 1.94 (15 H, s, C$_5$<u>Me</u>$_5$), 1.35 (3 H, d, <u>Me</u>CH, $^3J_{HH}$ = 8.2 Hz), 0.82–0.80 (3 H, overlapping m, CHCH<u>Me</u>$_2$), -0.12 (3 H, d, CHCH<u>Me</u>$_2$, $^3J_{HH}$ = 7.0 Hz) ppm. ^{13}C{^{1}H} NMR (C_6D_5Br, 125.7 MHz, 298 K): 159.2 (<u>C</u>H$_{meso}$), 148.5 (br. d, *o*-<u>C</u>$_6$F$_5$, $^1J_{CF}$ = 245.7 Hz), 138.6 (br. d, *p*-<u>C</u>$_6$F$_5$, $^1J_{CF}$ = 231.7 Hz), 136.1 (br. d, *m*-<u>C</u>$_6$F$_5$, $^1J_{CF}$= 230.6 Hz), 123.6 (<u>C</u>HCHMe$_2$), 109.4 (Me<u>C</u>H), 34.5 (CH<u>C</u>HMe$_2$), 24.9 (CHCH<u>Me</u>$_2$), 18.5 (<u>Me</u>CH), 17.6 (CHCH<u>Me</u>$_2$), 12.5 (C$_5$<u>Me</u>$_5$) ppm (*i*-<u>C</u>$_6$F$_5$ were not observed).

***Exo*-20-[BAr$^F{}_4$]**: ^{1}H NMR (C_6D_5Br, 399.9 Hz, 298 K): 7.11–7.09 (1 H, m, C<u>H</u>$_{meso}$) 6.02 (1 H, dd, C<u>H</u>CHMe$_2$, $^3J_{HH}$ = 14.0 Hz, 7.0 Hz), 5.94 (1 H, app. dd, MeC<u>H</u>, $^3J_{HH}$ = 14.0 Hz, 6.1 Hz), 2.19–2.14 (1 H, m CHC<u>H</u>Me$_2$), 1.15–1.13 (3 H, m, <u>Me</u>CH), 0.82-0.80 (3 H, overlapping m, CHCH<u>Me</u>$_2$), -0.04 (3 H, d, CHCH<u>Me</u>$_2$, $^3J_{HH}$ = 6.7 Hz) ppm. No ^{13}C{^{1}H} NMR spectroscopic data could be obtained due to the low concentration. Low concentration of both allyl complexes did not allow full characterisation of the amidinate supporting ligand.

Common data: ^{19}F NMR (C_6D_5Br, 470.4 MHz, 298 K): –112.0 (d, *o*-C$_6$H$_3$<u>F</u>$_2$, $^1J_{CF}$ = 109.1 Hz), –131.7 (m, *o*-C$_6$<u>F</u>$_5$), –162.1 (m, *p*-C$_6$<u>F</u>$_5$), –166.0 (m, *m*-C$_6$<u>F</u>$_5$) ppm. ^{11}B NMR (C_6D_5Br, 160.4 MHz, 298 K): –16.3 ppm. IR (NaCl plates, Nujol mull, cm^{-1}): 3410 (m, (NH)), 3351 (w), 2923 (s), 2619 (w), 2359 (w), 2282 (w), 1644 (m), 1455 (s), 1377 (m), 1261 (w), 1086 (m), 1019 (w), 908 (w), 797 (m), 726 (w), 683 (w), 659 (w), 640 (w), 602 (w). A satisfactory elemental analysis could not be obtained.

[Cp*Ti{HNC(Ph)N^{i}Pr$_2$}{η-CH$_2$(CH)$_2$CH^{i}Pr}][BAr$^F{}_4$] (21-[BAr$^F{}_4$]). To a stirring fluorobenzene (3 mL) solution of Cp*Ti{NC(Ph)N^{i}Pr$_2$}Me$_2$ (**3.05**, 0.100 g, 0.24 mmol) and 2,4-hexadiene (27 µL, 0.24 mmol) was added dropwise a fluorobenzene (2 mL) solution of [Ph$_3$C][BAr$^F{}_4$] (0.220 g, 0.24 mmol). After 3 h, pentane (10 mL) was added resulting in the formation of a dark green oil. The pentane/fluorobenzene was decanted away and the oil washed with pentane (3 ×

5 mL). The remaining solid was dried *in vacuo* to yield [Cp*Ti{HNC(Ph)N^{i}Pr$_2$}{η-CH$_2$(CH)$_2$CH^{i}Pr}][BAr$^{F}{}_4$] as a green solid. Yield: 0.06 g (40%).

^{1}H NMR (C$_6$D$_5$Br, 499.9 Hz, 298 K): 7.36–7.26 (4 H, C$_{Ar}$H), 6.85 (1 H, d, C$_{Ar}$H, ^1J = 6.9 Hz), 4.52 (1 H, s, NH, $^1J_{NH}$ = 60.3 Hz), 4.34 (1 H, dd, TiCHCH, $^3J_{HH}$ = 7.8 Hz, 13.5 Hz), 3.64–3.56 (2 H, overlapping m, NCHMe$_2$, TiCHCH), 3.39 (1 H, sept, NCHMe$_2$, $^3J_{HH}$ = 7.1 Hz), 3.26 (1 H, dt, TiCH$_2$CH, $^3J_{HH}$ = 9.8 Hz, 13.4 Hz), 2.44–2.34 (2 H, m, TiCH$_2$CH), 1.87–1.83 (1 H, m, TiCHCHMe$_2$), 1.71 (15 H, s, C$_5$Me$_5$), 1.37 (3 H, d, NCHMe$_2$, $^3J_{HH}$ = 7.1 Hz), 1.30 (3 H, d, NCHMe$_2$, $^3J_{HH}$ = 7.1 Hz), 1.26 (3 H, d, TiCHCHMe$_2$, $^3J_{HH}$ = 6.9 Hz), 0.89-0.83 (9 H, m, overlapping doublets, NCHMe$_2$, TiCHCHMe$_2$) ppm. ^{13}C{^{1}H} NMR (C$_6$D$_5$Br, 125.7 MHz, 298 K): 170.3 (NC), 148.8 (br. d, *o*-C$_6$F$_5$, $^1J_{CF}$ = 244.5 Hz), 138.8 (br. d, *p*-C$_6$F$_5$, $^1J_{CF}$ = 235.2 Hz), 136.7 (br. d, *m*-C$_6$F$_5$, $^1J_{CF}$ = 232.7 Hz), 135.0 (NCC$_{Ar}$), 128.5 (C$_{Ar}$H), 128.0 (C$_{Ar}$H), 126.8 (C$_{Ar}$H), 124.7 (C$_5$Me$_5$), 116.6 (TiCHCH), 114.2 (TiCH$_2$CH), 109.8 (TiCHCH), 85.7 (TiCH$_2$CH), 54.9 (NCHMe$_2$), 45.7 (NCHMe$_2$), 32.3 (TiCHCHMe$_2$), 27.5 (NCHMe$_2$), 25.4 (TiCHCHMe$_2$), 20.7 (NCHMe$_2$), 19.7 (NCHMe$_2$), 19.2 (TiCHCHMe$_2$), 18.7 (NCHMe$_2$), 12.5 (C$_5$Me$_5$) (*i*-C$_6$F$_5$ were not observed) ppm. ^{19}F NMR (C$_6$D$_5$Br, 470.4 MHz, 298 K): –131.4 (m, o-C$_6$F$_5$), –161.8 (m, p-C$_6$F$_5$), –165.6 (m, m-C$_6$F$_5$) ppm. ^{11}B NMR (C$_6$D$_5$Br, 160.4 MHz, 298 K): -16.0 ppm. IR (NaCl plates, Nujol mull, cm^{-1}): 3413 (m, (NH)), 1643 (m), 1581 (w), 1455 (w), 1341 (w), 1315 (w), 1260 (s), 1180 (w), 1090 (s), 1017 (s), 923 (w), 893 (w), 798 (s), 727 (w), 702 (w), 683 (w), 661 (m), 610 (w), 602 (m), 573 (w). A satisfactory elemental analysis could not be obtained.

NMR tube scale Cp*Ti{NC(NMe$_2$)$_2$}Me$_2$ in presence of 2,4-hexadiene and [Ph$_3$C][BAr$^{F}{}_4$]. To a solution of Cp*Ti{NC(NMe$_2$)$_2$}Me$_2$ (**1.58**, 0.010 g, 0.03 mmol) and 2,4-hexadiene (3.5 μL, 0.03 mmol) in CD$_2$Cl$_2$ (0.3 mL) a solution of [Ph$_3$C][BAr$^{F}{}_4$] (0.028 g, 0.003 mmol) in CD$_2$Cl$_2$ (0.2 mL) was added. The solution was transferred into a NMR tube and NMR spectra run within 5 minutes. The reaction was monitored over time and showed in 30 minutes the presence of **23-[BAr$^{F}{}_4$]** and ***endo*-24 -[BAr$^{F}{}_4$]** in a 0.81: 0.19 ratio, respectively.

[Cp*Ti{NC(NMe$_2$)$_2$}{η-CH$_2$(CH)$_2$CH^{i}Pr}][BAr$^F_4$] (23-[BAr$^F_4$]).

^{1}H NMR (CD_2Cl_2, 499.9 MHz, 298 K): 4.07–3.95 (2 H, m, TiCHC<u>H</u>, TiC<u>H</u>CH), 3.76–3.68 (1 H, m, TiCH$_2$C<u>H</u>), 3.55 (1 H, dd, TiC<u>H$_2$</u>CH, $^2J_{HH}$ = 5.9 Hz, $^3J_{HH}$ = 14.5 Hz), 3.37 (1 H, s, N<u>H</u>), 3.31–3.27 (1 H, m, TiC<u>H$_2$</u>CH), 2.81 (12 H, s, N<u>Me$_2$</u>), 2.14–2.11 (1 H, m, TiCHC<u>H</u>Me$_2$), 1.90 (15 H, s, C$_5$<u>Me$_5$</u>), 1.21–1.19 (3 H, m, TiCHCH<u>Me$_2$</u>), 1.06–1.03 (3 H, m, TiCHCH<u>Me$_2$</u>) ppm. ^{13}C{^{1}H} NMR (CD_2Cl_2, 125.7 Hz, 298 K): 167.4 (N<u>C</u>), 148.2 (br. d, *o*-<u>C$_6$</u>F$_5$, $^1J_{CF}$ = 251.1 Hz), 138.6 (br. d, *p*-<u>C$_6$</u>F$_5$, $^1J_{CF}$ = 237.9 Hz), 136.1 (br. d, *m*-<u>C$_6$</u>F$_5$, $^1J_{CF}$ = 236.1 Hz), 125.1 (<u>C$_5$Me$_5$</u>), 118.9 (TiCH<u>C</u>H), 114.0 (TiCH$_2$<u>C</u>H), 107.8 (Ti<u>C</u>HCH), 80.1 (Ti<u>C</u>H$_2$CH), 40.0 (N<u>Me$_2$</u>), 32.3 (TiCH<u>C</u>HMe$_2$), 27.0 (TiCHCH<u>Me$_2$</u>), 22.3 (TiCHCH<u>Me$_2$</u>), 12.5 (C$_5$<u>Me$_5$</u>) ppm (*i*-<u>C$_6$</u>F$_5$ were not observed).

[Cp*Ti{NC(NMe$_2$)$_2$}{η^3-CH$_3$(CH)$_3$^{i}Pr}][BAr$^F_4$] (*endo*-24 -[BAr$^F_4$]).

Endo-allyl: ^{1}H NMR (CD_2Cl_2, 499.9 MHz, 298 K): 8.38 (1 H, t, CH$_{meso}$, $^3J_{HH}$ = 13.8 Hz), 4.74 (1 H, dq, C<u>H</u>Me, $^3J_{HH}$ = 7.1 and 13.8 Hz), 4.46 (1 H, dd, C<u>H</u>CHMe$_2$, $^3J_{HH}$ = 6.8 and 13.8 Hz), 2.95 (12 H, s, N<u>Me$_2$</u>), 2.15 (15 H, s, C$_5$<u>Me$_5$</u>), 2.03–2.00 (1 H, m, CHC<u>H</u>Me$_2$), 1.18 (3 H, d, CH<u>Me</u>), 0.90 (3 H, d, CHCH<u>Me$_2$</u>, $^3J_{HH}$ = 6.4 Hz), 0.34 (3 H, d, CHCH<u>Me$_2$</u>, $^3J_{HH}$ = 6.4 Hz) ppm. ^{13}C{^{1}H} NMR (CD_2Cl_2, 125.7 MHz, 298 K): 167.0 (N<u>C</u>), 148.2 (br. d, *o*-<u>C$_6$</u>F$_5$, $^1J_{CF}$ = 251.1 Hz), 138.6 (br. d, *p*-<u>C$_6$</u>F$_5$, $^1J_{CF}$ = 237.9 Hz), 136.1 (br. d, *m*-<u>C$_6$</u>F$_5$, $^1J_{CF}$ = 236.1 Hz), 127.4 (<u>C$_5$Me$_5$</u>), 121.6 (<u>C</u>HCHMe$_2$), 106.7 (Me<u>C</u>H), 42.9 (N<u>Me$_2$</u>), 34.5 (CH<u>C</u>HMe$_2$), 24.8 (CHCH<u>Me$_2$</u>), 20.6 (CHCH<u>Me$_2$</u>), 19.4 (<u>Me</u>CH), 12.3 (C$_5$<u>Me$_5$</u>) ppm (*i*-<u>C$_6$</u>F$_5$ were not observed).

Common data: ^{19}F NMR (CD_2Cl_2, 470.4 MHz, 298 K): –133.1 (m, *o*-C$_6$<u>F$_5$</u>), –163.3 (m, *p*-C$_6$<u>F$_5$</u>), –167.3 (m, *m*-C$_6$<u>F$_5$</u>) ppm. ^{11}B NMR (CD_2Cl_2, 160.4 MHz, 298 K): -16.7 ppm.

Reaction of Cp*Ti{NC(N^{i}BuMe)$_2$}Me$_2$ (1.56) with [Ph$_3$C][BAr$^F_4$] and 2,4-hexadiene. To a stirring fluorobenzene (3 mL) solution of Cp*Ti{NC(N^{i}BuMe)$_2$}Me$_2$ (**1.56**, 0.03g, 0.073 mmol) and 2,4-hexadiene (83 µL, 0.073 mmol) was added dropwise a fluorobenzene (2 mL) solution of [Ph$_3$C][BAr$^F_4$] (0.067 g, 0.073 mmol). After 3 h, pentane (10 mL) was added resulting in the formation of a dark green oil. The pentane/fluorobenzene was decanted away and the oil washed with pentane (3 × 5 mL). The remaining solid was dried *in vacuo* to yield the *endo*- and *exo*-allyl

[Cp*Ti{NC(N^{i}BuMe)$_2$}{η^3-CH(Me)(CH)$_2$^{i}Pr}][BAr$^{F}_4$] and [Cp*Ti{NC(N(^{i}BuMe)$_2$}{η-CH$_2$(CH)$_3$^{i}Pr}][BAr$^{F}_4$] as a green solid in a 0.53 : 0.13 : 0.34 ratio, respectively. Yield: 0.030 g (36%).

Major species: [Cp*Ti{NC(N^{i}BuMe)$_2$}{η^3-CH(Me)(CH)$_2$^{i}Pr}][BAr$^{F}_4$] (*endo*-25-[BAr$^{F}_4$]).

^{1}H NMR (C$_6$D$_5$Br, 499.9 Hz, 298 K): 8.23 (1 H, t, C$\underline{H}_{meso}$, $^3J_{HH}$ = 13.8 Hz), 4.54 (1 H, dq, MeC$\underline{H}$, $^3J_{HH}$ = 13.8 Hz, 6.1 Hz), 4.31 (1 H, dd, C$\underline{H}$CHMe$_2$, $^3J_{HH}$ = 13.8 Hz, 7.7 Hz), 2.94–2.85 (4 H, m, NC$\underline{H}_2$CHMe$_2$), 2.79 (6 H, s, N$\underline{Me}$), 2.09–2.07 (1 H, m, CHC$\underline{H}$Me$_2$), 1.95 (15 H, s, C$_5\underline{Me}_5$), 1.93–1.89 (2 H, m, NCH$_2$C$\underline{H}$Me$_2$), 1.10 (3 H, d, $\underline{Me}$CH, $^3J_{HH}$ = 6.1 Hz), 0.93–0.91 (15 H, overlapping d, CHCH$\underline{Me}_2$, NCH$_2$CH$\underline{Me}_2$), 0.32 (3 H, d, CHCH$\underline{Me}_2$, $^3J_{HH}$ = 6.0 Hz). ^{13}C{^{1}H} NMR (C$_6$D$_5$Br, 125.7 MHz, 298 K): 161.8 (N$\underline{C}$), 148.5 (br. d, *o*-$\underline{C}_6$F$_5$, $^1J_{CF}$ = 244.7 Hz), 138.3 (br. d, *p*-$\underline{C}_6$F$_5$, $^1J_{CF}$ = 235.6 Hz), 136.4 (br. d, *m*-$\underline{C}_6$F$_5$, $^1J_{C\,F}$ = 238.1 Hz), 127.6 ($\underline{C}_5$Me$_5$), 121.1 ($\underline{C}$HCHMe$_2$), 106.6 (Me$\underline{C}$H), 59.6 (N$\underline{C}$H$_2$CHMe$_2$), 38.3 (N$\underline{Me}$), 34.4 (CH$\underline{C}$HMe$_2$), 26.2 (NCH$_2\underline{C}$HMe$_2$), 24.6 (CHCH$\underline{Me}_2$), 20.4 (CHCH$\underline{Me}_2$), 19.5 ($\underline{Me}$CH), 19.4 (NCH$_2$CH$\underline{Me}_2$), 12.3 (C$_5\underline{Me}_5$) ppm (C$\underline{H}_{meso}$ and *i*-$\underline{C}_6$F$_5$ were not observed).

Minor species: [Cp*Ti{NC(N^{i}BuMe)$_2$}{η^3-CH(Me)(CH)$_2$^{i}Pr}][BAr$^{F}_4$] (*exo*-25-[BAr$^{F}_4$])

^{1}H NMR (C$_6$D$_5$Br, 499.9 Hz, 298 K): 7.15–7.12 (1 H, m, C$\underline{H}_{meso}$), 6.44 (1 H, dd, C$\underline{H}$CHMe$_2$, $^3J_{HH}$ = 14.3 Hz, 8.9 Hz), 5.98 (1 H, dq, MeC$\underline{H}$, $^3J_{HH}$ = 14.3 Hz, 6.2 Hz), 2.94–2.83 (10 H, m, NC$\underline{H}_2$CHMe$_2$, N$\underline{Me}$), 2.19–2.17 (1 H, m, CHC$\underline{H}$Me$_2$), 1.93 (15 H, s, C$_5\underline{Me}_5$), 1.89–1.78 (2 H, m, NCH$_2$C$\underline{H}$Me$_2$), 1.19 (3 H, d, $\underline{Me}$CH, $^3J_{HH}$ = 6.2 Hz), 0.98–0.91 (12 H, overlapping doublet, NCH$_2$CH$\underline{Me}_2$), 0.88 (3 H, m, CHCH$\underline{Me}_2$), 0.16 (3 H, d, CHCH$\underline{Me}_2$, $^3J_{HH}$ = 7.3 Hz) ppm. ^{13}C{^{1}H} NMR (C$_6$D$_5$Br, 125.7 MHz, 298 K): 161.7 (N$\underline{C}$), 148.5 (br. d, *o*-$\underline{C}_6$F$_5$, $^1J_{CF}$ = 244.7 Hz), 138.3 (br. d, *p*-$\underline{C}_6$F$_5$, $^1J_{CF}$ = 235.6 Hz), 136.4 (br. d, *m*-$\underline{C}_6$F$_5$, $^1J_{CF}$ = 238.1 Hz), 127.5 ($\underline{C}_5$Me$_5$), 120.0 ($\underline{C}$HCHMe$_2$), 104.6 (Me$\underline{C}$H), 59.6 (N$\underline{C}$H$_2$CHMe$_2$), 38.8 (N$\underline{Me}$), 32.0 (CH$\underline{C}$HMe$_2$), 26.4 (NCH$_2\underline{C}$HMe$_2$), 22.3 (CHCH$\underline{Me}_2$), 20.3 (CHCH$\underline{Me}_2$), 19.7 (NCH$_2$CH$\underline{Me}_2$), 19.4(NCH$_2$CH$\underline{Me}_2$), 17.10 ($\underline{Me}$CH), 12.5 (C$_5\underline{Me}_5$) ppm (C$\underline{H}_{meso}$ and *i*-$\underline{C}_6$F$_5$ were not observed).

Minor species: [Cp*Ti{HNC(N(^{i}BuMe)$_2$}{η-CH$_2$(CH)$_3$^{i}Pr}][BAr$^{F}_4$] (26-[BAr$^{F}_4$]).

^{1}H NMR (C_6D_5Br, 499.9 Hz, 298 K): 3.93–3.84 (2 H, m, TiC<u>H</u>CH, TiCHC<u>H</u>), 3.61-3.54 (1 H, m, TiCH$_2$C<u>H</u>), 3.50 (1 H, dd, TiC<u>H$_2$</u>CH, $^2J_{HH}$ = 5.6 Hz, $^3J_{HH}$ = 13.3 Hz), 3.18 (1 H, dd, TiC<u>H$_2$</u>CH, $^2J_{HH}$ = 5.6 Hz, $^3J_{HH}$ = 9.6 Hz), 3.05 (1 H, s, N<u>H</u>, $^1J_{NH}$ = 60.9 Hz), 2.66 (2 H, app. d, NC<u>H$_2$</u>CHMe$_2$, $^3J_{HH}$ = 9.1 Hz), 2.61 (2 H, app. d, NC<u>H$_2$</u>CHMe$_2$, $^3J_{HH}$ = 6.8 Hz), 2.01–1.99 (1 H, m, TiCHC<u>H</u>Me$_2$), 1.81–1.76 (2 H, m, NCH$_2$C<u>H</u>Me$_2$), 1.73 (15 H, s, C$_5$<u>Me$_5$</u>), 1.23 (3 H, d, TiCHCH<u>Me$_2$</u>, $^3J_{HH}$ = 6.6 Hz), 0.87 (3 H, d, TiCHCH<u>Me$_2$</u>, $^3J_{HH}$ = 6.6 Hz) 0.84 (6 H, d, NCH$_2$CH<u>Me$_2$</u>, $^3J_{HH}$ = 6.3 Hz), 0.80 (6 H, d, NCH$_2$CH<u>Me$_2$</u>, $^3J_{HH}$ = 6.3 Hz) ppm. ^{13}C{^{1}H} NMR (C_6D_5Br, 125.7 MHz, 298 K): 169.0 (N<u>C</u>), 148.5 (br. d, *o*-<u>C$_6$</u>F$_5$, $^1J_{CF}$ = 244.7 Hz), 138.3 (br. d, *p*-<u>C$_6$</u>F$_5$, $^1J_{CF}$ = 235.6 Hz), 136.4 (br. d, *m*-<u>C$_6$</u>F$_5$, $^1J_{CF}$ = 238.1 Hz), 124.3 (C$_5$<u>Me$_5$</u>), 118.3 (TiCH<u>C</u>H), 114.0 (TiCH$_2$<u>C</u>H), 107.4 (Ti<u>C</u>HCH), 80.9 (Ti<u>C</u>H$_2$CH), 59.3 (N<u>C</u>H$_2$CHMe$_2$), 37.7 (N<u>Me</u>), 32.3 (CH<u>C</u>HMe$_2$), 27.3 (CHCH<u>Me$_2$</u>), 26.1 (NCH$_2$<u>C</u>HMe$_2$), 24.4 (CHCH<u>Me$_2$</u>), 19.6 (NCH$_2$CH<u>Me$_2$</u>), 19.4 (NCH$_2$CH<u>Me$_2$</u>), 12.0 (C$_5$<u>Me$_5$</u>) ppm (*i*-C$_6$F$_5$ were not observed).

Common data: ^{19}F NMR (C_6D_5Br, 470.4 MHz, 298 K): –131.4 (m, *o*-C$_6$<u>F$_5$</u>), –161.8 (m, *p*-C$_6$<u>F$_5$</u>), –165.7 (m, *m*-C$_6$<u>F$_5$</u>) ppm. ^{11}B NMR (C_6D_5Br, 160.4 MHz, 298 K): -16.1 ppm. IR (NaCl plates, Nujol mull, cm^{-1}): 3424 (m, (NH)), 1513 (m), 1462 (s), 1376 (m), 1260 (s), 1087 (m), 1020 (m), 978 (w), 798 (s). A satisfactory elemental analysis could not be obtained.

Reaction of Cp*Ti{NC(N(Xyl)CH$_2$)$_2$}Me$_2$ (3.06) with [Ph$_3$C][BAr$^{F}_4$] and 2,4-hexadiene. To a stirring fluorobenzene (3 mL) solution of Cp*Ti{NC(N(Xyl)CH$_2$)$_2$}Me$_2$ (**3.06**, 0.030 g, 0.059 mmol) and 2,4-hexadiene (6.8 µL, 0.059 mmol) was added dropwise a fluorobenzene (2 mL) solution of [Ph$_3$C][BAr$^{F}_4$] (0.055 g, 0.059 mmol). After 3 h, pentane (10 mL) was added resulting in the formation of a dark green oil. The pentane/fluorobenzene was decanted away and the oil washed with pentane (3 × 5 mL). The remaining solid was dried *in vacuo* to yield [Cp*Ti{HNC(N(Xyl)CH$_2$)$_2$}{η-CH$_2$(CH)$_3$^{i}Pr}][BAr$^{F}_4$] and the *exo*-allyl of [Cp*Ti{NC(N(Xyl)CH$_2$)$_2$}{η^3-CH(Me)(CH)$_2$^{i}Pr}][BAr$^{F}_4$] as a green solid in a 0.83 : 0.16 ratio. Yield: 0.049 g (66%).

Major species: [Cp*Ti{HNC(N(Xyl)CH_2)$_2$}{η-CH_2(CH)$_3$^{i}Pr}][BAr^F_4] (27-[BAr^F_4]).

^{1}H NMR (C_6D_5Br, 499.9 Hz, 298 K): 7.31–7.17 (4 H, m, $C_{Ar}\underline{H}$), 7.11–7.16 (2 H, m, $C_{Ar}\underline{H}$), 3.64–3.61 (3 H, m, $NC\underline{H}_2$, $N\underline{H}$, $^1J_{NH}$ = 61.9 Hz), 3.55–3.42 (4 H, m, $NC\underline{H}_2$, $TiC\underline{H}CH$, $TiCHC\underline{H}$), 3.25 (1 H, app. dt, $TiCH_2C\underline{H}$, $^3J_{HH}$ = 13.8 Hz, 9.4 Hz), 2.50–2.46 (1 H, m, $TiC\underline{H}_2CH$), 2.33 (6 H, s, $C_{Ar}\underline{Me}$), 2.10 (6 H, s, $C_{Ar}\underline{Me}$), 1.82–1.77 (1 H, m, $TiCHC\underline{H}Me_2$), 1.56 (1 H, m, $TiC\underline{H}_2CH$), 1.36 (15 H, s, $C_5\underline{Me}_5$), 1.28 (3 H, d, $TiCHCH\underline{Me}_2$, $^3J_{HH}$ = 6.8 Hz), 0.82 (3 H, d, $TiCHCH\underline{Me}_2$, $^3J_{HH}$ = 6.6 Hz) ppm. $^{13}C\{^1H\}$ NMR (C_6D_5Br, 125.7 MHz, 298 K): 164.5 ($N\underline{C}$), 148.5 (br. d, *o*-$\underline{C}_6F_5$, $^1J_{CF}$ = 243.8 Hz), 138.3 (br. d, *p*-$\underline{C}_6F_5$, $^1J_{CF}$ = 235.5 Hz), 136.4 (br. d, *m*-$\underline{C}_6F_5$, $^1J_{CF}$ = 232.8 Hz), 137.7 ($N\underline{C}_{Ar}$), 137.3 ($\underline{C}_{Ar}Me$), 133.4 ($C_{Ar}\underline{H}$), 130.2 ($C_{Ar}\underline{H}$), 122.8 ($\underline{C}_5Me_5$), 115.1 ($TiCH\underline{C}H$), 111.7 ($TiCH_2\underline{C}H$), 107.6 ($Ti\underline{C}HCH$), 82.3 ($Ti\underline{C}H_2CH$), 47.3 ($N\underline{C}H_2$), 32.4 ($TiCH\underline{C}HMe_2$), 27.3 ($TiCHCH\underline{Me}_2$), 24.9 ($TiCHCH\underline{Me}_2$), 18.2 ($C_{Ar}\underline{Me}$), 17.8 ($C_{Ar}\underline{Me}$), 11.5 ($C_5\underline{Me}_5$) ppm (*i*-$\underline{C}_6F_5$ were not observed).

Minor species: [Cp*Ti{NC(N(Xyl)CH_2)$_2$}{η^3-CH(Me)(CH)$_2$^{i}Pr}][BAr^F_4] (*exo*-28-[BAr^F_4]).

^{1}H NMR (C_6D_5Br, 499.9 Hz, 298 K): 7.31–7.17 (4 H, m, $C_{Ar}\underline{H}$), 7.11–7.16 (2 H, m, $C_{Ar}\underline{H}$), 6.81 (1 H, t, $C\underline{H}_{meso}$, $^3J_{HH}$ = 13.9 Hz), 5.79–5.72 (1 H, m, $C\underline{H}CHMe_2$), 5.36 (1 H, dq, $MeC\underline{H}$, $^3J_{HH}$ = 13.9 Hz, 6.0 Hz), 3.89 (4 H, s, $NC\underline{H}_2$), 2.61 (6 H, s, $C_{Ar}\underline{Me}$), 2.52 (6 H, s, $C_{Ar}\underline{Me}$), 2.17–2.10 (1 H, m, $CHC\underline{H}Me_2$), 1.63 (15 H, s, $C_5\underline{Me}_5$), 0.84–0.80 (3 H, m, $CHCH\underline{Me}_2$), 0.77 (3 H, d, $\underline{Me}CH$, $^3J_{HH}$ = 6.0 Hz), -0.14 (3 H, d, $CHCH\underline{Me}_2$, $^3J_{HH}$ = 6.6 Hz) ppm. $^{13}C\{^1H\}$ NMR (C_6D_5Br, 125.7 MHz, 298 K): 156.6 ($\underline{C}H_{meso}$), 154.7 ($N\underline{C}$), 148.5 (br. d, *o*-$\underline{C}_6F_5$, $^1J_{CF}$ = 243.8 Hz), 138.3 (br. d, *p*-$\underline{C}_6F_5$, $^1J_{CF}$ = 235.5 Hz), 136.4 (br. d, *m*-$\underline{C}_6F_5$, $^1J_{CF}$ = 232.8 Hz), 137.2 ($N\underline{C}_{Ar}$), 136.7 ($\underline{C}_{Ar}Me$), 135.4 ($\underline{C}_{Ar}H$), 129.6 ($\underline{C}_5Me_5$), 129.2 ($\underline{C}_{Ar}H$), 122.6 ($\underline{C}HCHMe_2$), 107.6 ($Me\underline{C}H$), 46.1 ($N\underline{C}H_2$), 32.4 ($CH\underline{C}HMe_2$), 26.9 ($CHCH\underline{Me}_2$), 19.7 ($CHCH\underline{Me}_2$), 18.5 ($C_{Ar}\underline{Me}$), 18.3 ($C_{Ar}\underline{Me}$), 18.2 ($\underline{Me}CH$), 12.1 ($C_5\underline{Me}_5$) ppm ($\underline{C}H_{meso}$ and *i*-$\underline{C}_6F_5$ were not observed).

Common data: ^{19}F NMR (C_6D_5Br, 470.4 MHz, 298 K): –131.4 (m, *o*-$C_6\underline{F}_5$), –161.9 (m, *p*-$C_6\underline{F}_5$), –165.7 (m, *m*-$C_6\underline{F}_5$) ppm. ^{11}B NMR (C_6D_5Br, 160.4 MHz, 298 K): -15.9 ppm. IR (NaCl plates, Nujol mull, cm^{-1}): 3285 (m, NH), 1643 (s), 1598 (w),

1514 (m), 1463 (m), 1380 (w), 1341 (m), 1260 (s), 1173 (w), 1086 (m), 1015 (m), 874 (m), 789 (s), 728 (m), 703 (w), 684 (m), 661 (m), 610 (w), 572 (w), 545 (w). A satisfactory elemental analysis could not be obtained.

Low temperature NMR tube scale reaction of Cp*Ti{NC(N(Xyl)CH$_2$)$_2$}Me$_2$ (3.06) with [Ph$_3$C][BAr$^F_4$] and 2,4-hexadiene. To a C_6D_5Br solution (0.3 mL) of Cp*Ti{NC(N(Xyl)CH$_2$)$_2$}Me$_2$ (**3.06**, 0.010 g, 0.020 mmol) and 2,4-hexadiene (2.3 µL, 0.020 mmol) was added a C_6D_5Br solution (0.2 mL) of [Ph$_3$C][BAr$^F_4$] (0.018 g, 0.020 mmol) at –30 ºC. The NMR spectra were recorded within 5 minutes at –30 ºC, indicating the formation of the *endo*-allyl [Cp*Ti{NC(N(Xyl)CH$_2$)$_2$}{η^3-CH(Me)(CH)$_2$^{i}Pr}][BAr$^F_4$] in a 55% spectroscopic yield.

[Cp*Ti{NC(N(Xyl)CH$_2$)$_2$}{η^3-CH(Me)(CH)$_2$^{i}Pr}][BAr$^F_4$] (*endo*-28-[BAr$^F_4$]).

^{1}H NMR (C_6D_5Br, 400.2 MHz, 243 K): 7.80 (1 H, t, C$\underline{H}_{meso}$, $^3J_{HH}$ = 14.8 Hz), 7.35–7.03 (21 H, m, $C_{Ar}\underline{H}$, $\underline{Ph}_3CMe$), 4.46 (1 H, dq, MeC$\underline{H}$, $^3J_{HH}$ = 14.8 Hz, 8.7 Hz), 3.91 (1H, dd, C$\underline{H}$CHMe$_2$, $^3J_{HH}$ = 14.8 Hz, 8.7 Hz), 3.68 (4 H, s, NCH$_2$), 2.56 (6 H, s, $C_{Ar}\underline{Me}$), 2.45 (6 H, s, $C_{Ar}\underline{Me}$), 2.24 (3 H, s, $Ph_3C\underline{Me}$), 1.88–1.84 (1 H, m, CHC$\underline{H}$Me$_2$), 1.63 (15 H, s, $C_5\underline{Me}_5$) 0.85 (3 H, d, CHCHMe$_2$, $^3J_{HH}$ = 6.5 Hz), 0.25 (3 H, d, $\underline{Me}$CH, $^3J_{HH}$ = 5.2 Hz), -0.36 (3 H, d, CHCHMe$_2$, $^3J_{HH}$ = 6.6 Hz) ppm. ^{19}F NMR (C_6D_5Br, 470.4 MHz, 243 K): –131.2 (m, *o*-$C_6\underline{F}_5$), –161.7 (m, *p*-$C_6\underline{F}_5$), –165.8 (m, *m*-$C_6\underline{F}_5$) ppm. ^{11}B NMR (C_6D_5Br, 160.4 MHz, 243 K): –16.0 ppm.

Typical procedure for 1-hexene polymerisation

To a solution of Ti{NCN(Dipp)CH$_2$C$_6$H$_4$}Me$_2$ (**3**, 5 mg, 0.009 mmol) and [Ph$_3$C][BAr$^F_4$] (9 mg, 0.009 mmol) in C_6D_5Br was added 1-hexene (60 µL, 0.49 mmol). The total volume was always 0.5 mL. The mixture was immediately transferred to a *J*. Young NMR tube and a ^{1}H NMR spectrum was recorded within 5 minutes. The sample was quenched with MeOH (0.2 mL) and run through a silica plug in pentane to remove any residual titanium species. The resulting polymer was analysed by GPC, by weight and NMR spectroscopy. The ^{1}H and ^{13}C{^{1}H} NMR spectra agree with literature.[18-20]

NMR tube scale reaction of 15-[BAr$^F_4$] and Ph$_3$PO. To a solution of [Cp*Ti{NCN(Dipp)CH$_2$C$_6$H$_4$}Me$_2$ (**3**, 0.020 g, 0.04 mmol) and [Ph$_3$C][BAr$^F_4$]

(0.036 g, 0.04 mmol) in C_6D_5Br (0.3 mL) was added a solution of 2,4-hexadiene (4.6 μL, 0.04 mmol) in C_6D_5Br (0.2 mL) resulting in the formation of a dark green solution. To this solution, Ph_3PO (0.017 g, 0.06 mmol) was added resulting in a dark brown solution. The NMR spectra were recorded within 5 minutes indicating the formation of (*E*)-5-methyl-1,3-hexadiene and a paramagnetic species, Ph_3CMe and $[BAr^F{}_4]^-$ (as previously recorded).

(*E*)-5-methyl-1,3-hexadiene: ^{1}H NMR (C_6D_5Br, 400.2 MHz, 298 K): 6.43–6.31 (1 H, m, CH_2CH), 6.10–6.04 (1 H, m, $CHCH$), 5.65 (1 H, dd, $CHCHMe_2$, $^3J_{HH}$ = 15.9 Hz, 6.6 Hz), 5.15 (1 H, d, CH_2CH, $^3J_{HH}$ = 17.4 Hz), 5.02 (1 H, d, CH_2CH, $^3J_{HH}$ = 10.1 Hz), 2.33–2.25 (1 H, m, $CHCHMe_2$), 1.01–0.98 (6 H, m, $CHCHMe_2$) ppm. $^{13}C\{^1H\}$ NMR (C_6D_5Br, 100.6 MHz, 298 K): 142.1 (CH^iPr), 138.1 (CH_2CH), 130.6 ($CHCH$), 115.0 (CH_2CH), 31.4 ($CHMe_2$), 22.7 ($CHMe_2$) ppm.

Ph_3CMe: $^{13}C\{^1H\}$ NMR (C_6D_5Br, 100.6 MHz, 298 K): ^{1}H NMR (C_6D_5Br, 400.2 MHz, 298 K): 7.50–7.26 (15 H, Ph_3CMe), 2.24 (3 H, Ph_3CMe) ppm. $^{13}C\{^1H\}$ NMR (C_6D_5Br, 100.6 MHz, 298 K): 149.2 (Ph_3CMe), 138.1 (Ph_3CMe), 128.1 (Ph_3CMe), 126.3 (Ph_3CMe), 52.2 (Ph_3CMe), 30.7 (Ph_3CMe) ppm

Low temperature NMR tube scale reaction of 15-[BAr$^F{}_4$] with Ph_3PO. To a dark green solution of **15-[BAr$^F{}_4$]** in C_6D_5Br (0.3 mL), generated *in situ* by the reaction of $[Cp^*Ti\{NCN(Dipp)CH_2C_6H_4\}Me_2$ (**3**, 0.020 g, 0.04 mmol) and $[Ph_3C][BAr^F{}_4]$ (0.036 g, 0.04 mmol), followed by the addition of 2,4-hexadiene (4.6 μL, 0.04 mmol) in C_6D_5Br (0.2 mL), was added a solution of Ph_3PO (0.017 g, 0.06 mmol) in C_6D_5Br (0.1 mL) at –30 ºC. The NMR spectra were recorded within 3 minutes at –30 ºC, indicating formation of **29-[BAr$^F{}_4$]** in a 50% spectroscopic yield.

^{1}H NMR (C_6D_5Br, 400.2 MHz, 243 K): 7.59–7.23 (30 H, Ph_3CMe, $OPPh_3$), 3.85–3.79 (1 H, m, $TiCHCH$), 3.60–3.51 (1 H, m, $TiCH_2CH$), 3.32 (1 H, dd, $TiCHCH$, $^3J_{HH}$ = 14.1 Hz, 8.1 Hz), 3.20 (1 H, dd, $TiCH_2CH$, $^2J_{HH}$ = 6.7 Hz, $^3J_{HH}$ = 10.4 Hz), 2.74 (1 H, dd, $TiCH_2CH$, $^2J_{HH}$ = 6.7 Hz, $^3J_{HH}$ = 13.6 Hz), 2.24 (Ph_3CMe), 1.93–1.82 (1 H, m, $TiCHCHMe_2$), 1.67 (15 H, s, C_5Me_5), 1.09 (3 H, d, $TiCHCHMe_2$, $^3J_{HH}$ = 6.6 Hz), 0.58 (3 H, d, $TiCHCHMe_2$, $^3J_{HH}$ = 6.6 Hz). $^{13}C\{^1H\}$ NMR (C_6D_5Br, 100.6 MHz, 243 K): 148.5 (br. d, *o*-C_6F_5, $^1J_{CF}$ = 244.8 Hz), 149.1 (Ph_3CMe), 138.3 (br. d, *p*-C_6F_5, $^1J_{CF}$ = 234.2 Hz), 138.2 (Ph_3CMe), 136.4 (br. d, *m*-C_6F_5, $^1J_{CF}$ = 231.9 Hz),

135.1 (*p*-OP<u>Ph</u>$_3$), 135.0 (*i*-OP<u>Ph</u>$_3$), 132.6 (d, $^2J_{CP}$ = 10.6 Hz, *o*-OP<u>Ph</u>$_3$), 129.8 (*m*-OP<u>Ph</u>$_3$), 128.2 (<u>Ph</u>$_3$CMe), 126.2 (<u>Ph</u>$_3$CMe), 123.6 (<u>C</u>$_5$Me$_5$), 117.3 (TiCH<u>C</u>H), 114.0 (TiCH$_2$<u>C</u>H), 106.8 (Ti<u>C</u>HCH), 78.0 (Ti<u>C</u>H$_2$CH), 52.5 (Ph$_3$<u>C</u>Me), 32.0 (TiCH<u>C</u>HMe$_2$), 30.7 (Ph$_3$C<u>Me</u>), 27.6 (TiCHCH<u>Me</u>$_2$), 23.5 (TiCHCH<u>Me</u>$_2$), 12.9 (C$_5$<u>Me</u>$_5$) ppm (*i*-<u>C</u>$_6$F$_5$ were not observed). ^{19}F NMR (C_6D_5Br, 376.5 MHz, 243 K): –131.3 (m, *o*-C$_6$<u>F</u>$_5$), -161.7 (m, *p*-C$_6$<u>F</u>$_5$), –165.9 (m, *m*-C$_6$<u>F</u>$_5$) ppm. ^{11}B NMR (C_6D_5Br, 128.4 MHz, 243 K): –15.9 ppm. ^{31}P{^{1}H} NMR (C_6D_5Br, 121.4 MHz, 243 K): 53.2 ppm.

6.8 Experimental details and characterising data for Chapter Four

Ap^1–Ap^3 (4.03–4.05) were prepared according to literature synthesis.[21, 22] The example procedure is giving here for Ap^1 (**4.03**). THF (20 mL) was added to magnesium turnings (1.28 g, 0.38 mol). 1-Br-2,4,6-Me$_3$C$_6$H$_2$ (5.4 mL, 0.35 mol) was then added and the solution was cooled to 0 ºC. To the resulting suspension, 1,2-dibromoethane (0.2 mL) was added and the solution was slowly warmed to room temperature and then heated at 50 ºC for 12 hours. The reaction mixture was filtered and the filtrate was directly used in the consecutive step. 2,6-diboromopyridine (7.91 g, 0.34 mol), tricyclohexylphosphane (0.021 g, 0.075 mmol) and [NiBr$_2$(dme)] (0.012 g, 0.0375 mmol) were added to a Schlenk tube and dissolved in THF (20 mL) and the reaction mixture cooled to 0 ºC. The filtrate from the previous step was then slowly added over an hour period. The solution was allowed to warm to room temperature upon a beige precipitate was observed. The reaction mixture was heated to 50 ºC and stirred overnight. To the cooled reaction mixture, H_2O (30 mL) and CH_2Cl_2 (30 mL) was added and the organic phase was collected. The inorganic phase was washed with CH_2Cl_2 (2 × 15 mL) and the organic phases were combined and washed with brine (30 mL). The organic layer was dried with Na_2SO_4 and the solvent was removed under reduced pressure. The white precipitate was washed with *n*-hexane (20 mL) affording the mono-bromide compound. Yield: 8.19 g (86%). The newly formed compound (3.0 g, 10.9 mmol) was combined in a Schlenk with 1,3-bis(diphenylphosphanyl)propane (0.16 g, 0.40 mmol), tris(dibenzylideneacetone) dipalladium(0) (0.18, 0.20 mmol) and sodium *tert*-butoxide (1.18 g, 12.3 mmol) and dissolved in toluene (20 mL). The resulting mixture was heated to 95 ºC for 48 h. The reaction mixture was cooled to room temperature and H_2O (20 mL) and Et_2O (20 mL) were added. The organic phase was extracted and the remaining inorganic phase was washed with Et_2O (2 × 15 mL). The combined organic layers were washed with a

brine solution and then dried with Na_2SO_4. The solvent was removed under reduced pressure resulting in a red solid which was purified using silica chromatography (eluent: CH_2Cl_2), yielding **4.03** as an off-white solid. Yield: 2.7 g (75%). The compounds ^{1}H NMR spectrum matched the spectrum previously reported.[21, 22]

Ap^{1}Li (30). This compound was prepared by adaptation of a literature synthesis of a similar compound.[21] To a diethyl ether (30 mL) solution of **4.03** (1.5 g, 4.5 mmol) at 0 ºC was added ^{n}BuLi (2.84 mL, 1.6 M in hexane, 4.5 mmol). The solution was allowed to slowly warm to room temperature and stirred for a further 2 h after which time the volatiles were removed *in vacuo*. The resulting off-white solid was washed with hexane and dried *in vacuo* yielding **30**. Yield: 1.30 g (84%).

^{1}H NMR (C_6D_6, 499.9 MHz, 293 K): 6.93–6.87 (3 H, m, $C_{Py}\underline{H}$, $C_{Ar}\underline{H}$), 6.72 (2 H, s, $C_{Ar}\underline{H}$), 5.92 (1 H, br.s, $C_{Py}\underline{H}$), 5.75 (1 H, d, $^3J_{HH}$ = 8.8 Hz, $C_{Py}\underline{H}$), 2.27 (3 H, s, $C_{Ar}\underline{Me}$), 2.20 (3 H, s, $C_{Ar}\underline{Me}$), 2.02 (3 H, s, $C_{Ar}\underline{Me}$), 1.99 (6 H, s, $C_{Ar}\underline{Me}$) ppm. ^{13}C{^{1}H} NMR (C_6D_6, 125.7 MHz, 293 K): 167.1 ($N\underline{C}_{Py}N$), 157.4 ($N\underline{C}_{Py}C_{Ar}$), 138.8 ($\underline{C}_{Py}H$), 138.1 ($N\underline{C}_{Ar}$), 137.0 ($NC_{Py}\underline{C}_{Ar}$), 135.7 ($\underline{C}_{Ar}Me$), 129.8 ($\underline{C}_{Ar}H$), 128.9 ($\underline{C}_{Ar}H$), 128.2 ($\underline{C}_{Ar}Me$), 128.3 ($\underline{C}_{Ar}Me$), 128.0 ($\underline{C}_{Ar}Me$), 107.4 ($\underline{C}_{Py}H$), 105.9 ($\underline{C}_{py}H$), 21.2 ($C_{Ar}\underline{Me}$), 21.1 ($C_{Ar}\underline{Me}$), 19.9 ($C_{Ar}\underline{Me}$), 18.5 ($C_{Ar}\underline{Me}$) ppm. EI-MS: *m/z* = 335 $[M]^+$, 329 $[M–Li]^+$. Anal. found (calcd. for $C_{23}H_{25}N_2Li$): C, 81.91 (82.12); N, 8.16 (8.33); H, 7.38 (7.49)%. IR (NaCl plates, Nujol mull, cm^{-1}): 2721 (w), 1597 (s), 1541 (m), 1463 (m), 1378 (m), 1254 (w), 1220 (1), 1163 (w), 1153 (w), 991 (w), 855(w), 787 (w), 738 (w), 601 (w).

Ap^{2}Li (4.06). This compound was prepared according to literature synthesis.[21] To a diethyl ether (30 mL) solution of **4.04** (0.98 g, 2.2 mmol) at 0 ºC was added ^{n}BuLi (1.34 mL, 1.6 M in hexane, 2.2 mmol). The solution was allowed to slowly warm to room temperature and stirred for a further 2 h after which time the volatiles were removed *in vacuo*. The resulting off-white solid was washed with hexane and dried *in vacuo* yielding **4.06**. Yield: 0.46 g (46%). The compounds ^{1}H NMR spectrum matched the spectrum previously reported.[21]

Ap^{3}Li 31. This compound was prepared by adaptation of a literature synthesis of a similar compound.[21] To a diethyl ether (30 mL) solution of **4.05** (0.90 g, 2.2 mmol) at 0 °C was added ^{n}BuLi (1.4 mL, 1.6 M in hexane , 2.2 mmol). The solution was allowed to slowly warm to room temperature and stirred for a further 2 h after which

time the volatiles were removed *in vacuo*. The resulting off-white solid was washed with hexane and dried *in vacuo* yielding **31**. Yield: 0.55 g (60%).

^{1}H NMR (C_6D_6, 400.2 MHz, 298 K): 7.09 (2 H, s, $C_{Ar}\underline{H}$), 6.91–6.87 (3 H, m, $C_{Py}\underline{H}$, $C_{Ar}\underline{H}$), 6.03 (1 H, d, $C_{Py}\underline{H}$, $^{3}J_{HH}$ = 7.8 Hz), 5.69 (1 H, d, $C_{Py}\underline{H}$, $^{3}J_{HH}$ = 8.3 Hz), 2.99–2.85 (3 H, m, $C\underline{H}Me_2$), 2.26 (3 H, s, $C_{Ar}\underline{Me}$), 1.97 (6 H, s, $C_{Ar}\underline{Me}$), 1.35 (6 H, d, $C_{Ar}CH\underline{Me}_2$, $^{3}J_{HH}$ = 6.8 Hz), 1.14 (6 H, d, $C_{Ar}CH\underline{Me}_2$, $^{3}J_{HH}$ = 6.9 Hz,), 0.98 (6 H, d, $C_{Ar}CH\underline{Me}_2$, $^{3}J_{HH}$ = 6.9 Hz) ppm. $^{13}C\{^{1}H\}$ NMR (C_6D_6, 100.6 MHz, 293 K): 167.5 ($N\underline{C}_{Py}N$), 157.3 ($N\underline{C}_{Py}C_{Ar}$), 148.9 ($\underline{C}_{Ar}CHMe_2$), 146.8 ($N\underline{C}_{Ar}$), 144.3 ($\underline{C}_{Ar}CHMe_2$), 138.5 ($\underline{C}_{py}H$), 137.1 ($NC_{Py}\underline{C}_{Ar}$), 133.9 ($\underline{C}_{Ar}Me$), 132.2 ($\underline{C}_{Ar}Me$), 130.0 ($\underline{C}_{Ar}H$), 121.2 ($\underline{C}_{Ar}H$), 107.6 ($\underline{C}_{Py}H$), 105.4 ($\underline{C}_{py}H$), 34.9 ($C_{Ar}\underline{C}HMe_2$), 30.6 ($C_{Ar}\underline{C}HMe_2$), 24.7 ($C_{Ar}CH\underline{Me}_2$), 24.5 ($C_{Ar}CH\underline{Me}_2$), 24.3 ($C_{Ar}CH\underline{Me}_2$), 21.0 ($C_{Ar}\underline{Me}$), 17.9 ($C_{Ar}\underline{Me}$) ppm. EI-MS: *m/z* = 413 $[M–Li]^{+}$. Anal. found (calcd. for $C_{30}H_{40}N_2$): C, 82.60 (82.72); N, 6.56 (6.43); H, 9.35 (9.26)%. IR (NaCl plates, Nujol mull, cm^{-1}): 1583 (m), 1548 (w), 1460 (s), 1376 (m), 1364 (m), 1260 (w), 1157 9w), 1099 (w), 956 (w), 855 (w), 794 (w), 720 (w).

$(Ap^1)Ti\{NC(Ph)N^iPr_2\}Cl_2$ (32). To a Schlenk tube, **30** (0.50 g, 1.5 mmol) and $Ti\{NC(Ph)N^iPr_2\}Cl_3$ (**4.02**, 0.53 g, 1.5 mmol) were added. The Schlenk tube was cooled down to –78 °C and cold diethyl ether (15 mL) was added. The resulting solution was stirred and allowed to slowly warm to room temperature where upon a colour change to red was observed. The mixture was subsequently stirred for further 16 h after which time the volatiles were removed *in vacuo*. The red solid was extracted into benzene (15 mL) and separated from the insoluble LiCl salt by filtration. The solvent was removed *in vacuo* and the red solid was washed with pentane (3 × 5 mL) giving $(Ap^1)Ti\{NC(Ph)N^iPr_2\}Cl_2$. Yield: 0.81 g (83%).

^{1}H NMR (Toluene-d_8, 400.2 MHz, 213 K): 6.86–6.79 (8 H, m, $C_{Py}\underline{H}$, $C_{Ar}\underline{H}$), 6.50 (2 H, s, $C_{Ar}\underline{H}$), 6.25 (1 H, d, $C_{Py}\underline{H}$, $^{3}J_{HH}$ = 8.6 Hz), 5.30 (1 H, d, $C_{Py}\underline{H}$, $^{3}J_{HH}$ = 8.6 Hz), 3.01 (1 H, sept, $NC\underline{H}Me_2$, $^{3}J_{HH}$ = 7.0 Hz), 2.64 (6 H, s, $C_{Ar}\underline{Me}$), 2.60–2.56 (1 H, m, $NC\underline{H}Me_2$), 2.23 (3 H, s, $C_{Ar}\underline{Me}$), 2.12 (3 H, s, $C_{Ar}\underline{Me}$), 2.07 (6 H, s, $C_{Ar}\underline{Me}$), 1.70 (6 H, d, $NCH\underline{Me}_2$, $^{3}J_{HH}$ = 7.0 Hz), 0.18 (6 H, d, $NCH\underline{Me}_2$, $^{3}J_{HH}$ = 7.0 Hz) ppm. $^{13}C\{^{1}H\}$ NMR (Toluene-d_8, 100.6 MHz, 213 K): 164.9 ($N\underline{C}_{Py}N$), 161.8 ($N\underline{C}C_{Ar}$), 157.6 ($N\underline{C}_{Py}Ar$), 146.0 ($N\underline{C}_{Ar}$), 141.8 ($\underline{C}_{Py}H$), 137.2 ($\underline{C}_{Ar}Me$), 136.1 ($\underline{C}_{Ar}Me$), 136.6 ($NC_{Py}\underline{C}_{Ar}$), 136.5 ($NC\underline{C}_{Ar}$), 134.0 ($\underline{C}_{Ar}Me$), 132.4 ($\underline{C}_{Ar}Me$), 129.0 ($\underline{C}_{Ar}H$), 125.4

($\underline{C}_{Ar}H$), 116.6 ($\underline{C}_{Py}H$), 99.2 ($\underline{C}_{Py}H$), 53.1 ($N\underline{C}HMe_2$), 49.1 ($N\underline{C}HMe_2$), 21.7 ($C_{Ar}\underline{Me}$), 21.5 ($C_{Ar}\underline{Me}$), 21.4 ($C_{Ar}\underline{Me}$), 20.4 ($NCH\underline{Me}_2$), 19.3 ($NCH\underline{Me}_2$), 19.2 ($C_{Ar}\underline{Me}$) ppm. EI-MS: *m/z* = 447 $[M–(NC(Ph)N^iPr)]^+$, 329 $[C_9H_{11}NC_5H_3NC_9H_{11}]^+$. Anal. found (calcd. for $C_{36}H_{44}N_4TiCl_2$): C, 66.28 (66.36); N, 8.48 (8.60); H, 6.87 (6.81)%.IR (NaCl plates, Nujol mull, cm^{-1}): 2853 (s), 1581 (w), 1562 (w), 1519 (m), 1455 (m), 1373 (w), 1336 (w), 1261 (w), 12421 (w), 1221 (w), 1164 (m), 1101 (w), 1031 (m), 1020 (m), 867 (w), 799 (w), 784 (w), 583 (m). Diffraction-quality crystals were grown from a dilute pentane solution at room temperature.

$(Ap^2)Ti\{NC(Ph)N^iPr_2\}Cl_2$ (33). To a Schlenk tube, **4.06** (0.400 g, 0.87 mmol) and $Ti\{NC(Ph)N^iPr_2\}Cl_3$ (**4.02**, 0.309 g, 0.87 mmol) were added. The Schlenk tube was cooled down to −78 ºC and cold diethyl ether (15 mL) was added. The resulting solution was stirred and allowed to slowly warm to room temperature where upon a colour change to red was observed. The mixture was subsequently stirred for further 16 h after which time the volatiles were removed *in vacuo*. The red solid was extracted into benzene (15 mL) and separated from the insoluble LiCl salt by filtration. The solvent was removed *in vacuo* and the red solid was washed with pentane (3 × 5 mL) yielding **33**. Yield: 0.260 g (40%).

^{1}H NMR (toluene-d_8, 400.2 MHz, 223 K): 7.32 (2 H, s, $C_{Ar}\underline{H}$), 7.15–6.81 (8 H, m, $C_{Ar}\underline{H}$), 6.59 (1 H, m, $C_{Py}\underline{H}$), 6.43 (1 H, d, $C_{Py}\underline{H}$, $^3J_{HH}$ = 7.9 Hz), 5.38 (1 H, d, $C_{Py}\underline{H}$, $^3J_{HH}$ = 7.9 Hz), 3.55– 3.48 (2 H, m, $C_{Ar}C\underline{H}Me_2$), 3.44–4.40 (2 H, m, $C_{Ar}C\underline{H}Me_2$), 3.01–2.92 (1 H, m, $NC\underline{H}Me_2$), 2.82–2.75 (1 H, m, $C_{Ar}C\underline{H}Me_2$), 2.63–2.56 (1 H, m, $NC\underline{H}Me_2$), 1.77 (6 H, d, $C_{Ar}CH\underline{Me}_2$, $^3J_{HH}$ = 7.4 Hz), 1.67 (6 H, d, $NCH\underline{Me}_2$, $^3J_{HH}$ = 7.6 Hz), 1.22–1.20 (12 H, m, $C_{Ar}CH\underline{Me}_2$), 1.09 (6H, d, $C_{Ar}CH\underline{Me}_2$, $^3J_{HH}$ = 6.7 Hz), 1.00 (6 H, d, $C_{Ar}CH\underline{Me}_2$, $^3J_{HH}$ = 6.8 Hz), 0.23 (6 H, d, $NCH\underline{Me}_2$, $^3J_{HH}$ = 6.9 Hz) ppm. $^{13}C\{^1H\}$ NMR (toluene-d_8, 100.6 MHz, 223 K): 165.0 ($N\underline{C}_{Py}N$), 161.8 ($N\underline{C}C_{Ar}$), 156.2 ($N\underline{C}_{Py}C_{Ar}$), 148.5 ($\underline{C}_{Ar}CHMe_2$), 147.4 ($N\underline{C}_{Ar}$), 146.4 ($\underline{C}_{Ar}CHMe_2$), 146.2 ($NC\underline{C}_{Ar}$), 146.0 ($NC_{Py}\underline{C}_{Ar}$), 142.5 ($\underline{C}_{Ar}CHMe_2$), 139.8 ($\underline{C}_{Py}H$), 134.1 ($\underline{C}_{Ar}H$), 128.8 ($\underline{C}_{Ar}H$), 127.8 ($\underline{C}_{Ar}H$), 124.1 ($\underline{C}_{Ar}H$), 123.7 ($\underline{C}_{Ar}H$), 118.3 ($\underline{C}_{Py}H$), 99.8 ($\underline{C}_{Py}H$), 52.5 ($N\underline{C}HMe_2$), 48.4 ($N\underline{C}HMe_2$), 34.5 ($C_{Ar}\underline{C}HMe_2$), 30.7 ($C_{Ar}\underline{C}HMe_2$), 28.0 ($C_{Ar}\underline{C}HMe_2$), 26.5 ($C_{Ar}CH\underline{Me}_2$), 24.5 ($C_{Ar}CH\underline{Me}_2$), 24.2 ($C_{Ar}CH\underline{Me}_2$), 23.9 ($C_{Ar}CH\underline{Me}_2$), 23.2 ($C_{Ar}CH\underline{Me}_2$), 19.7 ($NCH\underline{Me}_2$), 18.3 ($NCH\underline{Me}_2$) ppm. EI-MS: *m/z* = 203 $[NC(Ph)N^iPr_2]^+$, 455 $[Ap^2]^+$, 538 $[M–NC(N^iPr_2)Ph–Cl]^+$, 572 $[M–NC(Ph)N^iPr_2]^+$, Anal. found (calcd. for $C_{45}H_{62}N_4TiCl_2$): C 69.35, (69.49); N, 7.36 (7.20); H,7.87

(8.04)%. IR (NaCl plates, Nujol mull, cm^{-1}): 1643 (w), 1585 (w), 1564 (w), 1517 (m), 1493 (w), 1460 (s), 1374 (m), 1343 (w), 1259 (w), 1153 (w), 1102 (w), 1031 (w), 800 (w), 783 (w), 692 (w). Diffraction-quality crystals were grown from a dilute pentane solution at room temperature.

(Ap^3)Ti{NC(Ph)N^{i}Pr$_2$}Cl$_2$ (34). To a Schlenk tube, **31** (0.50 g, 1.2 mmol) and Ti{NC(Ph)N^{i}Pr$_2$}Cl$_3$ (**4.02**, 0.43 g, 1.2 mmol) were added. The Schlenk tube was cooled down to −78 ^{o}C and cold diethyl ether (15 mL) was added. The resulting solution was stirred and allowed to slowly warm up to room temperature where upon a colour change to red was observed. The mixture was subsequently stirred for further 16 h after which time the volatiles were removed *in vacuo*. The red solid was extracted into benzene (15 mL) and separated from the insoluble LiCl salt by filtration. The solvent was removed *in vacuo* and the red solid was washed with pentane (3 × 5 mL) yielding the titled compound **34**. Yield: 0.69 g (79%).

^{1}H NMR (C_6D_6, 400.2 MHz, 213 K): 7.33 (2 H, s, $C_{Ar}\underline{H}$), 6.83–6.77 (6 H, m, $C_{Py}\underline{H}$, $C_{Ar}\underline{H}$), 6.57 (1 H, d, $C_{Py}\underline{H}$, $^3J_{HH}$ = 8.0 Hz), 6.44 (2 H, s, $C_{Ar}\underline{H}$), 5.33 (1 H, d, $C_{Py}\underline{H}$, $^3J_{HH}$ = 8.0 Hz), 3.46–3.42 (2 H, m, $C_{Ar}C\underline{H}Me_2$), 3.01–2.97 (1 H, m, $NC\underline{H}Me_2$), 2.80-2.73 (1 H, m, $C_{Ar}C\underline{H}Me_2$), 2.57–2.52 (1 H, m, $NC\underline{H}Me_2$), 2.21 (3 H, s, $C_{Ar}\underline{Me}$), 2.05 (6 H, s, $C_{Ar}\underline{Me}$), 1.80 (6 H, d, $C_{Ar}CH\underline{Me}_2$, $^3J_{HH}$ = 6.5 Hz), 1.66 (6 H, d, $NCH\underline{Me}_2$, $^3J_{HH}$ = 6.8 Hz), 1.25 (6 H, d, $C_{Ar}CH\underline{Me}$, $^3J_{HH}$ = 6.5 Hz), 1.20 (6 H, d, $C_{Ar}CH\underline{Me}_2$, $^3J_{HH}$ = 6.8 Hz), 0.16 (6 H, d, $NCH\underline{Me}_2$, $^3J_{HH}$ = 6.8 Hz) ppm. $^{13}C\{^1H\}$ NMR (C_6D_6, 100.6 MHz, 213 K): 163.8 ($N\underline{C}_{Py}N$), 160.7 ($N\underline{C}C_{Ar}$), 156.2 ($N\underline{C}_{Py}C_{Ar}$), 148.6 ($\underline{C}_{Ar}CHMe_2$), 146.4 ($N\underline{C}_{Ar}$), 144.9 ($\underline{C}_{Ar}CHMe_2$), 139.4 ($\underline{C}_{py}H$), 136.7 ($NC\underline{C}_{Ar}$), 136.1($NC_{py}\underline{C}_{Ar}$) 133.1 ($\underline{C}_{Ar}Me$), 131.5 ($\underline{C}_{Ar}Me$), 128.7 ($\underline{C}_{Ar}H$), 128.2 ($\underline{C}_{Ar}H$), 125.0 ($\underline{C}_{Ar}H$), 120.2 ($\underline{C}_{Ar}H$), 117.9 ($\underline{C}_{Py}H$), 98.5 ($\underline{C}_{py}H$), 52.2 ($N\underline{C}HMe_2$), 48.2 ($N\underline{C}HMe_2$), 34.5 ($C_{Ar}\underline{C}HMe_2$), 30.7 ($C_{Ar}\underline{C}HMe_2$), 26.6 ($C_{Ar}CH\underline{Me}_2$), 24.0 ($C_{Ar}CH\underline{Me}_2$), 23.0 ($C_{Ar}CH\underline{Me}_2$), 21.7 ($C_{Ar}\underline{Me}$), 19.6 ($C_{Ar}\underline{Me}$), 18.5 ($NCH\underline{Me}_2$), 18.4 ($NCH\underline{Me}_2$). MS: *m/z* = 413 $[Ap^3]^+$. Anal. found (calcd. for $C_{42}H_{56}N_4TiCl_2$): C, 68.73 (68.57); N, 7.51 (7.62); H, 7.69 (7.67) %. IR (NaCl plates, Nujol mull, cm^{-1}): 1644 (w), 1580 (m), 1514 (m), 1455 (m), 1402 (m), 1376 (m), 1259 (w), 1222 (w), 1184 (w), 1150 (w), 1101 (w), 1064 (w), 1031 (m), 999 (w), 890 (w), 874 (m), 800 (w), 784 (w), 749 (w), 722 9w), 704 (w), 784 (w), 694 (w), 665 (w), 585 (w). Diffraction-quality crystals were grown from a dilute pentane solution at room temperature.

(Ap^1)Ti{NC(Ph)N^{i}Pr$_2$}Me$_2$ (35). To a stirring toluene (20 mL) solution of Ap^1Ti{NC(Ph)N^{i}Pr$_2$}Cl$_2$ (**32**, 0.55 g, 0.80 mmol) at 0 ºC was added dropwise MeMgBr (0.52 mL, 3.0 M in THF, 1.57 mmol) and the resulting solution was allowed to warm up to room temperature and stirred for a further 16 h. The volatiles were then removed *in vacuo* and the oily solid was then extracted into pentane (20 mL) with the addition of dioxane (3 mL) to remove any MgBrCl compound. (Ap^1)Ti{NC(Ph)N^{i}Pr$_2$}Me$_2$ was isolated as an olive green solid following removal of pentane *in vacuo*. Yield: 0.32 g (66%).

^{1}H NMR (Toluene-d_8, 400.2 MHz, 223 K): 6.93–6.89 (5 H, m, C$_{Py}$H, C$_{Ar}$H), 6.83 (2 H, s, C$_{Ar}$H), 6.75 (2 H, s, C$_{Ar}$H), 6.16 (1 H, d, C$_{Py}$H, $^3J_{HH}$ = 7.0 Hz), 5.48 (1 H, d, C$_{Py}$H, $^3J_{HH}$ = 6.9 Hz), 3.28 (1 H, m, NCHMe$_2$), 2.80 (1 H, br. s, NCHMe$_2$), 2.47 (6 H, s, C$_{Ar}$Me), 2.30 (3 H, s, C$_{Ar}$Me), 2.13 (3 H, s, C$_{Ar}$Me), 2.05 (6 H, s, C$_{Ar}$Me), 1.73 (6 H, d, NCHMe$_2$, $^3J_{HH}$ = 6.2 Hz), 1.11 (6 H, s, TiMe), 0.42 (6 H, d, NCHMe$_2$, $^3J_{HH}$ = 6.2 Hz) ppm. ^{13}C{^{1}H} NMR (Toluene-d_8, 100.6 MHz, 223 K): 167.7 (NC$_{Py}$N), 159.7 (NCC$_{Ar}$), 157.2 (NC$_{Py}$C$_{Ar}$), 144.6 (NC$_{Ar}$), 141.3 (C$_{Py}$H), 137.8 (NCC$_{Ar}$), 137.3 (C$_{Ar}$Me), 137.2 (C$_{Ar}$Me), 136.0 (NC$_{Py}$C$_{Ar}$), 133.0 (C$_{Ar}$Me), 132.5 (C$_{Ar}$Me), 128.4 (C$_{Ar}$H), 128.3 (C$_{Ar}$H), 124.8 (C$_{Ar}$H), 112.3 (C$_{Py}$H), 100.6 (C$_{Py}$H), 55.4 (TiMe), 51.7 (NCHMe$_2$), 47.3 (NCHMe$_2$), 21.3 (C$_{Ar}$Me), 21.2 (C$_{Ar}$Me), 20.8 (C$_{Ar}$Me), 19.8 (NCHMe$_2$), 19.6 (NCHMe$_2$), 18.6 (C$_{Ar}$Me) ppm. EI-MS: *m/z* = 77 [TiMe$_2$]$^+$, 329 [Ap^1]$^+$. IR (NaCl plates, Nujol mull, cm^{-1}): 2854 (s), 1581 (s), 1549 (s), 1452 (m), 1352 (m), 1332 (m), 1150 (w), 1034 (w), 794 (m), 782 (m). A satisfactory elemental analysis could not be obtained.

(Ap^1)Ti{NC(Ph)N^{i}Pr$_2$}(CH$_2$Ph)$_2$ (36). To a stirring benzene (20 mL) solution of (Ap^1)Ti{NC(Ph)N^{i}Pr$_2$}Cl$_2$ (**32**, 0.50 g, 0.77 mmol) at 5 ºC was added dropwise BnMgCl (1.53 mL, 1.0 M in Et$_2$O, 1.53 mmol) and the resulting solution was stirred for 16 h. The volatiles were then removed *in vacuo* and the oily solid was then extracted into pentane (20 mL) with the addition of dioxane (3 mL) to remove any coordinating MgCl$_2$ salt. (Ap^1)Ti{NC(Ph)N^{i}Pr$_2$}(CH$_2$Ph)$_2$ was isolated as an orange solid following removal of pentane *in vacuo*. Yield: 0.362 g (62%).

^{1}H NMR (C$_6$D$_6$, 400.2 MHz, 298 K): 7.37 (3 H, s, C$_{Ar}$H), 7.29 (4 H, t, PhCH$_2$, $^3J_{HH}$ = 7.6 Hz), 7.26–7.22 (1 H, m, C$_{Py}$H), 7.09–7.05 (3 H, m, C$_{Ar}$H) 7.01 (2 H, s, C$_{Ar}$H), 6.80 (4 H, d, CH$_2$Ph, $^3J_{HH}$ = 7.1 Hz), 6.77–6.75 (2 H, m, *p*-CH$_2$Ph), 6.48 (1 H,

d, $C_{Py}\underline{H}$, $^3J_{HH}$ = 7.5 Hz), 5.80 (1 H, d, $C_{Py}\underline{H}$, $^3J_{HH}$ = 7.9 Hz), 4.48 (1 H, br., $NC\underline{H}Me_2$), 3.39 (1 H, br. s, $NC\underline{H}Me_2$), 3.06 (4 H, s, $PhC\underline{H}_2$), 2.63 (6 H, s, $C_{Ar}\underline{Me}$), 2.45 (6 H, s, $C_{Ar}\underline{Me}$), 2.18 (6 H, s, $C_{Ar}\underline{Me}$), 1.14 (6 H, br. s, $NCH\underline{Me}_2$), 0.83 (6 H, br. s, $NCH\underline{Me}_2$) ppm. $^{13}C\{^1H\}$ NMR (C_6D_6, 100.6 MHz, 298 K): 167.4 ($N\underline{C}_{Py}N$), 161.4 ($N\underline{C}C_{Ar}$), 157.6 ($N\underline{C}_{Py}C_{Ar}$), 150.1 (*i*-$\underline{Ph}CH_2$), 145.5 ($N\underline{C}_{Ar}$), 141.2 ($\underline{C}_{Py}H$), 139.7 ($\underline{C}_{Ar}Me$), 137.4 ($NC_{Py}\underline{C}_{Ar}$), 136.3 ($NC\underline{C}_{Ar}$), 133.5 ($\underline{C}_{Ar}Me$), 133.4 ($\underline{C}_{Ar}Me$), 129.3 ($\underline{C}_{Ar}H$), 128.9 ($\underline{C}_{Ar}H$), 128.1 (*m*-$\underline{Ph}CH_2$), 127.9 ($\underline{C}_{Ar}H$), 127.7 ($\underline{C}_{Ar}H$), 127.2 (*o*-$\underline{Ph}CH_2$), 127.0 ($\underline{C}_{Ar}H$), 120.9 (*p*-$\underline{Ph}CH_2$), 113.7 ($\underline{C}_{Py}H$), 101.7 ($\underline{C}_{Py}H$), 83.0 ($Ph\underline{C}H_2$), 48.4 ($N\underline{C}HMe_2$), 21.2 ($C_{Ar}\underline{Me}$), 21.1 ($C_{Ar}\underline{Me}$), 21.0 ($NCH\underline{Me}_2$), 20.6 ($NCH\underline{Me}_2$), 18.8 ($C_{Ar}\underline{Me}$) ppm. EI-MS: *m/z* = 329[*M*–Ap^1–CH_2Ph]$^+$, 315 [Ap^1]$^+$, 91 [$PhCH_2$]$^+$. IR (NaCl plates, Nujol mull, cm^{-1}): 1582 (w), 1529 (w), 1456 (m), 1377 (m), 1312 (w), 1261 (w), 1153 (w), 1133 (w), 1098 (w), 875 (vw), 796 (w), 742 (m), 722 (m), 697 (w) 690 (w). A satisfactory elemental analysis could not be obtained.

(Ap^2)Ti{NC(Ph)N^{i}Pr$_2$}Me$_2$ (37). To a stirring benzene (20 mL) solution of (Ap^2)Ti{NC(Ph)N^{i}Pr$_2$}Cl$_2$ (**33**, 0.60 g, 0.77 mmol) at 5 °C was added dropwise MeLi (0.96 mL, 1.6 M in Et_2O, 1.5 mmol) and the resulting solution was allowed to warm up to room temperature and stirred for a further 16 h. The volatiles were then removed *in vacuo* and the oily solid was then extracted into pentane (20 mL) to filter away from the insoluble LiCl salt. (Ap^2)Ti{NC(Ph)N^{i}Pr$_2$}Me$_2$ was isolated as an olive green solid following removal of pentane *in vacuo*. Yield: 0.41 g (72%).

^{1}H NMR (Toluene-d_8, 400.2 MHz, 213 K): 7.29 (2 H, s, $C_{Ar}\underline{H}$), 7.15–7.00 (8 H, m, $C_{Ar}\underline{H}$), 6.58 (1 H, m, $C_{Py}\underline{H}$), 6.45 (1 H, d, $C_{Py}\underline{H}$, $^3J_{HH}$ = 6.8 Hz), 5.54 (1 H, d, $C_{Py}\underline{H}$, $^3J_{HH}$ = 7.6 Hz), 3.43–3.32 (4 H, m, $NC\underline{H}Me_2$, $C_{Ar}C\underline{H}Me_2$), 3.27–3.22 (1 H, m, $NC\underline{H}Me_2$), 2.89–2.76 (2 H, m, $C_{Ar}C\underline{H}Me_2$), 1.67 (6 H, d, $NCH\underline{Me}_2$, $^3J_{HH}$ = 6.4 Hz), 1.58 (6 H, d, $C_{Ar}CH\underline{Me}_2$, $^3J_{HH}$ = 6.2 Hz), 1.22 (12 H, d, $C_{Ar}CH\underline{Me}_2$, $^3J_{HH}$ = 6.4 Hz), 1.18 (6 H, d, $C_{Ar}CH\underline{Me}_2$, $^3J_{HH}$ = 6.4 Hz), 1.07 (12 H, m, $C_{Ar}CH\underline{Me}_2$, $Ti\underline{Me}$), 0.45 (6 H, d, $NCH\underline{Me}_2$, $^3J_{HH}$ = 6.4 Hz) ppm. $^{13}C\{^1H\}$ NMR (Toluene-d_8, 100.6 MHz, 213 K): 168.4 ($N\underline{C}_{Py}N$), 159.1 ($N\underline{C}C_{Ar}$), 156.4 ($N\underline{C}_{Py}C_{Ar}$), 148.8 ($\underline{C}_{Ar}CHMe_2$), 147.7 ($N\underline{C}_{Ar}$), 146.6 ($\underline{C}_{Ar}CHMe_2$), 146.3 ($N\underline{C}_{Ar}$), 145.1 ($NC\underline{C}_{Ar}$), 143.3 ($\underline{C}_{Ar}CHMe_2$), 140.3 ($\underline{C}_{Py}H$),139.8 ($NC_{Py}\underline{C}_{Ar}$), 134.1 ($\underline{C}_{Ar}H$), 129.1 ($\underline{C}_{Ar}H$), 126.8 ($\underline{C}_{Ar}H$), 123.7 ($\underline{C}_{Ar}H$), 120.5 ($\underline{C}_{Ar}H$),114.6 ($\underline{C}_{Py}H$), 101.5 ($\underline{C}_{Py}H$), 57.3 ($Ti\underline{Me}$), 51.6 ($N\underline{C}HMe_2$), 47.3 ($N\underline{C}HMe_2$), 34.8 ($C_{Ar}\underline{C}HMe_2$), 31.0 ($C_{Ar}\underline{C}HMe_2$), 28.5 ($C_{Ar}\underline{C}HMe_2$), 27.0

($C_{Ar}CH\underline{Me}_2$), 24.3 ($C_{Ar}CH\underline{Me}_2$), 24.2 ($C_{Ar}CH\underline{Me}_2$), 24.1 ($C_{Ar}CH\underline{Me}_2$), 22.9 ($C_{Ar}CH\underline{Me}_2$), 19.4 ($NCH\underline{Me}_2$), 19.3 ($NCH\underline{Me}_2$) ppm. MS: *m/z* = 445 $[Ap^2]^+$, 281 [*M*-Ap^2]. IR (NaCl plates, Nujol mull, cm^{-1}): 1573 (w), 1460 (m), 1377 (w), 1260 (w), 1094 (w), 799 (w). A satisfactory elemental analysis could not be obtained.

(Ap^2)Ti{NC(Ph)N^{i}Pr$_2$}(CH_2Ph)$_2$ (38). To a stirring benzene (20 mL) solution of (Ap^2)Ti{NC(Ph)N^{i}Pr$_2$}Cl_2 (**33**, 0.41 g, 0.53 mmol) at 5 °C was added dropwise BnMgCl (1.1 mL, 1.0 M in Et_2O, 1.1 mmol) and the resulting solution was stirred for 16 h. The volatiles were then removed *in vacuo* and the oily solid was then extracted into pentane (20 mL) with the addition of dioxane (3 mL) to remove any coordinating $MgCl_2$ salt. (Ap^2)Ti{NC(Ph)N^{i}Pr$_2$}(CH_2Ph)$_2$ was isolated as an orange solid following removal of pentane *in vacuo*. Yield: 0.18 g (42%).

^{1}H NMR (C_6D_6, 499.9 MHz, 298 K): 7.28 (2 H, s, $C_{Ar}\underline{H}$), 7.14–7.10 (3 H, m, $C_{Ar}\underline{H}$), 7.02–6.98 (5 H, m, $C_{Py}\underline{H}$, *m*-$\underline{Ph}CH_2$), 6.92–6.90 (3 H, m, $C_{Ar}\underline{H}$), 6.78 (2 H, t, *p*-$\underline{Ph}CH_2$, $^3J_{HH}$ = 7.2 Hz), 6.57–6.55 (3 H, m, $C_{Ar}\underline{H}$, $C_{Py}\underline{H}$), 6.38 (4 H, d, *o*-$\underline{Ph}CH_2$, $^3J_{HH}$ = 7.4 Hz), 5.63 (1 H, d, $C_{Py}\underline{H}$, $^3J_{HH}$ = 8.5 Hz), 4.67 (1 H, br. s, $NC\underline{H}Me_2$), 3.37 (2 H, sept, $C_{Ar}CH\underline{Me}_2$, $^3J_{HH}$ = 6.9 Hz), 3.23–3.18 (1 H, m, $NC\underline{H}Me_2$), 3.08 (2 H, sept, $C_{Ar}CH\underline{Me}_2$, $^3J_{HH}$ = 6.9 Hz), 2.95–2.88 (1 H, m, $C_{Ar}CH\underline{Me}_2$), 2.68 (4 H, overlapping doublets, $PhC\underline{H}_2$, $^3J_{HH}$ = 5.8 Hz, $^2J_{HH}$ = 8.9 Hz), 1.35–1.32 (12 H, m, $C_{Ar}CH\underline{Me}_2$), 1.20 (6 H, d, $C_{Ar}CH\underline{Me}_2$, $^3J_{HH}$ = 6.9 Hz), 1.10 (6 H, d, $C_{Ar}CH\underline{Me}_2$, $^3J_{HH}$ = 6.9 Hz), 0.93 (6 H, d, $C_{Ar}CH\underline{Me}_2$, $^3J_{HH}$ = 6.9 Hz), 0.85 (6 H, d, $NCH\underline{Me}_2$, $^3J_{HH}$ = 6.0 Hz), 0.66 (6 H, d, $NCH\underline{Me}_2$, $^3J_{HH}$ = 7.0 Hz) ppm. $^{13}C\{^1H\}$ NMR (C_6D_6, 125.7 MHz, 213 K): 168.5 ($N\underline{C}_{Py}N$), 161.3 ($N\underline{C}C_{Ar}$), 157.7 ($N\underline{C}_{Py}C_{Ar}$), 150.0 (*i*-$\underline{Ph}CH_2$), 147.7 ($\underline{C}_{Ar}CHMe_2$), 146.5 ($N\underline{C}_{Ar}$), 144.5 ($\underline{C}_{Ar}CHMe_2$), 140.5 ($\underline{C}_{Py}H$), 140.0 ($NC\underline{C}_{Ar}$), 135.9 ($NC_{Py}\underline{C}_{Ar}$), 128.5 (*m*-$\underline{Ph}CH_2$), 128.4 ($\underline{C}_{Ar}H$), 127.7 ($\underline{C}_{Ar}H$), 127.4 (*o*-$\underline{Ph}CH_2$), 126.0 ($\underline{C}_{Ar}H$), 124.4 ($\underline{C}_{Ar}H$), 121.5 ($\underline{C}_{Ar}H$), 121.2 (*p*-$\underline{Ph}CH_2$), 116.2 ($\underline{C}_{Py}H$), 104.3 ($\underline{C}_{Py}H$), 82.5 ($Ph\underline{C}H_2$), 48.8 (2 × $N\underline{C}HMe_2$), 35.5 ($C_{Ar}C\underline{H}Me_2$), 31.7 ($C_{Ar}C\underline{H}Me_2$), 29.0 ($C_{Ar}C\underline{H}Me_2$), 27.4 ($C_{Ar}CH\underline{Me}_2$), 25.3 ($C_{Ar}CH\underline{Me}_2$), 23.5 ($NCH\underline{Me}_2$), 23.0 ($C_{Ar}CH\underline{Me}_2$), 21.0 ($NCH\underline{Me}_2$) ppm. MS: *m/z* = 329 [*M*–Ap^2–CH_2Ph]$^+$, 455 $[Ap^2]^+$. IR (NaCl plates, Nujol mull, cm^{-1}): 1590 (w), 1522 (m), 1460 (s), 1377 (s), 1347 (w), 1312 (w), 1261 (w), 1205 (w), 1153 (w), 1098 (w), 1026 (w), 797 (w), 788 (w), 742 (w), 722 9w), 697 (w). A satisfactory elemental analysis could not be obtained.

$(Ap^3)Ti\{NC(Ph)N^iPr_2\}Me_2$ (39). To a stirring benzene (20 mL) solution of $(Ap^3)Ti\{NC(Ph)N^iPr_2\}Cl_2$ (**34**, 0.59 g, 0.81 mmol) at 5 ^{0}C was added dropwise MeLi (1.0 mL, 1.6 M in Et_2O, 1.62 mmol) and the resulting solution was allowed to warm to room temperature and stirred for a further 16 h. The volatiles were then removed *in vacuo* and the oily solid was then extracted into pentane (20 mL) to filter away from the insoluble LiCl salt. $(Ap^3)Ti\{NC(Ph)N^iPr_2\}Me_2$ was isolated as an olive green solid following removal of pentane *in vacuo*. Yield: 0.39 g (69%).

^{1}H NMR (Toluene-d_8, 400.2 MHz, 213 K): 7.29 (2 H, s, $C_{Ar}\underline{H}$), 7.01–6.88 (5 H, m, $C_{Ar}\underline{H}$), 6.71(3 H, s, $C_{Ar}\underline{H}$, $C_{Py}\underline{H}$), 6.44 (1 H, d, $C_{Py}\underline{H}$, $^3J_{HH}$ = 7.5 Hz), 5.52 (1 H, d, $C_{Py}\underline{H}$, $^3J_{HH}$ = 7.5 Hz), 3.40–3.33 (2 H, m, $NC\underline{H}Me_2$), 3.31–3.25 (1 H, m, $C_{Ar}C\underline{H}Me_2$), 2.85–2.74 (2 H, m, $C_{Ar}C\underline{H}Me_2$), 2.30 (3 H, s, $C_{Ar}\underline{Me}$), 2.05 (6 H, s, $C_{Ar}\underline{Me}$), 1.72 (6 H, d, $NCH\underline{Me}_2$, $^3J_{HH}$ = 5.8 Hz), 1.62 (6 H, d, $C_{Ar}CH\underline{Me}_2$, $^3J_{HH}$ = 6.2 Hz), 1.27–1.23 (12 H, m, $C_{Ar}CH\underline{Me}_2$), 1.14 (6 H, s, $Ti\underline{Me}$), 0.41 (6 H, d, $NCH\underline{Me}_2$, $^3J_{HH}$ = 5.8 Hz) ppm. $^{13}C\{^1H\}$ NMR (Toluene-d_8, 100.6 MHz, 213 K): 167.2 ($N\underline{C}_{Py}N$), 159.3 ($N\underline{C}C_{Ar}$), 156.4($N\underline{C}_{Py}C_{Ar}$), 148.8($N\underline{C}_{Ar}$), 146.6 ($\underline{C}_{Ar}CHMe_2$), 144.3 ($\underline{C}_{Ar}CHMe_2$), 140.4 ($\underline{C}_{Py}H$), 140.3 ($NC\underline{C}_{Ar}$), 139.6 ($NC_{Py}\underline{C}_{Ar}$), 137.7 ($\underline{C}_{Ar}H$), 136.9 ($\underline{C}_{Ar}Me$), 133.5 ($\underline{C}_{Ar}Me$), 132.7 ($\underline{C}_{Ar}H$), 132.2 ($\underline{C}_{Ar}H$), 128.3 ($\underline{C}_{Ar}H$), 127.0 ($\underline{C}_{Ar}H$), 124.0 ($\underline{C}_{Ar}H$), 120.4 ($\underline{C}_{Ar}H$), 114.4 ($\underline{C}_{Py}H$), 100.5 ($\underline{C}_{Py}H$), 56.4 ($Ti\underline{Me}$), 51.5 ($NC\underline{H}Me_2$), 47.0 ($NC\underline{H}Me_2$), 34.7 ($C_{Ar}\underline{C}HMe_2$), 31.0 ($C_{Ar}\underline{C}HMe_2$), 27.2 ($C_{Ar}CH\underline{Me}_2$), 24.3 ($C_{Ar}CH\underline{Me}_2$), 22.8 ($C_{Ar}CH\underline{Me}_2$), 21.0 ($C_{Ar}\underline{Me}$), 19.5 ($NCH\underline{Me}_2$), 19.3 ($NCH\underline{Me}_2$), 18.8 ($C_{Ar}\underline{Me}$) ppm. MS: *m/z* = 693 $[M]^+$, 413 $[Ap^3]^+$. IR (NaCl plates, Nujol mull, cm^{-1}): 1557 (s), 1444 (s), 1404 (w), 1369 (s), 1332 (w), 1284 (m), 1258 (m), 1225 (w), 1188 (m), 1063 (w), 1034 (w), 1024 (w), 944 (w), 657 (w), 917 (w), 889 (w), 864 (w), 782 (w), 746 (w), 696 (w), 667 (w). A satisfactory elemental analysis could not be obtained.

NMR tube scale synthesis of $[(Ap^1)Ti\{NCN(Dipp)CH_2C_6H_4\}Cl_2(NHMe_2)$ (**40**). $(SiMe_3)NCN(Dipp)CH_2C_6H_4$ was prepared following literature synthesis.[23] To a solution of $(Ap^1)TiCl_3(NHMe_2)$ (**1.75**, 0.020 g, 0.038 mmol) in C_6D_6 (0.3 mL) was added a solution of $(SiMe_3)NCN(Dipp)CH_2C_6H_4$ (0.014 g, 0.038 mmol) in C_6D_6 (0.2 mL). The reaction was transferred to an NMR tube and the NMR spectra recorded after 16 h. Impurities up to 30% spectroscopic yield were observed. Diffraction-quality crystals of **40** were grown from a benzene solution at room temperature.

^{1}H NMR (C_6D_6, 400.2 MHz, 298 K): 7.01–6.70 (12 H, m, $C_{Py}\underline{H}$, $C_{Ar}\underline{H}$, $C_{Dipp}\underline{H}$), 6.28 (1 H, d, $C_{Py}\underline{H}$, $^{3}J_{HH}$ = 7.5 Hz), 5.49 (1 H, d, $C_{Py}\underline{H}$, $^{3}J_{HH}$ = 7.4 Hz), 4.19 (2H, s, $NC\underline{H}_2$), 2.72 (2H, sept, $C_{Dipp}CH\underline{Me}_2$, $^{3}J_{HH}$ = 6.9 Hz), 2.47 (6 H, s, $C_{Ar}\underline{Me}$), 2.34 (6 H, s, $NH\underline{Me}_2$), 2.28–2.06 (9 H, m, $C_{Ar}\underline{Me}$), 1.37 (6 H, d, $C_{Dipp}CH\underline{Me}_2$, $^{3}J_{HH}$ = 6.9 Hz), 0.88 (6 H, d, $C_{Dipp}CH\underline{Me}_2$, $^{3}J_{HH}$ = 6.9 Hz) ppm.

NMR tube scale synthesis of [(Ap^{1})Ti{NC(Ph)N^{i}Pr$_2$}Me][BAr$^{F}_4$] (41-[BAr$^{F}_4$]). To a solution of (Ap^{1})Ti{NC(Ph)N^{i}Pr$_2$}Me$_2$ (**35**, 0.010 g, 0.016 mmol) in C_6D_5Br (0.5 mL) was added [Ph_3C][BAr$^{F}_4$] (0.015 g, 0.016 mmol) resulting in the formation of a dark brown solution. The solution was transferred to an NMR tube and the NMR spectra recorded after 5 minutes.

^{1}H NMR (C_6D_5Br, 400.2 MHz, 298 K): 7.36–7.26 (14 H, m, $C_{py}\underline{H}$, $\underline{Ph}CMe$), 7.06 (2 H, s, $C_{Ar}\underline{H}$), 6.96 (2 H, s, $C_{Ar}\underline{H}$), 6.91 (2 H, d, $\underline{Ph}_3CMe$, $^{3}J_{HH}$ = 7.5 Hz), 6.42 (1 H, d, $C_{Py}\underline{H}$, $^{3}J_{HH}$ = 8.0 Hz), 6.08 (1 H, d, $C_{Py}\underline{H}$, $^{3}J_{HH}$ = 8.4 Hz), 3.65–3.55 (2 H, m, $NC\underline{H}Me$), 2.46 (3 H, s, $C_{Ar}\underline{Me}$), 2.39 (3 H, s, $C_{Ar}\underline{Me}$), 2.24 (3 H, s, $Ph_3C\underline{Me}$), 2.18 (12 H, br. s, $C_{Ar}\underline{Me}$), 1.62 (3 H, s, $Ti\underline{Me}$), 1.37 (6H, br.,N $CH\underline{Me}_2$,), 0.94 (6 H, d, $NCH\underline{Me}_2$, $^{3}J_{HH}$ = 6.3 Hz) ppm. ^{19}F NMR (C_6D_5Br, 376.5 MHz, 298 K): –131.3 (m, *o*-$C_6\underline{F}_5$), –161.9 (m, *p*-$C_6\underline{F}_5$), –165.7(m, *m*-$C_6\underline{F}_5$) ppm. ^{11}B NMR (C_6D_5Br, 128.4 MHz, 298 K): –16.0 ppm.

NMR tube scale synthesis of [(Ap^{2})Ti{NC(Ph)N^{i}Pr$_2$}Me][BAr$^{F}_4$] (42-[BAr$^{F}_4$]). To a solution of (Ap^{2})Ti{NC(Ph)N^{i}Pr$_2$}Me$_2$ (**37**, 0.010 g, 0.014 mmol) in C_6D_5Br (0.5 mL) was added [Ph_3C][BAr$^{F}_4$] (0.012 g, 0.014 mmol) resulting in the formation of a dark brown solution. The solution was transferred to an NMR tube and the NMR spectra recorded after 5 minutes.

^{1}H NMR (C_6D_5Br, 400.2 MHz, 298 K): 7.40–7.26 (26 H, m, $C_{Ar}\underline{H}$, $C_{Py}\underline{H}$, $\underline{Ph}_3CMe$), 6.76 (1 H, d, $C_{Py}\underline{H}$, $^{3}J_{HH}$ = 8.3 Hz), 6.20 (1 H, d, $C_{Py}\underline{H}$, $^{3}J_{HH}$ = 8.3 Hz), 3.61–3.55 (2 H, m, $NC\underline{H}Me_2$), 3.35 (2 H, br. s, $C_{Ar}C\underline{H}Me_2$), 3.09–2.94 (2 H, m, $C_{Ar}C\underline{H}Me_2$), 2.64 (1 H, br. s, $C_{Ar}C\underline{H}Me_2$), 2.24 (3 H, s, $Ph_3C\underline{Me}$), 1.72 (3 H, s, $Ti\underline{Me}$), 1.40–0.84 (42 H, m, $C_{Ar}CH\underline{Me}_2$, $NCH\underline{Me}_2$) ppm. ^{19}F NMR (C_6D_5Br, 376.5 MHz, 298 K): –131.4 (m, *o*-$C_6\underline{F}_5$), –161.9 (m, *p*-$C_6\underline{F}_5$), –165.8(m, *m*-$C_6\underline{F}_5$) ppm. ^{11}B NMR (C_6D_5Br, 128.4 MHz, 298 K): –16.0 ppm.

NMR tube scale synthesis of [(Ap^{1})Ti{NC(Ph)N^{i}Pr$_2$}Me(OPPh$_3$)][BAr$^{F}_4$] (43-[BAr$^{F}_4$]). To a solution of (Ap^{1})Ti{NC(Ph)N^{i}Pr$_2$}Me$_2$ (**35**, 0.011 g, 0.018 mmol) and Ph$_3$PO (0.005 g, 0.018 mmol) in C_6D_5Br (0.5 mL) was added [Ph$_3$C][BAr$^{F}_4$] (0.017 g, 0.018 mmol) resulting in the formation of a dark brown solution. The resulting solution was transferred to an NMR tube and the NMR spectra recorded after 5 minutes.

^{1}H NMR (C_6D_5Br, 400.2 MHz, 298 K): 7.61 (8 H, br, $C_{Ar}\underline{H}$, $\underline{Ph}_3CMe$, $OP\underline{Ph}_3$), 7.39-7.26 (32 H, m, $C_{Ar}\underline{H}$, $C_{Py}\underline{H}$, $\underline{Ph}_3CMe$, $OP\underline{Ph}_3$), 6.27 (1H, d, $C_{Py}\underline{H}$, $^{3}J_{HH}$ = 7.2 Hz), 5.65 (1 H, d, $C_{Py}\underline{H}$, $^{3}J_{HH}$ = 7.2 Hz), 4.03 (1 H, br. s, $NC\underline{H}Me_2$), 3.61–3.51 (1H, m, $NC\underline{H}Me_2$), 2.45 (3 H, s, $C_{Ar}\underline{Me}$), 2.42 (3 H, s, $C_{Ar}\underline{Me}$), 2.31 (3 H, s, $C_{Ar}\underline{Me}$), 2.24 (3 H, s, $Ph_3C\underline{Me}$), 2.15 (3 H, s, $C_{Ar}\underline{Me}$), 1.94 (3 H, s, $C_{Ar}\underline{Me}$), 1.79 (3 H, s, $C_{Ar}\underline{Me}$), 1.49 (3 H, d, $NCH\underline{Me}_2$, $^{3}J_{HH}$ = 6.9 Hz), 1.43 (3 H, d, $NCH\underline{Me}_2$, $^{3}J_{HH}$ = 6.9 Hz), 1.11 (3 H, s, $Ti\underline{Me}$), 1.00–0.93 (6 H, m, $NCH\underline{Me}_2$) ppm. ^{19}F NMR (C_6D_5Br, 376.5 MHz, 298 K): –131.4 (m, *o*-$C_6\underline{F}_5$), –161.9 (m, *p*-$C_6\underline{F}_5$), –165.7 (m, *m*-$C_6\underline{F}_5$) ppm. ^{11}B NMR (C_6D_5Br, 128.4 MHz, 298 K): –15.9 ppm. ^{31}P{^{1}H} NMR (C_6D_5Br, 162.0 MHz, 298 K): 48.7 ppm.

NMR tube scale synthesis of [(Ap^{2})Ti{NC(Ph)N^{i}Pr$_2$}(Me)(OPPh$_3$)] [BAr$^{F}_4$] (44-[BAr$^{F}_4$]). To a solution of (Ap^{2})Ti{NC(Ph)N^{i}Pr$_2$}Me$_2$ (**37**, 0.030 g, 0.040 mmol) and Ph$_3$PO (0.011 g, 0.040 mmol) in C_6D_5Br (0.5 mL) was added [Ph$_3$C][BAr$^{F}_4$] (0.036 g, 0.040 mmol) resulting in the formation of a dark red solution. The solution was transferred to an NMR tube and the NMR spectra recorded after 5 minutes.

^{1}H NMR (C_6D_5Br, 400.2 MHz, 298 K): 7.58 (4 H, t, $OP\underline{Ph}_3$, $^{3}J_{HH}$ = 7.1 Hz), 7.45-7.23 (39 H, m, $C_{Ar}\underline{H}$, $C_{Py}\underline{H}$, $\underline{Ph}_3CMe$, $OP\underline{Ph}_3$), 6.52 (1 H, d, $C_{Py}\underline{H}$, $^{3}J_{HH}$ = 7.1 Hz), 5.72 (1 H, d, $C_{Py}\underline{H}$, $^{3}J_{HH}$ = 7.3 Hz), 3.64 (1 H, br.s, $NC\underline{H}Me_2$), 3.48–3.40 (1 H, m, $NC\underline{H}Me_2$), 3.21–3.03 (4 H, m, $C_{Ar}C\underline{H}Me_2$), 2.80 (1 H, sept, $C_{Ar}C\underline{H}Me_2$, $^{3}J_{HH}$ = 6.2 Hz), 2.24 (3 H, s, $Ph_3C\underline{Me}$), 1.48–1.43 (9 H, m, $NCH\underline{Me}_2$, $C_{Ar}CH\underline{Me}_2$), 1.32–1.21 (12 H, m, $C_{Ar}CH\underline{Me}_2$), 1.16 (3 H, s, $Ti\underline{Me}$), 1.11 (3 H, d, $C_{Ar}CH\underline{Me}_2$, $^{3}J_{HH}$ = 6. Hz), 1.02–0.95 (9 H, m, $NCH\underline{Me}_2$, $C_{Ar}CH\underline{Me}_2$), 0.90–0.83 (9 H, m, $CH\underline{Me}_2$) ppm. ^{19}F NMR (C_6D_5Br, 376.5 MHz, 298 K): –131.4 (m, *o*-$C_6\underline{F}_5$), –161.9 (m, *p*-$C_6\underline{F}_5$), -165.8(m, *m*-$C_6\underline{F}_5$) ppm. ^{11}B NMR (C_6D_5Br, 128.4 MHz, 298 K): -16.0 ppm. ^{31}P{^{1}H} NMR (C_6D_5Br, 162.0 MHz, 298 K): 48.5 ppm.

NMR tube scale synthesis of [(Ap^1)Ti{NC(Ph)N^{i}Pr$_2$}{MeC(N^{i}Pr$_2$)$_2$}] [BAr$^F{}_4$] (45-[BAr$^F{}_4$]). To a solution of (Ap^1)Ti{NC(Ph)N^{i}Pr$_2$}Me$_2$ (**35**, 0.03 g, 0.049 mmol) and diisopropylcarbodiimide (7.6 µL, 0.049 mmol) in C_6D_5Br (0.5 mL) was added [Ph_3C][BAr$^F{}_4$] (0.045 g, 0.049 mmol) resulting in the formation of a dark red solution. The solution was transferred to an NMR tube and the NMR spectra recorded after 5 minutes, showing the quantitative formation of **45-[BAr$^F{}_4$]**.

^{1}H NMR (C_6D_5Br, 400.2 MHz, 298 K): 7.42–7.26 (20 H, m, $\underline{Ph}_3CMe$, $C_{Ar}\underline{H}$), 7.04 (2 H, s, $C_{Ar}\underline{H}$), 6.96 (2 H, s, $C_{Ar}\underline{H}$), 6.42 (1 H, d, $C_{Py}\underline{H}$, $^3J_{HH}$ = 7.1 Hz), 5.76 (1 H, d, $C_{Py}\underline{H}$, $^3J_{HH}$ = 8.1 Hz), 3.71–3.56 (2 H, m, MeCNC$\underline{H}$Me$_2$), 3.46–3.40 (2H, m, NC$\underline{H}$Me$_2$), 2.46–2.37 (12 H, m, $C_{Ar}\underline{Me}$), 2.25 (3 H, s, $Ph_3C\underline{Me}$), 1.93 (3 H, s, $\underline{Me}$CNCHMe$_2$), 1.85 (6 H, s, $C_{Ar}\underline{Me}$), 1.47 (6 H, d, MeCNCH$\underline{Me}_2$, $^3J_{HH}$ = 6.8 Hz), 1.03 (6 H, d, MeCNCH$\underline{Me}_2$, $^3J_{HH}$ = 6.2 Hz), 0.91 (6 H, d, NCH$\underline{Me}_2$, $^3J_{HH}$ = 6.7 Hz), 0.71 (6 H, d, NCH$\underline{Me}_2$, $^3J_{HH}$ = 6.7 Hz) ppm. ^{13}C{^{1}H} NMR (C_6D_5Br, 100.6 MHz, 298 K): 174.5 (Me$\underline{C}$NCHMe$_2$), 164.5 (N$\underline{C}_{Py}$N), 164.1 (N$\underline{C}C_{Ar}$), 155.7 (N$\underline{C}_{Py}C_{Ar}$), 149.1 ($Ph_3\underline{C}$Me), 148.8 (br., d, *o*-$\underline{C}_6F_5$, $^1J_{CF}$ = 242.6 Hz), 142.1 (N$\underline{C}_{Ar}$), 142.0 ($\underline{C}_{py}$H), 139.1 ($\underline{C}_{Ar}$Me), 138.8 (br., d, *p*-$\underline{C}_6F_5$, $^1J_{CF}$ = 195.3 Hz), 138.2 ($\underline{Ph}_3$CMe), 137.4 (N$C_{Py}\underline{C}_{Ar}$), 136.2 (br., d, *m*-$\underline{C}_6F_5$, $^1J_{CF}$ = 186.8 Hz), 136.0 (N$\underline{C}_{Ar}$), 135.8 ($\underline{C}_{Ar}$Me), 135.0 ($\underline{C}_{Ar}$Me), 133.0 ($\underline{C}_{Ar}$Me), 130.1 ($\underline{C}_{Ar}$H), 129.6 ($\underline{C}_{Ar}$H), 129.1 ($\underline{C}_{Ar}$H), 129.0 ($\underline{Ph}_3$CMe), 128.6 ($\underline{C}_{Ar}$H), 128.2 ($\underline{Ph}_3$CMe), 126.2 ($\underline{Ph}_3$CMe), 125.3 ($\underline{C}_{Ar}$H), 114.9 ($\underline{C}_{Py}$H), 104.1 ($\underline{C}_{Py}$H), 52.7 (MeCN$\underline{C}$HMe$_2$), 52.5 ($Ph_3\underline{C}$Me), 50.8 (N$\underline{C}$HMe$_2$), 30.7 ($Ph_3C\underline{Me}$), 24.4 (MeCNCH$\underline{Me}_2$), 24.1 (NCH$\underline{Me}_2$), 24.0 (NCH$\underline{Me}_2$), 21.3 ($C_{Ar}\underline{Me}$), 21.2 ($C_{Ar}\underline{Me}$), 21.1 ($C_{Ar}\underline{Me}$), 20.3 (MeCNCH$\underline{Me}_2$), 17.8 ($C_{Ar}\underline{Me}$), 12.1 ($\underline{Me}$CNCHMe$_2$) ppm (*i*-$\underline{C}_6F_5$ were not observed). ^{19}F NMR (C_6D_5Br, 376.5 MHz, 298 K): –131.4 (m, *o*-$C_6\underline{F}_5$), –162.0 (m, *p*-$C_6\underline{F}_5$), –165.8 (m, *m*-$C_6\underline{F}_5$) ppm. ^{11}B NMR (C_6D_5Br, 128.4 MHz, 298 K): –15.9 ppm.

NMR tube scale synthesis of [(Ap^2)Ti{NC(Ph)N^{i}Pr$_2$}{MeC(N^{i}Pr)$_2$}] [BAr$^F{}_4$] ([46-[BAr$^F{}_4$]). To a solution of (Ap^2)Ti{NC(Ph)N^{i}Pr$_2$}Me$_2$ (**37**, 0.030 g, 0.040 mmol) and ^{i}PrNCN^{i}Pr (6.3 µL, 0.040 mmol) in C_6D_5Br (0.5 mL) was added [Ph_3C][BAr$^F{}_4$] (0.036 g, 0.040 mmol) resulting in the formation of a dark red solution. The solution was transferred to an NMR tube and the NMR spectra recorded after 5 minutes, forming **46-[BAr$^F{}_4$]** quantitatively.

^{1}H NMR (C_6D_5Br, 400.2 MHz, 298 K): 7.41–7.26 (28 H, m, $C_{Ar}\underline{H}$, $C_{Py}\underline{H}$, $\underline{Ph}_3CMe$), 6.61 (1 H, d, $C_{Py}\underline{H}$, $^{3}J_{HH}$ = 7.6 Hz), 5.89 (1 H, d, $C_{Py}\underline{H}$, $^{3}J_{HH}$ = 8.0 Hz), 3.86 (1 H, br.m, $NC\underline{H}Me_2$), 3.68 (1 H, sept, $NC\underline{H}Me_2$, $^{3}J_{HH}$ = 7.2), 3.31 (2 H, sept, $MeCNC\underline{H}Me_2$, $^{3}J_{HH}$ = 6.3), 3.13–2.92 (5 H, m, $C_{Ar}C\underline{H}Me_2$), 2.24 (3 H, s, $Ph_3C\underline{Me}$), 1.87 (3 H, s, $\underline{Me}CNCHMe_2$), 1.49–1.42 (18 H, m, $NCH\underline{Me}_2$, $C_{Ar}CH\underline{Me}_2$), 1.26 (6 H, m, $C_{Ar}CH\underline{Me}_2$, $^{3}J_{HH}$ = 6.8 Hz), 1.22 (6 H, m, $C_{Ar}CH\underline{Me}_2$, $^{3}J_{HH}$ = 6.8 Hz), 1.14 (6 H, m, $C_{Ar}CH\underline{Me}_2$, $^{3}J_{HH}$ = 7.0 Hz), 1.04 (6 H, m, $NCH\underline{Me}_2$, $^{3}J_{HH}$ = 7.0 Hz), 0.94 (6 H, m, $MeCNCH\underline{Me}_2$, $^{3}J_{HH}$ = 7.0 Hz), 0.71 (6 H, m, $MeCNCH\underline{Me}_2$, $^{3}J_{HH}$ = 6.8 Hz) ppm. $^{13}C\{^{1}H\}$ NMR (C_6D_5Br, 100.6 MHz, 298 K): 174.3 ($MeCNCHMe_2$), 166.4 ($NC_{Py}N$), 165.2 (NCC_{Ar}), 156.0 ($NC_{Py}C_{Ar}$), 150.7 (NC_{Ar}), 149.2 (Ph_3CMe), 148.8 (br., d, *o*-C_6F_5, $^{1}J_{CF}$ = 249.8 Hz), 146.3 ($C_{Ar}CHMe_2$), 144.2 (NCC_{Ar}), 143.7 ($C_{Ar}CHMe_2$), 143.1 ($NC_{py}C_{Ar}$), 141.2 ($C_{Ar}CHMe_2$), 138.6 (br., d, *p*-C_6F_5, $^{1}J_{CF}$ = 235.8 Hz), 136.7 (br., d, *m*-C_6F_5, $^{1}J_{CF}$= 245.4 Hz), 133.5 ($C_{Py}H$), 130.7 ($C_{Ar}H$), 129.8 ($C_{Ar}H$), 129.0 (Ph_3CMe), 128.6 ($C_{Ar}H$), 128.2 (Ph_3CMe), 127.7 ($C_{Ar}H$), 124.1 ($C_{Ar}H$), 121.5 ($C_{Ar}H$), 116.6 ($C_{Py}H$), 106.9 ($C_{Py}H$), 53.5 ($NCHMe_2$), 50.3 ($MeCNCHMe_2$), 50.7 (Ph_3CMe), 50.2 ($NCHMe_2$), 34.9 ($C_{Ar}CHMe_2$), 31.0 ($C_{Ar}CHMe_2$), 30.4 (Ph_3CMe), 28.7 ($C_{Ar}CHMe_2$), 26.1 ($C_{Ar}CHMe_2$), 25.7 ($C_{Ar}CHMe_2$), 24.1 ($NCHMe_2$), 24.0 ($MeCNCHMe_2$), 23.5 ($C_{Ar}CHMe_2$), 21.1 ($NCHMe_2$), 20.9 ($MeCNCHMe_2$), 13.3 ($MeCNCHMe_2$) ppm (*i*-C_6F_5 were not observed). ^{19}F NMR (C_6D_5Br, 376.5 MHz, 298 K): –131.8 (m, *o*-C_6F_5), –162.3 (m, *p*-C_6F_5), -166.1 (m, *m*-C_6F_5) ppm. ^{11}B NMR (C_6D_5Br, 128.4 MHz, 298 K): –16.4 ppm.

NMR tube scale synthesis of [(Ap^{2})Ti{NC(Ph)N^{i}Pr$_2$}(CH$_2$Ph)][BAr$^{F}_4$] (47-[BAr$^{F}_4$]). To a solution of (Ap^{2})Ti{NC(Ph)N^{i}Pr$_2$}(CH$_2$Ph)$_2$ (**38**, 0.030 g, 0.034 mmol) in C_6D_5Br (0.5 mL) was added [Ph_3C][BAr$^{F}_4$] (0.031 g, 0.034 mmol) resulting in the formation of a dark brown solution. The solution was transferred to an NMR tube and the NMR spectra recorded after 5 minutes.

^{1}H NMR (C_6D_5Br, 400.2 MHz, 298 K): 7.58–7.54 (1 H, m, $C_{Ar}\underline{H}$), 7.46–7.08 (30 H, m, $C_{Ar}\underline{H}$, $C_{Py}\underline{H}$, $\underline{Ph}_3CCH_2\underline{Ph}$, $\underline{Ph}CH_2$), 6.91–6.84 (6 H, m, $C_{Py}\underline{H}$, $\underline{Ph}_3CCH_2\underline{Ph}$), 6.14 (1 H, d, $C_{Py}\underline{H}$, $^{3}J_{HH}$ = 8.4 Hz), 4.04 (2H, s, $Ph_3CC\underline{H}_2Ph$), 3.64 (1 H, br. s, $NC\underline{H}Me_2$), 3.53–3.49 (2 H, m, $NC\underline{H}Me_2$,$C_{Ar}C\underline{H}Me_2$), 3.22–2.99 (5 H, m, $C_{Ar}C\underline{H}Me_2$, $PhC\underline{H}_2$), 2.60 (1 H, br. m, $C_{Ar}C\underline{H}Me_2$), 1.48 (6 H, d, $C_{Ar}CH\underline{Me}_2$, $^{3}J_{HH}$ = 6.6 Hz), 1.39–1.04 (30 H, $NCH\underline{Me}_2$, $C_{Ar}CH\underline{Me}_2$), 0.92 (6 H, br. s, $NCH\underline{Me}_2$) ppm. ^{19}F NMR (C_6D_5Br,

376.5 MHz, 298 K): –131.4 (m, *o*-$C_6\underline{F}_5$), –162.0 (m, *p*-$C_6\underline{F}_5$), –165.8 (m, *m*-$C_6\underline{F}_5$) ppm. ^{11}B NMR (C_6D_5Br, 128.4 MHz, 298 K): –16.0 ppm.

NMR tube scale synthesis of [(Ap^1)Ti{NC(Ph)N^{i}Pr$_2$}(CH$_2$Ph)(OPPh$_3$)] [BAr$^F_4$] (48-[BAr$^F_4$]). To a solution of (Ap^1)Ti{NC(Ph)N^{i}Pr$_2$}(CH$_2$Ph)$_2$ (**36**, 0.030 g, 0.039 mmol) and Ph_3PO (0.011 g, 0.039 mmol) in C_6D_5Br (0.5 mL) was added [Ph_3C][BAr$^F_4$] (0.037 g, 0.039 mmol) resulting in the formation of a dark brown solution. The solution was transferred to an NMR tube and the NMR spectra recorded after 5 minutes, showing the quantitative formation of **48-[BAr$^F_4$]**.

^{1}H NMR (C_6D_5Br, 400.2 MHz, 298 K): 7.61 (4 H, t, OP$\underline{Ph}_3$, $^3J_{HH}$ = 7.7 Hz), 7.41-6.75 (46 H, m, $C_{Ar}\underline{H}$, $C_{Py}\underline{H}$, $\underline{Ph}CCH_2\underline{Ph}$, OP$\underline{Ph}_3$, $CH_2\underline{Ph}$), 6.64 (2 H, d, $C_{Ar}\underline{H}$, $^3J_{HH}$ = 7.6 Hz), 6.31 (1 H, d, $C_{Py}\underline{H}$, $^3J_{HH}$ = 6.9 Hz), 5.71 (1 H, d, $C_{Py}\underline{H}$, $^3J_{HH}$ = 8.1 Hz), 4.78 (1 H, br.m , $NC\underline{H}Me_2$), 4.04 (2 H, s, $PhCC\underline{H}_2Ph$), 3.54 (1 H, sept, $NC\underline{H}Me_2$, $^3J_{HH}$ = 6.9 Hz), 3.15 (1 H, d, $PhC\underline{H}_2$, $^2J_{HH}$ = 10.0 Hz), 2.70 (1 H, d, $PhC\underline{H}_2$, $^2J_{HH}$ = 10.0 Hz), 2.47 (3 H, s, $C_{Ar}\underline{Me}$), 2.43 (3 H, s, $C_{Ar}\underline{Me}$), 2.42 (3 H, s, $C_{Ar}\underline{Me}$), 2.11 (3 H, s, $C_{Ar}\underline{Me}$), 1.98 (3 H, s, $C_{Ar}\underline{Me}$), 1.86 (3 H, s, $C_{Ar}\underline{Me}$), 1.31 (3 H, d, $NCH\underline{Me}_2$, $^3J_{HH}$ = 6.6 Hz), 1.20 (3 H, d, $NCH\underline{Me}_2$, $^3J_{HH}$ = 6.6 Hz), 0.92 (3 H, d, $NCH\underline{Me}_2$, $^3J_{HH}$ = 6.6 Hz), 0.87 (3 H, d, $NCH\underline{Me}_2$, $^3J_{HH}$ = 6.6 Hz) ppm. ^{13}C{^{1}H} NMR (C_6D_5Br, 100.6 MHz, 298 K): 166.7 ($NC_{Py}N$), 163.9 ($N\underline{C}C_{Ar}$), 156.6 ($N\underline{C}_{Py}C_{Ar}$), 148.9 (br., d, *o*-$\underline{C}_6F_5$, $^1J_{CF}$ = 241.8 Hz), 148.2 (*i*-$Ph_3CCH_2\underline{Ph}$), 148.1 (*i*-$CH_2\underline{Ph}$), 147.0 (*i*-$\underline{Ph}_3CCH_2Ph$), 144.3 ($\underline{C}_{Py}H$), 144.2 ($N\underline{C}_{Ar}$), 142.4 ($NC_{Py}\underline{C}_{Ar}$),138.7 ($\underline{Ph}_3CCH_2\underline{Ph}$), 138.6 (br., d, *p*-$\underline{C}_6F_5$, $^1J_{CF}$ = 239.8 Hz), 136.8 (br., d, *m*-$\underline{C}_6F_5$, $^1J_{CF}$ = 235.9 Hz), 136.1 (*p*-OP$\underline{Ph}_3$), 135.6 ($NC\underline{C}_{Ar}$), 135.1 ($\underline{C}_{Ar}Me$), 134.4 (*i*-OP$\underline{Ph}_3$), 133.3 (*m*-$CH_2\underline{Ph}$), 132.8 (d, $^2J_{CP}$ = 11.4 Hz, *o*-OP$\underline{Ph}_3$), 132.6 ($\underline{C}_{Ar}H$), 132.5 (*o*-$CH_2\underline{Ph}$), 131.8 ($\underline{C}_{Ar}Me$), 131.7 ($\underline{C}_{Ar}Me$), 131.5 ($\underline{Ph}_3CCH_2\underline{Ph}$), 129.4 (d, $^2J_{CP}$ = 11.2 Hz, *m*-OP$\underline{Ph}_3$), 129.1 ($\underline{Ph}_3CCH_2\underline{Ph}$) 129.0 ($\underline{C}_{Ar}H$), 128.9 ($\underline{C}_{Ar}H$), 128.5 ($\underline{C}_{Ar}H$), 127.9 ($\underline{Ph}_3CCH_2\underline{Ph}$), 127.6 ($\underline{C}_{Ar}H$), 126.2 ($\underline{Ph}_3CCH_2\underline{Ph}$), 125.7 (*p*-$CH_2\underline{Ph}$), 124.8 ($\underline{Ph}_3CCH_2\underline{Ph}$), 123.1 ($\underline{C}_{Ar}H$), 114.5 ($\underline{C}_{Py}H$), 102.3 ($\underline{C}_{Py}H$), 86.0 ($Ti\underline{C}H_2$), 58.8 ($Ph_3\underline{C}CH_2Ph$), 50.7 ($NC\underline{H}Me_2$), 46.6 ($Ph_3C\underline{C}H_2Ph$), 22.2 ($NCH\underline{Me}_2$), 22.1 ($NCH\underline{Me}_2$), 21.4 ($C_{Ar}\underline{Me}$), 21.0 ($NCH\underline{Me}_2$), 20.9 ($C_{Ar}\underline{Me}$), 20.8 ($C_{Ar}\underline{Me}$), 20.7 ($NCH\underline{Me}_2$), 20.0 ($C_{Ar}\underline{Me}$), 19.1 ($C_{Ar}\underline{Me}$), 19.0 ($C_{Ar}\underline{Me}$) ppm (*i*-$\underline{C}_6F_5$ were not observed). ^{19}F NMR (C_6D_5Br, 376.5 MHz, 298 K): -131.4 (m, *o*-$C_6\underline{F}_5$), –161.9 (m, *p*-$C_6\underline{F}_5$), –165.8 (m, *m*-$C_6\underline{F}_5$) ppm. ^{11}B NMR (C_6D_5Br, 128.4 MHz, 298 K): –15.9 ppm. ^{31}P{^{1}H} NMR (C_6D_5Br, 162.0 MHz, 298 K): 50.1 ppm.

Li{[MeC(NDipp)$_2$] (49). To a toluene (25 mL) solution of bis(2,6-diisopropylphenyl)carboiimide (0.500 g, 1.38 mmol) at 0 ^{o}C was added dropwise MeLi (0.86 mL, 1.6 M in diethyl ether, 1.38 mmol) and the resulting solution was allowed to warm to room temperature and subsequently stirred for 16 h. The volatiles were then removed *in vacuo* and the white solid was extracted into *n*-hexanes (20 mL). The *n*-hexanes were removed *in vacuo* and the resulting solid was dried *in vacuo* resulting **49** as a white powder. Yield: 0.423 g (80%).

^{1}H NMR (C_6D_6, 400.2 MHz, 298 K): 7.07 (6 H, s, $C_{Dipp}\underline{H}$), 3.35 (4 H, sept, $C_{Dipp}C\underline{H}Me_2$, $^{3}J_{HH}$ = 6.9 Hz), 1.39 (3 H, s, $\underline{Me}CNC_{Dipp}$), 1.20 (12 H, d, $C_{Dipp}CH\underline{Me}_2$, $^{3}J_{HH}$ = 6.9 Hz), 1.06 (12 H, d, $C_{Dipp}CH\underline{Me}_2$, $^{3}J_{HH}$ = 6.9 Hz) ppm. ^{13}C{^{1}H} NMR (C_6D_6, 100.6 MHz, 298 K): 170.8 ($Me\underline{C}NC_{Dipp}$), 145.5 (*i*-$MeCN\underline{C}_{Dipp}$), 142.9 ($\underline{C}_{Dipp}CHMe_2$), 124.3 ($\underline{C}_{Dipp}H$), 124.0 ($\underline{C}_{Dipp}H$), 28.9 ($C_{Dipp}\underline{C}HMe_2$), 24.3 ($C_{Dipp}CH\underline{Me}_2$), 24.0 ($C_{Dipp}CH\underline{Me}_2$), 16.9 ($\underline{Me}CNC_{Dipp}$) ppm. EI-MS: *m/z* = 378 [*M*–Li]$^{+}$, 335 [*M*–^{i}Pr]$^{+}$. Anal. found (calcd. for $C_{26}H_{39}N_2$): C, 80.89 (81.00); N, 7.19 (7.29); H, 9.78 (9.70) %. IR (NaCl plates, Nujol mull, cm^{-1}): 1502 (s), 1463 (s), 1435 (s), 1404 (m), 1379 (s), 1361 (s), 1314 (m), 1255 (w), 1098 (w), 1056 (w), 793 (m).

Ti{NC(Ph)N^{i}Pr$_2$}{MeC(NDipp)$_2$}Cl$_2$ (50). To a Schlenk tube, Li{[MeC(NDipp)$_2$] (**49**, 0.50 g, 1.3 mmol) and Ti{NC(Ph)N^{i}Pr$_2$}Cl$_3$ (**4.02**, 0.47 g, 1.3 mmol) were added. The Schlenk tube was cooled down to –78 ^{o}C and cold diethyl ether (15 mL) was added. The resulting solution was stirred and allowed to slowly warm to room temperature where upon a colour change to orange/red was observed. The mixture was subsequently stirred for further 16 h after which time the volatiles were removed *in vacuo*. The orange/red solid was extracted into benzene (15 mL) and separated from the insoluble LiCl salt by filtration. The solvent was removed *in vacuo* and the dark yellow solid was washed with pentane (3 × 5 mL) giving complex **50**. Yield: 0.61 g (67%).

^{1}H NMR ($C_6D_5CD_3$, 499.9 MHz, 298 K): 7.13–7.10 (5 H, m, $C_{Ar}\underline{H}$), 7.00–6.98 (6 H, m, $C_{Dipp}\underline{H}$), 3.70 (4 H, sept, $C_{Dipp}C\underline{H}Me_2$, $^{3}J_{HH}$ = 6.9 Hz), 3.39–3.21 (2 H, m, $NC\underline{H}Me_2$), 1.53 (6 H, br. s, $NCH\underline{Me}_2$), 1.42 (3 H, s, $\underline{Me}CNC_{Dipp}$), 1.36 (12 H, d, $C_{Dipp}CH\underline{Me}_2$, $^{3}J_{HH}$ = 6.9 Hz), 1.22 (12 H, d, $C_{Dipp}CH\underline{Me}_2$, $^{3}J_{HH}$ = 6.9 Hz), 0.55 (6 H, d, $NCH\underline{Me}_2$, $^{3}J_{HH}$ = 6.0 Hz) ppm. ^{13}C{^{1}H} NMR ($C_6D_5CD_3$, 125.7 MHz, 298 K): 180.0 ($Me\underline{C}NC_{Dipp}$), 163.2 ($N\underline{C}C_{Ar}$), 144.0 (*i*-$MeCN\underline{C}_{Dipp}$), 142.9 ($\underline{C}_{Dipp}CHMe_2$), 129.1

(NC$\underline{C}_{Ar}$), 129.0 ($\underline{C}_{Ar}$H), 128.2 ($\underline{C}_{Ar}$H), 126.4 ($\underline{C}_{Dipp}$H), 126.3 ($\underline{C}_{Dipp}$H), 123.7 ($\underline{C}_{Ar}$H), 52.4 (N$\underline{C}$HMe$_2$), 49.6 (N$\underline{C}$HMe$_2$), 28.6 (C$_{Dipp}\underline{C}$HMe$_2$), 24.8 (C$_{Dipp}\underline{C}$HMe$_2$), 24.7 (C$_{Dipp}\underline{C}$HMe$_2$), 23.3 (NCH$\underline{Me}_2$), 22.5 (NCH$\underline{Me}_2$), 15.4 ($\underline{Me}$CNC$_{Dipp}$) ppm. EI-MS: *m/z* = 698 $[M]^+$, 495 $[M–NC(Ph)N^iPr]^+$. Anal. found (calcd. for $C_{39}H_{56}N_4TiCl_2$): C, 66.84 (66.95); N, 8.01(8.14); H, 8.07 (8.19) %. IR (NaCl plates, Nujol mull, cm^{-1}): 1641 (w), 1515 (m), 1463 (m), 1368 (m), 1348 (w), 1322 (w), 1217 (w), 1180 (w), 151 (w), 1100 (w), 1056 (m), 1018 (w), 893 (w), 846 (w), 794 (m), 782 (m), 749 (w), 741 (w), 721 (w), 697 (w), 666 (w).

Ti{NC(Ph)N^{i}Pr$_2$}{MeC(NDipp)$_2$}Me$_2$ (51). To a stirring benzene (20 mL) solution of Ti{NC(Ph)N^{i}Pr$_2$}{MeC(NDipp)$_2$}Cl$_2$ (**50**, 1.0 g, 1.5 mmol) at 5 °C was added dropwise MeLi (1.9 mL, 1.6 M in Et$_2$O, 3.1 mmol) and the resulting solution was allowed to warm up to room temperature and stirred for a further 16 h. The volatiles were then removed *in vacuo* and the oily solid was then extracted into pentane (20 mL) to filter away from the insoluble LiCl salt. Complex **51** was isolated as an olive green solid following removal of pentane *in vacuo*. Yield: 0.56 g (60%).

^{1}H NMR (Toluene-d_8, 400.2 MHz, 223 K): 7.16–6.96 (11 H, m, C$_{Ar}\underline{H}$, C$_{Dipp}\underline{H}$), 3.72-3.69 (4 H, m, C$_{Dipp}$C$\underline{H}$Me$_2$), 3.52–3.46 (1 H, m, NC$\underline{H}$Me$_2$), 2.81–2.75 (1 H, m, NC$\underline{H}$Me$_2$), 1.61 (6 H, d, NCH$\underline{Me}_2$, $^3J_{HH}$ = 5.9 Hz), 1.50 (3 H, s, $\underline{Me}$CNC$_{Dipp}$), 1.38 (12 H, d, C$_{Dipp}$CH$\underline{Me}_2$, $^3J_{HH}$ = 7.2 Hz), 1.32 (12 H, d, C$_{Dipp}$CH$\underline{Me}_2$, $^3J_{HH}$ = 7.2 Hz), 1.07 (6 H, s, Ti$\underline{Me}$), 0.55 (6 H, d, NCH$\underline{Me}_2$, $^3J_{HH}$ = 5.9 Hz) ppm. ^{13}C{^{1}H} NMR (Toluene-d_8, 100.6 MHz, 223 K): 181.4 (Me$\underline{C}$NC$_{Dipp}$), 160.1 (N$\underline{C}$C$_{Ar}$), 143.8 ($\underline{C}_{Dipp}$CHMe$_2$), 143.3 (*i*-MeCN$\underline{C}_{Dipp}$), 142.2 (NC$\underline{C}_{Ar}$), 129.6 ($\underline{C}_{Ar}$H), 129.0 ($\underline{C}_{Ar}$H), 128.7 ($\underline{C}_{Dipp}$H), 127.9 ($\underline{C}_{Dipp}$H), 123.5 ($\underline{C}_{Ar}$H), 58.2 (Ti$\underline{Me}$), 51.8 (NC$\underline{H}$Me$_2$), 47.1 (NC$\underline{H}$Me$_2$), 28.1 (C$_{Dipp}$C$\underline{H}$Me$_2$), 24.7 (C$_{Dipp}$CH$\underline{Me}_2$), 24.6 (C$_{Dipp}$CH$\underline{Me}_2$) 19.6 (NCH$\underline{Me}_2$), 19.5 (NCH$\underline{Me}_2$), 15.3 ($\underline{Me}$CNC$_{Dipp}$) ppm. EI-MS: *m/z* = 77 $[TiMe_2]^+$, 455 $[M – (NC(Ph)N^iPr_2)]^+$. Anal. found (calcd. for $C_{41}H_{62}N_4Ti$): C, 74.52 (74.74); N, 8.45 (8.50); H, 9.68 (9.49)%. IR (NaCl plates, Nujol mull, cm^{-1}): 2924 (s), 1553 (m), 1462 (m), 1377 (w), 1338 (w), 1319 (w), 1259 (m), 1097 (w), 1023 (w), 794 (w). Diffraction-quality crystals were grown from a dilute pentane solution at room temperature.

Reaction of Li[hpp] and Ti{NC(Ph)N^{i}Pr$_2$}Cl$_3$ (4.02). To a solution of hpp (0.250 g, 1.80 mmol) in THF (10 mL) at –78 ºC was added dropwise ^{n}BuLi (1.12 mL, 1.6 M in

hexane, 1.80 mmol). The solution was allowed to warm to room temperature and stirred overnight. This solution was added over a period of 20 minutes to a solution of **4.02** (0.64 g, 1.80 mmol) at –78 ºC in THF (5 mL) and allowed to warm to room temperature. The volatiles were then removed *in vacuo* and the orange solid was washed with pentane. A number of products were observed by NMR spectroscopy and could not be separated. Diffraction-quality crystals of **52** were grown from a benzene solution at room temperature.

NMR tube scale synthesis of [Ti{NC(Ph)N^{i}Pr$_2$}{MeC(NDipp)$_2$}Me] [BAr$^{F}_4$] (53-[BAr$^{F}_4$]). To a solution of Ti{NC(Ph)N^{i}Pr$_2$}{MeC(NDipp)$_2$}Me$_2$ (**51**, 0.010 g, 0.015 mmol) in C_6D_5Br (0.3 mL) was added a solution of [Ph$_3$C][BAr$^{F}_4$] (0.014 g, 0.015 mmol) in C_6D_5Br (0.3 mL) resulting in the formation of a dark red solution. The solution was transferred to an NMR tube and the NMR spectra recorded after 5 minutes, showing quantitative formation of **53-[BAr$^{F}_4$]**.

^{1}H NMR (C_6D_5Br, 400.2 MHz, 298 K): 7.46–7.26 (26 H, m, Ph$_3$CMe, C$_{Ar}$H, C$_{Dipp}$H), 3.69–3.58 (2 H, m, NCHMe$_2$), 3.20 (2 H, br. s, C$_{Dipp}$CHMe$_2$), 2.96 (2 H, br. m, C$_{Dipp}$CHMe$_2$), 2.24 (3H, s, Ph$_3$CMe), 1.87 (3 H, s, TiMe), 1.77 (3H, s, MeCNC$_{Dipp}$), 1.47 (6 H, d, NCHMe$_2$, $^{3}J_{HH}$ = 6.8), 1.36–1.31 (12 H, m, C$_{Dipp}$CHMe$_2$), 1.09–1.05 (12H, m, C$_{Dipp}$CHMe$_2$), 1.00 (6H, d, NCHMe$_2$, $^{3}J_{HH}$ = 6.8) ppm. ^{19}F NMR (C_6D_5Br, 376.5 MHz, 298 K): –131.3 (m, *o*-C$_6$F$_5$), –161.9 (m, *p*-C$_6$F$_5$), –165.7(m, *m*-C$_6$F$_5$) ppm. ^{11}B NMR (C_6D_5Br, 128.4 MHz, 298 K): –16.0 ppm.

Synthesis of [Ti{NC(Ph)N^{i}Pr$_2$}{MeC(NDipp)$_2$CMe}{MeC(N^{i}Pr$_2$)$_2$}][BAr$^{F}_4$] (54-[BAr$^{F}_4$]). To a stirring fluorobenzene (3 mL) solution of Ti{NC(Ph)N^{i}Pr$_2$}{(NDipp)$_2$CMe}Me$_2$ (**51**, 0.040 g, 0.067 mmol) and diisopropylcarboiimide (9.4 µL, 0.067 mmol) was added dropwise a fluorobenzene (2 mL) solution of [Ph$_3$C][BAr$^{F}_4$] (0.056 g, 0.067 mmol). After 1 h, pentane (5 mL) was added resulting in the formation of a dark red oil. The pentane/fluorobenzene was decanted away and the oil washed with pentane (3 × 3 mL). The remaining solid was dried *in vacuo* to yield **54-[BAr$^{F}_4$]** as a red solid. Yield: 45 mg (52%).

^{1}H NMR (C_6D_5Br, 499.9 MHz, 298 K): 7.36–7.22 (11 H, m, C$_{Ar}$H, C$_{Dipp}$H), 3.59 (2 H, br., NCHMe$_2$), 3.33 (6 H, br, C$_{Dipp}$CHMe$_2$, MeCNCHMe$_2$), 1.98 (3 H, s, MeCNCHMe$_2$), 1.62 (3 H, s, MeCNC$_{Dipp}$), 1.45 (6 H, d, NCHMe$_2$, $^{3}J_{HH}$ = 6.1 Hz) 1.35 (12 H, d, C$_{Dipp}$CHMe$_2$, $^{3}J_{HH}$ = 6.7 Hz), 1.29 (12 H, C$_{Dipp}$CHMe$_2$, $^{3}J_{HH}$ = 6.7 Hz),

0.99 (6 H, d, NCH$\underline{Me}_2$, $^3J_{HH}$ = 6.1 Hz), 0.83 (6 H, d, MeCNCH$\underline{Me}_2$, $^3J_{HH}$ = 6.3 Hz), 0.76 (6 H, d, MeCNCH$\underline{Me}_2$, $^3J_{HH}$ = 6.7 Hz) ppm. $^{13}C\{^1H\}$ NMR (C_6D_5Br, 125.7 MHz, 298 K): 181.5 (Me$\underline{C}NC_{Dipp}$), 174.5 (Me$\underline{C}NCHMe_2$), 165.6 (N$\underline{C}C_{Ar}$), 148.8 (br., d, *o*-$\underline{C}_6F_5$, $^1J_{CF}$ = 240.9 Hz), 142.9 (*i*-MeCN$\underline{C}_{Dipp}$), 141.0 ($\underline{C}_{Dipp}CHMe_2$), 138.5 (br., d, *p*-$\underline{C}_6F_5$, $^1J_{CF}$ = 230.2 Hz), 137.5 (NC$\underline{C}_{Ar}$), 136.5 (br., d, *m*-$\underline{C}_6F_5$, $^1J_{CF}$ = 235.9 Hz), 129.1 ($\underline{C}_{Ar}H$), 128.5 ($\underline{C}_{Ar}H$), 127.8 ($\underline{C}_{Dipp}H$), 125.8 ($\underline{C}_{Ar}H$), 124.6 ($\underline{C}_{Dipp}H$), 51.1 (MeCN$\underline{C}HMe_2$), 49.5 (N$\underline{C}HMe_2$), 28.4 ($C_{Dipp}\underline{C}HMe_2$), 25.1 ($C_{Dipp}CH\underline{Me}_2$), 24.3 ($C_{Dipp}CH\underline{Me}_2$), 23.8 (MeCNCH$\underline{Me}_2$), 23.5 (MeCNCH$\underline{Me}_2$), 21.7 (NCH$\underline{Me}_2$), 20.6 (NCH$\underline{Me}_2$), 17.1 ($\underline{Me}CNC_{Dipp}$), 12.5 ($\underline{Me}CNCHMe_2$) ppm (*i*-$\underline{C}_6F_5$ were not observed). ^{19}F NMR (C_6D_5Br, 470.4 MHz, 298 K): –131.3 (m, *o*-$C_6\underline{F}_5$), –161.9 (m, *p*-$C_6\underline{F}_5$), –165.7 (m, *m*-$C_6\underline{F}_5$) ppm. ^{11}B NMR (C_6D_5Br, 160.4 MHz, 298 K): –16.0 ppm. Anal. found (calcd. for $C_{71}H_{75}BF_{20}N_6Ti$): C, 59.03, (58.85); N, 5.63 (5.80); H, 4.93 (5.08)%. IR (NaCl plates, Nujol mull, cm^{-1}): 2924 (s), 1540 (m), 1513 (w), 1460 (s), 1377 (m), 1317 (w), 1260 (w), 1084 (m), 1022 (w), 979 (s), 795 (m), 744 (m), 660 (w).

Ti{NC(Ph)N^{i}Pr$_2$}{MeC^{i}PrN$_2$}Cl$_2$ (4.07). Li[MeC(N^{i}Pr)$_2$] (1.00 g, 6.76 mmol) and Ti{NC(Ph)(N^{i}Pr$_2$)}Cl_3 (**4.02**, 2.42 g, 6.76 mmol) were placed in the same Schlenk tube. The Schlenk tube was cooled down to 5 °C and cold benzene (15 mL) was added. The resulting solution was slowly warmed room temperature and stirred for 12 h. The volatiles were removed under reduced pressure and the resulting solid was extracted into benzene (15 mL). After the filtration, the volatiles were removed *in vacuo* affording **4.07** as an orange solid. Yield: 2.23g (71%). The compounds ^1H NMR spectrum matched the spectrum previously reported.[24]

Ti{NC(Ph)N^{i}Pr$_2$}{PhC(NSiMe$_3$)$_2$}Cl$_2$ (4.08). Li[PhC(NSiMe$_3$)$_2$] (2.00 g, 7.40 mmol) and Ti{NC(Ph)(N^{i}Pr$_2$)}Cl_3 (**4.02**, 2.64 g, 7.40 mmol) were placed in the same schlenk. The schlenk was cooled down to 5 ^{0}C and cold benzene (15 mL) was added to the schlenk. The reaction mixture was allowed to slowly warm up to room temperature and stirred for 12 h. The volatiles were removed under reduced pressure and the resulting solid was extracted into diethyl ether (15 mL). After the filtration, the volatiles were removed *in vacuo* and the resulting orange solid was washed with cold pentane (3 × 5 mL), affording the title compound **4.08** as a pure orange solid. Yield: 2.14 (50%). The compounds ^1H NMR spectrum atched the spectrum previously reported.[24]

$(Ap^1)_2TiCl_2$ (55). To a stirring toluene solution (5 mL) of $TiCl_4$ (0.133 mL, 1.22 mmol) was added a toluene solution (10 mL) of **30** (1.0 g, 2.43 mmol), and an immediate colour change to purple was observed. The reaction mixture was stirred for 3 h. All volatiles were removed under reduced pressure. The purple solid was extracted into benzene (3 × 10 mL). Benzene was removed *in vacuo* resulting in **55** as a purple powder. Yield: 0.489 g (52%).

^{1}H NMR (C_6D_6, 499.9 MHz, 298 K): 6.82–6.80 (6 H, m, $C_{Ar}\underline{H}$, $C_{Py}\underline{H}$), 6.43 (4 H, s, $C_{Ar}\underline{H}$), 6.24 (2 H, d, $C_{py}\underline{H}$, $^3J_{HH}$ = 8.8 Hz), 5.42 (2 H, d, $C_{py}\underline{H}$, $^3J_{HH}$ = 8.8 Hz), 2.40 (6 H, s, $C_{Ar}\underline{Me}$), 2.29 (12 H, s, $C_{Ar}\underline{Me}$), 2.26 (12 H, s, $C_{Ar}\underline{Me}$), 2.16 (6 H, s, $C_{Ar}\underline{Me}$) ppm. $^{13}C\{^1H\}$ NMR (C_6D_6, 125.7 MHz, 298 K): 162.3 ($N\underline{C}_{Py}N$), 155.0 ($N\underline{C}_{Py}C_{Ar}$), 142.8 ($N\underline{C}_{Ar}$), 140.7 ($NC_{Py}\underline{C}_{Ar}$), 137.1 ($\underline{C}_{Ar}Me$), 136.4 ($\underline{C}_{Ar}Me$), 135.7 ($\underline{C}_{Ar}Me$), 133.4 ($\underline{C}_{Ar}Me$), 128.6 ($\underline{C}_{Ar}H$), 128.2 ($\underline{C}_{Ar}H$), 118.7 ($\underline{C}_{Py}H$), 100.2 ($\underline{C}_{Py}H$), 21.7 ($C_{Ar}\underline{Me}$), 21.1 ($C_{Ar}\underline{Me}$), 21.0 ($C_{Ar}\underline{Me}$), 19.0 ($C_{Ar}\underline{Me}$) ppm. MS: *m/z* = 392 $[Ap^1]^+$. Anal. found (calcd. for $C_{46}H_{44}N_4TiCl_2$): C, 70.77 (71.04); N, 6.98 (7.20); H, 6.70 (6.40)%. IR (NaCl plates, Nujol mull, cm^{-1}): 1640 (w), 1613 (m), 1584 (s), 1563 (m), 1454 (s), 1377 (m), 1337 (w), 1298 (w), 1260 (m), 1215 (m), 1151 (m), 1085 (w), 1065 (w), 1031 (w), 895 (m), 847 (w), 797 (m), 545 (m).

$Ti\{PhC(NSiMe_3)_2\}_2Cl_2$ (4.09). The bis-benzamidinate complex was synthesised as described in literature.[25-27] Bis(trimethylsilyl)amine (5 mL, 24.0 mmol) in *n*-hexanes (10 mL) was cooled to −10 ºC and *n*-butyl lithium (15 mL, 24.0 mmol) was added dropwise over a period of 1 h. The reaction mixture was allowed to warm up to room temperature and stirred for 16 h. The solution volume was reduced to 50% and the resulting off-white solid was collected and dried under reduced pressure. $Li[N(SiMe_3)_2]$ (3.48 g, 20.8 mmol) was dissolved in diethyl ether (10 mL) and benzonitrile (2.15 mL, 20.8 mmol) was added. The reaction mixture was stirred at room temperature for 48 h and the resulting solid was recrystallized from *n*-hexanes. $Li[PhC(NSiMe_3)_2]$ (1.00 g, 3.7 mmol) was dissolved in toluene (10 mL) and added to a solution of $TiCl_4$ (0.20 mL, 1.85 mmol) in toluene (5 mL) and stirred for 16 h. The solvent was reduced to 50% and slow cooling of the reaction mixture to −30 ºC overnight induced the formation of red crystals. The crystals were cold filtered and dried *in vacuo* yielding the title compound **4.09**. Yield: 0.53 g (49%). The ^{1}H NMR spectrum matched the spectrum previously reported.[25]

Ti{PhC(NSiMe$_3$)$_2$}$_2$Me$_2$ (4.10). This complex was synthesised as described in literature.[27, 28] Methyl lithium (1.6 M in Et_2O, 1.0 mL, 1.66 mmol) was slowly added to a solution of Ti{PhC(NSiMe$_3$)$_2$}Cl$_2$ (**4.09**, 0.53 g, 0.83 mmol) in benzene (5 mL) at 5 ºC. The reaction was stirred for 16 h and the byproduct, LiCl, was separated by filtration and the solvent was removed under reduced vacuum. The orange solid was recrystallised from pentane, giving **4.10** as orange crystals. Yield: 0.43 g (86%). The compounds ^{1}H NMR spectrum matched the spectrum previously reported.[28]

Ti{NC(Ph)N^{i}Pr$_2$}$_2$Cl$_2$ (4.11). A THF solution of MeMgCl (5.9 mL, 3.0 M, 17.8 mmol) was added to a solution of di*iso*propylamine (2.5mL, 17.8 mmol) in toluene (20 mL) and heated to 80 °C for 2 h resulting in a off-white precipitate. The reaction mixture was cooled to 0 °C, benzonitrile (1.8 mL, 17.8 mmol) was added and the mixture was allowed to warm to room temperature and subsequently stirred for 2 days. $TiCl_4$ (0.97 mL, 8.9 mmol) was dissolved in toluene and the Grignard-containing solution was added slowly at room temperature. The reaction was stirred for a further 16 h and dioxane was added. The solution was filtered away from the solid and the volatiles removed *in vacuo* to give **4.11** as a light-brown solid. Yield: 3.5 g (65%). Single crystals suitable for X-ray diffraction were grown from a benzene solution at room temperature. The compounds ^{1}H NMR spectrum matched the spectrum previously reported.[29]

Ti{NC(Ph)N^{i}Pr$_2$}$_2$Me$_2$ (4.12). To a solution of Ti{NC(Ph)N^{i}Pr$_2$}$_2$Cl$_2$ (**4.11**, 1.0 g, 1.9 mmol) in THF (10 mL) a THF solution of MeMgCl (1.3 mL, 3.9 mmol, 3.0M) was added at room temperature. The reaction mixture was stirred overnight and all volatlies were removed under reduced pressure. The solid was extracted into pentane and dioxane (2 mL) was added. The resulting solution was filtered and dried *in vacuo* resulting in **4.12** as a dark brown solid. Yield: 0.408 g (44%). The compounds ^{1}H NMR spectrum matched the spectrum previously reported.[29]

6.9 Experimental details and characterising data for Chapter Five

6.9.1 Characterising data

NMR tube scale synthesis of [(i Bu)$_2$Al]O[iBuAl(BHT)] (56). To a C_6D_5 solution (0.2 mL) of DiBAlO (0.156 mL, 0.045 mmol, 10 wt% in toluene) was added a C_6D_5

solution (0.3 mL) of BHT-H (0.01 g, 0.045 mmol) and the NMR spectra were recorded within 5 minutes showing quantitative formation of **56**.

^{1}H NMR (C_6D_5Br, 400.2 MHz, 298 K): 7.11 (2 H, s, $OC_6\underline{H}_2{}^{t}Bu_2Me$), 2.28 (3 H, s, $OC_6H_2{}^{t}Bu_2\underline{Me}$), 2.02 (2 H, appt. sept, $Al(CH_2C\underline{H}Me_2)_2$, $^{3}J_{HH}$ = 6.7 Hz), 1.66–1.61 (1 H, m, $AlCH_2C\underline{H}Me_2$), 1.49 (18 H, s, $OC_6H_2{}^{t}\underline{Bu}_2Me$), 1.03 (12 H, d, $Al(CH_2CH\underline{Me}_2)_2$, $^{3}J_{HH}$ = 6.7 Hz), 0.86 (6 H, d, $AlCH_2CHMe_2$, $^{3}J_{HH}$ = 6.5 Hz), 0.41 (4 H, d, $Al(C\underline{H}_2CHMe_2)_2$, $^{3}J_{HH}$ = 6.7 Hz) ($AlC\underline{H}_2CHMe_2$ was not observed) ppm. $^{13}C\{^{1}H\}$ NMR (C_6D_5Br, 100.6 MHz, 298 K): 153.7 ($O\underline{C}_6H_2{}^{t}Bu_2Me$), 138.1 (*o*-$O\underline{C}_6H_2{}^{t}Bu_2Me$), 127.3 (*p*-$O\underline{C}_6H_2{}^{t}Bu_2Me$), 126.1 (*m*-$O\underline{C}_6H_2{}^{t}Bu_2Me$), 34.7 ($OC_6H_2{}^{t}\underline{Bu}_2Me$), 32.0 ($OC_6H_2{}^{t}\underline{Bu}_2Me$), 28.9 ($AlCH_2\underline{C}HMe_2$), 28.2 ($Al(CH_2CH\underline{Me}_2)_2$), 25.8 ($Al(CH_2\underline{C}HMe_2)_2$), 24.9 ($AlCH_2CH\underline{Me}_2$), 23.9 ($Al(\underline{C}H_2CHMe_2)_2$) ($AlC\underline{H}_2CHMe_2$ was not observed) ppm.

NMR tube scale synthesis of [^{i}BuAlBHT]$_2$O (57). To a C_6D_5 solution (0.2 mL) of DiBAlO (0.156 mL, 0.045 mmol, 10 wt% in toluene) was added a C_6D_5 solution (0.3 mL) of BHT-H (0.02 g, 0.09 mmol) and heated to 85 ºC for 36 h. The reaction was monitored by ^{1}H NMR spectroscopy and after 36 h showed formation of **57**, **56** and unreacted BHT-H in a ratio of 0.75 : 0.20 : 0.05, respectively. The same ^{1}H NMR spectrum of **56** was observed.

57: ^{1}H NMR (C_6D_5Br, 400.2 MHz, 298 K): 7.22 (4 H, s, $OC_6\underline{H}_2{}^{t}Bu_2Me$), 2.33 (6 H, s, $OC_6H_2{}^{t}Bu_2\underline{Me}$), 1.89–1.88 (1 H, m, $AlCH_2C\underline{H}Me_2$), 1.69–1.67 (1 H, m, $AlCH_2C\underline{H}Me_2$), 1.66 (36 H, s, $OC_6\underline{H}_2{}^{t}Bu_2Me$), 0.85 (6 H, d, $AlCH_2CH\underline{Me}_2$, $^{3}J_{HH}$ = 6.4 Hz), 0.77 (6 H, d, $AlCH_2CH\underline{Me}_2$, $^{3}J_{HH}$ = 6.7 Hz), 0.45 (2 H, d, $AlC\underline{H}_2CHMe_2$, $^{3}J_{HH}$ = 7.5 Hz) (2 H $AlC\underline{H}_2CHMe_2$ were not observed) ppm. $^{13}C\{^{1}H\}$ NMR (C_6D_5Br, 100.6 MHz, 298 K): 152.6 ($O\underline{C}_6H_2{}^{t}Bu_2Me$), 138.0 (*o*-$O\underline{C}_6H_2{}^{t}Bu_2Me$), 126.9 (*p*-$O\underline{C}_6H_2{}^{t}Bu_2Me$), 126.1 (*m*-$O\underline{C}_6H_2{}^{t}Bu_2Me$), 34.8 ($OC_6H_2{}^{t}\underline{Bu}_2Me$), 31.8 ($OC_6H_2{}^{t}\underline{Bu}_2Me$), 27.2 ($AlCH_2CH\underline{Me}_2$), 24.5 ($AlCH_2CH\underline{Me}_2$), 24.8 ($AlCH_2\underline{C}HMe_2$), 23.3 ($AlCH_2\underline{C}HMe_2$), 21.7 (br, $Al\underline{C}H_2CHMe_2$), 21.3 ($OC_6H_2{}^{t}Bu_2\underline{Me}$) ($Al\underline{C}H_2CHMe_2$ were not observed) ppm.

NMR tube scale synthesis of [(Ap^{1})Ti{NC(Ph)N^{i}Pr$_2$}BHT][BAr$^{F}_4$] (58-[BAr$^{F}_4$]). To a solution of (Ap^{1})Ti{NC(Ph)N^{i}Pr$_2$}Me$_2$ (**35**, 0.020 g, 0.026 mmol) and BHT-H (0.006 g, 0.026 mmol) in C_6D_5Br (0.3 mL) was added a C_6D_5Br solution (0.2 mL) of [Ph_3C][BAr$^{F}_4$] (0.024 g, 0.026 mmol). The resulting dark red solution was transferred

to an NMR tube and the NMR spectra recorded after 5 minutes, showing formation of **58-[BAr$^{F}_{4}$]** and unreacted BHT-H.

^{1}H NMR (C_6D_5Br, 400.2 MHz, 298 K): 7.42–7.34 (11 H, m, $C_{Ar}\underline{H}$, $C_{Py}\underline{H}$, $\underline{Ph}_3CMe$), 7.31–7.24 (9 H, m, $C_{Ar}\underline{H}$, $C_{Py}\underline{H}$, $\underline{Ph}_3CMe$), 7.14–7.02 (10 H, $C_{Ar}\underline{H}$, $C_{Py}\underline{H}$, $\underline{Ph}_3CMe$, $OC_6\underline{H}_2{}^{t}Bu_2Me$), 6.85 (2 H, d, $C_{Ar}\underline{H}$, $^{3}J_{HH}$ = 6.9 Hz), 6.47 (1 H, d, $C_{Py}\underline{H}$, $^{3}J_{HH}$ = 7.4 Hz), 6.14 (1 H, d, $C_{Py}\underline{H}$, $^{3}J_{HH}$ = 7.4 Hz), 3.80–3.62 (1 H, br m, $NC\underline{H}Me_2$), 3.46 (1 H, sept, $NC\underline{H}Me_2$, $^{3}J_{HH}$ = 7.0 Hz), 2.49 (3 H, s, $C_{Ar}\underline{Me}$), 2.48 (3 H, s, $C_{Ar}\underline{Me}$), 2.39 (3 H, s, $C_{Ar}\underline{Me}$), 2.36 (6 H, s, $C_{Ar}\underline{Me}$, $OC_6H_2{}^{t}Bu_2\underline{Me}$), 2.23 (3 H, s, $Ph_3C\underline{Me}$), 2.19 (3 H, s, $C_{Ar}\underline{Me}$), 2.16 (3 H, s, $C_{Ar}\underline{Me}$), 1.41 (3 H, d, $NCH\underline{Me}_2$, $^{3}J_{HH}$ = 6.7 Hz), 1.34 (3 H, d, $NCH\underline{Me}_2$, $^{3}J_{HH}$ = 6.7 Hz), 1.14 (18 H, s, $OC_6H_2{}^{t}\underline{Bu}_2Me$), 0.92 (3 H, d, $NCH\underline{Me}_2$, $^{3}J_{HH}$ = 6.7 Hz), 0.87 (3 H, d, $NCH\underline{Me}_2$, $^{3}J_{HH}$ = 6.7 Hz) ppm. $^{13}C\{^{1}H\}$ NMR (C_6D_5Br, 100.6 MHz, 298 K): 167.7 ($N\underline{C}_{Py}N$), 162.4 (*i*-$O\underline{C}_6H_2{}^{t}Bu_2Me$), 161.6 ($N\underline{C}C_{Ar}$), 156.6 ($N\underline{C}_{Py}C_{Ar}$), 148.9 (br., d, *o*-$\underline{C}_6F_5$, $^{1}J_{CF}$ = 243.9 Hz), 147.0 ($\underline{Ph}_3CMe$), 144.2 ($\underline{C}_{Py}H$), 140.7 ($N\underline{C}_{Ar}$), 139.8 ($NC\underline{C}_{Ar}$), 138.8 (br., d, *p*-$\underline{C}_6F_5$, $^{1}J_{CF}$ = 233.8 Hz), 137.7 ($NC_{Py}\underline{C}_{Ar}$), 137.0 ($\underline{C}_{Ar}Me$), 136.8 (br., d, *m*-$\underline{C}_6F_5$, $^{1}J_{CF}$ = 233.1 Hz), 136.4 (*o*-$O\underline{C}_6H_2{}^{t}Bu_2Me$), 135.9 ($\underline{C}_{Ar}Me$), 135.8 ($\underline{C}_{Ar}Me$), 133.7 ($\underline{C}_{Ar}Me$), 133.3 (*p*-$O\underline{C}_6H_3{}^{t}BuMe$), 131.7 ($\underline{C}_{Ar}H$), 130.8 ($\underline{C}_{Ar}H$), 129.0 ($\underline{C}_{Ar}H$), 128.8 ($\underline{C}_{Ar}H$), 128.6 ($\underline{Ph}_3CMe$), 128.5 ($\underline{Ph}_3CMe$), 127.6 ($\underline{Ph}_3CMe$), 126.6 ($\underline{C}_{Ar}H$), 125.9 ($\underline{C}_{Ar}H$), 125.8 ($\underline{C}_{Ar}H$), 114.4 ($\underline{C}_{Py}H$), 105.9 ($\underline{C}_{Py}H$), 53.6 ($N\underline{C}HMe_2$), 50.0 ($N\underline{C}HMe_2$), 46.5 ($Ph_3\underline{C}Me$), 31.7 ($OC_6H_2{}^{t}\underline{Bu}_2Me$), 30.4 ($Ph_3C\underline{Me}$), 21.7 ($C_{Ar}\underline{Me}$), 21.6 ($C_{Ar}\underline{Me}$), 21.2 ($NCH\underline{Me}_2$), 21.0 ($C_{Ar}\underline{Me}$), 20.8 ($C_{Ar}\underline{Me}$), 20.6 ($C_{Ar}\underline{Me}$), 20.5 ($NCH\underline{Me}_2$), 20.3 (2 × $NCH\underline{Me}_2$), 18.8 ($OC_6H_2{}^{t}Bu_2\underline{Me}$), 18.6 ($C_{Ar}\underline{Me}$) ppm (*i*-$\underline{C}_6F_5$ were not observed). ^{19}F NMR (C_6D_5Br, 376.5 MHz, 298 K): –131.4 (m, *o*-$C_6\underline{F}_5$), –162.2 (m, *p*-$C_6\underline{F}_5$), –166.0 (m, *m*-$C_6\underline{F}_5$) ppm. ^{11}B NMR (C_6D_5Br, 128.4 MHz, 298 K): –16.1 ppm.

[(Ap^{2})Ti{NC(Ph)N^{i}Pr$_2$}BHT][BAr$^{F}_{4}$] 59-[BAr$^{F}_{4}$]. To a solution of (Ap^{2})Ti{NC(Ph)N^{i}Pr$_2$}Me$_2$ (**37**, 0.030 g, 0.04 mmol) and BHT-H (0.09 g, 0.04 mmol) in fluorobenzene (2 mL) was added a fluorobenzene solution (1 mL) of [Ph$_3$C][BAr$^{F}_{4}$] (0.038 g, 0.04 mmol). After 10 minutes, pentane (8 mL) was added resulting in the formation of a pale red solid. The pentane/fluorobenzene was decanted and the solid washed further with pentane (5 mL). The pale red solid was dried *in vacuo* yielding [(Ap^{2})Ti{NC(Ph)N^{i}Pr$_2$}BHT][BAr$^{F}_{4}$]. Yield: 0.033 g (55%)

^{1}H NMR (C_6D_5Br, 400.2 MHz, 298 K): 7.49–7.25 (10 H, m, $C_{Ar}\underline{H}$, $C_{Py}\underline{H}$), 7.12–7.09 (4 H, m, $OC_6\underline{H}_2{}^{t}$BuMe, $C_{Ar}\underline{H}$), 6.69 (1 H, d, $C_{Py}\underline{H}$, $^{3}J_{HH}$ = 6.8 Hz), 6.17 (1 H, d, $C_{Py}\underline{H}$, $^{3}J_{HH}$ = 7.6 Hz), 4.12 (1 H, br.m, $NC\underline{H}Me_2$), 3.60 (1 H, sept, $NC\underline{H}Me_2$, $^{3}J_{HH}$ = 6.9 Hz), 3.27 (1 H, sept, $C_{Ar}C\underline{H}Me_2$, $^{3}J_{HH}$ = 6.5 Hz), 3.16–3.07 (2 H, overlapping sept, $C_{Ar}C\underline{H}Me_2$), 2.95–2.89 (1 H, m, $C_{Ar}C\underline{H}Me_2$), 2.51 (1 H, sept, $C_{Ar}C\underline{H}Me_2$, $^{3}J_{HH}$ = 6.5 Hz), 2.43 (3 H, s, $OC_6H_2{}^{t}Bu\underline{Me}$), 1.49 (6 H, d, $C_{Ar}CH\underline{Me}_2$, $^{3}J_{HH}$ = 7.1 Hz), 1.41 (3 H, d, $C_{Ar}CH\underline{Me}_2$, $^{3}J_{HH}$ = 6.6 Hz), 1.34–1.26 (12 H, m, $C_{Ar}CH\underline{Me}_2$), 1.23 (18 H, s, $OC_6H_2{}^{t}\underline{Bu}$Me), 1.21–1.14 (15 H, m, $C_{Ar}CH\underline{Me}_2$, $NCH\underline{Me}_2$), 0.98 (3 H, d, $NCH\underline{Me}_2$, $^{3}J_{HH}$ = 6.9 Hz), 0.90 (3 H, d, $NCH\underline{Me}_2$, $^{3}J_{HH}$ = 6.9 Hz) ppm. ^{13}C{^{1}H} NMR ($C_6D_5CD_3$, 100.6 MHz, 298 K): 166.9 ($N\underline{C}_{Py}N$), 165.0 ($N\underline{C}C_{Ar}$), 162.0 (*i*-$O\underline{C}_6H_2{}^{t}$BuMe), 156.7 ($N\underline{C}_{Py}C_{Ar}$), 148.9 (br., d, *o*-$\underline{C}_6F_5$, $^{1}J_{CF}$ = 240.9 Hz), 151.1 ($N\underline{C}_{Ar}$), 146.8 ($\underline{C}_{Ar}CHMe_2$), 144.3 ($NC\underline{C}_{Ar}$), 143.3 ($\underline{C}_{Ar}CHMe_2$), 142.8 ($\underline{C}_{Ar}CHMe_2$), 142.5 ($NC_{Py}\underline{C}_{Ar}$), 141.1 ($\underline{C}_{Py}H$), 138.7 (br., d, *p*-$\underline{C}_6F_5$, $^{1}J_{CF}$ = 236.8 Hz), 136.8 (br., d, *m*-$\underline{C}_6F_5$, $^{1}J_{CF}$ = 233.8 Hz), 136.0 (*o*-$O\underline{C}_6H_2{}^{t}$BuMe), 132.5 (*p*-$O\underline{C}_6H_2{}^{t}$BuMe), 130.9 ($\underline{C}_{Ar}H$), 130.8 ($\underline{C}_{Ar}H$), 129.0 ($\underline{C}_{Ar}H$), 128.1 ($\underline{C}_{Ar}H$), 127.9 (*o*-$\underline{C}_6H_5$), 126.2 (*m*-$O\underline{C}_6H_2{}^{t}$BuMe), 125.3 ($\underline{C}_{Ar}H$), 121.2 ($\underline{C}_{Ar}H$), 116.2 ($\underline{C}_{Py}H$), 108.6 ($\underline{C}_{Py}H$), 53.0 ($N\underline{C}HMe_2$), 51.3 ($N\underline{C}HMe_2$), 34.8 ($OC_6H_2{}^{t}\underline{Bu}_2$Me), 31.4 ($OC_6H_2{}^{t}\underline{Bu}$Me), 30.9 (2 × $C_{Ar}\underline{C}HMe_2$), 29.6 ($C_{Ar}\underline{C}HMe_2$), 28.9 ($C_{Ar}\underline{C}HMe_2$), 26.1 ($C_{Ar}CH\underline{Me}_2$), 26.0 ($C_{Ar}CH\underline{Me}_2$), 25.9 ($NCH\underline{Me}_2$), 25.4 ($NCH\underline{Me}_2$), 24.5 ($C_{Ar}CH\underline{Me}_2$), 24.4 ($C_{Ar}CH\underline{Me}_2$), 24.1 ($C_{Ar}CH\underline{Me}_2$), 24.0 ($C_{Ar}CH\underline{Me}_2$), 23.6 ($C_{Ar}CH\underline{Me}_2$), 23.2 ($C_{Ar}CH\underline{Me}_2$), 21.8 ($C_{Ar}CH\underline{Me}_2$), 21.7 ($NCH\underline{Me}_2$), 21.6 ($NCH\underline{Me}_2$), 21.2 ($OC_6H_2{}^{t}Bu\underline{Me}$), 20.5 ($C_{Ar}CH\underline{Me}_2$) ppm (*i*-$\underline{C}_6F_5$ were not observed). ^{19}F NMR (C_6D_5Br, 376.5 MHz, 298 K): –131.2 (m, *o*-$C_6\underline{F}_5$), –161.7 (m, *p*-$C_6\underline{F}_5$), –165.9 (m, *m*-$C_6\underline{F}_5$) ppm. ^{11}B NMR (C_6D_5Br, 128.4 MHz, 298 K): –16.2 ppm. IR (NaCl plates, Nujol mull, cm^{-1}): 2924 (s), 1642 (w), 1594(w). 1514 (m), 1463 (s), 1377 (m), 1273 (w), 1214 (w), 1194 (w), 1162 (w), 1084 (m), 979 (s), 862 (w), 799 (w), 744 (m), 696 (w), 683 (m), 661 (w). A satisfactory elemental analysis could not be obtained.

6.8.2 Ethylene oligomerisation procedures

NMR tube scale: An example procedure is shown here. A solution of (Ap^1)Ti{NC(Ph)N^{i}Pr$_2$}Me_2 (**35**, 0.005 g, 0.008 mmol) and [Ph_3C][$BAr^F{}_4$] (0.008 g, 0.008 mmol) in C_6D_5Br (0.5 mL) was freeze-pump-thaw-degassed three times. The solution was then exposed to ethylene at a pressure of *ca*. 2.0 atm. A ^{1}H NMR

spectrum was obtained within 3 minutes of the addition. The sample was quenched with MeOH (0.2 mL) and run through a silica plug in pentane to remove any residual titanium species. The resulting polymer was analysed by GPC and NMR spectroscopy.

Small scale: A solution of $(Ap^1)Ti\{NC(Ph)N^iPr_2\}Me_2$ (**35**, 0.02 g, 0.033 mmol) and $[Ph_3C][BAr^F{}_4]$ (0.030 g, 0.033 mmol) in C_6D_5Br (2.0 mL) was freeze-pump-thaw-degassed three times. The solution was then exposed to ethylene at a pressure of *ca*. 3.0 atm for 30 minutes. The solution was stirred for further 30 minutes and an ^1H NMR spectrum was obtained showing the formation of oligomers and polymer.

High Throughput Experiments: The catalytic ethylene oligomerisation experiments were performed at the High Throughput Experimentation facility of ETH Zurich (HTE@ETH) on an Endeavour autoclave system (Biotage) operated inside a glove box (H_2O and O_2 levels were < 0.5 ppm). The ethylene feed was passed through activated Cu/Al_2O_3 sorbent and activated 4 Å molecular sieves before entering the autoclave system. For all experiments the stirring rate was set at 800 rpm. Toluene was saturated with nitrogen and purified by passing through a double activated alumina column and stored over activated Selexsorb CD® sorbent inside a glovebox. DiBAlO was purchased from Sigma as a 10 wt. % in toluene stored under nitrogen. Stock solutions were prepared using volumetric flasks. Gas chromatography was performed on a Thermo Fischer Trace GC 2000 equipped with a flame ionization detector, using a ZB-5 column (L: 30 m, i.d.: 0.25 mm, DF = 0.25 µm) with guardian and helium as the carrier gas with a constant flow of 1.1 mL min^{-1}. The GC-MS was calibrated with a solution of hexane, 1-octene, n-hexadecane and eicosane to allow quantitative analysis of the liquid oligomers.

Glass liners were charged with appropriate amounts of DiBAlO, an internal standard (decalin) and $[Ph_3C][Bar^F{}_4]$ in toluene and loaded into an 8-parallel autoclave. The reactors were leak tested with nitrogen (5.5 bar) and subsequently heated and pressurized with ethylene to desired conditions. Once temperature and pressure stabilised, a toluene solution containing the metal complex was quickly injected and the injector system washed with additional 0.5 mL of toluene. In all runs the total volume of the reaction mixture was 4 mL.

Stock solutions were prepared for $[Ph_3C][BAr^F{}_4]$, DiBAlO, BHT-H and for complexes **35**, **37**. Full detail of conditions are given in the Appendix.

6.10 References

1. R. A. Collins, A. F. Russell, R. T. W. Scott, R. Bernardo, G. H. J. van Doremaele, A. Berthoud and P. Mountford, *Organometallics*, 2017, **36**, 2167-2181.
2. M. Blumer, *Anal. Chem.*, 1957, **29**, 1039-1041.
3. A. R. Ali, H. Ghosh and B. K. Patel, *Tetrahedron Lett.*, 2010, **51**, 1019-1021.
4. U. Zucchini, E. Albizzati and U. Giannini, *J. Organomet. Chem.*, 1971, **26**, 357-372.
5. R. Scott, *DPhil Thesis*, University of Oxford, 2013.
6. Z. Otwinowski and W. Minor, *Processing of X-ray Diffraction Data Collected in Oscillation Mode*, Academic Press, New York, 1997.
7. A. Altomare, G. Cascarano, C. Giacovazzo and A. Guagliardi, *J. Appl. Crystallogr.*, 1994, **27**, 1045-1050.
8. L. Platinus and G. Chapuis, *J. Appl. Cryst.*, 2007, **40**, 284.
9. P. W. Betteridge, J. R. Carruthers, R. I. Cooper, K. Prout and D. J. Watkin, *J. Appl. Crystallogr.*, 2003, **36**, 1487.
10. F. C. Lin, S. S. Stivala and J. A. Biesenberger, *J. Appl. Polym. Sci.*, 1973, **17**, 1073-1090.
11. F. C. Lin, S. S. Stivala and J. A. Biesenberger, *J. Appl. Polym. Sci.*, 1973, **17**, 3465-3476.
12. M. J. Frisch, G. W. Trucks, H. B. Schlegel, G. E. Scuseria, M. A. Robb, J. R. Cheeseman, G. Scalmani, V. Barone, G. A. Petersson, H. Nakatsuji, X. Li, M. Caricato, A. V. Marenich, J. Bloino, B. G. Janesko, R. Gomperts, B. Mennucci, H. P. Hratchian, J. V. Ortiz, A. F. Izmaylov, J. L. Sonnenberg, Williams, F. Ding, F. Lipparini, F. Egidi, J. Goings, B. Peng, A. Petrone, T. Henderson, D. Ranasinghe, V. G. Zakrzewski, J. Gao, N. Rega, G. Zheng, W. Liang, M. Hada, M. Ehara, K. Toyota, R. Fukuda, J. Hasegawa, M. Ishida, T. Nakajima, Y. Honda, O. Kitao, H. Nakai, T. Vreven, K. Throssell, J. A. Montgomery Jr., J. E. Peralta, F. Ogliaro, M. J. Bearpark, J. J. Heyd, E. N. Brothers, K. N. Kudin, V. N. Staroverov, T. A. Keith, R. Kobayashi, J. Normand, K. Raghavachari, A. P. Rendell, J. C. Burant, S. S. Iyengar, J. Tomasi, M. Cossi, J. M. Millam, M. Klene, C. Adamo, R. Cammi, J. W.

Ochterski, R. L. Martin, K. Morokuma, O. Farkas, J. B. Foresman and D. J. Fox, *Gaussian 16 Rev. B.01*, Wallingford, CT, 2016.

13. F. Weigend and R. Ahlrichs, *Phys. Chem. Chem. Phys*, 2005, **7**, 3297-3305.
14. S. Grimme, J. Antony, S. Ehrlich and H. Krieg, *J. Chem. Phys.*, 2010, **132**, 154104.
15. A. M. Lee, N. C. Handy and S. M. Colwell, *J. Chem. Phys.*, 1995, **103**, 10095-10109.
16. R. J. Ditchfield, *J. Chem. Phys.*, 1972, **56**, 5688-5691.
17. W. Kutzelnigg, U. Fleischer and M. Schindler, *IGLOO-II*, Springer-Verlag: Berlin, 1990.
18. B. D. Ward, S. Bellemin-Laponnaz and L. H. Gade, *Angew. Chem. Int. Ed.*, 2005, **44**, 1668-1671.
19. K. Il, Z. Jia‐Min and C. Hoeil, *J. Polym. Sci., Part A: Polym. Chem.*, 2000, **38**, 1687-1697.
20. N. Kawahara, J. Saito, S. Matsuo, H. Kaneko, T. Matsugi, Y. Toda and N. Kashiwa, *Polymer*, 2007, **48**, 425-428.
21. N. M. Scott, T. Schareina, O. Tok and R. Kempe, *Eur. J. Inorg. Chem.*, 2004, 3297-3304.
22. W. P. Kretschmer, A. Meetsma, B. Hessen, T. Schmalz, S. Qayyum and R. Kempe, *Chem. - Eur. J.*, 2006, **12**, 8969-8978.
23. H. Bigmore, *DPhil Thesis*, University of Oxford, 2007.
24. L. Clark, *Part II Thesis*, University of Oxford, 2008.
25. V. Volkis, E. Nelkenbaum, A. Lisovskii, G. Hasson, R. Semiat, M. Kapon, M. Botoshansky, Y. Eishen and M. S. Eisen, *J. Am. Chem. Soc.*, 2003, **125**, 2179-2194.
26. D. G. Dick, J. J. H. Edema, R. Duchateau and S. Gambarotta, *Inorg. Chem.*, 1993, **32**, 1959-1962.
27. V. Volkis, C. Averbuj and M. S. Eisen, *J. Organomet. Chem.*, 2007, **692**, 1940-1950.
28. J. C. Flores, J. C. W. Chien and M. D. Rausch, *Organometallics*, 1995, **14**, 1827-1833.
29. A. Heath, *DPhil Thesis*, University of Oxford, 2011.

Appendix

A1 Addition experimental data for Chapter Five

Table A1. Summary of amounts and conditions in the ethylene oligomerisation with **35** and **37** of experiments described in Chapter Five.

Chemical	Amount (μmol)	Final conc. in RM (mM)	T (°C)	Pressure (bar)	Time (sec)	α	Productivity (mol of liquid C_2H_4 Ti mol^{-1} h^{-1} bar^{-1})
35	8×10^{-2}	2×10^{-2}	40	2	1060	0.57	7.78×10^4
$[Ph_3C][BAr^F{}_4]$	0.16	4×10^{-2}					
DiBAlO	0.4	0.1					
Decalin	19	4.76					
35	8×10^{-2}	2×10^{-2}	40	5	838	0.55	1.44×10^5
$[Ph_3C][BAr^F{}_4]$	0.16	4×10^{-2}					
DiBAlO	0.4	0.1					
Decalin	19	4.76					
35	8×10^{-2}	2×10^{-2}	40	10	917	0.58	4.96×10^4
$[Ph_3C][BAr^F{}_4]$	0.16	4×10^{-2}					
DiBAlO	0.4	0.1					
Decalin	19	4.76					
35	8×10^{-2}	2×10^{-2}	40	15	788	0.58	3.83×10^4
$[Ph_3C][BAr^F{}_4]$	0.16	4×10^{-2}					
DiBAlO	0.4	0.1					
Decalin	19	4.76					
35	8×10^{-2}	2×10^{-2}	50	5	739	0.59	5.95×10^4
$[Ph_3C][BAr^F{}_4]$	0.16	4×10^{-2}					
DiBAlO	0.4	0.1					
Decalin	19	4.76					
35	8×10^{-2}	2×10^{-2}	60	5	689	–	5.01×10^2
$[Ph_3C][BAr^F{}_4]$	0.16	4×10^{-2}					
DiBAlO	0.4	0.1					
Decalin	19	4.76					
35	8×10^{-2}	2×10^{-2}	70	5	643	–	2.16×10^2
$[Ph_3C][BAr^F{}_4]$	0.16	4×10^{-2}					
DiBAlO	0.4	0.1					
Decalin	19	4.76					
35	8×10^{-2}	2×10^{-2}	40	5	643	0.59	2.01×10^4
$[Ph_3C][BAr^F{}_4]$	0.16	4×10^{-2}					
DiBAlO	0.4	0.1					
BHT-H	0.8	0.2					
Decalin	19	4.76					
35	8×10^{-2}	2×10^{-2}	40	5	616	0.59	8.64×10^3
$[Ph_3C][BAr^F{}_4]$	0.16	4×10^{-2}					
DiBAlO	0.4	0.1					
BHT-H	1.6	0.4					
Decalin	19	4.76					

35	0.16	4×10^{-2}					
$[Ph_3C][BAr^F{}_4]$	0.32	8×10^{-2}	40	5	589	0.56	6.11×10^4
Decalin	19	4.76					
35	0.16	4×10^{-2}					
$[Ph_3C][BAr^F{}_4]$	0.32	2×10^{-2}	40	5	317	0.59	1.15×10^4
BHT-H	0.8	0.2					
Decalin	19	4.76					
37	2×10^{-2}	5×10^{-3}					
$[Ph_3C][BAr^F{}_4]$	4×10^{-2}	1×10^{-2}	40	5	627	0.40	5.15×10^5
DiBAlO	0.4	0.1					
Decalin	19	4.76					
37	4×10^{-2}	1×10^{-2}					
$[Ph_3C][BAr^F{}_4]$	8×10^{-2}	2×10^{-2}	50	5	536	0.40	5.73×10^4
DiBAlO	0.4	0.1					
Decalin	19	4.76					
37	4×10^{-2}	1×10^{-2}					
$[Ph_3C][BAr^F{}_4]$	8×10^{-2}	2×10^{-2}	60	5	513	0.43	2.67×10^4
DiBAlO	0.4	0.1					
Decalin	19	4.76					
37	4×10^{-2}	1×10^{-2}					
$[Ph_3C][BAr^F{}_4]$	8×10^{-2}	2×10^{-2}	70	5	458	–	5.07×10^3
DiBAlO	0.4	0.1					
Decalin	19	4.76					
37	2×10^{-2}	5×10^{-3}					
$[Ph_3C][BAr^F{}_4]$	4×10^{-2}	1×10^{-2}	40	2	798	0.37	4.55×10^5
DiBAlO	0.4	0.1					
Decalin	19	4.76					
37	2×10^{-2}	5×10^{-3}					
$[Ph_3C][BAr^F{}_4]$	4×10^{-2}	1×10^{-2}	40	4	766	0.36	4.25×10^5
DiBAlO	0.4	0.1					
Decalin	19	4.76					
37	2×10^{-2}	5×10^{-3}					
$[Ph_3C][BAr^F{}_4]$	4×10^{-2}	1×10^{-2}	40	8	755	0.37	1.86×10^5
DiBAlO	0.4	0.1					
Decalin	19	4.76					
37	8×10^{-2}	2×10^{-2}					
$[Ph_3C][BAr^F{}_4]$	0.16	4×10^{-2}					
DiBAlO	0.4	0.1	40	5	854	0.37	3.76×10^4
BHT-H	0.8	0.2					
Decalin	19	4.76					
37	8×10^{-2}	2×10^{-2}					
$[Ph_3C][BAr^F{}_4]$	0.16	4×10^{-2}					
DiBAlO	0.4	0.1	40	5	820	0.37	4.78×10^4
BHT-H	1.6	0.4					
Decalin	19	4.76					

A2 Additional data for BHT-H sensitivity of 37 in ethylene oligomerisation in Chapter Five

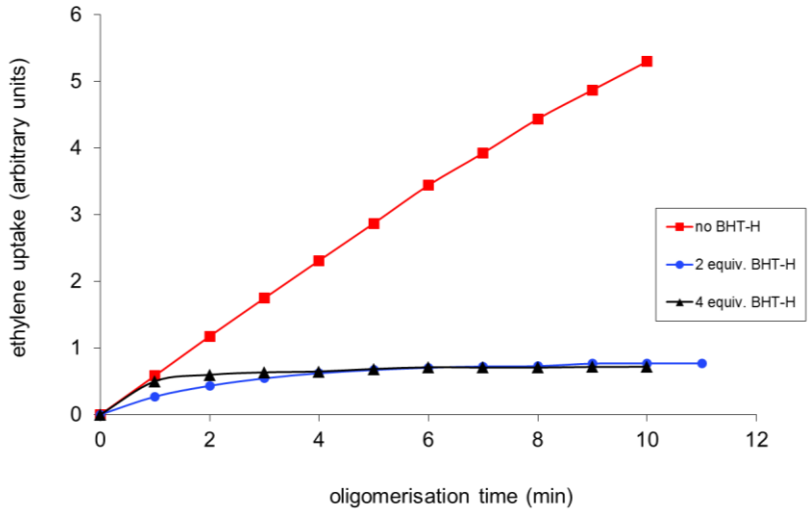

Figure A1. Ethylene uptake of **37** (0.02 μmol) with $[Ph_3C][BAr^F{}_4]$ (0.04 μmol) and DiBAlO (0.4 μmol) with varying amounts of BHT-H.

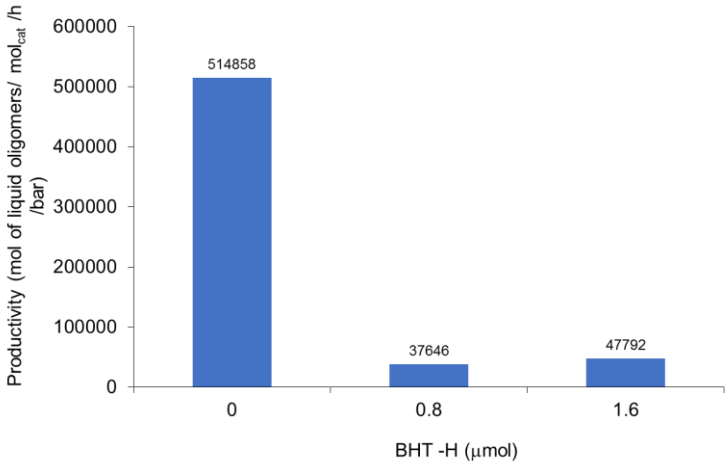

Figure A2. Productivity towards liquid oligomers in the oligomerisation of ethylene with **37** (0.02 μmol) with $[Ph_3C][BAr^F{}_4]$ (0.04 μmol) and DIBAL-O (0.4 μmol) with varying amounts of BHT-H.

A3 Additional data for BHT-H sensitivity of 35 in ethylene oligomerisation in the absence of DiBAlO

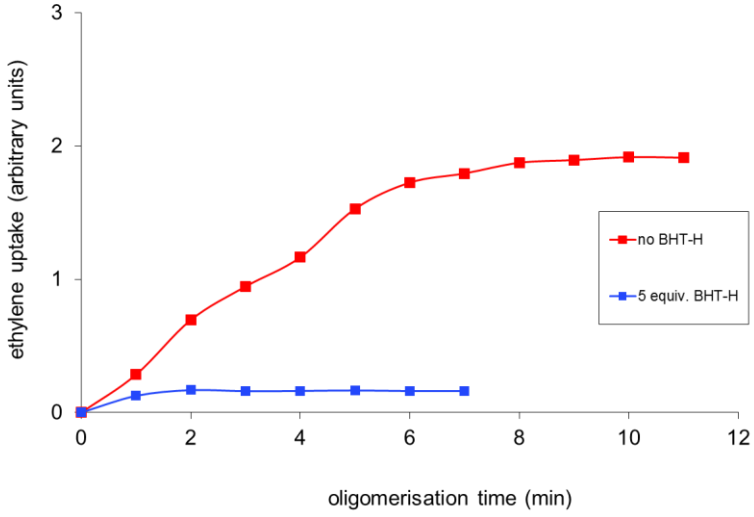

Figure A3. Ethylene uptake of **35** (0.16 μmol) with $[Ph_3C][BAr^F_4]$ (0.32 μmol) with varying amounts of BHT-H.

A4 Example calculation of productivity

The productivity calculated below is for the experiment from Table 5.4, Entry 1.

Table A2. GC data and conversion to mmol of compound.

Compound	Retention time (min)	Area	$A_{compound}/ A_{I.S}$	$m_{compound}$ (mmol)	mmol of C_2 in C_x fraction
C4	2.14	528263.1	19.76	1.216	2.431
C6	2.74	736028.2	27.54	1.369	4.107
C8	6.68	581161.5	21.74	0.669	2.675
C10	9.96	496840.7	18.59	0.457	2.287
Decaline (I.S.)	10.58 and 10.94	26729	1.00	–	–
C12	11.46	377311.9	14.12	0.289	1.737
C14	12.48	276241.5	10.33	0.182	1.271
C16	13.32	183263.7	6.86	0.072	0.574
C18	14.18	118449.9	4.43	0.041	0.371
C20	15.23	71795.3	2.68	0.026	0.255
C22	16.76	44347.6	1.66	0.013	0.139

$m_{compound}$ was calculated following Equation A1, where C is the intercept always equal zero and *f* is the correction factor obtained from the calibration curve (y = *f*x)

$$m_{compound} = \frac{\frac{A_{compound}}{A_{I.S.}} - C}{f \; x \; m_{I.S}} \qquad \textbf{Equation A1}$$

The data for C_4 was not considered, as it is only representative of what is dissolved in solution.

The mmol of C_2 in the C_x fraction was calculated by multiplying $m_{compound}$ with the number of carbons in each oligomer. The total number of mmol of liquid C_2H_4 is the sum of the C_x fractions (excluding C_4) which equals to 13.415 mmol in this case. The productivity was calculated following Equation A2.

$$Productivity = \frac{total\ mol\ of\ liquid\ C_2H_4}{mol\ of\ cat\ x\ pressure\ x\ hour} \qquad \textbf{Equation A2}$$

A5 Example calculation predicted mol(*n*) fractions and wt%

Example calculation of mol(*n*) and wt% including C_4 values, Table 5.4, Entry 3.

Table A3. Calculation of mol(*n*) and weight percentage (%) using the Schulz-Flory distribution and α derived from ln(mol(*n*)/*R*) *vs n*

n	Calc. mol(*n*)/*R*[a]	Calc. normalised mol(*n*)[b]	Calc. wt%[c]
2	0.24	0.60	45.5
3	0.09	0.24	27.0
4	0.04	0.09	14.3
5	0.01	0.04	7.1
6	0.01	0.01	3.4
7	0.002	0.005	1.6
8	0.001	0.002	0.7
9	0.0004	0.0009	0.3
10	0.0001	0.0004	0.1
11	0.0001	0.0001	0.1

[a] mol(*n*)/R = $(1-\alpha)\alpha^{n-1}$, where α = 0.40; [b] normalised by dividing through Σ(calc. mol(*n*)/*R*); [c] wt(%) = 100 × [(mol(n) × Mw)/Σ(mol(n) × Mw)]